Alpha

The Emergent Fine-Structure Constant

Mehrdad Pajuhaan*
(Dated: April 27, 2026)

We present a conditional shell-geometric selection mechanism for the fine-structure coupling within the Relator framework on the paired spaces $\mathbb{C}$ and $\mathbb{R}^3$. Starting from the kinematical lock $R\omega = c$, the construction fixes the minimal pinned electron branch, its matching-shell geometry, the scalar cavity–shell slowdown block $\mathcal{D}_{\mathrm{C}}(\alpha)$, the vector shell constant Λ_{geom}, and the universal single-log coefficient $\mathcal{C}_{\log} = 1/3$. The Alpha Lock Point then selects the coupling through the compatibility condition between the scalar shell law and the vector shell geometry. No measured value of α, no QED anomaly coefficient, and no fitted parameter enters this primary closure.

The resulting finite-rank realization places the emergent coupling in the immediate neighborhood of the accepted fine-structure benchmark, while keeping all benchmark comparisons external to the derivation. As a secondary consequence, the same scalar branch, lifted through the ALP map and the operational orbital slowdown map, generates a pure-photonic electron $g-2$ series. Its first benchmarked coefficients provide a stringent cross-check against the universal QED sequence, and its higher coefficients, beginning with the twelfth-order pure-photonic term $A_1^{(12)}$, are falsifiable predictions of the specified no-free-parameter shell realization.

Why α can be treated as an emergent quantity in the present framework.
The central proposal of this paper is that, on the minimal electron branch, the fine-structure constant need not be inserted as an external input, but can arise from a closed geometric–dynamical equilibrium. The framework is based on a minimal set of explicit postulates stated below, not on hidden tuning or phenomenological fitting of α itself. Its first kinematic ingredient is the Relator light-lock

$$R\,\omega = c,$$

which ties the internal phase-evolution scale of the Schrödinger wavefunction to the speed of light. Its second structural ingredient is that the electron is not modeled as a point source from the outset, but as a Gaussian, equivalently maximum-entropy, branch in an internal complex space $\mathbb{C}$, while the observable phenomenology is read in the orthogonal physical space $\mathbb{R}^3$. In this setting the familiar particle–field image in $\mathbb{R}^3$ is treated as an emergent projection of a more primitive object in $\mathbb{C}$. The corresponding vector image takes the form of a Dirac-type loop, and that projection fixes a *purely geometric quantity*, denoted Λ_{geom}, from the internal geometry of the branch rather than from external fitting.

From the same construction one obtains a closed least-action equation for the one-particle Relator branch. This equation is differential, explicit, and rapidly solvable, and it provides the scalar and vector data that enter the coupled closure studied in the main text. Within the resolved orders analyzed here, the resulting coefficient structure matches the expected QED pattern at the level documented later in the paper, while higher orders remain structurally accessible within the same scheme. In parallel, the electron g_2 factor is interpreted as a derived observable associated with *self-induced time dilation* on the same branch; it serves as a stringent cross-check of the construction, but it is not the primary claim of the paper. The primary claim is that α is selected by a balance law between the scalar, Coulombic sector and the vector, magnetic sector of the electron. Once the geometric quantity Λ_{geom} is inserted into that balance through the ALP (Alpha Lock Point) closure, the value of α is no longer free, and becomes a derived equilibrium quantity of the theory. In this sense, the key mechanism identified in the paper is that

$$R\,\omega = c, \qquad \Lambda_{\mathrm{geom}}, \qquad \text{and the ALP closure}$$

combine into a single structure in which the fine-structure constant appears as an emergent quantity rather than as an externally prescribed parameter.

Code and reproducibility: For reproducibility, the numerical scripts and supporting code used in this work are available in the public repository `https://github.com/pajuhaan/AlphaEmergent`. The repository contains the implementations used to generate the numerical solutions, diagnostic scans, and tables reported in the paper.

* pajuhaan@gmail.com

Part I
Foundations

I. INTRODUCTION AND MAIN RESULTS

The fine-structure coupling α occupies a distinguished place in modern physics. It governs atomic spectra, relativistic wave equations, and electromagnetic interaction strengths, yet in standard practice it enters as a measured dimensionless input rather than as a quantity selected by an internal geometric closure law [1–3]. Its numerical value is known with extraordinary precision [4–8], while the question of its origin remains open. In ordinary formulations of QED, perturbation theory predicts radiative dependence on α after the coupling has been specified; it does not, by itself, select the numerical value of α from an internal equilibrium of the electron branch.

The construction developed here addresses this origin problem by fixing, within the stated postulate set, a kinematical selection principle before the coupled shell problem is solved. This principle ties phase evolution, spatial propagation, and relativistic causality across the paired spaces $\mathbb{C}$ and $\mathbb{R}^3$. In RELATOR this role is carried by the lock $R\omega = c$. Within the explicit postulate set adopted later in sections II and III, this relation enters as a branch-admissibility condition rather than as a fitted condition on α. It places luminal phase transport inside the electron-branch kinematics and fixes a definite geometric relation between internal phase rotation in $\mathbb{C}$ and observable propagation in $\mathbb{R}^3$.

Within this locked branch class, the minimal electron branch is built from a Gaussian generator distribution in $\mathbb{C}$. This choice is consistent with the special role of Gaussian and maximum-entropy states in wave mechanics and statistical inference [9–11]. The observable shell data then arise from a projected one-loop reduction in $\mathbb{R}^3$.

The central result of this paper is conditional on the explicit postulates, branch calibrations, scalar evaluator, and vector-shell datum stated below. Once the branch has been constructed and reduced to its matching shell, α is not inserted as an external numerical input. It is selected as the admissible shell equilibrium at which the Coulombic scalar block and the gauge-invariant transverse inductive shell response close consistently. Equivalently, within the baseline shell closure, the admissible point is the one at which the canonical single-log shell coefficient takes its internally derived shell-geometric value 1/3.

Primary claim. Under the stated shell postulates, the minimal electron-branch reductions, a specified scalar evaluator, and a fixed vector-shell input, the Alpha Lock Point selects a unique admissible coupling α_* whenever the scalar admissibility hypotheses hold.

Primary firewall. No measured value of α, no QED anomaly coefficient, and no fitted parameter enters the primary scalar–vector lock.

Current realization. The printed value of α_* is a realization-level output of the current rank-5 scalar evaluator and the reduced vector input $\Lambda^{(\mathrm{th})}_{\mathrm{geom}}$. It is not asserted to be a certified operator-limit value.

Falsifiable continuation. After the primary lock has been fixed, the same scalar realization generates a secondary mass-independent A_1 electron-anomaly sequence. The higher coefficients beginning with $A_1^{(12)}$ are conditional outputs of the specified realization. Disagreement with future independent pure-photonic calculations outside the combined realization, truncation, and independent-calculation budgets would falsify that specified realization.

The paper has two technical tasks. First, it establishes that the RELATOR construction supplies the infrared structures needed later in the argument, including charge quantization, the Dirac limit, and the tree-level result $g = 2$. These structures fix branch data and consistency conditions; they do not import a numerical value of α. Second, it constructs the scalar slowdown block $\mathcal{D}_{\mathrm{C}}(\alpha)$, the gauge-invariant vector shell response, the logarithmic shell coefficient $\mathcal{C}_{\log}$, and the baseline shell lock of the minimal electron branch. These ingredients are built from the explicit assumptions and branch selections introduced in sections II to IV, and their closure determines the internal lock output α_*.

The numerical value reported below should be read with this logical split in mind. The value of α_* reported for the present realization is a QED-independent output of the geometric lock. The displayed digits have realization-level status and are controlled by two independently improvable ingredients; the reduced vector-geometric input used for $\Lambda^{(\mathrm{th})}_{\mathrm{geom}}$ and the scalar evaluator $\mathcal{D}_{\mathrm{C}}(\alpha)$. A QED-assisted branch is used only as a one-way reference check and not as part of the primary derivation.

The geometric one-loop electron setting used throughout the paper is shown in fig. 4. The geometric lock and the resulting internal fine-structure coupling are developed in sections IX and X, and the fixed notation is collected in table I.

Theorem 1 (Electron branch theorem)**.** *Under the standing postulates of sections II and III, together with the maximum-entropy generator construction and the minimal one-loop calibration of section IV, the minimal electron branch constructed in this paper is characterized by a Gaussian generator profile of width*

$$\sigma_{\mathbb{C}} = \frac{R}{\sqrt{\pi}}, \tag{1}$$

and a first-node matching shell

$$r_* = \pi R, \qquad \eta = \frac{R}{r_*} = \frac{1}{\pi}. \tag{2}$$

After gauging the compact carrier phase, imposing the corresponding canonical quantization, and taking the minimal spinorial infrared completion, with the charge-orientation convention fixed in section V, the same branch carries a quantized charge slot, an infrared Dirac reduction, and a tree-level magnetic-moment normalization with $g = 2$. The resulting shell data are the inputs to the emergent-α construction.

Proof. The Gaussian width follows from the maximum-entropy generator sheet together with the minimal one-loop calibration. In the notation of section IV, the Gaussian first-moment calculation gives the generator angular scale $L_{\mathbb{C}}$, and the minimal one-loop calibration fixes

$$L_{\mathbb{C}} = \frac{1}{2} mcR.$$

Substitution into the width computation in proposition 12 gives

$$\sigma_{\mathbb{C}} = \frac{R}{\sqrt{\pi}},$$

which is Eq. (1).

The matching shell is the first positive node of the regular isotropic radial Helmholtz mode. By proposition 16, the regular origin-normalized profile is

$$S_{\mathrm{Helm}}(r) = j_0(k_{\mathrm{base}} r) = \frac{\sin(k_{\mathrm{base}} r)}{k_{\mathrm{base}} r}.$$

Its positive zeros satisfy $k_{\mathrm{base}} r = p\pi$ with $p = 1, 2, \ldots$. The first-node selection therefore gives $k_{\mathrm{base}} r_* = \pi$. Since the minimal branch has $k_{\mathrm{base}} = R^{-1}$, proposition 17 yields

$$r_* = \frac{\pi}{k_{\mathrm{base}}} = \pi R, \qquad \eta = \frac{R}{r_*} = \frac{1}{\pi}.$$

This proves Eq. (2).

The charge statement is the compact-phase quantization result of theorem 4, which gives

$$Q_k = k q_0, \qquad k \in \mathbb{Z}.$$

The electron sector is the minimal negative-charge sector fixed by the charge-orientation convention in section V. The infrared first-order spinorial completion is theorem 5, which gives the minimally coupled Dirac form on the four-component spinor representative. Finally, the tree-level magnetic normalization follows from the geometric normalization in corollary 3 and from the Pauli reduction in theorem 6. Both routes give the coefficient multiplying $Q/(2m)$ as

$$g = 2.$$

Therefore the stated branch data follow from the cited postulates, branch-selection steps, and infrared reductions. □

Theorem 2 (Alpha lock theorem)**.** *Assume the standing postulates of sections II and III, the minimal electron branch of sections IV and V, the scalar slowdown block $\mathcal{D}_{\mathrm{C}}(\alpha)$ from section VI, the exact operator-level vector-shell constant Λ_{geom} from section VII, and the baseline shell-lock closure Eq.* (464)*. Let the dimensionless scalar target be*

$$\mathfrak{D}_* = \mathfrak{D}_{\mathrm{lock}}(\Lambda_{\mathrm{geom}}) = \frac{3}{2}\,\mathsf{K}_{ALP}\Lambda_{\mathrm{geom}}\left(1 + \frac{\mathsf{K}_{ALP}\Lambda_{\mathrm{geom}}}{2\pi^2}\right). \tag{3}$$

Here K_{ALP} *and* $\Lambda_{\rm geom}$ *are dimensionless shell inputs, with* K_{ALP} *fixed by Eqs.* (428) *and* (430) *and* $\Lambda_{\rm geom}$ *fixed by the vector-shell construction. Assume further that the admissibility condition Eq.* (492) *holds with this value of* $\mathfrak{D}_*$ *for the chosen scalar evaluator. Then the scalar mother branch has a unique admissible lock root* $\alpha_* \in (0,1)$ *such that*

$$\mathcal{D}_{\rm C}(\alpha_*) = \mathfrak{D}_*. \tag{4}$$

Equivalently, with

$$\zeta_* = \frac{\mathsf{K}_{ALP}\Lambda_{\rm geom}}{2\pi^2},$$

the scalar and vector shell sectors close at the baseline logarithmic shell equilibrium

$$\frac{\pi^2}{\mathfrak{D}_*}\,\zeta_*(1+\zeta_*) = \frac{1}{3}. \tag{5}$$

Proof. The baseline shell-lock closure is the zeroth-discrepancy ALP equation of Eq. (464). By theorem 20, inserting $C_\chi = 2\pi^2$ and

$$\zeta = \frac{\mathsf{K}_{\rm ALP}\Lambda_{\rm geom}}{2\pi^2}$$

gives the scalar target

$$\mathfrak{D}_{\rm lock}(\Lambda_{\rm geom}) = \frac{3}{2}\,\mathsf{K}_{\rm ALP}\Lambda_{\rm geom}\left(1 + \frac{\mathsf{K}_{\rm ALP}\Lambda_{\rm geom}}{2\pi^2}\right).$$

This is exactly the quantity denoted by $\mathfrak{D}_*$ in Eq. (3). The hypotheses of theorem 21 are the positivity of this scalar target, membership of this target in the admissible scalar domain, radicand positivity at the target, and placement of the resulting positive branch in $0 < \alpha < 1$. These are precisely the admissibility assumptions stated here through Eq. (492). Therefore theorem 21 gives exactly one admissible physical branch root

$$\alpha_* = \pi\,\frac{\mathfrak{D}_*}{\sqrt{\mathfrak{R}_{\rm moth}(\mathfrak{D}_*)}} \in (0,1),$$

and this root satisfies

$$\mathcal{D}_{\rm C}(\alpha_*) = \mathfrak{D}_*.$$

This proves Eq. (4) and uniqueness on the chosen admissible scalar branch.

It remains only to verify the displayed logarithmic equilibrium. From

$$\zeta_* = \frac{\mathsf{K}_{\rm ALP}\Lambda_{\rm geom}}{2\pi^2},$$

one has

$$\mathsf{K}_{\rm ALP}\Lambda_{\rm geom} = 2\pi^2\zeta_*.$$

Substituting this identity into Eq. (3) gives

$$\begin{aligned}\mathfrak{D}_* &= \frac{3}{2}\left(2\pi^2\zeta_*\right)(1+\zeta_*)\\ &= 3\pi^2\zeta_*(1+\zeta_*).\end{aligned}$$

Dividing both sides by $3\mathfrak{D}_*$ gives

$$\frac{\pi^2}{\mathfrak{D}_*}\,\zeta_*(1+\zeta_*) = \frac{1}{3},$$

which is Eq. (5). □

Numerical realization and reference-only checks. The present realization uses the theorem-level reduced vector input $\Lambda_{\rm geom}^{(\rm th)}$ together with the current rank-5 scalar evaluator for $\mathcal{D}_{\rm C}(\alpha)$. This choice gives the following realization-level internal lock output

$$\alpha_* = 0.007\,297\,352\,565\,050\,600, \qquad \alpha_*^{-1} = 137.035\,999\,163\,494\,704. \tag{6}$$

The numbers in Eq. (6) are rounded central values of the specified reduced realization. Their arithmetic residuals and working-precision stability are audited in section X and appendix C. They do not include a certified operator-limit uncertainty for the unresolved scalar and vector tails.

A separate one-way reference check reconstructs a comparison scalar slowdown branch from the retained external universal pure-photonic QED coefficients of the electron $g/2$ factor, denoted $g_{e,2}$, and then feeds that reconstructed branch into the same theorem-level geometric target $\mathfrak{D}_*^{(\rm th)}$. Using the retained coefficients through $M = 5$, one obtains

$$\alpha_{\rm QED\to D}^{[5]} = 0.007\,297\,352\,564\,484\,953, \qquad \left(\alpha_{\rm QED\to D}^{[5]}\right)^{-1} = 137.035\,999\,174\,116\,901. \tag{7}$$

The numbers in Eq. (7) are rounded central diagnostic values obtained from the retained $M = 5$ external benchmark coefficient set. Their precision is limited by the retained benchmark inputs and by the truncation order of the reference branch. This reference-assisted value plays no role in the primary derivation. It serves only as an external consistency check on the same theorem-level geometric target, using a comparison scalar branch reconstructed from retained QED data.

The values in Eqs. (6) and (7) inherit the realization-level status of both the reduced vector input $\Lambda_{\rm geom}^{(\rm th)}$ and the scalar evaluator. They are not presented as the final exact operator-limit value of the physical fine-structure constant. Improved first-principles evaluations of the vector shell constant, or operator-level improvements of the scalar mother law beyond the current truncation, will propagate into the realized numerical value of α_*. The local sensitivity of the lock to the vector representative is quantified in proposition 55, and the arithmetic and rank-stability audits are recorded in section X and appendix C. The QED-induced cross-check is developed in section XI B.

Remark. Within the stated Relator framework on the paired spaces $\mathbb{C}$ and $\mathbb{R}^3$, the internal derivation is self-contained. The main text contains the load-bearing definitions, propositions, theorems, and proofs needed for the downstream results summarized in theorems 1 and 2. The appendices provide extended calculations, deterministic error audits, implementation-level formulas, reference-only diagnostic maps, and reproducibility material. No appendix imports a measured value of α or a QED coefficient into the primary lock.

For reference, the dependency graph of the primary closure is

$$\begin{gathered}
\text{standing postulates and fixed notation} \\
\Downarrow \\
\text{minimal generator branch and matching shell} \\
\Downarrow \\
\text{infrared charge, Dirac, and tree-level magnetic structure} \\
\Downarrow \\
\mathcal{D}_{\rm C}(\alpha), \quad \Lambda_{\rm geom}, \quad \mathcal{C}_{\rm log} \\
\Downarrow \\
\mathfrak{D}_{\rm lock}(\Lambda_{\rm geom}) = \mathfrak{D}_* \\
\Downarrow \\
\mathcal{D}_{\rm C}(\alpha_*) = \mathfrak{D}_*.
\end{gathered}$$

Equivalently,

$$\text{postulates} \Longrightarrow \text{branch} \Longrightarrow \text{scalar and vector shell data} \Longrightarrow \text{ALP target} \Longrightarrow \alpha_*.$$

Sections II and III fix the postulates, notation, and paired-space kinematics. Sections IV and V construct the minimal electron branch and derive its infrared gauge structure. Sections VI to VIII build the scalar and vector shell blocks and establish the logarithmic shell lock. Finally, sections IX and X determine the admissible geometric-lock root for the specified scalar evaluator and vector representative, and evaluate the resulting internal value of α_*.

The logical order of the paper is strict. The branch is constructed first, its shell quantities are derived next, and the shell equilibrium is solved only at the end. External benchmarks, retained QED coefficients, and measured values of α enter only after the last arrow in the graph above, as comparisons or reference-only diagnostics. The value of α_* is therefore an output of the closure, not an inserted input or a benchmark-matched parameter.

II. STANDING POSTULATES AND FIXED NOTATION

A. Minimal postulate set

The derivation developed below rests on a standing postulate set that fixes the kinematical arena and the admissible shell class. These assumptions do not include the minimal electron branch, the numerical value of α, the scalar slowdown evaluator, the vector-shell constant, any QED anomaly coefficient, or the final scalar–vector shell closure. All of those objects are introduced or derived later within the stated framework.

Assumption 1 (Split generator–propagation arena). *The basic arena is the orthogonal split*

$$\mathbb{C} \oplus \mathbb{R}^3. \tag{8}$$

The factor $\mathbb{C}$ is the internal generator space that carries the primitive phase source. The factor $\mathbb{R}^3$ is the observed propagation and measurement space. The split is structural; the internal factor $\mathbb{C}$ is neither an additional observed spatial dimension nor a second copy of physical three-space.

Assumption 2 (Relator lock and rate decomposition). *There exists a branch radius parameter $R > 0$, with SI dimension of length, a total phase rate $\omega > 0$, and nonnegative split phase-rate magnitudes $\omega_{\mathbb{C}} \geq 0$ and $\omega_{\mathbb{R}^3} \geq 0$. All three rates are measured with respect to one common branch time parameter and have SI dimension T^{-1}. The angular phase itself is dimensionless. These rates are associated with the orthogonal $\mathbb{C}$- and $\mathbb{R}^3$-sectors of the split arena $\mathbb{C} \oplus \mathbb{R}^3$, and satisfy*

$$\omega^2 = \omega_{\mathbb{C}}^2 + \omega_{\mathbb{R}^3}^2, \qquad R\,\omega = c. \tag{9}$$

The equality $R\,\omega = c$ fixes the branch kinematical scale using the SI light speed c. By itself, it is not the observed velocity of a point particle in $\mathbb{R}^3$, and it does not identify R with an empirical electromagnetic length scale. When a worldline is introduced later, the corresponding rest-branch rate is interpreted as a proper-time rate only on the rest branch. We then define the dimensionless master slowdown variable by

$$\mathcal{D}_{\text{total}} = \left(\frac{\omega_{\mathbb{R}^3}}{\omega}\right)^2, \qquad 1 - \mathcal{D}_{\text{total}} = \left(\frac{\omega_{\mathbb{C}}}{\omega}\right)^2, \qquad 0 \leq \mathcal{D}_{\text{total}} \leq 1. \tag{10}$$

This decomposition is the standing kinematical input for the later shell closure. At this stage $\mathcal{D}_{\text{total}}$ is only a dimensionless split-rate variable; it is not yet the scalar slowdown law of the electron branch. The rest-branch normalization and the coherent one-loop realization are derived later from the relativistic rest-branch argument and from the generator reduction.

The symbol R is, at this stage, only a branch-level radius parameter. It is not fixed here by α, by a measured charge, by the electron mass, or by any empirical electromagnetic radius. Its minimal one-loop realization, together with its relation to the Gaussian width and the first-node shell, is derived later.

Assumption 3 (Shell admissibility and gauge regularity). *Every admissible stationary branch considered in this paper admits a smooth matching shell*

$$\Sigma_{r_*} = \{r = r_*\} \simeq \mathbb{S}^2, \qquad r_* > 0,$$

together with a collar whose thickness is controlled by a positive branch width scale $\sigma_{\mathbb{C}}$. At this postulate level, $\sigma_{\mathbb{C}}$ is only a regularity scale for the admissible shell class. On the minimal electron branch, its value is derived later from the generator construction and the one-loop branch selection.

Tangential shell data on Σ_{r_*} are represented by angular fields on $\mathbb{S}^2$. They belong to $H^1_{\tan}(\mathbb{S}^2)$, hence also to $L^2_{\tan}(\mathbb{S}^2)$, are globally single-valued on the matching sphere, and carry no singular string or monopole-type surface defect. For every such datum $X_{\tan}$, the weak surface divergences of $X_{\tan}$ and $\star X_{\tan}$ lie in $L^2(\mathbb{S}^2)$ and have zero mean. The surface Hodge potentials are the unique zero-mean weak solutions of

$$\Delta_{\mathbb{S}^2} h_{\text{ex}} = \operatorname{div}_{\mathbb{S}^2} X_{\tan}, \qquad \Delta_{\mathbb{S}^2} h_{\text{co}} = -\operatorname{div}_{\mathbb{S}^2}(\star X_{\tan}), \qquad \int_{\mathbb{S}^2} h_{\text{ex}}\,\mathrm{d}\Omega = \int_{\mathbb{S}^2} h_{\text{co}}\,\mathrm{d}\Omega = 0.$$

Elliptic regularity on the smooth closed surface $\mathbb{S}^2$ gives

$$h_{\text{ex}}, h_{\text{co}} \in H^2(\mathbb{S}^2)/\mathbb{R}.$$

Thus the standard surface Hodge decomposition is

$$X_{\tan} = \nabla_{\mathbb{S}^2} h_{\mathrm{ex}} + \star\nabla_{\mathbb{S}^2} h_{\mathrm{co}}, \qquad h_{\mathrm{ex}}, h_{\mathrm{co}} \in H^2(\mathbb{S}^2)/\mathbb{R}, \tag{11}$$

with equality in $H^1_{\tan}(\mathbb{S}^2)$. *Here* $\star$ *denotes the Hodge rotation on the oriented sphere induced by the outward normal convention. The first term is the exact surface-gradient component, and the second term is the coexact surface divergence-free component. The harmonic one-form sector is absent on* $\mathbb{S}^2$, *since* $H^1_{\mathrm{dR}}(\mathbb{S}^2) = 0$*; see, for example, [12, 13].*

The admitted shell gauge transformations are represented by smooth globally single-valued scalar functions on the matching sphere. Thus a pure tangential gauge datum has the form $\nabla_{\mathbb{S}^2}\lambda$, *with* λ *single-valued on* $\mathbb{S}^2$. *This is a regularity restriction on the admissible shell class, not a gauge fixing and not a fitted condition. The geometric tangential-transverse shell projector is therefore the standard* $L^2_{\tan}(\mathbb{S}^2)$*-orthogonal Hodge projector*

$$\Pi_{\mathrm{TT}} X_{\tan} = \star\nabla_{\mathbb{S}^2} h_{\mathrm{co}} = X_{\tan} - \nabla_{\mathbb{S}^2} h_{\mathrm{ex}},$$

where h_{ex} *and* h_{co} *are the Hodge potentials of* $X_{\tan}$. *Since the exact and coexact Hodge subspaces are* $L^2_{\tan}$*-orthogonal,* Π_{TT} *is bounded, self-adjoint, and idempotent. If* $X_{\tan} = \nabla_{\mathbb{S}^2}\lambda$, *then the zero-mean exact potential is*

$$h_{\mathrm{ex}} = \lambda - \frac{1}{4\pi}\int_{\mathbb{S}^2} \lambda \,\mathrm{d}\Omega, \qquad h_{\mathrm{co}} = 0,$$

and hence

$$\Pi_{\mathrm{TT}} \nabla_{\mathbb{S}^2}\lambda = 0.$$

Thus pure tangential gradient data lie in the null space of Π_{TT}. *The operator* Π_{TT} *is a geometric operator associated with the shell regularity assumption, not an independently fitted shell object.*

Assumption 4 (Exterior vacuum regularity)**.** *Outside the matching shell, the exterior field associated with any admissible shell-reduced interior branch is a stationary source-free vacuum field on* $r > r_*$. *It has finite energy and belongs to the decaying exterior branch at spatial infinity. In the axisymmetric reductions used later, scalar representatives of tangential shell traces are written in the polar-cosine variable* $\upsilon = \cos\vartheta$. *Endpoint regularity is imposed in the flux-compatible form*

$$f(\upsilon) = \sqrt{1-\upsilon^2}\,\widetilde{f}(\upsilon),$$

whenever a tangential vector trace carries the standard polar endpoint factor. The reduced profile $\widetilde{f}$, *or equivalently the energy-dual representative obtained after the endpoint factor has been removed, is required to extend real-analytically to an open neighborhood of the closed interval* $[-1, 1]$.

The odd shell expansions used later in the construction of $\Delta\Lambda_{\mathrm{out}}$ *are defined only for traces in this exterior-regularity class. Equivalently, when the odd toroidal basis and the flux pairing are introduced, admissible exterior data are restricted to the coefficient class for which the displayed exterior-energy series and the* $\Delta\Lambda_{\mathrm{out}}$ *series are absolutely convergent. This summability requirement is part of the exterior-domain assumption, not a conclusion derived at the postulate level. For the exact Maxwell trace of the filamentary carrier used later, the endpoint factorization and the square-summability needed for the exact* $\Delta\Lambda_{\mathrm{out}}$ *construction are checked separately in lemma 18 and theorem 12. This exterior regularity condition fixes the admissible function class for* $\Delta\Lambda_{\mathrm{out}}$*; it does not tune* $\Delta\Lambda_{\mathrm{out}}$ *to any value of* α.

These four assumptions are intentionally lean. The Gaussian generator profile, the minimal electron branch, and the first-node shell $r_* = \pi R$ are derived later from the generator construction and the branch-selection steps. The charge slot follows later from the compact phase sector and its canonical quantization. The infrared Dirac limit is derived later within the stated local first-order infrared operator class. The tree-level result $g = 2$ then follows from the minimal spin normalization and, independently, from the Pauli reduction of the minimally coupled Dirac equation. No measured magnetic anomaly or QED radiative coefficient enters that tree-level statement. None of these objects belongs to the standing postulate set. The schematic hierarchy in fig. 1 is organizational only and adds no further assumption. The higher-family boxes in that figure are placeholders only; they are neither generator-winding labels nor shell-node labels.

B. Fixed notation and conventions

We now fix the notation for the shell geometry, scalar reduction, vector reduction, and the auxiliary operators used in those constructions. Only symbols that remain active in the paper are recorded here. Composite quantities whose

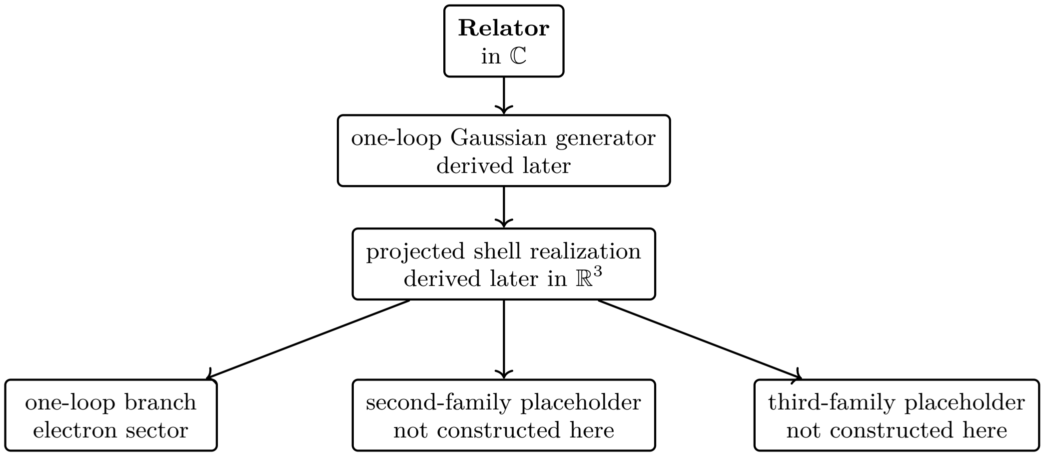

FIG. 1. Organizational schematic of the branch hierarchy used in the paper. Only the minimal electron branch enters the present construction. The muon and tau boxes are conditional family placeholders for downstream extensions; they are neither generator-winding sectors nor shell-node sectors, and they add no standing assumption.

full assembly is introduced later are described here only by role, dimension, and notation. The appearance of such a symbol in this subsection does not promote it to a standing postulate or a numerical input to the closure.

$$\upsilon = \cos\vartheta \in [-1,1], \qquad \eta = \frac{R}{r_*} > 0, \qquad \ell = \frac{\sigma_{\mathbb{C}}}{r_*} > 0. \tag{12}$$

At this stage $r_* > 0$ and $\sigma_{\mathbb{C}} > 0$ are symbolic branch quantities, while η, ℓ, and υ are dimensionless. Accordingly, r_* and $\sigma_{\mathbb{C}}$ carry SI dimension $[L]$. Their minimal electron-branch values are derived later and are not part of the standing notation.

Here $\vartheta \in [0,\pi]$ denotes the polar angle on $\mathbb{S}^2$, whereas $\theta \in [0, 2\pi)$ denotes the azimuthal coordinate on the oriented loop $\mathbb{S}^1$. The parameter ℓ always denotes the shell-bandwidth ratio entering the tangential-transverse shell-admission construction. The scalar symbol x denotes the dimensionless coupling variable in scalar-lock, QED-series, and coupling-variable contexts,

$$x = \frac{\alpha}{\pi}.$$

This is only a change of variable once α is treated as the unknown coupling; it does not assign a numerical value to α. Spacetime coordinates x^μ and spatial coordinates $\mathbf{x}$, when used, remain distinct by index and boldface notation. Whenever the parity-restricted exterior axisymmetric multipole expansion is used, the harmonic degree is indexed by odd integers,

$$j \in \{1, 3, 5, \dots\}.$$

This odd-degree convention belongs only to that restricted exterior sector; it is not a global removal of even modes from the full shell data.

TABLE I: Canonical notation and symbol definitions.

Symbol	Meaning	Dimension and notation rule
Spaces and kinematics		
$\mathbb{C}$	generator space	geometric space; internal phase sector; its radial coordinate has dimension $[L]$
$\mathbb{R}^3$	propagation space	geometric space; observed Euclidean three-space with coordinates of dimension $[L]$
R	Relator radius	$[L]$; branch-level generator radius
ω	total phase rate	$[T^{-1}]$; total rate in Eq. (9); ω is reserved for rate-like or frequency-like quantities
$\omega_{\mathbb{C}}$	$\mathbb{C}$ phase rate	$[T^{-1}]$; generator-side share
$\omega_{\mathbb{R}^3}$	$\mathbb{R}^3$ phase rate	$[T^{-1}]$; propagation-side share

Continued on next page

TABLE I continued from previous page

Symbol	Meaning	Dimension and notation rule
$\omega_{\rm ph}$	physical phase rate	$[T^{-1}]$; gauge-invariant local phase-rate representative
$\omega_{\rm dot}$	dot/clock phase rate	$[T^{-1}]$; clock-rate member of the Relator rate family
$\mathcal{D}_{\rm total}$	master slowdown	dimensionless; split-rate variable defined in Eq. (10) before the electron branch is selected
$\mathcal{D}_{\rm C}(\alpha)$	scalar slowdown evaluator	dimensionless function of the unknown coupling; derived from the Coulombic shell block
$\Delta\mathcal{D}_{\Lambda}$	vector slowdown correction	dimensionless; derived from the inductive shell response
$x=\alpha/\pi$	scalar coupling variable	dimensionless; used in scalar-lock, QED-series, and coupling-variable contexts; x^μ and $\mathbf{x}$ remain coordinate notation
Shell geometry and shell data		
$\mathbb{S}^1$	oriented loop / compact phase circle	dimensionless angular manifold; positive orientation in θ
$\mathbb{S}^2$	matching sphere	dimensionless angular sphere after radius extraction; outward normal toward $r>r_*$
r_*	matching radius	$[L]$; branch-dependent shell radius; minimal value derived later
$\sigma_{\mathbb{C}}$	branch width parameter	$[L]$; Gaussian width after the minimal generator branch is fixed
η	shell-radius ratio	dimensionless; $\eta=R/r_*$
ℓ	shell-bandwidth ratio	dimensionless; $\ell=\sigma_{\mathbb{C}}/r_*$
υ	polar-cosine coordinate	dimensionless; $\upsilon=\cos\vartheta\in[-1,1]$
$\rho_\perp(\upsilon)$	normalized shell cylindrical radius	dimensionless; cylindrical radius of a normalized shell point; ρ remains the $\mathbb{C}$ radial coordinate
$\varpi_{\rm col}(\xi)$	half-Gaussian collar weight	dimensionless; collar weight on $\xi\geq 0$
$N_{\rm col}$	L^2-mass of the collar weight	dimensionless; $N_{\rm col}=\Vert\varpi_{\rm col}\Vert^2_{L^2(0,\infty)}$
$\mathscr{A}_{\rm sh}$	generic tangential shell trace	shell datum; generic tangential trace used in shell-admission functionals
$\mathscr{A}_{\parallel}^{\rm coll}$	collar-averaged branch shell trace	shell datum; tangential branch trace obtained by collar reduction
$\mathscr{A}_{\rm TT}^{\rm coll}$	TT-cleaned branch shell trace	shell datum; tangential-transverse representative after applying $\Pi_{\rm TT}$
$\mathcal{S}$	Hamilton–Jacobi action	$[ML^2T^{-1}]$; action-valued field; $\nabla\mathcal{S}$ has SI momentum units
$\mathbf{A}$	electromagnetic vector potential	$[MLT^{-1}Q_{\rm el}^{-1}]$; SI vector potential in $\mathbb{R}^3$
$\mathbf{P}_{\rm mech}$	gauge-invariant mechanical momentum	$[MLT^{-1}]$; $\mathbf{P}_{\rm mech}=\nabla\mathcal{S}-Q\mathbf{A}$, with the sign carried by the charge Q
$\lambda_{\rm g}$	electromagnetic gauge-transform scalar	action per charge in SI units; gauge scalar in electromagnetic transformations
$\lambda_{\rm sh}$	shell-averaged gauge scalar	same units as $\lambda_{\rm g}$; gauge scalar obtained after collar reduction
$h_{\rm ex}$	exact Hodge potential	zero-mean scalar on $\mathbb{S}^2$; exact potential in the shell Hodge decomposition
$h_{\rm co}$	coexact Hodge potential	zero-mean scalar on $\mathbb{S}^2$; coexact potential in the shell Hodge decomposition
β_U	local toroidal one-form	one-form; local toroidal form used in the toroidal Hodge calculation
Scalar evaluator and visible finite-rank data		
$\mathfrak{R}_{\rm moth}(D)$	scalar mother radicand	dimensionless; radicand of the retained admissible scalar branch
$\Theta_{1,\rm eff}$	effective first static load	dimensionless; static first-order coefficient entering $\mathfrak{R}_{\rm moth}(D)$
$B_{11}^{\rm glue}$	visible static glued load	dimensionless; two-channel visible static coefficient
$B_{11}^{(3,\rho)}$	three-channel static completion load	dimensionless; reduced static load in the no-free-parameter static completion
$A_{\rm vis,0}$	common visible dynamic baseline	dimensionless; common baseline entering the visible dynamic amplitudes $A_{\rm uv}^{(N)}$ and $A_{\rm ir}^{(N)}$
$A_{\rm uv}^{(N)}$	visible UV dynamic amplitude	dimensionless; finite-N visible dynamic amplitude
$A_{\rm ir}^{(N)}$	visible IR dynamic amplitude	dimensionless; finite-N visible dynamic amplitude
$s_{\rm uv}$	visible UV pole scale	dimensionless; pole scale in the visible two-mode dynamic block
$s_{\rm ir}$	visible IR pole scale	dimensionless; pole scale in the visible two-mode dynamic block
χ_N	visible dynamic cross coefficient	dimensionless; finite-N off-diagonal coefficient in the visible dynamic block
$\Phi_{\rm dyn}^{(N)}(D)$	visible dynamic response	dimensionless; finite-N dynamic block entering the scalar mother radicand
$\mathcal{G}_{e\gamma}^{\rm gl,N}(D)$	visible glued dynamic evaluator	dimensionless; two-mode realization-level evaluator for $\Phi_{\rm dyn}^{(N)}(D)$
Vector quantities and lock maps		
$\Lambda_{\rm ind}$	filamentary reference core	dimensionless; leading logarithmic loop-core contribution
$\Delta\Lambda_{\rm UV\to IR}(\ell;\mathscr{A}_{\rm sh})$	admitted UV-to-IR transfer	dimensionless; shell functional of ℓ and a supplied tangential shell trace $\mathscr{A}_{\rm sh}$
$\Delta\Lambda_{\rm out}(\eta)$	exterior shell subtraction	dimensionless; signed exterior vacuum functional at radius ratio η
$\Lambda_{\rm geom}$	vector geometric constant	dimensionless; exact branch-fixed vector self-return invariant
$\Lambda_{\rm geom}^{(N)}$	finite-rank vector representative	dimensionless; Galerkin finite-rank representative of $\Lambda_{\rm geom}$

Continued on next page

TABLE I continued from previous page

Symbol	Meaning	Dimension and notation rule
$\Lambda_{\rm geom}^{(\rm th)}$	reduced vector representative	dimensionless; current reduced vector-shell representative used in the numerical realization
$\mathscr{R}_w(\rho)$	$\mathbb{C}$ radial density ratio	dimensionless; local ratio $w(\rho)/w_{\mathbb{C}}(\rho)$ in the entropy proof
$\mathsf{G}_{c\ell}$	collar–log gluing operator	operator; collar–log gluing object in scalar-shell evaluation contexts
$g_{c\ell}$	collar–log scalar overlap	dimensionless; scalar overlap associated with the reduced collar–log gluing calculation
$\mathfrak{D}_{\rm lock}(\Lambda)$	scalar target map	dimensionless; baseline scalar target map assembled from the ALP closure
$\mathfrak{D}_*$	exact scalar target value	dimensionless; exact vector-input scalar target $\mathfrak{D}_{\rm lock}(\Lambda_{\rm geom})$
$\mathfrak{D}_*^{(\rm th)}$	current reduced scalar target	dimensionless; reduced target $\mathfrak{D}_{\rm lock}(\Lambda_{\rm geom}^{(\rm th)})$
$\mathsf{K}_{\rm ALP}$	central ALP scalar coefficient	dimensionless; scalar coefficient entering the ALP target map
Projectors, admission operators, and geometric constants		
$\Pi_{\rm TT}$	geometric tangential-transverse shell projector	dimensionless operator; $L^2_{\rm tan}$-orthogonal projector onto the divergence-free tangential sector
$\mathbb{Q}_\chi(\ell)$	shell-admission operator	dimensionless operator; bandwidth-dependent admission map
$\overline{\mathbb{Q}_\chi}(\ell)$	normalized shell-admission operator	dimensionless operator; normalized shell-admission map
$P_{IR}^{(\chi)}(\ell;\mathscr{A}_{\rm sh})$	scalar admitted weight	dimensionless Rayleigh quotient associated with a nonzero tangential shell trace $\mathscr{A}_{\rm sh}$
$\mathcal{C}_{\log}$	shell logarithmic coefficient	dimensionless; common logarithmic coefficient from the shell calculation
$C_{\rm uni}$	uniform shell constant	dimensionless; scalar shell constant
$C_{\rm UV}^{(\rm Gauss)}$	Gaussian UV constant	dimensionless; Gaussian finite part entering the shell transfer calculation
C_χ	shell angular constant	dimensionless; fixed geometric shell constant

Two sesquilinear shell pairings are used repeatedly. Both are fixed as unnormalized reduced pairings. Whenever a Rayleigh quotient is formed with the same pairing in numerator and denominator, any common positive angular normalization factor cancels identically. For 2π-periodic loop data $f,g\in L^2(0,2\pi)$ on $\mathbb{S}^1$, we use the loop pairing

$$\langle f,g\rangle_\theta=\int_0^{2\pi}\overline{f(\theta)}\,g(\theta)\,\mathrm{d}\theta. \tag{13}$$

For scalar amplitudes representing axisymmetric flux-compatible tangential shell data on $\mathbb{S}^2$, written after removal of the standard polar endpoint factor in the form

$$f(\upsilon)=\sqrt{1-\upsilon^2}\,\widetilde{f}(\upsilon),\qquad g(\upsilon)=\sqrt{1-\upsilon^2}\,\widetilde{g}(\upsilon),\qquad \widetilde{f},\widetilde{g}\in L^2(-1,1), \tag{14}$$

with the factorization understood almost everywhere, we define

$$\langle f,g\rangle_{\rm flux}=\int_{-1}^{1}\frac{\overline{f(\upsilon)}\,g(\upsilon)}{1-\upsilon^2}\,\mathrm{d}\upsilon=\int_{-1}^{1}\overline{\widetilde{f}(\upsilon)}\,\widetilde{g}(\upsilon)\,\mathrm{d}\upsilon. \tag{15}$$

Thus the map $f\mapsto\widetilde{f}$ is an isometric identification of the flux-compatible class with $L^2(-1,1)$. Hence

$$\langle f,f\rangle_{\rm flux}=\|\widetilde{f}\|^2_{L^2(-1,1)}\geq 0,$$

with equality only if $f=0$ almost everywhere. The apparent endpoint singularity in $(1-\upsilon^2)^{-1}$ is therefore removable on the flux-compatible class.

The pairing Eq. (13) is used for loop tangential shell amplitudes and the associated Rayleigh quotients. The weighted pairing Eq. (15) is used for the reduced exterior shell subtraction. It is the pullback of the standard $L^2(-1,1)$ pairing under the endpoint factorization. It is compatible with the standard axisymmetric vector-spherical-harmonic conventions on $\mathbb{S}^2$, provided the same endpoint factor and the same unnormalized angular convention are used throughout; see, for example, [13, 14].

Although the symbols $\Pi_{\rm TT}$, $\mathbb{Q}_\chi(\ell)$, and $P_{IR}^{(\chi)}(\ell;\mathscr{A}_{\rm sh})$ are listed together in table I, they play distinct roles. The first is the geometric $L^2_{\rm tan}$-orthogonal projector onto the divergence-free tangential sector fixed by the admissible gauge-regular shell class. The second is a bandwidth-dependent shell-admission operator. The third is the scalar Rayleigh quotient generated by that operator on a nonzero tangential shell trace $\mathscr{A}_{\rm sh}$. Their exact definitions are given later in their natural settings. None of the three is a fitted parameter.

The orientation conventions are fixed once and for all. The loop $\mathbb{S}^1$ carries the positive orientation of increasing azimuth θ, and the normal on $\mathbb{S}^2$ is the outward unit normal pointing into the exterior region $r>r_*$. All later sign choices refer to these orientations. In particular, $\Delta\Lambda_{\mathrm{UV}\to\mathrm{IR}}$ carries the positive admitted-transfer sign, whereas $\Delta\Lambda_{\mathrm{out}}$ is defined later as the signed exterior-subtraction functional. The negative sign in $\Delta\Lambda_{\mathrm{out}}$ is therefore fixed by orientation and subtraction convention; it is not introduced as an adjustable sign. The exact formulas are stated later, and these conventions remain unchanged throughout the paper.

Definition II.1 (Operational matching shell)**.** In the present paper, a shell is neither a microscopic material boundary of a particle nor an empirical radius inserted from outside the closure. Instead, it is an effective matching surface $r = r_*$ in the observed space $\mathbb{R}^3$, where the interior branch is represented by shell data and an exterior source-free field. For the minimal branch constructed later, the generator-side profile in $\mathbb{C}$ is Gaussian and has no compact support. The radius r_* therefore marks the first geometrically distinguished matching interface between the interior branch, the local shell data, and the exterior vacuum field, rather than a literal material boundary.

Remark (Scope of the present paper). The present work studies the shell reduction of the minimal one-loop electron branch and the coupled scalar–vector equilibrium defined on that shell. It does not address the deeper dynamical selection of the electron rest mass. Once the branch has been constructed, its observable infrared data are organized at the shell level. After the scalar evaluator and the vector-shell input have been specified, the admissible value of α is selected by shell-level closure within the stated postulates and branch choices. No measured value of α, no electron-anomaly coefficient, and no additional rest-mass input beyond the earlier branch normalization enter this final selection step.

C. Logical status of the main objects

The principal objects of the paper are classified as standing postulates, definitions, derived shell objects, summary objects, reduced representatives, numerical realizations, and external benchmarks. This classification fixes the role each object plays inside the closure. In particular, it prevents a derived, reduced, or numerical representative from being mistaken either for defining shell data or for an independent input to the closure.

TABLE II. Logical-status ledger for the principal objects used in the shell closure. Standing postulates, derived objects, summary objects, reduced representatives, numerical realizations, and external benchmarks are kept distinct throughout the paper.

Object	Status	Basis
$\mathbb{C} \oplus \mathbb{R}^3$	standing postulate	assumption 1
$R\omega = c$, rate split	standing postulate	assumption 2
$\mathcal{D}_{\mathrm{total}}$	kinematic definition	Eq. (10)
Π_{TT}	derived shell operator	shell Hodge class of assumption 3
$r_*, \sigma_{\mathbb{C}}, \eta, \ell$	derived branch data	minimal-branch construction in section IV
$\mathcal{D}_{\mathrm{C}}(\alpha)$	primary scalar object	scalar mother law
$\Lambda_{\mathrm{ind}}, \Delta\Lambda_{\mathrm{UV}\to\mathrm{IR}}, \Delta\Lambda_{\mathrm{out}}$	primary vector-side ingredients	vector-shell construction
$\mathcal{C}_{\log}$	derived logarithmic coefficient	two-path shell calculation
Λ_{geom}	conditional exact summary invariant	exact vector-shell return under the stated vector hypotheses
$\Lambda_{\mathrm{geom}}^{(N)}$	finite-rank Galerkin realization	Galerkin vector evaluator
$\Lambda_{\mathrm{geom}}^{(\mathrm{th})}$	theorem-level reduced representative	reduced vector evaluator
$\Lambda \mapsto \mathfrak{D}_{\mathrm{lock}}(\Lambda)$	summary target map	baseline ALP closure
charge spectrum $Q = kq_0$	derived theorem-level statement	canonical phase quantization of the compact phase sector
infrared Dirac equation	derived theorem-level statement	minimal first-order infrared completion
tree-level $g = 2$	derived theorem-level statement	spin normalization and Pauli reduction
α_*	conditional lock root	scalar law, fixed vector input, and admissibility
α_{ref}, CODATA, QED coefficients	external benchmarks	comparison only

Definition II.2 (Primary objects of the shell closure)**.** The primary objects entering the shell closure are

$$\mathcal{D}_{\mathrm{C}}(\alpha), \qquad \Lambda_{\mathrm{ind}}, \qquad \Delta\Lambda_{\mathrm{UV}\to\mathrm{IR}}(\ell; \mathscr{A}_{\mathrm{sh}}), \qquad \Delta\Lambda_{\mathrm{out}}(\eta), \qquad \mathcal{C}_{\log}.$$

Here primary means load-bearing within the shell closure. It does not mean postulated, fitted, or numerically imported. Each listed item is introduced later either as a defining shell object or as a theorem-level derived shell quantity.

More specifically, $\mathcal{D}_{\mathrm{C}}(\alpha)$ is the scalar slowdown branch extracted from the scalar shell problem, with α treated as the unknown coupling. The functional $\Delta\Lambda_{\mathrm{UV}\to\mathrm{IR}}(\ell; \mathscr{A}_{\mathrm{sh}})$ is the admitted ultraviolet-to-infrared shell transfer associated with a nonzero tangential shell trace $\mathscr{A}_{\mathrm{sh}}$ at bandwidth ratio ℓ. The functional $\Delta\Lambda_{\mathrm{out}}(\eta)$ is the signed exterior shell-subtraction functional at shell-radius ratio η. The quantity Λ_{ind} is the intrinsic filamentary reference carried into the vector shell chain and is not adjusted to the lock output. The coefficient $\mathcal{C}_{\log}$ is the logarithmic shell coefficient fixed later by the two-path shell calculation, not by importing a QED logarithm. Branch-fixed specializations obtained by freezing ℓ, η, or the shell trace do not replace these primary objects.

Definition II.3 (Summary objects)**.** A summary object is any assembled quantity or map built from primary shell objects, fixed geometric constants, and explicit remainder terms, with no new shell-level input. In the present paper the principal examples are the operator-level vector-shell invariant $\Lambda_{\rm geom}$ and the target map $\Lambda \mapsto \mathfrak{D}_{\rm lock}(\Lambda)$. Reduced or finite-rank representatives of a summary object inherit their meaning from the corresponding exact or conditional-exact summary object and are identified by explicit superscripts, rank labels, or realization statements. A summary object is therefore derived rather than primary, and any representative of a summary object remains derived rather than constituting a new shell-level input.

Definition II.4 (Reduced representative, numerical realization, and external benchmark)**.** A reduced representative is a theorem-level or model-reduced expression that descends from an exact shell object under stated hypotheses. It is not a new shell-level input. A numerical realization is a finite-rank or otherwise implementation-level evaluation of an exact object or of a stated reduced representative. It may be used to produce a reported number, yet it does not replace the exact object from which it descends. Examples include $\Lambda_{\rm geom}^{(N)}$, finite-rank scalar evaluators, and the printed numerical value of α_* obtained from specified scalar and vector inputs. The quantity $\Lambda_{\rm geom}^{(\rm th)}$ is treated as a reduced vector representative, not as the exact operator-level invariant $\Lambda_{\rm geom}$.

An external benchmark is a value imported only for comparison after the internal shell closure has been evaluated. Examples include measured or adjusted values of α, recoil determinations, electron-moment determinations, CODATA adjustments, and perturbative QED coefficients. Such quantities are not part of the standing postulates and do not enter the primary closure.

Remark. The distinction between shell-level objects and reduced representatives is especially important for $\Delta\Lambda_{\rm out}$, $\Delta\Lambda_{\rm UV\to IR}$, and $\mathcal{C}_{\rm log}$. These objects are fixed first at the shell level. Any reduced formula or evaluator attached to them is introduced only afterwards as a derived representative, with its hypotheses and range of validity stated explicitly.

Remark. The classifications introduced in this subsection concern logical role rather than analytic domain or coordinate convention. They record whether an object is postulated, defined, derived, reduced, numerical, or external. They introduce no additional dynamical assumption, no value of α, no charge spectrum, no scalar evaluator, and no new shell closure.

III. GENERATOR SPACE $\mathbb{C}$ AND RELATOR KINEMATICS

A. $\mathbb{C}$ and the split $\mathbb{C} \oplus \mathbb{R}^3$

We now make explicit the geometric meaning of the split arena fixed in assumption 1. The point of this subsection is not to introduce a new dynamical law, a value of α, or a shell evaluator. Its purpose is to explain why $\mathbb{C}$ is the natural minimal metric lift of the compact complex phase carried by a quantum branch, and why the direction sphere of the observed $\mathbb{R}^3$-factor is naturally encoded by the minimal projective spinorial lift.

The logical distinction is important. The complex value line of a coarse-grained wavefunction will be denoted by $\mathbb{C}_{\rm ph}$. It is an auxiliary phase-amplitude line attached to a representative ψ. The generator plane $\mathbb{C}$, by contrast, is the autonomous metric carrier used by the Relator branch construction. The two are not identified pointwise. The compact phase of $\mathbb{C}_{\rm ph}$ motivates the $\mathbb{S}^1$ carrier direction in $\mathbb{C}$, while the radial coordinate in $\mathbb{C}$ is an independent branch-scale coordinate. Likewise, $\mathbb{R}^3$ is not obtained from a single complex line alone. A single complex line carries a circle of phases. Observed spatial directions arise only after the minimal two-component projective lift, whose complex-ray quotient is

$$\mathbb{CP}^1 := \big(\mathbb{C}^2 \setminus \{0\}\big)/\mathbb{C}^\times \simeq \mathbb{S}^2.$$

The observed radial coordinate then gives the metric cone over this direction sphere, which is Euclidean $\mathbb{R}^3$. This explains the split as a minimal generator-projection arena. It is not a derivation of physical three-space from a scalar complex value line alone.

Definition III.1 (Auxiliary complex phase fibre)**.** Let a coarse-grained scalar branch representative be defined on a nodal-free region by

$$\psi(t, \mathbf{x}) \in \mathbb{C}_{\rm ph} \setminus \{0\}.$$

The auxiliary phase fibre is the punctured complex value line $\mathbb{C}_{\mathrm{ph}} \setminus \{0\}$, with polar decomposition

$$\psi = |\psi|\, e^{i\varphi_{\mathrm{ph}}}, \qquad \varphi_{\mathrm{ph}} \in \mathbb{R}/2\pi\mathbb{Z}. \tag{16}$$

Equivalently, in the Madelung notation used later,

$$\psi = \sqrt{\rho_\psi}\, e^{i\mathcal{S}/\hbar}, \qquad \varphi_{\mathrm{ph}} = \mathcal{S}/\hbar \mod 2\pi.$$

The modulus $|\psi|$ is the normalization-dependent amplitude of the wavefunction representative. It is not the generator-plane radius in $\mathbb{C}$.

Proposition 1 (Canonical compact phase carried by a non-nodal branch)**.** *On every simply connected nodal-free region of a scalar branch, the normalized phase*

$$U_\psi(t,\mathbf{x}) := \frac{\psi(t,\mathbf{x})}{|\psi(t,\mathbf{x})|} = e^{i\mathcal{S}(t,\mathbf{x})/\hbar} \tag{17}$$

is a well-defined map into $U(1) \simeq \mathbb{S}^1$. Under an electromagnetic gauge transformation

$$\psi \mapsto e^{iq\lambda_{\mathrm{g}}/\hbar}\psi, \qquad \mathbf{A} \mapsto \mathbf{A} + \nabla\lambda_{\mathrm{g}}, \qquad \Phi \mapsto \Phi - \partial_t\lambda_{\mathrm{g}},$$

where $q\lambda_{\mathrm{g}}$ has SI units of action, it transforms by multiplication with a $U(1)$-valued phase,

$$U_\psi \mapsto e^{iq\lambda_{\mathrm{g}}/\hbar}U_\psi.$$

Thus the compact phase circle is forced by the complex Schrödinger representative and gauge covariance. No metric radius in $\mathbb{C}$ is fixed by this statement.

Proof. Since $\psi \neq 0$ on the region under consideration, the quotient $\psi/|\psi|$ is pointwise defined and has unit modulus. Hence $U_\psi \in U(1)$. On a simply connected nodal-free region the $U(1)$-valued map admits a continuous real phase lift, so

$$U_\psi = e^{i\mathcal{S}/\hbar}.$$

Under

$$\psi \mapsto e^{iq\lambda_{\mathrm{g}}/\hbar}\psi,$$

the modulus is unchanged, since

$$\left|e^{iq\lambda_{\mathrm{g}}/\hbar}\psi\right| = |\psi|.$$

Therefore

$$\frac{\psi}{|\psi|} \mapsto \frac{e^{iq\lambda_{\mathrm{g}}/\hbar}\psi}{\left|e^{iq\lambda_{\mathrm{g}}/\hbar}\psi\right|} = e^{iq\lambda_{\mathrm{g}}/\hbar}\frac{\psi}{|\psi|}.$$

This proves the stated $U(1)$ transformation law. The construction uses only the normalized phase and does not assign any length scale to the modulus of ψ. □

Definition III.2 (Autonomous generator lift)**.** The autonomous generator lift replaces the auxiliary phase circle of $\mathbb{C}_{\mathrm{ph}}$ by a metric carrier with an independent radial coordinate. The lift is required to satisfy the following minimal properties.

1. It carries a nontrivial continuous orthogonal $U(1)$ phase action whose nonzero orbits are circles.
2. It has one positive radial invariant measuring branch scale.
3. It is the lowest-dimensional real Euclidean vector carrier with these two properties.

The resulting carrier is a Euclidean real two-plane, equivalently a complex line. In this paper it is denoted by $\mathbb{C}$. Its angular coordinate records the internal generator phase, while its radial coordinate records generator scale. This lift promotes the compact phase from an auxiliary value-space coordinate to an autonomous geometric carrier. It does not identify the generator radius with $|\psi|$.

Proposition 2 (Minimality of the generator plane)**.** *A nontrivial continuous orthogonal $U(1)$ phase action cannot be represented on a one-dimensional real Euclidean carrier. The smallest real Euclidean carrier that supports a nontrivial compact $U(1)$ phase orbit together with an independent positive radial invariant is a real two-plane, equivalently a complex line.*

Proof. A Euclidean carrier with an orthogonal compact phase action carries a continuous group homomorphism from $U(1)$ into the orthogonal group of the carrier. In real dimension one this target group is

$$O(1) = \{\pm 1\}.$$

The group $U(1)$ is connected, while $O(1)$ is discrete. Hence the image of any continuous homomorphism

$$U(1) \longrightarrow O(1)$$

is connected and therefore consists of a single point. The action is trivial. Thus a one-dimensional real Euclidean carrier cannot support a nontrivial continuous $U(1)$ phase orbit.

In real dimension two, the standard rotation representation

$$e^{i\beta} \longmapsto \begin{pmatrix} \cos\beta & -\sin\beta \\ \sin\beta & \cos\beta \end{pmatrix}$$

is nontrivial and orthogonal. Its nonzero orbits are circles of fixed Euclidean radius. Writing this radius as $\rho > 0$ and the orbit coordinate as φ, one obtains polar coordinates

$$(\rho, \varphi) \in (0, \infty) \times \big(\mathbb{R}/2\pi\mathbb{Z}\big).$$

Filling in the regular point $\rho = 0$ gives the Euclidean plane with its usual complex coordinate. Thus a complex line is the minimal real Euclidean generator carrier of a compact phase together with a radial scale. ☐

Definition III.3 (Generator space)**.** The generator space $\mathbb{C}$ is the internal factor of the split arena fixed in assumption 1, understood as the autonomous metric lift of the compact phase fibre described above. The notation $\mathbb{C}$ denotes the standard complex plane regarded as a real Euclidean two-plane with its fixed metric structure. Every nonzero point $z \in \mathbb{C} \setminus \{0\}$ has the polar representation

$$z = \rho e^{i\varphi_{\mathbb{C}}}, \qquad \rho = |z| > 0, \qquad \varphi_{\mathbb{C}} \in \mathbb{R}/2\pi\mathbb{Z}, \tag{18}$$

and the Euclidean line element is

$$\mathrm{d}s^2_{\mathbb{C}} = \mathrm{d}\rho^2 + \rho^2 \mathrm{d}\varphi^2_{\mathbb{C}}. \tag{19}$$

Thus

$$\mathbb{C} \setminus \{0\} \simeq (0, \infty) \times \big(\mathbb{R}/2\pi\mathbb{Z}\big).$$

At $\rho = 0$, the angular coordinate $\varphi_{\mathbb{C}}$ is undefined, whereas the Euclidean metric extends regularly across the origin. The radial variable ρ is the generator-plane radius and has SI dimension of length. The angular coordinate $\varphi_{\mathbb{C}}$ is dimensionless and carries the internal generator phase. The word amplitude, when used for ρ, refers only to this generator-coordinate convention. It is not the pointwise modulus of the coarse-grained wavefunction ψ.

Definition III.4 (Projective observation directions)**.** A single complex generator line carries the compact phase circle. To obtain observed spatial directions in a rotationally covariant way, use the minimal two-component complex lift and retain only the complex ray

$$[\varsigma] \in \mathbb{CP}^1 := \big(\mathbb{C}^2 \setminus \{0\}\big)/\mathbb{C}^\times, \qquad \varsigma = \begin{pmatrix} \varsigma_1 \\ \varsigma_2 \end{pmatrix}.$$

Equivalently, one may choose the normalized representative

$$\varsigma^\dagger \varsigma = 1$$

and then identify

$$\varsigma \sim e^{i\beta} \varsigma.$$

The vector ς is an auxiliary projective coordinate for observed directions. It is not the Dirac spinor and it is not an additional physical spin degree of freedom introduced at this stage.

Let the Pauli matrices be

$$\sigma_1 = \begin{pmatrix} 0 & 1 \\ 1 & 0 \end{pmatrix}, \qquad \sigma_2 = \begin{pmatrix} 0 & -i \\ i & 0 \end{pmatrix}, \qquad \sigma_3 = \begin{pmatrix} 1 & 0 \\ 0 & -1 \end{pmatrix}.$$

The associated projective direction is

$$n_a([\varsigma]) = \frac{\varsigma^\dagger \sigma_a \varsigma}{\varsigma^\dagger \varsigma}, \qquad a = 1, 2, 3. \tag{20}$$

Proposition 3 (Emergence of the observed direction sphere)**.** *The map in Eq.* (20) *is well defined on* $\mathbb{CP}^1$*, satisfies*

$$n_1([\varsigma])^2 + n_2([\varsigma])^2 + n_3([\varsigma])^2 = 1, \tag{21}$$

and induces the standard identification

$$\mathbb{CP}^1 \simeq \mathbb{S}^2.$$

It is rotationally covariant under the adjoint action of $SU(2)$*. More precisely, for every* $U \in SU(2)$ *there is a unique* $R(U) \in SO(3)$ *such that*

$$n([U\varsigma]) = R(U)\, n([\varsigma]).$$

The two-component complex lift is minimal in the projective sense; one complex component gives $\mathbb{CP}^0$*, a point, while two complex components give the first nontrivial projective direction sphere. Adding an observed radial coordinate gives the metric cone*

$$\mathrm{Cone}(\mathbb{S}^2) := \big([0,\infty) \times \mathbb{S}^2\big) / \big(\{0\} \times \mathbb{S}^2\big),$$

which is Euclidean $\mathbb{R}^3$*.*

Proof. First we verify that the map is projectively well defined. If $\lambda \in \mathbb{C}^\times$, then

$$n_a([\lambda\varsigma]) = \frac{(\lambda\varsigma)^\dagger \sigma_a (\lambda\varsigma)}{(\lambda\varsigma)^\dagger(\lambda\varsigma)} = \frac{|\lambda|^2 \varsigma^\dagger \sigma_a \varsigma}{|\lambda|^2 \varsigma^\dagger \varsigma} = n_a([\varsigma]).$$

Hence n_a depends only on the complex ray $[\varsigma] \in \mathbb{CP}^1$.

Next, using the Pauli identity

$$\sum_{a=1}^{3} (\sigma_a)_{\alpha\beta} (\sigma_a)_{\gamma\delta} = 2\delta_{\alpha\delta}\delta_{\beta\gamma} - \delta_{\alpha\beta}\delta_{\gamma\delta},$$

we compute

$$\begin{aligned}
\sum_{a=1}^{3} (\varsigma^\dagger \sigma_a \varsigma)^2 &= \bar{\varsigma}_\alpha \varsigma_\beta \bar{\varsigma}_\gamma \varsigma_\delta \sum_{a=1}^{3} (\sigma_a)_{\alpha\beta} (\sigma_a)_{\gamma\delta} \\
&= 2\bar{\varsigma}_\alpha \varsigma_\beta \bar{\varsigma}_\beta \varsigma_\alpha - \bar{\varsigma}_\alpha \varsigma_\alpha \bar{\varsigma}_\gamma \varsigma_\gamma \\
&= 2\left(\sum_{\alpha=1}^{2} |\varsigma_\alpha|^2\right)\left(\sum_{\beta=1}^{2} |\varsigma_\beta|^2\right) - (\varsigma^\dagger\varsigma)^2 \\
&= (\varsigma^\dagger\varsigma)^2.
\end{aligned}$$

Dividing by $(\varsigma^\dagger\varsigma)^2$ gives Eq. (21), so $n([\varsigma]) \in \mathbb{S}^2$.

Conversely, every direction

$$n = (\sin\vartheta\cos\phi, \sin\vartheta\sin\phi, \cos\vartheta) \in \mathbb{S}^2$$

is obtained from the normalized spinor

$$\varsigma(\vartheta,\phi)=\begin{pmatrix}\cos(\vartheta/2)\\ e^{i\phi}\sin(\vartheta/2)\end{pmatrix}.$$

Indeed,

$$\begin{aligned}\varsigma^\dagger\sigma_1\varsigma&=2\Re(\bar\varsigma_1\varsigma_2)=\sin\vartheta\cos\phi,\\ \varsigma^\dagger\sigma_2\varsigma&=2\Im(\bar\varsigma_1\varsigma_2)=\sin\vartheta\sin\phi,\\ \varsigma^\dagger\sigma_3\varsigma&=|\varsigma_1|^2-|\varsigma_2|^2=\cos\vartheta.\end{aligned}$$

Thus the map is onto $\mathbb{S}^2$.

It remains to identify the fibres. For any normalized spinor ς, the rank-one projector onto its complex line is

$$P_\varsigma:=\varsigma\varsigma^\dagger.$$

Using the Pauli matrices and $\varsigma^\dagger\varsigma=1$, direct matrix multiplication gives

$$P_\varsigma=\frac{1}{2}\left(I_2+\sum_{a=1}^{3}n_a([\varsigma])\sigma_a\right).$$

Therefore two normalized spinors with the same direction n have the same rank-one projector and hence span the same complex line. They differ by one overall phase. Consequently

$$\mathbb{S}^3/U(1)\simeq\mathbb{CP}^1\simeq\mathbb{S}^2.$$

We now verify rotational covariance. The real vector space of traceless Hermitian 2×2 matrices has basis $\{\sigma_a\}_{a=1}^3$ and inner product

$$\langle X,Y\rangle_{\mathrm{P}}:=\frac{1}{2}\operatorname{tr}(XY).$$

For $U\in SU(2)$, conjugation $X\mapsto U^\dagger XU$ preserves this inner product and maps traceless Hermitian matrices to traceless Hermitian matrices. Therefore there is a real orthogonal matrix $R(U)$ such that

$$U^\dagger\sigma_aU=R(U)_{ab}\sigma_b.$$

Since $SU(2)$ is connected and $R(I_2)=I_3$, one has $R(U)\in SO(3)$. Hence

$$n_a([U\varsigma])=\frac{\varsigma^\dagger U^\dagger\sigma_aU\varsigma}{\varsigma^\dagger\varsigma}=R(U)_{ab}\frac{\varsigma^\dagger\sigma_b\varsigma}{\varsigma^\dagger\varsigma}=R(U)_{ab}n_b([\varsigma]).$$

This proves the stated covariance.

The minimality statement follows from projective dimension. A one-component complex lift has projectivization

$$\mathbb{CP}^0=\big(\mathbb{C}\setminus\{0\}\big)/\mathbb{C}^\times,$$

which is a single point and carries no direction sphere. The first projective lift with a nontrivial continuum of directions is the two-component lift, whose quotient is $\mathbb{CP}^1\simeq\mathbb{S}^2$.

Finally, define

$$\mathrm{Cone}(\mathbb{S}^2)=\big([0,\infty)\times\mathbb{S}^2\big)/\big(\{0\}\times\mathbb{S}^2\big).$$

The map

$$[(r,n)]\longmapsto r\,n$$

is well defined from this cone to $\mathbb{R}^3$, since all pairs $(0,n)$ map to the same zero vector. For $r>0$, every nonzero vector in Euclidean three-space has the unique polar representation

$$\mathbf{x}=r\,n,\qquad r=|\mathbf{x}|>0,\qquad n=\mathbf{x}/r\in\mathbb{S}^2.$$

The endpoint $r = 0$ gives the origin. On $r > 0$, the Euclidean metric is recovered from

$$\mathrm{d}\mathbf{x} = n\,\mathrm{d}r + r\,\mathrm{d}n, \qquad n \cdot n = 1, \qquad n \cdot \mathrm{d}n = 0,$$

so

$$|\mathrm{d}\mathbf{x}|^2 = \mathrm{d}r^2 + r^2|\mathrm{d}n|^2 = \mathrm{d}r^2 + r^2\mathrm{d}\Omega^2.$$

Hence the metric cone over the projective direction sphere is Euclidean $\mathbb{R}^3$. □

Remark (Why a single complex line is not enough for $\mathbb{R}^3$)*.* The generator line $\mathbb{C}$ supplies a compact phase orbit and an internal radial scale. By itself,

$$\mathbb{C} \setminus \{0\} \simeq (0, \infty) \times \mathbb{S}^1,$$

which does not contain the direction sphere $\mathbb{S}^2$. The passage to observed three-dimensional directions therefore uses the minimal projective spinorial lift

$$\mathbb{C}^2 \setminus \{0\} \longrightarrow \mathbb{CP}^1 \simeq \mathbb{S}^2.$$

This is why the present split should be read as a generator-projection decomposition. The internal generator phase lives in $\mathbb{C}$, while observed directions are read through the projective $\mathbb{S}^2$ image.

Definition III.5 (Observed propagation space)**.** The observed propagation space is the $\mathbb{R}^3$-factor of the split arena fixed in assumption 1. It is identified with Euclidean three-space, equivalently with the metric cone over the projective direction sphere described in proposition 3,

$$\mathbb{R}^3 \simeq \mathrm{Cone}(\mathbb{S}^2) = \big([0, \infty) \times \mathbb{S}^2\big)/\big(\{0\} \times \mathbb{S}^2\big).$$

For $\mathbf{x} \in \mathbb{R}^3 \setminus \{0\}$, define

$$r = |\mathbf{x}| > 0, \qquad n = \mathbf{x}/r \in \mathbb{S}^2.$$

Then

$$\mathbb{R}^3 \setminus \{0\} \simeq (0, \infty) \times \mathbb{S}^2,$$

and the Euclidean metric takes the form

$$\mathrm{d}s^2_{\mathbb{R}^3} = \mathrm{d}r^2 + r^2\mathrm{d}\Omega^2. \tag{22}$$

No single angular chart on $\mathbb{S}^2$ is used globally. At $r = 0$, the angular variables are undefined, whereas the Euclidean metric remains regular. Time is not part of the present split geometry. This arena is a spatial bookkeeping device rather than a spacetime metric. Time enters later through phase evolution, rate decomposition, and worldline dynamics. Throughout the paper, ρ denotes the radial coordinate in $\mathbb{C}$, whereas r denotes the observed radial coordinate in $\mathbb{R}^3$.

Definition III.6 (Split kinematical arena)**.** The kinematical arena is the orthogonal direct sum $\mathbb{C} \oplus \mathbb{R}^3$ fixed in Eq. (8). Under the standard identification of an orthogonal direct sum with the corresponding Cartesian product, its points are pairs

$$(z, \mathbf{x}) \in \mathbb{C} \oplus \mathbb{R}^3. \tag{23}$$

The generator component z carries the autonomous phase-scale lift, while the observed component $\mathbf{x}$ lies in the projective propagation space. The bookkeeping metric is block diagonal:

$$\mathrm{d}s^2 = \mathrm{d}s^2_{\mathbb{C}} + \mathrm{d}s^2_{\mathbb{R}^3}. \tag{24}$$

There are no off-diagonal $\mathbb{C}$-$\mathbb{R}^3$ terms at the kinematical level. This orthogonality is the convention used for the later rate decomposition. It does not preclude branch relations, projection maps, shell reductions, or lock equations that depend on data from both sectors.

Remark. The block metric Eq. (24) is a kinematical product metric on the split arena. It is neither a five-dimensional physical spacetime metric nor an additional observed spatial geometry. Observable propagation, shell geometry, and measured fields live in $\mathbb{R}^3$. The factor $\mathbb{C}$ supplies the autonomous internal phase carrier and branch-scale coordinate. The $\mathbb{R}^3$-directions may be read as the minimal projective spinorial image $\mathbb{CP}^1 \simeq \mathbb{S}^2$, while the observed radial coordinate completes the Euclidean propagation space.

Definition III.7 (Generator radius)**.** The symbol $R > 0$ is the branch-level radius parameter already appearing in the RELATOR lock. It is not fixed here by α, by a measured charge, by the electron mass, or by an empirical electromagnetic radius. When the generator sector is later reduced to a coherent one-loop carrier, the same radius parameter is represented in $\mathbb{C}$ by the Euclidean circle

$$\Gamma_R := \{z \in \mathbb{C} \mid |z| = R\}, \tag{25}$$

where $|z|$ is the Euclidean norm induced by Eq. (19). Equivalently,

$$\Gamma_R \simeq \mathbb{S}^1, \qquad z(\varphi_{\mathbb{C}}) = Re^{i\varphi_{\mathbb{C}}}.$$

The full generator profile remains two-dimensional in $\mathbb{C}$. The circle Γ_R records only the collective carrier representative of the branch radius within the coherent one-loop representation. The minimal electron-branch construction later fixes the relations among R, $\sigma_{\mathbb{C}}$, and r_*. It does not turn Γ_R into a material boundary of the generator profile or into an empirical input surface.

Remark (Angular notation)*.* The coordinate $\varphi_{\mathbb{C}}$ is the polar angle on the generator plane. The auxiliary phase angle φ_{ph} belongs to the complex value line $\mathbb{C}_{\mathrm{ph}}$ of a coarse-grained representative. The collective carrier phase θ_0 is introduced later only after the coherent one-loop reduction has been carried out. The symbol θ is reserved for oriented loop coordinates in later shell formulas. These angular variables are not identified unless an explicit reduction states the identification and preserves the stated orientation convention.

Remark (Logical status of this subsection)*.* The objects $\mathbb{C}$, $\mathbb{R}^3$, and the split $\mathbb{C} \oplus \mathbb{R}^3$ remain the standing kinematical arena of the paper. The added phase-fibre and projective-spinor arguments explain why this arena is a minimal natural choice rather than an arbitrary doubling of space. They do not introduce the Gaussian generator profile, do not fix $\sigma_{\mathbb{C}}/R$, do not impose the first-node shell $r_* = \pi R$, do not choose the electron branch, do not quantize charge, do not define the scalar slowdown law, do not compute the vector-shell invariant, and do not select α. Those objects are introduced or derived only in the later sections where their hypotheses and reductions are stated.

B. The lock $R\omega = c$

At the coarse-grained branch level, with spin degrees of freedom suppressed because they do not enter the lock kinematics of this subsection, a charged branch is represented by a scalar phase representative

$$\psi\colon I \times \mathbb{R}^3 \to \mathbb{C}_{\mathrm{ph}},$$

where $I \subset \mathbb{R}$ is the time interval and $\mathbb{C}_{\mathrm{ph}} \simeq \mathbb{C}$ is a complex phase–amplitude line. This value space is not the metric generator plane $\mathbb{C}$ itself, and no identification between $\mathbb{C}_{\mathrm{ph}}$ and $\mathbb{C}$ is assumed here. For each fixed $t \in I$, $\psi(t, \cdot)$ assigns to every observed spatial point $\mathbf{x} \in \mathbb{R}^3$ a complex branch amplitude. Its pointwise modulus has the normalization-dependent units of a wave amplitude, whereas only its phase enters the gauge-covariant kinematics developed below.

The collective radius R is the branch-level generator radius associated with the coherent one-loop reduction. It is not identified with $|\psi(t, \mathbf{x})|$, and $|\psi|$ is not used as a radial coordinate on $\mathbb{C}$. Any comparison between the phase of ψ and the internal generator phase is deferred until that coherent branch reduction has been invoked.

At finer resolution, R and ω are interpreted as collective descriptors of microscopic generator constituents in $\mathbb{C}$. That construction is derived later in section IV A. In particular, the collective one-loop radius is obtained from the generator measure rather than from the pointwise modulus of the wavefunction. The present subsection therefore fixes the kinematical and gauge-covariant language, not the microscopic branch construction itself.

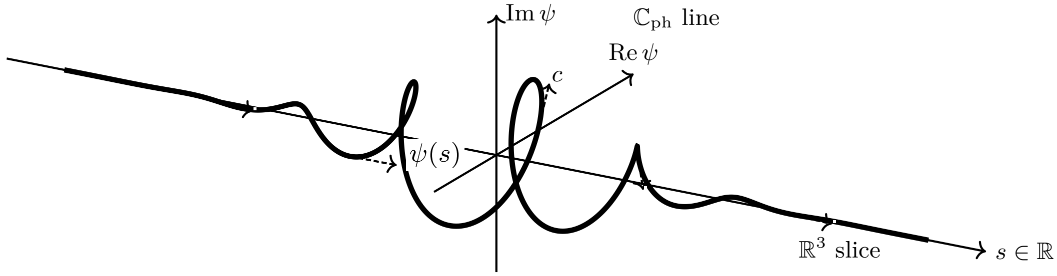

FIG. 2. Coarse-grained branch picture. A one-dimensional slice $s \mapsto \psi(t_0, \mathbf{x}(s))$, where $s \in \mathbb{R}$ parametrizes a fixed line $\mathbf{x}(s) \subset \mathbb{R}^3$, is drawn as a helical curve in the product of that observed line and the complex phase–amplitude line of the scalar representative. The dashed tangents indicate local phase transport. The label c is not the Euclidean speed of the plotted curve; it marks the later branch-lock convention $R\omega = c$. The figure is schematic. It illustrates the bookkeeping split between an observed line in $\mathbb{R}^3$ and the complex value line of the scalar representative, not a literal embedding of $\mathbb{C} \oplus \mathbb{R}^3$ into Euclidean three-space.

Proposition 4 (Gauge-covariant Schrödinger branch equation)**.** *Let ψ be C^1 in t and C^2 in $\mathbf{x}$ on the region under consideration. Let Φ and $\mathbf{A}$ be C^1 there, and let $\lambda_{\rm g}$ be C^2 there. In SI units, consider a coarse-grained charged branch whose infrared scalar representative satisfies*

$$i\hbar\,\partial_t\psi = \left[\frac{1}{2m}\Big(-i\hbar\nabla - q\mathbf{A}\Big)^2 + q\Phi + V_{\rm GI}\right]\psi, \qquad V_{\rm GI}(t,\mathbf{x}) \in \mathbb{R}, \tag{26}$$

where q is a signed generic branch charge parameter in this subsection and $V_{\rm GI}$ is a real gauge-inert scalar potential with SI units of energy. No charge quantization is assumed in this subsection. Equivalently, with

$$D_t := \partial_t + \frac{iq}{\hbar}\Phi, \qquad D_a := \partial_a - \frac{iq}{\hbar}A_a, \qquad \mathbf{D}^2 := \sum_{a=1}^{3} D_a D_a,$$

one may write

$$i\hbar\,D_t\psi = -\frac{\hbar^2}{2m}\,\mathbf{D}^2\psi + V_{\rm GI}\psi.$$

Under the SI gauge transformation

$$\mathbf{A} \mapsto \mathbf{A} + \nabla\lambda_{\rm g}, \qquad \Phi \mapsto \Phi - \partial_t\lambda_{\rm g}, \qquad \psi \mapsto e^{\,iq\lambda_{\rm g}/\hbar}\psi, \tag{27}$$

where $\lambda_{\rm g}$ has units such that $q\lambda_{\rm g}$ has units of action, one has

$$D_t'\psi' = e^{\,iq\lambda_{\rm g}/\hbar}D_t\psi, \qquad \mathbf{D}'\psi' = e^{\,iq\lambda_{\rm g}/\hbar}\mathbf{D}\psi.$$

This convention is equivalent to the covariant four-potential convention

$$A_\mu = \left(\frac{\Phi}{c}, -\mathbf{A}\right), \qquad \partial_\mu = \left(\frac{1}{c}\partial_t, \nabla\right), \qquad A_\mu \mapsto A_\mu - \partial_\mu\lambda_{\rm g}.$$

Hence Eq. (26) is gauge covariant. On any simply connected nodal-free region where $\psi = \sqrt{\rho_\psi}\,e^{\,i\mathcal{S}/\hbar}$ with $\rho_\psi = |\psi|^2 > 0$, one may choose the smooth transformed phase branch so that

$$\mathcal{S} \mapsto \mathcal{S} + q\lambda_{\rm g}. \tag{28}$$

Proof. The covariant-derivative form is the identity

$$-i\hbar D_a = -i\hbar\partial_a - qA_a, \qquad -\hbar^2\mathbf{D}^2 = \sum_{a=1}^{3}(-i\hbar D_a)^2 = \big(-i\hbar\nabla - q\mathbf{A}\big)^2.$$

We now verify the gauge-covariance identities explicitly.

For the time derivative,

$$\begin{aligned}
D_t'\psi' &= \left(\partial_t + \frac{iq}{\hbar}\Phi'\right)\left(e^{iq\lambda_{\rm g}/\hbar}\psi\right) \\
&= \left(\partial_t + \frac{iq}{\hbar}(\Phi - \partial_t\lambda_{\rm g})\right)\left(e^{iq\lambda_{\rm g}/\hbar}\psi\right) \\
&= e^{iq\lambda_{\rm g}/\hbar}\left[\partial_t\psi + \frac{iq}{\hbar}(\partial_t\lambda_{\rm g})\psi + \frac{iq}{\hbar}\Phi\psi - \frac{iq}{\hbar}(\partial_t\lambda_{\rm g})\psi\right] \\
&= e^{iq\lambda_{\rm g}/\hbar}\left(\partial_t + \frac{iq}{\hbar}\Phi\right)\psi \\
&= e^{iq\lambda_{\rm g}/\hbar}D_t\psi.
\end{aligned}$$

For the spatial derivative, for each Cartesian component $a = 1, 2, 3$,

$$\begin{aligned}
D_a'\psi' &= \left(\partial_a - \frac{iq}{\hbar}A_a'\right)\left(e^{iq\lambda_{\rm g}/\hbar}\psi\right) \\
&= \left(\partial_a - \frac{iq}{\hbar}(A_a + \partial_a\lambda_{\rm g})\right)\left(e^{iq\lambda_{\rm g}/\hbar}\psi\right) \\
&= e^{iq\lambda_{\rm g}/\hbar}\left[\partial_a\psi + \frac{iq}{\hbar}(\partial_a\lambda_{\rm g})\psi - \frac{iq}{\hbar}A_a\psi - \frac{iq}{\hbar}(\partial_a\lambda_{\rm g})\psi\right] \\
&= e^{iq\lambda_{\rm g}/\hbar}\left(\partial_a - \frac{iq}{\hbar}A_a\right)\psi \\
&= e^{iq\lambda_{\rm g}/\hbar}D_a\psi.
\end{aligned}$$

Hence

$$\mathbf{D}'\psi' = e^{iq\lambda_{\rm g}/\hbar}\mathbf{D}\psi.$$

Applying the same identity once more to each component gives

$$D_a'D_a'\psi' = D_a'\big(e^{iq\lambda_{\rm g}/\hbar}D_a\psi\big) = e^{iq\lambda_{\rm g}/\hbar}D_aD_a\psi.$$

Summing over a yields

$$\mathbf{D}'^2\psi' = e^{iq\lambda_{\rm g}/\hbar}\mathbf{D}^2\psi.$$

Therefore the transformed equation is exactly $e^{iq\lambda_{\rm g}/\hbar}$ times the original one, so Eq. (26) is gauge covariant.

Finally, on a simply connected nodal-free region, $\rho_\psi' = |\psi'|^2 = \rho_\psi$, and

$$\psi' = e^{iq\lambda_{\rm g}/\hbar}\psi = \sqrt{\rho_\psi}\, e^{i(\mathcal{S}+q\lambda_{\rm g})/\hbar}.$$

Since the phase on such a region is defined only up to an additive constant multiple of $2\pi\hbar$, one may choose the continuous transformed branch so that

$$\mathcal{S}' = \mathcal{S} + q\lambda_{\rm g}.$$

This proves Eq. (28). □

Definition III.8 (Gauge-invariant mechanical momentum)**.** On any simply connected nodal-free region where the phase $\mathcal{S}$ is chosen smoothly, and with q denoting the signed generic branch charge parameter used in proposition 4, the gauge-invariant mechanical momentum is

$$\mathbf{P}_{\rm mech} \equiv \nabla\mathcal{S} - q\mathbf{A}. \tag{29}$$

It is gauge invariant because

$$\nabla\mathcal{S}' - q\mathbf{A}' = \nabla(\mathcal{S} + q\lambda_{\rm g}) - q(\mathbf{A} + \nabla\lambda_{\rm g}) = \nabla\mathcal{S} - q\mathbf{A}.$$

Definition III.9 (Gauge-invariant local phase rate and spatial winding rate)**.** On any simply connected nodal-free region of a branch with fixed $R > 0$, the gauge-invariant local phase rate is

$$\omega_{\rm ph} \equiv -\frac{1}{\hbar}\big(\partial_t \mathcal{S} + q\Phi\big), \tag{30}$$

and the local spatial winding-rate vector is

$$\boldsymbol{\omega}^{\rm loc}_{\mathbb{R}^3}(t,\mathbf{x}) \equiv \frac{\mathbf{P}_{\rm mech}(t,\mathbf{x})}{mR}, \qquad \omega^{\rm loc}_{\mathbb{R}^3}(t,\mathbf{x}) \equiv \big\|\boldsymbol{\omega}^{\rm loc}_{\mathbb{R}^3}(t,\mathbf{x})\big\|\,. \tag{31}$$

When a branch-level scalar rate is needed, we write

$$p_{\rm br} \geq 0$$

for the chosen shell-reduced or branch-representative magnitude of $\mathbf{P}_{\rm mech}$, and set

$$\omega_{\mathbb{R}^3} \equiv \frac{p_{\rm br}}{mR}.$$

In a pointwise reading one may take $p_{\rm br} = \|\mathbf{P}_{\rm mech}(t,\mathbf{x})\|$; in the shell closure it is the shell-reduced scalar representative specified by the relevant shell construction.

Proposition 5 (Madelung form in gauge-invariant variables)**.** *Let ψ be C^1 in t and C^2 in $\mathbf{x}$ on a simply connected nodal-free region, and let Φ, $\mathbf{A}$, and $V_{\rm GI}$ be C^1 there. Assume*

$$\rho_\psi = |\psi|^2 > 0, \qquad \psi = \sqrt{\rho_\psi}\, e^{\,i\mathcal{S}/\hbar}.$$

Then the Schrödinger Eq. (26) *is equivalent to*

$$\partial_t \rho_\psi + \nabla\cdot\Big(\frac{\rho_\psi}{m}\,\mathbf{P}_{\rm mech}\Big) = 0, \tag{32}$$

and

$$-\partial_t \mathcal{S} = \frac{\mathbf{P}^2_{\rm mech}}{2m} + q\Phi + V_{\rm GI} - \frac{\hbar^2}{2m}\,\frac{\nabla^2\sqrt{\rho_\psi}}{\sqrt{\rho_\psi}}, \tag{33}$$

where

$$\mathbf{P}_{\rm mech} = \nabla\mathcal{S} - q\mathbf{A}.$$

Equivalently,

$$\hbar\,\omega_{\rm ph} = \frac{\mathbf{P}^2_{\rm mech}}{2m} + V_{\rm GI} - \frac{\hbar^2}{2m}\,\frac{\nabla^2\sqrt{\rho_\psi}}{\sqrt{\rho_\psi}},$$

which is manifestly gauge invariant.

Proof. Set

$$u = \sqrt{\rho_\psi}, \qquad S = \mathcal{S}, \qquad \mathbf{P}_{\rm mech} = \nabla S - q\mathbf{A}.$$

Since $u > 0$ on the nodal-free region, division by u is legitimate.

First,

$$\partial_t \psi = e^{\,iS/\hbar}\left(\partial_t u + \frac{i}{\hbar} u\,\partial_t S\right),$$

so

$$i\hbar\,\partial_t\psi = e^{\,iS/\hbar}\left(i\hbar\,\partial_t u - u\,\partial_t S\right).$$

Next,

$$
\begin{aligned}
\big(-i\hbar\nabla - q\mathbf{A}\big)\psi &= -i\hbar\, e^{\,iS/\hbar}\left(\nabla u + \frac{i}{\hbar}u\,\nabla S\right) - q\mathbf{A}\,u\,e^{\,iS/\hbar} \\
&= e^{\,iS/\hbar}\big(u(\nabla S - q\mathbf{A}) - i\hbar\,\nabla u\big) \\
&= e^{\,iS/\hbar}\big(u\,\mathbf{P}_{\text{mech}} - i\hbar\,\nabla u\big).
\end{aligned}
$$

Apply the operator once more componentwise. Writing $(\mathbf{P}_{\text{mech}})_a$ for the Cartesian components of $\mathbf{P}_{\text{mech}}$,

$$
\begin{aligned}
\big(-i\hbar\nabla - q\mathbf{A}\big)^2\psi &= \sum_{a=1}^{3}\big(-i\hbar\partial_a - qA_a\big)\Big(e^{\,iS/\hbar}\big(u(\mathbf{P}_{\text{mech}})_a - i\hbar\,\partial_a u\big)\Big) \\
&= e^{\,iS/\hbar}\sum_{a=1}^{3}\big[(\mathbf{P}_{\text{mech}})_a\big(u(\mathbf{P}_{\text{mech}})_a - i\hbar\,\partial_a u\big) - i\hbar\,\partial_a\big(u(\mathbf{P}_{\text{mech}})_a - i\hbar\,\partial_a u\big)\big] \\
&= e^{\,iS/\hbar}\big[u\,\mathbf{P}_{\text{mech}}^2 - i\hbar\,\mathbf{P}_{\text{mech}}\cdot\nabla u - i\hbar\,\nabla\cdot(u\mathbf{P}_{\text{mech}}) - \hbar^2\nabla^2 u\big] \\
&= e^{\,iS/\hbar}\Big[u\,\mathbf{P}_{\text{mech}}^2 - \hbar^2\nabla^2 u - i\hbar\Big(2\,\mathbf{P}_{\text{mech}}\cdot\nabla u + u\,\nabla\cdot\mathbf{P}_{\text{mech}}\Big)\Big].
\end{aligned}
$$

Substituting these identities into Eq. (26) gives

$$
\begin{aligned}
&i\hbar\,\partial_t\psi - \left[\frac{1}{2m}\big(-i\hbar\nabla - q\mathbf{A}\big)^2 + q\Phi + V_{\text{GI}}\right]\psi \\
&\quad = e^{\,iS/\hbar}\left\{i\hbar\left[\partial_t u + \frac{1}{m}\mathbf{P}_{\text{mech}}\cdot\nabla u + \frac{u}{2m}\nabla\cdot\mathbf{P}_{\text{mech}}\right]\right. \\
&\qquad\qquad \left. + u\left[-\partial_t S - \frac{\mathbf{P}_{\text{mech}}^2}{2m} - q\Phi - V_{\text{GI}} + \frac{\hbar^2}{2m}\frac{\nabla^2 u}{u}\right]\right\}.
\end{aligned}
$$

Since

$$
\partial_t\rho_\psi = 2u\,\partial_t u, \qquad \nabla\cdot\Big(\frac{\rho_\psi}{m}\mathbf{P}_{\text{mech}}\Big) = \frac{2u}{m}\mathbf{P}_{\text{mech}}\cdot\nabla u + \frac{u^2}{m}\nabla\cdot\mathbf{P}_{\text{mech}},
$$

the imaginary bracket is

$$
\partial_t u + \frac{1}{m}\mathbf{P}_{\text{mech}}\cdot\nabla u + \frac{u}{2m}\nabla\cdot\mathbf{P}_{\text{mech}} = \frac{1}{2u}\left[\partial_t\rho_\psi + \nabla\cdot\Big(\frac{\rho_\psi}{m}\mathbf{P}_{\text{mech}}\Big)\right].
$$

Therefore the Schrödinger equation implies Eqs. (32) and (33) by vanishing of the imaginary and real parts.

Conversely, assume that Eqs. (32) and (33) hold. Replacing the two square brackets in the displayed identity above by those equations shows that the full right-hand side vanishes identically. Hence ψ satisfies Eq. (26). This proves the equivalence.

Finally, by Eq. (30),

$$
\hbar\,\omega_{\text{ph}} = -\partial_t S - q\Phi.
$$

Substituting Eq. (33) into this identity yields the displayed gauge-invariant form. □

Remark (Energy normalization). The quantity ω_{ph} is gauge invariant. Its absolute value is nevertheless shifted by any additive constant in the gauge-inert part of the Hamiltonian. The energy zero must therefore be fixed before ω_{ph} can be identified with an intrinsic branch frequency. That choice normalizes the rest representative; it is not a fit to α or to a radiative correction.

Proposition 6 (Relativistic rest-branch identification of the internal phase rate)**.** *Assume that the field-free rest branch is normalized by the relativistic rest dispersion*

$$
E^2 = m^2c^4 + \|\mathbf{P}_{\text{mech}}\|^2c^2, \qquad \mathbf{P}_{\text{mech}} = 0.
$$

Thus $E_0 = mc^2$. Assume also that the scalar representative used here is not rest-energy-subtracted; the gauge-inert energy zero is fixed so that, in a field-free representative,

$$
q\Phi = 0, \qquad \mathbf{P}_{\text{mech}} = 0, \qquad \psi(t,\mathbf{x}) = e^{-imc^2t/\hbar}\psi_0(\mathbf{x}).
$$

This fixes the rest-phase normalization of the representative. It does not determine the electron rest mass and does not introduce a value of α. Equivalently, if the scalar Eq. (26) is used literally for this rest carrier, the gauge-inert scalar term contains the corresponding constant rest-energy offset on the rest branch. Then

$$\omega_{\mathbb{C}} = \omega_{\mathrm{ph}}^{\mathrm{rest}} = \frac{mc^2}{\hbar}. \tag{34}$$

Proof. On the field-free rest branch the relativistic dispersion gives

$$E_0 = mc^2.$$

The de Broglie phase law $E = \hbar\omega$ therefore gives the carrier frequency

$$\omega_0 = \frac{E_0}{\hbar} = \frac{mc^2}{\hbar}.$$

In a field-free gauge one may write

$$\psi(t, \mathbf{x}) = e^{-imc^2 t/\hbar}\psi_0(\mathbf{x}), \qquad \mathcal{S} = -mc^2 t + S_0(\mathbf{x}), \qquad \Phi = 0.$$

Hence

$$\omega_{\mathrm{ph}}^{\mathrm{rest}} = -\frac{1}{\hbar}\big(\partial_t \mathcal{S} + q\Phi\big) = \frac{mc^2}{\hbar}.$$

Since ω_{ph} is gauge invariant by Eqs. (28) and (30), the same value holds in every gauge representative. This proves Eq. (34). □

Corollary 1 (Rest-dispersion identity for the reduced Compton radius)**.** *Let*

$$R_{\mathrm{C}} := \frac{\hbar}{mc} \tag{35}$$

be the reduced Compton radius associated with the same rest branch. Then

$$R_{\mathrm{C}}\omega_{\mathbb{C}} = c. \tag{36}$$

This identity motivates the Relator lock, while the branch-level radius R remains the collective generator radius specified by the coherent branch construction.

Proof. Using Eqs. (34) and (35),

$$R_{\mathrm{C}}\omega_{\mathbb{C}} = \frac{\hbar}{mc}\,\frac{mc^2}{\hbar} = c.$$

This proves Eq. (36). □

Definition III.10 (Total rate, projected rates, and rate admissibility)**.** For the stationary one-loop branch under consideration, let $\omega_{\mathbb{C}}$ denote the branch-level internal phase-rotation rate, and let $\omega_{\mathbb{R}^3} \geq 0$ denote the scalar magnitude of the observed projected rate. Equivalently, if $\boldsymbol{\omega}_{\mathbb{R}^3}^{\mathrm{br}}$ denotes the branch-level projected-rate vector, then

$$\omega_{\mathbb{R}^3} = \left\|\boldsymbol{\omega}_{\mathbb{R}^3}^{\mathrm{br}}\right\|.$$

By the block metric on $\mathbb{C} \oplus \mathbb{R}^3$, the total rate is defined as the Euclidean norm of the orthogonal pair $(\omega_{\mathbb{C}}, \boldsymbol{\omega}_{\mathbb{R}^3}^{\mathrm{br}})$. Therefore

$$\omega^2 = \omega_{\mathbb{C}}^2 + \omega_{\mathbb{R}^3}^2. \tag{37}$$

On the field-free stationary rest branch, $\omega_{\mathbb{C}}$ agrees with $\omega_{\mathrm{ph}}^{\mathrm{rest}}$ by Eq. (34). A stationary branch is rate-admissible if its projected rates are real, with $\omega > 0$, $\omega_{\mathbb{C}}^2 \geq 0$, and $\omega_{\mathbb{R}^3}^2 \geq 0$.

Definition III.11 (Relator lock)**.** A stationary coherent one-loop branch is called RELATOR-locked when its collective generator radius and total branch rate satisfy

$$R\omega = c. \tag{38}$$

This condition is the branch-level admissibility condition motivated by the rest-dispersion identity Eq. (36). It is imposed on the collective branch pair (R, ω) and does not by itself identify R with an empirical radius.

Remark (Status of the lock). The identity Eq. (38) does not follow from the Schrödinger equation alone. It is the RELATOR branch-admissibility condition used to extend the relativistic rest normalization to coherent one-loop branches. It is not a fit to α, to the electron anomaly, or to an empirical radius. Its microscopic realization within the generator reduction is obtained later from the coherent annular construction; see proposition 13.

Proposition 7 (Observed rate fraction and slowdown)**.** *For every rate-admissible stationary branch satisfying the Relator lock, let $p_{\rm br} \geq 0$ be the branch-level mechanical-momentum magnitude used in the projected-rate definition,*

$$\omega_{\mathbb{R}^3} = \frac{p_{\rm br}}{mR}.$$

Then the observed rate fraction is

$$\Omega_{\mathbb{R}^3} \equiv \frac{\omega_{\mathbb{R}^3}}{\omega} = \frac{p_{\rm br}}{mc}, \tag{39}$$

and the master slowdown variable is

$$\mathcal{D}_{\rm total} \equiv \Omega^2_{\mathbb{R}^3} = \frac{p^2_{\rm br}}{m^2c^2}. \tag{40}$$

In a pointwise local reading, $p_{\rm br}$ may be replaced by $\|\mathbf{P}_{\rm mech}(t, \mathbf{x})\|$. In the shell closure, $p_{\rm br}$ is the shell-reduced representative fixed by the scalar or vector shell construction. Equivalently,

$$1 - \mathcal{D}_{\rm total} = \left(\frac{\omega_{\mathbb{C}}}{\omega}\right)^2. \tag{41}$$

Consequently,

$$0 \leq \Omega_{\mathbb{R}^3} \leq 1, \qquad 0 \leq \mathcal{D}_{\rm total} \leq 1, \qquad 0 \leq p_{\rm br} \leq mc.$$

If the pointwise representative $p_{\rm br} = \|\mathbf{P}_{\rm mech}(t, \mathbf{x})\|$ is chosen, the last bound becomes the corresponding pointwise bound on $\|\mathbf{P}_{\rm mech}(t, \mathbf{x})\|$. The same identities give

$$\omega = \frac{c}{R}, \qquad \omega_{\mathbb{R}^3} = \frac{c}{R}\sqrt{\mathcal{D}_{\rm total}}.$$

Proof. By definition of the branch-level projected rate,

$$\omega_{\mathbb{R}^3} = \frac{p_{\rm br}}{mR}.$$

Using the Relator lock Eq. (38), one has

$$\omega = \frac{c}{R}.$$

Therefore

$$\frac{\omega_{\mathbb{R}^3}}{\omega} = \frac{p_{\rm br}}{mc},$$

which proves Eq. (39). Squaring gives Eq. (40). Dividing the orthogonal rate split Eq. (37) by $\omega^2 > 0$ gives

$$\left(\frac{\omega_{\mathbb{C}}}{\omega}\right)^2 + \left(\frac{\omega_{\mathbb{R}^3}}{\omega}\right)^2 = 1,$$

hence Eq. (41). Since the projected squared rates are nonnegative on a rate-admissible branch, the normalized squared rates lie in $[0, 1]$. The bounds on $\Omega_{\mathbb{R}^3}$, $\mathcal{D}_{\rm total}$, and $p_{\rm br}$ follow from Eqs. (39) and (40). The pointwise bound on $\|\mathbf{P}_{\rm mech}\|$ follows only under the pointwise representative choice. Finally, $\omega_{\mathbb{R}^3} = \omega\sqrt{\mathcal{D}_{\rm total}}$ together with $\omega = c/R$ gives the stated projected scale. □

Remark. The bound $p_{\mathrm{br}} \le mc$, equivalent to $0 \le \mathcal{D}_{\mathrm{total}} \le 1$ through Eq. (40), is not a consequence of the Schrödinger equation by itself. It is the kinematical admissibility condition induced by the locked split. A pointwise bound on $\|\mathbf{P}_{\mathrm{mech}}\|$ is obtained only when p_{br} is chosen to be the pointwise mechanical-momentum magnitude.

Remark. The quantity $\mathcal{D}_{\mathrm{total}}$ measures the propagation share of the locked rate split. When $\mathcal{D}_{\mathrm{total}}$ is close to one, most of the squared total rate is carried by the projected $\mathbb{R}^3$ sector. When $\mathcal{D}_{\mathrm{total}}$ is small, the internal generator contribution dominates. At this stage $\mathcal{D}_{\mathrm{total}}$ is purely kinematical and gauge invariant; it is not yet the scalar mother law $\mathcal{D}_{\mathrm{C}}(\alpha)$.

Definition III.12 (Bookkeeping vectors for the slowdown)**.** The gauge-invariant local quantity behind the shell slowdown is the minimally coupled mechanical momentum

$$\mathbf{P}_{\mathrm{mech}} = \nabla \mathcal{S} - q\mathbf{A}, \qquad \mathcal{D}_{\mathrm{total}} = \frac{p_{\mathrm{br}}^2}{m^2c^2}. \tag{42}$$

Here p_{br} is the branch-level or shell-reduced magnitude extracted from $\mathbf{P}_{\mathrm{mech}}$ by the representative specified in the relevant shell construction. In a pointwise local reading one may instead define $\mathcal{D}_{\mathrm{total}}^{\mathrm{loc}} = \|\mathbf{P}_{\mathrm{mech}}(t,\mathbf{x})\|^2/(m^2c^2)$. Under the shell gauge transformation

$$\mathbf{A} \mapsto \mathbf{A} + \nabla\lambda_{\mathrm{g}}, \qquad \mathcal{S} \mapsto \mathcal{S} + q\lambda_{\mathrm{g}},$$

one has

$$\nabla(\mathcal{S} + q\lambda_{\mathrm{g}}) - q(\mathbf{A} + \nabla\lambda_{\mathrm{g}}) = \nabla\mathcal{S} - q\mathbf{A}.$$

Hence $\mathbf{P}_{\mathrm{mech}}$ is gauge invariant. The induced quantity $\mathcal{D}_{\mathrm{total}}$ is gauge invariant whenever p_{br} is obtained from $\mathbf{P}_{\mathrm{mech}}$ by a gauge-invariant pointwise, branch-level, or shell-reduced representative. The scalar and vector shell blocks introduced later are therefore not independent gauge-dependent fields. They are dimensionless representatives of two channel contributions to the same invariant slowdown quantity $\mathcal{D}_{\mathrm{total}}$.

On the matching shell, introduce dimensionless vectors $\boldsymbol{\mathcal{D}}_{\mathrm{C}}$ and $\boldsymbol{\mathcal{D}}_{\Lambda}$ in an auxiliary Euclidean bookkeeping space and represent the dimensionless quantity $\mathcal{D}_{\mathrm{total}}$ by the auxiliary norm

$$\mathcal{D}_{\mathrm{total}} = \left\| \underbrace{\boldsymbol{\mathcal{D}}_{\mathrm{C}}}_{\substack{\text{scalar}\\ \text{part}}} + \underbrace{\boldsymbol{\mathcal{D}}_{\Lambda}}_{\substack{\text{vector}\\ \text{part}}} \right\|. \tag{43}$$

Here the scalar part denotes the Coulombic shell contribution, while the vector part denotes the inductive transverse shell contribution. The norm in Eq. (43) is the auxiliary bookkeeping norm; it is not a new physical norm on $\mathbb{R}^3$, not a new Hilbert-space norm on the wavefunction, and it does not introduce additional dynamical degrees of freedom.

Assuming $\mathcal{D}_{\mathrm{C}} > 0$, define

$$\mathcal{D}_{\mathrm{C}} \equiv \|\boldsymbol{\mathcal{D}}_{\mathrm{C}}\|, \qquad \Delta\mathcal{D}_{\Lambda} \equiv \widehat{\boldsymbol{\mathcal{D}}_{\mathrm{C}}}\cdot\boldsymbol{\mathcal{D}}_{\Lambda}, \qquad \widehat{\boldsymbol{\mathcal{D}}_{\mathrm{C}}} \equiv \frac{\boldsymbol{\mathcal{D}}_{\mathrm{C}}}{\mathcal{D}_{\mathrm{C}}}. \tag{44}$$

Proposition 8 (First-order resolution of the slowdown)**.** *Assume $\mathcal{D}_{\mathrm{C}} > 0$. Then, in the regime*

$$\frac{\|\boldsymbol{\mathcal{D}}_{\Lambda}\|}{\mathcal{D}_{\mathrm{C}}} \to 0$$

with $\mathcal{D}_{\mathrm{C}}$ held fixed, one has

$$\mathcal{D}_{\mathrm{total}} = \mathcal{D}_{\mathrm{C}} + \Delta\mathcal{D}_{\Lambda} + O\left(\frac{\|\boldsymbol{\mathcal{D}}_{\Lambda}\|^2}{\mathcal{D}_{\mathrm{C}}}\right). \tag{45}$$

More precisely, there exist constants $c_0 > 0$ and $C > 0$, independent of $\boldsymbol{\mathcal{D}}_{\Lambda}$, such that whenever

$$\frac{\|\boldsymbol{\mathcal{D}}_{\Lambda}\|}{\mathcal{D}_{\mathrm{C}}} \le c_0,$$

one has

$$|\mathcal{D}_{\mathrm{total}} - \mathcal{D}_{\mathrm{C}} - \Delta\mathcal{D}_{\Lambda}| \le C\,\frac{\|\boldsymbol{\mathcal{D}}_{\Lambda}\|^2}{\mathcal{D}_{\mathrm{C}}}.$$

Proof. Starting from Eq. (43),

$$\mathcal{D}_{\text{total}} = \sqrt{(\boldsymbol{\mathcal{D}}_{\text{C}} + \boldsymbol{\mathcal{D}}_{\Lambda})\cdot(\boldsymbol{\mathcal{D}}_{\text{C}} + \boldsymbol{\mathcal{D}}_{\Lambda})} = \sqrt{\mathcal{D}_{\text{C}}^2 + 2\mathcal{D}_{\text{C}}\,\Delta\mathcal{D}_{\Lambda} + \|\boldsymbol{\mathcal{D}}_{\Lambda}\|^2}.$$

Hence

$$\mathcal{D}_{\text{total}} = \mathcal{D}_{\text{C}}\sqrt{1+\varepsilon}, \qquad \varepsilon \equiv \frac{2\Delta\mathcal{D}_{\Lambda}}{\mathcal{D}_{\text{C}}} + \frac{\|\boldsymbol{\mathcal{D}}_{\Lambda}\|^2}{\mathcal{D}_{\text{C}}^2}.$$

Since

$$\Delta\mathcal{D}_{\Lambda} = \widehat{\boldsymbol{\mathcal{D}}_{\text{C}}}\cdot\boldsymbol{\mathcal{D}}_{\Lambda}, \qquad \|\widehat{\boldsymbol{\mathcal{D}}_{\text{C}}}\| = 1,$$

the Cauchy–Schwarz inequality gives

$$|\Delta\mathcal{D}_{\Lambda}| \le \|\boldsymbol{\mathcal{D}}_{\Lambda}\|.$$

Therefore, with

$$\delta \equiv \frac{\|\boldsymbol{\mathcal{D}}_{\Lambda}\|}{\mathcal{D}_{\text{C}}},$$

one has

$$|\varepsilon| \le 2\delta + \delta^2.$$

If $\delta \le \frac{1}{4}$, then

$$|\varepsilon| \le \frac{1}{2} + \frac{1}{16} = \frac{9}{16} < 1.$$

Let $g(t) = \sqrt{1+t}$. By Taylor's theorem at $t = 0$,

$$g(\varepsilon) = 1 + \frac{\varepsilon}{2} + \frac{g''(\xi_\varepsilon)}{2}\,\varepsilon^2$$

for some ξ_ε between 0 and ε. Since

$$g''(t) = -\frac{1}{4}(1+t)^{-3/2},$$

and since $|\varepsilon| \le 9/16$, one has

$$|g''(\xi_\varepsilon)| \le \frac{1}{4}\left(1 - \frac{9}{16}\right)^{-3/2} = \frac{1}{4}\left(\frac{16}{7}\right)^{3/2}.$$

Thus there is a constant $C_1 > 0$, independent of $\boldsymbol{\mathcal{D}}_{\Lambda}$, such that

$$\sqrt{1+\varepsilon} = 1 + \frac{\varepsilon}{2} + R_\varepsilon, \qquad |R_\varepsilon| \le C_1\varepsilon^2.$$

Multiplying by $\mathcal{D}_{\text{C}}$ gives

$$\mathcal{D}_{\text{total}} = \mathcal{D}_{\text{C}} + \frac{\mathcal{D}_{\text{C}}\varepsilon}{2} + \mathcal{D}_{\text{C}}R_\varepsilon = \mathcal{D}_{\text{C}} + \Delta\mathcal{D}_{\Lambda} + \frac{\|\boldsymbol{\mathcal{D}}_{\Lambda}\|^2}{2\mathcal{D}_{\text{C}}} + \mathcal{D}_{\text{C}}R_\varepsilon.$$

Moreover,

$$\mathcal{D}_{\text{C}}|\varepsilon|^2 \le \mathcal{D}_{\text{C}}(2\delta+\delta^2)^2 \le C_2\,\mathcal{D}_{\text{C}}\,\delta^2 = C_2\,\frac{\|\boldsymbol{\mathcal{D}}_{\Lambda}\|^2}{\mathcal{D}_{\text{C}}}$$

for some constant $C_2 > 0$ valid whenever $\delta \le \frac{1}{4}$. Hence

$$|\mathcal{D}_{\text{C}}R_\varepsilon| \le C_1C_2\,\frac{\|\boldsymbol{\mathcal{D}}_{\Lambda}\|^2}{\mathcal{D}_{\text{C}}}.$$

Therefore

$$|\mathcal{D}_{\text{total}} - \mathcal{D}_{\text{C}} - \Delta\mathcal{D}_{\Lambda}| \le \left(\frac{1}{2} + C_1C_2\right)\frac{\|\boldsymbol{\mathcal{D}}_{\Lambda}\|^2}{\mathcal{D}_{\text{C}}}.$$

This proves Eq. (45). □

Remark. Equation (45) is a first-order bookkeeping expansion about the nonzero baseline $\boldsymbol{\mathcal{D}}_{\text{C}}$, not an independent postulate. It prepares the later separation between the Coulombic scalar shell block $\mathcal{D}_{\text{C}}$ and the inductive vector correction $\Delta\mathcal{D}_{\Lambda}$; see sections VI and VII.

C. Coarse graining, shell variables, and admissible regularity

The eventual α-lock closure is not imposed directly on bulk fields. Instead, it is formulated in terms of shell-level data extracted at the matching radius r_*, either by collar reduction of tangential bulk fields or by one-sided exterior traces on the shell. In the present subsection we fix the corresponding shell geometry and admissible regularity. The vector-shell representatives introduced here enter later into $\Delta\Lambda_{\mathrm{UV}\to\mathrm{IR}}$ and $\Delta\Lambda_{\mathrm{out}}$. The scalar law defining $\mathcal{D}_{\mathrm{C}}(\alpha)$ is introduced separately in section VI. No value of α, no scalar slowdown law, and no vector-shell invariant is fixed in this subsection.

Definition III.13 (Matching shell and collar)**.** Let $r_* > 0$ be the matching radius of the stationary branch under consideration, and let $\mathbb{S}^2$ denote the dimensionless unit sphere of directions,

$$\mathbb{S}^2 := \{\Omega \in \mathbb{R}^3 \;\big|\; |\Omega| = 1\}.$$

Fix once and for all a dimensionless auxiliary collar half-width $c_{\mathrm{col}} > 0$, held fixed and not varied to tune the lock, such that

$$c_{\mathrm{col}}\sigma_{\mathbb{C}} < r_*. \tag{46}$$

Define the matching shell and its collar by

$$\Sigma_{r_*} = \{r_*\Omega \;\big|\; \Omega \in \mathbb{S}^2\}, \tag{47}$$

and

$$\mathcal{C}(r_*) = \{\mathbf{x} \in \mathbb{R}^3 \;;\; ||\mathbf{x}| - r_*| \le c_{\mathrm{col}}\sigma_{\mathbb{C}}\}. \tag{48}$$

The condition Eq. (46) ensures that the collar remains in the region of positive radius. In particular, every point $\mathbf{x} \in \mathcal{C}(r_*)$ can be written uniquely as $r\Omega$ with $r > 0$ and $\Omega \in \mathbb{S}^2$, so the radial projection to Σ_{r_*} is well defined. The specific branch value of r_* is fixed later; for the electron branch it is shown to equal πR. This later value is not assumed in the collar definition.

Definition III.14 (Collar reduction to the shell)**.** Let

$$a := r_* - c_{\mathrm{col}}\sigma_{\mathbb{C}}, \qquad b := r_* + c_{\mathrm{col}}\sigma_{\mathbb{C}}.$$

Let $u_\parallel$ be a tangential field on $\mathcal{C}(r_*)$, meaning that $u_\parallel(r,\Omega)\cdot\Omega = 0$ for almost every $(r,\Omega) \in [a,b]\times\mathbb{S}^2$. For each fixed $\Omega \in \mathbb{S}^2$, the tangent spaces of the concentric spheres along the ray $r \mapsto r\Omega$ coincide as vector subspaces of $\mathbb{R}^3$,

$$T_{r\Omega}\Sigma_r = T_{r_*\Omega}\Sigma_{r_*} = \{v \in \mathbb{R}^3 \;;\; v\cdot\Omega = 0\}.$$

We therefore identify tangential vectors along a fixed ray by viewing them as elements of this common plane. The collar reduction is then defined by

$$\langle u_\parallel\rangle_{\mathrm{collar}}(\Omega) = \frac{1}{b-a}\int_a^b u_\parallel(r,\Omega)\,\mathrm{d}r = \frac{1}{2c_{\mathrm{col}}\sigma_{\mathbb{C}}}\int_{r_*-c_{\mathrm{col}}\sigma_{\mathbb{C}}}^{r_*+c_{\mathrm{col}}\sigma_{\mathbb{C}}} u_\parallel(r,\Omega)\,\mathrm{d}r, \tag{49}$$

where $\Omega \in \mathbb{S}^2$ labels the shell point $r_*\Omega \in \Sigma_{r_*}$. In particular,

$$\mathscr{A}_\parallel^{\mathrm{coll}} = \langle A_\parallel\rangle_{\mathrm{collar}}. \tag{50}$$

This is the shell-reduction map used in the present subsection. It should not be confused with the Gaussian collar extension E_ℓ that appears later inside the shell-admission operator $\mathbb{Q}_\chi(\ell)$. The present map reduces physical bulk data to shell data; the later operator E_ℓ acts on shell data that have already been extracted. Neither operation introduces an adjustable shell coupling or a value of α.

Definition III.15 (Axisymmetric exterior shell trace)**.** When the branch is axisymmetric with respect to a fixed symmetry axis, shell data on $\Sigma_{r_*} \cong \mathbb{S}^2$ are written as functions of the fixed polar-cosine coordinate $\upsilon = \cos\vartheta \in [-1,1]$ from Eq. (12), where ϑ is the polar angle with respect to that axis. Let $B_\vartheta^{\mathrm{ext}}(r,\upsilon)$ denote the polar component of the stationary source-free exterior magnetic field. Its one-sided exterior shell trace is

$$b_*^{\mathrm{ext}}(\upsilon) := B_\vartheta^{\mathrm{ext}}(r_*^+,\upsilon). \tag{51}$$

For a regular axisymmetric exterior vacuum field, this trace is understood in the endpoint-regular form

$$b_*^{\mathrm{ext}}(v) = \sqrt{1-v^2}\, h_*^{\mathrm{ext}}(v),$$

where h_*^{ext} is smooth and, in the admissible analytic class used later, extends real-analytically to a neighborhood of $[-1,1]$. The corresponding flux-compatible datum is

$$\beta_*^{\mathrm{ext}}(v) := \sqrt{1-v^2}\, b_*^{\mathrm{ext}}(v).$$

The dimensionless exterior datum used later in $\Delta\Lambda_{\mathrm{out}}$ is obtained from this endpoint-regular shell trace after the common SI prefactor has been removed. This removal is a normalization convention for the exterior functional and is not a numerical fit.

Proposition 9 (Boundedness of collar reduction)**.** *Let*

$$a := r_* - c_{\mathrm{col}}\sigma_{\mathbb{C}} > 0, \qquad b := r_* + c_{\mathrm{col}}\sigma_{\mathbb{C}}, \qquad L := b - a = 2c_{\mathrm{col}}\sigma_{\mathbb{C}}.$$

For every tangential field $u_\parallel \in L^2_{\mathrm{tan}}(\mathcal{C}(r_*))$, the collar reduction $\langle u_\parallel \rangle_{\mathrm{collar}}$ belongs to $L^2_{\mathrm{tan}}(\Sigma_{r_*})$ and satisfies

$$\|\langle u_\parallel \rangle_{\mathrm{collar}}\|_{L^2_{\mathrm{tan}}(\Sigma_{r_*})} \le \frac{r_*}{a\sqrt{L}}\, \|u_\parallel\|_{L^2_{\mathrm{tan}}(\mathcal{C}(r_*))}. \tag{52}$$

In particular, the same bound holds for every $u_\parallel \in H^1_{\mathrm{tan}}(\mathcal{C}(r_*))$.

Proof. Using the parametrization $\Sigma_{r_*} = \{r_*\Omega \; ; \; \Omega \in \mathbb{S}^2\}$, the shell norm is

$$\|v\|^2_{L^2_{\mathrm{tan}}(\Sigma_{r_*})} = r_*^2 \int_{\mathbb{S}^2} |v(\Omega)|^2 \,\mathrm{d}\Omega.$$

Similarly,

$$\|u_\parallel\|^2_{L^2_{\mathrm{tan}}(\mathcal{C}(r_*))} = \int_a^b \int_{\mathbb{S}^2} |u_\parallel(r,\Omega)|^2\, r^2 \,\mathrm{d}\Omega \,\mathrm{d}r.$$

For each fixed $\Omega \in \mathbb{S}^2$, Cauchy–Schwarz in the radial variable gives

$$\left|\langle u_\parallel \rangle_{\mathrm{collar}}(\Omega)\right|^2 = \left| \frac{1}{L}\int_a^b u_\parallel(r,\Omega)\,\mathrm{d}r \right|^2 \le \frac{1}{L}\int_a^b |u_\parallel(r,\Omega)|^2 \,\mathrm{d}r.$$

Integrating over $\mathbb{S}^2$ and multiplying by r_*^2 yields

$$\|\langle u_\parallel \rangle_{\mathrm{collar}}\|^2_{L^2_{\mathrm{tan}}(\Sigma_{r_*})} \le \frac{r_*^2}{L}\int_{\mathbb{S}^2}\int_a^b |u_\parallel(r,\Omega)|^2 \,\mathrm{d}r\,\mathrm{d}\Omega.$$

Since $r \ge a$ on the collar, one has

$$|u_\parallel(r,\Omega)|^2 \le \frac{1}{a^2}\, |u_\parallel(r,\Omega)|^2 r^2.$$

Therefore

$$\|\langle u_\parallel \rangle_{\mathrm{collar}}\|^2_{L^2_{\mathrm{tan}}(\Sigma_{r_*})} \le \frac{r_*^2}{La^2}\int_a^b\int_{\mathbb{S}^2} |u_\parallel(r,\Omega)|^2 r^2 \,\mathrm{d}\Omega\,\mathrm{d}r = \frac{r_*^2}{La^2}\|u_\parallel\|^2_{L^2_{\mathrm{tan}}(\mathcal{C}(r_*))}.$$

Taking square roots gives Eq. (52). The H^1 statement follows from the continuous inclusion

$$H^1_{\mathrm{tan}}(\mathcal{C}(r_*)) \hookrightarrow L^2_{\mathrm{tan}}(\mathcal{C}(r_*)).$$

$\square$

Proposition 9 shows that collar averaging defines a bounded linear map from $L^2_{\tan}(\mathcal{C}(r_*))$ to $L^2_{\tan}(\Sigma_{r_*})$, with explicit norm control given by Eq. (52). Thus the passage from a finite-thickness collar field to an effective shell representative introduces no uncontrolled norm loss. The later $H^1_{\tan}$ fields therefore lie automatically in its domain.

The shell reduction and the associated axisymmetric exterior trace are shown schematically in fig. 3. The figure summarizes the two shell representatives used later; the collar-averaged tangential field on Σ_{r_*} and the exterior magnetic shell trace $b_*^{\mathrm{ext}}(\upsilon)$. It is conceptual, introduces no additional assumption, and is not part of the proof.

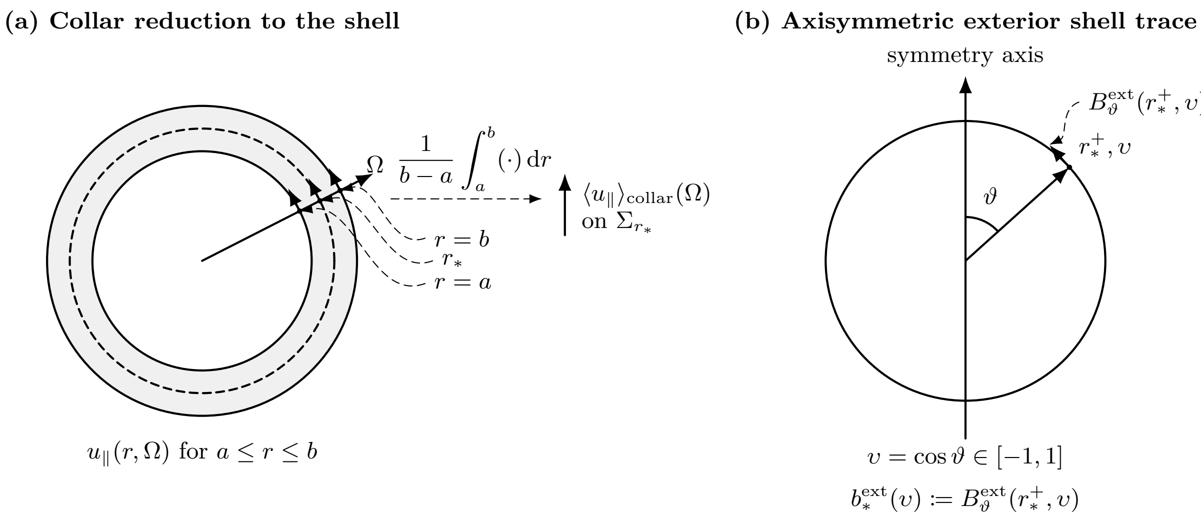

FIG. 3. Schematic shell reduction and axisymmetric exterior trace at the matching radius. Panel (a) shows the collar $\mathcal{C}(r_*)$ and the radial averaging map that sends a tangential bulk field $u_\parallel(r,\Omega)$ to its shell representative $\langle u_\parallel\rangle_{\mathrm{collar}}(\Omega)$ on Σ_{r_*}. Panel (b) shows the one-sided exterior magnetic shell trace $b_*^{\mathrm{ext}}(\upsilon)=B_\vartheta^{\mathrm{ext}}(r_*^+,\upsilon)$ in the axisymmetric exterior sector. The figure is schematic, introduces no additional assumption, and is not part of the proof.

Definition III.16 (Shell-admissible branch)**.** A stationary branch is called shell-admissible at $r=r_*$ if the following shell representatives are well defined and satisfy the stated regularity conditions. These conditions define the admissible shell domain; they do not select a value of α.

1. The shell density trace

$$\rho_* := \rho_\psi\big|_{\Sigma_{r_*}}$$

   belongs to $H^1(\Sigma_{r_*})$.

2. Tangential shell traces belong to $H^1_{\tan}(\Sigma_{r_*})$.

3. The gauge-invariant mechanical momentum admits an L^2 trace on Σ_{r_*},

$$\mathbf{P}_{\mathrm{mech}}\big|_{\Sigma_{r_*}} \in L^2(\Sigma_{r_*};\mathbb{R}^3),$$

   with SI units of momentum. Any scalar momentum scale p_* or p_{br} used later is obtained from this trace only after the corresponding shell-reduction or matching rule has been stated.

4. Collar-reduced tangential traces such as Eq. (50) are well defined in the sense of proposition 9, with the collar parameter fixed as a reduction convention rather than a fitted shell datum.

5. In the exterior vacuum sector, the axisymmetric exterior trace has the endpoint-regular form

$$b_*^{\mathrm{ext}}(\upsilon)=\sqrt{1-\upsilon^2}\,h_*^{\mathrm{ext}}(\upsilon),$$

   where h_*^{ext} extends real-analytically to a neighborhood of $[-1,1]$. Equivalently, the flux-compatible datum

$$\beta_*^{\mathrm{ext}}(\upsilon):=\sqrt{1-\upsilon^2}\,b_*^{\mathrm{ext}}(\upsilon)=(1-\upsilon^2)h_*^{\mathrm{ext}}(\upsilon)$$

   is real-analytic near $[-1,1]$ and vanishes at $\upsilon=\pm1$. This analytic class is an exterior regularity domain for the shell expansion and is not tuned to α.

These are the shell-level regularity requirements inherited from assumptions 3 and 4.

The shell data carried forward are precisely the representatives fixed above. The gauge-invariant projected collar field $\mathscr{A}_{\mathrm{TT}}^{\mathrm{coll}} = \Pi_{\mathrm{TT}}\mathscr{A}_{\parallel}^{\mathrm{coll}}$ and the exterior trace $b_*^{\mathrm{ext}}(v)$, after the stated SI normalization is removed where appropriate, feed the vector shell channel. The density trace ρ_* and the gauge-invariant mechanical-momentum trace $\mathbf{P}_{\mathrm{mech}}|_{\Sigma_{r_*}}$ feed the scalar shell channel. Their exact roles in $\mathcal{D}_{\mathrm{C}}(\alpha)$, $\Delta\Lambda_{\mathrm{UV}\to\mathrm{IR}}$, $\Delta\Lambda_{\mathrm{out}}$, and $\mathcal{C}_{\log}$ are specified only when those objects are constructed.

Remark. The analyticity requirement is stronger than smoothness. It is imposed on the exterior vacuum representative as the admissible regularity class for the exterior shell expansion. This choice is compatible with the source-free analytic elliptic character of the stationary exterior Maxwell problem on $r > r_*$, whereas the interior branch enters only through shell data at $r = r_*$. The resulting regularity yields absolute convergence of the parity-restricted odd shell spectral expansion defining $\Delta\Lambda_{\mathrm{out}}$. The choice fixes the exterior function class; it is not adjusted to obtain a target value of $\Delta\Lambda_{\mathrm{out}}$ or α.

Proposition 10 (Gauge compatibility of collar reduction)**.** *Let $\mathbf{A}$ be a gauge potential on $\mathcal{C}(r_*)$ whose tangential component belongs to $L^2_{\tan}(\mathcal{C}(r_*))$, and let $\lambda_{\mathrm{g}} \in H^1(\mathcal{C}(r_*))$ be a single-valued admissible gauge function. Set*

$$\mathbf{A}' = \mathbf{A} + \nabla\lambda_{\mathrm{g}}.$$

Let $\mathscr{A}_{\parallel}^{\mathrm{coll}}$ and $\mathscr{A}_{\parallel}^{\mathrm{coll}\prime}$ denote the collar reductions of the tangential components of $\mathbf{A}$ and $\mathbf{A}'$, respectively. Then there exists $\lambda_{\mathrm{sh}} \in H^1(\Sigma_{r_*})$, with the same SI units as λ_{g}, given by

$$\lambda_{\mathrm{sh}}(\Omega) = \frac{r_*}{2c_{\mathrm{col}}\sigma_{\mathbb{C}}} \int_{r_*-c_{\mathrm{col}}\sigma_{\mathbb{C}}}^{r_*+c_{\mathrm{col}}\sigma_{\mathbb{C}}} \frac{\lambda_{\mathrm{g}}(r,\Omega)}{r}\,\mathrm{d}r, \qquad \Omega \in \mathbb{S}^2,$$

such that

$$\mathscr{A}_{\parallel}^{\mathrm{coll}\prime} = \mathscr{A}_{\parallel}^{\mathrm{coll}} + \nabla_{\Sigma_{r_*}}\lambda_{\mathrm{sh}} \qquad \text{in } L^2_{\tan}(\Sigma_{r_*}).$$

The projector Π_{TT} on Σ_{r_*} is understood through radial pullback to the unit sphere $\mathbb{S}^2$. This pullback changes the metric scale but not the exact/coexact Hodge splitting. Consequently, the projected collar representative is gauge invariant within the admissible shell-gauge class,

$$\Pi_{\mathrm{TT}}\mathscr{A}_{\parallel}^{\mathrm{coll}\prime} = \Pi_{\mathrm{TT}}\mathscr{A}_{\parallel}^{\mathrm{coll}}. \tag{53}$$

Proof. Write

$$a = r_* - c_{\mathrm{col}}\sigma_{\mathbb{C}}, \qquad b = r_* + c_{\mathrm{col}}\sigma_{\mathbb{C}}, \qquad L = b - a = 2c_{\mathrm{col}}\sigma_{\mathbb{C}}.$$

We first treat the case $\lambda_{\mathrm{g}} \in C^\infty(\overline{\mathcal{C}(r_*)})$. In spherical coordinates one has

$$\nabla\lambda_{\mathrm{g}} = (\partial_r\lambda_{\mathrm{g}})\,\hat{r} + \frac{1}{r}\,\nabla_{\mathbb{S}^2}\lambda_{\mathrm{g}}.$$

Hence the tangential component of $\nabla\lambda_{\mathrm{g}}$ on the sphere of radius r is

$$(\nabla\lambda_{\mathrm{g}})_{\parallel}(r,\Omega) = \frac{1}{r}\,\nabla_{\mathbb{S}^2}\lambda_{\mathrm{g}}(r,\Omega).$$

By linearity of the collar reduction,

$$\begin{aligned}
\mathscr{A}_{\parallel}^{\mathrm{coll}\prime} &= \mathscr{A}_{\parallel}^{\mathrm{coll}} + \big((\nabla\lambda_{\mathrm{g}})_{\parallel}\big)^{\mathrm{coll}} \\
&= \mathscr{A}_{\parallel}^{\mathrm{coll}} + \frac{1}{L}\int_a^b \frac{1}{r}\,\nabla_{\mathbb{S}^2}\lambda_{\mathrm{g}}(r,\Omega)\,\mathrm{d}r \\
&= \mathscr{A}_{\parallel}^{\mathrm{coll}} + \frac{1}{L}\,\nabla_{\mathbb{S}^2}\left(\int_a^b \frac{\lambda_{\mathrm{g}}(r,\Omega)}{r}\,\mathrm{d}r\right).
\end{aligned}$$

On Σ_{r_*}, the surface gradient satisfies

$$\nabla_{\Sigma_{r_*}} = \frac{1}{r_*}\,\nabla_{\mathbb{S}^2}.$$

Therefore

$$\begin{aligned}\mathscr{A}_{\|}^{\mathrm{coll}\prime} &= \mathscr{A}_{\|}^{\mathrm{coll}} + \nabla_{\Sigma_{r_*}}\left(\frac{r_*}{L}\int_a^b \frac{\lambda_{\mathrm{g}}(r,\Omega)}{r}\,\mathrm{d}r\right)\\ &= \mathscr{A}_{\|}^{\mathrm{coll}} + \nabla_{\Sigma_{r_*}}\lambda_{\mathrm{sh}}.\end{aligned}$$

This proves the identity for smooth λ_{g}.

Next define, for smooth λ_{g},

$$T\lambda_{\mathrm{g}}(\Omega) = \frac{r_*}{L}\int_a^b \frac{\lambda_{\mathrm{g}}(r,\Omega)}{r}\,\mathrm{d}r.$$

We show that T extends boundedly from $H^1(\mathcal{C}(r_*))$ to $H^1(\Sigma_{r_*})$. For the L^2 part, Cauchy–Schwarz gives

$$\begin{aligned}\|T\lambda_{\mathrm{g}}\|^2_{L^2(\Sigma_{r_*})} &= r_*^2\int_{\mathbb{S}^2}\left|\frac{r_*}{L}\int_a^b \frac{\lambda_{\mathrm{g}}(r,\Omega)}{r}\,\mathrm{d}r\right|^2\mathrm{d}\Omega\\ &\le \frac{r_*^4}{L}\int_{\mathbb{S}^2}\int_a^b \frac{|\lambda_{\mathrm{g}}(r,\Omega)|^2}{r^2}\,\mathrm{d}r\,\mathrm{d}\Omega\\ &\le \frac{r_*^4}{La^4}\int_{\mathbb{S}^2}\int_a^b |\lambda_{\mathrm{g}}(r,\Omega)|^2 r^2\,\mathrm{d}r\,\mathrm{d}\Omega\\ &= \frac{r_*^4}{La^4}\|\lambda_{\mathrm{g}}\|^2_{L^2(\mathcal{C}(r_*))}.\end{aligned}$$

For the surface gradient, the smooth identity above yields

$$\nabla_{\Sigma_{r_*}}T\lambda_{\mathrm{g}} = \frac{1}{L}\int_a^b \frac{1}{r}\,\nabla_{\mathbb{S}^2}\lambda_{\mathrm{g}}(r,\Omega)\,\mathrm{d}r.$$

Hence

$$\begin{aligned}\|\nabla_{\Sigma_{r_*}}T\lambda_{\mathrm{g}}\|^2_{L^2(\Sigma_{r_*})} &= r_*^2\int_{\mathbb{S}^2}\left|\frac{1}{L}\int_a^b \frac{1}{r}\,\nabla_{\mathbb{S}^2}\lambda_{\mathrm{g}}(r,\Omega)\,\mathrm{d}r\right|^2\mathrm{d}\Omega\\ &\le \frac{r_*^2}{L}\int_{\mathbb{S}^2}\int_a^b \frac{|\nabla_{\mathbb{S}^2}\lambda_{\mathrm{g}}(r,\Omega)|^2}{r^2}\,\mathrm{d}r\,\mathrm{d}\Omega\\ &\le \frac{r_*^2}{L}\int_{\mathbb{S}^2}\int_a^b |\nabla\lambda_{\mathrm{g}}(r,\Omega)|^2\,\mathrm{d}r\,\mathrm{d}\Omega\\ &\le \frac{r_*^2}{La^2}\|\nabla\lambda_{\mathrm{g}}\|^2_{L^2(\mathcal{C}(r_*))}.\end{aligned}$$

Therefore T extends uniquely to a bounded linear map

$$T : H^1(\mathcal{C}(r_*)) \to H^1(\Sigma_{r_*}).$$

We define $\lambda_{\mathrm{sh}} \coloneqq T\lambda_{\mathrm{g}}$, so $\lambda_{\mathrm{sh}} \in H^1(\Sigma_{r_*})$.

Since

$$\mathcal{C}(r_*) = \{\mathbf{x} \in \mathbb{R}^3\ ;\ a \le |\mathbf{x}| \le b\}$$

is a bounded C^∞ annulus, the standard density theorem yields

$$C^\infty(\overline{\mathcal{C}(r_*)}) \text{ is dense in } H^1(\mathcal{C}(r_*)).$$

Choose a sequence

$$\lambda_{\mathrm{g},n} \in C^\infty(\overline{\mathcal{C}(r_*)}) \qquad \text{with} \qquad \lambda_{\mathrm{g},n} \to \lambda_{\mathrm{g}} \quad \text{in } H^1(\mathcal{C}(r_*)).$$

For each n, the smooth identity gives

$$\big((\nabla\lambda_{\mathrm{g},n})_\parallel\big)^{\mathrm{coll}} = \nabla_{\Sigma_{r_*}}\lambda_{\mathrm{sh},n}.$$

Moreover, by proposition 9 applied to $(\nabla(\lambda_{\mathrm{g},n}-\lambda_{\mathrm{g},m}))_\parallel$,

$$\big\|\big((\nabla\lambda_{\mathrm{g},n})_\parallel\big)^{\mathrm{coll}} - \big((\nabla\lambda_{\mathrm{g},m})_\parallel\big)^{\mathrm{coll}}\big\|_{L^2_{\tan}(\Sigma_{r_*})} \le \frac{r_*}{a\sqrt{L}}\,\|\nabla(\lambda_{\mathrm{g},n}-\lambda_{\mathrm{g},m})\|_{L^2(\mathcal{C}(r_*))}.$$

Hence

$$\big((\nabla\lambda_{\mathrm{g},n})_\parallel\big)^{\mathrm{coll}} \to \big((\nabla\lambda_{\mathrm{g}})_\parallel\big)^{\mathrm{coll}} \qquad \text{in } L^2_{\tan}(\Sigma_{r_*}),$$

while boundedness of T gives

$$\lambda_{\mathrm{sh},n} \to \lambda_{\mathrm{sh}} \qquad \text{in } H^1(\Sigma_{r_*}).$$

Passing to the limit in the smooth identity yields

$$\big((\nabla\lambda_{\mathrm{g}})_\parallel\big)^{\mathrm{coll}} = \nabla_{\Sigma_{r_*}}\lambda_{\mathrm{sh}} \qquad \text{in } L^2_{\tan}(\Sigma_{r_*}).$$

By linearity of the collar reduction,

$$\mathscr{A}_\parallel^{\mathrm{coll}\prime} = \mathscr{A}_\parallel^{\mathrm{coll}} + \big((\nabla\lambda_{\mathrm{g}})_\parallel\big)^{\mathrm{coll}} = \mathscr{A}_\parallel^{\mathrm{coll}} + \nabla_{\Sigma_{r_*}}\lambda_{\mathrm{sh}}.$$

Since Σ_{r_*} is a smooth compact sphere, $C^\infty(\Sigma_{r_*})$ is dense in $H^1(\Sigma_{r_*})$. Choose $\lambda_n \in C^\infty(\Sigma_{r_*})$ with

$$\lambda_n \to \lambda_{\mathrm{sh}} \qquad \text{in } H^1(\Sigma_{r_*}).$$

Then

$$\nabla_{\Sigma_{r_*}}\lambda_n \to \nabla_{\Sigma_{r_*}}\lambda_{\mathrm{sh}} \qquad \text{in } L^2_{\tan}(\Sigma_{r_*}).$$

The radial pullback of $\nabla_{\Sigma_{r_*}}\lambda_n$ to the unit sphere is a smooth exact tangential gradient. By assumption 3, every such single-valued exact gradient lies in the null space of Π_{TT}. Hence

$$\Pi_{\mathrm{TT}}\nabla_{\Sigma_{r_*}}\lambda_n = 0 \qquad \text{for every } n.$$

Because Π_{TT} is bounded on $L^2_{\tan}(\Sigma_{r_*})$ under the same pullback convention, passing to the limit gives

$$\Pi_{\mathrm{TT}}\nabla_{\Sigma_{r_*}}\lambda_{\mathrm{sh}} = \lim_{n\to\infty}\Pi_{\mathrm{TT}}\nabla_{\Sigma_{r_*}}\lambda_n = 0.$$

Applying Π_{TT} to the identity above proves Eq. (53). □

Remark. The raw collar-reduced field $\mathscr{A}_\parallel^{\mathrm{coll}}$ is not gauge invariant. The gauge-invariant vector-shell representative is $\mathscr{A}_{\mathrm{TT}}^{\mathrm{coll}} = \Pi_{\mathrm{TT}}\mathscr{A}_\parallel^{\mathrm{coll}}$, and this is the object on which the later shell-admission operator $\mathbb{Q}_\chi(\ell)$ acts. Together with the exterior trace $b_*^{\mathrm{ext}}(\upsilon)$, after the stated SI normalization is removed where appropriate, it feeds the vector shell channel. The representatives ρ_* and $\mathbf{P}_{\mathrm{mech}}|_{\Sigma_{r_*}}$ feed the scalar shell channel. No gauge-dependent raw potential enters the primary vector-shell invariant.

Remark. The present subsection closes the kinematical shell-reduction layer used in the primary electron-branch construction. From this point onward, each load-bearing object in the primary closure is either a derived shell scalar, a derived shell vector functional, or a coupled map assembled from them. Later branch selections, operator reductions, and numerical realizations may still be introduced with their stated logical status. They are not additional kinematical postulates for the shell-extraction layer.

Part II
The self-contained electron branch

IV. GAUSSIAN GENERATOR MICROSTATE AND ONE-LOOP REDUCTION

This section constructs the minimal branch data used later in the electron shell closure. The logical status of the ingredients is kept explicit. The Gaussian generator sheet is derived within a radial maximum-entropy class with fixed normalization and a fixed second radial moment, in the sense of Shannon and Jaynes [10, 11]. The microscopic luminal rule, the coherent annular reduction, the minimal one-loop calibration, and the first-node pinning are branch-selection conditions within the standing kinematical framework. They are not additional standing postulates, and they do not encode a value of α. The branch ratios used in the later shell construction are derived at the end of the section in Eq. (85).

A. Maximum-entropy Gaussian state on $\mathbb{C}$

We begin with the rotationally invariant sector of generator ensembles on $\mathbb{C}$. Since the standing postulates introduce no preferred direction in $\mathbb{C}$, the minimal stationary branch is evaluated in the radial sector. This is a symmetry-sector selection for the minimal branch, not a separate dynamical postulate. At the variational stage, the retained generator data are the normalization and a single radial second moment. No mass value, charge value, value of α, spin normalization, or shell-lock condition enters this variational step. The total generator mass parameter m is reintroduced only after the maximizing probability density has been fixed.

The radial restriction can also be justified directly by rotational symmetrization. Let $W(\rho,\varphi_{\mathbb{C}}) \geq 0$ be any areal probability density on $\mathbb{C}$ such that

$$\int_{\mathbb{C}} W\,\mathrm{d}^2 z = 1, \qquad \int_{\mathbb{C}} |z|^2 W\,\mathrm{d}^2 z = \sigma_{\mathbb{C}}^2, \qquad W \ln\frac{W}{W_*} \in L^1(\mathbb{C}),$$

for some constant reference areal density $W_* > 0$. Define its angular average by

$$W_{\mathrm{rad}}(\rho) := \frac{1}{2\pi}\int_0^{2\pi} W(\rho,\varphi_{\mathbb{C}})\,\mathrm{d}\varphi_{\mathbb{C}}.$$

Then W_{rad} is a radial areal density with the same normalization and the same second radial moment as W, because

$$2\pi\int_0^{\infty} \rho\, W_{\mathrm{rad}}(\rho)\,\mathrm{d}\rho = \int_0^{\infty}\int_0^{2\pi} \rho\, W(\rho,\varphi_{\mathbb{C}})\,\mathrm{d}\varphi_{\mathbb{C}}\,\mathrm{d}\rho = \int_{\mathbb{C}} W\,\mathrm{d}^2 z = 1,$$

and

$$2\pi\int_0^{\infty} \rho^3 W_{\mathrm{rad}}(\rho)\,\mathrm{d}\rho = \int_0^{\infty}\int_0^{2\pi} \rho^3 W(\rho,\varphi_{\mathbb{C}})\,\mathrm{d}\varphi_{\mathbb{C}}\,\mathrm{d}\rho = \int_{\mathbb{C}} |z|^2 W\,\mathrm{d}^2 z = \sigma_{\mathbb{C}}^2.$$

Moreover, since $u \mapsto u \ln u$ is convex on $[0,\infty)$, Jensen's inequality applied pointwise in ρ to $u(\varphi_{\mathbb{C}}) = W(\rho,\varphi_{\mathbb{C}})/W_*$ gives

$$\frac{1}{2\pi}\int_0^{2\pi} W(\rho,\varphi_{\mathbb{C}}) \ln\frac{W(\rho,\varphi_{\mathbb{C}})}{W_*}\,\mathrm{d}\varphi_{\mathbb{C}} \geq W_{\mathrm{rad}}(\rho)\ln\frac{W_{\mathrm{rad}}(\rho)}{W_*}$$

for almost every ρ. Multiplying by $2\pi\rho$ and integrating in ρ yields

$$-\int_{\mathbb{C}} W_{\mathrm{rad}} \ln\frac{W_{\mathrm{rad}}}{W_*}\,\mathrm{d}^2 z \geq -\int_{\mathbb{C}} W \ln\frac{W}{W_*}\,\mathrm{d}^2 z.$$

Hence angular symmetrization does not decrease the entropy at fixed normalization and fixed second radial moment. The maximum-entropy problem may therefore be restricted to radial densities without loss of any maximizer.

Definition IV.1 (Radial generator probability density)**.** A radial generator probability density is a measurable function

$$w(\rho) \geq 0, \qquad \rho \in [0,\infty),$$

normalized with respect to the $\mathbb{C}$ area measure

$$2\pi \int_0^\infty \rho\, w(\rho)\, \mathrm{d}\rho = 1. \tag{54}$$

Its second radial moment is

$$M_2[w] \coloneqq 2\pi \int_0^\infty \rho^3 w(\rho)\, \mathrm{d}\rho. \tag{55}$$

Definition IV.2 (Entropy functional on $\mathbb{C}$)**.** Fix a positive constant reference scale $w_* > 0$ with the same physical dimension as w, namely an areal density on $\mathbb{C}$. This reference scale only makes the logarithm dimensionless and is not a physical input to the branch selection. For a radial generator density w, define

$$\mathcal{S}_{\mathbb{C}}[w] = -2\pi \int_0^\infty \rho\, w(\rho)\, \ln\frac{w(\rho)}{w_*}\, \mathrm{d}\rho, \tag{56}$$

with the standard convention $0 \ln 0 = 0$. For a prescribed moment label $\sigma_{\mathbb{C}} > 0$, let

$$\mathcal{A}_{\sigma_{\mathbb{C}}} = \left\{ w \geq 0 \;\middle|\; \begin{array}{c} 2\pi \displaystyle\int_0^\infty \rho\, w(\rho)\, \mathrm{d}\rho = 1, \\ M_2[w] = \sigma_{\mathbb{C}}^2, \\ \rho\, w(\rho) \ln\dfrac{w(\rho)}{w_*} \in L^1(0,\infty), \quad \text{with the same convention } 0\ln 0 = 0 \end{array} \right\}. \tag{57}$$

At this stage $\sigma_{\mathbb{C}}$ is only the fixed second-moment scale of the variational class. Its relation to R is not fixed until the minimal one-loop calibration in Condition IV.2. Replacing w_* by κw_*, with any constant $\kappa > 0$, shifts $\mathcal{S}_{\mathbb{C}}$ by the additive constant $\ln \kappa$, because the normalization Eq. (54) is fixed. Hence the maximizer on $\mathcal{A}_{\sigma_{\mathbb{C}}}$ is independent of the choice of constant reference scale.

Theorem 3 (Maximum-entropy radial state on $\mathbb{C}$)**.** *For fixed $\sigma_{\mathbb{C}} > 0$, among all radial generator probability densities $w \in \mathcal{A}_{\sigma_{\mathbb{C}}}$, the unique maximizer of $\mathcal{S}_{\mathbb{C}}$ is*

$$w_{\mathbb{C}}(\rho) = \frac{1}{\pi \sigma_{\mathbb{C}}^2} \exp\!\left(-\frac{\rho^2}{\sigma_{\mathbb{C}}^2}\right). \tag{58}$$

This theorem fixes the Gaussian shape at fixed radial second moment. It does not fix the branch value of $\sigma_{\mathbb{C}}$, its relation to R, the generator mass parameter m, or any value of α. With the normalization and second-moment convention of Eqs. (54) *and* (55)*,*

$$M_2[w_{\mathbb{C}}] = \sigma_{\mathbb{C}}^2,$$

so $\sigma_{\mathbb{C}}$ is the root-mean-square radial width of the two-dimensional generator sheet. Equivalently, if $z = x_1 + i x_2$ is any orthonormal Cartesian chart on $\mathbb{C}$, then

$$\int_{\mathbb{C}} x_1^2 w_{\mathbb{C}}\, \mathrm{d}^2 z = \int_{\mathbb{C}} x_2^2 w_{\mathbb{C}}\, \mathrm{d}^2 z = \frac{\sigma_{\mathbb{C}}^2}{2}.$$

Proof. We first determine any stationary point under the normalization and second-moment constraints. Consider

$$\mathcal{J}[w] = \mathcal{S}_{\mathbb{C}}[w] - \lambda_0 \left(2\pi \int_0^\infty \rho\, w(\rho)\, \mathrm{d}\rho - 1\right) - \lambda_2 \left(2\pi \int_0^\infty \rho^3 w(\rho)\, \mathrm{d}\rho - \sigma_{\mathbb{C}}^2\right).$$

Let h be a compactly supported bounded variation for which $w + \varepsilon h$ remains positive for all sufficiently small ε. Then

$$\frac{\mathrm{d}}{\mathrm{d}\varepsilon} \mathcal{J}[w + \varepsilon h]\Big|_{\varepsilon=0} = -2\pi \int_0^\infty \rho \Big[\ln\frac{w(\rho)}{w_*} + 1 + \lambda_0 + \lambda_2 \rho^2\Big] h(\rho)\, \mathrm{d}\rho.$$

Since h is arbitrary, stationarity gives

$$\ln\frac{w(\rho)}{w_*} + 1 + \lambda_0 + \lambda_2 \rho^2 = 0 \qquad \text{for almost every } \rho > 0.$$

Hence

$$w(\rho) = C\, e^{-\lambda_2 \rho^2}, \qquad C \coloneqq w_* e^{-1-\lambda_0}.$$

The normalization and finite second-moment constraints force $\lambda_2 > 0$; otherwise the radial integrals either diverge or fail to define a probability density with finite second moment. Using

$$\int_0^\infty \rho\, e^{-\lambda_2 \rho^2}\, \mathrm{d}\rho = \frac{1}{2\lambda_2}, \qquad \int_0^\infty \rho^3 e^{-\lambda_2 \rho^2}\, \mathrm{d}\rho = \frac{1}{2\lambda_2^2},$$

the constraints give

$$1 = 2\pi C \int_0^\infty \rho\, e^{-\lambda_2 \rho^2}\, \mathrm{d}\rho = \frac{\pi C}{\lambda_2}, \qquad \sigma_{\mathbb{C}}^2 = 2\pi C \int_0^\infty \rho^3 e^{-\lambda_2 \rho^2}\, \mathrm{d}\rho = \frac{\pi C}{\lambda_2^2}.$$

Therefore

$$C = \frac{\lambda_2}{\pi}, \qquad \lambda_2 = \sigma_{\mathbb{C}}^{-2},$$

and the only stationary point is

$$w_{\mathbb{C}}(\rho) = \frac{1}{\pi \sigma_{\mathbb{C}}^2} \exp\!\left(-\frac{\rho^2}{\sigma_{\mathbb{C}}^2} \right).$$

This stationary density indeed belongs to $\mathcal{A}_{\sigma_{\mathbb{C}}}$. Its normalization is

$$2\pi \int_0^\infty \rho\, \frac{1}{\pi \sigma_{\mathbb{C}}^2} e^{-\rho^2/\sigma_{\mathbb{C}}^2}\, \mathrm{d}\rho = \frac{2}{\sigma_{\mathbb{C}}^2} \int_0^\infty \rho e^{-\rho^2/\sigma_{\mathbb{C}}^2}\, \mathrm{d}\rho = \frac{2}{\sigma_{\mathbb{C}}^2} \cdot \frac{\sigma_{\mathbb{C}}^2}{2} = 1.$$

Its second radial moment is

$$2\pi \int_0^\infty \rho^3\, \frac{1}{\pi \sigma_{\mathbb{C}}^2} e^{-\rho^2/\sigma_{\mathbb{C}}^2}\, \mathrm{d}\rho = \frac{2}{\sigma_{\mathbb{C}}^2} \int_0^\infty \rho^3 e^{-\rho^2/\sigma_{\mathbb{C}}^2}\, \mathrm{d}\rho = \frac{2}{\sigma_{\mathbb{C}}^2} \cdot \frac{\sigma_{\mathbb{C}}^4}{2} = \sigma_{\mathbb{C}}^2.$$

The entropy integral is finite because

$$\rho\, w_{\mathbb{C}}(\rho) \ln \frac{w_{\mathbb{C}}(\rho)}{w_*} = \rho\, w_{\mathbb{C}}(\rho) \left[-\ln(\pi \sigma_{\mathbb{C}}^2 w_*) - \frac{\rho^2}{\sigma_{\mathbb{C}}^2} \right],$$

and both $\int_0^\infty \rho w_{\mathbb{C}}(\rho)\, \mathrm{d}\rho$ and $\int_0^\infty \rho^3 w_{\mathbb{C}}(\rho)\, \mathrm{d}\rho$ are finite.

It remains to prove global maximality and uniqueness. Define

$$\mathrm{d}\mu(\rho) \coloneqq 2\pi \rho\, \mathrm{d}\rho.$$

For any $w \in \mathcal{A}_{\sigma_{\mathbb{C}}}$, one has

$$\ln w_{\mathbb{C}}(\rho) = -\ln(\pi \sigma_{\mathbb{C}}^2) - \frac{\rho^2}{\sigma_{\mathbb{C}}^2}.$$

Hence

$$\begin{aligned} \mathcal{S}_{\mathbb{C}}[w] - \mathcal{S}_{\mathbb{C}}[w_{\mathbb{C}}] &= -\int_0^\infty w \ln \frac{w}{w_*}\, \mathrm{d}\mu + \int_0^\infty w_{\mathbb{C}} \ln \frac{w_{\mathbb{C}}}{w_*}\, \mathrm{d}\mu \\ &= -\int_0^\infty w \ln \frac{w}{w_{\mathbb{C}}}\, \mathrm{d}\mu - \int_0^\infty (w - w_{\mathbb{C}}) \ln \frac{w_{\mathbb{C}}}{w_*}\, \mathrm{d}\mu. \end{aligned}$$

Since

$$\ln \frac{w_{\mathbb{C}}}{w_*} = -\ln(\pi \sigma_{\mathbb{C}}^2 w_*) - \frac{\rho^2}{\sigma_{\mathbb{C}}^2},$$

the second integral vanishes because w and $w_{\mathbb{C}}$ have the same normalization and the same second radial moment. Therefore

$$\mathcal{S}_{\mathbb{C}}[w] - \mathcal{S}_{\mathbb{C}}[w_{\mathbb{C}}] = -\int_0^\infty w(\rho)\, \ln \frac{w(\rho)}{w_{\mathbb{C}}(\rho)}\, \mathrm{d}\mu(\rho).$$

To make the sign explicit, set

$$\mathscr{R}_w(\rho) = \frac{w(\rho)}{w_{\mathbb{C}}(\rho)},$$

with the standard convention $0 \ln 0 = 0$. Since $w_{\mathbb{C}}(\rho) > 0$ for every $\rho \geq 0$, this ratio is defined $\mathrm{d}\mu$-almost everywhere. Since w and $w_{\mathbb{C}}$ have the same normalization,

$$\int_0^\infty w_{\mathbb{C}}(\rho)\big(\mathscr{R}_w(\rho) - 1\big)\, \mathrm{d}\mu(\rho) = 0.$$

Hence

$$\int_0^\infty w \ln \frac{w}{w_{\mathbb{C}}}\, \mathrm{d}\mu = \int_0^\infty w_{\mathbb{C}}(\rho)\big(\mathscr{R}_w(\rho) \ln \mathscr{R}_w(\rho) - \mathscr{R}_w(\rho) + 1\big)\, \mathrm{d}\mu(\rho) \geq 0,$$

because $s \ln s - s + 1 \geq 0$ for $s \geq 0$, with equality only at $s = 1$. Therefore

$$\mathcal{S}_{\mathbb{C}}[w] - \mathcal{S}_{\mathbb{C}}[w_{\mathbb{C}}] \leq 0,$$

with equality if and only if $w = w_{\mathbb{C}}$ almost everywhere. Hence $w_{\mathbb{C}}$ is the unique maximizer on $\mathcal{A}_{\sigma_{\mathbb{C}}}$.

Finally, let $z = x_1 + ix_2$ be any orthonormal Cartesian chart on $\mathbb{C}$. Since

$$w_{\mathbb{C}}(x_1, x_2) = \frac{1}{\pi\sigma_{\mathbb{C}}^2} \exp\left(-\frac{x_1^2 + x_2^2}{\sigma_{\mathbb{C}}^2}\right)$$

is rotationally invariant, one has

$$\int_{\mathbb{C}} x_1^2 w_{\mathbb{C}}\, \mathrm{d}^2 z = \int_{\mathbb{C}} x_2^2 w_{\mathbb{C}}\, \mathrm{d}^2 z.$$

Moreover,

$$\int_{\mathbb{C}} (x_1^2 + x_2^2) w_{\mathbb{C}}\, \mathrm{d}^2 z = \int_{\mathbb{C}} |z|^2 w_{\mathbb{C}}\, \mathrm{d}^2 z = M_2[w_{\mathbb{C}}] = \sigma_{\mathbb{C}}^2.$$

Therefore

$$\int_{\mathbb{C}} x_1^2 w_{\mathbb{C}}\, \mathrm{d}^2 z = \int_{\mathbb{C}} x_2^2 w_{\mathbb{C}}\, \mathrm{d}^2 z = \frac{\sigma_{\mathbb{C}}^2}{2}.$$

This proves the final sentence of the theorem statement. □

Definition IV.3 (Gaussian generator mass sheet)**.** After a positive total generator mass parameter $m > 0$ has been assigned to the normalized Gaussian density as an overall mass normalization, the areal mass density on $\mathbb{C}$ is

$$\rho_m(\rho) = m\, w_{\mathbb{C}}(\rho) = \frac{m}{\pi\sigma_{\mathbb{C}}^2} \exp\left(-\frac{\rho^2}{\sigma_{\mathbb{C}}^2}\right), \qquad 2\pi \int_0^\infty \rho\, \rho_m(\rho)\, \mathrm{d}\rho = m. \tag{59}$$

In polar coordinates on $\mathbb{C}$, the local areal mass element is

$$\mathrm{d}m_{\mathrm{loc}} = \rho_m(\rho)\, \rho\, \mathrm{d}\rho\, \mathrm{d}\varphi_{\mathbb{C}}.$$

The corresponding radially integrated mass element is

$$\mathrm{d}m = \int_0^{2\pi} \mathrm{d}m_{\mathrm{loc}} = 2\pi\rho\, \rho_m(\rho)\, \mathrm{d}\rho. \tag{60}$$

This definition normalizes the generator sheet by a mass parameter. It does not derive the observed electron rest mass, and it does not select the numerical value of m.

Condition IV.1 (Microscopic luminal generator rule)**.** In the minimal one-loop branch construction, the following internal generator-side kinematical rule is adopted as part of the branch-selection package. Each microscopic generator element at radius $\rho > 0$ is assigned the tangential speed scale c in $\mathbb{C}$, relative to the chosen positive orientation of the generator plane. This is an internal kinematical rule; it is not the velocity of an observed massive point particle in $\mathbb{R}^3$, not a statement about signal propagation in observed space, and not a fit to α, $g-2$, or a measured lepton mass.

The local oriented tangential momentum element is defined by

$$\mathrm{d}\mathbf{p}_{\mathrm{tan}}^{\mathrm{loc}} = c\,\mathrm{d}m_{\mathrm{loc}}\,\hat{\mathbf{t}}_{\mathbb{C}},$$

where $\hat{\mathbf{t}}_{\mathbb{C}}$ is the unit tangent compatible with the chosen orientation. Its radially integrated positive magnitude is

$$\mathrm{d}p_{\mathrm{tan}} = \int_0^{2\pi} \left|\mathrm{d}\mathbf{p}_{\mathrm{tan}}^{\mathrm{loc}}\right| = c\,\mathrm{d}m. \tag{61}$$

The corresponding local angular rate is

$$\omega_{\mathrm{dot}}(\rho) = \frac{c}{\rho}. \tag{62}$$

The constant c is the same SI speed scale that appears in the Relator lock. It is not inferred from a measured generator motion. The singular behavior of $\omega_{\mathrm{dot}}(\rho)$ at $\rho = 0$ is harmless for the quantities used below. Indeed, for every $\delta > 0$,

$$\int_0^{\delta} \omega_{\mathrm{dot}}(\rho)\,\mathrm{d}m = \int_0^{\delta} \frac{c}{\rho}\,2\pi\rho\,\rho_m(\rho)\,\mathrm{d}\rho = 2\pi c \int_0^{\delta} \rho_m(\rho)\,\mathrm{d}\rho \le 2\pi c\,\delta \sup_{0\le\rho\le\delta} \rho_m(\rho) < \infty,$$

because ρ_m is continuous at the origin by Eq. (59). The full Gaussian sheet is used below only through finite radial moments such as $\int \rho\,\mathrm{d}m$, whereas collective angular rates are assigned only to coherent annular reductions whose support is compactly contained in $(0,\infty)$.

Proposition 11 (First radial moment and generator first moment)**.** *For the Gaussian sheet Eq.* (59)*, the first radial moment is*

$$\langle\rho\rangle_{\mathbb{C}} := \frac{1}{m}\int_0^{\infty} \rho\,\mathrm{d}m = \frac{\sqrt{\pi}}{2}\,\sigma_{\mathbb{C}}. \tag{63}$$

Under the microscopic luminal generator rule Condition IV.1, the associated oriented generator first-moment functional is not the net linear momentum of the rotationally symmetric sheet, whose angular average vanishes. It is the positive magnitude of the axial moment relative to the chosen orientation,

$$L_{\mathbb{C}} := \int_0^{\infty} \rho\,\mathrm{d}p_{\mathrm{tan}} = \int_0^{\infty} \rho\,c\,\mathrm{d}m = \frac{\sqrt{\pi}}{2}\,mc\,\sigma_{\mathbb{C}}. \tag{64}$$

This is a generator-level kinematical first moment with the dimensions of angular momentum. At this stage it is not a spin operator, not the relativistic mechanical momentum of an observed point particle, not the net tangential momentum of the sheet, and not an independently measured angular momentum. Reversing the chosen loop orientation reverses the associated axial direction, while $L_{\mathbb{C}}$ denotes the positive magnitude used in the minimal branch calibration.

Proof. To separate the vanishing tangential linear momentum from the nonvanishing axial first moment, write the local microscopic tangential momentum element in polar coordinates on $\mathbb{C}$ as

$$\mathrm{d}\mathbf{p}_{\mathrm{tan}}^{\mathrm{loc}} = c\,\rho_m(\rho)\,\rho\,\mathrm{d}\rho\,\mathrm{d}\varphi_{\mathbb{C}}\,\hat{\mathbf{t}}_{\mathbb{C}}(\varphi_{\mathbb{C}}),$$

where

$$\hat{\mathbf{t}}_{\mathbb{C}}(\varphi_{\mathbb{C}}) = \big(-\sin\varphi_{\mathbb{C}}, \cos\varphi_{\mathbb{C}}\big)$$

is the positively oriented unit tangent on the generator plane. Then

$$\int_0^{2\pi} \hat{\mathbf{t}}_{\mathbb{C}}(\varphi_{\mathbb{C}})\,\mathrm{d}\varphi_{\mathbb{C}} = \left(-\int_0^{2\pi} \sin\varphi_{\mathbb{C}}\,\mathrm{d}\varphi_{\mathbb{C}}, \int_0^{2\pi} \cos\varphi_{\mathbb{C}}\,\mathrm{d}\varphi_{\mathbb{C}}\right) = (0,0),$$

and therefore the net tangential linear momentum of the rotationally symmetric sheet vanishes,

$$\int_0^\infty \int_0^{2\pi} \mathrm{d}\mathbf{p}_{\tan}^{\mathrm{loc}} = c \int_0^\infty \rho_m(\rho)\,\rho \left(\int_0^{2\pi} \hat{\mathbf{t}}_{\mathbb{C}}(\varphi_{\mathbb{C}})\,\mathrm{d}\varphi_{\mathbb{C}} \right) \mathrm{d}\rho = 0.$$

By contrast, the local axial angular-momentum element has positive magnitude

$$\mathrm{d}L_{\mathbb{C}}^{\mathrm{loc}} = \rho \left| \mathrm{d}\mathbf{p}_{\tan}^{\mathrm{loc}} \right| = \rho\, c\, \rho_m(\rho)\, \rho\, \mathrm{d}\rho\, \mathrm{d}\varphi_{\mathbb{C}}.$$

After integrating over $\varphi_{\mathbb{C}}$, this becomes

$$\mathrm{d}L_{\mathbb{C}} = \int_0^{2\pi} \mathrm{d}L_{\mathbb{C}}^{\mathrm{loc}} = \rho\, c\, \mathrm{d}m.$$

Using Eq. (60),

$$\langle \rho \rangle_{\mathbb{C}} = \frac{1}{m} \int_0^\infty \rho\, \mathrm{d}m = \frac{2}{\sigma_{\mathbb{C}}^2} \int_0^\infty \rho^2 e^{-\rho^2/\sigma_{\mathbb{C}}^2}\, \mathrm{d}\rho.$$

Set

$$u = \frac{\rho^2}{\sigma_{\mathbb{C}}^2}, \qquad \rho = \sigma_{\mathbb{C}} \sqrt{u}, \qquad \mathrm{d}\rho = \frac{\sigma_{\mathbb{C}}}{2\sqrt{u}}\, \mathrm{d}u.$$

Then

$$\int_0^\infty \rho^2 e^{-\rho^2/\sigma_{\mathbb{C}}^2}\, \mathrm{d}\rho = \frac{\sigma_{\mathbb{C}}^3}{2} \int_0^\infty u^{1/2} e^{-u}\, \mathrm{d}u = \frac{\sigma_{\mathbb{C}}^3}{2}\, \Gamma\!\left(\frac{3}{2}\right) = \frac{\sqrt{\pi}}{4} \sigma_{\mathbb{C}}^3.$$

Therefore

$$\langle \rho \rangle_{\mathbb{C}} = \frac{2}{\sigma_{\mathbb{C}}^2} \cdot \frac{\sqrt{\pi}}{4} \sigma_{\mathbb{C}}^3 = \frac{\sqrt{\pi}}{2} \sigma_{\mathbb{C}},$$

which proves Eq. (63).

Using Eq. (61),

$$L_{\mathbb{C}} = \int_0^\infty \rho\, \mathrm{d}p_{\tan} = c \int_0^\infty \rho\, \mathrm{d}m = mc\, \langle \rho \rangle_{\mathbb{C}} = \frac{\sqrt{\pi}}{2}\, mc\, \sigma_{\mathbb{C}},$$

which is Eq. (64). □

Condition IV.2 (Minimal one-loop calibration)**.** The minimal one-loop branch is selected by the calibration

$$L_{\mathbb{C}} = \frac{1}{2}\, mc\, R. \tag{65}$$

This is a branch-selection condition. It does not follow from the maximum-entropy variational problem and is not a numerical fit to α, to $g-2$, to a measured spin value, or to a measured lepton mass. It also does not identify R with the reduced Compton radius and does not insert $\hbar/2$ as an external datum. Its role is to set the generator first-moment scale equal to one half of mcR for the single collective radius R of the minimal one-loop branch. The rational factor $1/2$ is therefore part of the explicit minimal branch calibration, and the later spin-sector normalization is conditional on this calibration.

Proposition 12 (Width of the Gaussian sheet)**.** *For a branch with fixed collective radius R, and conditional on the branch-selection calibration Condition IV.2, the Gaussian width is fixed uniquely relative to R as*

$$\sigma_{\mathbb{C}} = \frac{R}{\sqrt{\pi}} \tag{66}$$

and therefore

$$\varepsilon := \frac{\sigma_{\mathbb{C}}}{R} = \frac{1}{\sqrt{\pi}}. \tag{67}$$

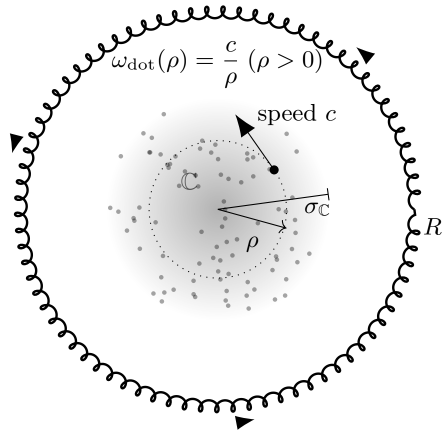

FIG. 4. Generator-side geometry on $\mathbb{C}$. After the minimal one-loop calibration, the maximum-entropy Gaussian generator sheet has width $\sigma_{\mathbb{C}} = R/\sqrt{\pi}$. The coherent carrier representative is shown at radius R, and a representative microscopic element is shown at radius ρ with tangential speed scale c. This speed is not an observed particle velocity in $\mathbb{R}^3$. The figure is schematic and displays generator-side bookkeeping only. Charge assignment and current normalization are introduced later.

Proof. Insert Eq. (64) into Eq. (65). This gives

$$\frac{\sqrt{\pi}}{2}\, mc\, \sigma_{\mathbb{C}} = \frac{1}{2}\, mc\, R.$$

Cancelling the common nonzero factor $\frac{1}{2}mc$ yields

$$\sqrt{\pi}\, \sigma_{\mathbb{C}} = R,$$

which is Eq. (66). Dividing by R gives Eq. (67). □

Remark. The role of Condition IV.2 is to calibrate the generator width against the single collective radius R. After division by mcR, it is a dimensionless branch-selection rule, not a numerical fit. The factor 1/2 is part of the minimal-branch calibration, not an inserted measured spin value. Its interpretation within the charge-spin sector is discussed later.

Figure 4 summarizes the generator-side geometry. It displays the maximum-entropy Gaussian sheet on $\mathbb{C}$, the carrier circle $|z| = R$, and the microscopic luminal generator rule. The figure is schematic and is not part of the derivation. Charge assignment, current normalization, and the specialization $Q = \pm e$ are introduced later in section V.

B. Collective reduction to the one-loop branch

The Gaussian sheet has noncompact support and is therefore not itself a one-dimensional carrier. The loop used later in the shell construction is a collective reduction of the Gaussian microstate. Within the minimal one-loop branch class considered here, this reduction is restricted to lock-compatible annular representatives and to the minimal nonzero azimuthal winding sector. It belongs to the branch-selection layer; it does not introduce a measured value of α, a QED loop coefficient, or an empirical lepton datum.

Definition IV.4 (Coherent annular reduction)**.** A coherent annular reduction is a positive Borel probability measure μ_{coh} on $(0, \infty)$, normalized by

$$\int_{(0,\infty)} \mathrm{d}\mu_{\mathrm{coh}}(\rho) = 1. \tag{68}$$

Its support is required to satisfy

$$\operatorname{supp}\mu_{\mathrm{coh}} \subset [\rho_-, \rho_+] \subset (0, \infty), \qquad 0 < \rho_- \le \rho_+ < \infty. \tag{69}$$

The associated collective rate is defined by the branch-reduction convention that linearly averages the microscopic angular rates,

$$\omega = \int_{(0,\infty)} \omega_{\mathrm{dot}}(\rho)\, \mathrm{d}\mu_{\mathrm{coh}}(\rho) = c \int_{(0,\infty)} \frac{1}{\rho}\, \mathrm{d}\mu_{\mathrm{coh}}(\rho). \tag{70}$$

This averaging convention is part of the coherent annular reduction and is not a fit to any external frequency or coupling.

The harmonic-radius functional of the coherent annular reduction is

$$\mathcal{R}_{\mathrm{H}}[\mu_{\mathrm{coh}}] \coloneqq \left(\int_{(0,\infty)} \frac{1}{\rho}\, \mathrm{d}\mu_{\mathrm{coh}}(\rho) \right)^{-1}.$$

A coherent annular reduction is compatible with the calibrated branch radius R only when this harmonic radius equals that same branch radius, namely

$$\mathcal{R}_{\mathrm{H}}[\mu_{\mathrm{coh}}] = R. \tag{71}$$

This compatibility condition matches the radius used in the one-loop calibration to the lock-preserving radius exported by the annular reduction. It is a branch-consistency condition, not an adjustable radial fit. The compatible class is nonempty. For example, the Dirac point measure

$$\mu_{\mathrm{coh}} = \delta_R$$

has support $\{R\} \subset (0,\infty)$, satisfies

$$\int_{(0,\infty)} \mathrm{d}\mu_{\mathrm{coh}} = 1, \qquad \int_{(0,\infty)} \frac{1}{\rho}\, \mathrm{d}\mu_{\mathrm{coh}}(\rho) = \frac{1}{R},$$

and therefore satisfies Eq. (71). More general coherent annular reductions may have finite radial width, provided their harmonic radius is R.

This measure encodes only the radial coarse graining of the phase-coherent annular representative. It is not identified with the full Gaussian area measure $2\pi\rho\, w_{\mathbb{C}}(\rho)\, \mathrm{d}\rho$, and it is not an additional probability law for the whole generator sheet. The Gaussian sheet fixes the width $\sigma_{\mathbb{C}}$ through the maximum-entropy result and the one-loop calibration, whereas μ_{coh} records the annular reduction whose harmonic radius is exported to the carrier description. No uniqueness of μ_{coh} is asserted here, and no reconstruction map from the full Gaussian sheet to μ_{coh} is used below. Only the existence of at least one compatible annular reduction is required.

Proposition 13 (Lock-preserving harmonic radius and uniqueness of the radius functional)**.** *Let ω be the collective rate associated with μ_{coh} through Eq.* (70)*, and recall*

$$\frac{1}{\mathcal{R}_{\mathrm{H}}[\mu_{\mathrm{coh}}]} = \int_{(0,\infty)} \frac{1}{\rho}\, \mathrm{d}\mu_{\mathrm{coh}}(\rho). \tag{72}$$

Then $\mathcal{R}_{\mathrm{H}}[\mu_{\mathrm{coh}}]$ is well defined and satisfies

$$\rho_- \le \mathcal{R}_{\mathrm{H}}[\mu_{\mathrm{coh}}] \le \rho_+.$$

If the annular reduction is compatible with the calibrated branch radius, so that $\mathcal{R}_{\mathrm{H}}[\mu_{\mathrm{coh}}] = R$, then the lock identity holds,

$$R\,\omega = c \tag{73}$$

Moreover, let $\mathcal{R}[\mu_{\mathrm{coh}}] > 0$ be any radius functional defined on coherent annular reductions and satisfying

$$\mathcal{R}[\mu_{\mathrm{coh}}]\,\omega = c$$

for every admissible coherent annular reduction, where ω is the collective rate defined by Eq. (70)*. Then necessarily*

$$\mathcal{R}[\mu_{\mathrm{coh}}] = \mathcal{R}_{\mathrm{H}}[\mu_{\mathrm{coh}}] = \left(\int_{(0,\infty)} \frac{1}{\rho}\, \mathrm{d}\mu_{\mathrm{coh}}(\rho) \right)^{-1}.$$

Proof. Since

$$\operatorname{supp}\mu_{\mathrm{coh}} \subset [\rho_-, \rho_+] \subset (0, \infty),$$

one has

$$\frac{1}{\rho_+} \le \frac{1}{\rho} \le \frac{1}{\rho_-} \qquad \text{for } \mu_{\mathrm{coh}}\text{-almost every } \rho.$$

Integrating and using

$$\int_{(0,\infty)} \mathrm{d}\mu_{\mathrm{coh}}(\rho) = 1$$

gives

$$\frac{1}{\rho_+} \le \int_{(0,\infty)} \frac{1}{\rho}\, \mathrm{d}\mu_{\mathrm{coh}}(\rho) \le \frac{1}{\rho_-}.$$

Hence the integral in Eq. (72) is finite and strictly positive, so $\mathcal{R}_{\mathrm{H}}[\mu_{\mathrm{coh}}]$ is well defined and

$$\rho_- \le \mathcal{R}_{\mathrm{H}}[\mu_{\mathrm{coh}}] \le \rho_+.$$

Using the microscopic luminal rule Eq. (62) in the collective average Eq. (70) gives

$$\omega = c \int_{(0,\infty)} \frac{1}{\rho}\, \mathrm{d}\mu_{\mathrm{coh}}(\rho) = \frac{c}{\mathcal{R}_{\mathrm{H}}[\mu_{\mathrm{coh}}]}.$$

If the annular reduction is compatible, then $\mathcal{R}_{\mathrm{H}}[\mu_{\mathrm{coh}}] = R$, and therefore

$$\omega = \frac{c}{R},$$

which is equivalent to Eq. (73).

Finally, let $\mathcal{R}[\mu_{\mathrm{coh}}] > 0$ be any radius functional with the property

$$\mathcal{R}[\mu_{\mathrm{coh}}]\, \omega = c$$

for every admissible coherent annular reduction. Substituting the already proved identity

$$\omega = \frac{c}{\mathcal{R}_{\mathrm{H}}[\mu_{\mathrm{coh}}]}$$

yields

$$\mathcal{R}[\mu_{\mathrm{coh}}] = \frac{c}{\omega} = \left(\int_{(0,\infty)} \frac{1}{\rho}\, \mathrm{d}\mu_{\mathrm{coh}}(\rho) \right)^{-1} = \mathcal{R}_{\mathrm{H}}[\mu_{\mathrm{coh}}],$$

which proves uniqueness of the harmonic radius within the stated single-radius closure class. □

Definition IV.5 (Collective carrier phase)**.** The collective carrier phase is the angular variable

$$\theta_0 \in \mathbb{R}/2\pi\mathbb{Z}, \tag{74}$$

parametrizing the carrier circle $\Gamma_R \subset \mathbb{C}$. Let t_{br} denote the branch evolution parameter used for internal phase transport, with SI units of time. Whenever θ_0 is differentiated with respect to t_{br}, the derivative is understood through any smooth local lift $\widetilde{\theta}_0$ of θ_0 to $\mathbb{R}$. Any two such local lifts differ by an additive constant in $2\pi\mathbb{Z}$, so their derivatives agree. For a compatible coherent annular reduction, the locked branch convention therefore reads

$$\frac{\mathrm{d}\theta_0}{\mathrm{d}t_{\mathrm{br}}} := \frac{\mathrm{d}\widetilde{\theta}_0}{\mathrm{d}t_{\mathrm{br}}} = \omega = \frac{c}{R}. \tag{75}$$

When the branch center is later represented by a timelike worldline, t_{br} is identified with the corresponding rest-frame, equivalently proper-time, parameter only within that worldline convention. Until then, t_{br} denotes only the internal branch evolution parameter, and dot notation is avoided for θ_0.

Proposition 14 (Azimuthal Fourier modes on the carrier circle)**.** *Parametrize the carrier circle by*

$$z(\theta_0) = Re^{i\theta_0}, \qquad 0 \le \theta_0 < 2\pi.$$

In this subsection the carrier Hilbert space is taken to be the normalized angular phase space

$$L^2\left(\mathbb{R}/2\pi\mathbb{Z}, \frac{\mathrm{d}\theta_0}{2\pi}\right).$$

This choice uses the angular parametrization of the carrier and is distinct from the arc-length space $L^2(\Gamma_R; \mathrm{d}s)$. Then for every

$$f \in L^2\left(\mathbb{R}/2\pi\mathbb{Z}, \frac{\mathrm{d}\theta_0}{2\pi}\right)$$

there exists a unique sequence $(c_n)_{n\in\mathbb{Z}} \in \ell^2(\mathbb{Z})$ such that

$$f = \sum_{n\in\mathbb{Z}} c_n\, e^{in\theta_0} \qquad \text{in } L^2\left(\mathbb{R}/2\pi\mathbb{Z}, \frac{\mathrm{d}\theta_0}{2\pi}\right), \tag{76}$$

with Fourier coefficients

$$c_n = \frac{1}{2\pi}\int_0^{2\pi} f(\theta_0)e^{-in\theta_0}\,\mathrm{d}\theta_0, \qquad \sum_{n\in\mathbb{Z}} |c_n|^2 = \|f\|^2_{L^2(\mathbb{R}/2\pi\mathbb{Z},\mathrm{d}\theta_0/2\pi)}.$$

The basis mode $e^{in\theta_0}$ has winding number n. In particular, $n = 0$ is constant, and the minimal nonzero winding sectors are $n = \pm 1$.

Proof. With the normalized measure $\mathrm{d}\theta_0/(2\pi)$, the family $\{e^{in\theta_0}\}_{n\in\mathbb{Z}}$ is orthonormal because

$$\frac{1}{2\pi}\int_0^{2\pi} e^{i(n-m)\theta_0}\,\mathrm{d}\theta_0 = \delta_{nm}.$$

By the Fourier–Plancherel theorem on $L^2(\mathbb{R}/2\pi\mathbb{Z}, \mathrm{d}\theta_0/2\pi)$, this orthonormal family is complete. Hence every f in the normalized angular Hilbert space has a unique coefficient sequence $(c_n)_{n\in\mathbb{Z}} \in \ell^2(\mathbb{Z})$ such that

$$f = \sum_{n\in\mathbb{Z}} c_n e^{in\theta_0} \qquad \text{in } L^2\left(\mathbb{R}/2\pi\mathbb{Z}, \frac{\mathrm{d}\theta_0}{2\pi}\right),$$

and Parseval's identity gives

$$\sum_{n\in\mathbb{Z}} |c_n|^2 = \|f\|^2_{L^2(\mathbb{R}/2\pi\mathbb{Z},\mathrm{d}\theta_0/2\pi)}.$$

The coefficient formula in Eq. (76) is the orthogonal projection of f onto the basis vector $e^{in\theta_0}$.

For the basis mode $f_n(\theta_0) = e^{in\theta_0}$, the winding number is

$$\frac{1}{2\pi i}\int_0^{2\pi} f_n(\theta_0)^{-1}\,\partial_{\theta_0} f_n(\theta_0)\,\mathrm{d}\theta_0 = \frac{1}{2\pi i}\int_0^{2\pi} in\,\mathrm{d}\theta_0 = n.$$

Hence $n = 0$ is the constant mode, while the minimal nonzero winding sectors are $n = \pm 1$. □

Definition IV.6 (One-loop branch)**.** The Fourier decomposition separates the winding sectors. The one-loop branch is the branch-selection choice that retains the minimal nonzero azimuthal winding sector. Here one-loop means one closed carrier winding in the generator phase sector; it is not a QED loop order and does not import any radiative coefficient. After fixing the positive orientation, we represent this sector by

$$f_1(\theta_0) = e^{i\theta_0}. \tag{77}$$

The mode $e^{-i\theta_0}$ has winding number -1 and represents the opposite orientation. At the present stage the two orientations are equivalent, and charge and current conventions are fixed later.

Remark. The Gaussian sheet and the one-loop carrier play different logical roles. The Gaussian is the maximum-entropy generator microstate on $\mathbb{C}$, whereas the one-loop carrier is its minimal closed azimuthal reduction. The maximum-entropy theorem fixes the Gaussian shape at prescribed $\sigma_{\mathbb{C}}$, while the minimal one-loop calibration fixes the ratio $\sigma_{\mathbb{C}}/R$. A compatible annular reduction then exports the lock-preserving pair (R, ω), with $\omega = c/R$. The carrier is neither a rigid material ring nor an empirical radius inserted into the shell closure.

After the $n = 1$ azimuthal sector has been selected, the carrier-level construction depends only on the Gaussian width $\sigma_{\mathbb{C}}$, the calibrated collective radius R, the carrier circle Γ_R, and the lock-preserving rate $\omega = c/R$. By proposition 13, every compatible coherent annular reduction satisfies

$$\omega = \frac{c}{\mathcal{R}_{\mathrm{H}}[\mu_{\mathrm{coh}}]} = \frac{c}{R}.$$

Thus the detailed radial profile of μ_{coh} does not enter the minimal carrier-level construction beyond the compatibility condition $\mathcal{R}_{\mathrm{H}}[\mu_{\mathrm{coh}}] = R$. No unique compatible annular reduction is required, and no additional tunable radial profile is carried into the primary shell closure.

C. Electron branch selection

We now select the free minimal geometric branch that is identified with the electron only after the charge sector has been fixed. At this stage, the label electron refers only provisionally to the minimal one-loop, first-node branch and carries no charge-sign assignment. The generator side has already selected the minimal circulating sector $n = 1$. On the propagation side, the free minimal branch is required to carry no preferred spatial direction in $\mathbb{R}^3$. This selects the rotationally invariant propagation sector. We therefore first identify the isotropic propagation mode and then choose its first regular shell node. The result is the minimal geometric branch used later in the shell closure. It does not introduce a value of α, a measured lepton mass, or any QED input.

Proposition 15 (Minimal isotropic scalar propagation sector)**.** *For the scalar propagation factor of a free stationary branch on $\mathbb{R}^3$ with no preferred spatial direction, the angular dependence must lie in the rotationally invariant sector of the spherical-harmonic decomposition. This sector is exactly the orbital mode $L_{\mathrm{orb}} = 0$. Consequently the minimal angular propagation sector is the isotropic s-wave sector.*

Proof. Let $U(r, \Omega)$ denote the scalar propagation factor. Rotational invariance means

$$U(r, R\Omega) = U(r, \Omega) \qquad \text{for every } r > 0,\ \Omega \in \mathbb{S}^2,\ R \in SO(3).$$

Fix $r > 0$. The action of $SO(3)$ on $\mathbb{S}^2$ is transitive. Hence for any $\Omega_1, \Omega_2 \in \mathbb{S}^2$, there exists $R \in SO(3)$ such that $R\Omega_1 = \Omega_2$. Therefore

$$U(r, \Omega_2) = U(r, R\Omega_1) = U(r, \Omega_1),$$

so $\Omega \mapsto U(r, \Omega)$ is constant on $\mathbb{S}^2$. Constant functions on $\mathbb{S}^2$ are precisely the $L_{\mathrm{orb}} = 0$ spherical-harmonic sector. Hence the only rotationally invariant angular sector is $L_{\mathrm{orb}} = 0$, which is the isotropic s-wave sector.

The Helmholtz equation introduced next operates within this already selected isotropic sector. Rotational invariance fixes the angular sector, whereas the Helmholtz condition fixes the radial propagation representative. □

Definition IV.7 (Base shell wavenumber)**.** The base shell wavenumber is defined from the total locked branch rate by

$$k_{\mathrm{base}} := \frac{\omega}{c}. \tag{78}$$

Since $\omega > 0$ and $c > 0$, one has

$$k_{\mathrm{base}} > 0.$$

It has SI units of inverse length. This is a branch-geometric wavenumber used to define the free propagation representative. It is not an observed de Broglie wavenumber, not a measured inverse length, and not a fitted input. On a Relator-locked branch, $R\omega = c$, and therefore

$$k_{\mathrm{base}} = \frac{1}{R}. \tag{79}$$

Definition IV.8 (Regular isotropic radial Helmholtz problem)**.** After the isotropic angular sector has been selected, the free stationary scalar propagation representative of the minimal branch is chosen to be the regular s-wave solution of the scalar Helmholtz equation with base wavenumber k_{base}. This is a propagation-side branch-selection equation; it is not a consequence of rotational invariance alone, and it does not import a measured wavelength or a value of α.

For base wavenumber k_{base}, the radial profile $S_{\mathrm{Helm}}(r)$ is required to satisfy the $L_{\mathrm{orb}} = 0$ radial reduction of the scalar Helmholtz equation

$$(\Delta_{\mathbb{R}^3} + k_{\mathrm{base}}^2)U = 0, \qquad U(r, \Omega) = S_{\mathrm{Helm}}(r).$$

Since

$$\Delta_{\mathbb{R}^3} U = \frac{1}{r^2}\frac{\mathrm{d}}{\mathrm{d}r}\left(r^2 \frac{\mathrm{d}S_{\mathrm{Helm}}}{\mathrm{d}r}\right) = S''_{\mathrm{Helm}}(r) + \frac{2}{r}S'_{\mathrm{Helm}}(r),$$

the radial equation on $(0, \infty)$ is

$$S''_{\mathrm{Helm}}(r) + \frac{2}{r}S'_{\mathrm{Helm}}(r) + k_{\mathrm{base}}^2 S_{\mathrm{Helm}}(r) = 0, \qquad r > 0. \tag{80}$$

The selected branch is further required to admit a smooth extension to $r = 0$ with

$$S_{\mathrm{Helm}}(0) = 1, \qquad S'_{\mathrm{Helm}}(0) = 0. \tag{81}$$

Here $L_{\mathrm{orb}} = 0$ denotes the orbital index and is not to be confused with the shell bandwidth ℓ.

Proposition 16 (Regular origin-normalized isotropic shell mode)**.** *The unique function $S_{\mathrm{Helm}} \in C^\infty([0, \infty))$ whose restriction to $(0, \infty)$ satisfies Eq.* (80) *and whose origin data satisfy Eq.* (81) *is*

$$S_{\mathrm{Helm}}(r) = j_0(k_{\mathrm{base}} r), \qquad j_0(s) := \begin{cases} \dfrac{\sin s}{s}, & s \neq 0, \\ 1, & s = 0. \end{cases} \tag{82}$$

Proof. Set

$$v(r) := r\, S_{\mathrm{Helm}}(r).$$

Then, for $r > 0$,

$$v'(r) = S_{\mathrm{Helm}}(r) + rS'_{\mathrm{Helm}}(r), \qquad v''(r) = 2S'_{\mathrm{Helm}}(r) + rS''_{\mathrm{Helm}}(r).$$

Multiplying Eq. (80) by r gives

$$rS''_{\mathrm{Helm}}(r) + 2S'_{\mathrm{Helm}}(r) + k_{\mathrm{base}}^2 r S_{\mathrm{Helm}}(r) = 0,$$

hence

$$v''(r) + k_{\mathrm{base}}^2 v(r) = 0, \qquad r > 0.$$

Because S_{Helm} extends smoothly to $r = 0$ and satisfies Eq. (81), one has

$$v(0) = 0, \qquad v'(0) = S_{\mathrm{Helm}}(0) = 1.$$

The unique solution of

$$v'' + k_{\mathrm{base}}^2 v = 0, \qquad v(0) = 0, \qquad v'(0) = 1,$$

is

$$v(r) = \frac{\sin(k_{\mathrm{base}} r)}{k_{\mathrm{base}}}.$$

Therefore, for $r > 0$,

$$S_{\mathrm{Helm}}(r) = \frac{v(r)}{r} = \frac{\sin(k_{\mathrm{base}} r)}{k_{\mathrm{base}} r}.$$

To verify the origin data explicitly, expand at $r = 0$

$$\frac{\sin(k_{\text{base}}r)}{k_{\text{base}}r} = 1 - \frac{k_{\text{base}}^2 r^2}{6} + O(r^4).$$

Hence the quotient has a smooth extension to $r = 0$, with

$$S_{\text{Helm}}(0) = 1, \qquad S'_{\text{Helm}}(0) = 0.$$

This extension is exactly $j_0(k_{\text{base}}r)$. It is the unique smooth solution satisfying Eqs. (80) and (81). □

Definition IV.9 (First-node matching shell)**.** The minimal free branch is selected by first-node pinning. The matching shell is placed at the first positive zero of the regular isotropic radial mode S_{Helm}. Thus the matching shell Σ_{r_*} is fixed by

$$k_{\text{base}}r_* = \pi. \tag{83}$$

This is a geometric branch-selection condition, not a material boundary condition and not an empirical radius fit. The zero of $r\,S_{\text{Helm}}(r)$ at $r = 0$ encodes regularity at the origin and does not define a shell. The higher positive zeros

$$k_{\text{base}}r = p\pi, \qquad p = 2, 3, \ldots,$$

define higher-node branch candidates and are not used in the minimal branch considered here.

Proposition 17 (Minimal first-node shell radius)**.** *For the first-node matching shell of definition IV.9, and using the locked branch relation $k_{\text{base}} = 1/R$, one has*

$$r_* = \pi R, \qquad \eta \coloneqq \frac{R}{r_*} = \frac{1}{\pi}. \tag{84}$$

Proof. Since $\omega > 0$ and $c > 0$, Eq. (78) gives

$$k_{\text{base}} > 0.$$

By Eq. (82), for $r > 0$,

$$S_{\text{Helm}}(r) = \frac{\sin(k_{\text{base}}r)}{k_{\text{base}}r}.$$

For $r > 0$, the denominator $k_{\text{base}}r$ is strictly positive. Hence the positive zeros of S_{Helm} are exactly the positive zeros of $\sin(k_{\text{base}}r)$, namely the radii satisfying

$$k_{\text{base}}r = p\pi, \qquad p = 1, 2, 3, \ldots.$$

The value at $r = 0$ is the removable regular value $S_{\text{Helm}}(0) = 1$, so $r = 0$ is not a node. The first positive zero therefore corresponds to $p = 1$, which is precisely Eq. (83). Using Eq. (79),

$$r_* = \frac{\pi}{k_{\text{base}}} = \pi R.$$

Therefore

$$\eta = \frac{R}{r_*} = \frac{1}{\pi},$$

which proves Eq. (84). □

Definition IV.10 (Minimal electron-branch geometry)**.** The minimal branch geometry later used for the electron sector combines

1. the minimal nonzero winding sector $|n| = 1$ on the collective generator loop Γ_R, with the positive carrier orientation represented by $n = 1$;
2. the first positive regular shell node $r_* = \pi R$ of $S_{\text{Helm}}(r)$.

TABLE III. Logical-status ledger for the branch data constructed in section IV.

Object	Status	Dependency
radial variational class $\mathcal{A}_{\sigma_{\mathbb{C}}}$	definition	fixed normalization and second radial moment
Gaussian density $w_{\mathbb{C}}$	derived theorem	maximum entropy at fixed $\sigma_{\mathbb{C}}$
mass sheet ρ_m	definition	overall mass normalization, not mass selection
microscopic luminal rule	branch-selection condition	internal $\mathbb{C}$ kinematics, not observed velocity in $\mathbb{R}^3$
minimal one-loop calibration	branch-selection condition	Eq. (65), not a spin datum
width ratio $\varepsilon = \sigma_{\mathbb{C}}/R$	derived branch datum	Gaussian first moment and one-loop calibration
coherent annular measure μ_{coh}	reduction representative	compact support and compatible harmonic radius
harmonic radius $\mathcal{R}_{\mathrm{H}}[\mu_{\mathrm{coh}}]$	derived representative	lock-preserving average of $1/\rho$
compatibility $\mathcal{R}_{\mathrm{H}}[\mu_{\mathrm{coh}}] = R$	branch-consistency condition	calibrated collective radius
winding sector $n = 1$	branch-selection condition	minimal carrier winding, not a QED loop order
first-node shell radius $r_* = \pi R$	derived branch datum	Helmholtz mode, lock, and first-node pinning
branch ratios η, ℓ	derived branch data	Eq. (85)

At this stage, this is only a geometric branch selection. The charge quantum number is a separate compact-phase momentum quantum number introduced later. The negative minimal charge sector is identified with the electron only in section V. Thus the carrier orientation $n = 1$ is not the electron charge sign, and the label electron in this definition is only a later sector label, not an input to the charge construction. Higher winding sectors and higher radial nodes define higher branch candidates and are not used in the present paper.

Corollary 2 (Geometric electron-branch ratios)**.** *For the minimal branch geometry later used for the electron sector,*

$$\varepsilon = \frac{\sigma_{\mathbb{C}}}{R} = \frac{1}{\sqrt{\pi}}, \qquad \eta = \frac{R}{r_*} = \frac{1}{\pi}, \qquad \ell = \frac{\sigma_{\mathbb{C}}}{r_*} = \varepsilon\eta = \frac{1}{\pi\sqrt{\pi}}. \tag{85}$$

Proof. From Eq. (66) one has

$$\varepsilon = \frac{\sigma_{\mathbb{C}}}{R} = \frac{1}{\sqrt{\pi}}.$$

From Eq. (84) one has

$$\eta = \frac{R}{r_*} = \frac{1}{\pi}.$$

Therefore

$$\ell = \frac{\sigma_{\mathbb{C}}}{r_*} = \frac{\sigma_{\mathbb{C}}}{R}\frac{R}{r_*} = \varepsilon\eta = \frac{1}{\pi\sqrt{\pi}}.$$

This proves Eq. (85). □

Remark (Exported branch data)*.* The only branch ratios exported to the later shell construction are those in Eq. (85). They are derived branch data, conditional on the radial maximum-entropy class, the microscopic luminal generator rule, the minimal one-loop calibration, the locked base wavenumber, and the first-node shell selection. No value of α, no charge assignment, and no QED coefficient enters these ratios. Unless a different branch is stated explicitly, all later uses of $\sigma_{\mathbb{C}}$, r_*, η, and ℓ refer to these minimal-branch values.

V. GAUGE COUPLING, CHARGE QUANTIZATION, DIRAC LIMIT, AND $g = 2$

This section supplies the infrared gauge structure used later in the vector shell channel. Its ingredients have distinct logical status. The compact collective phase, the gauge convention, the charge scale q_0, and the covariant phase derivative are definitions. The gauged lock action represents the infrared phase-lock sector on a prescribed worldline. Charge conservation follows from that phase-lock action, whereas integer charge quantization appears only after canonical quantization of the single-valued compact phase sector. The worldline current and the effective loop current are induced currents used for the infrared and shell-source descriptions, respectively. The minimal local spinorial equation and the tree-level value $g = 2$ are infrared consequences of the stated completion conditions.

The charge unit q_0 is a fundamental gauge scale of the compact phase sector. The quantization result fixes an integer spectrum in units of q_0; it does not determine the laboratory numerical value of that unit. The generator inputs needed here are the coherent loop degree of freedom summarized in fig. 4 and, for the geometric $g = 2$ normalization, the minimal one-loop calibration Eq. (65). The inertial parameter m enters only through the infrared normalization of the branch. The prescribed worldline used below is an infrared representative of the already selected branch. It is not varied in the gauged phase-lock sector, and no Lorentz-force equation is derived in this section.

The generator geometry relevant for this section is summarized in fig. 4. The Gaussian sheet supplies the generator mass distribution used in the calibrated branch normalization, whereas the coherent loop at radius R supplies the compact phase degree of freedom gauged below.

A. Gauged phase and conserved momentum

We now introduce a prescribed smooth timelike worldline $x^\mu(\tau) \in \mathbb{R}^{1,3}$, where τ is proper time, as the infrared worldline representative of the collective loop. With the metric convention fixed below, this means

$$\eta_{\mu\nu}\dot{x}^\mu \dot{x}^\nu = c^2.$$

In this subsection the worldline is treated as prescribed. No worldline equation of motion is derived, and no electromagnetic field equation is imposed. We retain the compact collective phase

$$\theta_0(\tau) \in \mathbb{R}/2\pi\mathbb{Z}$$

introduced in definition IV.5. Throughout this subsection, a dot denotes $\mathrm{d}/\mathrm{d}\tau$. In this proper-time worldline convention, the rate c/R is the rest-frame branch rate of the coherent loop; it is not the coordinate-time frequency of a moving laboratory trajectory. We use the SI four-potential convention

$$x^\mu = (ct, \mathbf{x}), \qquad \partial_\mu = \frac{\partial}{\partial x^\mu} = \left(\frac{1}{c}\partial_t, \nabla\right), \qquad A_\mu = \left(\frac{\Phi}{c}, -\mathbf{A}\right), \tag{86}$$

where $\mathbf{A}$ is the ordinary SI three-vector potential. Thus the spatial covariant components of A_μ are $-A_i$, while later three-vector formulas use $\mathbf{A} = (A_1, A_2, A_3)$. With these conventions,

$$A_\mu \, \mathrm{d}x^\mu = \Phi \, \mathrm{d}t - \mathbf{A} \cdot \mathrm{d}\mathbf{x}. \tag{87}$$

The four-volume element used below is

$$\mathrm{d}^4x = \mathrm{d}x^0 \, \mathrm{d}^3\mathbf{x} = c \, \mathrm{d}t \, \mathrm{d}^3\mathbf{x}. \tag{88}$$

Definition V.1 (Gauge charge scale)**.** Let $q_0 > 0$ denote the fundamental gauge charge scale carried by the compact collective phase. At this stage q_0 is an intrinsic scale of the phase degree of freedom and fixes the unit in which the conserved phase momentum is later expressed as a charge. It is not a measured laboratory input, not a value inferred from α, and is not yet assigned the conventional name e.

Definition V.2 (Gauge transformation of the collective phase)**.** For any smooth single-valued gauge function $\lambda_\mathrm{g}(x)$, chosen with SI units of magnetic flux, equivalently action per charge, so that $q_0\lambda_\mathrm{g}/\hbar$ is dimensionless, define

$$A_\mu \mapsto A_\mu - \partial_\mu \lambda_\mathrm{g}, \qquad \theta_0 \mapsto \theta_0 - \frac{q_0}{\hbar}\,\lambda_\mathrm{g}\big(x(\tau)\big) \quad \text{in } \mathbb{R}/2\pi\mathbb{Z}. \tag{89}$$

The conjugate action variable J is taken to be gauge invariant. The shift of θ_0 is independent of θ_0 itself, so this is the canonical momentum convention associated with a gauge translation of the compact phase coordinate at fixed prescribed worldline. The gauge scale $q_0 > 0$ fixes the unit of charge. The sign of the branch charge is not fixed by the orientation of this coordinate shift; it is encoded in the conserved momentum J through Eq. (94).

With the convention $A_\mu = (\Phi/c, -\mathbf{A})$ and $x^0 = ct$, this is equivalent to the three-vector transformation

$$\Phi \mapsto \Phi - \partial_t \lambda_\mathrm{g}, \qquad \mathbf{A} \mapsto \mathbf{A} + \nabla \lambda_\mathrm{g}. \tag{90}$$

This sign convention is chosen so that the induced worldline coupling for a signed charge Q takes the standard SI form

$$-Q \int A_\mu \, \mathrm{d}x^\mu = \int \left(Q\mathbf{A} \cdot \frac{\mathrm{d}\mathbf{x}}{\mathrm{d}t} - Q\Phi\right) \mathrm{d}t$$

when the worldline is parametrized by coordinate time.

Definition V.3 (Gauge-covariant phase derivative)**.** The worldline gauge-covariant derivative of the collective phase is

$$D_\tau\theta_0 \coloneqq \dot{\theta}_0 - \frac{q_0}{\hbar}\,\dot{x}^\mu A_\mu\big(x(\tau)\big). \tag{91}$$

Proposition 18 (Gauge invariance of the covariant phase derivative)**.** *The quantity $D_\tau\theta_0$ defined in Eq.* (91) *is invariant under Eq.* (89)*.*

Proof. Under Eq. (89),

$$\theta_0(\tau) \mapsto \theta_0(\tau) - \frac{q_0}{\hbar}\lambda_{\mathrm{g}}(x(\tau)).$$

Differentiating along the worldline gives

$$\dot{\theta}_0 \mapsto \dot{\theta}_0 - \frac{q_0}{\hbar}\frac{\mathrm{d}}{\mathrm{d}\tau}\lambda_{\mathrm{g}}(x(\tau)) = \dot{\theta}_0 - \frac{q_0}{\hbar}\,\dot{x}^\mu\partial_\mu\lambda_{\mathrm{g}}.$$

At the same time,

$$A_\mu \mapsto A_\mu - \partial_\mu\lambda_{\mathrm{g}} \quad\Longrightarrow\quad \dot{x}^\mu A_\mu \mapsto \dot{x}^\mu A_\mu - \dot{x}^\mu\partial_\mu\lambda_{\mathrm{g}}.$$

Substituting both transformations into Eq. (91) shows that the two shifts cancel exactly. Hence $D_\tau\theta_0$ is gauge invariant. □

Definition V.4 (Gauged lock action)**.** Let τ denote proper time along a prescribed smooth timelike worldline $x^\mu(\tau)$, and let $J(\tau)$ be the action variable canonically conjugate to the compact phase $\theta_0(\tau) \in \mathbb{R}/2\pi\mathbb{Z}$, with dimensions of action. In the present subsection, $x^\mu(\tau)$ and $A_\mu(x)$ are treated as background data, and the variation is taken only with respect to J and with respect to a local real lift of θ_0. Thus the action below derives the phase-lock constraint and the conserved phase momentum, not the Lorentz-force equation and not Maxwell dynamics.

Let $I \subset \mathbb{R}$ be any connected proper-time interval on which a smooth real lift of θ_0 has been chosen. Writing again $\theta_0 : I \to \mathbb{R}$ for that lift on I, define the local gauged lock constraint action by

$$S_{\mathrm{lock}}^{\mathrm{gauged}} = \int_I \mathrm{d}\tau\; J(\tau)\left(D_\tau\theta_0(\tau) - \frac{c}{R}\right). \tag{92}$$

Different lifts on the same connected interval differ by an additive constant $2\pi n$, with $n \in \mathbb{Z}$. Hence the Euler–Lagrange equations obtained from compactly supported variations on I are independent of the chosen lift. This is the first-order phase-lock constraint sector of the branch action. It is not the full relativistic worldline action for $x^\mu(\tau)$.

Because $D_\tau\theta_0$ is gauge invariant by proposition 18, because J is gauge invariant by the convention of definition V.2, and because R is a geometric scalar, the integrand in Eq. (92) is pointwise gauge invariant along the prescribed worldline. Hence the action $S_{\mathrm{lock}}^{\mathrm{gauged}}$ is gauge invariant. This statement concerns only the phase-lock sector, with x^μ and A_μ treated as background data.

Proposition 19 (Lock equation and conserved conjugate momentum)**.** *Holding $x^\mu(\tau)$ and $A_\mu(x)$ fixed and varying only J and a local lift of the compact phase θ_0, with compactly supported variations in τ, the phase-sector Euler–Lagrange equations of Eq.* (92) *are*

$$D_\tau\theta_0 = \frac{c}{R}, \qquad \dot{J} = 0. \tag{93}$$

Proof. Write

$$L\big(\theta_0, \dot{\theta}_0, J\big) = J\left(D_\tau\theta_0 - \frac{c}{R}\right) = J\left(\dot{\theta}_0 - \frac{q_0}{\hbar}\,\dot{x}^\mu A_\mu - \frac{c}{R}\right).$$

A variation with respect to J gives

$$\delta_J S_{\mathrm{lock}}^{\mathrm{gauged}} = \int \mathrm{d}\tau\; \delta J\left(D_\tau\theta_0 - \frac{c}{R}\right).$$

Since δJ is arbitrary, one obtains

$$D_\tau\theta_0 = \frac{c}{R}.$$

For variations of θ_0, one has

$$\delta_{\theta_0} S^{\text{gauged}}_{\text{lock}} = \int \mathrm{d}\tau\, J\,\delta\dot{\theta}_0 = \Big[J\,\delta\theta_0\Big]_{\tau_i}^{\tau_f} - \int \mathrm{d}\tau\, \dot{J}\,\delta\theta_0.$$

The boundary term vanishes for compactly supported variations. Since $\delta\theta_0$ is otherwise arbitrary, one obtains

$$\dot{J} = 0.$$

This proves Eq. (93). □

Definition V.5 (Classical charge parameter carried by the collective phase)**.** Once the gauge scale q_0 has been fixed, the classical charge parameter carried by the branch is

$$Q = \frac{q_0}{\hbar}\, J. \tag{94}$$

By Eq. (93), Q is constant along the worldline. Since $q_0 > 0$, the sign of Q is determined by the sign of the conserved conjugate momentum J. At this classical stage Q is a conserved signed charge parameter, not yet an integer quantum number and not yet identified with $\pm e$. Charge quantization is a separate statement and arises only after quantization of the compact phase sector.

Proposition 20 (Worldline interaction term and induced distributional current)**.** *Expanding Eq.* (92) *and using Eq.* (94) *gives, after imposing the phase-sector equation $\dot{J} = 0$ so that Q is constant on the segment, the standard worldline interaction term*

$$S_{\text{int}} = -\,Q \int A_\mu\, \mathrm{d}x^\mu. \tag{95}$$

With the convention

$$S_{\text{int}} = -\int \mathrm{d}^4x\, j^\mu(x)\, A_\mu(x), \tag{96}$$

this identifies the induced distributional worldline current of the prescribed infrared representative,

$$j^\mu(x) = Q \int \mathrm{d}\tau\, \dot{x}^\mu(\tau)\, \delta^{(4)}\big(x - x(\tau)\big), \tag{97}$$

where Q is signed and $\delta^{(4)}$ is normalized with respect to the four-volume element $\mathrm{d}^4x = \mathrm{d}x^0\,\mathrm{d}^3\mathbf{x}$ fixed in Eq. (88)*.*

In the $x^0 = ct$ convention, j^μ is the current density paired with the four-volume element $\mathrm{d}^4x = c\,\mathrm{d}t\,\mathrm{d}^3\mathbf{x}$. Thus each component of j^μ has SI units of charge density,

$$[j^\mu] = \mathrm{C\,m^{-3}},$$

and j^μ is related to the conventional electromagnetic current $J^\mu_{\text{conv}} = (c\rho_{\text{ch}}, \mathbf{J}_{\text{conv}})$ by

$$j^\mu = \frac{1}{c} J^\mu_{\text{conv}}, \qquad j^0 = \rho_{\text{ch}}, \qquad j^i = \frac{1}{c} J^i_{\text{conv}}. \tag{98}$$

Indeed, using $\mathrm{d}^4x = c\,\mathrm{d}t\,\mathrm{d}^3\mathbf{x}$ and $A_\mu = (\Phi/c, -\mathbf{A})$, one has

$$j^\mu A_\mu = \rho_{\text{ch}} \frac{\Phi}{c} - \frac{\mathbf{J}_{\text{conv}}}{c} \cdot \mathbf{A}.$$

Hence

$$-\int \mathrm{d}^4x\, j^\mu A_\mu = -\int c\,\mathrm{d}t\,\mathrm{d}^3\mathbf{x} \left(\rho_{\text{ch}} \frac{\Phi}{c} - \frac{\mathbf{J}_{\text{conv}}}{c} \cdot \mathbf{A}\right) = \int \mathrm{d}t\,\mathrm{d}^3\mathbf{x}\,\big(\mathbf{J}_{\text{conv}} \cdot \mathbf{A} - \rho_{\text{ch}}\Phi\big),$$

which is the standard SI interaction convention.

For the restriction of the worldline current to a smooth segment $[\tau_i, \tau_f]$, define

$$j^\mu_{[\tau_i,\tau_f]}(x) := Q \int_{\tau_i}^{\tau_f} \mathrm{d}\tau\, \dot{x}^\mu(\tau)\, \delta^{(4)}\big(x - x(\tau)\big).$$

Then, in the sense of distributions,

$$\partial_\mu j^\mu_{[\tau_i,\tau_f]}(x) = Q\,\delta^{(4)}\big(x - x(\tau_i)\big) - Q\,\delta^{(4)}\big(x - x(\tau_f)\big).$$

Consequently, on every open spacetime region whose test functions vanish near the segment endpoints, one has

$$\partial_\mu j^\mu_{[\tau_i,\tau_f]} = 0.$$

In particular, if the full prescribed worldline has no endpoint in the spacetime region under consideration, the full current j^μ satisfies

$$\partial_\mu j^\mu = 0. \tag{99}$$

This conservation statement is distributional and local to the region in which no endpoint source is present. It is the standard worldline current; see, for example, [14].

Proof. Insert Eq. (91) into Eq. (92). The term linear in A_μ is, before imposing the phase-sector equation,

$$S_{\text{int}} = -\int \mathrm{d}\tau\; Q(\tau)\,\dot{x}^\mu(\tau) A_\mu(x(\tau)), \qquad Q(\tau) := \frac{q_0}{\hbar} J(\tau).$$

The Euler–Lagrange equation for θ_0 gives $\dot{J} = 0$, hence $Q(\tau) = Q$ is constant on shell. Therefore

$$S_{\text{int}} = -Q \int A_\mu\,\mathrm{d}x^\mu,$$

which proves Eq. (95). To identify the current distributionally, let $a_\mu \in C_c^\infty(\mathbb{R}^{1,3})$ be a test four-potential. Then, with $\delta^{(4)}$ normalized relative to d^4x,

$$\int \mathrm{d}^4x\,\left[Q\int \mathrm{d}\tau\;\dot{x}^\mu(\tau)\,\delta^{(4)}\big(x - x(\tau)\big)\right] a_\mu(x) = Q\int \mathrm{d}\tau\;\dot{x}^\mu(\tau)\,a_\mu(x(\tau)).$$

Hence the A_μ-linear part of the action is represented distributionally by

$$S_{\text{int}}[a] = -\int \mathrm{d}^4x\,j^\mu(x)\,a_\mu(x), \qquad j^\mu(x) = Q\int \mathrm{d}\tau\;\dot{x}^\mu(\tau)\,\delta^{(4)}\big(x - x(\tau)\big),$$

which is exactly Eq. (97).

For the divergence of the current restricted to the segment $[\tau_i, \tau_f]$, define

$$j^\mu_{[\tau_i,\tau_f]}(x) := Q\int_{\tau_i}^{\tau_f} \mathrm{d}\tau\;\dot{x}^\mu(\tau)\,\delta^{(4)}\big(x - x(\tau)\big).$$

Let $\varphi \in C_c^\infty(\mathbb{R}^{1,3})$ be a test function. Then

$$\begin{aligned}
\langle \partial_\mu j^\mu_{[\tau_i,\tau_f]}, \varphi\rangle &= -\langle j^\mu_{[\tau_i,\tau_f]}, \partial_\mu\varphi\rangle \\
&= -Q\int_{\tau_i}^{\tau_f} \mathrm{d}\tau\;\dot{x}^\mu(\tau)\,\partial_\mu\varphi(x(\tau)) \\
&= -Q\int_{\tau_i}^{\tau_f} \mathrm{d}\tau\;\frac{\mathrm{d}}{\mathrm{d}\tau}\varphi(x(\tau)) \\
&= Q\,\varphi(x(\tau_i)) - Q\,\varphi(x(\tau_f)).
\end{aligned}$$

Hence

$$\partial_\mu j^\mu_{[\tau_i,\tau_f]}(x) = Q\,\delta^{(4)}\big(x - x(\tau_i)\big) - Q\,\delta^{(4)}\big(x - x(\tau_f)\big)$$

in the sense of distributions. This proves the segment formula. The full conservation statement Eq. (99) then follows immediately on every spacetime region containing no worldline endpoint. □

Remark. Once the scale q_0 has been fixed, the classical charge parameter Q is not introduced as a second independent primitive. It is the conserved momentum conjugate to the compact collective phase, expressed in units of q_0. The same signed quantity Q determines the distributional worldline current and provides the charge parameter used later in the loop-current normalization of the shell vector sector.

B. Charge quantization

The collective phase is compact. Quantization is performed on the single-valued periodic sector of that phase coordinate. With the operator identification

$$\hat{Q} = \frac{q_0}{\hbar}\,\hat{J},$$

the compact phase representation yields an integer charge spectrum in units of the intrinsic scale q_0. This step quantizes charge relative to q_0; it does not insert a measured value of e, a measured value of α, or any QED coefficient.

Proposition 21 (Momentum operator on the compact phase circle)**.** *On the Hilbert space*

$$L^2\left(\mathbb{R}/2\pi\mathbb{Z},\, \frac{\mathrm{d}\theta_0}{2\pi}\right), \tag{100}$$

with domain $H^1_{\mathrm{per}}(\mathbb{R}/2\pi\mathbb{Z})$, the canonical momentum operator

$$\hat{J} = -\,i\hbar\,\frac{\partial}{\partial\theta_0} \tag{101}$$

is self-adjoint and has pure point spectrum $\hbar\mathbb{Z}$. A complete orthonormal set of eigenfunctions is

$$\varphi_k(\theta_0) = e^{ik\theta_0}, \qquad k \in \mathbb{Z}, \tag{102}$$

with eigenvalue equation

$$\hat{J}\,\varphi_k = k\hbar\,\varphi_k. \tag{103}$$

Proof. Define the Fourier-series unitary map

$$U : L^2\left(\mathbb{R}/2\pi\mathbb{Z},\, \frac{\mathrm{d}\theta_0}{2\pi}\right) \longrightarrow \ell^2(\mathbb{Z}), \qquad (U\psi)_k = \frac{1}{2\pi}\int_0^{2\pi} \psi(\theta_0)e^{-ik\theta_0}\,\mathrm{d}\theta_0.$$

Then $\psi \in H^1_{\mathrm{per}}(\mathbb{R}/2\pi\mathbb{Z})$ if and only if

$$U\psi = (c_k)_{k\in\mathbb{Z}} \qquad \text{with} \qquad \sum_{k\in\mathbb{Z}} k^2|c_k|^2 < \infty.$$

On this domain,

$$U\hat{J}U^{-1}(c_k)_{k\in\mathbb{Z}} = (k\hbar\, c_k)_{k\in\mathbb{Z}}.$$

Hence $\hat{J}$ is unitarily equivalent to the multiplication operator

$$M(c_k)_{k\in\mathbb{Z}} := (k\hbar\, c_k)_{k\in\mathbb{Z}}$$

on

$$D(M) = \left\{ (c_k) \in \ell^2(\mathbb{Z}) \;\middle|\; \sum_{k\in\mathbb{Z}} k^2|c_k|^2 < \infty \right\}.$$

Since the multiplier $k\hbar$ is real, M is self-adjoint. Therefore $\hat{J}$ is self-adjoint.

For each $k \in \mathbb{Z}$, let $e^{(k)} \in \ell^2(\mathbb{Z})$ be the standard basis vector,

$$e^{(k)}_m = \delta_{km}.$$

Then

$$Me^{(k)} = k\hbar\, e^{(k)}.$$

Since $\{e^{(k)}\}_{k\in\mathbb{Z}}$ is a complete orthonormal basis of $\ell^2(\mathbb{Z})$, the spectrum of M, and therefore the spectrum of $\hat{J}$, is pure point and equals $\hbar\mathbb{Z}$.

Transporting the basis back by U^{-1} gives

$$U^{-1}e^{(k)}(\theta_0) = e^{ik\theta_0} = \varphi_k(\theta_0).$$

Thus $\{\varphi_k\}_{k\in\mathbb{Z}}$ is a complete orthonormal set in $L^2(\mathbb{R}/2\pi\mathbb{Z}, \mathrm{d}\theta_0/(2\pi))$, and

$$\hat{J}\,\varphi_k = k\hbar\,\varphi_k.$$

This proves Eq. (103). □

Remark (Single-valued phase sector). The periodic domain $H^1_{\mathrm{per}}(\mathbb{R}/2\pi\mathbb{Z})$ implements single-valued wavefunctions on the compact phase circle. The present model introduces no additional flat holonomy and no twisted boundary condition. Hence the spectrum is the integer spectrum $k \in \mathbb{Z}$, with no shifted sector $k + \nu_{\mathrm{hol}}$.

Theorem 4 (Quantized charge spectrum). *On the same domain as $\hat{J}$, define the charge operator*

$$\hat{Q} := \frac{q_0}{\hbar}\,\hat{J}. \tag{104}$$

Then $\hat{Q}$ is self-adjoint and has pure point spectrum

$$Q_k = k\,q_0, \qquad k \in \mathbb{Z}. \tag{105}$$

In particular, charge is quantized in integer units of the fundamental gauge charge scale q_0. The theorem fixes the integer spectrum relative to q_0, whereas the later notation $q_0 \equiv e$ is only the conventional naming of the minimal charge magnitude and not an empirical numerical input.

Proof. By definition Eq. (104),

$$\hat{Q} = \frac{q_0}{\hbar}\hat{J}$$

on the same domain $H^1_{\mathrm{per}}(\mathbb{R}/2\pi\mathbb{Z})$ as $\hat{J}$. Since $q_0/\hbar \in \mathbb{R}$ and $\hat{J}$ is self-adjoint by proposition 21, $\hat{Q}$ is self-adjoint as a real scalar multiple of $\hat{J}$.

Applying $\hat{Q}$ to the complete orthonormal eigenbasis $\{\varphi_k\}_{k\in\mathbb{Z}}$ from proposition 21 gives

$$\hat{Q}\,\varphi_k = \frac{q_0}{\hbar}(k\hbar)\varphi_k = kq_0\,\varphi_k.$$

Thus $\{\varphi_k\}_{k\in\mathbb{Z}}$ is a complete orthonormal eigenbasis of $\hat{Q}$. Therefore the spectrum of $\hat{Q}$ is pure point and equals

$$\sigma(\hat{Q}) = \{kq_0 \mid k \in \mathbb{Z}\}.$$

This proves Eq. (105). □

Proposition 22 (Compatibility of compact-phase and field gauge phases). *Let*

$$a_{\mathrm{g}}(x) := \frac{q_0}{\hbar}\lambda_{\mathrm{g}}(x).$$

The collective coordinate transforms as

$$\theta_0 \mapsto \theta_0 - a_{\mathrm{g}}(x(\tau)).$$

For each fixed value of τ, the number $a_{\mathrm{g}}(x(\tau))$ is a real shift on the compact phase circle. On wavefunctions on that circle, the corresponding active unitary action at that value of τ is the pullback by the inverse coordinate shift,

$$(U_{\mathrm{g}}(\tau)\psi)(\theta_0) = \psi(\theta_0 + a_{\mathrm{g}}(x(\tau)))\,. \tag{106}$$

Therefore, on the charge eigenstate $\varphi_k(\theta_0) = e^{ik\theta_0}$,

$$U_{\mathrm{g}}(\tau)\varphi_k = e^{ikq_0\lambda_{\mathrm{g}}(x(\tau))/\hbar}\,\varphi_k = e^{iQ_k\lambda_{\mathrm{g}}(x(\tau))/\hbar}\,\varphi_k. \tag{107}$$

Thus the compact-phase gauge convention induces the same phase factor later used for an infrared field of charge Q_k, evaluated along the prescribed worldline.

Proof. Since the transformed coordinate is

$$\theta_0' = \theta_0 - a_{\rm g},$$

a scalar wavefunction on the circle transforms by pullback,

$$\psi'(\theta_0) = \psi(\theta_0 + a_{\rm g}(x(\tau))).$$

This map preserves the normalized measure $\mathrm{d}\theta_0/(2\pi)$, because it is a rigid translation on $\mathbb{R}/2\pi\mathbb{Z}$. Therefore

$$\int_0^{2\pi} |(U_{\rm g}\psi)(\theta_0)|^2 \frac{\mathrm{d}\theta_0}{2\pi} = \int_0^{2\pi} |\psi(\theta_0 + a_{\rm g})|^2 \frac{\mathrm{d}\theta_0}{2\pi} = \int_0^{2\pi} |\psi(\theta_0)|^2 \frac{\mathrm{d}\theta_0}{2\pi},$$

so $U_{\rm g}$ is unitary.

Applying this unitary to $\varphi_k(\theta_0) = e^{ik\theta_0}$ gives

$$(U_{\rm g}(\tau)\varphi_k)(\theta_0) = e^{ik(\theta_0 + a_{\rm g}(x(\tau)))} = e^{ikq_0\lambda_{\rm g}(x(\tau))/\hbar} e^{ik\theta_0}.$$

Since $Q_k = kq_0$, this is exactly

$$U_{\rm g}(\tau)\varphi_k = e^{iQ_k\lambda_{\rm g}(x(\tau))/\hbar}\varphi_k.$$

This proves Eq. (107). □

Definition V.6 (Electron and positron sectors)**.** By convention, the minimal negative-charge sector $k = -1$ is identified with the electron charge sector,

$$Q_{\rm e} = -\, q_0 \equiv -e, \tag{108}$$

whereas the minimal positive-charge sector $k = +1$ is identified with the positron charge sector,

$$Q_{\rm p} = +\, q_0 \equiv +e. \tag{109}$$

The symbol $e > 0$ denotes the conventional name for the elementary charge magnitude. The identification $q_0 \equiv e$ is therefore only a naming convention for the minimal charge quantum in the $k = \pm 1$ sectors. It fixes the charge-sign labels used below; it does not insert a measured numerical value of e, α, or any QED coefficient, and it does not determine the fine-structure coupling.

Remark (Charge quantum number versus winding number)*.* The charge quantum number k is distinct from the generator winding number n introduced in definition IV.6. The integer n labels the geometric degree of the carrier map

$$\theta_0 \longmapsto e^{in\theta_0}$$

used in the one-loop branch selection. By contrast, k labels the eigenvalue of the canonical momentum operator

$$\hat{J} = -i\hbar\,\partial_{\theta_0}$$

acting on quantum states over the compact phase circle. Thus n is a configuration-space winding label, whereas k is a phase-space momentum label and, after quantization, a charge label. In the minimal electron branch, the carrier orientation is fixed by $n = 1$, whereas the electron charge sector is $k = -1$. These signs are not identified.

Remark. The result Eq. (105) is structurally analogous to the Kaluza–Klein relation between electric charge and momentum along a compact coordinate [15, 16]. The analogy is purely structural. The compact variable here is the collective internal phase θ_0, not an additional spacetime dimension, and no Kaluza–Klein radius or higher-dimensional metric is introduced.

Proposition 23 (Loop charge measure and shell-source current)**.** *On the collective loop $\Gamma_R \subset \mathbb{C}$, a branch of signed total charge Q is represented for shell-source bookkeeping by the distribution*

$$\rho_Q(\rho, \theta_0) = \frac{Q}{2\pi R}\,\delta(\rho - R), \tag{110}$$

with respect to the polar area measure $\rho\,\mathrm{d}\rho\,\mathrm{d}\theta_0$. Equivalently, for every test function $f \in C_c^\infty([0,\infty) \times \mathbb{R}/2\pi\mathbb{Z})$,

$$\int_0^{2\pi}\int_0^{\infty} \rho_Q(\rho,\theta_0)\,f(\rho,\theta_0)\,\rho\,\mathrm{d}\rho\,\mathrm{d}\theta_0 = \frac{Q}{2\pi}\int_0^{2\pi} f(R,\theta_0)\,\mathrm{d}\theta_0.$$

In particular,

$$\int_0^{2\pi}\int_0^{\infty} \rho_Q(\rho,\theta_0)\,\rho\,\mathrm{d}\rho\,\mathrm{d}\theta_0 = Q. \tag{111}$$

With respect to arc length $s = R\theta_0$, the corresponding uniform signed line charge density is

$$\lambda_Q = \frac{Q}{2\pi R}.$$

Along solutions of the phase-sector Eq. (93), equivalently $D_\tau\theta_0 = c/R$, the gauge-invariant shell-source current, defined as transported charge through an oriented radial cut per unit proper time, is

$$I_{\text{shell}} = \frac{Q}{2\pi}\,D_\tau\theta_0 = \frac{Q\,\omega}{2\pi} = \frac{Q\,c}{2\pi R}. \tag{112}$$

Its sign is the sign of Q relative to the chosen positive loop orientation.

Proof. For any test function f,

$$\begin{aligned}\int_0^{2\pi}\int_0^{\infty} \rho_Q(\rho,\theta_0)\,f(\rho,\theta_0)\,\rho\,\mathrm{d}\rho\,\mathrm{d}\theta_0 &= \frac{Q}{2\pi R}\int_0^{2\pi}\int_0^{\infty} \delta(\rho-R)\,f(\rho,\theta_0)\,\rho\,\mathrm{d}\rho\,\mathrm{d}\theta_0 \\ &= \frac{Q}{2\pi R}\int_0^{2\pi} f(R,\theta_0)\,R\,\mathrm{d}\theta_0 \\ &= \frac{Q}{2\pi}\int_0^{2\pi} f(R,\theta_0)\,\mathrm{d}\theta_0.\end{aligned}$$

This proves the distributional identity. Choosing $f \in C_c^\infty([0,\infty)\times\mathbb{R}/2\pi\mathbb{Z})$ equal to 1 on a neighborhood of the support of ρ_Q gives Eq. (111).

The corresponding uniform signed line charge density with respect to arc length $s = R\theta_0$ is

$$\lambda_Q = \frac{Q}{2\pi R}.$$

Over a proper-time increment $\mathrm{d}\tau$, the gauge-invariant phase advance transports the carrier through the arc length

$$\mathrm{d}s = R\,D_\tau\theta_0\,\mathrm{d}\tau.$$

The transported charge through an oriented radial cut is therefore

$$\mathrm{d}Q_{\text{cross}} = \lambda_Q\,\mathrm{d}s = \frac{Q}{2\pi R}R\,D_\tau\theta_0\,\mathrm{d}\tau = \frac{Q}{2\pi}\,D_\tau\theta_0\,\mathrm{d}\tau.$$

Dividing by $\mathrm{d}\tau$ gives

$$I_{\text{shell}} = \frac{\mathrm{d}Q_{\text{cross}}}{\mathrm{d}\tau} = \frac{Q}{2\pi}\,D_\tau\theta_0.$$

By proposition 18, this current is gauge invariant. Using Eq. (93),

$$D_\tau\theta_0 = \frac{c}{R},$$

and the locked-branch rate convention

$$\omega = \frac{c}{R},$$

one obtains

$$I_{\text{shell}} = \frac{Q}{2\pi}\,D_\tau\theta_0 = \frac{Q\,\omega}{2\pi} = \frac{Q\,c}{2\pi R},$$

which is exactly Eq. (112). Since $D_\tau\theta_0 > 0$ on the locked phase sector, the sign of I_{shell} is the sign of Q relative to the chosen positive loop orientation. □

Remark. Equation (112) is the only loop-current formula needed later in the shell vector sector. In the electron charge sector one sets $Q = -e$ by Eq. (108), whereas the carrier orientation remains the previously fixed positive one-loop orientation. The resulting shell source is therefore a negatively charged carrier loop whose current sign is opposite to the chosen positive orientation. This sign assignment descends from the compact-phase charge sector; it is not fitted to the vector-shell response.

C. Infrared Dirac limit

The charge sector above is worldline-based. To connect it with standard low-energy relativistic physics, we now pass to a minimal local infrared field representative. Only the infrared content needed later in the paper is retained. This step imposes an infrared completion criterion for a branch of fixed signed charge Q. It does not introduce a measured value of e, a measured value of α, a QED anomaly coefficient, or a microscopic ontology for the generator sheet.

Definition V.7 (Gauge-covariant momentum operator)**.** We use the Minkowski metric

$$\eta^{\mu\nu} = \mathrm{diag}(1, -1, -1, -1). \tag{113}$$

The coordinate convention is $x^\mu = (ct, \mathbf{x})$, so that

$$\partial_\mu = \left(\frac{1}{c}\partial_t, \nabla\right).$$

For a branch of fixed signed charge Q, acting first on charged scalar fields

$$u \in C^1(\mathbb{R}^{1,3}; \mathbb{C}), \qquad u \mapsto e^{\,iQ\lambda_{\mathrm{g}}/\hbar}u,$$

define the gauge-covariant four-momentum operator

$$\Pi_\mu = i\hbar\,\partial_\mu - QA_\mu, \qquad \Pi^\mu := \eta^{\mu\nu}\Pi_\nu. \tag{114}$$

With the convention $A_\mu = (\Phi/c, -\mathbf{A})$, the spatial covariant components satisfy

$$\Pi_i = i\hbar\partial_i + QA_i^{\mathrm{vec}} = -\big(p_i - QA_i^{\mathrm{vec}}\big), \qquad p_i = -i\hbar\partial_i,$$

where A_i^{vec} denotes the Cartesian components of the ordinary three-vector potential $\mathbf{A}$. The physical minimally coupled three-momentum is therefore carried by the raised spatial components,

$$\Pi^i = p_i - QA_i^{\mathrm{vec}}.$$

Whenever the composite expression $\Pi_\mu\Pi^\mu$ is used below, it is understood to act on charged scalar fields in $C^2(\mathbb{R}^{1,3}; \mathbb{C})$, with the operator product taken in the displayed order.

Proposition 24 (Gauge covariance of Π_μ and the scalar infrared equation)**.** *Under the gauge transformation*

$$A_\mu \mapsto A_\mu - \partial_\mu\lambda_{\mathrm{g}}, \qquad u \mapsto e^{\,iQ\lambda_{\mathrm{g}}/\hbar}u,$$

with Q held fixed as the branch charge, the operator $\Pi_\mu = i\hbar\partial_\mu - QA_\mu$ transforms covariantly,

$$\Pi_\mu u \mapsto e^{\,iQ\lambda_{\mathrm{g}}/\hbar}\,\Pi_\mu u. \tag{115}$$

If $u \in C^2(\mathbb{R}^{1,3}; \mathbb{C})$, then

$$\big(\Pi_\mu\Pi^\mu - m^2c^2\big)u \mapsto e^{\,iQ\lambda_{\mathrm{g}}/\hbar}\big(\Pi_\mu\Pi^\mu - m^2c^2\big)u.$$

Proof. Let

$$u' = e^{\,iQ\lambda_{\mathrm{g}}/\hbar}u, \qquad A'_\mu = A_\mu - \partial_\mu\lambda_{\mathrm{g}}.$$

Then

$$\Pi'_\mu u' = \big(i\hbar\partial_\mu - QA'_\mu\big)e^{\,iQ\lambda_{\mathrm{g}}/\hbar}u.$$

Expanding the derivative gives

$$\Pi'_\mu u' = i\hbar\left(\frac{iQ}{\hbar}\,\partial_\mu\lambda_{\mathrm{g}}\,e^{\,iQ\lambda_{\mathrm{g}}/\hbar}u + e^{\,iQ\lambda_{\mathrm{g}}/\hbar}\partial_\mu u\right) - Q(A_\mu - \partial_\mu\lambda_{\mathrm{g}})e^{\,iQ\lambda_{\mathrm{g}}/\hbar}u.$$

The terms proportional to $\partial_\mu\lambda_{\mathrm{g}}$ cancel, leaving

$$\Pi'_\mu u' = e^{\,iQ\lambda_{\mathrm{g}}/\hbar}\big(i\hbar\partial_\mu - QA_\mu\big)u = e^{\,iQ\lambda_{\mathrm{g}}/\hbar}\Pi_\mu u,$$

which proves Eq. (115).

Since the metric $\eta^{\mu\nu}$ is constant, raising the index preserves the same gauge phase factor. Indeed,

$$\Pi'^{\mu}u' = \eta^{\mu\nu}\Pi'_{\nu}u' = \eta^{\mu\nu}e^{\,iQ\lambda_{\rm g}/\hbar}\Pi_{\nu}u = e^{\,iQ\lambda_{\rm g}/\hbar}\Pi^{\mu}u.$$

Applying Π'_{μ} once more, and using the already proved covariance of Π'_{μ}, gives

$$\Pi'_{\mu}\Pi'^{\mu}u' = \Pi'_{\mu}\Big(e^{\,iQ\lambda_{\rm g}/\hbar}\Pi^{\mu}u\Big) = e^{\,iQ\lambda_{\rm g}/\hbar}\Pi_{\mu}\Pi^{\mu}u.$$

Subtracting

$$m^2c^2u' = e^{\,iQ\lambda_{\rm g}/\hbar}m^2c^2u$$

yields the stated covariance of the second-order equation. □

For a complex scalar infrared field representative $u \in C^2(\mathbb{R}^{1,3};\mathbb{C})$, the associated second-order relativistic mass-shell equation is

$$\big(\Pi_{\mu}\Pi^{\mu} - m^2c^2\big)u = 0, \tag{116}$$

where m is the infrared inertial parameter of the branch, and where $\Pi_{\mu}\Pi^{\mu}$ denotes the ordered differential expression built from Eq. (114). This equation is used only as an infrared representative motivating the first-order completion below. It is not asserted as the microscopic ontology of the branch, and it does not determine the electron rest mass, the charge scale q_0, or the value of α.

Definition V.8 (Minimal spinorial infrared completion)**.** A minimal spinorial infrared completion is a local, first-order, Lorentz-covariant completion criterion. One seeks a differential operator

$$\mathcal{L} = \Gamma^{\mu}\Pi_{\mu} - mc\,\mathbf{1}_V, \tag{117}$$

acting componentwise on smooth spinor fields

$$\Psi \in C^1(\mathbb{R}^{1,3};V),$$

where V is a finite-dimensional complex vector space and the coefficient matrices

$$\Gamma^{\mu} \in \mathrm{End}_{\mathbb{C}}(V)$$

are constant. Its principal symbol is

$$\sigma(\mathcal{L},p) = \Gamma^{\mu}p_{\mu}, \tag{118}$$

and is required to satisfy

$$\sigma(\mathcal{L},p)^2 = (p_{\mu}p^{\mu})\mathbf{1}_V \qquad \text{for every covector } p_{\mu}. \tag{119}$$

The minimality condition is that the unital complex subalgebra of $\mathrm{End}_{\mathbb{C}}(V)$ generated by the constant matrices Γ^{μ} acts irreducibly on V. Once Eq. (119) yields the Clifford relations, this is equivalent to an irreducible complex representation of $\mathrm{Cl}_{1,3}(\mathbb{C})$. The square condition in Eq. (119) is a principal-symbol condition. It is not an assertion that the fully gauged first-order operator squares to the scalar equation without lower-order electromagnetic curvature terms. This definition is an infrared representation criterion, not a standing postulate about the microscopic generator sheet.

Theorem 5 (Dirac infrared limit)**.** *Let $\mathcal{L}$ be a minimal spinorial infrared completion in the sense of definition V.8, for a branch of fixed signed charge Q and infrared inertial parameter m. Then the coefficient matrices satisfy*

$$\Gamma^{\mu}\Gamma^{\nu} + \Gamma^{\nu}\Gamma^{\mu} = 2\eta^{\mu\nu}\mathbf{1}_V. \tag{120}$$

Hence the assignment $e^{\mu} \mapsto \Gamma^{\mu}$ extends to an irreducible complex representation of the Clifford algebra $\mathrm{Cl}_{1,3}(\mathbb{C})$*. By the standard classification of complex Clifford algebras,*

$$\mathrm{Cl}_{1,3}(\mathbb{C}) \cong \mathrm{Mat}_4(\mathbb{C}),$$

every irreducible complex representation is four-dimensional and unique up to equivalence. After choosing a basis of V and fixing any standard 4×4 gamma-matrix system $\{\gamma^\mu\}_{\mu=0}^3$, there exists an invertible constant matrix $S \in \mathrm{GL}(4, \mathbb{C})$ such that

$$\Gamma^\mu = S\gamma^\mu S^{-1}, \tag{121}$$

where

$$\gamma^\mu\gamma^\nu + \gamma^\nu\gamma^\mu = 2\eta^{\mu\nu}\mathbf{1}_4. \tag{122}$$

After the field redefinition $\widetilde{\Psi} = S^{-1}\Psi$, and dropping the tilde afterwards, the infrared field equation for a branch of charge Q takes the standard minimally coupled Dirac form

$$\big(\gamma^\mu\Pi_\mu - mc\big)\Psi = 0, \tag{123}$$

with Ψ a four-component complex spinor [2, 17, 18].

Proof. For any covector p_μ, the principal symbol of $\mathcal{L}$ is

$$\sigma(\mathcal{L}, p) = \Gamma^\mu p_\mu.$$

By Eq. (119),

$$(\Gamma^\mu p_\mu)^2 = (p_\mu p^\mu)\mathbf{1}_V \qquad \text{for all } p_\mu.$$

Let p_μ and q_μ be arbitrary covectors. Evaluating Eq. (119) at $p_\mu + q_\mu$ gives

$$\big(\Gamma^\mu(p_\mu + q_\mu)\big)^2 = (p_\mu + q_\mu)(p^\mu + q^\mu)\,\mathbf{1}_V.$$

Expanding both sides yields

$$(\Gamma^\mu p_\mu)^2 + (\Gamma^\mu p_\mu)(\Gamma^\nu q_\nu) + (\Gamma^\mu q_\mu)(\Gamma^\nu p_\nu) + (\Gamma^\mu q_\mu)^2 = (p_\mu p^\mu + 2p_\mu q^\mu + q_\mu q^\mu)\,\mathbf{1}_V.$$

Subtracting the identities at p_μ and at q_μ gives

$$(\Gamma^\mu p_\mu)(\Gamma^\nu q_\nu) + (\Gamma^\mu q_\mu)(\Gamma^\nu p_\nu) = 2p_\mu q^\mu\,\mathbf{1}_V.$$

Renaming dummy indices in the second term gives

$$(\Gamma^\mu p_\mu)(\Gamma^\nu q_\nu) + (\Gamma^\nu q_\nu)(\Gamma^\mu p_\mu) = 2p_\mu q^\mu\,\mathbf{1}_V.$$

Choosing the coordinate covectors $p_\mu = \delta^\alpha_\mu$ and $q_\mu = \delta^\beta_\mu$, so that $p_\mu q^\mu = \eta^{\alpha\beta}$, yields

$$\Gamma^\alpha\Gamma^\beta + \Gamma^\beta\Gamma^\alpha = 2\eta^{\alpha\beta}\mathbf{1}_V,$$

which is Eq. (120).

By the universal property of the complex Clifford algebra, the assignment $e^\mu \mapsto \Gamma^\mu$ extends uniquely to a unital algebra homomorphism

$$\rho_\Gamma : \mathrm{Cl}_{1,3}(\mathbb{C}) \to \mathrm{End}_{\mathbb{C}}(V).$$

The minimality hypothesis in definition V.8 states exactly that this representation is irreducible.

By the standard classification $\mathrm{Cl}_{1,3}(\mathbb{C}) \cong \mathrm{Mat}_4(\mathbb{C})$, every irreducible complex representation is four-dimensional and unique up to equivalence. Choose a basis of V, identify $V \simeq \mathbb{C}^4$, and fix any standard gamma-matrix system $\{\gamma^\mu\}_{\mu=0}^3$ satisfying Eq. (122). Representation equivalence then yields an invertible constant matrix $S \in \mathrm{GL}(4, \mathbb{C})$ such that

$$\Gamma^\mu = S\gamma^\mu S^{-1}.$$

Because S is constant in spacetime and acts only in spinor space, while Q and A_μ are scalar coefficients, one has for every smooth spinor field $\widetilde{\Psi}$

$$\Pi_\mu(S\widetilde{\Psi}) = i\hbar\,\partial_\mu(S\widetilde{\Psi}) - QA_\mu S\widetilde{\Psi} = S(i\hbar\,\partial_\mu\widetilde{\Psi} - QA_\mu\widetilde{\Psi}) = S\Pi_\mu\widetilde{\Psi}.$$

Hence

$$S^{-1}\mathcal{L}S = S^{-1}\Gamma^\mu S\,\Pi_\mu - mc\,\mathbf{1}_4 = \gamma^\mu\Pi_\mu - mc\,\mathbf{1}_4.$$

If $\mathcal{L}\Psi = 0$ and $\widetilde{\Psi} = S^{-1}\Psi$, then

$$(\gamma^\mu\Pi_\mu - mc)\widetilde{\Psi} = 0.$$

Renaming $\widetilde{\Psi}$ as Ψ gives Eq. (123). $\square$

Remark. Theorem 5 is infrared in scope. It identifies the unique irreducible local first-order completion with the required principal symbol. It does not claim that the Dirac field is the microscopic ontology of the branch. The scale m enters only as the infrared inertial parameter in this completion and is not dynamically selected here. In an electromagnetic background, squaring the operator produces lower-order Pauli terms proportional to $F_{\mu\nu}$. These terms arise from the noncommutativity of gauge-covariant momenta and are analyzed below. They are not QED radiative anomaly coefficients and are not inputs to the α-lock closure.

D. Tree-level magnetic moment and $g = 2$

The tree-level magnetic normalization appears here in two compatible infrared readings. Geometrically, an effective axial bookkeeping moment is assigned to the collective loop current on $\mathbb{C}$ for shell-source normalization. Algebraically, the same tree-level coefficient is read from the Pauli term obtained in the infrared reduction of the minimally coupled Dirac operator. The two readings agree in the signed coefficient multiplying $Q/(2m)$, and that coefficient is $g = 2$. This is a tree-level normalization statement, not the insertion of a measured anomalous magnetic moment.

Proposition 25 (Effective geometric magnetic moment of the collective loop)**.** *Choose an auxiliary bookkeeping axial unit $\hat{\mathbf{n}}_{\mathbb{C}}$ perpendicular to the oriented carrier plane. This unit fixes the sign convention of the internal carrier orientation and is not an observed spatial direction in $\mathbb{R}^3$. For the purpose of shell vector normalization, the charged collective loop Γ_R is assigned the effective geometric magnetic moment*

$$\boldsymbol{\mu}_{\mathbb{C}} = I_{\text{shell}}\,\pi R^2\,\hat{\mathbf{n}}_{\mathbb{C}} = \frac{Q\,c\,R}{2}\,\hat{\mathbf{n}}_{\mathbb{C}}. \tag{124}$$

Equivalently, the signed scalar moment relative to the chosen orientation is

$$\mu_{\mathbb{C}} = \frac{Q\,c\,R}{2}.$$

Thus, in the electron sector $Q = -e$, the effective moment is opposite to the chosen positive axial orientation, while in the positron sector it is aligned with that orientation. This is a shell-normalization bookkeeping moment associated with the effective loop source. It is not an additional measured magnetic moment, not a microscopic magnetic moment in observed space, and not an anomalous magnetic moment inserted into the theory.

Proof. For a loop of signed current I_{shell} and oriented area vector

$$\pi R^2 \hat{\mathbf{n}}_{\mathbb{C}},$$

the magnetic moment is

$$\boldsymbol{\mu}_{\mathbb{C}} = I_{\text{shell}}\,\pi R^2 \hat{\mathbf{n}}_{\mathbb{C}}.$$

Using the loop current Eq. (112),

$$\boldsymbol{\mu}_{\mathbb{C}} = \frac{Q\,\omega}{2\pi}\,\pi R^2 \hat{\mathbf{n}}_{\mathbb{C}} = \frac{Q\,\omega R^2}{2}\,\hat{\mathbf{n}}_{\mathbb{C}}.$$

The Relator lock $R\omega = c$ then gives

$$\boldsymbol{\mu}_{\mathbb{C}} = \frac{Q\,c\,R}{2}\,\hat{\mathbf{n}}_{\mathbb{C}}.$$

This proves Eq. (124). □

Corollary 3 (Geometric tree-level normalization of $g = 2$)**.** *If the effective infrared spin scale of the minimal one-loop branch is normalized by the minimal generator first moment*

$$\mathbf{S}_{\text{eff}} \equiv L_{\mathbb{C}}\,\hat{\mathbf{n}}_{\mathbb{C}}, \tag{125}$$

with $L_{\mathbb{C}}$ fixed by Eq. (65)*, then*

$$\boldsymbol{\mu}_{\mathbb{C}} = \frac{Q}{m}\,\mathbf{S}_{\text{eff}} = 2\,\frac{Q}{2m}\,\mathbf{S}_{\text{eff}}. \tag{126}$$

Hence, conditional on the effective spin-scale convention Eq. (125) *and on the minimal one-loop calibration Eq.* (65)*, the coefficient multiplying* $Q/(2m)$ *in the geometric normalization is*

$$g = 2. \tag{127}$$

This is a tree-level statement.

Proof. By Eq. (124) and the minimal one-loop normalization Eq. (65),

$$\boldsymbol{\mu}_{\mathbb{C}} = \frac{Q\,c\,R}{2}\,\hat{\mathbf{n}}_{\mathbb{C}}, \qquad \mathbf{S}_{\text{eff}} = L_{\mathbb{C}}\,\hat{\mathbf{n}}_{\mathbb{C}} = \frac{1}{2}mcR\,\hat{\mathbf{n}}_{\mathbb{C}}.$$

Hence

$$\boldsymbol{\mu}_{\mathbb{C}} = \frac{Q}{m}\,\mathbf{S}_{\text{eff}} = 2\,\frac{Q}{2m}\,\mathbf{S}_{\text{eff}},$$

which is exactly the standard tree-level form with $g = 2$. □

Proposition 26 (Squared Dirac operator and Pauli term)**.** *Let*

$$\sigma^{\mu\nu} \equiv \frac{i}{2}\,[\gamma^\mu, \gamma^\nu], \qquad F_{\mu\nu} \equiv \partial_\mu A_\nu - \partial_\nu A_\mu. \tag{128}$$

With the convention $A_\mu = (\Phi/c, -\mathbf{A})$ *and* $x^0 = ct$*, and with* $\epsilon_{123} = +1$*, the field-strength components are*

$$F_{0i} = \frac{E_i}{c}, \qquad F_{ij} = -\,\epsilon_{ijk}B_k, \tag{129}$$

where

$$\mathbf{E} = -\nabla\Phi - \partial_t\mathbf{A}, \qquad \mathbf{B} = \nabla \times \mathbf{A}.$$

Then the minimally coupled Dirac operator satisfies

$$\left(\gamma^\mu \Pi_\mu\right)^2 = \Pi_\mu \Pi^\mu - \frac{Q\hbar}{2}\,\sigma^{\mu\nu}F_{\mu\nu}. \tag{130}$$

Proof. We first verify the field-strength components in the stated SI convention. Since $x^0 = ct$, one has $\partial_0 = c^{-1}\partial_t$. Also $A_0 = \Phi/c$ and $A_i = -A_i^{\text{vec}}$, where A_i^{vec} are the Cartesian components of $\mathbf{A}$. Therefore

$$F_{0i} = \partial_0 A_i - \partial_i A_0 = -\frac{1}{c}\partial_t A_i^{\text{vec}} - \frac{1}{c}\partial_i\Phi = \frac{1}{c}\left(-\partial_i\Phi - \partial_t A_i^{\text{vec}}\right) = \frac{E_i}{c}.$$

Likewise,

$$F_{ij} = \partial_i A_j - \partial_j A_i = -\partial_i A_j^{\text{vec}} + \partial_j A_i^{\text{vec}} = -\epsilon_{ijk}B_k.$$

Use the decompositions

$$\gamma^\mu\gamma^\nu = \frac{1}{2}\{\gamma^\mu, \gamma^\nu\} + \frac{1}{2}[\gamma^\mu, \gamma^\nu], \qquad \Pi_\mu\Pi_\nu = \frac{1}{2}\{\Pi_\mu, \Pi_\nu\} + \frac{1}{2}[\Pi_\mu, \Pi_\nu].$$

Since the contraction of a symmetric tensor in μ, ν with an antisymmetric one vanishes, one obtains

$$\begin{aligned}(\gamma^\mu\Pi_\mu)^2 &= \gamma^\mu\gamma^\nu\Pi_\mu\Pi_\nu \\ &= \frac{1}{4}\{\gamma^\mu, \gamma^\nu\}\{\Pi_\mu, \Pi_\nu\} + \frac{1}{4}[\gamma^\mu, \gamma^\nu][\Pi_\mu, \Pi_\nu].\end{aligned}$$

Using $\{\gamma^\mu, \gamma^\nu\} = 2\eta^{\mu\nu}\mathbf{1}$, the symmetric part is

$$\frac{1}{4}\{\gamma^\mu, \gamma^\nu\}\{\Pi_\mu, \Pi_\nu\} = \frac{1}{2}\eta^{\mu\nu}\{\Pi_\mu, \Pi_\nu\} = \Pi_\mu\Pi^\mu.$$

Next, for every test spinor u,

$$\begin{aligned}[\Pi_\mu, \Pi_\nu]u &= [i\hbar\partial_\mu - QA_\mu,\ i\hbar\partial_\nu - QA_\nu]u \\ &= -\,i\hbar Q\,(\partial_\mu A_\nu - \partial_\nu A_\mu)\,u \\ &= -\,i\hbar Q\,F_{\mu\nu}\,u.\end{aligned}$$

Hence

$$[\Pi_\mu, \Pi_\nu] = -\,i\hbar Q\,F_{\mu\nu}.$$

Using $[\gamma^\mu, \gamma^\nu] = -2i\,\sigma^{\mu\nu}$, the antisymmetric part becomes

$$\frac{1}{4}[\gamma^\mu, \gamma^\nu][\Pi_\mu, \Pi_\nu] = \frac{1}{4}(-2i\,\sigma^{\mu\nu})(-i\hbar Q\,F_{\mu\nu}) = -\frac{Q\hbar}{2}\,\sigma^{\mu\nu}F_{\mu\nu}.$$

Adding the two pieces yields Eq. (130). □

Theorem 6 (Infrared Pauli reduction and $g = 2$)**.** *For a branch of fixed signed charge Q, choose the standard Dirac representation for convenience. Assume a nonrelativistic infrared regime after subtraction of the rest energy. More precisely, on the retained wave packets,*

$$i\hbar\partial_t - Q\Phi = O(c^0), \qquad \boldsymbol{\pi} = \mathbf{p} - Q\mathbf{A} = O(c^0), \qquad Q\Phi = O(c^0),$$

as $c \to \infty$, with smooth external electromagnetic fields and with the derivatives of the fields bounded at the same infrared order. After factoring out the rest energy according to

$$\Psi(t, \mathbf{x}) = e^{-imc^2 t/\hbar}\begin{pmatrix}\varphi(t, \mathbf{x})\\ \chi(t, \mathbf{x})\end{pmatrix},$$

the upper two spinor components satisfy, to leading nonrelativistic order,

$$i\hbar\partial_t\varphi = \left[\frac{1}{2m}\big(\mathbf{p} - Q\mathbf{A}\big)^2 + Q\Phi - \frac{Q\hbar}{2m}\,\boldsymbol{\sigma}\cdot\mathbf{B}\right]\varphi + O(c^{-2}), \qquad \mathbf{p} = -\,i\hbar\nabla. \tag{131}$$

Equivalently, with

$$\mathbf{S} = \frac{\hbar}{2}\boldsymbol{\sigma}, \tag{132}$$

the leading magnetic interaction takes the standard tree-level form

$$H_{\text{mag}} = -\,\boldsymbol{\mu}\cdot\mathbf{B}, \qquad \boldsymbol{\mu} = g\,\frac{Q}{2m}\,\mathbf{S}, \qquad g = 2. \tag{133}$$

For the electron sector $Q = -e$, this convention gives a magnetic moment antiparallel to the spin direction.

Proof. Choose the standard Dirac representation,

$$\gamma^0 = \begin{pmatrix}\mathbf{1} & 0\\ 0 & -\mathbf{1}\end{pmatrix}, \qquad \gamma^i = \begin{pmatrix}0 & \sigma^i\\ -\sigma^i & 0\end{pmatrix},$$

and define

$$\boldsymbol{\pi} \coloneqq \mathbf{p} - Q\mathbf{A} = -\,i\hbar\nabla - Q\mathbf{A}.$$

Multiplying Eq. (123) by $c\gamma^0$ gives the Hamiltonian form

$$i\hbar\partial_t\Psi = \big[c\,\boldsymbol{\alpha}\cdot\boldsymbol{\pi} + \beta mc^2 + Q\Phi\big]\,\Psi, \qquad \boldsymbol{\alpha} = \gamma^0\boldsymbol{\gamma}, \qquad \beta = \gamma^0.$$

Indeed, with $A_\mu = (\Phi/c, -\mathbf{A})$, the raised spatial components give the physical three-momentum

$$\boldsymbol{\pi} = \mathbf{p} - Q\mathbf{A}, \qquad \mathbf{p} = -i\hbar\nabla.$$

After extracting the rest energy,

$$\Psi(t,\mathbf{x}) = e^{-imc^2t/\hbar}\begin{pmatrix}\varphi(t,\mathbf{x})\\ \chi(t,\mathbf{x})\end{pmatrix},$$

the Hamiltonian equation becomes the coupled block system

$$(i\hbar\partial_t - Q\Phi)\varphi = c\,\boldsymbol{\sigma}\cdot\boldsymbol{\pi}\,\chi, \tag{134}$$

$$(i\hbar\partial_t - Q\Phi + 2mc^2)\chi = c\,\boldsymbol{\sigma}\cdot\boldsymbol{\pi}\,\varphi. \tag{135}$$

In the nonrelativistic regime after subtraction of the rest energy, the lower component is smaller by one power of c^{-1}. From Eq. (135),

$$\chi = \big(2mc^2 + i\hbar\partial_t - Q\Phi\big)^{-1}\,c\,\boldsymbol{\sigma}\cdot\boldsymbol{\pi}\,\varphi.$$

On the retained wave packets, $i\hbar\partial_t - Q\Phi = O(c^0)$ and $\boldsymbol{\pi} = O(c^0)$. Hence

$$\big(2mc^2 + i\hbar\partial_t - Q\Phi\big)^{-1} = \frac{1}{2mc^2} + O(c^{-4})$$

as an operator on the retained infrared class. Therefore

$$\chi = \frac{1}{2mc}\,\boldsymbol{\sigma}\cdot\boldsymbol{\pi}\,\varphi + O(c^{-3}). \tag{136}$$

Substituting Eq. (136) into Eq. (134) yields

$$(i\hbar\partial_t - Q\Phi)\varphi = \frac{1}{2m}(\boldsymbol{\sigma}\cdot\boldsymbol{\pi})^2\varphi + O(c^{-2}).$$

Now compute

$$\begin{aligned}(\boldsymbol{\sigma}\cdot\boldsymbol{\pi})^2 &= \sigma_i\sigma_j\,\pi_i\pi_j\\ &= (\delta_{ij} + i\epsilon_{ijk}\sigma_k)\pi_i\pi_j\\ &= \boldsymbol{\pi}^{\,2} + i\epsilon_{ijk}\sigma_k\pi_i\pi_j\\ &= \boldsymbol{\pi}^{\,2} + \frac{i}{2}\epsilon_{ijk}\sigma_k[\pi_i,\pi_j].\end{aligned}$$

Since, in this three-vector calculation, A_i^{vec} denotes the Cartesian components of the ordinary vector potential $\mathbf{A}$, not the covariant spatial component $A_i = -A_i^{\text{vec}}$, one has

$$\pi_i = p_i - QA_i^{\text{vec}} = -\,i\hbar\partial_i - QA_i^{\text{vec}}.$$

Therefore

$$[\pi_i,\pi_j] = [-\,i\hbar\partial_i - QA_i^{\text{vec}}, -\,i\hbar\partial_j - QA_j^{\text{vec}}] = i\hbar Q\,(\partial_i A_j^{\text{vec}} - \partial_j A_i^{\text{vec}}) = i\hbar Q\,\epsilon_{ijk}B_k.$$

Consequently,

$$\frac{i}{2}\epsilon_{ijk}\sigma_k[\pi_i,\pi_j] = \frac{i}{2}\epsilon_{ijk}\sigma_k\big(i\hbar Q\,\epsilon_{ij\ell}B_\ell\big) = -\frac{\hbar Q}{2}\big(\epsilon_{ijk}\epsilon_{ij\ell}\big)\sigma_k B_\ell = -Q\hbar\,\boldsymbol{\sigma}\cdot\mathbf{B},$$

because

$$\epsilon_{ijk}\epsilon_{ij\ell} = 2\delta_{k\ell}.$$

Hence

$$(\boldsymbol{\sigma}\cdot\boldsymbol{\pi})^2 = \boldsymbol{\pi}^{\,2} - Q\hbar\,\boldsymbol{\sigma}\cdot\mathbf{B}.$$

Therefore

$$i\hbar\partial_t\varphi = \left[\frac{1}{2m}\big(\mathbf{p} - Q\mathbf{A}\big)^2 + Q\Phi - \frac{Q\hbar}{2m}\,\boldsymbol{\sigma}\cdot\mathbf{B}\right]\varphi + O(c^{-2}),$$

which is Eq. (131).

Finally, using

$$\mathbf{S} = \frac{\hbar}{2}\boldsymbol{\sigma},$$

the leading magnetic term becomes

$$H_{\mathrm{mag}} = -\frac{Q}{m}\,\mathbf{S}\cdot\mathbf{B} = -\left(2\,\frac{Q}{2m}\,\mathbf{S}\right)\cdot\mathbf{B}.$$

Hence the tree-level gyromagnetic factor is $g = 2$; see [2, 17, 19, 20]. □

The geometric loop normalization and the infrared Dirac–Pauli reduction therefore yield the same tree-level coefficient $g = 2$ multiplying the signed factor $Q/(2m)$. This is only a coefficient-level agreement. No stronger identification between the bookkeeping spin scale $\mathbf{S}_{\mathrm{eff}}$ and the spin operator $\mathbf{S}$ is required here, and no anomalous magnetic moment is inserted.

Definition V.9 (Pauli slot and anomalous magnetic moment)**.** The anomalous magnetic moment is

$$a \equiv \frac{g-2}{2}. \tag{137}$$

For operator classification only, we use natural-unit mass-dimension counting while keeping all displayed coefficients in SI conventions. Within the local parity-even magnetic-dipole class, and excluding derivatives acting on Ψ and on $F_{\mu\nu}$, the retained infrared magnetic slot is the Pauli bilinear. At this stage a is a formal coefficient slot for an anomalous contribution, not a measured value. With

$$\bar{\Psi} \equiv \Psi^{\dagger}\gamma^{0},$$

we write its coefficient convention as

$$\mathscr{L}^{\mathrm{slot}}_{\mathrm{Pauli}} = \varsigma_{\mathrm{P}}\, a\, \frac{Q\hbar}{4m}\,\bar{\Psi}\,\sigma^{\mu\nu}F_{\mu\nu}\Psi, \qquad \varsigma_{\mathrm{P}} = \pm 1. \tag{138}$$

Here $F_{0i} = E_i/c$ and $F_{ij} = -\epsilon_{ijk}B_k$ follow the SI convention fixed in Eq. (129). With these conventions both $Q\hbar B/m$ and $Q\hbar E/(mc)$ have dimensions of energy. Hence $Q\hbar F_{\mu\nu}/m$ has the correct energy dimension in both the magnetic and electric components. If Ψ is normalized with the usual SI field dimension $[\Psi] = L^{-3/2}$, then $\mathscr{L}^{\mathrm{slot}}_{\mathrm{Pauli}}$ has dimensions of energy density. The sign ς_{P} is fixed by the action-to-Hamiltonian convention. Only the coefficient slot proportional to $aQ\hbar/(4m)$ is used later; no measured value of a, no QED value of a, and no coefficient from the electron anomaly is inserted here.

Proposition 27 (Uniqueness of the retained Pauli magnetic slot)**.** *Within the local infrared operator class fixed in definition V.9, namely Lorentz-scalar, gauge-invariant, parity-even magnetic-dipole terms linear in $F_{\mu\nu}$ and with no derivatives acting on Ψ or on $F_{\mu\nu}$, the only retained dimension-five bilinear slot is*

$$\bar{\Psi}\,\sigma^{\mu\nu}F_{\mu\nu}\Psi$$

up to an overall real coefficient and the action-to-Hamiltonian sign convention. This is a classification statement within the restricted infrared slot, not a derivation of a numerical anomalous moment.

Proof. A local bilinear without derivatives has the form

$$\bar{\Psi}\,\mathcal{O}\,\Psi,$$

where $\mathcal{O}$ is built from the Dirac matrices. The independent Lorentz bilinear types are scalar, pseudoscalar, vector, axial vector, and antisymmetric tensor. To contract linearly with the antisymmetric field strength $F_{\mu\nu}$ and obtain a Lorentz scalar without introducing any extra fixed tensor, the spinor bilinear must also carry two antisymmetric Lorentz indices. Thus the only candidates are

$$\bar{\Psi}\,\sigma^{\mu\nu}\Psi\,F_{\mu\nu} \qquad \text{and} \qquad \bar{\Psi}\,\sigma^{\mu\nu}\gamma^5\Psi\,F_{\mu\nu}.$$

Equivalently, the second term may be written as a contraction with the dual field strength. With the four-dimensional orientation fixed by $\epsilon^{0123} = +1$, the standard identity is

$$\sigma^{\mu\nu}\gamma^5 = \frac{i}{2}\epsilon^{\mu\nu\rho\sigma}\sigma_{\rho\sigma},$$

with the corresponding sign changed if the four-dimensional orientation is reversed. The first bilinear gives the magnetic-dipole Pauli slot in the nonrelativistic magnetic reduction. The second is the parity-odd electric-dipole slot and is excluded by the parity-even restriction in definition V.9. Therefore the retained parity-even magnetic slot is unique within the stated local infrared class and is precisely

$$\bar{\Psi}\,\sigma^{\mu\nu}F_{\mu\nu}\Psi.$$

□

Remark. For the later α derivation, this section supplies only the quantized charge slot $Q = kq_0$, the shell-source loop current Eq. (112), the tree-level magnetic normalization encoded by $g = 2$, and the formal Pauli coefficient slot Eq. (138). No measured value of e, no measured value of α, no measured magnetic anomaly, and no QED anomaly coefficient enters this input layer.

E. Heuristic geometric picture of the one-loop electron branch

This subsection is heuristic and does not enter the derivation. It introduces no postulate, no shell-closure definition, and no numerical input. The scalar and vector channels used in the paper are defined by the operator equations stated in the surrounding sections, and every quantitative claim rests on those equations. The discussion below is only a geometric mnemonic for fig. 5.

In this mnemonic reading, $\mathbb{C}$ and $\mathbb{R}^3$ remain distinct. The generator side is pictured as the maximum-entropy Gaussian sheet together with its coherent one-loop carrier, rather than as a rigid wire or a sharp material torus. The only load-bearing data carried forward from this picture are the derived width $\sigma_{\mathbb{C}}$, the collective radius R, and the matching shell r_*. The split-rate balance itself is not assumed in this heuristic picture; it is fixed later by the scalar and vector shell equations and by the coupled closure.

Near the coherent carrier, the Gaussian sheet is most naturally visualized as a filamentary one-loop core together with a Gaussian transverse dressing. This picture motivates the later separation between the filamentary Maxwell source and the finite-width collar effects. In the Relator construction, R is fixed by the lock and by the internal phase kinematics; no independent identification with a laboratory Compton scale is assumed at this stage.

The projected image in $\mathbb{R}^3$ should not be read as a rigid material torus or as a solid body embedded in an ambient medium. It is only a kinematic trace of the projected branch geometry. A Gaussian-dressed circulating branch in $\mathbb{C}$ is represented heuristically in $\mathbb{R}^3$ by a toroidal tube of transverse scale $\sigma_{\mathbb{C}}$. Because the Gaussian profile has infinite support, this torus marks the dominant core region rather than a hard boundary. The matching shell then surrounds the toroidal core region used in the mnemonic picture.

This is the intended reading of fig. 5. Panel (a) shows the generator-side mnemonic in $\mathbb{C}$, together with the already derived minimal-branch width $\sigma_{\mathbb{C}} = R/\sqrt{\pi}$ from Eq. (66). Panel (b) shows the corresponding projected toroidal mnemonic in $\mathbb{R}^3$, enclosed by the already derived matching shell $r_* = \pi R$ from Eq. (84). The figure asserts no literal map $\mathbb{C} \to \mathbb{R}^3$. In the exact vector construction, the exterior shell datum is the polar magnetic component B_ϑ^{ext} on that sphere, equivalently the shell trace $b_*^{\text{ext}}(\upsilon)$. The Gaussian profile enters only through the collar scale $\sigma_{\mathbb{C}}$, the extension operator E_ℓ, the shell-admission operator $\mathbb{Q}_\chi(\ell)$, and the renormalized shell-return kernel. It does not enter by replacing the exact Maxwell source with a smeared current at this stage. This separation prevents double counting of finite-width effects.

The intended mnemonic is that of a closed feedback branch. The carrier circulates, supplies the effective shell source, and the returned shell response is evaluated on the same branch. This language remains heuristic only; the quantitative content is carried entirely by the scalar and vector shell operators.

Remark. This subsection is included only to aid intuition. None of its geometric phrasing is used as an independent axiom in the derivation. The load-bearing content remains the scalar shell law, the vector shell functional, and the shell operators associated with them.

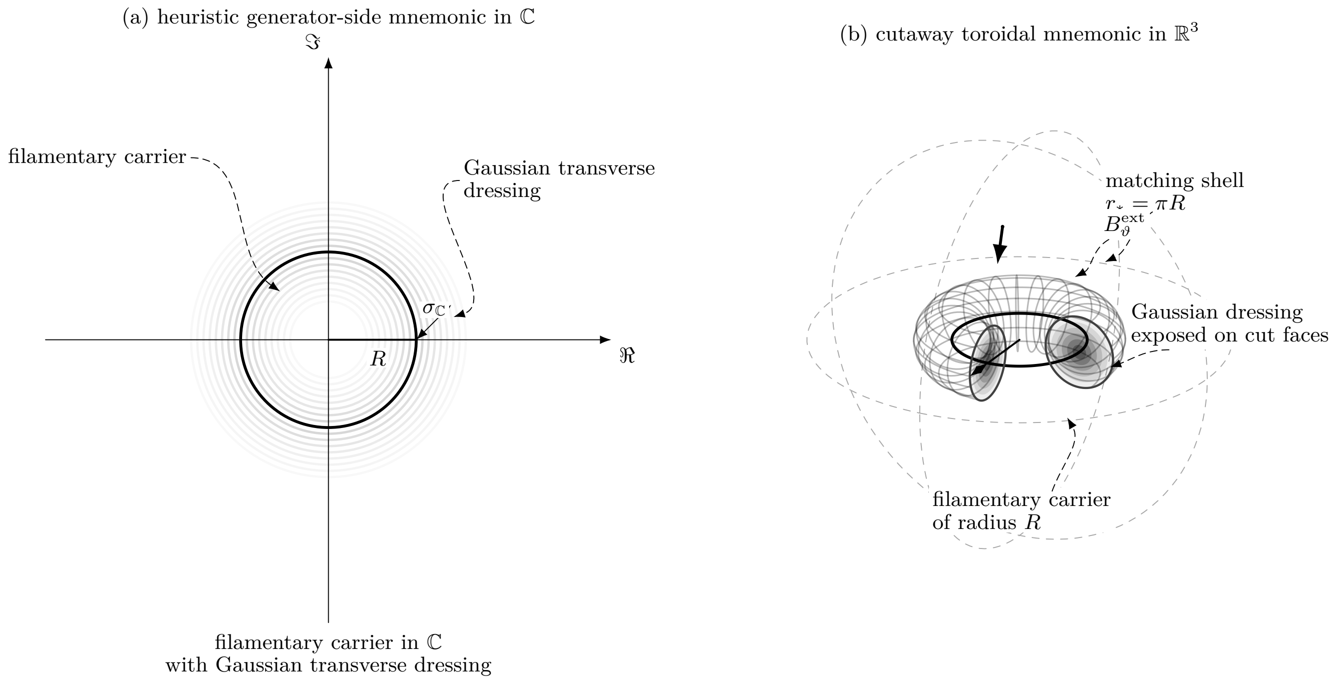

FIG. 5. Heuristic generator-side and projected branch mnemonics. Panel (a) shows the filamentary carrier of radius R in $\mathbb{C}$ with Gaussian transverse dressing of width $\sigma_{\mathbb{C}}$. Panel (b) shows the corresponding projected toroidal mnemonic in $\mathbb{R}^3$, enclosed by the matching shell $r_* = \pi R$. In the exact vector construction, the exterior shell datum is the polar magnetic trace $B_\vartheta^{\mathrm{ext}}$ on that sphere. The figure is schematic and serves intuition only. Finite-width effects enter the exact construction through $\sigma_{\mathbb{C}}$, the extension operator E_ℓ, the shell-admission operator $\mathbb{Q}_\chi(\ell)$, and the renormalized shell-return kernel.

Part III
Scalar and Vector Channels of the Electron

VI. MATCHING SHELL AND THE SCALAR SLOWDOWN BLOCK

This section fixes the scalar side of the emergent-α construction. The defining scalar-side object is a boundary-coupled scalar cavity pinned to the minimal-branch shell and coupled to a strictly positive self-adjoint glued shell bath. Eliminating the shell reaction field gives the scalar slowdown branch $\mathcal{D}_{\mathrm{C}}(\alpha)$. The scalar shell matching rule below is a branch-level matching condition, while the mother cavity–shell pencil is the defining operator-level scalar law.

The scalar sector is kept separate from the vector shell channel. No vector quantity enters the definition of $\mathcal{D}_{\mathrm{C}}$. Once the scalar branch has been fixed, the later shell lock compares it with an independently computed vector input. The vector channel is not determined inside the scalar definition.

The dependency order in this section is as follows. The minimal branch fixes r_*, η_0, ℓ_0. The scalar matching rule fixes the Coulomb anchor $\mathcal{D}_{\mathrm{C}}^{(0)} = x$ on the Compton-baseline shell. The mother cavity–shell pencil, together with the strictly positive glued shell bath, defines the scalar branch $\mathcal{D}_{\mathrm{C}}(\alpha)$. Finite visible, static-hidden, and Lanczos–Jacobi constructions are finite-rank evaluators of that scalar branch. External numerical orientation points are used only after the scalar evaluator has been fixed.

A. Matching shell and branch pinning

The scalar block is built on the matching shell selected in the minimal branch construction. We recall here only the geometric data needed for the scalar derivation, namely the locked one-loop radius, the first-node shell, and the fixed dimensionless ratios exported to the shell problem. This subsection introduces no new branch postulate, no value of α, no QED coefficient, and no empirical scalar input.

Definition VI.1 (Pinned scalar shell data)**.** The scalar shell problem used in this section is pinned to the minimal branch geometry obtained in propositions 16 and 17 and corollary 2. The relevant regular isotropic radial profile is therefore the previously derived mode $j_0(k_{\mathrm{base}} r)$, with branch-geometric base wavenumber $k_{\mathrm{base}} = R^{-1}$, and the pinned shell is its first positive node. This pinning was already fixed in the minimal branch construction; it is not a material cavity boundary and not an empirical radius fit.

In the notation used below,

$$r_* = \pi R, \qquad \eta_0 \equiv \frac{R}{r_*} = \frac{1}{\pi}. \tag{139}$$

With the previously derived minimal-branch width $\sigma_{\mathbb{C}} = R/\sqrt{\pi}$, one has

$$\frac{\sigma_{\mathbb{C}}}{R} = \frac{1}{\sqrt{\pi}}, \qquad \ell_0 \equiv \frac{\sigma_{\mathbb{C}}}{r_*} = \frac{1}{\pi\sqrt{\pi}} = \frac{\eta_0}{\sqrt{\pi}}. \tag{140}$$

No new scalar symbol is introduced here for $\sigma_{\mathbb{C}}/R$. This ratio is written explicitly in the scalar discussion below, so that ε_0 retains its standard SI meaning as the vacuum permittivity throughout this section. When no ambiguity arises, the unsubscripted shell ratios η and ℓ are specialized to the minimal-branch values η_0 and ℓ_0.

Proposition 28 (Rest-frequency normalization and symbolic reduced-Compton baseline)**.** *Adopt the infrared rest-frequency normalization*

$$\omega_{\mathbb{C}} = \frac{mc^2}{\hbar}. \tag{141}$$

For a locked stationary branch with this internal normalization and projected branch-rate magnitude $\omega_{\mathbb{R}^3}$, the orthogonal rate split gives

$$\omega^2 = \left(\frac{mc^2}{\hbar}\right)^2 + \omega_{\mathbb{R}^3}^2. \tag{142}$$

When a nonzero projected share is retained, the branch no longer sits at the zero-projected symbolic reduced-Compton baseline. The lock then relates its collective radius to the projected branch-rate magnitude by

$$R = \frac{c}{\omega} = \frac{\hbar}{mc}\left(1 + \frac{\hbar^2\omega_{\mathbb{R}^3}^2}{m^2c^4}\right)^{-1/2}, \qquad r_* = \pi R. \tag{143}$$

This identity is purely kinematical; it does not select $\omega_{\mathbb{R}^3}$, m, or α.

The scalar Coulomb normalization anchor used below is evaluated at the zero-projected symbolic reduced-Compton baseline,

$$\omega_{\mathbb{R}^3} = 0. \tag{144}$$

This baseline serves only as a normalization anchor for the scalar Coulomb block. It is not the final locked branch with nonzero scalar slowdown, and it is not a fitted reference to a measured value of α. Whenever this anchor is used, r_* denotes the baseline shell radius associated with the zero-projected normalization, not a redefinition of the nonzero-slowdown locked branch radius. In that baseline,

$$\omega = \omega_{\mathbb{C}} = \frac{mc^2}{\hbar}, \qquad R = R_{\mathrm{C}} \equiv \frac{\hbar}{mc}, \qquad r_* = \pi\, R_{\mathrm{C}}. \tag{145}$$

Here R_{C} is the symbolic reduced Compton radius associated with the same infrared inertial parameter m. No measured rest mass is introduced.

Proof. The adopted rest-frequency normalization gives

$$\omega_{\mathbb{C}} = \frac{mc^2}{\hbar}.$$

For any locked stationary branch with this internal normalization, the orthogonal rate split gives

$$\omega^2 = \omega_{\mathbb{C}}^2 + \omega_{\mathbb{R}^3}^2 = \left(\frac{mc^2}{\hbar}\right)^2 + \omega_{\mathbb{R}^3}^2.$$

The lock $R\omega = c$ then yields

$$R = \frac{c}{\sqrt{(mc^2/\hbar)^2 + \omega_{\mathbb{R}^3}^2}} = \frac{\hbar}{mc}\left(1 + \frac{\hbar^2\omega_{\mathbb{R}^3}^2}{m^2c^4}\right)^{-1/2}.$$

The pinned first-node relation gives $r_* = \pi R$, which is the displayed formula Eq. (143).

The symbolic reduced-Compton baseline is the special zero-projected case

$$\omega_{\mathbb{R}^3} = 0.$$

Therefore

$$\omega = \omega_{\mathbb{C}} = \frac{mc^2}{\hbar}, \qquad R = \frac{c}{mc^2/\hbar} = \frac{\hbar}{mc}, \qquad r_* = \pi\frac{\hbar}{mc}.$$

This proves Eqs. (142), (143) and (145). □

B. Gauge-invariant scalar dilation on the pinned shell

We now formulate the scalar block $\mathcal{D}_{\mathrm{C}}$ in the form used both for the derivation and for later computation. The guiding point is that the scalar block is not an ad hoc closed formula. It is the shell-reduced scalar-channel representative of the gauge-invariant slowdown variable of RELATOR, extracted from the pinned scalar shell problem and from the positive self-adjoint shell-bath construction defined later in this section. No measured value of α, no QED coefficient, and no fitted scalar parameter enters this definition layer.

Remark. The quantity $\mathcal{D}_{\mathrm{C}}$ denotes the scalar-shell contribution to the full gauge-invariant slowdown variable $\mathcal{D}_{\mathrm{total}}$ introduced in Eq. (10). At the branch level the full observable is represented as

$$\mathcal{D}_{\mathrm{total}} = \left(\frac{\omega_{\mathbb{R}^3}}{\omega}\right)^2 = \frac{p_{\mathrm{br}}^2}{m^2c^2},$$

where p_{br} is the chosen gauge-invariant branch or shell representative extracted from

$$\mathbf{P}_{\mathrm{mech}} = \nabla\mathcal{S} - Q\mathbf{A}.$$

In a pointwise local reading one may use $\mathcal{D}_{\mathrm{total}}^{\mathrm{loc}} = \|\mathbf{P}_{\mathrm{mech}}\|^2/(m^2c^2)$. The present subsection isolates the purely scalar Coulombic shell channel. The resulting quantity $\mathcal{D}_{\mathrm{C}}$ is therefore a gauge-invariant scalar-channel slowdown representative rather than a full-space electromagnetic self-energy.

Definition VI.2 (Shell-weighted radial inner product)**.** For radial functions on $0 \le r \le r_*$, define

$$\langle f, g\rangle_* := \int_0^{r_*} \overline{f(r)}\, g(r)\, r^2\, \mathrm{d}r = r_*^3 \int_0^1 \overline{f(r_* y)}\, g(r_* y)\, y^2\, \mathrm{d}y, \qquad y := \frac{r}{r_*}. \tag{146}$$

Definition VI.3 (Pinned scalar ground line)**.** The normalized pinned s-wave is

$$u_0(r) = \mathcal{N}\, j_0(k_{\mathrm{base}} r), \qquad k_{\mathrm{base}} = \frac{\pi}{r_*}, \qquad 4\pi\langle u_0, u_0\rangle_* = 1. \tag{147}$$

In the reduced cavity coordinate $y = r/r_*$, define the reduced line variable

$$v(y) := y\, u_0(r_* y). \tag{148}$$

A convenient complete orthonormal Dirichlet eigenbasis of $L^2(0,1)$ is

$$\phi_n(y) = \sqrt{2}\sin(n\pi y), \qquad n \ge 1. \tag{149}$$

Using $k_{\mathrm{base}} = \pi/r_*$ and $j_0(z) = \sin z/z$, one has

$$v(y) = \mathcal{N}\, y\, j_0(\pi y) = \mathcal{N}\, \frac{\sin(\pi y)}{\pi} = \frac{\mathcal{N}}{\sqrt{2}\,\pi}\, \phi_1(y). \tag{150}$$

Hence v is smooth on $[0,1]$, vanishes at both endpoints, and therefore

$$v \in H^2(0,1) \cap H_0^1(0,1) \subset L^2(0,1).$$

Define the normalized reduced ground line by

$$v_0(y) := \sqrt{4\pi r_*^3}\, v(y). \tag{151}$$

Lemma 1 (Normalization and ground-mode expectation of y^2)**.** *For the mode Eq.* (147)*,*

$$\mathcal{N}^2 = \frac{\pi}{2 r_*^3}, \tag{152}$$

and the normalized radial expectation of $y^2 = r^2/r_*^2$ is

$$\langle y^2\rangle_0 := 4\pi \int_0^{r_*} r^2 |u_0(r)|^2 \frac{r^2}{r_*^2}\, \mathrm{d}r = \frac{1}{3} - \frac{1}{2\pi^2}. \tag{153}$$

Moreover, the normalized reduced line defined in Eq. (151) *satisfies*

$$\int_0^1 |v_0(y)|^2\, \mathrm{d}y = 1, \qquad v_0(y) = \phi_1(y), \tag{154}$$

and, for $0 < r \le r_*$, equivalently $0 < y \le 1$,

$$u_0(r) = \frac{1}{\sqrt{4\pi r_*^3}}\, \frac{\phi_1(y)}{y}, \qquad y = \frac{r}{r_*}. \tag{155}$$

Proof. Write $y = r/r_*$. Using the explicit ground radial mode in Eq. (147),

$$u_0(r) = \mathcal{N}\, \frac{\sin(\pi y)}{\pi y}, \qquad r = r_* y, \qquad \mathrm{d}r = r_*\, \mathrm{d}y.$$

Hence

$$4\pi \int_0^{r_*} r^2 |u_0(r)|^2\, \mathrm{d}r = 4\pi \mathcal{N}^2 r_*^3 \int_0^1 y^2 \frac{\sin^2(\pi y)}{\pi^2 y^2}\, \mathrm{d}y = \frac{4\pi \mathcal{N}^2 r_*^3}{\pi^2} \int_0^1 \sin^2(\pi y)\, \mathrm{d}y.$$

Since

$$\int_0^1 \sin^2(\pi y)\, \mathrm{d}y = \frac{1}{2},$$

the normalization condition gives

$$1 = \frac{4\pi\mathcal{N}^2 r_*^3}{\pi^2} \cdot \frac{1}{2} = \frac{2\mathcal{N}^2 r_*^3}{\pi},$$

hence

$$\mathcal{N}^2 = \frac{\pi}{2r_*^3}.$$

This proves Eq. (152).

For the expectation value,

$$\langle y^2\rangle_0 = 4\pi \int_0^{r_*} r^2 |u_0(r)|^2 \frac{r^2}{r_*^2}\, \mathrm{d}r = \frac{4\pi\mathcal{N}^2 r_*^3}{\pi^2} \int_0^1 y^2 \sin^2(\pi y)\, \mathrm{d}y.$$

Now

$$\begin{aligned}
\int_0^1 y^2 \sin^2(\pi y)\, \mathrm{d}y &= \frac{1}{2}\int_0^1 y^2\, \mathrm{d}y - \frac{1}{2}\int_0^1 y^2 \cos(2\pi y)\, \mathrm{d}y \\
&= \frac{1}{6} - \frac{1}{2}\left[\frac{y^2\sin(2\pi y)}{2\pi} + \frac{2y\cos(2\pi y)}{(2\pi)^2} - \frac{2\sin(2\pi y)}{(2\pi)^3}\right]_0^1 \\
&= \frac{1}{6} - \frac{1}{4\pi^2}.
\end{aligned}$$

Substituting Eq. (152), we obtain

$$\langle y^2\rangle_0 = \frac{4\pi}{\pi^2}\cdot\frac{\pi}{2}\left(\frac{1}{6} - \frac{1}{4\pi^2}\right) = \frac{1}{3} - \frac{1}{2\pi^2}.$$

Finally, by Eq. (151),

$$v_0(y) = \sqrt{4\pi r_*^3}\, y\, u_0(r_* y).$$

Therefore

$$\int_0^1 |v_0(y)|^2\, \mathrm{d}y = 4\pi r_*^3 \int_0^1 y^2 |u_0(r_* y)|^2\, \mathrm{d}y = 4\pi \int_0^{r_*} r^2 |u_0(r)|^2\, \mathrm{d}r = 1.$$

Thus v_0 is normalized in $L^2(0,1)$. Using the explicit form of u_0, we also get

$$v_0(y) = \sqrt{4\pi r_*^3}\, y\, \mathcal{N}\, \frac{\sin(\pi y)}{\pi y} = \sqrt{4\pi r_*^3}\, \mathcal{N}\, \frac{\sin(\pi y)}{\pi} = \sqrt{2}\, \sin(\pi y) = \phi_1(y),$$

where $\mathcal{N}^2 = \pi/(2r_*^3)$ was used. This proves Eq. (154). For $0 < y \le 1$, the same identity gives

$$u_0(r_* y) = \frac{v_0(y)}{\sqrt{4\pi r_*^3}\, y} = \frac{1}{\sqrt{4\pi r_*^3}}\, \frac{\phi_1(y)}{y}.$$

Equivalently, with $y = r/r_*$,

$$u_0(r) = \frac{1}{\sqrt{4\pi r_*^3}}\, \frac{\phi_1(y)}{y}, \qquad 0 < r \le r_*,$$

which proves Eq. (155). □

Definition VI.4 (Gauge-invariant scalar shell dilation)**.** On the scalar side, the shell slowdown block is the scalar-channel representative of the gauge-invariant slowdown observable restricted to the Coulombic shell channel. We define

$$\mathcal{D}_{\mathrm{C}} := \frac{p_*^2}{m^2 c^2}, \tag{156}$$

where p_* is the shell-matched scalar momentum scale associated with the one-sided scalar shell representative. Thus $\mathcal{D}_{\mathrm{C}}$ is the scalar Coulombic contribution to

$$\left(\frac{\omega_{\mathbb{R}^3}}{\omega}\right)^2$$

after isolation of the Coulombic shell channel.

The scale p_* is not obtained by taking a pointwise derivative of the pinned Dirichlet mode at its node. When a nodal-free scalar collar representative is used and the one-sided trace exists, p_*^2 is the one-sided shell trace of the gauge-invariant mechanical momentum square,

$$p_*^2 = \operatorname*{tr}_{r\to r_*^-} \|\mathbf{P}_{\mathrm{mech}}\|^2, \qquad \mathbf{P}_{\mathrm{mech}} = \nabla\mathcal{S} - Q\mathbf{A}. \tag{157}$$

The pinned Dirichlet mode supplies the scalar cavity shape and the shell susceptibility, whereas the scalar momentum scale itself is fixed below by the shell matching rule.

In the purely electrostatic scalar channel, assume the magnetic field vanishes on the collar and the collar is simply connected. Then $\nabla \times \mathbf{A} = 0$ implies $\mathbf{A} = \nabla a$ for a single-valued scalar a on the collar. The gauge transformation with $\lambda_{\mathrm{g}} = -a$ sets $\mathbf{A}' = 0$. In that gauge one may evaluate the same gauge-invariant representative as

$$\mathcal{D}_{\mathrm{C}} = \frac{\mathrm{tr}_{r\to r_*^-} \|\nabla\mathcal{S}\|^2}{m^2c^2} = \delta_C^2, \qquad \delta_C := \frac{\left(\mathrm{tr}_{r\to r_*^-} \|\nabla\mathcal{S}\|^2\right)^{1/2}}{mc}. \tag{158}$$

Condition VI.1 (Scalar shell matching rule)**.** In the purely Coulombic shell sector, the scalar shell momentum scale is fixed by the branch-level leading nonrelativistic matching condition

$$\frac{p_*^2}{2m} = U_{\mathrm{far}}(r_*). \tag{159}$$

This condition is the scalar Coulomb-anchor matching rule for the pinned shell. It is not an empirical fit, and it is not the final scalar–vector lock equation. Here $U_{\mathrm{far}}(r_*)$ is the positive electrostatic field energy stored in the exterior region $r \geq r_*$ for total charge magnitude $|Q| = q_0$, later denoted by e in the minimal $k = \pm 1$ sectors. The use of $p_*^2/(2m)$ is the leading Coulomb-anchor reading of the relativistic kinetic energy in the scalar channel. More precisely, as $p_*/(mc) \to 0$,

$$mc^2\left(\sqrt{1+\frac{p_*^2}{m^2c^2}} - 1\right) = \frac{p_*^2}{2m} - \frac{p_*^4}{8m^3c^2} + O\!\left(\frac{p_*^6}{m^5c^4}\right). \tag{160}$$

This uses the charge quantum defined earlier and does not insert a measured numerical value of e, a measured value of α, a rest-mass benchmark, or any QED coefficient.

Proposition 29 (Far-field Coulomb anchor)**.** *Under the shell matching rule Eq.* (159)*, let the symbolic dimensionless coupling variable associated with the compact charge scale q_0 be*

$$\alpha := \frac{q_0^2}{4\pi\varepsilon_0\hbar c}, \tag{161}$$

where ε_0 is the SI vacuum permittivity. At this stage α is an unknown dimensionless coupling variable, not a measured input. Then the purely exterior Coulomb anchor is

$$\mathcal{D}_{\mathrm{C}}^{(0)} := \frac{2U_{\mathrm{far}}(r_*)}{mc^2} = \alpha\frac{R_{\mathrm{C}}}{r_*}, \qquad R_{\mathrm{C}} \equiv \frac{\hbar}{mc}. \tag{162}$$

In particular, on the symbolic reduced-Compton baseline shell $r_* = \pi R_{\mathrm{C}}$,

$$\mathcal{D}_{\mathrm{C}}^{(0)} = \frac{\alpha}{\pi} := x. \tag{163}$$

Proof. By the shell matching rule,

$$\mathcal{D}_{\mathrm{C}}^{(0)} = \frac{2U_{\mathrm{far}}(r_*)}{mc^2}.$$

For a charge of magnitude q_0, the exterior Coulomb field magnitude is

$$|\mathbf{E}(r)| = \frac{q_0}{4\pi\varepsilon_0 r^2}, \qquad r \geq r_*.$$

Hence

$$U_{\rm far}(r_*) = \int_{r_*}^{\infty} \frac{\varepsilon_0}{2} |\mathbf{E}(r)|^2 \, 4\pi r^2 \, \mathrm{d}r = \int_{r_*}^{\infty} \frac{\varepsilon_0}{2} \left(\frac{q_0}{4\pi\varepsilon_0 r^2} \right)^2 4\pi r^2 \, \mathrm{d}r = \frac{q_0^2}{8\pi\varepsilon_0 r_*}.$$

Therefore

$$\mathcal{D}_{\rm C}^{(0)} = \frac{q_0^2}{4\pi\varepsilon_0 r_* mc^2} = \frac{q_0^2}{4\pi\varepsilon_0 \hbar c} \frac{\hbar}{mc} \frac{1}{r_*} = \alpha \frac{R_{\rm C}}{r_*}.$$

On the Compton-baseline pinned scalar shell $r_* = \pi R_{\rm C}$, this gives

$$\mathcal{D}_{\rm C}^{(0)} = \frac{\alpha}{\pi} = x.$$

□

Definition VI.5 (Uniform interior Coulomb baseline)**.** The standard spherically symmetric interior Coulomb baseline used in the scalar channel is the positive charge-magnitude potential-energy profile

$$\mathcal{V}_{\rm bulk}(r) = \frac{q_0^2}{8\pi\varepsilon_0 r_*} \left(3 - \frac{r^2}{r_*^2} \right), \qquad 0 \leq r \leq r_*. \tag{164}$$

Here ε_0 is the SI vacuum permittivity. In the minimal $k = \pm 1$ sectors one may write $q_0 \equiv e$. This is a naming convention for the charge unit and does not insert a measured value of e. The sign of the branch charge does not enter this scalar Coulomb baseline, because this profile is built from the positive quadratic charge scale $Q^2 = q_0^2$. It is a scalar-channel baseline profile, not an additional electromagnetic self-energy definition.

Definition VI.6 (Uniform near-shell coefficient)**.** The shell-averaged interior baseline is

$$U_{\rm near}(r_*) \equiv 4\pi \int_0^{r_*} r^2 |u_0(r)|^2 \mathcal{V}_{\rm bulk}(r) \, \mathrm{d}r. \tag{165}$$

Let

$$R_{\rm C} \equiv \frac{\hbar}{mc}$$

denote the symbolic reduced-Compton baseline radius obtained in the zero-projected-share limit. The associated dimensionless uniform near-shell coefficient is

$$C_{\rm uni} \equiv \frac{1}{\alpha mc^2} U_{\rm near}(r_*) \Big|_{r_* = \pi R_{\rm C}}. \tag{166}$$

Proposition 30 (Uniform near-shell coefficient and Coulomb-anchor load)**.** *In the symbolic Compton-baseline pinned scalar shell problem, the uniform near-shell coefficient is*

$$C_{\rm uni} = \frac{1}{\pi} \left(\frac{4}{3} + \frac{1}{4\pi^2} \right). \tag{167}$$

Moreover, for the pinned s-wave shell geometry, the uniform interior load is tied to the Coulomb anchor by

$$\frac{2U_{\rm near}(r_*)}{mc^2} = 2\pi \, C_{\rm uni} \, \mathcal{D}_{\rm C}^{(0)}. \tag{168}$$

Proof. By lemma 1, the normalized pinned ground state satisfies

$$4\pi \int_0^{r_*} r^2 |u_0(r)|^2 \, \mathrm{d}r = 1, \qquad \langle y^2 \rangle_0 = 4\pi \int_0^{r_*} r^2 |u_0(r)|^2 \frac{r^2}{r_*^2} \, \mathrm{d}r = \frac{1}{3} - \frac{1}{2\pi^2}.$$

Insert the uniform interior Coulomb baseline

$$\mathcal{V}_{\rm bulk}(r) = \frac{q_0^2}{8\pi\varepsilon_0 r_*}\left(3 - \frac{r^2}{r_*^2}\right)$$

into the definition of $U_{\rm near}$. Then

$$\begin{aligned} U_{\rm near}(r_*) &= 4\pi \int_0^{r_*} r^2 |u_0(r)|^2 \mathcal{V}_{\rm bulk}(r)\,\mathrm{d}r \\ &= \frac{q_0^2}{8\pi\varepsilon_0 r_*}\left(3 - \langle y^2\rangle_0\right) \\ &= \frac{q_0^2}{8\pi\varepsilon_0 r_*}\left(\frac{8}{3} + \frac{1}{2\pi^2}\right). \end{aligned}$$

In the symbolic Compton-baseline pinned scalar shell problem,

$$r_* = \pi R_{\rm C}, \qquad R_{\rm C} = \frac{\hbar}{mc}, \qquad \frac{q_0^2}{4\pi\varepsilon_0 \hbar c} = \alpha.$$

Therefore

$$\begin{aligned} C_{\rm uni} &= \frac{1}{\alpha mc^2} U_{\rm near}(r_*)\Big|_{r_*=\pi R_{\rm C}} \\ &= \frac{1}{\alpha mc^2}\frac{q_0^2}{8\pi\varepsilon_0\, \pi R_{\rm C}}\left(\frac{8}{3} + \frac{1}{2\pi^2}\right) \\ &= \frac{1}{2\pi}\left(\frac{8}{3} + \frac{1}{2\pi^2}\right) = \frac{1}{\pi}\left(\frac{4}{3} + \frac{1}{4\pi^2}\right). \end{aligned}$$

This proves Eq. (167).

The exterior Coulomb anchor is

$$\mathcal{D}_{\rm C}^{(0)} = \frac{2U_{\rm far}(r_*)}{mc^2} = \frac{q_0^2}{4\pi\varepsilon_0 r_* mc^2}.$$

Hence

$$\frac{2U_{\rm near}(r_*)}{mc^2} = \left(\frac{8}{3} + \frac{1}{2\pi^2}\right)\mathcal{D}_{\rm C}^{(0)}.$$

Since

$$2\pi C_{\rm uni} = \frac{8}{3} + \frac{1}{2\pi^2},$$

one obtains

$$\frac{2U_{\rm near}(r_*)}{mc^2} = 2\pi\, C_{\rm uni}\, \mathcal{D}_{\rm C}^{(0)}.$$

This proves Eq. (168). □

Definition VI.7 (Core static scalar load and self-consistent uniform shell load)**.** The core static scalar load associated with the uniform interior baseline is

$$\Theta_{1,\rm core} := 2\pi\, C_{\rm uni} = \frac{8}{3} + \frac{1}{2\pi^2}. \tag{169}$$

The closure-level uniform near-load map is

$$\Xi(\mathcal{D}_{\rm C}) \equiv \Theta_{1,\rm core}\,\mathcal{D}_{\rm C} = 2\pi\, C_{\rm uni}\,\mathcal{D}_{\rm C}. \tag{170}$$

This is the self-consistent replacement of the Coulomb-anchor load by the scalar slowdown variable $\mathcal{D}_{\rm C}$. It is a scalar-channel closure map used later. By itself it neither solves the scalar–vector lock nor introduces an additional fitted parameter.

C. Mother cavity–shell pencil

The defining operator-level object is not a closed one-line radicand formula. It is a linear cavity–shell pencil. The scalar block $\mathcal{D}_{\mathrm{C}}$ is recovered only after elimination of the shell reaction field, namely through a Feshbach reduction of this mother system. Thus the abstract scalar law is fixed before any finite-rank evaluator or numerical realization is introduced.

Lemma 2 (Reduced-line transform of the pinned radial cavity)**.** *Let*

$$(U_{\mathrm{red}}u)(y) := \sqrt{4\pi r_*^3}\, y\, u(r_* y), \qquad 0 < y < 1. \tag{171}$$

Then U_{red} is a unitary map from $L^2((0,r_*), 4\pi r^2\,\mathrm{d}r)$ onto $L^2(0,1;\mathrm{d}y)$, with inverse

$$(U_{\mathrm{red}}^{-1}w)(r) = \frac{1}{\sqrt{4\pi r_*^3}} \frac{w(r/r_*)}{r/r_*}, \qquad 0 < r < r_*. \tag{172}$$

Let the pinned radial cavity operator be

$$K_{\mathrm{rad}} := -k_{\mathrm{base}}^{-2}\left(\partial_r^2 + \frac{2}{r}\partial_r\right), \tag{173}$$

with domain

$$\mathrm{Dom}(K_{\mathrm{rad}}) := \Big\{ u \in L^2((0,r_*), 4\pi r^2\,\mathrm{d}r)\ ;\ ru \in H^2(0,r_*) \cap H_0^1(0,r_*) \Big\}. \tag{174}$$

Then

$$U_{\mathrm{red}} K_{\mathrm{rad}} U_{\mathrm{red}}^{-1} = K_0, \qquad K_0 := -\pi^{-2}\partial_y^2, \qquad \mathrm{Dom}(K_0) = H^2(0,1)\cap H_0^1(0,1). \tag{175}$$

The operator K_0 is the nonnegative self-adjoint Dirichlet realization on $L^2(0,1;\mathrm{d}y)$, with eigenbasis $\phi_n(y) = \sqrt{2}\sin(n\pi y)$ and eigenvalues n^2. Consequently K_{rad} is nonnegative and self-adjoint on $L^2((0,r_*), 4\pi r^2\,\mathrm{d}r)$ by unitary equivalence. Moreover,

$$U_{\mathrm{red}} u_0 = \phi_1. \tag{176}$$

Proof. Let $r = r_* y$. Then

$$\int_0^1 |(U_{\mathrm{red}}u)(y)|^2\,\mathrm{d}y = 4\pi r_*^3 \int_0^1 y^2 |u(r_* y)|^2\,\mathrm{d}y = 4\pi \int_0^{r_*} r^2 |u(r)|^2\,\mathrm{d}r,$$

so U_{red} is isometric. The inverse formula Eq. (172) is immediate, hence U_{red} is unitary.

Writing

$$u(r) = \frac{1}{\sqrt{4\pi r_*^3}} \frac{w(y)}{y}, \qquad y = \frac{r}{r_*},$$

one computes

$$\partial_r u(r) = \frac{1}{\sqrt{4\pi r_*^3}} \frac{1}{r_*}\left(\frac{w'(y)}{y} - \frac{w(y)}{y^2}\right),$$

and

$$\partial_r^2 u(r) = \frac{1}{\sqrt{4\pi r_*^3}} \frac{1}{r_*^2}\left(\frac{w''(y)}{y} - \frac{2w'(y)}{y^2} + \frac{2w(y)}{y^3}\right).$$

Therefore

$$\frac{2}{r}\partial_r u(r) = \frac{1}{\sqrt{4\pi r_*^3}} \frac{1}{r_*^2}\left(\frac{2w'(y)}{y^2} - \frac{2w(y)}{y^3}\right),$$

so the singular terms cancel and

$$\left(-\partial_r^2 - \frac{2}{r}\partial_r\right) u(r) = \frac{1}{\sqrt{4\pi r_*^3}}\, \frac{1}{r_*^2 y}\, \big(-w''(y)\big).$$

Since $r_* = \pi/k_{\mathrm{base}}$, equivalently $r_*^2 = \pi^2/k_{\mathrm{base}}^2$, one obtains

$$U_{\mathrm{red}} K_{\mathrm{rad}} U_{\mathrm{red}}^{-1} w = -\pi^{-2}\partial_y^2 w = K_0 w.$$

Moreover,

$$w(y) = \sqrt{4\pi r_*^3}\, y\, u(r_* y) = \sqrt{4\pi r_*}\, (ru)(r_* y).$$

Hence

$$ru \in H^2(0,r_*) \cap H_0^1(0,r_*) \quad\iff\quad w \in H^2(0,1) \cap H_0^1(0,1),$$

which proves the domain statement.

Let

$$w_n := \langle w, \phi_n\rangle_{L^2(0,1)}, \qquad w = \sum_{n\ge 1} w_n \phi_n \quad \text{in } L^2(0,1).$$

If $w \in H^2(0,1) \cap H_0^1(0,1)$, then $\phi_n \in H^2(0,1) \cap H_0^1(0,1)$, $\phi_n'' = -(n\pi)^2\phi_n$, and integration by parts twice gives

$$\begin{aligned}
\langle K_0 w, \phi_n\rangle_{L^2} &= -\pi^{-2} \int_0^1 w''(y)\, \overline{\phi_n(y)}\, \mathrm{d}y \\
&= -\pi^{-2} \Big[w'(y)\overline{\phi_n(y)} - w(y)\overline{\phi_n'(y)} \Big]_0^1 - \pi^{-2} \int_0^1 w(y)\, \overline{\phi_n''(y)}\, \mathrm{d}y \\
&= n^2 \langle w, \phi_n\rangle_{L^2} = n^2 w_n,
\end{aligned}$$

because $w(0) = w(1) = \phi_n(0) = \phi_n(1) = 0$. Therefore

$$K_0 w = \sum_{n\ge 1} n^2 w_n \phi_n \quad \text{in } L^2(0,1), \qquad \sum_{n\ge 1} n^4 |w_n|^2 = \|K_0 w\|_{L^2(0,1)}^2 < \infty.$$

Conversely, if $\sum_{n\ge 1} n^4 |w_n|^2 < \infty$, then the partial sums $w^{(N)} = \sum_{n=1}^N w_n \phi_n$ satisfy

$$\|w^{(N)} - w^{(M)}\|_{L^2}^2 = \sum_{n=M+1}^{N} |w_n|^2,$$

$$\|(w^{(N)} - w^{(M)})'\|_{L^2}^2 = \pi^2 \sum_{n=M+1}^{N} n^2 |w_n|^2,$$

$$\|(w^{(N)} - w^{(M)})''\|_{L^2}^2 = \pi^4 \sum_{n=M+1}^{N} n^4 |w_n|^2.$$

Hence $(w^{(N)})_N$ is Cauchy in $H^2(0,1)$. Since each $w^{(N)} \in H^2(0,1) \cap H_0^1(0,1)$, the limit belongs to $H^2(0,1) \cap H_0^1(0,1)$. Thus

$$\operatorname{Dom}(K_0) = \left\{ w = \sum_{n\ge 1} w_n \phi_n \ ;\ \sum_{n\ge 1} n^4 |w_n|^2 < \infty \right\}, \qquad K_0 w = \sum_{n\ge 1} n^2 w_n \phi_n.$$

Therefore, under the Fourier–sine unitary map $w \mapsto (w_n)_{n\geq 1}$, the operator K_0 is unitarily equivalent to multiplication by the real sequence $(n^2)_{n\geq 1}$ on the domain

$$\left\{ (w_n) \in \ell^2 \ ; \ \sum_{n\geq 1} n^4 |w_n|^2 < \infty \right\}.$$

Hence K_0 is nonnegative and self-adjoint. The self-adjointness of K_{rad} then follows from the unitary equivalence already proved.

Finally, by Eq. (151),

$$(U_{\mathrm{red}} u_0)(y) = \phi_1(y).$$

This proves Eq. (176). □

Definition VI.8 (Reduced cavity line space and reduced bulk load)**.** We identify the reduced cavity with

$$\mathcal{H}_{\mathrm{cav}} := L^2(0, 1; \mathrm{d}y), \tag{177}$$

using the unitary map U_{red} of Eq. (171). The associated Dirichlet basis is Eq. (149), and

$$K_0 \phi_n = n^2 \phi_n, \qquad n \geq 1. \tag{178}$$

The reduced bulk Coulomb operator is multiplication by

$$V_{\mathrm{bulk}}^{\mathrm{red}}(y) := 3 - y^2. \tag{179}$$

The multiplication operator $V_{\mathrm{bulk}}^{\mathrm{red}}$ is bounded and self-adjoint on $\mathcal{H}_{\mathrm{cav}}$, and satisfies

$$2I_{\mathrm{cav}} \leq V_{\mathrm{bulk}}^{\mathrm{red}} \leq 3I_{\mathrm{cav}}.$$

Definition VI.9 (Shell bath, source vector, and derivative trace)**.** The shell-bath coordinates in this definition are dimensionless reduced coordinates. To avoid confusion with the physical generator radius ρ on $\mathbb{C}$, we write the collar coordinate as $\xi \in \mathbb{R}_+$ and the logarithmic-line coordinate as $t \in \mathbb{R}_+$. This t is an internal logarithmic coordinate of the shell bath and is not physical time. The shell-bath Hilbert space is

$$\mathcal{H}_{\mathrm{sh}} := \mathcal{H}_{\mathrm{coll}} \oplus \mathcal{H}_{\mathrm{log}} := L^2(\mathbb{R}_+, \mathrm{d}\xi) \oplus L^2(\mathbb{R}_+, \mathrm{d}t). \tag{180}$$

On $\mathcal{H}_{\mathrm{coll}}$, define the dimensionless collar operator

$$H_{\mathrm{coll}} := \ell_0^{-2}(-\partial_\xi^2 + \xi^2), \tag{181}$$

with Dirichlet boundary condition at $\xi = 0$ and operator domain

$$\mathrm{Dom}(H_{\mathrm{coll}}) = \Big\{ f \in H_0^1(\mathbb{R}_+) \ ; \ -f'' + \xi^2 f \in L^2(\mathbb{R}_+) \Big\}. \tag{182}$$

Equivalently, for this half-line harmonic oscillator realization,

$$\mathrm{Dom}(H_{\mathrm{coll}}) = \Big\{ f \in H^2(\mathbb{R}_+) \cap H_0^1(\mathbb{R}_+) \ ; \ \xi^2 f \in L^2(\mathbb{R}_+) \Big\}.$$

The operator H_{coll} is the self-adjoint Friedrichs realization of the closed quadratic form

$$h_{\mathrm{coll}}[f] = \ell_0^{-2} \int_0^\infty \big(|f'(\xi)|^2 + \xi^2 |f(\xi)|^2 \big) \, \mathrm{d}\xi, \qquad f \in H_0^1(\mathbb{R}_+), \quad \xi f \in L^2(\mathbb{R}_+).$$

In particular,

$$H_{\mathrm{coll}} \geq 0$$

as a self-adjoint operator.

On $\mathcal{H}_{\log}$, define

$$L_{\log} := -\partial_t^2 + \frac{1}{4}, \qquad \mathrm{Dom}(L_{\log}) = H^2(\mathbb{R}_+) \cap H_0^1(\mathbb{R}_+). \tag{183}$$

This is the self-adjoint Dirichlet half-line realization of $-\partial_t^2 + 1/4$, and

$$L_{\log} \geq \frac{1}{4} I_{\log}.$$

For the abstract scalar reduction, let $\mathsf{G}_{c\ell} : \mathcal{H}_{\log} \to \mathcal{H}_{\mathrm{coll}}$ be bounded and define

$$\mathbb{L}_{\mathrm{sh}}^{\mathrm{gl}} = \begin{pmatrix} H_{\mathrm{coll}} & \mathsf{G}_{c\ell} \\ \mathsf{G}_{c\ell}{}^* & L_{\log} \end{pmatrix}, \qquad \mathrm{Dom}(\mathbb{L}_{\mathrm{sh}}^{\mathrm{gl}}) = \mathrm{Dom}(H_{\mathrm{coll}}) \oplus \mathrm{Dom}(L_{\log}). \tag{184}$$

Since

$$\begin{pmatrix} 0 & \mathsf{G}_{c\ell} \\ \mathsf{G}_{c\ell}{}^* & 0 \end{pmatrix}$$

is a bounded self-adjoint perturbation of $H_{\mathrm{coll}} \oplus L_{\log}$, the block operator $\mathbb{L}_{\mathrm{sh}}^{\mathrm{gl}}$ is self-adjoint on the displayed domain. The scalar mother law assumes the strict glued-bath lower bound

$$\mathbb{L}_{\mathrm{sh}}^{\mathrm{gl}} \geq c_{\mathrm{sh}} I_{\mathrm{sh}} \quad \text{for some } c_{\mathrm{sh}} > 0. \tag{185}$$

This is an explicit positivity hypothesis for the abstract shell bath. It is fixed before the scalar branch is solved and is not tuned to a measured value of α or to a QED coefficient. The finite evaluators introduced later specify reduced representatives of this glued bath. In the abstract scalar law, the D-dependence enters through the shifted resolvent $(\mathbb{L}_{\mathrm{sh}}^{\mathrm{gl}} + DI_{\mathrm{sh}})^{-1}$. Static overlap formulas such as $g_{c\ell}(D)$ introduced later belong to a particular reduced evaluator and are not a second definition of the abstract glued-bath operator. Let $J_{\mathrm{sh}} : \mathbb{C} \to \mathcal{H}_{\mathrm{sh}}$ be the fixed shell source injection, chosen as part of the abstract shell-bath realization before the scalar branch is solved, and write

$$j_{\mathrm{sh}} := J_{\mathrm{sh}}(1) \in \mathcal{H}_{\mathrm{sh}}. \tag{186}$$

The source vector is not adjusted against a measured value of α or against any QED benchmark. Define the derivative trace by

$$T_\partial u := u'(1^-), \qquad u \in \mathrm{Dom}(K_0). \tag{187}$$

For notational brevity, set

$$\tau u := j_{\mathrm{sh}}\, T_\partial u \in \mathcal{H}_{\mathrm{sh}}, \qquad u \in \mathrm{Dom}(K_0). \tag{188}$$

Lemma 3 (Continuity of the boundary derivative functional)**.** *For every $u \in \mathrm{Dom}(K_0)$, expanded as*

$$u = \sum_{n\geq 1} u_n \phi_n, \qquad K_0 u = \sum_{n\geq 1} n^2 u_n \phi_n,$$

the derivative trace satisfies

$$T_\partial u = \sqrt{2}\,\pi \sum_{n\geq 1} (-1)^n n\, u_n \tag{189}$$

and the estimate

$$|T_\partial u| \leq \frac{\pi^2}{\sqrt{3}}\, \|K_0 u\|_{\mathcal{H}_{\mathrm{cav}}}. \tag{190}$$

In particular, T_∂ is continuous on $\mathrm{Dom}(K_0)$ equipped with the graph norm of K_0, and τ is a graph-norm continuous map from $\mathrm{Dom}(K_0)$ to $\mathcal{H}_{\mathrm{sh}}$.

Proof. Let

$$u_n := \langle u, \phi_n \rangle_{\mathcal{H}_{\mathrm{cav}}}, \qquad u = \sum_{n\ge 1} u_n \phi_n \quad \text{in } \mathcal{H}_{\mathrm{cav}}.$$

Since $u \in \mathrm{Dom}(K_0)$, the Fourier characterization of the Dirichlet domain proved in lemma 2 gives

$$K_0 u = \sum_{n\ge 1} n^2 u_n \phi_n \quad \text{in } \mathcal{H}_{\mathrm{cav}}, \qquad \sum_{n\ge 1} n^4 |u_n|^2 = \|K_0 u\|^2_{\mathcal{H}_{\mathrm{cav}}} < \infty.$$

For $N \ge 1$, set

$$u^{(N)} := \sum_{n=1}^{N} u_n \phi_n.$$

Then

$$\|u - u^{(N)}\|^2_{L^2(0,1)} = \sum_{n>N} |u_n|^2,$$

$$\|(u - u^{(N)})'\|^2_{L^2(0,1)} = \pi^2 \sum_{n>N} n^2 |u_n|^2,$$

$$\|(u - u^{(N)})''\|^2_{L^2(0,1)} = \pi^4 \sum_{n>N} n^4 |u_n|^2.$$

Hence $u^{(N)} \to u$ in $H^2(0,1)$. In one dimension, the trace map $H^2(0,1) \to \mathbb{C}$, $w \mapsto w'(1)$, is continuous. Therefore

$$T_\partial u = u'(1^-) = \lim_{N\to\infty} (u^{(N)})'(1).$$

Since

$$\phi_n'(1) = \sqrt{2}\, n\pi \cos(n\pi) = \sqrt{2}\, (-1)^n n\pi,$$

one has

$$(u^{(N)})'(1) = \sqrt{2}\,\pi \sum_{n=1}^{N} (-1)^n n\, u_n.$$

Moreover, by Cauchy–Schwarz,

$$\sum_{n\ge 1} |n\, u_n| = \sum_{n\ge 1} \frac{1}{n}\,(n^2 |u_n|) \le \left(\sum_{n\ge 1} \frac{1}{n^2}\right)^{1/2} \left(\sum_{n\ge 1} n^4 |u_n|^2\right)^{1/2} < \infty.$$

Hence the series for $T_\partial u$ converges absolutely, and passing to the limit $N \to \infty$ yields

$$T_\partial u = \sqrt{2}\,\pi \sum_{n\ge 1} (-1)^n n\, u_n,$$

which is Eq. (189).

Using the same identity and Cauchy–Schwarz again,

$$|T_\partial u| \le \sqrt{2}\,\pi \left(\sum_{n\ge 1} \frac{1}{n^2}\right)^{1/2} \left(\sum_{n\ge 1} n^4 |u_n|^2\right)^{1/2}.$$

Since

$$\sum_{n\ge 1}\frac{1}{n^2}=\frac{\pi^2}{6},\qquad \sum_{n\ge 1}n^4|u_n|^2=\|K_0u\|^2_{\mathcal{H}_{\mathrm{cav}}},$$

one obtains

$$|T_\partial u|\le \frac{\pi^2}{\sqrt{3}}\,\|K_0u\|_{\mathcal{H}_{\mathrm{cav}}},$$

which is Eq. (190). Since $\tau u=j_{\mathrm{sh}}T_\partial u$ with fixed $j_{\mathrm{sh}}\in\mathcal{H}_{\mathrm{sh}}$, the graph-norm continuity of τ follows immediately. □

Definition VI.10 (Mother cavity–shell saddle functional)**.** Let $x=\alpha/\pi>0$, where α is the symbolic compact-charge coupling variable, and let $\kappa>0$ be dimensionless, with the scalar slowdown written as

$$D=\mathcal{D}_{\mathrm{C}}=x\kappa.$$

The parameter κ is the scalar dilation unknown of the mother pencil, not a fitted constant. All operators and pairings in the reduced mother pencil are dimensionless. In particular, K_0, $V^{\mathrm{red}}_{\mathrm{bulk}}$, $\mathbb{L}^{\mathrm{gl}}_{\mathrm{sh}}$, and the shifted argument $x\kappa$ have been normalized by the pinned shell scales before the reduced pencil is written. Define the quadratic cavity–shell saddle functional by

$$\begin{aligned}\mathfrak{L}_{\mathrm{C}}[u,\chi_{\mathrm{sh}};\kappa,x]\coloneqq{}&\Big\langle u,\,\Big(K_0-\kappa^{-2}I_{\mathrm{cav}}+\frac{x}{\kappa}V^{\mathrm{red}}_{\mathrm{bulk}}\Big)\,u\Big\rangle_{\mathcal{H}_{\mathrm{cav}}}\\&-\Big\langle\chi_{\mathrm{sh}},(\mathbb{L}^{\mathrm{gl}}_{\mathrm{sh}}+x\kappa I_{\mathrm{sh}})\chi_{\mathrm{sh}}\Big\rangle_{\mathcal{H}_{\mathrm{sh}}}\\&-2\sqrt{\frac{x}{\kappa}}\,\eta_0\,\Re\Big(\overline{T_\partial u}\,\langle j_{\mathrm{sh}},\chi_{\mathrm{sh}}\rangle_{\mathcal{H}_{\mathrm{sh}}}\Big),\end{aligned}\tag{191}$$

where I_{sh} denotes the identity operator on $\mathcal{H}_{\mathrm{sh}}$, $u\in\mathrm{Dom}(K_0)$, and $\chi_{\mathrm{sh}}\in\mathrm{Dom}(\mathbb{L}^{\mathrm{gl}}_{\mathrm{sh}})$.

Proposition 31 (Mother cavity–shell pencil in weak form)**.** *The Euler–Lagrange equations of $\mathfrak{L}_{\mathrm{C}}$, understood in the sense of real Gâteaux variations along arbitrary complex directions, are*

$$(\mathbb{L}^{\mathrm{gl}}_{\mathrm{sh}}+x\kappa I_{\mathrm{sh}})\chi_{\mathrm{sh}}+\sqrt{\frac{x}{\kappa}}\,\eta_0\,\tau u=0,\tag{192}$$

and

$$\Big\langle v,\,\Big(K_0-\kappa^{-2}I_{\mathrm{cav}}+\frac{x}{\kappa}V^{\mathrm{red}}_{\mathrm{bulk}}\Big)\,u\Big\rangle_{\mathcal{H}_{\mathrm{cav}}}-\sqrt{\frac{x}{\kappa}}\,\eta_0\,\overline{T_\partial v}\,\langle j_{\mathrm{sh}},\chi_{\mathrm{sh}}\rangle_{\mathcal{H}_{\mathrm{sh}}}=0\tag{193}$$

for every $v\in\mathrm{Dom}(K_0)$.

Proof. Set

$$A_{x,\kappa}\coloneqq K_0-\kappa^{-2}I_{\mathrm{cav}}+\frac{x}{\kappa}V^{\mathrm{red}}_{\mathrm{bulk}},\qquad c_{x,\kappa}\coloneqq\sqrt{\frac{x}{\kappa}}\,\eta_0.$$

For $\zeta\in\mathrm{Dom}(\mathbb{L}^{\mathrm{gl}}_{\mathrm{sh}})$, consider the real variation $\chi_{\mathrm{sh}}\mapsto\chi_{\mathrm{sh}}+\varepsilon\zeta$, $\varepsilon\in\mathbb{R}$. Then

$$\frac{\mathrm{d}}{\mathrm{d}\varepsilon}\mathfrak{L}_{\mathrm{C}}[u,\chi_{\mathrm{sh}}+\varepsilon\zeta;\kappa,x]\Big|_{\varepsilon=0}=-2\,\Re\Big\langle\zeta,\,(\mathbb{L}^{\mathrm{gl}}_{\mathrm{sh}}+x\kappa I_{\mathrm{sh}})\chi_{\mathrm{sh}}+c_{x,\kappa}\,j_{\mathrm{sh}}T_\partial u\Big\rangle_{\mathcal{H}_{\mathrm{sh}}}.$$

Stationarity for every ζ implies, by testing with both ζ and $i\zeta$,

$$(\mathbb{L}^{\mathrm{gl}}_{\mathrm{sh}}+x\kappa I_{\mathrm{sh}})\chi_{\mathrm{sh}}+c_{x,\kappa}\,j_{\mathrm{sh}}T_\partial u=0,$$

which is Eq. (192), since $\tau u=j_{\mathrm{sh}}T_\partial u$.

Now let $v\in\mathrm{Dom}(K_0)$ and vary $u\mapsto u+\varepsilon v$, $\varepsilon\in\mathbb{R}$. One finds

$$\frac{\mathrm{d}}{\mathrm{d}\varepsilon}\mathfrak{L}_{\mathrm{C}}[u+\varepsilon v,\chi_{\mathrm{sh}};\kappa,x]\Big|_{\varepsilon=0}=2\,\Re\big(\langle v,A_{x,\kappa}u\rangle_{\mathcal{H}_{\mathrm{cav}}}-c_{x,\kappa}\,\overline{T_\partial v}\,\langle j_{\mathrm{sh}},\chi_{\mathrm{sh}}\rangle_{\mathcal{H}_{\mathrm{sh}}}\big).$$

Stationarity for every v, and again testing with both v and iv, gives

$$\langle v,A_{x,\kappa}u\rangle_{\mathcal{H}_{\mathrm{cav}}}-c_{x,\kappa}\,\overline{T_\partial v}\,\langle j_{\mathrm{sh}},\chi_{\mathrm{sh}}\rangle_{\mathcal{H}_{\mathrm{sh}}}=0,$$

which is Eq. (193). □

Remark. The sign pattern in Eqs. (192) and (193) is fixed by the saddle structure of $\mathfrak{L}_{\mathrm{C}}$. In particular, the shell variable χ_{sh} acts as a linear reaction field and must be eliminated by a Schur complement rather than by a naive positive-definite minimization.

Definition VI.11 (Scalar shell-memory function)**.** For every $D \geq 0$, define

$$m_{\mathrm{sh}}^{\mathrm{gl}}(D) := \left\langle j_{\mathrm{sh}}, (\mathbb{L}_{\mathrm{sh}}^{\mathrm{gl}} + DI_{\mathrm{sh}})^{-1} j_{\mathrm{sh}} \right\rangle_{\mathcal{H}_{\mathrm{sh}}}. \tag{194}$$

This is well defined at $D = 0$ because the strict lower bound in Eq. (185) makes $(\mathbb{L}_{\mathrm{sh}}^{\mathrm{gl}})^{-1}$ a bounded positive self-adjoint operator.

Lemma 4 (Exact elimination of the shell reaction field)**.** *If $x > 0$, $\kappa > 0$, and (u, χ_{sh}) satisfies Eqs.* (192) *and* (193)*, then*

$$\chi_{\mathrm{sh}} = -\sqrt{\frac{x}{\kappa}}\,\eta_0\,(\mathbb{L}_{\mathrm{sh}}^{\mathrm{gl}} + x\kappa I_{\mathrm{sh}})^{-1} \tau u. \tag{195}$$

Substitution into the cavity equation yields the reduced weak pencil

$$\left\langle v, \left(K_0 - \kappa^{-2} I_{\mathrm{cav}} + \frac{x}{\kappa} V_{\mathrm{bulk}}^{\mathrm{red}}\right) u \right\rangle_{\mathcal{H}_{\mathrm{cav}}} + \frac{x}{\kappa}\eta_0^2\, m_{\mathrm{sh}}^{\mathrm{gl}}(x\kappa)\, \overline{T_\partial v}\, T_\partial u = 0 \tag{196}$$

for every $v \in \mathrm{Dom}(K_0)$.

Proof. Equation (192) gives

$$(\mathbb{L}_{\mathrm{sh}}^{\mathrm{gl}} + x\kappa I_{\mathrm{sh}})\chi_{\mathrm{sh}} = -\sqrt{\frac{x}{\kappa}}\,\eta_0\,\tau u.$$

hence Eq. (195). Substituting this into Eq. (193), one finds

$$\left\langle v, \left(K_0 - \kappa^{-2} I_{\mathrm{cav}} + \frac{x}{\kappa} V_{\mathrm{bulk}}^{\mathrm{red}}\right) u \right\rangle_{\mathcal{H}_{\mathrm{cav}}} + \frac{x}{\kappa}\eta_0^2\, \overline{T_\partial v}\, \left\langle j_{\mathrm{sh}}, (\mathbb{L}_{\mathrm{sh}}^{\mathrm{gl}} + x\kappa I_{\mathrm{sh}})^{-1} j_{\mathrm{sh}} \right\rangle_{\mathcal{H}_{\mathrm{sh}}} T_\partial u = 0.$$

Using Eq. (194) yields Eq. (196). ☐

Remark. After elimination of the shell reaction field, the entire glued shell bath enters the reduced scalar problem only through the single scalar memory function $m_{\mathrm{sh}}^{\mathrm{gl}}(D)$, multiplying the boundary form $\overline{T_\partial v}\, T_\partial u$. This is the precise scalar Feshbach compression of the shell bath.

Definition VI.12 (Scalar shell-memory measure)**.** Let $E_{\mathbb{L}}(\sigma)$ be the spectral measure of $\mathbb{L}_{\mathrm{sh}}^{\mathrm{gl}}$, and let $j_{\mathrm{sh}} = J_{\mathrm{sh}}(1)$. Define the positive scalar measure

$$\mathrm{d}\mu_{\mathrm{sh}}^{\mathrm{gl}}(\sigma) := \left\langle j_{\mathrm{sh}}, \mathrm{d}E_{\mathbb{L}}(\sigma)\, j_{\mathrm{sh}} \right\rangle_{\mathcal{H}_{\mathrm{sh}}}. \tag{197}$$

Proposition 32 (Scalar Stieltjes shell-memory function)**.** *For every $D \geq 0$, the scalar shell-memory function Eq.* (194) *satisfies*

$$m_{\mathrm{sh}}^{\mathrm{gl}}(D) = \int_0^\infty \frac{\mathrm{d}\mu_{\mathrm{sh}}^{\mathrm{gl}}(\sigma)}{\sigma + D}. \tag{198}$$

Moreover, because J_{sh} is injective, one has $j_{\mathrm{sh}} = J_{\mathrm{sh}}(1) \neq 0$,

$$m_{\mathrm{sh}}^{\mathrm{gl}}(D) > 0 \qquad (D \geq 0), \tag{199}$$

and for every $D > 0$,

$$\frac{\mathrm{d}}{\mathrm{d}D} m_{\mathrm{sh}}^{\mathrm{gl}}(D) = -\int_0^\infty \frac{\mathrm{d}\mu_{\mathrm{sh}}^{\mathrm{gl}}(\sigma)}{(\sigma + D)^2} < 0. \tag{200}$$

Proof. By the spectral theorem,

$$(\mathbb{L}_{\mathrm{sh}}^{\mathrm{gl}} + DI_{\mathrm{sh}})^{-1} = \int_0^\infty \frac{\mathrm{d}E_{\mathbb{L}}(\sigma)}{\sigma + D}.$$

Hence

$$m_{\mathrm{sh}}^{\mathrm{gl}}(D) = \left\langle j_{\mathrm{sh}}, \left(\int_0^\infty \frac{\mathrm{d}E_{\mathbb{L}}(\sigma)}{\sigma + D}\right) j_{\mathrm{sh}} \right\rangle = \int_0^\infty \frac{\langle j_{\mathrm{sh}}, \mathrm{d}E_{\mathbb{L}}(\sigma) j_{\mathrm{sh}}\rangle}{\sigma + D},$$

which proves Eq. (198).

Since $\mathbb{L}_{\mathrm{sh}}^{\mathrm{gl}} > 0$, the measure $\mu_{\mathrm{sh}}^{\mathrm{gl}}$ is positive and finite, with total mass

$$\mu_{\mathrm{sh}}^{\mathrm{gl}}([0,\infty)) = \langle j_{\mathrm{sh}}, j_{\mathrm{sh}}\rangle_{\mathcal{H}_{\mathrm{sh}}} = \|j_{\mathrm{sh}}\|_{\mathcal{H}_{\mathrm{sh}}}^2 < \infty.$$

Because J_{sh} is an injection, one has $j_{\mathrm{sh}} \neq 0$, hence $\mu_{\mathrm{sh}}^{\mathrm{gl}}$ is not the zero measure. Since $\mathbb{L}_{\mathrm{sh}}^{\mathrm{gl}} \geq c_{\mathrm{sh}} I_{\mathrm{sh}}$, the support of $\mu_{\mathrm{sh}}^{\mathrm{gl}}$ is contained in $[c_{\mathrm{sh}}, \infty)$. Therefore for every $D \geq 0$,

$$\frac{1}{\sigma + D} > 0 \qquad \text{on } \operatorname{supp} \mu_{\mathrm{sh}}^{\mathrm{gl}},$$

and the integral

$$m_{\mathrm{sh}}^{\mathrm{gl}}(D) = \int_0^\infty \frac{\mathrm{d}\mu_{\mathrm{sh}}^{\mathrm{gl}}(\sigma)}{\sigma + D}$$

is strictly positive. This proves Eq. (199) including $D = 0$.

For differentiation, fix $D_0 \geq 0$. Since $\sigma \geq c_{\mathrm{sh}} > 0$ on the support, for D in a sufficiently small neighborhood of D_0 inside $[0, \infty)$ one has

$$\frac{1}{(\sigma + D)^2} \leq \frac{1}{c_{\mathrm{sh}}^2}.$$

The right-hand side is integrable with respect to the finite measure $\mu_{\mathrm{sh}}^{\mathrm{gl}}$. Dominated convergence therefore justifies differentiation for $D > 0$, and also gives the right derivative at $D = 0$. Hence

$$\frac{\mathrm{d}}{\mathrm{d}D} m_{\mathrm{sh}}^{\mathrm{gl}}(D) = -\int_0^\infty \frac{\mathrm{d}\mu_{\mathrm{sh}}^{\mathrm{gl}}(\sigma)}{(\sigma + D)^2} \qquad (D > 0).$$

Since $\mu_{\mathrm{sh}}^{\mathrm{gl}}$ is a nonzero positive measure and $(\sigma + D)^{-2} > 0$ on its support, the derivative is strictly negative:

$$\frac{\mathrm{d}}{\mathrm{d}D} m_{\mathrm{sh}}^{\mathrm{gl}}(D) < 0 \qquad (D > 0).$$

This proves Eq. (200). ☐

Theorem 7 (Mother pencil and reduced weak pencil)**.** *Let $x = \alpha/\pi > 0$, with α the symbolic compact-charge coupling variable, and let $\kappa > 0$ with $\mathcal{D}_{\mathrm{C}} = x\kappa$. The following two conditions are equivalent.*

$$\exists\, (u, \chi_{\mathrm{sh}}) \neq (0,0) \ \textit{such that}\ (192)\ \textit{and}\ (193)\ \textit{hold.} \tag{201}$$

$$\exists\, u \neq 0 \ \textit{such that}\ (196)\ \textit{holds.} \tag{202}$$

Moreover, for every nontrivial reduced solution u, the shell reaction field is reconstructed uniquely by Eq. (195)*. Since $\mathbb{L}_{\mathrm{sh}}^{\mathrm{gl}} + x\kappa I_{\mathrm{sh}} > 0$, one has $u = 0 \Rightarrow \chi_{\mathrm{sh}} = 0$, so every nontrivial mother solution has $u \neq 0$.*

Proof. By lemma 4, every nontrivial mother solution (u, χ_{sh}) satisfies the reduced weak pencil Eq. (196).

Conversely, let $u \neq 0$ satisfy Eq. (196). Define

$$\chi_{\mathrm{sh}} := -\sqrt{\frac{x}{\kappa}}\, \eta_0\, (\mathbb{L}_{\mathrm{sh}}^{\mathrm{gl}} + x\kappa I_{\mathrm{sh}})^{-1} \tau u.$$

Since

$$\mathbb{L}_{\mathrm{sh}}^{\mathrm{gl}} + x\kappa I_{\mathrm{sh}} \geq (c_{\mathrm{sh}} + x\kappa) I_{\mathrm{sh}} > 0,$$

this operator is self-adjoint and boundedly invertible. Its inverse maps $\mathcal{H}_{\mathrm{sh}}$ into $\mathrm{Dom}(\mathbb{L}_{\mathrm{sh}}^{\mathrm{gl}})$. Hence $\chi_{\mathrm{sh}} \in \mathrm{Dom}(\mathbb{L}_{\mathrm{sh}}^{\mathrm{gl}})$. By construction, Eq. (192) holds. Substituting the same χ_{sh} into Eq. (193) reproduces Eq. (196). Therefore the pair (u, χ_{sh}) satisfies Eqs. (192) and (193). This proves the equivalence of Eq. (201) and Eq. (202).

If $u = 0$, then Eq. (192) reduces to

$$(\mathbb{L}_{\mathrm{sh}}^{\mathrm{gl}} + x\kappa I_{\mathrm{sh}})\chi_{\mathrm{sh}} = 0.$$

Since $\mathbb{L}_{\mathrm{sh}}^{\mathrm{gl}} + x\kappa I_{\mathrm{sh}}$ is strictly positive, its kernel is trivial, so $\chi_{\mathrm{sh}} = 0$. Hence every nontrivial mother solution must have $u \neq 0$. □

Definition VI.13 (Physical scalar branch selection)**.** For fixed $x > 0$ and $\kappa > 0$, with $x = \alpha/\pi$ treated as an unknown symbolic coupling variable, define the reduced scalar Rayleigh functional

$$\mathcal{R}_{x,\kappa}[u] := \frac{\langle u, K_0 u\rangle_{\mathcal{H}_{\mathrm{cav}}} + \dfrac{x}{\kappa}\langle u, V_{\mathrm{bulk}}^{\mathrm{red}} u\rangle_{\mathcal{H}_{\mathrm{cav}}} + \dfrac{x}{\kappa}\eta_0^2 m_{\mathrm{sh}}^{\mathrm{gl}}(x\kappa)\, |T_\partial u|^2}{\|u\|_{\mathcal{H}_{\mathrm{cav}}}^2}, \qquad u \in \mathrm{Dom}(K_0) \setminus \{0\}. \tag{203}$$

By Eq. (190), the boundary term $|T_\partial u|^2$ is finite for every $u \in \mathrm{Dom}(K_0)$. Since $K_0 \geq 0$, $V_{\mathrm{bulk}}^{\mathrm{red}}(y) = 3 - y^2 \geq 2$ on $[0, 1]$, and $m_{\mathrm{sh}}^{\mathrm{gl}}(x\kappa) > 0$, the numerator is nonnegative and the functional is well defined.

The scalar mother branch used later in the primary closure is selected in two steps. First, for the given $x > 0$ and $\kappa > 0$, one requires the existence of a nontrivial reduced-pencil state $u \in \mathrm{Dom}(K_0) \setminus \{0\}$ satisfying Eq. (196). Second, among all such branches at fixed x, one selects the ground-state branch by imposing

$$\inf_{u \in \mathrm{Dom}(K_0)\setminus\{0\}} \mathcal{R}_{x,\kappa}[u] = \kappa^{-2}, \qquad \mathcal{D}_{\mathrm{C}} = x\kappa. \tag{204}$$

together with the Coulomb-anchor condition

$$\kappa(x) \to 1 \qquad \text{as } x \downarrow 0,$$

equivalently

$$\mathcal{D}_{\mathrm{C}}(x) = x + o(x) \qquad (x \downarrow 0).$$

This is the scalar branch-selection rule of the glued mother pencil, not a reduced numerical proxy and not a fit to a measured value of α.

Remark. The quotient $\mathcal{R}_{x,\kappa}$ is the scalar quadratic quotient associated with the reduced weak pencil Eq. (196). If $u \neq 0$ satisfies Eq. (196), then choosing $v = u$ gives

$$\begin{aligned} 0 &= \left\langle u, \left(K_0 - \kappa^{-2} I_{\mathrm{cav}} + \frac{x}{\kappa} V_{\mathrm{bulk}}^{\mathrm{red}}\right) u \right\rangle_{\mathcal{H}_{\mathrm{cav}}} + \frac{x}{\kappa}\eta_0^2 m_{\mathrm{sh}}^{\mathrm{gl}}(x\kappa)\, |T_\partial u|^2 \\ &= \langle u, K_0 u\rangle_{\mathcal{H}_{\mathrm{cav}}} + \frac{x}{\kappa}\langle u, V_{\mathrm{bulk}}^{\mathrm{red}} u\rangle_{\mathcal{H}_{\mathrm{cav}}} + \frac{x}{\kappa}\eta_0^2 m_{\mathrm{sh}}^{\mathrm{gl}}(x\kappa)\, |T_\partial u|^2 - \kappa^{-2}\|u\|_{\mathcal{H}_{\mathrm{cav}}}^2. \end{aligned}$$

Hence

$$\mathcal{R}_{x,\kappa}[u] = \kappa^{-2}.$$

The infimum condition in Eq. (204) is therefore an additional ground-state selection among nontrivial reduced-pencil branches at fixed x. No separate bounded self-adjoint operator on $\mathcal{H}_{\mathrm{cav}}$ is asserted here. The selection is carried directly by the weak pencil on $\mathrm{Dom}(K_0)$, whose derivative trace is controlled by Eq. (190). No form-domain extension to $\mathrm{Dom}(K_0^{1/2})$ is assumed here. Finite-dimensional or reduced evaluators introduced later implement this weak-pencil selection; they do not replace it.

D. Exact Feshbach reduction and ground-line law

The mother pencil is exact at the operator level, whereas its Feshbach reduction still carries operator-valued excited-sector data. To connect this structure to the scalar coefficient series, we first derive Feshbach laws that are exact on specified finite-dimensional Galerkin subspaces and then state the infinite-rank ground-line scalar law under the corresponding excited-sector block hypothesis. No measured value of α, no QED coefficient, and no finite-rank numerical proxy enters this reduction.

Definition VI.14 (Exact cavity matrix elements)**.** For each $D \geq 0$, with $D = 0$ interpreted through the bounded inverse $(\mathbb{L}_{\mathrm{sh}}^{\mathrm{gl}})^{-1}$ guaranteed by the strict lower bound Eq. (185), define the shell-memory matrix elements by

$$\widetilde{C}^{\mathrm{gl}}_{mn}(D) := \big\langle \tau\phi_m,\, (\mathbb{L}_{\mathrm{sh}}^{\mathrm{gl}} + DI_{\mathrm{sh}})^{-1}\tau\phi_n \big\rangle_{\mathcal{H}_{\mathrm{sh}}}, \qquad m, n \geq 1. \tag{205}$$

Then define the renormalized cavity matrix by

$$B_{mn}(D) := (V^{\mathrm{red}}_{\mathrm{bulk}})_{mn} + \eta_0^2\, \widetilde{C}^{\mathrm{gl}}_{mn}(D), \qquad m, n \geq 1. \tag{206}$$

Lemma 5 (Explicit shell-memory matrix elements)**.** *For every $D \geq 0$,*

$$\widetilde{C}^{\mathrm{gl}}_{mn}(D) = \overline{T\partial\phi_m}\, T\partial\phi_n\, m^{\mathrm{gl}}_{\mathrm{sh}}(D) = 2\pi^2 mn(-1)^{m+n}\, m^{\mathrm{gl}}_{\mathrm{sh}}(D). \tag{207}$$

Proof. By definition,

$$\tau\phi_n = j_{\mathrm{sh}}\, T\partial\phi_n.$$

Hence

$$\widetilde{C}^{\mathrm{gl}}_{mn}(D) = \big\langle j_{\mathrm{sh}} T\partial\phi_m,\, (\mathbb{L}_{\mathrm{sh}}^{\mathrm{gl}} + DI_{\mathrm{sh}})^{-1} j_{\mathrm{sh}} T\partial\phi_n \big\rangle_{\mathcal{H}_{\mathrm{sh}}} = \overline{T\partial\phi_m}\, T\partial\phi_n\, m^{\mathrm{gl}}_{\mathrm{sh}}(D).$$

Using Eq. (189) on the basis vectors,

$$T\partial\phi_n = \sqrt{2}\,\pi(-1)^n n,$$

so

$$\overline{T\partial\phi_m}\, T\partial\phi_n = 2\pi^2 mn(-1)^{m+n}.$$

This proves Eq. (207). $\square$

Lemma 6 (Reduced bulk matrix elements)**.** *For the reduced bulk potential $V^{\mathrm{red}}_{\mathrm{bulk}}(y) = 3 - y^2$,*

$$(V^{\mathrm{red}}_{\mathrm{bulk}})_{nn} = \frac{8}{3} + \frac{1}{2n^2\pi^2}, \tag{208}$$

and for $m \neq n$,

$$(V^{\mathrm{red}}_{\mathrm{bulk}})_{mn} = -\frac{8mn(-1)^{m+n}}{\pi^2(m^2 - n^2)^2}. \tag{209}$$

In particular,

$$(V^{\mathrm{red}}_{\mathrm{bulk}})_{11} = \frac{8}{3} + \frac{1}{2\pi^2} = 2\pi C_{\mathrm{uni}}. \tag{210}$$

Proof. By Eq. (149),

$$(V^{\mathrm{red}}_{\mathrm{bulk}})_{mn} = 2\int_0^1 (3 - y^2)\sin(m\pi y)\sin(n\pi y)\,\mathrm{d}y.$$

If $m = n$, then

$$(V^{\mathrm{red}}_{\mathrm{bulk}})_{nn} = 6\int_0^1 \sin^2(n\pi y)\,\mathrm{d}y - 2\int_0^1 y^2\sin^2(n\pi y)\,\mathrm{d}y.$$

Using

$$\int_0^1 \sin^2(n\pi y)\,\mathrm{d}y = \frac{1}{2}$$

and

$$\int_0^1 y^2 \sin^2(n\pi y)\,\mathrm{d}y = \frac{1}{6} - \frac{1}{4n^2\pi^2},$$

we obtain

$$(V_{\mathrm{bulk}}^{\mathrm{red}})_{nn} = 6 \cdot \frac{1}{2} - 2\left(\frac{1}{6} - \frac{1}{4n^2\pi^2}\right) = \frac{8}{3} + \frac{1}{2n^2\pi^2},$$

which proves Eq. (208).

If $m \neq n$, the constant part vanishes by the explicit Dirichlet orthogonality calculation

$$\begin{aligned}\int_0^1 \sin(m\pi y)\sin(n\pi y)\,\mathrm{d}y &= \frac{1}{2}\int_0^1 \Big[\cos((m-n)\pi y) - \cos((m+n)\pi y)\Big]\mathrm{d}y \\ &= \frac{1}{2}\left[\frac{\sin((m-n)\pi y)}{(m-n)\pi} - \frac{\sin((m+n)\pi y)}{(m+n)\pi}\right]_0^1 = 0,\end{aligned}$$

because $m \pm n$ are nonzero integers and $\sin(k\pi) = 0$ for every $k \in \mathbb{Z}$. Hence only the y^2-term remains:

$$(V_{\mathrm{bulk}}^{\mathrm{red}})_{mn} = -2\int_0^1 y^2 \sin(m\pi y)\sin(n\pi y)\,\mathrm{d}y.$$

Using

$$\sin(m\pi y)\sin(n\pi y) = \frac{1}{2}\Big(\cos((m-n)\pi y) - \cos((m+n)\pi y)\Big),$$

we get

$$\int_0^1 y^2 \sin(m\pi y)\sin(n\pi y)\,\mathrm{d}y = \frac{1}{2}\int_0^1 y^2\cos((m-n)\pi y)\,\mathrm{d}y - \frac{1}{2}\int_0^1 y^2\cos((m+n)\pi y)\,\mathrm{d}y.$$

For any nonzero integer k,

$$\int_0^1 y^2\cos(k\pi y)\,\mathrm{d}y = \left[\frac{y^2\sin(k\pi y)}{k\pi} + \frac{2y\cos(k\pi y)}{(k\pi)^2} - \frac{2\sin(k\pi y)}{(k\pi)^3}\right]_0^1 = \frac{2(-1)^k}{k^2\pi^2}.$$

Hence

$$\int_0^1 y^2 \sin(m\pi y)\sin(n\pi y)\,\mathrm{d}y = \frac{(-1)^{m+n}}{\pi^2}\left(\frac{1}{(m-n)^2} - \frac{1}{(m+n)^2}\right) = \frac{4mn(-1)^{m+n}}{\pi^2(m^2-n^2)^2}.$$

Therefore

$$(V_{\mathrm{bulk}}^{\mathrm{red}})_{mn} = -\frac{8mn(-1)^{m+n}}{\pi^2(m^2-n^2)^2},$$

which proves Eq. (209). Equation (210) is the case $n = 1$ of Eq. (208). □

Definition VI.15 (Excited-shell gaps)**.** For $n \geq 2$, define the reduced excited-shell gaps

$$\Delta_n := n^2 - 1. \tag{211}$$

Proposition 33 (Exact finite-rank Feshbach law)**.** *Let $x > 0$, $D > 0$, and $N \geq 2$. Restrict the reduced weak pencil Eq.* (196) *to the Galerkin subspace*

$$\mathcal{H}_N := \operatorname{span}\{\phi_1, \dots, \phi_N\},$$

by taking both trial and test functions in $\mathcal{H}_N$. Writing the scalar relation $D = \mathcal{D}_\mathrm{C} = x\kappa$, equivalently $\kappa = D/x$, the resulting finite-dimensional coefficient matrix is

$$[M_N(D; x)]_{mn} := \left(n^2 - \frac{x^2}{D^2}\right)\delta_{mn} + \frac{x^2}{D}\, B_{mn}(D), \qquad 1 \leq m, n \leq N. \tag{212}$$

Since $V_\mathrm{bulk}^\mathrm{red}$ is a real self-adjoint multiplication operator and, by Eq. (207)*,*

$$\widetilde{C}^\mathrm{gl}_{mn}(D) = 2\pi^2 mn(-1)^{m+n} m^\mathrm{gl}_\mathrm{sh}(D) = \widetilde{C}^\mathrm{gl}_{nm}(D),$$

the matrix $M_N(D; x)$ is real symmetric. Write M_N in block form relative to $1 \oplus E$, where $E = \{2, \dots, N\}$:

$$M_N = \begin{pmatrix} M^{(N)}_{11} & M^{(N)}_{1E} \\ M^{(N)}_{E1} & M^{(N)}_{EE} \end{pmatrix}.$$

Whenever $M^{(N)}_{EE}(D; x)$ is invertible, the restricted Galerkin system admits a nontrivial solution $u_N = \sum_{n=1}^N a_n \phi_n$ with $a_1 \neq 0$ if and only if

$$F_N(D; x) := M^{(N)}_{11}(D; x) - M^{(N)}_{1E}(D; x)\big(M^{(N)}_{EE}(D; x)\big)^{-1} M^{(N)}_{E1}(D; x) = 0. \tag{213}$$

This condition is exact on the chosen Galerkin subspace. It is not yet the infinite-rank scalar branch law.

Proof. Let

$$u_N = \sum_{n=1}^N a_n \phi_n \in \mathcal{H}_N.$$

Testing the reduced weak pencil Eq. (196) against $v = \phi_m$, $1 \leq m \leq N$, gives

$$\sum_{n=1}^N \left[\left(n^2 - \frac{x^2}{D^2}\right)\delta_{mn} + \frac{x^2}{D} B_{mn}(D)\right] a_n = 0, \qquad 1 \leq m \leq N,$$

which is exactly the matrix system $M_N(D; x)a = 0$.

Writing $a = (a_1, a_E)^T$, the block system is

$$M^{(N)}_{11} a_1 + M^{(N)}_{1E} a_E = 0, \qquad M^{(N)}_{E1} a_1 + M^{(N)}_{EE} a_E = 0.$$

If $M^{(N)}_{EE}$ is invertible, then

$$a_E = -\big(M^{(N)}_{EE}\big)^{-1} M^{(N)}_{E1} a_1.$$

Substitution into the first block equation yields

$$\Big[M^{(N)}_{11} - M^{(N)}_{1E}\big(M^{(N)}_{EE}\big)^{-1} M^{(N)}_{E1}\Big] a_1 = 0.$$

For $a_1 \neq 0$, this is equivalent to Eq. (213). Conversely, if Eq. (213) holds, one reconstructs a nontrivial Galerkin solution with $a_1 \neq 0$ by the same formula for a_E. □

Definition VI.16 (Infinite excited-sector coefficient blocks)**.** Let $\mathscr{C} \subset \mathbb{C}^\mathbb{N}$ denote the space of finitely supported coefficient sequences in the Dirichlet basis $\{\phi_n\}_{n \geq 1}$, and decompose it as

$$\mathscr{C} = \mathbb{C}e_1 \oplus \mathscr{C}(E), \qquad E = \{2, 3, \dots\}.$$

For each $D > 0$, let $B(D)$ denote the formal infinite matrix with entries $B_{mn}(D)$. At this stage the notation records only coefficient blocks; operator realization is imposed separately in proposition 34. Relative to the above decomposition, write

$$B(D) = \begin{pmatrix} B_{11}(D) & B_{1E}(D) \\ B_{E1}(D) & B_{EE}(D) \end{pmatrix}.$$

On the finitely supported excited-sector sequences, define

$$\Delta \equiv \operatorname{diag}(\Delta_n)_{n\geq 2}, \qquad \Delta_n = n^2 - 1. \tag{214}$$

In any Hilbert coefficient-space realization used below, Δ is understood as the positive self-adjoint multiplication operator associated with this diagonal sequence, with its natural domain.

Proposition 34 (Conditional exact ground-line scalar law)**.** *Let*

$$\varrho(D; x) \equiv 1 - \frac{x^2}{D^2}.$$

Assume that, for the given $D > 0$ and $x > 0$, the reduced weak pencil admits an exact coefficient realization on a Hilbert coefficient space

$$\mathfrak{h} = \mathbb{C}e_1 \oplus \mathfrak{h}(E), \qquad I_E := \mathrm{Id}_{\mathfrak{h}(E)},$$

containing the finitely supported sequences. In this realization, Δ is the positive self-adjoint multiplication operator defined by Eq. (214) *on its natural domain* $\mathrm{Dom}(\Delta) \subset \mathfrak{h}(E)$*. The formal blocks $B_{1E}(D)$, $B_{E1}(D)$, and $B_{EE}(D)$ extend to bounded maps*

$$B_{1E}(D) : \mathfrak{h}(E) \to \mathbb{C}, \qquad B_{E1}(D) : \mathbb{C} \to \mathfrak{h}(E), \qquad B_{EE}(D) : \mathfrak{h}(E) \to \mathfrak{h}(E).$$

Assume moreover that the excited-sector operator

$$M_{EE}(D; x) = \Delta + \varrho(D; x) I_E + \frac{x^2}{D} B_{EE}(D), \qquad \mathrm{Dom}(M_{EE}) = \mathrm{Dom}(\Delta),$$

is self-adjoint on $\mathfrak{h}(E)$ and has a bounded inverse on $\mathfrak{h}(E)$. Assume also that the selected scalar branch has nonzero ground-line coefficient $a_1 \neq 0$. Then the Schur scalar

$$\mathcal{Q}_E(D; x) := B_{1E}(D) \Big[\Delta + \varrho(D; x) I_E + \frac{x^2}{D} B_{EE}(D)\Big]^{-1} B_{E1}(D) \tag{215}$$

is well defined, and the ground-line equation is

$$\mathcal{D}_{\mathrm{C}} = x\sqrt{1 - \mathcal{D}_{\mathrm{C}}\, B_{11}(\mathcal{D}_{\mathrm{C}}) + x^2 \mathcal{Q}_E(\mathcal{D}_{\mathrm{C}}; x)}. \tag{216}$$

The positive square-root branch is selected by $\mathcal{D}_{\mathrm{C}}/x > 0$, equivalently by $\mathcal{D}_{\mathrm{C}} \sim x$ as $x \downarrow 0$. The symbol $\mathcal{Q}_E$ denotes an excited-sector Schur scalar. It is unrelated to the branch charge Q, to the charge scale q_0, and to any QED coefficient.

Proof. Under the stated coefficient-space hypothesis, let

$$a = a_1 e_1 + a_E \in \mathfrak{h}, \qquad a_1 \in \mathbb{C}, \qquad a_E \in \mathfrak{h}(E),$$

be the coefficient vector of the selected branch. By hypothesis, $a_1 \neq 0$, and the reduced weak pencil has the coefficient realization

$$M(D; x)_{mn} := \left(n^2 - \frac{x^2}{D^2}\right) \delta_{mn} + \frac{x^2}{D} B_{mn}(D), \qquad m, n \geq 1. \tag{217}$$

Relative to the decomposition $\mathfrak{h} = \mathbb{C}e_1 \oplus \mathfrak{h}(E)$, the equation

$$M(D; x) a = 0$$

is the block system

$$M_{11}(D; x) a_1 + M_{1E}(D; x) a_E = 0, \tag{218}$$

$$M_{E1}(D;x)a_1 + M_{EE}(D;x)a_E = 0. \tag{219}$$

The blocks are

$$M_{11}(D;x) = 1 - \frac{x^2}{D^2} + \frac{x^2}{D}B_{11}(D),$$

$$M_{1E}(D;x) = \frac{x^2}{D}B_{1E}(D), \qquad M_{E1}(D;x) = \frac{x^2}{D}B_{E1}(D),$$

and

$$M_{EE}(D;x) = \Delta + \varrho(D;x)I_E + \frac{x^2}{D}B_{EE}(D), \qquad \mathrm{Dom}(M_{EE}) = \mathrm{Dom}(\Delta).$$

Since $M_{EE}(D;x)$ is boundedly invertible on $\mathfrak{h}(E)$, Eq. (219) gives

$$a_E = -M_{EE}(D;x)^{-1}M_{E1}(D;x)a_1.$$

Substituting this expression into Eq. (218) yields

$$\Big[M_{11}(D;x) - M_{1E}(D;x)M_{EE}(D;x)^{-1}M_{E1}(D;x)\Big]a_1 = 0.$$

Because $a_1 \neq 0$, the Schur complement condition is

$$M_{11}(D;x) - M_{1E}(D;x)M_{EE}(D;x)^{-1}M_{E1}(D;x) = 0.$$

Substituting the explicit block formulas gives

$$1 - \frac{x^2}{D^2} + \frac{x^2}{D}B_{11}(D) - \frac{x^4}{D^2}B_{1E}(D)\Big[\Delta + \varrho(D;x)I_E + \frac{x^2}{D}B_{EE}(D)\Big]^{-1}B_{E1}(D) = 0.$$

By Eq. (215), this is

$$1 - \frac{x^2}{D^2} + \frac{x^2}{D}B_{11}(D) - \frac{x^4}{D^2}\mathcal{Q}_E(D;x) = 0.$$

Rearranging gives

$$\frac{D^2}{x^2} = 1 - D\,B_{11}(D) + x^2\mathcal{Q}_E(D;x).$$

Since $D > 0$ and $x > 0$, the right-hand side is

$$1 - D\,B_{11}(D) + x^2\mathcal{Q}_E(D;x) = \left(\frac{D}{x}\right)^2 > 0.$$

Hence the square root is real on the selected branch, and its positive value is uniquely fixed by

$$\sqrt{1 - D\,B_{11}(D) + x^2\mathcal{Q}_E(D;x)} = \frac{D}{x}.$$

Setting $D = \mathcal{D}_{\mathrm{C}}$ gives

$$\mathcal{D}_{\mathrm{C}} = x\sqrt{1 - \mathcal{D}_{\mathrm{C}}\,B_{11}(\mathcal{D}_{\mathrm{C}}) + x^2\mathcal{Q}_E(\mathcal{D}_{\mathrm{C}};x)},$$

which is Eq. (216). □

Remark (Exact versus purely ground-line reductions). Equation (216) is exact at the level of the ground-line Schur reduction, provided the coefficient-space realization and the excited-sector inverse in Eq. (215) exist. It is therefore stronger than the purely ground-line Stieltjes reduction obtained by discarding the excited cavity sector altogether. The latter is only a Rayleigh reduction on span$\{\phi_1\}$, whereas Eq. (216) still carries the excited-cavity Schur complement through $\mathcal{Q}_E$. It nevertheless remains conditional on the stated excited-sector hypothesis.

Definition VI.17 (Low-order scalar invariants)**.** By Eqs. (206), (207) and (210),

$$B_{11}(D) = 2\pi C_{\mathrm{uni}} + 2\pi^2\eta_0^2\, m_{\mathrm{sh}}^{\mathrm{gl}}(D).$$

Since $\mathbb{L}_{\mathrm{sh}}^{\mathrm{gl}} \geq c_{\mathrm{sh}} I_{\mathrm{sh}}$, the measure $\mu_{\mathrm{sh}}^{\mathrm{gl}}$ is supported in $[c_{\mathrm{sh}}, \infty)$. Hence, for $|D| < c_{\mathrm{sh}}$,

$$\frac{1}{\sigma + D} = \sum_{m\geq 0} \frac{(-D)^m}{\sigma^{m+1}}, \qquad \sigma \in \operatorname{supp} \mu_{\mathrm{sh}}^{\mathrm{gl}},$$

with uniform absolute convergence on the support. Using the Stieltjes representation Eq. (198), one obtains

$$m_{\mathrm{sh}}^{\mathrm{gl}}(D) = \sum_{m\geq 0} (-D)^m \int_0^\infty \sigma^{-m-1}\, \mathrm{d}\mu_{\mathrm{sh}}^{\mathrm{gl}}(\sigma), \qquad |D| < c_{\mathrm{sh}}.$$

Therefore $m_{\mathrm{sh}}^{\mathrm{gl}}$, and hence B_{11}, are real-analytic at $D = 0$.

Assume in addition that the composed excited-sector quantity $\mathcal{Q}_E(\mathcal{D}_{\mathrm{C}}(x); x)$ admits an expansion at $x = 0$ along the selected scalar branch. This is the only local expansion hypothesis still required for coefficient extraction; it is not an additional input to the scalar mother law. Write

$$B_{11}(D) = \sum_{m\geq 0} \beta_m D^m, \qquad \mathcal{Q}_E(\mathcal{D}_{\mathrm{C}}(x); x) = \mathfrak{q}_0 + \mathfrak{q}_1 x + \mathfrak{q}_2 x^2 + \cdots, \tag{220}$$

The coefficients $\mathfrak{q}_0, \mathfrak{q}_1, \mathfrak{q}_2, \ldots$ are excited-sector Schur coefficients and are unrelated to the gauge charge scale q_0, to the branch charge Q, and to QED perturbative coefficients. Write also

$$\mathcal{D}_{\mathrm{C}}(x) = \sum_{n\geq 1} c_n x^n, \qquad c_1 = 1. \tag{221}$$

Corollary 4 (Low-order coefficients of the scalar branch)**.** *Under the local expansion hypotheses in Eqs.* (220) *and* (221)*, the following are the coefficient identities of the formal power-series solution of Eq.* (216) *selected by* $c_1 = 1$*. If the series in Eqs.* (220) *and* (221) *converge in a neighborhood of* $x = 0$*, the same identities hold for the corresponding Taylor coefficients in that neighborhood. The first coefficients are*

$$c_2 = -\frac{\beta_0}{2}, \qquad c_3 = \frac{\beta_0^2}{8} - \frac{\beta_1}{2} + \frac{\mathfrak{q}_0}{2}, \qquad c_4 = \frac{\beta_0\beta_1}{2} - \frac{\beta_2}{2} + \frac{\mathfrak{q}_1}{2}, \tag{222}$$

and

$$c_5 = -\frac{\beta_0^4}{128} - \frac{3\beta_0^2\beta_1}{16} - \frac{\beta_0^2\mathfrak{q}_0}{16} + \frac{3\beta_0\beta_2}{4} + \frac{3\beta_1^2}{8} - \frac{\beta_1\mathfrak{q}_0}{4} - \frac{\beta_3}{2} - \frac{\mathfrak{q}_0^2}{8} + \frac{\mathfrak{q}_2}{2}. \tag{223}$$

Proof. Working formally in x, and analytically for sufficiently small x whenever the displayed series converge, write

$$\mathcal{D}_{\mathrm{C}}(x) = x + c_2 x^2 + c_3 x^3 + c_4 x^4 + c_5 x^5 + \cdots,$$

$$B_{11}(D) = \beta_0 + \beta_1 D + \beta_2 D^2 + \beta_3 D^3 + \cdots.$$

Squaring Eq. (216) gives

$$\left(\frac{\mathcal{D}_{\mathrm{C}}(x)}{x}\right)^2 = 1 - \mathcal{D}_{\mathrm{C}}(x)\, B_{11}(\mathcal{D}_{\mathrm{C}}(x)) + x^2 \mathcal{Q}_E(\mathcal{D}_{\mathrm{C}}(x); x). \tag{224}$$

Now

$$\left(\frac{\mathcal{D}_{\mathrm{C}}(x)}{x}\right)^2 = \left(1 + c_2 x + c_3 x^2 + c_4 x^3 + c_5 x^4 + \cdots\right)^2$$

$$= 1 + 2c_2 x + (c_2^2 + 2c_3)x^2 + (2c_2c_3 + 2c_4)x^3 + (2c_2c_4 + c_3^2 + 2c_5)x^4 + \cdots.$$

On the right-hand side of Eq. (224),

$$\mathcal{D}_{\mathrm{C}}(x)\,B_{11}(\mathcal{D}_{\mathrm{C}}(x)) = \beta_0 x + (\beta_0 c_2 + \beta_1)x^2 + (\beta_0 c_3 + 2\beta_1 c_2 + \beta_2)x^3$$

$$+(\beta_0 c_4 + \beta_1 c_2^2 + 2\beta_1 c_3 + 3\beta_2 c_2 + \beta_3)x^4 + \cdots,$$

so

$$1 - \mathcal{D}_{\mathrm{C}}(x)\,B_{11}(\mathcal{D}_{\mathrm{C}}(x)) + x^2 \mathcal{Q}_E(\mathcal{D}_{\mathrm{C}}(x); x) = 1 - \beta_0 x$$

$$+\big(-\beta_0 c_2 - \beta_1 + \mathfrak{q}_0\big)x^2 + \big(-\beta_0 c_3 - 2\beta_1 c_2 - \beta_2 + \mathfrak{q}_1\big)x^3$$

$$+\big(-\beta_0 c_4 - \beta_1 c_2^2 - 2\beta_1 c_3 - 3\beta_2 c_2 - \beta_3 + \mathfrak{q}_2\big)x^4 + \cdots.$$

Matching powers of x in Eq. (224) yields successively

$$2c_2 + \beta_0 = 0,$$

$$c_2^2 + 2c_3 + \beta_0 c_2 + \beta_1 - \mathfrak{q}_0 = 0,$$

$$2c_2 c_3 + 2c_4 + \beta_0 c_3 + 2\beta_1 c_2 + \beta_2 - \mathfrak{q}_1 = 0,$$

$$2c_2 c_4 + c_3^2 + 2c_5 + \beta_0 c_4 + \beta_1 c_2^2 + 2\beta_1 c_3 + 3\beta_2 c_2 + \beta_3 - \mathfrak{q}_2 = 0.$$

Solving these recursively gives

$$c_2 = -\frac{\beta_0}{2},$$

$$c_3 = \frac{\beta_0^2}{8} - \frac{\beta_1}{2} + \frac{\mathfrak{q}_0}{2},$$

$$c_4 = \frac{\beta_0\beta_1}{2} - \frac{\beta_2}{2} + \frac{\mathfrak{q}_1}{2},$$

and

$$c_5 = -\frac{\beta_0^4}{128} - \frac{3\beta_0^2\beta_1}{16} - \frac{\beta_0^2\mathfrak{q}_0}{16} + \frac{3\beta_0\beta_2}{4} + \frac{3\beta_1^2}{8} - \frac{\beta_1\mathfrak{q}_0}{4} - \frac{\beta_3}{2} - \frac{\mathfrak{q}_0^2}{8} + \frac{\mathfrak{q}_2}{2}.$$

This proves Eqs. (222) and (223). □

E. Visible truncations, static hidden completion, and finite-N dynamic diagnostics

The ground-line scalar law Eq. (216) is the scalar equation carried forward from the cavity–shell reduction. Practical evaluation requires a reduced representation of the shell response. The current realization uses a visible two-mode dynamic compression as a realization-level evaluator, not as a replacement for the abstract mother law. In this subsection we record the finite Gaussian-collar diagnostics used to assemble the current visible dynamic amplitudes, reinterpret the visible truncation from the mother-equation point of view, construct a no-free-parameter reduced algebraic static hidden-mode completion, and record finite-N diagnostics for the dynamic hidden sector. These are finite compressions of the glued/visible scalar evaluator; they are not asserted to be the full infinite derivative-trace bath and are not fitted to a measured value of α.

Definition VI.18 (Finite Gaussian collar matrix)**.** For $p \geq 0$ and $\ell > 0$, define

$$F_p(\ell) := \int_0^1 \exp\left[-\left(\frac{1-y}{\ell}\right)^2\right] \cos(p\pi y)\,\mathrm{d}y. \tag{225}$$

The finite Gaussian collar matrix is

$$C_{mn}(\ell) := mn\Big(F_{|m-n|}(\ell) + F_{m+n}(\ell)\Big), \qquad m, n \geq 1. \tag{226}$$

These coefficients are finite Gaussian-collar diagnostics. They are not the exact glued shell-memory matrix elements $\widetilde{C}^{\mathrm{gl}}_{mn}(D)$ of Eq. (205).

Lemma 7 (Closed form of the finite Gaussian collar profile)**.** *For $p \geq 0$ and $\ell > 0$, the integral Eq.* (225) *admits the closed form*

$$F_p(\ell) = \frac{\sqrt{\pi}\,\ell}{2} \exp\left[-\frac{(p\pi\ell)^2}{4}\right] \Re\left\{e^{ip\pi}\left[\operatorname{erf}\left(\frac{1}{\ell} + \frac{ip\pi\ell}{2}\right) - \operatorname{erf}\left(\frac{ip\pi\ell}{2}\right)\right]\right\}. \tag{227}$$

Proof. Write

$$F_p(\ell) = \Re \int_0^1 \exp\left[-\left(\frac{1-y}{\ell}\right)^2\right] e^{ip\pi y}\,\mathrm{d}y.$$

Set

$$s = \frac{1-y}{\ell}, \qquad y = 1 - \ell s, \qquad \mathrm{d}y = -\ell\,\mathrm{d}s.$$

Then $y = 0$ corresponds to $s = 1/\ell$, and $y = 1$ corresponds to $s = 0$. Hence

$$F_p(\ell) = \ell\,\Re\left\{e^{ip\pi}\int_0^{1/\ell} e^{-s^2 - ip\pi\ell s}\,\mathrm{d}s\right\}.$$

Let

$$a := p\pi\ell.$$

Completing the square gives

$$-s^2 - ias = -\left(s + \frac{ia}{2}\right)^2 - \frac{a^2}{4}.$$

Therefore

$$F_p(\ell) = \ell\, e^{-a^2/4} \Re\left\{e^{ip\pi}\int_0^{1/\ell} \exp\left[-\left(s + \frac{ia}{2}\right)^2\right] \mathrm{d}s\right\}.$$

Now set

$$u = s + \frac{ia}{2}, \qquad \mathrm{d}u = \mathrm{d}s.$$

Then

$$F_p(\ell) = \ell\, e^{-a^2/4} \Re\left\{e^{ip\pi}\int_{ia/2}^{1/\ell + ia/2} e^{-u^2}\,\mathrm{d}u\right\}.$$

Using

$$\int e^{-u^2}\,\mathrm{d}u = \frac{\sqrt{\pi}}{2}\operatorname{erf}(u),$$

one obtains

$$F_p(\ell) = \frac{\sqrt{\pi}\,\ell}{2} e^{-a^2/4} \Re\left\{e^{ip\pi}\left[\operatorname{erf}\left(\frac{1}{\ell} + \frac{ia}{2}\right) - \operatorname{erf}\left(\frac{ia}{2}\right)\right]\right\}.$$

Substituting back $a = p\pi\ell$ gives Eq. (227). ∎

The common visible dynamic baseline used in the current finite-rank scalar evaluator is

$$A_{\mathrm{vis},0} := \pi^2 C_{11}(\ell_0) + \frac{\gamma_E}{4}, \tag{228}$$

where $C_{11}(\ell_0)$ is the Gaussian collar coefficient defined in Eq. (226). This is the common visible dynamic baseline entering $A_{\mathrm{uv}}^{(N)}$ and $A_{\mathrm{ir}}^{(N)}$. It is not a tangential shell trace and not a direct-sum proxy. The associated visible dynamic scales are

$$s_{\mathrm{uv}} := \ln 2, \qquad s_{\mathrm{ir}} := \frac{1}{8\pi^2}. \tag{229}$$

Definition VI.19 (Visible two-mode dynamic compression)**.** In all finite-dimensional reduced blocks in this subsection, vectors are real column vectors, matrices act on the corresponding Euclidean spaces, the symbol $(\cdot)^T$ denotes transpose with respect to the standard Euclidean inner product, and $\|\cdot\|$ denotes the induced Euclidean operator norm whenever a matrix norm is used.

Assume

$$A_{\mathrm{uv}}^{(N)} > 0, \qquad A_{\mathrm{ir}}^{(N)} > 0, \qquad 0 \le \chi_{\mathrm{cross}}^{(N)} < \sqrt{s_{\mathrm{uv}} s_{\mathrm{ir}}}. \tag{230}$$

Let

$$u_N \in \mathbb{R}^2, \qquad u_N = \begin{pmatrix} \sqrt{A_{\mathrm{uv}}^{(N)}} \\ \sqrt{A_{\mathrm{ir}}^{(N)}} \end{pmatrix}, \qquad \chi_N := \chi_{\mathrm{cross}}^{(N)} \in \mathbb{R}. \tag{231}$$

Define

$$S_N \in \mathbb{R}^{2\times 2}, \qquad S_N = \begin{pmatrix} s_{\mathrm{uv}} & \chi_N \\ \chi_N & s_{\mathrm{ir}} \end{pmatrix}. \tag{232}$$

Then S_N is positive definite. The visible two-mode dynamic evaluator used in the manuscript is the finite representative

$$\mathcal{G}_{e\gamma}^{\mathrm{gl,N}}(D) = u_N^T (I_2 + D S_N)^{-1} u_N. \tag{233}$$

Equivalently, with

$$J_2 := S_N^{-1}, \qquad g_2 := S_N^{-1/2} u_N, \tag{234}$$

one has

$$\mathcal{G}_{e\gamma}^{\mathrm{gl,N}}(D) = g_2^T (J_2 + D I_2)^{-1} g_2. \tag{235}$$

The subscript in g_2 labels the visible two-mode block and is unrelated to the tree-level gyromagnetic statement $g = 2$.

Proposition 35 (Positivity and pole form of the visible two-mode dynamic block)**.** *Under Eq.* (230)*, the matrix S_N in Eq.* (232) *is positive definite. Consequently $I_2 + DS_N$ is positive definite for every $D \ge 0$, and $\mathcal{G}_{e\gamma}^{\mathrm{gl,N}}(D)$ is well defined. Moreover, with $J_2 = S_N^{-1}$ and $g_2 = S_N^{-1/2} u_N$, one has*

$$\mathcal{G}_{e\gamma}^{\mathrm{gl,N}}(D) = g_2^T (J_2 + D I_2)^{-1} g_2.$$

Proof. The first principal minor of S_N is $s_{\mathrm{uv}} > 0$. Its determinant is

$$\det S_N = s_{\mathrm{uv}} s_{\mathrm{ir}} - \chi_N^2.$$

By Eq. (230),

$$0 \le \chi_N < \sqrt{s_{\mathrm{uv}} s_{\mathrm{ir}}},$$

hence

$$\det S_N > 0.$$

Therefore S_N is positive definite by Sylvester's criterion. For $D \geq 0$ and any nonzero $z \in \mathbb{R}^2$,

$$z^T(I_2 + DS_N)z = \|z\|^2 + D\, z^T S_N z > 0,$$

so $I_2 + DS_N$ is positive definite.

Since $S_N > 0$, the positive square root $S_N^{1/2}$ and inverse S_N^{-1} exist. Also,

$$J_2 + DI_2 = S_N^{-1} + DI_2 = S_N^{-1}(I_2 + DS_N).$$

Hence

$$(J_2 + DI_2)^{-1} = (I_2 + DS_N)^{-1} S_N.$$

Therefore

$$\begin{aligned} g_2^T(J_2 + DI_2)^{-1} g_2 &= u_N^T S_N^{-1/2}(I_2 + DS_N)^{-1} S_N S_N^{-1/2} u_N \\ &= u_N^T (I_2 + DS_N)^{-1} u_N, \end{aligned}$$

because S_N commutes with $I_2 + DS_N$. This proves Eq. (235). □

Remark. The current article evaluator can therefore be viewed as a visible two-mode realization-level truncation within the mother-equation class. The missing operator-level information is not a different type of scalar law; it is the hidden-mode completion of the visible bath. Thus the visible block is a reduced representative of the mother law, not a new defining scalar law.

Definition VI.20 (Finite Gaussian-collar dynamic diagnostics)**.** For $N \geq 2$, define the finite visible excited-sector source vector $v^{(N)} \in \mathbb{R}^{N-1}$ by

$$v_n^{(N)} \equiv \frac{C_{1n}(\ell_0)}{\sqrt{\Delta_n}}, \qquad 2 \leq n \leq N. \tag{236}$$

For $N = 1$, the excited sector is empty.

For $N \geq 2$, define the finite Gaussian-collar dynamic matrix $M_{EE,\mathrm{dyn}}^{(N)} \in \mathbb{R}^{(N-1)\times(N-1)}$ by

$$(M_{EE,\mathrm{dyn}}^{(N)})_{mn} \equiv \frac{C_{mn}(\ell_0)}{\Delta_m \Delta_n}, \qquad 2 \leq m, n \leq N. \tag{237}$$

Whenever $I + tM_{EE,\mathrm{dyn}}^{(N)}$ is invertible on the finite excited sector, define

$$\Phi_N(t) \equiv (v^{(N)})^T (I + tM_{EE,\mathrm{dyn}}^{(N)})^{-1} v^{(N)}. \tag{238}$$

In the empty-sector case $N = 1$, set

$$\Phi_1(t) \equiv 0.$$

Lemma 8 (Finite-N Neumann diagnostics of the Gaussian-collar dynamic response)**.** *Let $v^{(N)}$, $M_{EE,\mathrm{dyn}}^{(N)}$, and $\Phi_N(t)$ be defined by definition VI.20. In the empty-sector case $N = 1$, one has*

$$\Phi_1(t) \equiv 0.$$

For $N \geq 2$, and with the convention that $\|M_{EE,\mathrm{dyn}}^{(N)}\|^{-1} = +\infty$ when $M_{EE,\mathrm{dyn}}^{(N)} = 0$, the Neumann series converges for

$$|t| < \|M_{EE,\mathrm{dyn}}^{(N)}\|^{-1}. \tag{239}$$

In this domain, for each fixed N, as $t \to 0$,

$$\Phi_N(t) = (v^{(N)})^T v^{(N)} - t\, (v^{(N)})^T M_{EE,\mathrm{dyn}}^{(N)} v^{(N)} + O_N(t^2). \tag{240}$$

Equivalently, the zeroth-order finite dynamic diagnostic is

$$\Delta A_{\mathrm{mix}}^{(N)} \equiv \frac{\gamma_E}{\pi^2}\, (v^{(N)})^T v^{(N)} = \frac{\gamma_E}{\pi^2} \sum_{n=2}^{N} \frac{C_{1n}(\ell_0)^2}{\Delta_n}, \tag{241}$$

The full finite-N coefficient of the linear-in-t correction is

$$-\frac{\gamma_E}{\pi^2}(v^{(N)})^T M^{(N)}_{EE,\mathrm{dyn}} v^{(N)}. \tag{242}$$

Its retained diagonal part is

$$\delta A_0^{(N)} \equiv -\frac{\gamma_E}{\pi^2}\sum_{n=2}^{N}\frac{C_{1n}(\ell_0)^2 C_{nn}(\ell_0)}{\Delta_n^3}. \tag{243}$$

The discarded off-diagonal part is the finite scalar

$$\delta A_{\mathrm{off}}^{(N)} \equiv -\frac{\gamma_E}{\pi^2}\sum_{\substack{m,n=2\\ m\neq n}}^{N}\frac{C_{1m}(\ell_0)C_{mn}(\ell_0)C_{1n}(\ell_0)}{\Delta_m^{3/2}\Delta_n^{3/2}}. \tag{244}$$

Thus

$$-\frac{\gamma_E}{\pi^2}(v^{(N)})^T M^{(N)}_{EE,\mathrm{dyn}} v^{(N)} = \delta A_0^{(N)} + \delta A_{\mathrm{off}}^{(N)}. \tag{245}$$

In the visible evaluator below, $\delta A_0^{(N)}$ is retained as a diagonal diagnostic, while $\delta A_{\mathrm{off}}^{(N)}$ is not included in the displayed two-mode amplitudes unless stated explicitly. This is a realization-level truncation choice. It is not an operator-level identity of the finite hidden sector, and it is not an infinite-rank convergence statement.

Proof. By Eq. (226), the entries $C_{mn}(\ell_0)$ are real and symmetric in m, n. Hence $M^{(N)}_{EE,\mathrm{dyn}}$ is a finite real symmetric matrix. If $|t|\,\|M^{(N)}_{EE,\mathrm{dyn}}\| < 1$, the Neumann series converges in operator norm and gives

$$(I + tM^{(N)}_{EE,\mathrm{dyn}})^{-1} = \sum_{k=0}^{\infty}(-t)^k \big(M^{(N)}_{EE,\mathrm{dyn}}\big)^k.$$

Therefore

$$\begin{aligned}\Phi_N(t) &= (v^{(N)})^T\left[\sum_{k=0}^{\infty}(-t)^k\big(M^{(N)}_{EE,\mathrm{dyn}}\big)^k\right]v^{(N)}\\ &= (v^{(N)})^T v^{(N)} - t\,(v^{(N)})^T M^{(N)}_{EE,\mathrm{dyn}} v^{(N)} + t^2\sum_{k=2}^{\infty}(-t)^{k-2}(v^{(N)})^T\big(M^{(N)}_{EE,\mathrm{dyn}}\big)^k v^{(N)}.\end{aligned}$$

For $|t|\,\|M^{(N)}_{EE,\mathrm{dyn}}\| < 1$, the remainder obeys

$$\left|t^2\sum_{k=2}^{\infty}(-t)^{k-2}(v^{(N)})^T\big(M^{(N)}_{EE,\mathrm{dyn}}\big)^k v^{(N)}\right| \le \frac{t^2\,\|v^{(N)}\|^2\,\|M^{(N)}_{EE,\mathrm{dyn}}\|^2}{1-|t|\,\|M^{(N)}_{EE,\mathrm{dyn}}\|}.$$

This proves Eq. (240).

Using Eq. (236),

$$(v^{(N)})^T v^{(N)} = \sum_{n=2}^{N}\frac{C_{1n}(\ell_0)^2}{\Delta_n}.$$

Multiplication by γ_E/π^2 gives Eq. (241).

Next,

$$\begin{aligned}(v^{(N)})^T M^{(N)}_{EE,\mathrm{dyn}} v^{(N)} &= \sum_{m,n=2}^{N}\frac{C_{1m}(\ell_0)C_{mn}(\ell_0)C_{1n}(\ell_0)}{\Delta_m^{3/2}\Delta_n^{3/2}}\\ &= \sum_{n=2}^{N}\frac{C_{1n}(\ell_0)^2 C_{nn}(\ell_0)}{\Delta_n^3} + \sum_{\substack{m,n=2\\ m\neq n}}^{N}\frac{C_{1m}(\ell_0)C_{mn}(\ell_0)C_{1n}(\ell_0)}{\Delta_m^{3/2}\Delta_n^{3/2}}.\end{aligned}$$

Multiplying by $-\gamma_E/\pi^2$ gives Eqs. (243) to (245). Since the sums are finite, the discarded off-diagonal diagnostic satisfies the explicit bound

$$|\delta A_{\mathrm{off}}^{(N)}| \le \frac{\gamma_E}{\pi^2} \sum_{\substack{m,n=2\\ m\neq n}}^{N} \frac{|C_{1m}(\ell_0)C_{mn}(\ell_0)C_{1n}(\ell_0)|}{\Delta_m^{3/2}\Delta_n^{3/2}}.$$

□

Definition VI.21 (Finite-N visible dynamic amplitudes)**.** For a fixed finite Gaussian-collar diagnostic rank N, define the diagonal retained correction by

$$\Delta A_{\mathrm{diag}}^{(N)} := -\eta_0^2\, \delta A_0^{(N)}. \tag{246}$$

The visible UV and IR dynamic amplitudes are

$$A_{\mathrm{uv}}^{(N)} := A_{\mathrm{vis},0} + \Delta A_{\mathrm{mix}}^{(N)} + \delta A_0^{(N)} + \Delta A_{\mathrm{diag}}^{(N)}, \tag{247}$$

and

$$A_{\mathrm{ir}}^{(N)} := A_{\mathrm{vis},0} - \Delta A_{\mathrm{mix}}^{(N)} + \delta A_0^{(N)} + \Delta A_{\mathrm{diag}}^{(N)}. \tag{248}$$

Finally, set

$$\chi_{\mathrm{cross}}^{(N)} := \big(\Delta A_{\mathrm{mix}}^{(N)}\big)^2. \tag{249}$$

Only ranks N for which the resulting amplitudes satisfy the admissibility conditions in Eq. (230) are used as visible two-mode dynamic evaluators. Otherwise the finite-N quantities remain diagnostics.

Remark. The quantities $\Delta A_{\mathrm{mix}}^{(N)}$ and $\delta A_0^{(N)}$ are therefore finite-N diagnostics of the visible hidden block. They are not primitive data of the mother equation. Only the first quantity is the full constant term of the finite Neumann expansion; the second retains only the diagonal part of the linear term.

Definition VI.22 (Minimal static glue used in the reduced evaluator)**.** For $D \ge 0$, define the reduced-evaluator collar–log overlap by

$$g_{c\ell}(D) := \int_0^\infty \exp\left[-\left(\frac{s}{\ell_0}\right)^2\right] \exp\left[-\sqrt{D+\frac{1}{4}}\, s\right] \mathrm{d}s. \tag{250}$$

This is a reduced finite-evaluator overlap. It is not a second definition of the abstract operator-level glued bath $\mathbb{L}_{\mathrm{sh}}^{\mathrm{gl}}$, whose scalar response enters the defining mother law through the shifted resolvent $(\mathbb{L}_{\mathrm{sh}}^{\mathrm{gl}} + DI_{\mathrm{sh}})^{-1}$. It is not adjusted to a measured value of α or to a QED coefficient.

Lemma 9 (Closed form of the minimal static glue)**.** *For every $D \ge 0$, the overlap Eq.* (250) *has the closed form*

$$g_{c\ell}(D) = \frac{\sqrt{\pi}\,\ell_0}{2} \exp\Big[\frac{\ell_0^2}{4}\Big(D+\frac{1}{4}\Big)\Big] \operatorname{erfc}\Big(\frac{\ell_0}{2}\sqrt{D+\frac{1}{4}}\Big). \tag{251}$$

Proof. Set

$$a := \sqrt{D+\frac{1}{4}}.$$

Then

$$g_{c\ell}(D) = \int_0^\infty \exp\left[-\frac{s^2}{\ell_0^2} - as\right] \mathrm{d}s.$$

Complete the square in the exponent:

$$-\frac{s^2}{\ell_0^2} - as = -\frac{1}{\ell_0^2}\left(s + \frac{a\ell_0^2}{2}\right)^2 + \frac{a^2\ell_0^2}{4}.$$

Hence

$$g_{c\ell}(D) = \exp\!\left(\frac{a^2\ell_0^2}{4}\right) \int_0^\infty \exp\!\left[-\frac{1}{\ell_0^2}\left(s + \frac{a\ell_0^2}{2}\right)^2\right] \mathrm{d}s.$$

Now introduce

$$u := \frac{1}{\ell_0}\left(s + \frac{a\ell_0^2}{2}\right), \qquad \mathrm{d}s = \ell_0\,\mathrm{d}u.$$

When $s = 0$, one has $u = \frac{a\ell_0}{2}$; when $s \to \infty$, one has $u \to \infty$. Therefore

$$g_{c\ell}(D) = \ell_0 \,\exp\!\left(\frac{a^2\ell_0^2}{4}\right) \int_{a\ell_0/2}^\infty e^{-u^2}\,\mathrm{d}u.$$

Using

$$\mathrm{erfc}(z) = \frac{2}{\sqrt{\pi}} \int_z^\infty e^{-u^2}\,\mathrm{d}u,$$

we obtain

$$g_{c\ell}(D) = \frac{\sqrt{\pi}\,\ell_0}{2} \exp\!\left(\frac{a^2\ell_0^2}{4}\right) \mathrm{erfc}\!\left(\frac{a\ell_0}{2}\right).$$

Since $a^2 = D + \frac{1}{4}$, this is exactly Eq. (251). □

Proposition 36 (Visible static two-channel truncation)**.** *Assume*

$$\Theta_1^{(\mathrm{coll})} > 0, \qquad \Theta_1^{(\mathrm{log})} > 0, \qquad 1 - \frac{g_{c\ell}(0)^2}{4}\,\Theta_1^{(\mathrm{coll})}\Theta_1^{(\mathrm{log})} > 0. \tag{252}$$

Then the visible static stiffness matrix

$$K_{\mathrm{vis}}^{(2)} := \begin{pmatrix} 1/\Theta_1^{(\mathrm{coll})} & g_{c\ell}(0)/2 \\ g_{c\ell}(0)/2 & 1/\Theta_1^{(\mathrm{log})} \end{pmatrix} \tag{253}$$

is positive definite, and the corresponding visible static coefficient is

$$B_{11}^{\mathrm{glue}} = \frac{\Theta_1^{(\mathrm{coll})} + \Theta_1^{(\mathrm{log})} - g_{c\ell}(0)\,\Theta_1^{(\mathrm{coll})}\Theta_1^{(\mathrm{log})}}{1 - \dfrac{g_{c\ell}(0)^2}{4}\Theta_1^{(\mathrm{coll})}\Theta_1^{(\mathrm{log})}}, \tag{254}$$

with

$$B_{11}^{\mathrm{glue}} > 0. \tag{255}$$

Hence

$$\Theta_1^{\mathrm{gl}} = \Theta_{1,\mathrm{core}} + B_{11}^{\mathrm{glue}}, \qquad \Theta_{1,\mathrm{core}} = 2\pi C_{\mathrm{uni}}. \tag{256}$$

Proof. Under Eq. (252), the principal minors of $K_{\mathrm{vis}}^{(2)}$ are positive; hence $K_{\mathrm{vis}}^{(2)}$ is positive definite. Introduce the visible source vector

$$t_{\mathrm{vis}} := \begin{pmatrix} 1 \\ 1 \end{pmatrix}. \tag{257}$$

The visible static load is the quadratic form

$$B_{11}^{\mathrm{glue}} = t_{\mathrm{vis}}^T \big(K_{\mathrm{vis}}^{(2)}\big)^{-1} t_{\mathrm{vis}}.$$

Now

$$\left(K^{(2)}_{\mathrm{vis}}\right)^{-1} = \frac{1}{\frac{1}{\Theta_1^{(\mathrm{coll})}\Theta_1^{(\log)}} - \frac{g_{c\ell}(0)^2}{4}} \begin{pmatrix} 1/\Theta_1^{(\log)} & -g_{c\ell}(0)/2 \\ -g_{c\ell}(0)/2 & 1/\Theta_1^{(\mathrm{coll})} \end{pmatrix}.$$

Contracting against t_{vis} gives

$$B^{\mathrm{glue}}_{11} = \frac{\frac{1}{\Theta_1^{(\mathrm{coll})}} + \frac{1}{\Theta_1^{(\log)}} - g_{c\ell}(0)}{\frac{1}{\Theta_1^{(\mathrm{coll})}\Theta_1^{(\log)}} - \frac{g_{c\ell}(0)^2}{4}}.$$

Multiplying numerator and denominator by $\Theta_1^{(\mathrm{coll})}\Theta_1^{(\log)}$ yields Eq. (254). Since $K^{(2)}_{\mathrm{vis}}$ is positive definite and $t_{\mathrm{vis}} \neq 0$, the quadratic form $t_{\mathrm{vis}}^T (K^{(2)}_{\mathrm{vis}})^{-1} t_{\mathrm{vis}}$ is strictly positive; hence Eq. (255) holds. Adding the core part gives Eq. (256). □

Definition VI.23 (Reduced static trace pair and common overlap mode)**.** Define the reduced-evaluator raw static trace profiles

$$f_c(s) := e^{-(s/\ell_0)^2}, \qquad f_\ell(s) := e^{-s/2}, \tag{258}$$

with norms

$$N_c := \int_0^\infty f_c(s)^2\,\mathrm{d}s = \sqrt{\frac{\pi}{8}}\,\ell_0, \qquad N_\ell := \int_0^\infty f_\ell(s)^2\,\mathrm{d}s = 1, \tag{259}$$

and normalized overlap

$$\rho_{\mathrm{stat}} \equiv \frac{g_{c\ell}(0)}{\sqrt{N_c N_\ell}}. \tag{260}$$

Let

$$a_{\mathrm{stat}} := \Theta_1^{(\mathrm{coll})}, \qquad b_{\mathrm{stat}} := \Theta_1^{(\log)}. \tag{261}$$

and define the static trace map

$$T_{\mathrm{stat}} : \mathbb{C}^2 \to L^2(\mathbb{R}_+, \mathrm{d}s), \qquad T_{\mathrm{stat}}\begin{pmatrix}\xi_c \\ \xi_\ell\end{pmatrix} := \xi_c\sqrt{\frac{a_{\mathrm{stat}}}{N_c}}\,f_c + \xi_\ell\sqrt{\frac{b_{\mathrm{stat}}}{N_\ell}}\,f_\ell. \tag{262}$$

Lemma 10 (Static trace Gram map and overlap bounds)**.** *Set*

$$a \equiv a_{\mathrm{stat}}, \qquad b \equiv b_{\mathrm{stat}}.$$

With T_{stat}, a, b, and ρ_{stat} defined in this way from definition VI.23, the Gram map $G_{\mathrm{stat}} = T^*_{\mathrm{stat}} T_{\mathrm{stat}}$ is

$$G_{\mathrm{stat}} = \begin{pmatrix} a & \sqrt{ab}\,\rho_{\mathrm{stat}} \\ \sqrt{ab}\,\rho_{\mathrm{stat}} & b \end{pmatrix}. \tag{263}$$

Moreover,

$$G_{\mathrm{stat}} = (1-\rho_{\mathrm{stat}})\begin{pmatrix} a & 0 \\ 0 & b\end{pmatrix} + \rho_{\mathrm{stat}}\begin{pmatrix}\sqrt{a} \\ \sqrt{b}\end{pmatrix}\begin{pmatrix}\sqrt{a} & \sqrt{b}\end{pmatrix}, \tag{264}$$

and

$$0 < \rho_{\mathrm{stat}} < 1. \tag{265}$$

Proof. Let $e_c = (1,0)^T$ and $e_\ell = (0,1)^T$. By definition,

$$T_{\mathrm{stat}} e_c = \sqrt{\frac{a}{N_c}}\,f_c, \qquad T_{\mathrm{stat}} e_\ell = \sqrt{\frac{b}{N_\ell}}\,f_\ell.$$

The raw trace norms and overlap are

$$\langle f_c, f_c\rangle = N_c, \qquad \langle f_\ell, f_\ell\rangle = N_\ell, \qquad \langle f_c, f_\ell\rangle = g_{c\ell}(0) = \rho_{\mathrm{stat}}\sqrt{N_c N_\ell}.$$

Therefore

$$\langle T_{\mathrm{stat}} e_c, T_{\mathrm{stat}} e_c\rangle = \frac{a}{N_c}\langle f_c, f_c\rangle = a,$$

$$\langle T_{\mathrm{stat}} e_\ell, T_{\mathrm{stat}} e_\ell\rangle = \frac{b}{N_\ell}\langle f_\ell, f_\ell\rangle = b,$$

and

$$\langle T_{\mathrm{stat}} e_c, T_{\mathrm{stat}} e_\ell\rangle = \sqrt{\frac{ab}{N_c N_\ell}}\,\langle f_c, f_\ell\rangle = \sqrt{ab}\,\rho_{\mathrm{stat}}.$$

These three identities give Eq. (263).

To prove the decomposition, expand the right-hand side of Eq. (264):

$$(1-\rho_{\mathrm{stat}})\begin{pmatrix} a & 0 \\ 0 & b\end{pmatrix} + \rho_{\mathrm{stat}}\begin{pmatrix} a & \sqrt{ab} \\ \sqrt{ab} & b\end{pmatrix} = \begin{pmatrix} a & \sqrt{ab}\,\rho_{\mathrm{stat}} \\ \sqrt{ab}\,\rho_{\mathrm{stat}} & b\end{pmatrix}.$$

This is exactly Eq. (263).

Finally, $f_c(s) = e^{-(s/\ell_0)^2}$ and $f_\ell(s) = e^{-s/2}$ are strictly positive and nonzero in $L^2(\mathbb{R}_+, \mathrm{d}s)$. Hence

$$\langle f_c, f_\ell\rangle > 0,$$

so $\rho_{\mathrm{stat}} > 0$. They are not proportional, because equality $e^{-(s/\ell_0)^2} = Ce^{-s/2}$ for all $s \geq 0$ would force a quadratic function of s to equal an affine function of s, which is impossible for $\ell_0 > 0$. Therefore the strict Cauchy–Schwarz inequality gives

$$\langle f_c, f_\ell\rangle < \|f_c\|_{L^2}\,\|f_\ell\|_{L^2} = \sqrt{N_c N_\ell}.$$

Dividing by $\sqrt{N_c N_\ell}$ yields

$$0 < \rho_{\mathrm{stat}} < 1,$$

which proves Eq. (265). □

Lemma 11 (Deflated visible loads)**.** *Assume Eqs.* (252) *and* (265)*. Let*

$$c_0 := \frac{g_{c\ell}(0)a_{\mathrm{stat}}b_{\mathrm{stat}}}{2}, \qquad a_{\mathrm{stat}}^{\perp} := a_{\mathrm{stat}} - \frac{c_0^2}{b_{\mathrm{stat}}}, \qquad b_{\mathrm{stat}}^{\perp} := b_{\mathrm{stat}} - \frac{c_0^2}{a_{\mathrm{stat}}}. \tag{266}$$

Then, with $a \equiv a_{\mathrm{stat}}$ and $b \equiv b_{\mathrm{stat}}$,

$$a_{\mathrm{stat}}^{\perp} = a\left(1 - \frac{g_{c\ell}(0)^2 ab}{4}\right) > 0, \qquad b_{\mathrm{stat}}^{\perp} = b\left(1 - \frac{g_{c\ell}(0)^2 ab}{4}\right) > 0. \tag{267}$$

Proof. Set $a \equiv a_{\mathrm{stat}}$ and $b \equiv b_{\mathrm{stat}}$. Using Eq. (266),

$$a_{\mathrm{stat}}^{\perp} = a - \frac{c_0^2}{b} = a - \frac{g_{c\ell}(0)^2 a^2 b}{4} = a\left(1 - \frac{g_{c\ell}(0)^2 ab}{4}\right),$$

and similarly

$$b_{\mathrm{stat}}^{\perp} = b - \frac{c_0^2}{a} = b\left(1 - \frac{g_{c\ell}(0)^2 ab}{4}\right).$$

The positivity follows from Eq. (252). □

Definition VI.24 (Canonical no-free-parameter algebraic static hidden-mode completion)**.** Assume Eqs. (252), (265) and (267). Define the renormalized visible source

$$t^{\perp} := \begin{pmatrix} \sqrt{a_{\rm stat}^{\perp}/a_{\rm stat}} \\ \sqrt{b_{\rm stat}^{\perp}/b_{\rm stat}} \\ 0 \end{pmatrix}. \tag{268}$$

and the three-channel symmetric static stiffness matrix

$$K_{\rm stat}^{(3,\rho)} = \begin{pmatrix} 1/a_{\rm stat}^{\perp} & g_{c\ell}(0)/2 & \sqrt{c_0} \\ g_{c\ell}(0)/2 & 1/b_{\rm stat}^{\perp} & \sqrt{c_0} \\ \sqrt{c_0} & \sqrt{c_0} & \Lambda_h \end{pmatrix}, \qquad \Lambda_h \equiv \frac{1}{1-\rho_{\rm stat}^2}. \tag{269}$$

The matrix $K_{\rm stat}^{(3,\rho)}$ is the no-free-parameter reduced algebraic static completion determined by the trace pair and overlap data. Its positivity is not asserted here as an automatic consequence of the preceding identities. Rather, positive definiteness of $K_{\rm stat}^{(3,\rho)}$ is the realization-level admissibility condition under which the reduced static completion is accepted. On that admissible domain, define the associated reduced static load by

$$B_{11}^{(3,\rho)} := (t^{\perp})^T \big(K_{\rm stat}^{(3,\rho)}\big)^{-1} t^{\perp}. \tag{270}$$

This load is part of the reduced algebraic static completion and is not the operator-level shell-memory function $m_{\rm sh}^{\rm gl}(D)$.

Remark. The completion Eqs. (269) and (270) is a canonical algebraic lift of the visible static block that restores the rank-one common overlap mode of Eq. (264) without introducing a fitted parameter. The operator-level content fixed directly in this construction is the trace pair (f_c, f_ℓ) and the Gram map Eq. (263). The three-channel matrix Eq. (269) is the corresponding no-free-parameter static completion at the reduced algebraic level.

Proposition 37 (Finite Lanczos–Jacobi representation of the hidden dynamic chain)**.** *Let $N \geq 2$ and assume $v^{(N)} \neq 0$. Let*

$$\mathcal{K}_N := \operatorname{span}\Big\{ v^{(N)},\, M_{EE,\rm dyn}^{(N)} v^{(N)},\, \big(M_{EE,\rm dyn}^{(N)}\big)^2 v^{(N)},\, \dots \Big\}, \tag{271}$$

and let $r_N := \dim \mathcal{K}_N$. Set

$$q_{\rm L,0}^{(N)} := \frac{v^{(N)}}{\|v^{(N)}\|}. \tag{272}$$

Applying Lanczos to the real symmetric matrix $M_{EE,\rm dyn}^{(N)}$ with starting vector $q_{\rm L,0}^{(N)}$ and carrying the process to completion on $\mathcal{K}_N$ yields a finite Jacobi matrix

$$J_{r_N}^{(N)} = \begin{pmatrix} a_{\rm L,0}^{(N)} & b_{\rm L,1}^{(N)} & 0 & \cdots \\ b_{\rm L,1}^{(N)} & a_{\rm L,1}^{(N)} & b_{\rm L,2}^{(N)} & \ddots \\ 0 & b_{\rm L,2}^{(N)} & a_{\rm L,2}^{(N)} & \ddots \\ \vdots & \ddots & \ddots & \ddots \end{pmatrix} \in \mathbb{R}^{r_N \times r_N}. \tag{273}$$

such that

$$\Phi_N(t) = \|v^{(N)}\|^2 e_1^T (I + tJ_{r_N}^{(N)})^{-1} e_1 \tag{274}$$

for every t such that $I + tM_{EE,\rm dyn}^{(N)}$ is invertible.

Proof. Since $M_{EE,\rm dyn}^{(N)}$ is a finite real symmetric matrix, the Krylov space $\mathcal{K}_N$ is finite dimensional. Let

$$Q_N : \mathbb{R}^{r_N} \to \mathbb{R}^{N-1}$$

be the Lanczos isometry whose columns form an orthonormal basis of $\mathcal{K}_N$, chosen so that

$$Q_N e_1 = q_{\rm L,0}^{(N)} = \frac{v^{(N)}}{\|v^{(N)}\|}.$$

Because the Lanczos process is carried to completion on $\mathcal{K}_N$, this subspace is $M^{(N)}_{EE,\mathrm{dyn}}$-invariant, and

$$Q_N^T M^{(N)}_{EE,\mathrm{dyn}} Q_N = J^{(N)}_{r_N}. \tag{275}$$

Hence

$$v^{(N)} = \|v^{(N)}\|\, Q_N e_1.$$

Therefore

$$\Phi_N(t) = (v^{(N)})^T (I + tM^{(N)}_{EE,\mathrm{dyn}})^{-1} v^{(N)} = \|v^{(N)}\|^2 e_1^T Q_N^T (I + tM^{(N)}_{EE,\mathrm{dyn}})^{-1} Q_N e_1.$$

Since $\mathcal{K}_N$ is $M^{(N)}_{EE,\mathrm{dyn}}$-invariant, there exists a unique real symmetric matrix $J^{(N)}_{r_N}$ on $\mathbb{R}^{r_N}$ such that

$$M^{(N)}_{EE,\mathrm{dyn}} Q_N = Q_N J^{(N)}_{r_N}. \tag{276}$$

Left-multiplying by Q_N^T and using $Q_N^T Q_N = I_{r_N}$ gives Eq. (275).

Hence

$$(I + tM^{(N)}_{EE,\mathrm{dyn}}) Q_N = Q_N (I + tJ^{(N)}_{r_N}).$$

Assume $I + tM^{(N)}_{EE,\mathrm{dyn}}$ is invertible. If $I + tJ^{(N)}_{r_N}$ were not invertible, there would exist $y \in \mathbb{R}^{r_N} \setminus \{0\}$ such that

$$(I + tJ^{(N)}_{r_N}) y = 0.$$

Then

$$(I + tM^{(N)}_{EE,\mathrm{dyn}})(Q_N y) = Q_N (I + tJ^{(N)}_{r_N}) y = 0.$$

Since Q_N is an isometry, $Q_N y \neq 0$, which contradicts the invertibility of $I + tM^{(N)}_{EE,\mathrm{dyn}}$. Therefore $I + tJ^{(N)}_{r_N}$ is invertible, and

$$(I + tM^{(N)}_{EE,\mathrm{dyn}})^{-1} Q_N = Q_N (I + tJ^{(N)}_{r_N})^{-1}.$$

Right-multiplying by Q_N^T and left-multiplying by Q_N^T then yields

$$Q_N^T (I + tM^{(N)}_{EE,\mathrm{dyn}})^{-1} Q_N = (I + tJ^{(N)}_{r_N})^{-1}.$$

Substituting this identity gives Eq. (274). □

Remark (Unregularized derivative trace and the role of finite collar diagnostics)*.* The exact derivative-trace memory matrix

$$\widetilde{C}^{\mathrm{gl}}_{mn}(D) = 2\pi^2 mn(-1)^{m+n} m^{\mathrm{gl}}_{\mathrm{sh}}(D)$$

is a rank-one boundary-memory form at fixed D. In the unregularized infinite excited sector, its ground-to-excited coefficients grow like n, so the corresponding coefficient vector is not an $\ell^2(E)$ vector without an additional collar regularization or a form-domain interpretation. This is why the finite Gaussian-collar quantities $C_{mn}(\ell_0)$ introduced above are diagnostic finite-rank evaluators rather than direct replacements of $\widetilde{C}^{\mathrm{gl}}_{mn}(D)$.

Remark. The representation Eqs. (273) and (274) is exact for each fixed finite N of the visible Gaussian-collar dynamic matrix Eq. (237). This finite matrix is built from the collar coefficients $C_{mn}(\ell_0)$, not from the unregularized rank-one derivative-trace coefficients $\widetilde{C}^{\mathrm{gl}}_{mn}(0)$ of Eq. (207). This distinction is essential. The unregularized derivative-trace model has

$$\widetilde{C}^{\mathrm{gl}}_{1n}(0) = 2\pi^2 n(-1)^{n+1} m^{\mathrm{gl}}_{\mathrm{sh}}(0),$$

so the associated infinite source vector is not naturally in $\ell^2(E)$. The visible dynamic evaluator used here is therefore a finite Gaussian-collar compression of the hidden dynamic sector. It is not claimed to be the full unregularized infinite derivative-trace bath.

Definition VI.25 (A refined no-free-parameter mother truncation)**.** For the fixed diagnostic rank N under consideration, let g_2 and J_2 denote the visible two-mode dynamic block extracted from the current realization through Eq. (234). The vector g_2 is unrelated to the gyromagnetic coefficient $g = 2$. Assume

$$0 \le \rho_{\rm dyn}^{(N)} := \frac{\chi_N}{\sqrt{s_{\rm uv} s_{\rm ir}}} < 1, \tag{277}$$

so that S_N is positive definite and $J_2 = S_N^{-1}$ is well defined. Define

$$\lambda_u^{(N)} \equiv \frac{1}{1 - (\rho_{\rm dyn}^{(N)})^2}, \qquad g_2^{\rm eff} \equiv \sqrt{\lambda_u^{(N)}}\, g_2. \tag{278}$$

Assume moreover that $K_{\rm stat}^{(3,\rho)}$ is positive definite. For $x > 0$ and $D \ge 0$, define the refined six-dimensional no-free-parameter reduced truncation by the spectral condition

$$\det \mathcal{M}_6^{\rm nf}(D; x) = 0. \tag{279}$$

with

$$\mathcal{M}_6^{\rm nf}(D; x) = \begin{pmatrix} \left(\dfrac{D}{x}\right)^2 - 1 + \Theta_{1,\rm core} D & \sqrt{D}\, (t^\perp)^T & D\, (g_2^{\rm eff})^T \\ \sqrt{D}\, t^\perp & -K_{\rm stat}^{(3,\rho)} & 0 \\ D\, g_2^{\rm eff} & 0 & J_2 + D I_2 \end{pmatrix}. \tag{280}$$

Proposition 38 (Schur reduction of the refined mother truncation)**.** *Under the assumptions of definition VI.25, and for every $D \ge 0$, the block $J_2 + D I_2$ is positive definite. If $\det \mathcal{M}_6^{\rm nf}(D; x) = 0$ and $D > 0$, the Schur complement of the lower two blocks of $\mathcal{M}_6^{\rm nf}(D; x)$ yields the reduced scalar law*

$$D = x\sqrt{1 - \left(\Theta_{1,\rm core} + B_{11}^{(3,\rho)}\right) D + D^2 (g_2^{\rm eff})^T (J_2 + D I_2)^{-1} g_2^{\rm eff}}. \tag{281}$$

The positive square-root branch is selected by the local condition $D \sim x > 0$.

Proof. Since $\rho_{\rm dyn}^{(N)} < 1$, the visible stiffness matrix S_N is positive definite, hence so is $J_2 = S_N^{-1}$. Therefore $J_2 + D I_2$ is positive definite and invertible for every $D \ge 0$.

Write $\mathcal{M}_6^{\rm nf}(D; x)$ in block form as

$$\mathcal{M}_6^{\rm nf}(D; x) = \begin{pmatrix} A(D; x) & B(D)^T \\ B(D) & C(D) \end{pmatrix},$$

where

$$A(D; x) = \left(\frac{D}{x}\right)^2 - 1 + \Theta_{1,\rm core} D,$$

$$B(D) = \begin{pmatrix} \sqrt{D}\, t^\perp \\ D\, g_2^{\rm eff} \end{pmatrix}, \qquad C(D) = \begin{pmatrix} -K_{\rm stat}^{(3,\rho)} & 0 \\ 0 & J_2 + D I_2 \end{pmatrix}.$$

The block

$$C(D) := \begin{pmatrix} -K_{\rm stat}^{(3,\rho)} & 0 \\ 0 & J_2 + D I_2 \end{pmatrix}$$

is invertible because $K_{\rm stat}^{(3,\rho)}$ is positive definite and $J_2 + D I_2$ is positive definite. Since the upper-left block $A(D; x)$ is scalar, the block-determinant identity gives

$$\det \mathcal{M}_6^{\rm nf}(D; x) = \det C(D) \left(A(D; x) - B(D)^T C(D)^{-1} B(D) \right).$$

Therefore, under the invertibility of $C(D)$,

$$\det \mathcal{M}_6^{\mathrm{nf}}(D;x) = 0 \qquad \Longleftrightarrow \qquad A(D;x) - B(D)^T C(D)^{-1} B(D) = 0.$$

Since

$$C(D)^{-1} = \begin{pmatrix} -\big(K_{\mathrm{stat}}^{(3,\rho)}\big)^{-1} & 0 \\ 0 & (J_2 + DI_2)^{-1} \end{pmatrix},$$

one obtains

$$B(D)^T C(D)^{-1} B(D) = -D\, B_{11}^{(3,\rho)} + D^2 (g_2^{\mathrm{eff}})^T (J_2 + DI_2)^{-1} g_2^{\mathrm{eff}}.$$

Hence the scalar Schur equation is

$$\left(\frac{D}{x}\right)^2 = 1 - \big(\Theta_{1,\mathrm{core}} + B_{11}^{(3,\rho)}\big) D + D^2 (g_2^{\mathrm{eff}})^T (J_2 + DI_2)^{-1} g_2^{\mathrm{eff}}.$$

Equivalently,

$$1 - \big(\Theta_{1,\mathrm{core}} + B_{11}^{(3,\rho)}\big) D + D^2 (g_2^{\mathrm{eff}})^T (J_2 + DI_2)^{-1} g_2^{\mathrm{eff}} = \left(\frac{D}{x}\right)^2 > 0.$$

Thus the radicand is strictly positive on every positive root, and the real square root is uniquely selected by

$$\frac{D}{x} > 0.$$

Taking that positive square root gives Eq. (281). □

Remark (Logical status of the refined truncation)*.* The static hidden mode Eq. (269) is a no-free-parameter reduced algebraic completion determined by the static trace pair and its Gram structure. The dynamic hidden block enters the present construction only through the visible two-mode compression g_2, J_2. The refined truncation Eq. (280) is therefore a richer realization-level completion than the original two-channel evaluator, while it remains a reduced truncation rather than the full operator-level solution of the mother equation. No measured value of α, no QED coefficient, and no external benchmark enters this completion.

F. Numerical realization of the scalar mother truncation

This subsection records only the internal scalar-sector numerics of the mother construction. No QED target coefficient is used here, and no reverse engineering from the electron g-factor is invoked. The tables display the fixed geometric input, the visible and hidden scalar-shell data, and the realization-level values of the scalar branch $\mathcal{D}_{\mathrm{C}}$. When a numerical value is displayed at an external orientation point, that point serves only as an argument at which the current scalar evaluator is sampled. It does not define, tune, or select the scalar law.

Unless the definition column provides an exact closed form, the printed decimals below are realization-level outputs of the current finite-rank evaluator at the stated input values. They are central computed values, not certified significant digits and not rigorous truncation or convergence bounds. Whenever two algebraically equivalent evaluations are listed side by side, their difference records an internal reproducibility residual of the current implementation, not an uncertainty estimate.

Remark (Reference point, conventions, and reproducibility)*.* The scalar tables that require a numerical argument are evaluated at the external orientation point defined by the CODATA 2022 fine-structure constant [8],

$$\alpha_{\mathrm{CODATA22}}^{-1} = 137.035999177(21), \qquad x_{\mathrm{ref}} \equiv \frac{\alpha_{\mathrm{CODATA22}}}{\pi}. \tag{282}$$

The parenthetical digits denote the one-standard-deviation uncertainty of the CODATA 2022 value. No uncertainty propagation is performed here, and every row evaluated at x_{ref} uses only the central value of $\alpha_{\mathrm{CODATA22}}$. The resulting decimals therefore record the value of the current scalar evaluator at that central argument. By themselves they do not quantify sensitivity to the CODATA uncertainty, to the finite-rank choice, or to later operator-level improvements. This orientation point is not used to define the scalar law, choose a branch, tune a truncation, or determine the later geometric lock. The numerical data are reproducible from the archived scalar-channel computation accompanying the manuscript. Auxiliary comparison routines exist in the computational archive, although no QED benchmark quantity is used in constructing the scalar tables below.

TABLE IV. Fixed shell geometry and realization-level static hidden-mode data for the refined mother truncation. Entries whose definition column gives an exact closed form are exact quantities displayed here in decimal form. The rows labelled "tab" and "rec" are two independent evaluations of the same reduced static quantity within the current implementation. The residual rows $\Delta B_{11}^{\rm glue}$ and $\Delta B_{11}^{(3,\rho)}$ are internal arithmetic consistency checks at the printed precision; they are not error bars.

Symbol	Def.	Value
η_0	$1/\pi$	0.31830988618379067153 7768
ℓ_0	$1/(\pi\sqrt{\pi})$	0.17958712212516656168 9082
$C_{\rm uni}$	$(1/\pi)(4/3+1/(4\pi^2))$	0.43247606518668743434 6462
$s_{\rm uv}$	$\log 2$	0.69314718055994530941 7232
$s_{\rm ir}$	$1/(8\pi^2)$	0.01266514795529222143 04849
$g_{c\ell}(0)$	static collar–log overlap	0.15140235122355889364 7073
N_c	$\sqrt{\pi/8}\,\ell_0$	0.11253953951963825869 4400
$\rho_{\rm stat}$	$g_{c\ell}(0)/\sqrt{N_c N_\ell}$	0.45131529584185576931 1888
Λ_h	$(1-\rho_{\rm stat}^2)^{-1}$	1.25578523975689906678 199
$\Theta_{1,\rm core}$	$2\pi\,C_{\rm uni}$	2.71732725848783555238 861
$\Theta_1^{(\rm coll)}$	$(\gamma_E/\pi^2)\,C_{11}(\ell_0)$	0.01607850686959103319 00000
$\Theta_1^{(\log)}$	$\eta_0^2/[8(1-\eta_0^2/4)]$	0.01299429735237808221 96273
$B_{11,\rm tab}^{\rm glue}$	tabulated visible 2-channel static load	0.02904120666648408568 40579
$B_{11,\rm rec}^{\rm glue}$	$t_{\rm vis}^{\mathsf T}(K_{\rm vis}^{(2)})^{-1}t_{\rm vis}$	0.02904120666648408568 58449
$\Delta B_{11}^{\rm glue}$	reconstructed − tabulated	$1.7869761488248702093 2124\times 10^{-21}$
$B_{11,\rm tab}^{(3,\rho)}$	tabulated 3-channel static completion	0.02904114778429781136 75691
$B_{11,\rm rec}^{(3,\rho)}$	$(t^\perp)^{\mathsf T}(K_{\rm stat}^{(3,\rho)})^{-1}t^\perp$	0.02904114778429781136 75691
$\Delta B_{11}^{(3,\rho)}$	reconstructed − tabulated	$3.8295949811777497507 6346\times 10^{-37}$
$\Theta_1^{(3,\rho)}$	$\Theta_{1,\rm core}+B_{11,\rm rec}^{(3,\rho)}$	2.74636840627213336375 618

TABLE V. Rank-dependent visible dynamic diagnostics extracted from the finite-rank scalar construction. The row $N=1$ uses the empty-sector convention of definition VI.20, so $\Delta A_{\rm mix}^{(1)}=\delta A_0^{(1)}=\chi_{\rm cross}^{(1)}=0$. For $N\geq 2$, the entries are finite-N Gaussian-collar diagnostics of the hidden sector. They are neither operator-level hidden-bath data nor fitted to an external value of α, and they do not by themselves establish monotone or rigorous convergence as $N\to\infty$.

N	$\Delta A_{\rm mix}^{(N)}$	$\delta A_0^{(N)}$	$\chi_{\rm cross}^{(N)}$
1	0	0	0
3	$5.6297544557207391\times10^{-3}$	$-3.9660140058889997\times10^{-4}$	$3.1694135231707515\times10^{-5}$
5	$6.4229315823120090\times10^{-3}$	$-4.0484921668976660\times10^{-4}$	$4.1254050111061048\times10^{-5}$
100	$6.4673176500784765\times10^{-3}$	$-4.0504733367299593\times10^{-4}$	$4.1826197587016588\times10^{-5}$

TABLE VI. Visible dynamic two-channel parameters. Here $\lambda_u^{(N)}:=(1-(\rho_{\rm dyn}^{(N)})^2)^{-1}$ is the visible-source quadratic renormalization factor used by the current scalar evaluator. With the convention $g_2^{\rm eff}=\sqrt{\lambda_u^{(N)}}\,g_2$, the induced dynamic quadratic kernel is scaled by $\lambda_u^{(N)}$. The symbol g_2 labels a two-mode scalar-evaluator vector; it is unrelated to the tree-level gyromagnetic statement $g=2$.

N	$A_{\rm uv}^{(N)}$	$A_{\rm ir}^{(N)}$	$\rho_{\rm dyn}^{(N)}$	$\lambda_u^{(N)}$
1	2.857661911487003679 40000	2.857661911487003679 40000	0	1.00000000000000000000 000
3	2.862935248665477394 80000	2.851675739754035916 66000	0.00033826809862918462 0000000	1.00000011442531964335 605
5	2.863721013654457602 27000	2.850875150489833584 19000	0.00044030000425725735 90000000	1.00000019386416507271 733
100	2.863765221678688080 86000	2.850830586378531127 85000	0.00044640651108518807 0000000	1.00000019927881285128 748

TABLE VII. First coefficients of the finite hidden dynamic Jacobi chain extracted from the higher-mode matrix in the representative finite diagnostic truncation $N = 100$. These coefficients describe the finite Gaussian-collar compression and not the full unregularized derivative-trace bath.

Symbol	Def.	Value
$\|v^{(100)}\|^2$	hidden dynamic source norm	0.11058235357030053635
$a^{(100)}_{\mathrm{L},0}$	first Jacobi diagonal coefficient	0.11874476222472424339
$b^{(100)}_{\mathrm{L},1}$	first Jacobi off-diagonal coefficient	0.01434871678338358206
$a^{(100)}_{\mathrm{L},1}$	second Jacobi diagonal coefficient	0.00937286363486739350
$b^{(100)}_{\mathrm{L},2}$	second Jacobi off-diagonal coefficient	0.00670541329129441449
$a^{(100)}_{\mathrm{L},2}$	third Jacobi diagonal coefficient	0.01271810767253984155

TABLE VIII. Diagnostic scalar roots evaluated at the external orientation point x_{ref}. The quantity $\mathcal{D}_{\mathrm{C}}^{(\mathrm{vis},N)}(x_{\mathrm{ref}})$ denotes the visible two-channel scalar truncation used in the current realization, whereas $\mathcal{D}_{\mathrm{C}}^{(\mathrm{nf},N)}(x_{\mathrm{ref}})$ denotes the refined no-free-parameter mother truncation with the three-channel static completion and the visible-source renormalization factor $\lambda_u^{(N)}$. In both truncations, the listed value is the positive root on the branch selected by $\mathcal{D}_{\mathrm{C}}(x) \sim x$ as $x \downarrow 0$. The point x_{ref} is not used to define, tune, rank-select, or validate either truncation. Here $\Delta\mathcal{D}_{\mathrm{C}}^{(N)}(x_{\mathrm{ref}}) := \mathcal{D}_{\mathrm{C}}^{(\mathrm{nf},N)}(x_{\mathrm{ref}}) - \mathcal{D}_{\mathrm{C}}^{(\mathrm{vis},N)}(x_{\mathrm{ref}})$. The difference $\Delta\mathcal{D}_{\mathrm{C}}^{(N)}(x_{\mathrm{ref}})$ is an evaluator-to-evaluator comparison at fixed x_{ref}; it is not an uncertainty bound and does not by itself quantify convergence in N.

N	$\mathcal{D}_{\mathrm{C}}^{(\mathrm{vis},N)}(x_{\mathrm{ref}})$	$\mathcal{D}_{\mathrm{C}}^{(\mathrm{nf},N)}(x_{\mathrm{ref}})$	$\Delta\mathcal{D}_{\mathrm{C}}^{(N)}(x_{\mathrm{ref}})$
1	$2.31545783632796834010 \times 10^{-3}$	$2.31545783648631566866 \times 10^{-3}$	$1.58347328553 \times 10^{-13}$
3	$2.31545783183517298386 \times 10^{-3}$	$2.31545783200165699383 \times 10^{-3}$	$1.66484009966 \times 10^{-13}$
5	$2.31545783173438515638 \times 10^{-3}$	$2.31545783190651795298 \times 10^{-3}$	$1.72132796594 \times 10^{-13}$
100	$2.31545783173168786041 \times 10^{-3}$	$2.31545783190420568565 \times 10^{-3}$	$1.72517825236 \times 10^{-13}$

TABLE IX. First coefficients of the scalar branch $\mathcal{D}_{\mathrm{C}}(x) = \sum_{n\geq 1} c_n x^n$ for representative visible truncations and for the refined mother truncation. These are the formal small-x coefficients of the positive branch selected by $\mathcal{D}_{\mathrm{C}}(x) \sim x$ as $x \downarrow 0$. They are obtained from the internal scalar-evaluator expansion around $x = 0$, not from the external orientation point x_{ref} and not from a numerical fit to sampled root values. The rows compare finite-rank realizations of that branch; they do not by themselves establish infinite-rank convergence.

Coefficient	$N = 1$ (vis)	$N = 5$ (vis)	$N = 100$ (vis)	$N = 100$ (refined)
c_1	1	1	1	1
c_2	-1.37318423257715981904	-1.37318423257715981904	-1.37318423257715981904	-1.37318420313606668188
c_3	3.80047937978626535441	3.80011555037140726825	3.80011537232787127937	3.80011590129876110426
c_4	-8.85667906170849485234	-8.85785467402324147604	-8.85787085895835474781	-8.85787245590036295736
c_5	24.72888434717861820061	24.73523387578082466951	24.73531230541546984406	24.73531936592802804793

Remark (Status of the scalar numerics). The numerical data above are internal to the scalar mother construction. The static sector is represented by two visible collar–log channels together with one hidden common static mode fixed by the trace geometry. The dynamic sector is represented by a finite-N Lanczos–Jacobi compression, with representative diagnostic $N = 100$ coefficients listed in table VII. These finite coefficients do not represent the full infinite hidden dynamic bath. The refined scalar table uses the convention

$$g_2^{\mathrm{eff}} = \sqrt{\lambda_u^{(N)}}\, g_2, \qquad \lambda_u^{(N)} = \left(1 - (\rho_{\mathrm{dyn}}^{(N)})^2\right)^{-1},$$

so the dynamic quadratic kernel in Eq. (281) is scaled by $\lambda_u^{(N)}$. Any later diagnostic lift using a different refined-kernel convention must state that convention separately and must not be conflated with the scalar tables displayed here. The implemented scalar block should therefore be read as a finite-rank realization of the cavity–shell mother pencil, not as a direct-sum proxy with ad hoc corrections and not as the full operator-level scalar solution. The external orientation point used in some rows is not an input to the scalar law, not a branch-selection condition, and not a truncation-tuning target. No measured α, no QED coefficient, and no electron g-factor benchmark is used to tune the displayed scalar data.

VII. VECTOR-CHANNEL GEOMETRIC CONSTANT

This section constructs the branch-fixed vector datum for the minimal electron branch. The data entering this construction have already been fixed by the preceding branch-selection steps. The coherent one-loop carrier has radius R, the transverse Gaussian organization has collar scale $\sigma_{\mathbb{C}}$, and the first-node matching shell is $r_* = \pi R$. These are derived or selected branch data, not new postulates of the vector channel.

Under the operator hypotheses stated below, these data define a transverse shell self-return problem on the vector side. Within the admissible shell-gauge class, pure tangential gradients are annihilated by Π_{TT}. The return equation and exterior subtraction are therefore formulated entirely on the tangential-transverse (TT) shell sector. The local admitted UV load is evaluated in the branch-fixed Coulomb-gauge Biot–Savart and collar convention specified below. In the branch-cyclic numerical realization, the full-load denominator is retained, so the displayed scalar admission quotient is a fixed-representative quotient rather than a quotient on gauge classes. The gauge-class version is obtained by replacing that denominator with the TT norm, as stated in Eq. (314).

The operator-level datum of the TT shell-return problem is the dimensionless geometric constant

$$\Lambda_{\mathrm{geom}}.$$

It is neither a pointwise observable nor a bare loop logarithm. It is not inferred from the α-lock, and it is not a function of the scalar slowdown block $\mathcal{D}_{\mathrm{C}}$. The reduced quantities introduced near the end of the section are numerical realizations of this vector datum; they do not redefine it.

The vector block is organized around a shell self-return problem. At the exact operator level derived below, assume that $\mathbb{G}_{\mathrm{sh}}(\eta_0, \ell_0)$ is defined on the odd flux space and that $\mathbb{I} - \mathbb{G}_{\mathrm{sh}}(\eta_0, \ell_0)$ is invertible there. Then the returned transverse shell field a_* is uniquely determined by

$$(\mathbb{I} - \mathbb{G}_{\mathrm{sh}}(\eta_0, \ell_0))\, a_* = J_\chi(\eta_0).$$

Here a_* is a shell field, while $\mathbf{a}_*$ denotes its coordinate vector in the normalized odd-toroidal basis used later. Likewise, $J_\chi(\eta_0)$ denotes the shell source as a field, while $\mathbf{J}_\chi(\eta_0)$ denotes its coefficient vector.

For that unique returned field, the associated dimensionless scalar invariant is

$$\Lambda_{\mathrm{geom}} = \Lambda_{\mathrm{ind}} + \Delta\Lambda_{\mathrm{UV}\to\mathrm{IR}}(\ell_0; \mathscr{A}_\parallel^{\mathrm{coll}}) - \frac{1}{2}\,\langle J_\chi(\eta_0), a_*\rangle_{\mathrm{flux}}.$$

Here $\Delta\Lambda_{\mathrm{UV}\to\mathrm{IR}}(\ell_0; \mathscr{A}_\parallel^{\mathrm{coll}})$ is evaluated with the branch-fixed full-load denominator. Its numerator is TT-cleaned through Π_{TT}, equivalently through $\mathscr{A}_{\mathrm{TT}}^{\mathrm{coll}} = \Pi_{\mathrm{TT}}\mathscr{A}_\parallel^{\mathrm{coll}}$. The term Λ_{ind} is the local filamentary logarithmic core of the branch, $\Delta\Lambda_{\mathrm{UV}\to\mathrm{IR}}(\ell_0; \mathscr{A}_{\mathrm{TT}}^{\mathrm{coll}})$ is the admitted Gaussian finite part inherited from the collar and evaluated on the branch-fixed TT shell trace, and the final overlap is the nonlocal shell-return correction produced by the transverse field generated by the projected ring source.

The dependency order in the vector channel is as follows. The minimal branch fixes $R, \sigma_{\mathbb{C}}, r_*, \eta_0, \ell_0$. The local vector analysis fixes the filamentary reference core Λ_{ind} and the Gaussian finite part $C_{\mathrm{UV}}^{(\mathrm{Gauss})}$. The normalized shell-admission construction turns $C_{\mathrm{UV}}^{(\mathrm{Gauss})}$ into the admitted load $\Delta\Lambda_{\mathrm{UV}\to\mathrm{IR}}(\ell_0; \mathscr{A}_{\mathrm{TT}}^{\mathrm{coll}})$. The exact Maxwell shell trace fixes the source $J_\chi(\eta_0)$ and the exterior subtraction $\Delta\Lambda_{\mathrm{out}}(\eta_0)$. Under the return-kernel and contraction hypotheses, the shell-memory operator $\mathbb{G}_{\mathrm{sh}}(\eta_0, \ell_0)$ fixes the exact return factor R_χ and hence Λ_{geom}. Reduced spectral formulas and finite odd-mode ledgers are numerical realizations of this chain, not additional definitions.

A. Meaning of the vector geometric constant

This subsection places Λ_{geom} within the Relator kinematics and records the coordinate form of the shell functional. The effective charge and loop current carried by the branch are not primitive variables. They are derived macroscopic gauge descriptors of the coherent one-loop organization built from the generator microstate in $\mathbb{C}$, the compact-phase charge sector, and the locked loop-current normalization. No measured charge value, measured value of α, QED coefficient, or empirical current is introduced here.

The slowdown variable $\mathcal{D}_{\mathrm{total}}$ and the gauge-invariant mechanical momentum $\mathbf{P}_{\mathrm{mech}}$ have already been fixed in Eqs. (10) and (29). The scalar shell block supplies the Coulombic shell representative of this gauge-invariant slowdown, whereas the vector shell block supplies the tangential divergence-free shell response. Pure tangential gauge gradients are removed by the geometric shell projector Π_{TT}. The quantity Λ_{geom} is therefore neither a rate nor a replacement for $\omega_{\mathbb{C}}$, and it is not a raw exterior magnetic energy. It is the exact shell-level vector self-return invariant of the minimal one-loop branch. Reduced or finite-dimensional evaluations of this invariant are separate realization-level objects.

After the odd flux space, the shell source, and the shell-memory operator have been introduced below, the vector functional on a real finite Galerkin block takes the coordinate form

$$\mathcal{L}_\Lambda[\mathbf{a}] = \underbrace{\Lambda_{\mathrm{ind}} + \Delta\Lambda_{\mathrm{UV}\to\mathrm{IR}}(\ell_0; \mathscr{A}^{\mathrm{coll}}_{\mathrm{TT}})}_{\substack{\text{branch-fixed}\\ \text{vector load}}} - \underbrace{\mathbf{J}_\chi^\top \mathbf{a}}_{\substack{\text{source–field}\\ \text{coupling}}} + \underbrace{\frac{1}{2}\,\mathbf{a}^\top(\mathbb{I}-\mathbb{G}_{\mathrm{sh}})\mathbf{a}}_{\substack{\text{shell-memory}\\ \text{quadratic form}}}.$$

Here $\mathbf{a}$ and $\mathbf{J}_\chi$ are real coordinate vectors on the chosen block, and $\mathbb{I}-\mathbb{G}_{\mathrm{sh}}$ denotes the real symmetric matrix representing $\mathbb{I}-\mathbb{G}_{\mathrm{sh}}(\eta_0,\ell_0)$ on that block. The exact Hilbert-space statement is written only after the odd flux space and the operator domain of $\mathbb{G}_{\mathrm{sh}}$ have been fixed.

In the stationary axisymmetric sector the source and the returned field may be taken real in this basis, so the flux pairing reduces to the Euclidean pairing on each finite Galerkin block. For a real variation $\delta\mathbf{a}$ and $\varepsilon \in \mathbb{R}$,

$$\begin{aligned}\mathcal{L}_\Lambda[\mathbf{a}+\varepsilon\delta\mathbf{a}] - \mathcal{L}_\Lambda[\mathbf{a}] &= -\varepsilon\,\mathbf{J}_\chi^\top\delta\mathbf{a}\\ &\quad + \frac{1}{2}\Big[(\mathbf{a}+\varepsilon\delta\mathbf{a})^\top(\mathbb{I}-\mathbb{G}_{\mathrm{sh}})(\mathbf{a}+\varepsilon\delta\mathbf{a}) - \mathbf{a}^\top(\mathbb{I}-\mathbb{G}_{\mathrm{sh}})\mathbf{a}\Big]\\ &= \varepsilon\,\delta\mathbf{a}^\top\Big((\mathbb{I}-\mathbb{G}_{\mathrm{sh}})\mathbf{a}-\mathbf{J}_\chi\Big) + \frac{\varepsilon^2}{2}\,\delta\mathbf{a}^\top(\mathbb{I}-\mathbb{G}_{\mathrm{sh}})\delta\mathbf{a},\end{aligned}$$

because $\mathbb{I}-\mathbb{G}_{\mathrm{sh}}$ is symmetric on the chosen real block. Therefore the first variation is

$$\delta\mathcal{L}_\Lambda[\mathbf{a}](\delta\mathbf{a}) = \delta\mathbf{a}^\top\Big((\mathbb{I}-\mathbb{G}_{\mathrm{sh}})\mathbf{a}-\mathbf{J}_\chi\Big),$$

and stationarity for every real $\delta\mathbf{a}$ is equivalent to

$$(\mathbb{I}-\mathbb{G}_{\mathrm{sh}})\mathbf{a}_* = \mathbf{J}_\chi.$$

Whenever $\mathbb{I}-\mathbb{G}_{\mathrm{sh}}$ is invertible on that block, the stationary point is unique and is given by

$$\mathbf{a}_* = (\mathbb{I}-\mathbb{G}_{\mathrm{sh}})^{-1}\mathbf{J}_\chi.$$

This invertibility is a shell-return hypothesis for the vector sector and is not a numerical fit.

Evaluating the functional at the stationary point gives

$$\begin{aligned}\mathcal{L}_\Lambda[\mathbf{a}_*] &= \Lambda_{\mathrm{ind}} + \Delta\Lambda_{\mathrm{UV}\to\mathrm{IR}}(\ell_0; \mathscr{A}^{\mathrm{coll}}_{\mathrm{TT}}) - \mathbf{J}_\chi^\top\mathbf{a}_* + \frac{1}{2}\,\mathbf{a}_*^\top(\mathbb{I}-\mathbb{G}_{\mathrm{sh}})\mathbf{a}_*\\ &= \Lambda_{\mathrm{ind}} + \Delta\Lambda_{\mathrm{UV}\to\mathrm{IR}}(\ell_0; \mathscr{A}^{\mathrm{coll}}_{\mathrm{TT}}) - \mathbf{J}_\chi^\top\mathbf{a}_* + \frac{1}{2}\,\mathbf{a}_*^\top\mathbf{J}_\chi\\ &= \Lambda_{\mathrm{ind}} + \Delta\Lambda_{\mathrm{UV}\to\mathrm{IR}}(\ell_0; \mathscr{A}^{\mathrm{coll}}_{\mathrm{TT}}) - \frac{1}{2}\,\mathbf{J}_\chi^\top\mathbf{a}_*,\end{aligned}$$

where the second line uses the stationary equation and the last line uses $\mathbf{a}_*^\top\mathbf{J}_\chi = \mathbf{J}_\chi^\top\mathbf{a}_*$ for real coordinate vectors. Accordingly, once the exact odd-flux operator problem below has been posed and solved under its stated hypotheses, the field-level invariant is

$$\Lambda_{\mathrm{geom}} = \Lambda_{\mathrm{ind}} + \Delta\Lambda_{\mathrm{UV}\to\mathrm{IR}}(\ell_0; \mathscr{A}^{\mathrm{coll}}_{\mathrm{TT}}) - \frac{1}{2}\,\langle J_\chi(\eta_0), a_*\rangle_{\mathrm{flux}}.$$

This is the dimensionless scalar invariant carried by the closed vector self-return of the branch. It is a vector-shell invariant, not a scalar-channel slowdown and not the final scalar–vector lock output.

The matching shell is not an arbitrary auxiliary sphere. It is the first-node surface selected by the minimal branch geometry, on which the branch tests whether its own transverse gauge-invariant return field closes consistently. Within the branch class used in this paper, the single loop is the minimal nonzero winding carrier compatible with axial symmetry and stationary current closure. Higher winding sectors or higher-node carriers belong to higher branch sectors and are not part of the minimal branch used for the electron sector.

A compact summary of the geometric chain is

$$\begin{aligned}\text{Gaussian generator sheet in } \mathbb{C} &\longrightarrow \text{coarse-grained one-loop carrier} \longrightarrow \text{effective shell source in } \mathbb{R}^3\\ &\longrightarrow \text{admitted transverse shell return} \longrightarrow \Lambda_{\mathrm{geom}}.\end{aligned}$$

The rest of the section resolves the branch-fixed ingredients entering this stationary reduction; the local core Λ_{ind}, the admitted Gaussian finite part $\Delta\Lambda_{\mathrm{UV}\to\mathrm{IR}}(\ell_0; \mathscr{A}^{\mathrm{coll}}_{\mathrm{TT}})$, the shell source $J_\chi(\eta_0)$, and the nonlocal shell return encoded by $\mathbb{G}_{\mathrm{sh}}$. These ingredients are derived within the vector shell construction. They are not adjusted to match a measured value of α or any QED benchmark.

B. Intrinsic core and exact shell admission

We now derive the branch-fixed local part of the vector mother equation. The local vector load consists of the filamentary logarithmic reference core $\Lambda_{\rm ind}$ and the universal Gaussian finite part $C_{\rm UV}^{(\rm Gauss)}$. The admitted contribution $\Delta\Lambda_{\rm UV\to IR}(\ell_0;\mathscr{A}_{\parallel}^{\rm coll})$ is obtained only after $C_{\rm UV}^{(\rm Gauss)}$ has been transported to the matching shell, tangential-transverse (TT) cleaned, and weighted by the shell-admission operator. None of these local quantities contains the nonlocal shell-memory inversion; that inversion enters only later through $\mathbb{G}_{\rm sh}$ and R_χ. The purpose of this subsection is therefore to derive these local inputs and the exact shell-admission framework before the shell-memory problem is solved. No measured value of α, no QED coefficient, and no fitted vector parameter enters this local vector-load layer.

Definition VII.1 (Filamentary reference and vector-branch geometry)**.** The coarse-grained vector source in $\mathbb{R}^3$ is represented by the effective one-loop filamentary skeleton whose centerline has radius R. Its transverse width is retained through the Gaussian collar scale $\sigma_{\mathbb{C}}$ inherited from the generator microstate in $\mathbb{C}$. This skeleton is a shell-source representative, not a microscopic material ring, not an empirical current loop, and not an additional observed spatial structure. In this local vector subsection we use the dimensionless ratios

$$\varepsilon_{\rm br}\equiv\frac{\sigma_{\mathbb{C}}}{R},\qquad \eta\equiv\frac{R}{r_*},\qquad \ell\equiv\frac{\sigma_{\mathbb{C}}}{r_*}=\varepsilon_{\rm br}\eta. \tag{283}$$

On the minimal branch geometry later used for the electron sector, these are the previously derived values

$$\varepsilon_{\rm br,0}=\frac{1}{\sqrt{\pi}},\qquad \eta_0=\frac{1}{\pi},\qquad \ell_0=\frac{1}{\pi\sqrt{\pi}}. \tag{284}$$

This local notation does not alter the earlier SI convention that ε_0 denotes the vacuum permittivity.

Definition VII.2 (Complete elliptic integrals)**.** For $m\in[0,1)$, the complete elliptic integrals of the first and second kind are

$$\mathrm{K}_{\rm ell}(m)=\int_0^{\pi/2}\frac{\mathrm{d}\varphi}{\sqrt{1-m\sin^2\varphi}},\qquad \mathrm{E}_{\rm ell}(m)=\int_0^{\pi/2}\sqrt{1-m\sin^2\varphi}\,\mathrm{d}\varphi. \tag{285}$$

Here m is the elliptic parameter. In the loop problem below one has $m=k^2$, where $k\in(0,1)$ is determined by the ratio of the tubular offset to the loop radius. This m is unrelated to the particle mass used elsewhere in the paper. As $m\uparrow 1$, $\mathrm{K}_{\rm ell}(m)$ develops the logarithmic divergence of the loop self-geometry, while $\mathrm{E}_{\rm ell}(m)$ remains finite.

Proposition 39 (Tubular regularization of the thin-loop tangential self-trace and circulation)**.** *Let*

$$\Gamma_R=\big\{(R\cos\phi,R\sin\phi,0)\,;\,0\le\phi<2\pi\big\}\subset\mathbb{R}^3$$

be the effective filamentary skeleton associated with the one-loop branch, oriented by increasing ϕ. The variables ϕ and θ used in this local loop calculation are ring azimuth parameters in $\mathbb{R}^3$; they are distinct from the compact generator phase θ_0. If Γ_R carries a steady current I in that orientation, its standard Coulomb-gauge magnetostatic vector potential in SI units is

$$\mathbf{A}(\mathbf{r})=\frac{\mu_0 I}{4\pi}\oint_{\Gamma_R}\frac{\mathrm{d}\boldsymbol{\ell}'}{|\mathbf{r}-\mathbf{r}'|}.$$

where μ_0 is the SI vacuum permeability. The vector potential $\mathbf{A}$ has units tesla–meter, equivalently weber per meter. The pointwise tangential trace is Coulomb-gauge representative data, whereas the closed circulation below is gauge invariant for smooth single-valued gauge functions on the tubular neighborhood. To regularize the self-trace, evaluate $\mathbf{A}$ on the binormal tubular offset

$$\mathbf{r}_a(\theta)=\big(R\cos\theta,R\sin\theta,a\big),\qquad a>0,$$

and denote the corresponding offset loop by

$$\Gamma_{R,a}=\big\{(R\cos\theta,R\sin\theta,a)\,;\,0\le\theta<2\pi\big\}.$$

The corresponding unit tangent is

$$\mathbf{t}(\theta)=(-\sin\theta,\cos\theta,0).$$

Define the regularized tangential trace on the offset loop by

$$A_{\parallel,a}^{\mathrm{ring}}(\theta) \coloneqq \mathbf{A}(\mathbf{r}_a(\theta)) \cdot \mathbf{t}(\theta).$$

By rotational symmetry, $A_{\parallel,a}^{\mathrm{ring}}(\theta)$ is independent of θ; we therefore write it simply as $A_{\parallel,a}^{\mathrm{ring}}$. One then has

$$A_{\parallel,a}^{\mathrm{ring}} = \frac{\mu_0 IR}{4\pi} \int_0^{2\pi} \frac{\cos\varphi}{\sqrt{a^2 + 4R^2 \sin^2(\varphi/2)}} \, \mathrm{d}\varphi. \tag{286}$$

Defining

$$k^2 = \frac{4R^2}{4R^2 + a^2}, \tag{287}$$

one has $0 < k < 1$, and the exact elliptic representation is

$$A_{\parallel,a}^{\mathrm{ring}} = \frac{\mu_0 I}{\pi k} \left[\left(1 - \frac{k^2}{2}\right) \mathrm{K}_{\mathrm{ell}}(k^2) - \mathrm{E}_{\mathrm{ell}}(k^2) \right]. \tag{288}$$

As $a/R \to 0$,

$$A_{\parallel,a}^{\mathrm{ring}} = \frac{\mu_0 I}{2\pi} \left[\ln\frac{8R}{a} - 2 + O\!\left(\frac{a^2}{R^2} \ln\frac{R}{a} \right) \right]. \tag{289}$$

In particular, identifying the tubular offset with the Gaussian transverse scale,

$$a = \sigma_{\mathbb{C}}, \tag{290}$$

gives

$$A_{\parallel}^{\mathrm{ring,reg}} = \frac{\mu_0 I}{2\pi} \left[\underbrace{\ln\frac{8R}{\sigma_{\mathbb{C}}} - 2}_{\substack{\textit{leading logarithmic} \\ \textit{filamentary core}}} + \underbrace{O\!\left(\frac{\sigma_{\mathbb{C}}^2}{R^2} \ln\frac{R}{\sigma_{\mathbb{C}}} \right)}_{\substack{\textit{local finite-width} \\ \textit{tubular remainder}}} \right]. \tag{291}$$

Equivalently, define the regularized vector potential on the offset loop by

$$\mathbf{A}_{\mathrm{reg}}(\theta) \coloneqq \mathbf{A}(\mathbf{r}_{\sigma_{\mathbb{C}}}(\theta)),$$

and denote that offset loop by

$$\Gamma_{R,\sigma_{\mathbb{C}}} = \big\{ (R\cos\theta, R\sin\theta, \sigma_{\mathbb{C}}) \,;\, 0 \le \theta < 2\pi \big\}.$$

Since $A_{\parallel}^{\mathrm{ring,reg}} = \mathbf{A}_{\mathrm{reg}}(\theta) \cdot \mathbf{t}(\theta)$ is constant along $\Gamma_{R,\sigma_{\mathbb{C}}}$, the regularized closed-loop circulation is

$$\oint_{\Gamma_{R,\sigma_{\mathbb{C}}}} \mathbf{A}_{\mathrm{reg}} \cdot \mathrm{d}\boldsymbol{\ell} = \mu_0 RI \left[\ln\frac{8R}{\sigma_{\mathbb{C}}} - 2 + O\!\left(\frac{\sigma_{\mathbb{C}}^2}{R^2} \ln\frac{R}{\sigma_{\mathbb{C}}} \right) \right]. \tag{292}$$

Proof. Parameterize the source loop by

$$\mathbf{r}'(\phi) = R(\cos\phi, \sin\phi, 0), \qquad \mathrm{d}\boldsymbol{\ell}' = R(-\sin\phi, \cos\phi, 0)\, \mathrm{d}\phi.$$

Fix the offset field point $\mathbf{r}_a(\theta)$. Writing $\phi = \theta + \varphi$, one finds

$$\mathbf{t}(\theta) \cdot \mathrm{d}\boldsymbol{\ell}' = R\cos\varphi \, \mathrm{d}\varphi,$$

and

$$|\mathbf{r}_a(\theta) - \mathbf{r}'(\theta + \varphi)|^2 = a^2 + 4R^2 \sin^2(\varphi/2).$$

Hence, from the SI Biot–Savart potential formula and the definition of $A^{\rm ring}_{\parallel,a}$,

$$A^{\rm ring}_{\parallel,a} = \frac{\mu_0 I R}{4\pi} \int_0^{2\pi} \frac{\cos\varphi}{\sqrt{a^2 + 4R^2 \sin^2(\varphi/2)}}\,\mathrm{d}\varphi,$$

which is Eq. (286).

Set $u = \varphi/2$. Then

$$A^{\rm ring}_{\parallel,a} = \frac{\mu_0 I R}{2\pi} \int_0^{\pi} \frac{\cos(2u)}{\sqrt{a^2 + 4R^2 \sin^2 u}}\,\mathrm{d}u.$$

The integrand is invariant under $u \mapsto \pi - u$, because

$$\cos(2(\pi - u)) = \cos(2u), \qquad \sin^2(\pi - u) = \sin^2 u.$$

Hence

$$\int_0^{\pi} \frac{\cos(2u)}{\sqrt{a^2 + 4R^2 \sin^2 u}}\,\mathrm{d}u = 2\int_0^{\pi/2} \frac{\cos(2u)}{\sqrt{a^2 + 4R^2 \sin^2 u}}\,\mathrm{d}u.$$

Now substitute $u \mapsto \pi/2 - u$. Then

$$\cos(2(\pi/2 - u)) = -\cos(2u) = 1 - 2\cos^2 u, \qquad \sin^2(\pi/2 - u) = \cos^2 u.$$

Therefore

$$\int_0^{\pi} \frac{\cos(2u)}{\sqrt{a^2 + 4R^2 \sin^2 u}}\,\mathrm{d}u = 2\int_0^{\pi/2} \frac{1 - 2\cos^2 u}{\sqrt{a^2 + 4R^2 \cos^2 u}}\,\mathrm{d}u.$$

Hence

$$A^{\rm ring}_{\parallel,a} = \frac{\mu_0 I R}{\pi} \int_0^{\pi/2} \frac{1 - 2\cos^2 u}{\sqrt{a^2 + 4R^2 \cos^2 u}}\,\mathrm{d}u.$$

With

$$k^2 = \frac{4R^2}{4R^2 + a^2},$$

one has

$$a^2 + 4R^2 \cos^2 u = \frac{4R^2}{k^2}\bigl(1 - k^2 \sin^2 u\bigr),$$

hence

$$A^{\rm ring}_{\parallel,a} = \frac{\mu_0 I k}{2\pi} \int_0^{\pi/2} \frac{1 - 2\cos^2 u}{\sqrt{1 - k^2 \sin^2 u}}\,\mathrm{d}u.$$

Using $1 - 2\cos^2 u = -1 + 2\sin^2 u$, together with

$$\int_0^{\pi/2} \frac{\mathrm{d}u}{\sqrt{1 - k^2 \sin^2 u}} = \mathrm{K}_{\rm ell}(k^2),$$

and

$$\mathrm{E}_{\rm ell}(k^2) = \mathrm{K}_{\rm ell}(k^2) - k^2 \int_0^{\pi/2} \frac{\sin^2 u}{\sqrt{1 - k^2 \sin^2 u}}\,\mathrm{d}u,$$

we obtain

$$\int_0^{\pi/2} \frac{\sin^2 u}{\sqrt{1 - k^2 \sin^2 u}}\,\mathrm{d}u = \frac{\mathrm{K}_{\rm ell}(k^2) - \mathrm{E}_{\rm ell}(k^2)}{k^2}.$$

Substituting this identity gives

$$A_{\parallel,a}^{\text{ring}} = \frac{\mu_0 I k}{2\pi}\left[-\mathrm{K}_{\text{ell}}(k^2) + \frac{2}{k^2}\left(\mathrm{K}_{\text{ell}}(k^2) - \mathrm{E}_{\text{ell}}(k^2)\right)\right] = \frac{\mu_0 I}{\pi k}\left[\left(1 - \frac{k^2}{2}\right)\mathrm{K}_{\text{ell}}(k^2) - \mathrm{E}_{\text{ell}}(k^2)\right],$$

which is Eq. (288).

For the thin-tube asymptotic, define the complementary modulus

$$k'^2 := 1 - k^2 = \frac{a^2}{4R^2 + a^2}.$$

As $a/R \to 0$, one has

$$k' = \frac{a}{\sqrt{4R^2 + a^2}} = \frac{a}{2R} + O\left(\frac{a^3}{R^3}\right),$$

$$\frac{1}{k} = 1 + O(k'^2), \qquad 1 - \frac{k^2}{2} = \frac{1}{2} + O(k'^2).$$

The standard complete-elliptic expansions for $k' \downarrow 0$ are

$$\mathrm{K}_{\text{ell}}(k^2) = \ln\frac{4}{k'} + O\left(k'^2 \ln\frac{1}{k'}\right), \qquad \mathrm{E}_{\text{ell}}(k^2) = 1 + O\left(k'^2 \ln\frac{1}{k'}\right).$$

Substituting these into Eq. (288) yields

$$A_{\parallel,a}^{\text{ring}} = \frac{\mu_0 I}{2\pi}\left[\ln\frac{4}{k'} - 2 + O\left(k'^2 \ln\frac{1}{k'}\right)\right].$$

Next,

$$\ln\frac{4}{k'} = \ln\frac{4\sqrt{4R^2 + a^2}}{a} = \ln\frac{8R}{a} + O\left(\frac{a^2}{R^2}\right),$$

and

$$k'^2 \ln\frac{1}{k'} = O\left(\frac{a^2}{R^2}\ln\frac{R}{a}\right).$$

Therefore

$$A_{\parallel,a}^{\text{ring}} = \frac{\mu_0 I}{2\pi}\left[\ln\frac{8R}{a} - 2 + O\left(\frac{a^2}{R^2}\ln\frac{R}{a}\right)\right], \qquad \frac{a}{R} \downarrow 0,$$

which is Eq. (289). Here the $O(\cdot)$ term is with respect to the dimensionless parameter a/R with R fixed. Substituting $a = \sigma_{\mathbb{C}}$ gives Eq. (291). Since $A_{\parallel}^{\text{ring,reg}}$ is constant along the offset loop $\Gamma_{R,\sigma_{\mathbb{C}}}$, the circulation is

$$\oint_{\Gamma_{R,\sigma_{\mathbb{C}}}} \mathbf{A}_{\text{reg}} \cdot \mathrm{d}\boldsymbol{\ell} = A_{\parallel}^{\text{ring,reg}}\,(2\pi R),$$

which gives Eq. (292). Finally, if λ_{g} is smooth and single-valued on a neighborhood of $\Gamma_{R,\sigma_{\mathbb{C}}}$, then

$$\oint_{\Gamma_{R,\sigma_{\mathbb{C}}}} \nabla\lambda_{\text{g}} \cdot \mathrm{d}\boldsymbol{\ell} = 0,$$

because the integral of an exact differential over a closed loop vanishes. Hence the closed circulation is gauge invariant within that gauge class. □

Remark (Meaning of $\mathbf{A}$ and its relation to the magnetic field)*.* The quantity $\mathbf{A}$ denotes the standard magnetostatic vector potential in the projected physical space $\mathbb{R}^3$. In SI units it has units tesla–meter, equivalently weber per meter. It is not the magnetic field itself; rather,

$$\mathbf{B} = \nabla \times \mathbf{A},$$

where $\mathbf{B}$ has units tesla. For an ideal thin filament, the pointwise self-field on the carrier is singular. Accordingly, the finite quantity extracted in the present calculation is not the local value of $\mathbf{B}$ on the loop, but the regularized tangential trace $A_{\parallel}^{\mathrm{ring,reg}}$, namely the component of $\mathbf{A}$ parallel to the loop tangent on the offset circle $\Gamma_{R,\sigma_{\mathbb{C}}}$. The earlier quantity $A_{\parallel,a}^{\mathrm{ring}}$ is the same tangential trace evaluated on the tubular offset at distance a; after the identification $a = \sigma_{\mathbb{C}}$ one obtains the regularized value $A_{\parallel}^{\mathrm{ring,reg}}$.

The closed-loop circulation

$$\oint_{\Gamma_{R,\sigma_{\mathbb{C}}}} \mathbf{A}_{\mathrm{reg}} \cdot \mathrm{d}\boldsymbol{\ell}$$

has units of magnetic flux. Because the integration path is closed, any gauge transformation $\mathbf{A} \mapsto \mathbf{A} + \nabla\lambda_{\mathrm{g}}$ with λ_{g} smooth and single-valued on a neighborhood of $\Gamma_{R,\sigma_{\mathbb{C}}}$ changes the integral by

$$\oint_{\Gamma_{R,\sigma_{\mathbb{C}}}} \nabla\lambda_{\mathrm{g}} \cdot \mathrm{d}\boldsymbol{\ell} = 0,$$

so the circulation is gauge-invariant. In regularized Stokes form it is the regularized self-flux linked by the offset loop. After division by the current I, it yields the regularized self-inductance

$$L_{\mathrm{self}}^{\mathrm{reg}} = \frac{1}{I} \oint_{\Gamma_{R,\sigma_{\mathbb{C}}}} \mathbf{A}_{\mathrm{reg}} \cdot \mathrm{d}\boldsymbol{\ell}.$$

In this sense, the bracketed term in Eqs. (289) and (292) is the dimensionless geometric factor controlling the strength of the loop's coupling to its own magnetic field.

Definition VII.3 (Filamentary reference core)**.** The filamentary reference core is the dimensionless leading logarithmic coefficient extracted from the gauge-invariant regularized circulation Eq. (292). Equivalently, in the Coulomb-gauge Biot–Savart representative Eq. (291), it is the leading bracket after the local tubular remainder has been separated. Thus

$$\Lambda_{\mathrm{ind}} \equiv \ln\frac{8R}{\sigma_{\mathbb{C}}} - 2. \tag{293}$$

On the minimal electron branch,

$$\Lambda_{\mathrm{ind}} = \ln(8\sqrt{\pi}) - 2. \tag{294}$$

Remark. The coefficient Λ_{ind} is a filamentary *reference core*. It is the leading logarithmic contribution extracted from the exact tubular regularization of the thin loop; it is not the full finite-width self-circulation of the dressed branch. The remainder

$$O\left(\frac{\sigma_{\mathbb{C}}^2}{R^2} \ln\frac{R}{\sigma_{\mathbb{C}}}\right)$$

is a local finite-width correction. In the theorem path of the present section, that remainder is not set to zero and is not identified a priori with the later Gaussian dressing unless such a matching is proved separately.

On the minimal branch geometry later used for the electron sector one has

$$\varepsilon_{\mathrm{br}} = \frac{\sigma_{\mathbb{C}}}{R} = \frac{1}{\sqrt{\pi}} \approx 0.564,$$

which is not an asymptotically small parameter. Therefore $\Lambda_{\mathrm{ind}} = \ln(8\sqrt{\pi}) - 2$ must be read as an extracted logarithmic reference core, not as a claim that the local tubular remainder is numerically negligible on that branch.

In particular, the exact theorem path uses Λ_{ind} only as the fixed filamentary logarithmic core. The finite transverse structure retained explicitly in the later vector channel is carried by $C_{\mathrm{UV}}^{(\mathrm{Gauss})}$, the Gaussian collar extension E_ℓ, the swirl-compliance operator $\mathbb{S}_\ell$, and the full shell-admission operator $\mathbb{Q}_\chi(\ell)$. This separation prevents double counting of finite-width effects.

Definition VII.4 (Normalized Gaussian collar density on the transverse normal plane)**.** Let $y \in \mathbb{R}^2$ denote a local transverse displacement from the carrier in a normal plane to the loop. The Euclidean norm $|y|$ is the local transverse distance from the carrier. The normalized Gaussian collar density of width $\sigma_{\mathbb{C}}$ is

$$g_{\sigma_{\mathbb{C}}}(y) = \frac{1}{\pi\sigma_{\mathbb{C}}^2} e^{-|y|^2/\sigma_{\mathbb{C}}^2}, \qquad y \in \mathbb{R}^2,$$

so that

$$\int_{\mathbb{R}^2} g_{\sigma_{\mathbb{C}}}(y)\, \mathrm{d}^2 y = 1.$$

The density $g_{\sigma_{\mathbb{C}}}$ has units of inverse area. Therefore any average taken against $g_{\sigma_{\mathbb{C}}}(y)\, \mathrm{d}^2 y$ is dimensionless whenever the integrand is dimensionless.

Lemma 12 (Gaussian finite part)**.** *The single-point Gaussian collar average of the local logarithm is*

$$\int_{\mathbb{R}^2} g_{\sigma_{\mathbb{C}}}(y)\, \ln\frac{\sigma_{\mathbb{C}}}{|y|}\, \mathrm{d}^2 y = \frac{\gamma_E}{2}, \tag{295}$$

where γ_E is the Euler–Mascheroni constant. The integral is absolutely convergent, dimensionless, and independent of $\sigma_{\mathbb{C}}$.

Proof. Write

$$I_{\mathrm{G}} = \int_{\mathbb{R}^2} g_{\sigma_{\mathbb{C}}}(y)\, \ln\frac{\sigma_{\mathbb{C}}}{|y|}\, \mathrm{d}^2 y = \frac{1}{\pi\sigma_{\mathbb{C}}^2} \int_{\mathbb{R}^2} e^{-|y|^2/\sigma_{\mathbb{C}}^2} \ln\frac{\sigma_{\mathbb{C}}}{|y|}\, \mathrm{d}^2 y.$$

The integral is absolutely convergent because the Gaussian factor gives exponential decay at infinity, while near $y = 0$ one has $\int_0^1 r|\ln r|\, \mathrm{d}r < \infty$.

In polar coordinates $s := |y|$, with $\mathrm{d}^2 y = 2\pi s\, \mathrm{d}s$, one finds

$$I_{\mathrm{G}} = \frac{2}{\sigma_{\mathbb{C}}^2} \int_0^\infty e^{-s^2/\sigma_{\mathbb{C}}^2} s \ln\frac{\sigma_{\mathbb{C}}}{s}\, \mathrm{d}s.$$

Now set

$$t = \frac{s^2}{\sigma_{\mathbb{C}}^2}, \qquad s\, \mathrm{d}s = \frac{\sigma_{\mathbb{C}}^2}{2}\, \mathrm{d}t.$$

Then

$$I_{\mathrm{G}} = \int_0^\infty e^{-t} \ln\frac{1}{\sqrt{t}}\, \mathrm{d}t = -\frac{1}{2}\int_0^\infty e^{-t} \ln t\, \mathrm{d}t.$$

The dependence on $\sigma_{\mathbb{C}}$ cancels exactly at this step. Using the standard Gamma-function identity

$$\int_0^\infty e^{-t} \ln t\, \mathrm{d}t = -\gamma_E,$$

one obtains

$$I_{\mathrm{G}} = \frac{\gamma_E}{2},$$

which proves Eq. (295). □

Theorem 8 (Gaussian UV constant)**.** *Let Y and Y' be independent transverse collar points with common density $g_{\sigma_{\mathbb{C}}}$. Define*

$$C_{\mathrm{UV}}^{(\mathrm{Gauss})} := \iint_{\mathbb{R}^2\times\mathbb{R}^2} g_{\sigma_{\mathbb{C}}}(y)\, g_{\sigma_{\mathbb{C}}}(y')\, \ln\frac{2\sigma_{\mathbb{C}}}{|y-y'|}\, \mathrm{d}^2 y\, \mathrm{d}^2 y'. \tag{296}$$

Then $C_{\mathrm{UV}}^{(\mathrm{Gauss})}$ is absolutely convergent and satisfies

$$C_{\mathrm{UV}}^{(\mathrm{Gauss})} = \frac{1}{2}(\ln 2 + \gamma_E) = \underbrace{\frac{1}{2}\ln 2}_{\substack{\textit{relative-width}\\ \textit{doubling term}}} + \underbrace{\frac{\gamma_E}{2}}_{\substack{\textit{single-point Gaussian}\\ \textit{finite part}}}. \tag{297}$$

Proof. Set

$$I_{\mathrm{UV}} := C_{\mathrm{UV}}^{(\mathrm{Gauss})}.$$

Because $g_{\sigma_{\mathbb{C}}}$ is Gaussian, the integrand in Eq. (296) decays exponentially for large $|y|$ and $|y'|$. Near the diagonal $y = y'$, the singularity is only logarithmic, and $\int_{|z|<1} |\ln|z||\,\mathrm{d}^2z < \infty$. Hence the double integral defining I_{UV} is absolutely convergent.

Introduce the relative variable

$$z := y - y'.$$

By Fubini's theorem,

$$I_{\mathrm{UV}} = \int_{\mathbb{R}^2} \left(\int_{\mathbb{R}^2} g_{\sigma_{\mathbb{C}}}(y)\, g_{\sigma_{\mathbb{C}}}(y-z)\,\mathrm{d}^2y \right) \ln\frac{2\sigma_{\mathbb{C}}}{|z|}\,\mathrm{d}^2z.$$

The inner integral is the Gaussian convolution. Since

$$g_{\sigma_{\mathbb{C}}}(y) = \frac{1}{\pi\sigma_{\mathbb{C}}^2} e^{-|y|^2/\sigma_{\mathbb{C}}^2},$$

one has

$$\int_{\mathbb{R}^2} g_{\sigma_{\mathbb{C}}}(y)\, g_{\sigma_{\mathbb{C}}}(y-z)\,\mathrm{d}^2y = \frac{1}{\pi^2\sigma_{\mathbb{C}}^4} \int_{\mathbb{R}^2} e^{-(|y|^2+|y-z|^2)/\sigma_{\mathbb{C}}^2}\,\mathrm{d}^2y.$$

Complete the square,

$$|y|^2 + |y-z|^2 = 2\left|y - \frac{z}{2}\right|^2 + \frac{|z|^2}{2},$$

to obtain

$$\int_{\mathbb{R}^2} g_{\sigma_{\mathbb{C}}}(y)\, g_{\sigma_{\mathbb{C}}}(y-z)\,\mathrm{d}^2y = \frac{e^{-|z|^2/(2\sigma_{\mathbb{C}}^2)}}{\pi^2\sigma_{\mathbb{C}}^4} \int_{\mathbb{R}^2} e^{-2|u|^2/\sigma_{\mathbb{C}}^2}\,\mathrm{d}^2u = \frac{1}{2\pi\sigma_{\mathbb{C}}^2} e^{-|z|^2/(2\sigma_{\mathbb{C}}^2)}.$$

Hence

$$I_{\mathrm{UV}} = \frac{1}{2\pi\sigma_{\mathbb{C}}^2} \int_{\mathbb{R}^2} e^{-|z|^2/(2\sigma_{\mathbb{C}}^2)} \ln\frac{2\sigma_{\mathbb{C}}}{|z|}\,\mathrm{d}^2z.$$

Now scale

$$z = \sqrt{2}\,\sigma_{\mathbb{C}}\,w, \qquad \mathrm{d}^2z = 2\sigma_{\mathbb{C}}^2\,\mathrm{d}^2w.$$

Then

$$I_{\mathrm{UV}} = \frac{1}{\pi} \int_{\mathbb{R}^2} e^{-|w|^2} \ln\frac{\sqrt{2}}{|w|}\,\mathrm{d}^2w = \frac{1}{2}\ln 2 + \frac{1}{\pi} \int_{\mathbb{R}^2} e^{-|w|^2} \ln\frac{1}{|w|}\,\mathrm{d}^2w.$$

The second term is exactly the single-point Gaussian finite part at unit width; by Eq. (295),

$$\frac{1}{\pi} \int_{\mathbb{R}^2} e^{-|w|^2} \ln\frac{1}{|w|}\,\mathrm{d}^2w = \frac{\gamma_E}{2}.$$

Therefore

$$C_{\mathrm{UV}}^{(\mathrm{Gauss})} = \frac{1}{2}\ln 2 + \frac{\gamma_E}{2} = \frac{1}{2}(\ln 2 + \gamma_E),$$

which proves Eq. (297). The decomposition displayed in Eq. (297) is then immediate. □

Remark. Up to this point the derivation is local on the transverse normal plane of the carrier. The shell enters only through the TT projector, the Gaussian collar lift, and the shell-admission chain. For a tangential shell trace $\mathscr{A}_{\mathrm{sh}}$, the admitted ultraviolet contribution will be

$$\Delta\Lambda_{\mathrm{UV}\to\mathrm{IR}}(\ell;\mathscr{A}_{\mathrm{sh}}) = C_{\mathrm{UV}}^{(\mathrm{Gauss})}\, P_{IR,\mathrm{full}}^{(\chi)}(\ell;\mathscr{A}_{\mathrm{sh}}),$$

with $P_{IR,\mathrm{full}}^{(\chi)}(\ell;\mathscr{A}_{\mathrm{sh}})$ defined in Eq. (313).

Definition VII.5 (Axisymmetric tangential shell space)**.** Let $\Sigma_{r_*} \subset \mathbb{R}^3$ be the matching shell, identified with $\mathbb{S}^2$ through the angular coordinates (ϑ, φ). We work throughout with dimensionless angular shell operators and with the dimensionless solid-angle measure

$$\mathrm{d}\Omega = \sin\vartheta\, \mathrm{d}\vartheta\, \mathrm{d}\varphi.$$

The symbol $H_{\tan}^{\mathrm{ax}}(\Sigma_{r_*})$ denotes the real L^2-based Hilbert space of axisymmetric tangential shell amplitudes

$$U(\vartheta) = U_\vartheta(\vartheta)\, \hat{\mathbf{e}}_\vartheta + U_\varphi(\vartheta)\, \hat{\mathbf{e}}_\varphi$$

such that

$$U_\vartheta, U_\varphi \in L^2\big((0,\pi), \sin\vartheta\, \mathrm{d}\vartheta\big).$$

Physical SI fields enter this space only after their common SI prefactors have been removed, as in the normalized shell trace $\widetilde{b}_\eta$ below. Thus the shell pairings in this subsection are reduced geometric pairings unless an SI prefactor is explicitly restored. Equip this space with the real shell pairing

$$\langle U, V\rangle_{\mathrm{sh}} = \int_{S^2_{r_*}} U\cdot V\, \mathrm{d}\Omega = 2\pi \int_0^\pi \big(U_\vartheta(\vartheta)V_\vartheta(\vartheta) + U_\varphi(\vartheta)V_\varphi(\vartheta)\big) \sin\vartheta\, \mathrm{d}\vartheta. \tag{298}$$

If the space is complexified, this pairing is extended sesquilinearly by conjugating the first entry. With the above convention that U and V are dimensionless shell amplitudes, $\langle U, V\rangle_{\mathrm{sh}}$ is dimensionless.

The measure $\mathrm{d}\Omega$ and the angular differential operators are dimensionless. Hence, when U and V are dimensionless shell amplitudes, the pairing is dimensionless. If U and V are SI-valued tangential traces, such as traces of the vector potential, the pairing carries the product of their physical units. All scalar Rayleigh quotients below are dimensionless because their numerators and denominators carry the same units, or because the common SI prefactor has first been removed. All tangential differential operators below are taken in this angular shell representation. Here $\nabla_{\tan}$ and $\div_{\tan}$ act on shell scalars and shell tangential fields in the standard way. We use the scalar Laplace–Beltrami sign convention

$$\Delta_{\tan} \coloneqq \div_{\tan}\nabla_{\tan}, \qquad -\Delta_{\tan} \geq 0$$

on nonconstant scalar spherical harmonics. The inverse $\Delta_{\tan}^{-1}$ used below is the inverse of $\Delta_{\tan}$ on the mean-zero axisymmetric scalar subspace. Thus, with the convention $-\Delta_{\tan} \geq 0$, this inverse is the inverse of a negative operator on nonconstant modes. The toroidal Hodge Laplacian introduced later is denoted separately by Δ_{tor}, with the same nonnegative convention for $-\Delta_{\mathrm{tor}}$.

Theorem 9 (Shell TT projector on the axisymmetric tangential shell space)**.** *Every $U \in H_{\tan}^{\mathrm{ax}}(S^2_{r_*})$ admits the orthogonal Hodge decomposition, in the reduced L^2-tangential sense,*

$$U = \underbrace{\nabla_{\tan} h_{\mathrm{ex}}}_{\substack{\textit{exact / gauge}\\ \textit{part}}} + \underbrace{\hat{\mathbf{n}} \times \nabla_{\tan} h_{\mathrm{co}}}_{\substack{\textit{coexact / physical}\\ \textit{TT part}}}, \qquad h_{\mathrm{ex}}, h_{\mathrm{co}} \in H^1_{\mathrm{ax}}(S^2_{r_*})/\mathbb{R}. \tag{299}$$

The potentials are therefore unique modulo additive constants. In the axisymmetric sector this decomposition is explicit; the exact part is purely meridional and the coexact part is purely toroidal. Equivalently,

$$U(\vartheta) = \underbrace{U_\vartheta(\vartheta)\, \hat{\mathbf{e}}_\vartheta}_{\substack{\textit{exact / gauge}\\ \textit{part}}} + \underbrace{U_\varphi(\vartheta)\, \hat{\mathbf{e}}_\varphi}_{\substack{\textit{coexact / physical}\\ \textit{TT part}}}. \tag{300}$$

On smooth axisymmetric tangential fields, the orthogonal projector onto the gauge-invariant tangential-transverse, equivalently tangential divergence-free, sector is

$$\Pi_{\mathrm{TT}} = \mathbb{I} - \nabla_{\tan}\Delta_{\tan}^{-1} \div_{\tan}. \tag{301}$$

Here $\Delta_{\tan}^{-1}$ is the inverse of $\Delta_{\tan} = \div_{\tan}\nabla_{\tan}$ on the mean-zero axisymmetric scalar subspace. For general $U \in H^{\mathrm{ax}}_{\tan}(\Sigma_{r_*})$, this formula is understood in the weak Hodge sense; first define the exact component $\nabla_{\tan}h_{\mathrm{ex}}$ by

$$\int_{S^2_{r_*}} \nabla_{\tan}h_{\mathrm{ex}} \cdot \nabla_{\tan}f \,\mathrm{d}\Omega = \int_{S^2_{r_*}} U \cdot \nabla_{\tan}f \,\mathrm{d}\Omega \qquad \textit{for all } f \in H^1_{\mathrm{ax}}(S^2_{r_*})/\mathbb{R}, \tag{302}$$

and then set

$$\Pi_{\mathrm{TT}}U \coloneqq U - \nabla_{\tan}h_{\mathrm{ex}}.$$

This weak definition agrees with Eq. (301) whenever $\div_{\tan}U$ is represented by an L^2 scalar.

$$\Pi_{\mathrm{TT}}^2 = \Pi_{\mathrm{TT}}, \qquad \Pi_{\mathrm{TT}}^* = \Pi_{\mathrm{TT}}, \qquad \Pi_{\mathrm{TT}}\nabla_{\tan}\lambda = 0 \quad \textit{for every } \lambda \in H^1_{\mathrm{ax}}(S^2_{r_*}), \tag{303}$$

and, explicitly,

$$\Pi_{\mathrm{TT}}\big(U_\vartheta(\vartheta)\,\hat{\mathbf{e}}_\vartheta + U_\varphi(\vartheta)\,\hat{\mathbf{e}}_\varphi\big) = U_\varphi(\vartheta)\,\hat{\mathbf{e}}_\varphi. \tag{304}$$

Moreover, Π_{TT} is the unique bounded self-adjoint idempotent on $H^{\mathrm{ax}}_{\tan}(S^2_{r_*})$ that annihilates all tangential gradients and acts as the identity on every axisymmetric tangential divergence-free field.

Proof. By the standard L^2 Hodge decomposition for tangential one-forms on a closed smooth sphere, see for example [12, 13], every L^2-tangential field on $S^2_{r_*}$ decomposes orthogonally into exact, coexact, and harmonic parts. Because

$$H^1_{\mathrm{dR}}(S^2) = 0,$$

the harmonic one-form sector is trivial. Hence every $U \in H^{\mathrm{ax}}_{\tan}(S^2_{r_*})$ admits the orthogonal decomposition

$$U = \nabla_{\tan}h_{\mathrm{ex}} + \hat{\mathbf{n}} \times \nabla_{\tan}h_{\mathrm{co}}, \qquad h_{\mathrm{ex}}, h_{\mathrm{co}} \in H^1_{\mathrm{ax}}(S^2_{r_*})/\mathbb{R},$$

and restricting to the axisymmetric sector gives Eq. (299).

In the angular shell representation, if $f = f(\vartheta)$ is axisymmetric, then

$$\nabla_{\tan}f = f'(\vartheta)\,\hat{\mathbf{e}}_\vartheta, \qquad \hat{\mathbf{n}} \times \nabla_{\tan}f = f'(\vartheta)\,\hat{\mathbf{e}}_\varphi.$$

Thus the exact part is purely meridional and the coexact part is purely toroidal. This yields Eq. (300).

We now show that the axisymmetric tangential divergence-free sector is precisely the toroidal sector. Let

$$U(\vartheta) = U_\vartheta(\vartheta)\,\hat{\mathbf{e}}_\vartheta + U_\varphi(\vartheta)\,\hat{\mathbf{e}}_\varphi$$

be axisymmetric. Then

$$\div_{\tan}\big(U_\varphi(\vartheta)\,\hat{\mathbf{e}}_\varphi\big) = 0,$$

while

$$\div_{\tan}\big(U_\vartheta(\vartheta)\,\hat{\mathbf{e}}_\vartheta\big) = \frac{1}{\sin\vartheta}\frac{d}{d\vartheta}\big(\sin\vartheta\,U_\vartheta(\vartheta)\big).$$

If U is divergence-free, then the toroidal component has zero surface divergence, and therefore the meridional component must satisfy

$$\frac{d}{d\vartheta}\big(\sin\vartheta\,U_\vartheta(\vartheta)\big) = 0.$$

Hence

$$\sin\vartheta\,U_\vartheta(\vartheta) = C$$

for some constant C. If $C \neq 0$, then

$$\int_0^\pi |U_\vartheta(\vartheta)|^2 \sin\vartheta\,\mathrm{d}\vartheta = |C|^2 \int_0^\pi \frac{\mathrm{d}\vartheta}{\sin\vartheta} = +\infty,$$

which contradicts $U \in H^{\mathrm{ax}}_{\tan}(S^2_{r_*})$. Thus $C = 0$, and

$$U_\vartheta(\vartheta) \equiv 0.$$

Therefore every axisymmetric tangential divergence-free field is purely toroidal.

Let

$$P_{\mathrm{ex}} = \nabla_{\tan}\Delta_{\tan}^{-1} \div_{\tan} .$$

Because $S^2_{r_*}$ is closed and has no boundary, one has

$$\int_{S^2_{r_*}} \div_{\tan} U \,\mathrm{d}\Omega = 0 \qquad \text{for every } U \in H^{\mathrm{ax}}_{\tan}(S^2_{r_*}).$$

Hence $\div_{\tan} U$ belongs to the mean-zero scalar subspace on which $\Delta_{\tan}^{-1}$ is defined. For

$$U = \nabla_{\tan} h_{\mathrm{ex}} + \hat{\mathbf{n}} \times \nabla_{\tan} h_{\mathrm{co}},$$

one has

$$\div_{\tan}\big(\hat{\mathbf{n}} \times \nabla_{\tan} h_{\mathrm{co}}\big) = 0, \qquad \div_{\tan}(\nabla_{\tan} h_{\mathrm{ex}}) = \Delta_{\tan} h_{\mathrm{ex}}.$$

Hence

$$\div_{\tan} U = \Delta_{\tan} h_{\mathrm{ex}}.$$

Since $\Delta_{\tan}^{-1}$ is taken on the orthogonal complement of the constants,

$$\Delta_{\tan}^{-1}\Delta_{\tan} h_{\mathrm{ex}} = h_{\mathrm{ex}} - \overline{h_{\mathrm{ex}}},$$

where $\overline{h_{\mathrm{ex}}}$ is the mean value of h_{ex} on the sphere. Taking the tangential gradient removes the constant and gives

$$P_{\mathrm{ex}} U = \nabla_{\tan}(h_{\mathrm{ex}} - \overline{h_{\mathrm{ex}}}) = \nabla_{\tan} h_{\mathrm{ex}}.$$

Therefore

$$(\mathbb{I} - P_{\mathrm{ex}})U = \hat{\mathbf{n}} \times \nabla_{\tan} h_{\mathrm{co}},$$

which is precisely the coexact divergence-free tangential part. Hence

$$\Pi_{\mathrm{TT}} = \mathbb{I} - P_{\mathrm{ex}} = \mathbb{I} - \nabla_{\tan}\Delta_{\tan}^{-1} \div_{\tan} .$$

Now P_{ex} is a projection. For any U,

$$P_{\mathrm{ex}}^2 U = \nabla_{\tan}\Delta_{\tan}^{-1} \div_{\tan} \left(\nabla_{\tan}\Delta_{\tan}^{-1} \div_{\tan} U\right) = \nabla_{\tan}\Delta_{\tan}^{-1}\Delta_{\tan}\Delta_{\tan}^{-1} \div_{\tan} U = P_{\mathrm{ex}} U.$$

Consequently,

$$\Pi_{\mathrm{TT}}^2 = (\mathbb{I} - P_{\mathrm{ex}})^2 = \mathbb{I} - P_{\mathrm{ex}} = \Pi_{\mathrm{TT}}.$$

The exact and coexact subspaces are orthogonal. For smooth axisymmetric potentials f and g, one has

$$\nabla_{\tan} f = f'(\vartheta)\hat{\mathbf{e}}_\vartheta, \qquad \hat{\mathbf{n}} \times \nabla_{\tan} g = g'(\vartheta)\hat{\mathbf{e}}_\varphi.$$

Therefore

$$\begin{aligned}\big\langle \nabla_{\tan} f,\, \hat{\mathbf{n}} \times \nabla_{\tan} g \big\rangle_{\mathrm{sh}} &= 2\pi \int_0^\pi f'(\vartheta) g'(\vartheta)\, \hat{\mathbf{e}}_\vartheta \cdot \hat{\mathbf{e}}_\varphi \,\sin\vartheta\,\mathrm{d}\vartheta \\ &= 2\pi \int_0^\pi f'(\vartheta) g'(\vartheta)\, 0 \,\sin\vartheta\,\mathrm{d}\vartheta = 0.\end{aligned}$$

Equivalently, if V is a smooth axisymmetric tangential divergence-free field, then for every smooth axisymmetric scalar f,

$$\begin{aligned}\langle \nabla_{\tan} f, V\rangle_{\mathrm{sh}} &= \int_{S^2_{r_*}} \nabla_{\tan} f \cdot V \,\mathrm{d}\Omega \\ &= -\int_{S^2_{r_*}} f \ \div_{\tan} V \,\mathrm{d}\Omega = 0,\end{aligned}$$

because the sphere has no boundary. By density, the same orthogonality holds in the L^2-tangential Hodge decomposition. Thus Π_{TT} is the orthogonal projection onto the coexact sector, and consequently

$$\Pi^*_{\mathrm{TT}} = \Pi_{\mathrm{TT}}, \qquad \Pi^2_{\mathrm{TT}} = \Pi_{\mathrm{TT}}.$$

For any $\lambda \in H^1_{\mathrm{ax}}(S^2_{r_*})$,

$$P_{\mathrm{ex}}\nabla_{\tan}\lambda = \nabla_{\tan}\Delta^{-1}_{\tan}\Delta_{\tan}\lambda = \nabla_{\tan}(\lambda - \overline{\lambda}) = \nabla_{\tan}\lambda,$$

and therefore

$$\Pi_{\mathrm{TT}}\nabla_{\tan}\lambda = (\mathbb{I} - P_{\mathrm{ex}})\nabla_{\tan}\lambda = 0.$$

This proves Eq. (303). The explicit formula Eq. (304) follows from the identification of the axisymmetric divergence-free sector with the toroidal sector.

Finally, let P be any bounded self-adjoint idempotent on $H^{\mathrm{ax}}_{\tan}(S^2_{r_*})$ such that

$$P\nabla_{\tan}\lambda = 0 \quad \text{for every } \lambda \in H^1_{\mathrm{ax}}(S^2_{r_*}),$$

and

$$PV = V \quad \text{for every axisymmetric tangential divergence-free field } V.$$

For any

$$U = \nabla_{\tan}h_{\mathrm{ex}} + \hat{\mathbf{n}} \times \nabla_{\tan}h_{\mathrm{co}},$$

one then has

$$PU = P\nabla_{\tan}h_{\mathrm{ex}} + P\big(\hat{\mathbf{n}} \times \nabla_{\tan}h_{\mathrm{co}}\big) = 0 + \hat{\mathbf{n}} \times \nabla_{\tan}h_{\mathrm{co}} = \Pi_{\mathrm{TT}}U.$$

Hence $P = \Pi_{\mathrm{TT}}$. The projector is unique. □

Remark. The projector entering the vector channel is therefore not an additional fitted object and it is not ℓ-dependent. Its role is purely geometric and gauge-theoretic; it removes pure tangential gauge-gradient data and retains the physical transverse shell content. It should not be confused with the earlier geometric emergence of the one-loop branch from $\mathbb{C}$ into its coarse-grained Dirac-ring image in $\mathbb{R}^3$. That earlier step produces the shell data; the present projector acts only after those shell data already exist. In the present Gaussian closure the explicit ℓ-dependence enters through the swirl-compliance operator $\mathbb{S}_\ell$; the notation E_ℓ is retained because it belongs to the same one-parameter shell admission family.

Definition VII.6 (Shell-admission operator)**.** Let

$$\mathcal{H}^{\mathrm{ax}}_{\mathrm{tor}}(S^2_{r_*}) := \operatorname{Ran}\Pi_{\mathrm{TT}} \subset H^{\mathrm{ax}}_{\tan}(S^2_{r_*})$$

denote the axisymmetric tangential divergence-free shell sector. Let $\xi \in [0,\infty)$ be the dimensionless transverse collar coordinate, measured in units of $\sigma_{\mathbb{C}}$. On the collar space

$$L^2([0,\infty)_\xi; H^{\mathrm{ax}}_{\tan}(S^2_{r_*})),$$

use the pairing

$$\langle F, G\rangle_{\mathrm{col}} = \int_0^\infty \langle F(\xi,\cdot), G(\xi,\cdot)\rangle_{\mathrm{sh}} \,\mathrm{d}\xi. \tag{305}$$

Define the half-Gaussian collar profile

$$\varpi_{\mathrm{col}}(\xi) = \frac{2}{\sqrt{\pi}} e^{-\xi^2}, \qquad \xi \geq 0. \tag{306}$$

It is normalized in $L^1([0,\infty))$,

$$\int_0^\infty \varpi_{\mathrm{col}}(\xi)\,\mathrm{d}\xi = 1,$$

and its L^2-mass is

$$N_{\mathrm{col}} := \int_0^\infty \varpi_{\mathrm{col}}(\xi)^2\,\mathrm{d}\xi = \frac{4}{\pi}\int_0^\infty e^{-2\xi^2}\,\mathrm{d}\xi = \sqrt{\frac{2}{\pi}}.$$

The Gaussian collar extension is

$$(E_\ell \mathscr{A}_{\mathrm{sh}})(\xi,\vartheta) = \varpi_{\mathrm{col}}(\xi)\,\mathscr{A}_{\mathrm{sh}}(\vartheta), \qquad \mathscr{A}_{\mathrm{sh}} \in H^{\mathrm{ax}}_{\mathrm{tan}}(S^2_{r_*}). \tag{307}$$

Its adjoint is

$$(E_\ell^* F)(\vartheta) = \int_0^\infty \varpi_{\mathrm{col}}(\xi)\,F(\xi,\vartheta)\,\mathrm{d}\xi. \tag{308}$$

The notation E_ℓ is retained because the extension is used inside the one-parameter shell-admission family. In the present Gaussian closure, E_ℓ itself is the fixed half-Gaussian lift in the dimensionless collar coordinate ξ, while the explicit ℓ-dependence enters through the compliance operator defined below.

Let $-\Delta_{\mathrm{tor}}$ be the nonnegative self-adjoint toroidal Hodge Laplacian on $\mathcal{H}^{\mathrm{ax}}_{\mathrm{tor}}(S^2_{r_*})$, with operator domain

$$\mathrm{Dom}(\Delta_{\mathrm{tor}}) \subset \mathcal{H}^{\mathrm{ax}}_{\mathrm{tor}}(S^2_{r_*}).$$

With the solid-angle shell normalization used here, Δ_{tor} is dimensionless. For $\ell \geq 0$, define by spectral calculus

$$\mathbb{S}_\ell = \underbrace{\big(-\ell^2\Delta_{\mathrm{tor}}\big)}_{\substack{\text{dimensionless}\\ \text{toroidal scale}}}\underbrace{\big(\mathbb{I} - \ell^2\Delta_{\mathrm{tor}}\big)^{-1}}_{\substack{\text{bounded resolvent}\\ \text{regularization}}}. \tag{309}$$

On the toroidal collar sector, $\mathbb{S}_\ell$ acts fiberwise,

$$\big((\mathbb{S}_\ell F)(\xi)\big)(\vartheta) = \big(\mathbb{S}_\ell(F(\xi,\cdot))\big)(\vartheta).$$

The unnormalized shell-space admission operator is

$$\mathbb{Q}_{\chi,\mathrm{sh}}(\ell) = \underbrace{\Pi_{\mathrm{TT}}}_{\substack{\text{TT filter}\\ \text{on shell data}}}\ \underbrace{E_\ell^*}_{\substack{\text{return from}\\ \text{Gaussian collar}}}\ \underbrace{\left(\mathbb{I} - \frac{1}{3}\,\mathbb{S}_\ell\right)}_{\substack{\text{swirl-compliance}\\ \text{weight}}}\ \underbrace{E_\ell}_{\substack{\text{Gaussian}\\ \text{extension}}}\ \underbrace{\Pi_{\mathrm{TT}}}_{\substack{\text{TT filter}\\ \text{on shell input}}}. \tag{310}$$

When no realization tag is needed, we write $\mathbb{Q}_\chi(\ell)$ for this shell-space operator locally.

Lemma 13 (Gaussian collar extension)**.** *The operator E_ℓ is bounded and satisfies*

$$\|E_\ell \mathscr{A}_{\mathrm{sh}}\|^2_{\mathrm{col}} = N_{\mathrm{col}}\,\|\mathscr{A}_{\mathrm{sh}}\|^2_{\mathrm{sh}}, \qquad \mathscr{A}_{\mathrm{sh}} \in H^{\mathrm{ax}}_{\mathrm{tan}}(S^2_{r_*}).$$

Its adjoint is given by Eq. (308)*, and*

$$E_\ell^* E_\ell = N_{\mathrm{col}}\,\mathbb{I} \qquad \text{on } H^{\mathrm{ax}}_{\mathrm{tan}}(S^2_{r_*}). \tag{311}$$

Proof. For $\mathscr{A}_{\mathrm{sh}} \in H^{\mathrm{ax}}_{\mathrm{tan}}(S^2_{r_*})$, one has

$$\|E_\ell \mathscr{A}_{\mathrm{sh}}\|^2_{\mathrm{col}} = \int_0^\infty \|\varpi_{\mathrm{col}}(\xi)\mathscr{A}_{\mathrm{sh}}\|^2_{\mathrm{sh}}\,\mathrm{d}\xi = \left(\int_0^\infty \varpi_{\mathrm{col}}(\xi)^2\,\mathrm{d}\xi\right)\|\mathscr{A}_{\mathrm{sh}}\|^2_{\mathrm{sh}} = N_{\mathrm{col}}\,\|\mathscr{A}_{\mathrm{sh}}\|^2_{\mathrm{sh}}.$$

Hence E_ℓ is bounded with

$$\|E_\ell\| = \sqrt{N_{\mathrm{col}}}.$$

For $F \in L^2([0,\infty)_\xi; H^{\mathrm{ax}}_{\tan}(S^2_{r_*}))$, the Bochner integral

$$\int_0^\infty \varpi_{\mathrm{col}}(\xi) F(\xi,\cdot)\,\mathrm{d}\xi$$

is well defined in $H^{\mathrm{ax}}_{\tan}(S^2_{r_*})$, because

$$\left\| \int_0^\infty \varpi_{\mathrm{col}}(\xi) F(\xi,\cdot)\,\mathrm{d}\xi \right\|_{\mathrm{sh}} \le \|\varpi_{\mathrm{col}}\|_{L^2(0,\infty)} \|F\|_{\mathrm{col}}.$$

Therefore

$$\begin{aligned}\langle E_\ell \mathscr{A}_{\mathrm{sh}}, F\rangle_{\mathrm{col}} &= \int_0^\infty \langle \varpi_{\mathrm{col}}(\xi)\mathscr{A}_{\mathrm{sh}}, F(\xi,\cdot)\rangle_{\mathrm{sh}}\,\mathrm{d}\xi \\ &= \left\langle \mathscr{A}_{\mathrm{sh}}, \int_0^\infty \varpi_{\mathrm{col}}(\xi) F(\xi,\cdot)\,\mathrm{d}\xi \right\rangle_{\mathrm{sh}}.\end{aligned}$$

This proves Eq. (308). Applying the adjoint formula to $F = E_\ell \mathscr{A}_{\mathrm{sh}}$ gives

$$E_\ell^* E_\ell \mathscr{A}_{\mathrm{sh}} = \int_0^\infty \varpi_{\mathrm{col}}(\xi)^2 \mathscr{A}_{\mathrm{sh}}\,\mathrm{d}\xi = N_{\mathrm{col}} \mathscr{A}_{\mathrm{sh}},$$

which is Eq. (311). □

Lemma 14 (Basic properties of $\mathbb{S}_\ell$ and $\mathbb{Q}_\chi(\ell)$)**.** *For every $\ell \ge 0$, the operator $\mathbb{S}_\ell$ is bounded and self-adjoint on $\mathcal{H}^{\mathrm{ax}}_{\mathrm{tor}}(S^2_{r_*})$, and its fiberwise lift is bounded and self-adjoint on*

$$L^2\big([0,\infty)_\xi; \mathcal{H}^{\mathrm{ax}}_{\mathrm{tor}}(S^2_{r_*})\big).$$

The shell-admission operator $\mathbb{Q}_\chi(\ell)$ is bounded and self-adjoint on $H^{\mathrm{ax}}_{\tan}(S^2_{r_*})$. Moreover,

$$0 \le \mathbb{S}_\ell \le \mathbb{I}, \qquad 0 \le \mathbb{Q}_\chi(\ell) \le N_{\mathrm{col}}\,\Pi_{\mathrm{TT}},$$

where the second inequality is understood in the quadratic-form sense on $H^{\mathrm{ax}}_{\tan}(S^2_{r_*})$. In particular, $\mathbb{Q}_\chi(\ell)$ is positive semidefinite and is not idempotent in general.

Proof. Let

$$T := -\Delta_{\mathrm{tor}} \ge 0$$

on $\mathcal{H}^{\mathrm{ax}}_{\mathrm{tor}}(S^2_{r_*})$. By the spectral theorem applied to T,

$$\mathbb{S}_\ell = \ell^2 T\big(\mathbb{I} + \ell^2 T\big)^{-1} = \int_0^\infty \frac{\ell^2\lambda}{1+\ell^2\lambda}\,\mathrm{d}E_T(\lambda),$$

with spectral multiplier

$$\lambda \longmapsto \frac{\ell^2\lambda}{1+\ell^2\lambda} \in [0,1].$$

Hence

$$0 \le \mathbb{S}_\ell \le \mathbb{I}, \qquad \frac{2}{3}\,\mathbb{I} \le \mathbb{I} - \frac{1}{3}\,\mathbb{S}_\ell \le \mathbb{I}.$$

Therefore

$$B_\ell := \mathbb{I} - \frac{1}{3}\,\mathbb{S}_\ell$$

is bounded, self-adjoint, and positive.

Since $\Pi_{\mathrm{TT}}\mathscr{A}_{\mathrm{sh},1} \in \mathcal{H}^{\mathrm{ax}}_{\mathrm{tor}}(S^2_{r_*})$, the collar lift $E_\ell \Pi_{\mathrm{TT}}\mathscr{A}_{\mathrm{sh},1}$ lies in the toroidal collar sector, where $B_\ell := \mathbb{I} - \frac{1}{3}\mathbb{S}_\ell$ is defined. For $\mathscr{A}_{\mathrm{sh},1}, \mathscr{A}_{\mathrm{sh},2} \in H^{\mathrm{ax}}_{\tan}(S^2_{r_*})$,

$$\begin{aligned}\langle \mathscr{A}_{\mathrm{sh},2}, \mathbb{Q}_\chi(\ell)\mathscr{A}_{\mathrm{sh},1}\rangle_{\mathrm{sh}} &= \Big\langle E_\ell \Pi_{\mathrm{TT}}\mathscr{A}_{\mathrm{sh},2},\, B_\ell E_\ell \Pi_{\mathrm{TT}}\mathscr{A}_{\mathrm{sh},1}\Big\rangle_{\mathrm{col}} \\ &= \Big\langle B_\ell E_\ell \Pi_{\mathrm{TT}}\mathscr{A}_{\mathrm{sh},2},\, E_\ell \Pi_{\mathrm{TT}}\mathscr{A}_{\mathrm{sh},1}\Big\rangle_{\mathrm{col}} \\ &= \langle \mathbb{Q}_\chi(\ell)\mathscr{A}_{\mathrm{sh},2}, \mathscr{A}_{\mathrm{sh},1}\rangle_{\mathrm{sh}},\end{aligned}$$

because B_ℓ is self-adjoint on the toroidal collar sector. Hence $\mathbb{Q}_\chi(\ell)$ is self-adjoint. Its boundedness follows from

$$\|\mathbb{Q}_\chi(\ell)\| \le \|\Pi_{\mathrm{TT}}\|\,\|E_\ell^*\|\,\|B_\ell\|\,\|E_\ell\|\,\|\Pi_{\mathrm{TT}}\| \le N_{\mathrm{col}}.$$

For $\mathscr{A}_{\mathrm{sh}} \in H^{\mathrm{ax}}_{\tan}(S^2_{r_*})$,

$$\langle \mathscr{A}_{\mathrm{sh}}, \mathbb{Q}_\chi(\ell)\mathscr{A}_{\mathrm{sh}}\rangle_{\mathrm{sh}} = \big\langle E_\ell \Pi_{\mathrm{TT}}\mathscr{A}_{\mathrm{sh}},\, B_\ell E_\ell \Pi_{\mathrm{TT}}\mathscr{A}_{\mathrm{sh}}\big\rangle_{\mathrm{col}} = \big\|B_\ell^{1/2} E_\ell \Pi_{\mathrm{TT}}\mathscr{A}_{\mathrm{sh}}\big\|^2_{\mathrm{col}} \ge 0.$$

Hence $\mathbb{Q}_\chi(\ell)$ is positive semidefinite.

Using $0 \le B_\ell \le \mathbb{I}$ and Eq. (311), we obtain

$$\langle \mathscr{A}_{\mathrm{sh}}, \mathbb{Q}_\chi(\ell)\mathscr{A}_{\mathrm{sh}}\rangle_{\mathrm{sh}} \le \|E_\ell \Pi_{\mathrm{TT}}\mathscr{A}_{\mathrm{sh}}\|^2_{\mathrm{col}} = \langle \Pi_{\mathrm{TT}}\mathscr{A}_{\mathrm{sh}}, E_\ell^* E_\ell \Pi_{\mathrm{TT}}\mathscr{A}_{\mathrm{sh}}\rangle_{\mathrm{sh}} = N_{\mathrm{col}}\langle \Pi_{\mathrm{TT}}\mathscr{A}_{\mathrm{sh}}, \Pi_{\mathrm{TT}}\mathscr{A}_{\mathrm{sh}}\rangle_{\mathrm{sh}}.$$

Since Π_{TT} is self-adjoint and idempotent,

$$\langle \Pi_{\mathrm{TT}}\mathscr{A}_{\mathrm{sh}}, \Pi_{\mathrm{TT}}\mathscr{A}_{\mathrm{sh}}\rangle_{\mathrm{sh}} = \langle \mathscr{A}_{\mathrm{sh}}, \Pi_{\mathrm{TT}}\mathscr{A}_{\mathrm{sh}}\rangle_{\mathrm{sh}}.$$

Therefore

$$\langle \mathscr{A}_{\mathrm{sh}}, \mathbb{Q}_\chi(\ell)\mathscr{A}_{\mathrm{sh}}\rangle_{\mathrm{sh}} \le N_{\mathrm{col}}\langle \mathscr{A}_{\mathrm{sh}}, \Pi_{\mathrm{TT}}\mathscr{A}_{\mathrm{sh}}\rangle_{\mathrm{sh}},$$

which is exactly the quadratic-form statement

$$0 \le \mathbb{Q}_\chi(\ell) \le N_{\mathrm{col}}\,\Pi_{\mathrm{TT}}.$$

Finally, $\mathbb{Q}_{\chi,\mathrm{sh}}(\ell)$ is not idempotent in general. At $\ell = 0$ one has $\mathbb{S}_0 = 0$. Since the Gaussian collar lift itself is independent of ℓ, this gives

$$\mathbb{Q}_{\chi,\mathrm{sh}}(0) = \Pi_{\mathrm{TT}} E_0^* E_0 \Pi_{\mathrm{TT}} = N_{\mathrm{col}}\,\Pi_{\mathrm{TT}}.$$

Because

$$N_{\mathrm{col}} = \sqrt{\frac{2}{\pi}} \neq 1,$$

it follows that

$$\big(\mathbb{Q}_{\chi,\mathrm{sh}}(0)\big)^2 = N_{\mathrm{col}}^2\,\Pi_{\mathrm{TT}} \neq N_{\mathrm{col}}\,\Pi_{\mathrm{TT}} = \mathbb{Q}_{\chi,\mathrm{sh}}(0).$$

Hence $\mathbb{Q}_{\chi,\mathrm{sh}}(\ell)$ cannot be idempotent for all $\ell \ge 0$. □

Definition VII.7 (Full shell-admission construction and normalized scalar admitted weight)**.** The operator $\mathbb{Q}_{\chi,\mathrm{sh}}(\ell)$ is the unnormalized shell-space admission operator. The sole normalization defect comes from the L^2-mass of the half-Gaussian collar lift,

$$N_{\mathrm{col}} = \int_0^\infty \varpi_{\mathrm{col}}(\xi)^2\,\mathrm{d}\xi = \sqrt{\frac{2}{\pi}}, \qquad E_\ell^* E_\ell = N_{\mathrm{col}}\,\mathbb{I}.$$

For scalar admission weights we therefore use the normalized shell-space admission operator

$$\overline{\mathbb{Q}_{\chi,\mathrm{sh}}}(\ell) := N_{\mathrm{col}}^{-1}\mathbb{Q}_{\chi,\mathrm{sh}}(\ell). \tag{312}$$

For any nonzero branch-fixed tangential shell-load representative $\mathscr{A}_{\rm sh} \in H^{\rm ax}_{\tan}(S^2_{r_*})$, define the normalized admitted full-load weight by

$$P^{(\chi)}_{IR,\rm full}(\ell; \mathscr{A}_{\rm sh}) = \frac{\langle \mathscr{A}_{\rm sh}, \overline{\mathbb{Q}_{\chi,\rm sh}}(\ell)\mathscr{A}_{\rm sh}\rangle_{\rm sh}}{\langle \mathscr{A}_{\rm sh}, \mathscr{A}_{\rm sh}\rangle_{\rm sh}}. \tag{313}$$

The denominator is the full shell norm of the chosen branch-load representative $\mathscr{A}_{\rm sh}$, not the TT-cleaned norm $\langle \Pi_{\rm TT}\mathscr{A}_{\rm sh}, \Pi_{\rm TT}\mathscr{A}_{\rm sh}\rangle_{\rm sh}$. This choice is deliberate in the branch-cyclic numerical realization; it measures the admitted TT–χ content as a fraction of the full coarse-grained shell load carried by the fixed branch representative.

This full-load quotient is not a gauge-class functional of an arbitrary vector-potential trace $\mathscr{A}_{\rm sh}$, because adding a tangential gauge gradient changes the denominator in general. It is used in this paper only after the branch shell-load representative has been fixed by the stated Coulomb-gauge Biot–Savart/collar convention. This convention fixes the branch representative and is not adjusted to a measured value of α or to a QED benchmark. If a quotient on gauge classes is needed, the corresponding TT-normalized quotient is

$$P^{(\chi)}_{IR,\rm TT}(\ell; \mathscr{A}_{\rm sh}) = \frac{\langle \mathscr{A}_{\rm sh}, \overline{\mathbb{Q}_{\chi,\rm sh}}(\ell)\mathscr{A}_{\rm sh}\rangle_{\rm sh}}{\langle \Pi_{\rm TT}\mathscr{A}_{\rm sh}, \Pi_{\rm TT}\mathscr{A}_{\rm sh}\rangle_{\rm sh}}, \qquad \Pi_{\rm TT}\mathscr{A}_{\rm sh} \neq 0. \tag{314}$$

For the distinguished collar-averaged tangential shell trace of the one-loop branch, we use its dimensionless branch-load representative and denote it by $\mathscr{A}^{\rm coll}_{\parallel}$. All common SI prefactors have been removed before this representative is inserted into the shell-admission quotient. We abbreviate

$$P^{(\chi)}_{IR}(\ell) \equiv P^{(\chi)}_{IR,\rm full}(\ell; \mathscr{A}^{\rm coll}_{\parallel}).$$

Its TT-cleaned representative is

$$\mathscr{A}^{\rm coll}_{\rm TT} := \Pi_{\rm TT}\mathscr{A}^{\rm coll}_{\parallel}.$$

Lemma 15 (Bounds for the normalized admitted weight). *For every nonzero tangential shell trace $\mathscr{A}_{\rm sh} \in H^{\rm ax}_{\tan}(S^2_{r_*})$,*

$$0 \leq P^{(\chi)}_{IR,\rm full}(\ell; \mathscr{A}_{\rm sh}) \leq 1. \tag{315}$$

Proof. By Eq. (312) and the quadratic-form bound $0 \leq \mathbb{Q}_{\chi,\rm sh}(\ell) \leq N_{\rm col}\Pi_{\rm TT}$, one has

$$0 \leq \overline{\mathbb{Q}_{\chi,\rm sh}}(\ell) \leq \Pi_{\rm TT}.$$

Therefore

$$0 \leq \langle \mathscr{A}_{\rm sh}, \overline{\mathbb{Q}_{\chi,\rm sh}}(\ell)\mathscr{A}_{\rm sh}\rangle_{\rm sh} \leq \langle \mathscr{A}_{\rm sh}, \Pi_{\rm TT}\mathscr{A}_{\rm sh}\rangle_{\rm sh}.$$

Since $\Pi_{\rm TT}$ is an orthogonal projector,

$$\langle \mathscr{A}_{\rm sh}, \Pi_{\rm TT}\mathscr{A}_{\rm sh}\rangle_{\rm sh} = \|\Pi_{\rm TT}\mathscr{A}_{\rm sh}\|^2_{\rm sh} \leq \|\mathscr{A}_{\rm sh}\|^2_{\rm sh} = \langle \mathscr{A}_{\rm sh}, \mathscr{A}_{\rm sh}\rangle_{\rm sh}.$$

Dividing by $\langle \mathscr{A}_{\rm sh}, \mathscr{A}_{\rm sh}\rangle_{\rm sh} > 0$ gives Eq. (315). $\square$

Before passing to the shell-return problem, one must reduce the local Gaussian finite part from the transverse collar picture to the shell sector. The constant $C^{(\rm Gauss)}_{\rm UV}$ computed above still lives on the local normal plane of the one-loop carrier. To enter the vector block it must be transported to the matching shell, cleaned of pure tangential gauge gradients, weighted by the toroidal shell response, and represented back on shell data. The next theorem states that, after Gaussian collar normalization by $N^{-1/2}_{\rm col}$, the entire reduction is encoded exactly by the normalized shell-admission operator $\overline{\mathbb{Q}_{\chi,\rm sh}}(\ell)$.

Theorem 10 (Shell-reduction identity for the normalized Gaussian UV transfer). *Let $\mathscr{A}_{\rm sh} \in H^{\rm ax}_{\tan}(S^2_{r_*})$ be any nonzero tangential shell trace. Define the normalized Gaussian collar lift by*

$$\overline{E}_\ell := N^{-1/2}_{\rm col} E_\ell, \qquad \overline{E}^*_\ell := N^{-1/2}_{\rm col} E^*_\ell.$$

Then

$$\overline{E}^*_\ell \overline{E}_\ell = \mathbb{I}, \qquad \overline{\mathbb{Q}_{\chi,\rm sh}}(\ell) = \Pi_{\rm TT}\, \overline{E}^*_\ell \Big(\mathbb{I} - \frac{1}{3}\,\mathbb{S}_\ell\Big) \overline{E}_\ell\, \Pi_{\rm TT}.$$

Define the normalized shell-reduced Gaussian UV quadratic form by

$$\mathcal{U}^{(\chi)}_{\mathrm{UV}\to\mathrm{IR}}(\ell;\mathscr{A}_{\mathrm{sh}}) = C^{(\mathrm{Gauss})}_{\mathrm{UV}} \Big\langle \underbrace{\overline{E}_\ell \Pi_{\mathrm{TT}} \mathscr{A}_{\mathrm{sh}}}_{\substack{\textit{TT-cleaned}\\ \textit{collar-normalized lift}}} , \underbrace{\Big(\mathbb{I} - \frac{1}{3}\,\mathbb{S}_\ell\Big)}_{\substack{\textit{swirl-compliance}\\ \textit{weight}}} \underbrace{\overline{E}_\ell \Pi_{\mathrm{TT}} \mathscr{A}_{\mathrm{sh}}}_{\substack{\textit{TT-cleaned}\\ \textit{collar-normalized lift}}} \Big\rangle_{\mathrm{col}}. \tag{316}$$

If $\mathscr{A}_{\mathrm{sh}}$ is a dimensionless shell amplitude, then this quadratic form is dimensionless. If $\mathscr{A}_{\mathrm{sh}}$ carries a physical SI unit, then $\mathcal{U}^{(\chi)}_{\mathrm{UV}\to\mathrm{IR}}(\ell;\mathscr{A}_{\mathrm{sh}})$ carries the squared unit of $\mathscr{A}_{\mathrm{sh}}$. In all cases the admitted load

$$\Delta\Lambda_{\mathrm{UV}\to\mathrm{IR}}(\ell;\mathscr{A}_{\mathrm{sh}}) = \frac{\mathcal{U}^{(\chi)}_{\mathrm{UV}\to\mathrm{IR}}(\ell;\mathscr{A}_{\mathrm{sh}})}{\langle \mathscr{A}_{\mathrm{sh}}, \mathscr{A}_{\mathrm{sh}}\rangle_{\mathrm{sh}}}$$

is dimensionless. It is well defined because $\Pi_{\mathrm{TT}}\mathscr{A}_{\mathrm{sh}} \in \mathcal{H}^{\mathrm{ax}}_{\mathrm{tor}}(S^2_{r_*})$, hence $\overline{E}_\ell \Pi_{\mathrm{TT}}\mathscr{A}_{\mathrm{sh}}$ lies in the toroidal collar sector on which $\mathbb{S}_\ell$ acts fiberwise.

Then

$$\mathcal{U}^{(\chi)}_{\mathrm{UV}\to\mathrm{IR}}(\ell;\mathscr{A}_{\mathrm{sh}}) = C^{(\mathrm{Gauss})}_{\mathrm{UV}} \,\langle \mathscr{A}_{\mathrm{sh}}, \overline{\mathbb{Q}_{\chi,\mathrm{sh}}}(\ell)\mathscr{A}_{\mathrm{sh}}\rangle_{\mathrm{sh}}.$$

Therefore the admitted Gaussian UV load associated with the branch-fixed full-load scalar admission convention is

$$\Delta\Lambda_{\mathrm{UV}\to\mathrm{IR}}(\ell;\mathscr{A}_{\mathrm{sh}}) = \frac{\mathcal{U}^{(\chi)}_{\mathrm{UV}\to\mathrm{IR}}(\ell;\mathscr{A}_{\mathrm{sh}})}{\langle \mathscr{A}_{\mathrm{sh}}, \mathscr{A}_{\mathrm{sh}}\rangle_{\mathrm{sh}}} = C^{(\mathrm{Gauss})}_{\mathrm{UV}} \, P^{(\chi)}_{IR,\mathrm{full}}(\ell;\mathscr{A}_{\mathrm{sh}}). \tag{317}$$

This is a dimensionless scalar load for the chosen branch-load representative $\mathscr{A}_{\mathrm{sh}}$. For the minimal-branch numerical realization,

$$P^{(\chi)}_{IR}(\ell) \equiv P^{(\chi)}_{IR,\mathrm{full}}(\ell;\mathscr{A}^{\mathrm{coll}}_{\parallel}), \qquad \Delta\Lambda_{\mathrm{UV}\to\mathrm{IR}}(\ell) \equiv \Delta\Lambda_{\mathrm{UV}\to\mathrm{IR}}(\ell;\mathscr{A}^{\mathrm{coll}}_{\parallel}).$$

If one instead wants a gauge-class quotient for arbitrary shell traces, the denominator in Eq. (317) *must be replaced by $\langle \Pi_{\mathrm{TT}}\mathscr{A}_{\mathrm{sh}}, \Pi_{\mathrm{TT}}\mathscr{A}_{\mathrm{sh}}\rangle_{\mathrm{sh}}$, as in Eq.* (314)*. For the distinguished collar trace $\mathscr{A}^{\mathrm{coll}}_{\parallel}$, namely the Gaussian collar-averaged tangential shell trace of the one-loop branch, we abbreviate*

$$\Delta\Lambda_{\mathrm{UV}\to\mathrm{IR}}(\ell) = \Delta\Lambda_{\mathrm{UV}\to\mathrm{IR}}(\ell;\mathscr{A}^{\mathrm{coll}}_{\parallel}) = C^{(\mathrm{Gauss})}_{\mathrm{UV}} \, P^{(\chi)}_{IR}(\ell).$$

Proof. By the definition Eq. (316),

$$\mathcal{U}^{(\chi)}_{\mathrm{UV}\to\mathrm{IR}}(\ell;\mathscr{A}_{\mathrm{sh}}) = C^{(\mathrm{Gauss})}_{\mathrm{UV}} \Big\langle \overline{E}_\ell \Pi_{\mathrm{TT}}\mathscr{A}_{\mathrm{sh}},\, \Big(\mathbb{I} - \frac{1}{3}\,\mathbb{S}_\ell\Big)\overline{E}_\ell \Pi_{\mathrm{TT}}\mathscr{A}_{\mathrm{sh}}\Big\rangle_{\mathrm{col}}.$$

Using the adjoint relation for $\overline{E}^*_\ell$ gives

$$\mathcal{U}^{(\chi)}_{\mathrm{UV}\to\mathrm{IR}}(\ell;\mathscr{A}_{\mathrm{sh}}) = C^{(\mathrm{Gauss})}_{\mathrm{UV}} \Big\langle \Pi_{\mathrm{TT}}\mathscr{A}_{\mathrm{sh}},\, \overline{E}^*_\ell\Big(\mathbb{I} - \frac{1}{3}\,\mathbb{S}_\ell\Big)\overline{E}_\ell \Pi_{\mathrm{TT}}\mathscr{A}_{\mathrm{sh}}\Big\rangle_{\mathrm{sh}}.$$

Since Π_{TT} is self-adjoint and idempotent,

$$\begin{aligned}\mathcal{U}^{(\chi)}_{\mathrm{UV}\to\mathrm{IR}}(\ell;\mathscr{A}_{\mathrm{sh}}) &= C^{(\mathrm{Gauss})}_{\mathrm{UV}} \Big\langle \mathscr{A}_{\mathrm{sh}},\, \Pi_{\mathrm{TT}}\overline{E}^*_\ell\Big(\mathbb{I} - \frac{1}{3}\,\mathbb{S}_\ell\Big)\overline{E}_\ell \Pi_{\mathrm{TT}}\mathscr{A}_{\mathrm{sh}}\Big\rangle_{\mathrm{sh}} \\ &= C^{(\mathrm{Gauss})}_{\mathrm{UV}} \,\langle \mathscr{A}_{\mathrm{sh}}, \overline{\mathbb{Q}_{\chi,\mathrm{sh}}}(\ell)\mathscr{A}_{\mathrm{sh}}\rangle_{\mathrm{sh}}.\end{aligned}$$

Dividing by $\langle \mathscr{A}_{\mathrm{sh}}, \mathscr{A}_{\mathrm{sh}}\rangle_{\mathrm{sh}} \neq 0$ and using Eq. (313) yields Eq. (317). □

Condition VII.1 (Branch-cyclic realization of the normalized TT–χ admission)**.** This condition gives the branch-cyclic scalar realization of the already defined normalized admission quotient for the distinguished minimal-branch trace. It is not a second definition of the shell-admission operator on the full tangential shell space.

Let $\ell > 0$, and let

$$\mathcal{H}_\chi := L^2((0,1),\mathrm{d}y), \qquad y = \frac{r}{r_*} \in [0,1], \qquad s(y) = 1 - y.$$

The first-node scalar branch on the pinned cavity carries the real cyclic amplitude

$$\mathfrak{a}_\chi(y) = y \sin(\pi y). \tag{318}$$

Define

$$\mathcal{N}_\chi = \int_0^1 y^2 \sin^2(\pi y)\, \mathrm{d}y, \qquad \psi_\chi(y) = \frac{\mathfrak{a}_\chi(y)}{\sqrt{\mathcal{N}_\chi}}. \tag{319}$$

The associated probability measure is

$$\mathrm{d}\mu_\chi(y) = |\psi_\chi(y)|^2\, \mathrm{d}y = \frac{y^2 \sin^2(\pi y)}{\mathcal{N}_\chi}\, \mathrm{d}y. \tag{320}$$

In the branch-cyclic realization used for the scalar admitted weight, the cyclic compression of the normalized shell-admission operator is represented on $\mathcal{H}_\chi$ by

$$\mathcal{W}_\ell \Big(\mathbb{I} - \frac{1}{3}\, \mathcal{S}_{\ell,\chi}\Big) \mathcal{W}_\ell, \tag{321}$$

where

$$(\mathcal{W}_\ell f)(y) = \exp\left[-\frac{1}{2}\left(\frac{1-y}{\ell}\right)^2\right] f(y), \tag{322}$$

and

$$\mathcal{S}_{\ell,\chi} = \mathcal{T}_{\ell,\chi}\big(\mathbb{I} + \mathcal{T}_{\ell,\chi}\big)^{-1}, \qquad (\mathcal{T}_{\ell,\chi} f)(y) = \frac{(1-y)^2}{\ell^2} f(y). \tag{323}$$

The branch-cyclic condition fixes the one-dimensional realization used to evaluate $P_{IR}^{(\chi)}(\ell)$ for the distinguished minimal-branch trace. It is a conditional realization of the already defined scalar quotient, not a second definition of the full shell-space operator and not a replacement for the shell-space Rayleigh quotient for arbitrary traces. The full shell-space operator remains $\overline{\mathbb{Q}_{\chi,\mathrm{sh}}}(\ell)$.

Lemma 16 (Cyclic multiplier identity under the branch-cyclic realization)**.** *In the branch-cyclic realization of Condition VII.1, the cyclic compression of $\overline{\mathbb{Q}_{\chi,\mathrm{sh}}}(\ell)$ is multiplication by*

$$W_\ell^{(\chi)}(y) = \exp\left[-\left(\frac{1-y}{\ell}\right)^2\right]\left[1 - \frac{1}{3}\frac{(1-y)^2}{(1-y)^2 + \ell^2}\right]. \tag{324}$$

Proof. By Eq. (322), the normalized Gaussian collar lift $\mathcal{W}_\ell$ is multiplication by

$$\exp\left[-\frac{1}{2}\left(\frac{1-y}{\ell}\right)^2\right].$$

Therefore the quadratic collar lift $\mathcal{W}_\ell^* \mathcal{W}_\ell = \mathcal{W}_\ell^2$ contributes the multiplier

$$\exp\left[-\left(\frac{1-y}{\ell}\right)^2\right].$$

Next, by Eq. (323), the operator $\mathcal{T}_{\ell,\chi}$ is multiplication by

$$\frac{(1-y)^2}{\ell^2}.$$

Hence

$$\mathcal{S}_{\ell,\chi} = \mathcal{T}_{\ell,\chi}\big(\mathbb{I} + \mathcal{T}_{\ell,\chi}\big)^{-1}$$

is multiplication by

$$\frac{\dfrac{(1-y)^2}{\ell^2}}{1+\dfrac{(1-y)^2}{\ell^2}} = \frac{(1-y)^2}{(1-y)^2+\ell^2}.$$

Hence

$$\mathbb{I} - \frac{1}{3}\,\mathcal{S}_{\ell,\chi}$$

is multiplication by

$$1 - \frac{1}{3}\,\frac{(1-y)^2}{(1-y)^2+\ell^2}.$$

Multiplying the Gaussian factor from Eq. (322) with the swirl factor from Eq. (323) inside the compressed operator Eq. (321) gives exactly Eq. (324). □

Lemma 17 (Normalization of the cyclic χ-admission measure)**.** *The normalization constant in Eq.* (319) *is*

$$\mathcal{N}_\chi = \frac{1}{6} - \frac{1}{4\pi^2}. \tag{325}$$

Hence $\mathrm{d}\mu_\chi$ *is a probability measure on* $[0,1]$.

Proof. Using

$$\sin^2(\pi y) = \frac{1}{2}\big(1-\cos(2\pi y)\big),$$

we compute

$$\begin{aligned}\mathcal{N}_\chi &= \int_0^1 y^2\sin^2(\pi y)\,\mathrm{d}y\\ &= \frac{1}{2}\int_0^1 y^2\,\mathrm{d}y - \frac{1}{2}\int_0^1 y^2\cos(2\pi y)\,\mathrm{d}y.\end{aligned}$$

The first integral is

$$\frac{1}{2}\int_0^1 y^2\,\mathrm{d}y = \frac{1}{6}.$$

For the second integral, two integrations by parts give

$$\int_0^1 y^2\cos(2\pi y)\,\mathrm{d}y = \left[\frac{y^2\sin(2\pi y)}{2\pi} + \frac{2y\cos(2\pi y)}{(2\pi)^2} - \frac{2\sin(2\pi y)}{(2\pi)^3}\right]_0^1 = \frac{1}{2\pi^2}.$$

Therefore

$$\mathcal{N}_\chi = \frac{1}{6} - \frac{1}{2}\frac{1}{2\pi^2} = \frac{1}{6} - \frac{1}{4\pi^2}.$$

Since $y^2\sin^2(\pi y) \geq 0$ and is not identically zero on $(0,1)$, $\mathcal{N}_\chi > 0$. Thus $\mathrm{d}\mu_\chi$ has total mass one. □

Theorem 11 (Conditional closed cyclic evaluation of the TT–χ admitted weight)**.** *For the distinguished collar-averaged shell trace* $\mathscr{A}_\parallel^{\mathrm{coll}}$ *of the minimal one-loop branch, and conditional on the branch-cyclic realization of Condition VII.1, the normalized scalar admitted weight is*

$$P_{IR}^{(\chi)}(\ell) := P_{IR,\mathrm{full}}^{(\chi)}(\ell;\mathscr{A}_\parallel^{\mathrm{coll}}) = \frac{\langle \mathscr{A}_\parallel^{\mathrm{coll}}, \overline{\mathbb{Q}_{\chi,\mathrm{sh}}}(\ell)\mathscr{A}_\parallel^{\mathrm{coll}}\rangle_{\mathrm{sh}}}{\langle \mathscr{A}_\parallel^{\mathrm{coll}}, \mathscr{A}_\parallel^{\mathrm{coll}}\rangle_{\mathrm{sh}}}. \tag{326}$$

Equivalently, since $\mathscr{A}^{\mathrm{coll}}_{\mathrm{TT}} = \Pi_{\mathrm{TT}}\mathscr{A}^{\mathrm{coll}}_{\parallel}$ *and* $\overline{\mathbb{Q}_{\chi,\mathrm{sh}}}(\ell) = \Pi_{\mathrm{TT}}\,\overline{\mathbb{Q}_{\chi,\mathrm{sh}}}(\ell)\,\Pi_{\mathrm{TT}}$*, the numerator may be written as*

$$\langle \mathscr{A}^{\mathrm{coll}}_{\parallel}, \overline{\mathbb{Q}_{\chi,\mathrm{sh}}}(\ell)\mathscr{A}^{\mathrm{coll}}_{\parallel}\rangle_{\mathrm{sh}} = \langle \mathscr{A}^{\mathrm{coll}}_{\mathrm{TT}}, \overline{\mathbb{Q}_{\chi,\mathrm{sh}}}(\ell)\mathscr{A}^{\mathrm{coll}}_{\mathrm{TT}}\rangle_{\mathrm{sh}}.$$

The denominator, however, remains the full shell norm of $\mathscr{A}^{\mathrm{coll}}_{\parallel}$*. Then, in this branch-cyclic realization and only for the distinguished branch-load representative,*

$$P^{(\chi)}_{IR}(\ell) = \int_0^1 W^{(\chi)}_{\ell}(y)\,\mathrm{d}\mu_\chi(y). \tag{327}$$

Equivalently,

$$P^{(\chi)}_{IR}(\ell) = \frac{\displaystyle\int_0^1 y^2\sin^2(\pi y)\left[1-\frac{1}{3}\frac{(1-y)^2}{(1-y)^2+\ell^2}\right]\exp\left[-\left(\frac{1-y}{\ell}\right)^2\right]\mathrm{d}y}{\displaystyle\int_0^1 y^2\sin^2(\pi y)\,\mathrm{d}y}. \tag{328}$$

In particular,

$$0 < P^{(\chi)}_{IR}(\ell) < 1 \qquad (\ell > 0). \tag{329}$$

Proof. Since

$$\overline{\mathbb{Q}_{\chi,\mathrm{sh}}}(\ell) = \Pi_{\mathrm{TT}}\,\overline{\mathbb{Q}_{\chi,\mathrm{sh}}}(\ell)\,\Pi_{\mathrm{TT}},$$

and Π_{TT} is self-adjoint and idempotent, the numerator in Eq. (326) satisfies

$$\begin{aligned}\langle \mathscr{A}^{\mathrm{coll}}_{\parallel}, \overline{\mathbb{Q}_{\chi,\mathrm{sh}}}(\ell)\mathscr{A}^{\mathrm{coll}}_{\parallel}\rangle_{\mathrm{sh}} &= \langle \Pi_{\mathrm{TT}}\mathscr{A}^{\mathrm{coll}}_{\parallel}, \overline{\mathbb{Q}_{\chi,\mathrm{sh}}}(\ell)\Pi_{\mathrm{TT}}\mathscr{A}^{\mathrm{coll}}_{\parallel}\rangle_{\mathrm{sh}}\\ &= \langle \mathscr{A}^{\mathrm{coll}}_{\mathrm{TT}}, \overline{\mathbb{Q}_{\chi,\mathrm{sh}}}(\ell)\mathscr{A}^{\mathrm{coll}}_{\mathrm{TT}}\rangle_{\mathrm{sh}}.\end{aligned}$$

Thus the TT projection is applied inside the admitted numerator. The denominator in Eq. (326) remains $\|\mathscr{A}^{\mathrm{coll}}_{\parallel}\|^2_{\mathrm{sh}}$, so the scalar is the admitted fraction of the full collar-averaged branch load.

Under the branch-cyclic realization Condition VII.1, the distinguished branch-fixed full-load representative is normalized by

$$\frac{\mathscr{A}^{\mathrm{coll}}_{\parallel}}{\|\mathscr{A}^{\mathrm{coll}}_{\parallel}\|_{\mathrm{sh}}} \quad\longmapsto\quad \psi_\chi.$$

This normalization uses the fixed full collar-trace norm of the chosen Coulomb-gauge/collar representative, not the TT-cleaned norm. Therefore the scalar quotient transported to $\mathcal{H}_\chi$ is the branch-fixed full-load quotient

$$P^{(\chi)}_{IR}(\ell) = P^{(\chi)}_{IR,\mathrm{full}}(\ell;\mathscr{A}^{\mathrm{coll}}_{\parallel}) = \big\langle \psi_\chi,\, \mathcal{W}_\ell\Big(\mathbb{I}-\frac{1}{3}\,\mathcal{S}_{\ell,\chi}\Big)\mathcal{W}_\ell\psi_\chi\big\rangle_{\mathcal{H}_\chi}.$$

Using the cyclic multiplier identity lemma 16, this becomes

$$P^{(\chi)}_{IR}(\ell) = \int_0^1 W^{(\chi)}_{\ell}(y)\,|\psi_\chi(y)|^2\,\mathrm{d}y = \int_0^1 W^{(\chi)}_{\ell}(y)\,\mathrm{d}\mu_\chi(y),$$

which proves Eq. (327). Inserting the explicit density

$$\mathrm{d}\mu_\chi(y) = \frac{y^2\sin^2(\pi y)}{\mathcal{N}_\chi}\,\mathrm{d}y$$

gives Eq. (328).

For $\ell > 0$ and $0 \le y \le 1$,

$$0 < \exp\left[-\left(\frac{1-y}{\ell}\right)^2\right] \le 1, \qquad 0 \le \frac{(1-y)^2}{(1-y)^2+\ell^2} \le 1.$$

Hence

$$0 < W_\ell^{(\chi)}(y) \le 1.$$

The equality $W_\ell^{(\chi)}(y) = 1$ can hold only at the endpoint $y = 1$, which has zero $\mathrm{d}\mu_\chi$-measure. Since $\mathrm{d}\mu_\chi$ is a probability measure and has positive density on every nonempty subinterval of $(0, 1)$,

$$0 < P_{IR}^{(\chi)}(\ell) < 1.$$

This proves Eq. (329). □

Corollary 5 (Minimal-branch value of the TT–χ admitted weight)**.** *On the minimal electron branch,*

$$\ell_0 = \frac{1}{\pi\sqrt{\pi}}.$$

A high-precision numerical evaluation of the one-dimensional integral Eq. (328) *gives*

$$P_{IR}^{(\chi)}(\ell_0) = 0.0857791925845556011097469\ldots \tag{330}$$

The displayed decimal is a realization-level quadrature value. The quantity $\delta_{\rm quad}$ used in the numerical ledger records the internal quadrature stopping criterion; it is not a theorem-level analytic error bound for the exact integral. This numerical value is not an external benchmark and is not fitted to α. Consequently, with

$$P_{IR}^{(\chi)}(\ell_0) = P_{IR,\mathrm{full}}^{(\chi)}(\ell_0; \mathscr{A}_\parallel^{\mathrm{coll}}),$$

the admitted Gaussian UV load on the minimal branch is

$$\Delta\Lambda_{\mathrm{UV}\to\mathrm{IR}}(\ell_0) \equiv \Delta\Lambda_{\mathrm{UV}\to\mathrm{IR}}(\ell_0; \mathscr{A}_\parallel^{\mathrm{coll}}) = C_{\mathrm{UV}}^{(\mathrm{Gauss})}\, P_{IR}^{(\chi)}(\ell_0). \tag{331}$$

Proof. Evaluating the explicit integral Eq. (328) at $\ell = \ell_0 = 1/(\pi\sqrt{\pi})$ gives the displayed realization-level number. The identity Eq. (331) then follows from Eq. (317). □

The closed cyclic formula Eq. (328) gives a direct visual diagnostic of the normalized χ-admission mechanism. With

$$p_\chi(y) = \frac{y^2 \sin^2(\pi y)}{\mathcal{N}_\chi},$$

one has

$$P_{IR}^{(\chi)}(\ell_0) = \int_0^1 W_{\ell_0}^{(\chi)}(y)\, p_\chi(y)\, \mathrm{d}y.$$

This is shown in fig. 6. Within the branch-cyclic realization, the small value of $P_{IR}^{(\chi)}(\ell_0)$ follows from the overlap between the near-shell Gaussian window and the first-node cyclic density, which is suppressed near $y = 1$.

Remark (Logical status of the admission objects)*.* The geometric projector Π_{TT}, the unnormalized shell-admission operator $\mathbb{Q}_\chi(\ell)$, the normalized operator $\overline{\mathbb{Q}_{\chi,\mathrm{sh}}}(\ell)$, and the scalar admitted weight $P_{IR}^{(\chi)}(\ell; \mathscr{A}_{\mathrm{sh}})$ are distinct objects. The first is an idempotent orthogonal projector. The second and third are positive admission operators and are not idempotent in general. The last is a scalar quotient, not a projector and not a shell operator.

On the minimal branch, $P_{IR}^{(\chi)}(\ell)$ means $P_{IR,\mathrm{full}}^{(\chi)}(\ell; \mathscr{A}_\parallel^{\mathrm{coll}})$. The TT-cleaned field $\mathscr{A}_{\mathrm{TT}}^{\mathrm{coll}} = \Pi_{\mathrm{TT}} \mathscr{A}_\parallel^{\mathrm{coll}}$ enters the numerator through $\overline{\mathbb{Q}_{\chi,\mathrm{sh}}}(\ell)$, while the denominator remains the full norm of $\mathscr{A}_\parallel^{\mathrm{coll}}$. The closed formula Eq. (328) is the branch-cyclic realization of this scalar quotient. It is not an auxiliary fit and not an independent scalar closure.

Figure 7 summarizes the geometry of the local vector load derived in this subsection. On the $\mathbb{C}$ side, the one-loop carrier and its Gaussian collar determine the filamentary reference core Λ_{ind}. On the shell side in $\mathbb{R}^3$, the same branch is represented only through its tangential shell data, and only the TT-cleaned shell content is admitted into the vector block. The central ribbon in the figure is therefore not a literal metric projection and not the action of Π_{TT} itself. It is only a schematic reminder that the local Gaussian collar data feed the exact shell-admission chain $\mathbb{Q}_\chi(\ell)$. The shell quantities drawn on the right are shown only to indicate the downstream continuation to the later shell-return analysis.

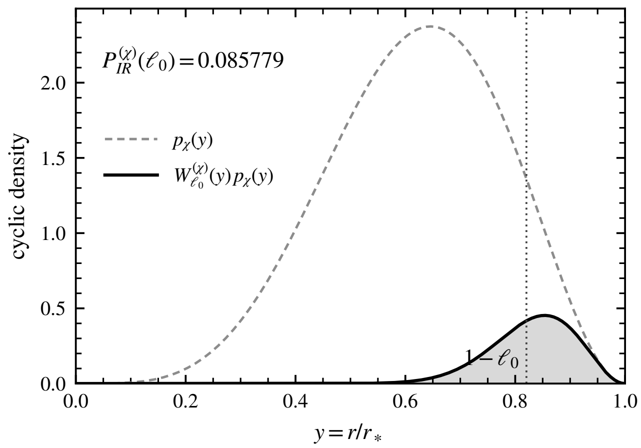

FIG. 6. Diagnostic profile behind the normalized χ-admission. The dashed curve is $p_\chi(y) = y^2 \sin^2(\pi y)/\mathcal{N}_\chi$, hence $\mathrm{d}\mu_\chi(y) = p_\chi(y)\mathrm{d}y$. The solid curve is the admitted density $W_{\ell_0}^{(\chi)}(y)p_\chi(y)$. Its area equals the scalar admitted weight $P_{IR}^{(\chi)}(\ell_0)$. The vertical dotted line marks $y = 1 - \ell_0$, indicating that the Gaussian shell window probes only the near-shell collar, where the first-node cyclic amplitude is already suppressed.

C. Exact shell source and energy-dual exterior subtraction

We now turn from the local Gaussian collar reduction to the part of the vector channel fixed by the exact magnetostatic shell trace of the filamentary carrier on the matching shell. The task of this subsection is twofold. First, it extracts the exact odd-toroidal shell source launched by the one-loop branch onto the shell in $\mathbb{R}^3$. Second, it computes the exact shell-normalized energy-dual exterior subtraction associated with that source. This is the first genuinely nonlocal part of the vector channel. It nevertheless remains fully branch-fixed, requires no shell-memory inversion, and introduces no measured value of α, no QED coefficient, and no fitted vector parameter.

At this stage the branch is read only through its exact magnetostatic shell trace in $\mathbb{R}^3$, after the common SI current factor has been removed. The only branch parameter entering the dimensionless shell formulas is the ring-to-shell ratio

$$\eta = \frac{R}{r_*}, \qquad 0 < \eta < 1.$$

The source shape extracted below is the exact shell datum that later feeds the shell-return operator and the exterior subtraction term $\Delta\Lambda_{\mathrm{out}}$.

Definition VII.8 (Exact shell field of the filamentary carrier)**.** Use the axisymmetric shell coordinate already fixed in Eq. (12),

$$\upsilon = \cos\vartheta \in [-1, 1].$$

Work first on the normalized shell $r_* = 1$. In these normalized units, the circular filamentary carrier has cylindrical radius $\eta = R/r_*$ with $0 < \eta < 1$. For a shell point with polar variable υ, write

$$\rho_\perp(\upsilon) = \sqrt{1 - \upsilon^2}, \qquad z(\upsilon) = \upsilon. \tag{332}$$

Define the associated elliptic parameter by

$$k(\upsilon)^2 = \frac{4\eta\,\rho_\perp(\upsilon)}{(\eta + \rho_\perp(\upsilon))^2 + z(\upsilon)^2}. \tag{333}$$

For every $\upsilon \in (-1, 1)$, one has

$$0 < k(\upsilon)^2 < 1.$$

Indeed, $\rho_\perp(\upsilon) > 0$ on $(-1, 1)$, and

$$(\eta + \rho_\perp(\upsilon))^2 + z(\upsilon)^2 - 4\eta\,\rho_\perp(\upsilon) = (\eta - \rho_\perp(\upsilon))^2 + z(\upsilon)^2.$$

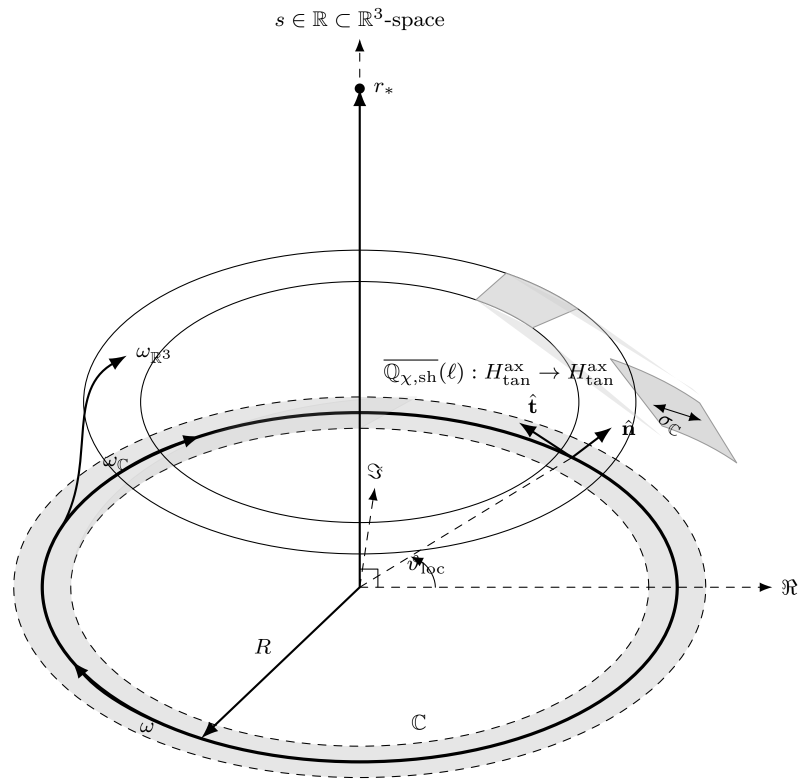

FIG. 7. *Intrinsic core and exact shell admission.* Left; the effective one-loop carrier of radius R with Gaussian collar width $\sigma_{\mathbb{C}}$. Extracting the leading logarithmic part of its regularized tangential self-circulation yields the filamentary reference core $\Lambda_{\mathrm{ind}} = \ln(8R/\sigma_{\mathbb{C}}) - 2$. Middle; a schematic reminder of the shell-admission chain from the local Gaussian collar picture to the matching shell $r = r_* = \pi R \subset \mathbb{R}^3$, with $\ell = \sigma_{\mathbb{C}}/r_*$ the corresponding shell bandwidth. The ribbon is not a literal map from $\mathbb{C}$ to $\mathbb{R}^3$, and it is not the action of Π_{TT}. Right; only the admitted tangential-transverse shell content is retained for the later shell-return problem. The arrows labelled by J_χ, a_*, and $\mathbb{G}_{\mathrm{sh}}$, together with the box Λ_{geom}, indicate that later continuation and are not part of the admission formula itself. The drawing is conceptual and not metrically to scale.

If the right-hand side were zero, then $\rho_\perp(\upsilon) = \eta$ and $z(\upsilon) = 0$, hence

$$1 = \rho_\perp(\upsilon)^2 + z(\upsilon)^2 = \eta^2,$$

which contradicts $0 < \eta < 1$. Therefore the complete elliptic integrals in Eqs. (334) and (335) are evaluated at admissible parameter values. For $\upsilon \in (-1, 1)$, define the cylindrical shell shape functions of the unit-current filamentary carrier by

$$\mathcal{B}_\rho(\eta;\upsilon) = \frac{z(\upsilon)}{2\pi\rho_\perp(\upsilon)\sqrt{(\eta+\rho_\perp(\upsilon))^2 + z(\upsilon)^2}} \left[-\mathrm{K}_{\mathrm{ell}}\big(k(\upsilon)^2\big) + \frac{\eta^2 + \rho_\perp(\upsilon)^2 + z(\upsilon)^2}{(\eta-\rho_\perp(\upsilon))^2 + z(\upsilon)^2}\,\mathrm{E}_{\mathrm{ell}}\big(k(\upsilon)^2\big)\right], \tag{334}$$

The displayed formula for $\mathcal{B}_\rho$ has an apparent axial singularity because of the factor $\rho_\perp(\upsilon)^{-1}$. Its endpoint values at $\upsilon = \pm 1$ are always understood by the smooth axial extension proved in lemma 18, not by direct substitution into the displayed quotient.

$$\mathcal{B}_z(\eta;\upsilon) = \frac{1}{2\pi\sqrt{(\eta+\rho_\perp(\upsilon))^2 + z(\upsilon)^2}} \left[\mathrm{K}_{\mathrm{ell}}\big(k(\upsilon)^2\big) + \frac{\eta^2 - \rho_\perp(\upsilon)^2 - z(\upsilon)^2}{(\eta-\rho_\perp(\upsilon))^2 + z(\upsilon)^2}\,\mathrm{E}_{\mathrm{ell}}\big(k(\upsilon)^2\big)\right], \tag{335}$$

where $\mathrm{K}_{\mathrm{ell}}$ and $\mathrm{E}_{\mathrm{ell}}$ are the complete elliptic integrals defined in Eq. (285). These are the exact Biot–Savart shell profiles of the circular filament after removal of the common SI factor $\mu_0 I/r_*$. Thus

$$[B_\rho] = [B_z] = \mathrm{T}, \qquad \left[\frac{\mu_0 I}{r_*}\right] = \mathrm{T}, \qquad [\mathcal{B}_\rho] = [\mathcal{B}_z] = 1.$$

By linearity in the current and dimensional scaling of the Biot–Savart field, the corresponding physical shell field for a nonzero signed current I, with the positive orientation fixed by increasing ring azimuth, is

$$B_\rho(r_*, \upsilon; \eta, I) = \frac{\mu_0 I}{r_*}\,\mathcal{B}_\rho(\eta; \upsilon), \qquad B_z(r_*, \upsilon; \eta, I) = \frac{\mu_0 I}{r_*}\,\mathcal{B}_z(\eta; \upsilon).$$

For the electron charge sector, $Q = -e$ and hence the effective loop current has the sign fixed earlier by $I = Qc/(2\pi R)$. The dimensionless shell shapes below are normalized by the same signed current I. Thus the sign of the physical current is removed from $\widetilde{b}_\eta$, while the chosen orientation fixes the sign convention of the basis coefficients. This normalization is a sign convention for the vector shell source and is not fitted to the exterior subtraction. In the shell frame, the polar tangential unit vector is

$$\hat{\mathbf{e}}_\vartheta = z(\upsilon)\,\hat{\mathbf{e}}_\rho - \rho_\perp(\upsilon)\,\hat{\mathbf{e}}_z.$$

Hence the shell-normalized tangential trace is

$$\underbrace{\widetilde{b}_\eta(\upsilon) = \frac{r_*}{\mu_0 I}\,B_\vartheta(r_*, \upsilon; \eta, I)}_{\substack{\text{shell-normalized}\\ \text{tangential trace}}} = \underbrace{\upsilon\,\mathcal{B}_\rho(\eta; \upsilon)}_{\substack{\text{radial component}\\ \text{projected tangentially}}} - \underbrace{\rho_\perp(\upsilon)\,\mathcal{B}_z(\eta; \upsilon)}_{\substack{\text{axial component}\\ \text{projected tangentially}}}. \tag{336}$$

Equivalently, in the earlier shell-trace notation,

$$b_*^{\mathrm{ext}}(\upsilon) = B_\vartheta^{\mathrm{ext}}(r_*^+, \upsilon) = \frac{\mu_0 I}{r_*}\,\widetilde{b}_\eta(\upsilon).$$

Lemma 18 (Endpoint regularity and flux compatibility of the exact shell trace)**.** *For every fixed* $0 < \eta < 1$*, the filament lies strictly inside the matching shell. There exists a function* $h_\eta \in C^\infty([-1, 1])$ *such that*

$$\widetilde{b}_\eta(\upsilon) = \rho_\perp(\upsilon)\,h_\eta(\upsilon), \qquad \rho_\perp(\upsilon) = \sqrt{1 - \upsilon^2}. \tag{337}$$

Consequently, the flux-compatible datum

$$\beta_\eta(\upsilon) \equiv \rho_\perp(\upsilon)\widetilde{b}_\eta(\upsilon) = (1 - \upsilon^2)\,h_\eta(\upsilon) \tag{338}$$

extends smoothly to $[-1, 1]$*, vanishes at* $\upsilon = \pm 1$*, and all flux and energy-dual shell moments used below are finite.*

Proof. The circular filament lies strictly inside the shell $r = r_*$. Hence the source-free Maxwell field is real analytic in Cartesian coordinates on a neighborhood of the shell, including neighborhoods of the north and south poles. Write the field near the symmetry axis in Cartesian form

$$\mathbf{B}(x, y, z) = B_x(x, y, z)\,\hat{\mathbf{e}}_x + B_y(x, y, z)\,\hat{\mathbf{e}}_y + B_z(x, y, z)\,\hat{\mathbf{e}}_z.$$

Axisymmetry about the z-axis implies that B_z is invariant under rotations in the (x, y)-plane, whereas (B_x, B_y) transforms as a planar vector. Therefore there exist smooth functions F_η and G_η, defined near $(\rho^2, z) = (0, \pm 1)$, such that

$$B_x(x, y, z) = x\,F_\eta(x^2 + y^2, z), \qquad B_y(x, y, z) = y\,F_\eta(x^2 + y^2, z), \qquad B_z(x, y, z) = G_\eta(x^2 + y^2, z).$$

Passing to cylindrical coordinates $\rho = \sqrt{x^2 + y^2}$ gives

$$B_\rho(\rho, z) = \frac{xB_x + yB_y}{\rho} = \rho\,F_\eta(\rho^2, z), \qquad B_z(\rho, z) = G_\eta(\rho^2, z).$$

Renaming F_η and G_η as H_ρ and H_z, one obtains

$$B_\rho(\rho, z) = \rho\,H_\rho(\rho^2, z), \qquad B_z(\rho, z) = H_z(\rho^2, z),$$

with H_ρ and H_z smooth near $\rho = 0$. On the normalized shell $r_* = 1$, one has

$$\hat{\mathbf{e}}_\vartheta = z\,\hat{\mathbf{e}}_\rho - \rho\,\hat{\mathbf{e}}_z,$$

and therefore

$$B_\vartheta = z\,B_\rho - \rho\,B_z.$$

Thus

$$B_\vartheta(\rho,z) = \rho\Big[z\,H_\rho(\rho^2,z) - H_z(\rho^2,z)\Big].$$

Restricting this identity to the normalized shell

$$\rho = \rho_\perp(\upsilon) = \sqrt{1-\upsilon^2}, \qquad z = z(\upsilon) = \upsilon,$$

and dividing by the common factor $\mu_0 I/r_*$, we get

$$\widetilde{b}_\eta(\upsilon) = \rho_\perp(\upsilon)\,h_\eta(\upsilon),$$

with $h_\eta \in C^\infty([-1,1])$. This proves Eq. (337).

Multiplying once more by $\rho_\perp(\upsilon)$ gives

$$\beta_\eta(\upsilon) = \rho_\perp(\upsilon)\widetilde{b}_\eta(\upsilon) = (1-\upsilon^2)\,h_\eta(\upsilon),$$

which is smooth on $[-1,1]$ and vanishes at $\upsilon = \pm 1$. Hence β_η is flux-compatible. Since $\mathcal{T}_j(\upsilon)$ is a polynomial multiple of $1-\upsilon^2$, both the flux pairings and the energy-dual moments used below are finite. □

Remark. The physical tangential shell trace is $B_\vartheta(r_*,\upsilon)$. The present definition introduces the dimensionless scalar shape $\widetilde{b}_\eta(\upsilon)$, obtained by removing the common SI factor $\mu_0 I/r_*$ before shell-mode projection. The corresponding flux-compatible datum is

$$\beta_\eta(\upsilon) = \rho_\perp(\upsilon)\widetilde{b}_\eta(\upsilon).$$

Thus the shell moments, the normalized source coefficients, and $\Delta\Lambda_{\mathrm{out}}$ defined below are dimensionless.

For orientation, it is useful to display the same minimal branch on both sides of the split $\mathbb{C}\oplus\mathbb{R}^3$. Figure 8 juxtaposes the collar-side organization inherited from the Gaussian generator state with the corresponding physical shell field on the matching sphere. The figure is diagnostic only. It introduces no additional shell datum and plays no role in the proof. Its purpose is simply to make the collar organization and the observed shell-source geometry visually explicit before the exact shell functional is written in mode coordinates.

The left panel should be read as a collar chart rather than as an ordinary physical-space picture. Its main message is that the shell loading is concentrated near the admitted boundary $\xi = 0$ and decays inward with the Gaussian collar weight. The black arrows there do *not* represent a physical magnetic field; they represent the gradient of the collar-side amplitude on the chart. The right panel is the observed-side counterpart in $\mathbb{R}^3$; it shows where the same branch places field strength on the matching shell, which way the field itself points there, and in which tangential direction the shell field becomes stronger. In this sense the two panels are complementary; the left panel displays how the branch is organized before shell projection, while the right panel displays the physical shell geometry that enters the exact vector functional and, ultimately, the computation of Λ_{geom}.

Definition VII.9 (Toroidal shell basis, flux pairing, and energy-dual moments)**.** Let

$$\mathcal{T}_j(\upsilon) = (1-\upsilon^2)P_j'(\upsilon), \qquad j = 1,2,\ldots. \tag{339}$$

where P_j is the Legendre polynomial of degree j. On the real flux-compatible class

$$f(\upsilon) = \rho_\perp(\upsilon)\,\widetilde{f}(\upsilon), \qquad g(\upsilon) = \rho_\perp(\upsilon)\,\widetilde{g}(\upsilon), \qquad \widetilde{f},\widetilde{g} \in L^2(-1,1),$$

we use the flux pairing

$$\langle f,g\rangle_{\mathrm{flux}} := \int_{-1}^{1} \frac{f(\upsilon)g(\upsilon)}{1-\upsilon^2}\,\mathrm{d}\upsilon = \int_{-1}^{1} \widetilde{f}(\upsilon)\widetilde{g}(\upsilon)\,\mathrm{d}\upsilon. \tag{340}$$

This agrees with the pairing fixed in Eq. (15). The apparent endpoint singularity is removable on this class. The functions $\mathcal{T}_j$ belong to the flux-compatible class and, by Eq. (341), form an orthogonal system under $\langle\cdot,\cdot\rangle_{\mathrm{flux}}$. The corresponding flux space is the closed span of these modes in the associated flux norm.

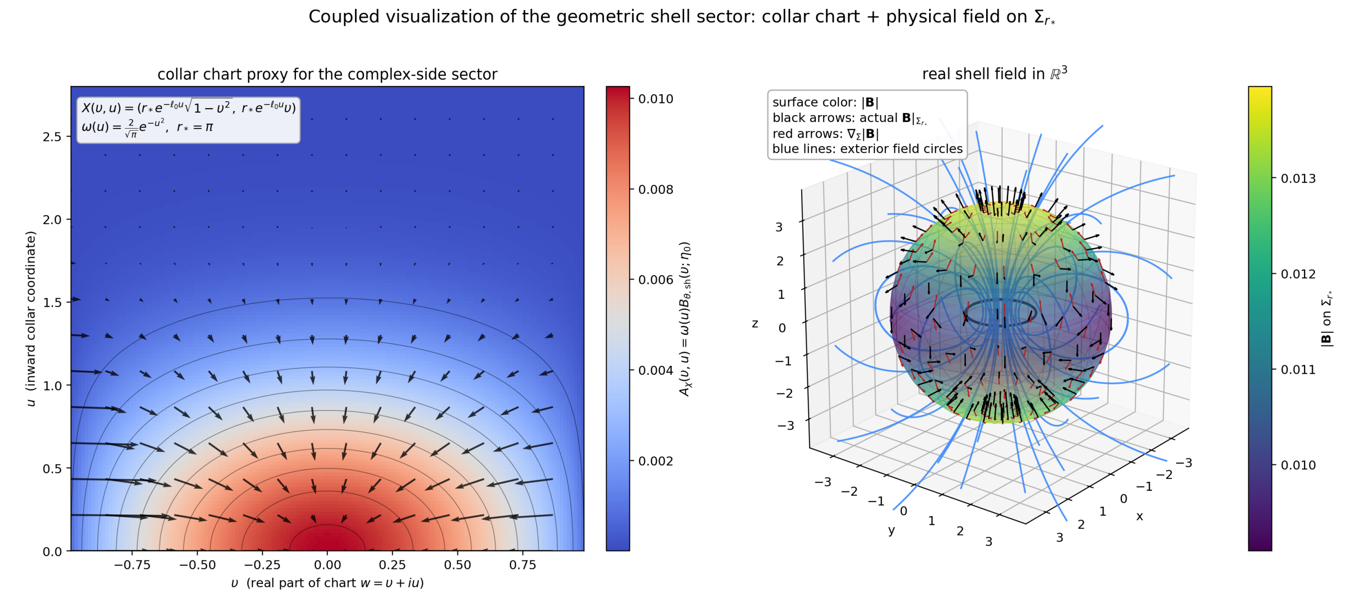

FIG. 8. Diagnostic visualization of the minimal one-loop branch. Left panel; a collar-side chart with complex coordinate $\zeta_{\mathrm{col}} = \upsilon + i\xi$. The horizontal coordinate $\upsilon \in [-1,1]$ labels meridional shell position, equivalently $\upsilon = \cos\vartheta$, whereas $\xi \geq 0$ is inward collar depth. The color scale shows the collar-side amplitude concentrated near the admitted shell boundary, and the black arrows show its chart gradient in the (υ, ξ) plane. Right panel; the physical matching shell $\Sigma_{r_*} \subset \mathbb{R}^3$ together with the exterior field generated by the corresponding filamentary ring carrier. The surface color shows shell-field strength, the black arrows show field direction on the shell, the red arrows show the surface gradient of shell-field strength, and the blue curves are representative exterior field lines of the axisymmetric ring field. The figure is diagnostic only and introduces no additional vector datum. It is included only to display the shell-source geometry before projection onto the odd toroidal shell basis.

On the same real sector, define the unweighted energy-dual pairing

$$[f,g]_{\mathrm{E}} = \int_{-1}^{1} f(\upsilon)g(\upsilon)\,\mathrm{d}\upsilon.$$

The corresponding energy-dual shell moments are

$$[\widetilde{b}_\eta, \mathcal{T}_j]_{\mathrm{E}} = \int_{-1}^{1} \widetilde{b}_\eta(\upsilon)\mathcal{T}_j(\upsilon)\,\mathrm{d}\upsilon.$$

This distinction is essential. The flux-compatible datum $\beta_\eta = \rho_\perp \widetilde{b}_\eta$ matches tangential shell traces, whereas the energy-dual pairing supplies the source moments used by the exterior shell-energy quadratic form. The parity restriction to the odd subsector is proved in lemma 20.

Lemma 19 (Flux orthogonality of the toroidal basis)**.** *For $j, k \geq 1$,*

$$\langle \mathcal{T}_j, \mathcal{T}_k \rangle_{\mathrm{flux}} = I_j\,\delta_{jk}, \qquad I_j = \frac{2j(j+1)}{2j+1}. \tag{341}$$

Proof. By definition of the flux pairing and of $\mathcal{T}_j$,

$$\langle \mathcal{T}_j, \mathcal{T}_k \rangle_{\mathrm{flux}} = \int_{-1}^{1} \frac{(1-\upsilon^2)P_j'(\upsilon)\,(1-\upsilon^2)P_k'(\upsilon)}{1-\upsilon^2}\,\mathrm{d}\upsilon = \int_{-1}^{1} (1-\upsilon^2)P_j'(\upsilon)P_k'(\upsilon)\,\mathrm{d}\upsilon.$$

Integrate by parts. Since $1-\upsilon^2 = 0$ at $\upsilon = \pm 1$ and P_j, P_k are bounded there, the boundary term vanishes and

$$\langle \mathcal{T}_j, \mathcal{T}_k \rangle_{\mathrm{flux}} = -\int_{-1}^{1} P_k(\upsilon)\,\frac{d}{d\upsilon}\Big((1-\upsilon^2)P_j'(\upsilon)\Big)\,\mathrm{d}\upsilon.$$

Now use the Legendre equation

$$\frac{d}{dv}\Big((1-v^2)P_j'(v)\Big) + j(j+1)P_j(v) = 0.$$

Hence

$$\langle \mathcal{T}_j, \mathcal{T}_k\rangle_{\text{flux}} = j(j+1)\int_{-1}^{1} P_j(v)P_k(v)\,\mathrm{d}v.$$

Using the standard Legendre orthogonality relation

$$\int_{-1}^{1} P_j(v)P_k(v)\,\mathrm{d}v = \frac{2}{2j+1}\,\delta_{jk},$$

we obtain Eq. (341). □

Proposition 40 (Energy-dual shell source moments)**.** *For $j \geq 1$, define the energy-dual shell moment of the exact Maxwell tangential shell trace by*

$$a_j^{\text{sh}}(\eta) = \frac{1}{I_j}\int_{-1}^{1} \widetilde{b}_\eta(v)\,\mathcal{T}_j(v)\,\mathrm{d}v, \qquad I_j = \frac{2j(j+1)}{2j+1}. \tag{342}$$

Equivalently,

$$a_j^{\text{sh}}(\eta) = \frac{1}{I_j}\int_{-1}^{1} \widetilde{b}_\eta(v)\,(1-v^2)P_j'(v)\,\mathrm{d}v. \tag{343}$$

The normalized amplitudes used in the shell-energy source are

$$\widehat{a}_j(\eta) = 2(j+1)\,\eta^{-1/2}\,a_j^{\text{sh}}(\eta). \tag{344}$$

This is the energy-dual normalization used by the shell-normalized exterior response in theorem 12. These amplitudes are dimensionless. They are not flux expansion coefficients of $\widetilde{b}_\eta$. They are the normalized shell-source amplitudes that enter Eqs. (352) *and* (356)*.*

Proof. By lemma 18,

$$\widetilde{b}_\eta(v) = \rho_\perp(v)\,h_\eta(v), \qquad \rho_\perp(v) = \sqrt{1-v^2},$$

with $h_\eta \in C^\infty([-1,1])$. Since

$$\mathcal{T}_j(v) = (1-v^2)P_j'(v) = \rho_\perp(v)^2 P_j'(v),$$

the energy-dual integrand is

$$\widetilde{b}_\eta(v)\mathcal{T}_j(v) = \rho_\perp(v)^3 h_\eta(v)P_j'(v),$$

which belongs to $L^1(-1,1)$. Hence $a_j^{\text{sh}}(\eta)$ is well defined. The expanded form Eq. (343) is simply Eq. (339) written out, and the normalized amplitudes $\widehat{a}_j(\eta)$ are then fixed by Eq. (344). □

Remark (Normalized-shell versus physical-shell coefficient conventions)*.* The coefficient $a_j^{\text{sh}}(\eta)$ in Eq. (342) is the normalized-shell theorem coefficient. The shell is first scaled to $r_* = 1$, and the common factor $\mu_0 I/r_*$ is removed from the Maxwell trace. The numerical tables may instead record the physical-shell rescaling

$$a_j^{\text{sh,phys}}(\eta) = \eta^{-(j+1)}a_j^{\text{sh}}(\eta),$$

because direct quadrature is performed on the physical shell $r_* = \eta^{-1}$. In that convention,

$$\widehat{a}_j(\eta) = 2(j+1)\eta^{j+1/2}a_j^{\text{sh,phys}}(\eta),$$

which is algebraically equivalent to Eq. (344). The theorem path therefore uses a_j^{sh}, whereas the low-mode numerical tables may display $a_j^{\text{sh,phys}}$.

Lemma 20 (Equatorial parity selection)**.** *For the equatorial filamentary carrier,*

$$\mathcal{B}_\rho(\eta;-\upsilon) = -\mathcal{B}_\rho(\eta;\upsilon), \qquad \mathcal{B}_z(\eta;-\upsilon) = \mathcal{B}_z(\eta;\upsilon), \qquad \widetilde{b}_\eta(-\upsilon) = \widetilde{b}_\eta(\upsilon).$$

Moreover,

$$\mathcal{T}_j(-\upsilon) = (-1)^{j+1}\mathcal{T}_j(\upsilon).$$

Hence, for every even j,

$$a_j^{\mathrm{sh}}(\eta) = 0.$$

Therefore only the odd toroidal modes contribute to the energy-dual shell source and to $\Delta\Lambda_{\mathrm{out}}$.

Proof. Since

$$\rho_\perp(-\upsilon) = \rho_\perp(\upsilon), \qquad z(-\upsilon) = -z(\upsilon), \qquad k(-\upsilon)^2 = k(\upsilon)^2,$$

the explicit formulas Eqs. (334) and (335) imply

$$\mathcal{B}_\rho(\eta;-\upsilon) = -\mathcal{B}_\rho(\eta;\upsilon), \qquad \mathcal{B}_z(\eta;-\upsilon) = \mathcal{B}_z(\eta;\upsilon).$$

Therefore, from Eq. (336),

$$\widetilde{b}_\eta(-\upsilon) = (-\upsilon)\,\mathcal{B}_\rho(\eta;-\upsilon) - \rho_\perp(-\upsilon)\,\mathcal{B}_z(\eta;-\upsilon) = \widetilde{b}_\eta(\upsilon),$$

so $\widetilde{b}_\eta$ is even.

Further,

$$P_j(-\upsilon) = (-1)^j P_j(\upsilon) \quad\Longrightarrow\quad P_j'(-\upsilon) = (-1)^{j+1}P_j'(\upsilon),$$

hence

$$\mathcal{T}_j(-\upsilon) = (-1)^{j+1}\mathcal{T}_j(\upsilon).$$

If j is even, then $\mathcal{T}_j$ is odd. Since $\widetilde{b}_\eta$ is even, the integrand in

$$a_j^{\mathrm{sh}}(\eta) = \frac{1}{I_j}\int_{-1}^{1} \widetilde{b}_\eta(\upsilon)\mathcal{T}_j(\upsilon)\,\mathrm{d}\upsilon$$

is odd, and therefore

$$a_j^{\mathrm{sh}}(\eta) = 0 \qquad \text{for every even } j.$$

This proves the parity selection for the energy-dual shell source. □

Definition VII.10 (Exact normalized energy-dual shell source)**.** Define the exact dimensionless odd-toroidal shell source coefficients by

$$J_j^{(\chi)}(\eta) = \sqrt{\frac{2\pi}{(j+1)(2j+1)}}\,\widehat{a}_j(\eta), \qquad j = 1,3,5,\ldots. \tag{345}$$

We also write

$$\mathbf{J}_\chi(\eta) := \big(J_j^{(\chi)}(\eta)\big)_{j=1,3,5,\ldots} \tag{346}$$

for the odd source sequence itself. Whenever the odd source sequence is nonzero and square-summable,

$$0 < \sum_{k\ \mathrm{odd}} \big(J_k^{(\chi)}(\eta)\big)^2 < \infty,$$

define the normalized weights by

$$w_j = \frac{\big(J_j^{(\chi)}(\eta)\big)^2}{\sum_{k\ \mathrm{odd}}\big(J_k^{(\chi)}(\eta)\big)^2}, \qquad \sum_{j\ \mathrm{odd}} w_j = 1. \tag{347}$$

The square-summability required here is proved in theorem 12.

Theorem 12 (Energy-dual exterior mode identity and shell subtraction)**.** *For each odd j, define the energy-dual exterior-response coefficient by*

$$d_j^{\mathrm{E}}(\eta) = \eta^{-1/2} a_j^{\mathrm{sh}}(\eta). \tag{348}$$

Define the corresponding energy-dual exterior harmonic mode by

$$\Phi_{j,\mathrm{E}}^{\mathrm{out}}(r, \upsilon) = \mu_0 I \, d_j^{\mathrm{E}}(\eta) \left(\frac{r_*}{r}\right)^{j+1} P_j(\upsilon), \qquad r \geq r_*. \tag{349}$$

This auxiliary harmonic mode is not the flux-matching exterior Maxwell continuation of the shell trace. It is the diagonal exterior harmonic mode assigned to the energy-dual shell coefficient $d_j^{\mathrm{E}}(\eta)$ under the shell-energy normalization used below. On exterior fields with finite magnetic energy, define the exterior energy inner product by

$$\langle \mathbf{B}, \mathbf{C} \rangle_{\mathrm{out},E} := \frac{1}{2\mu_0} \int_{r > r_*} \mathbf{B} \cdot \mathbf{C} \, \mathrm{d}V. \tag{350}$$

The word exterior in this theorem refers to this energy-dual exterior response, not to an additional fitted exterior field.

Let h_η be the smooth endpoint factor from lemma 18, so that

$$\widetilde{b}_\eta(\upsilon) = \rho_\perp(\upsilon) \, h_\eta(\upsilon), \qquad \rho_\perp(\upsilon) = \sqrt{1 - \upsilon^2}.$$

Define

$$H_\eta(\upsilon) = (1 - \upsilon^2) \widetilde{b}_\eta(\upsilon) = \rho_\perp(\upsilon)^3 h_\eta(\upsilon).$$

Then $H_\eta(\pm 1) = 0$ and $H'_\eta \in L^2(-1, 1)$. Consequently, the energy-dual moments satisfy

$$|a_j^{\mathrm{sh}}(\eta)| \leq \frac{\|H'_\eta\|_{L^2(-1,1)}}{I_j} \left(\frac{2}{2j+1}\right)^{1/2} \leq \sqrt{\frac{3}{2}} \, \|H'_\eta\|_{L^2(-1,1)} \, j^{-3/2}, \qquad j = 1, 3, 5, \ldots. \tag{351}$$

In particular,

$$\sum_{j=1,3,5,\ldots} \left(a_j^{\mathrm{sh}}(\eta)\right)^2 < \infty.$$

For each odd j, let

$$\mathbf{B}_{j,\mathrm{E}}^{\mathrm{out}} = -\nabla \Phi_{j,\mathrm{E}}^{\mathrm{out}}.$$

Its exterior energy is

$$U_j^{\mathrm{out}} = \frac{1}{2\mu_0} \int_{r > r_*} |\mathbf{B}_{j,\mathrm{E}}^{\mathrm{out}}|^2 \, \mathrm{d}V = 2\pi \mu_0 I^2 \, r_* \, \frac{j+1}{2j+1} \left(d_j^{\mathrm{E}}(\eta)\right)^2 = 2\pi \mu_0 I^2 \, r_* \, \eta^{-1} \, \frac{j+1}{2j+1} \left(a_j^{\mathrm{sh}}(\eta)\right)^2. \tag{352}$$

The family $\{\mathbf{B}_{j,\mathrm{E}}^{\mathrm{out}}\}_{j \text{ odd}}$ is orthogonal in the exterior energy inner product, and

$$U^{\mathrm{out}} := \sum_{j=1,3,5,\ldots} U_j^{\mathrm{out}} < \infty.$$

The exterior subtraction functional is defined with the vector-channel subtraction sign convention as the negative of the shell-normalized energy-dual exterior-response norm. This sign is fixed by the subtraction convention and is not adjustable,

$$\Delta\Lambda_{\mathrm{out}}(\eta) = - \underbrace{\frac{2}{\mu_0 I^2 r_*}}_{\substack{\textit{shell-energy} \\ \textit{normalization}}} U^{\mathrm{out}} = - \underbrace{\frac{2}{\mu_0 I^2 r_*}}_{\substack{\textit{shell-energy} \\ \textit{normalization}}} \sum_{j=1,3,5,\ldots} U_j^{\mathrm{out}}, \tag{353}$$

and therefore

$$\Delta\Lambda_{\mathrm{out}}(\eta) = -4\pi \, \eta^{-1} \sum_{j=1,3,5,\ldots} \frac{j+1}{2j+1} \left(a_j^{\mathrm{sh}}(\eta)\right)^2. \tag{354}$$

In particular, the normalized source vector belongs to ℓ^2,

$$\sum_{j=1,3,5,\dots} \big(J_j^{(\chi)}(\eta)\big)^2 < \infty. \tag{355}$$

Equivalently,

$$\Delta\Lambda_{\rm out}(\eta) = -\pi \sum_{j=1,3,5,\dots} \frac{\widehat{a}_j(\eta)^2}{(j+1)(2j+1)} = -\frac{1}{2} \sum_{j=1,3,5,\dots} \big(J_j^{(\chi)}(\eta)\big)^2 = -\frac{1}{2}\,\|\mathbf{J}_\chi(\eta)\|_{\ell^2}^2. \tag{356}$$

Hence

$$\Delta\Lambda_{\rm out}(\eta) \le 0, \qquad \Delta\Lambda_{\rm out}(\eta) = 0 \quad\Longleftrightarrow\quad \mathbf{J}_\chi(\eta) = 0. \tag{357}$$

Proof. By lemma 18,

$$\widetilde{b}_\eta(\upsilon) = \rho_\perp(\upsilon)\,h_\eta(\upsilon), \qquad h_\eta \in C^\infty([-1,1]).$$

Therefore

$$H_\eta(\upsilon) = (1-\upsilon^2)\widetilde{b}_\eta(\upsilon) = \rho_\perp(\upsilon)^3 h_\eta(\upsilon),$$

so $H_\eta(\pm 1) = 0$ and

$$H_\eta'(\upsilon) = -3\upsilon\,\rho_\perp(\upsilon)\,h_\eta(\upsilon) + \rho_\perp(\upsilon)^3 h_\eta'(\upsilon) \in L^2(-1,1).$$

Using Eq. (343),

$$a_j^{\rm sh}(\eta) = \frac{1}{I_j}\int_{-1}^{1} H_\eta(\upsilon)\,P_j'(\upsilon)\,\mathrm{d}\upsilon.$$

Integrating by parts, and using $H_\eta(\pm 1) = 0$, gives

$$a_j^{\rm sh}(\eta) = -\frac{1}{I_j}\int_{-1}^{1} H_\eta'(\upsilon)\,P_j(\upsilon)\,\mathrm{d}\upsilon.$$

Hence

$$|a_j^{\rm sh}(\eta)| \le \frac{1}{I_j}\,\|H_\eta'\|_{L^2(-1,1)}\,\|P_j\|_{L^2(-1,1)} = \frac{\|H_\eta'\|_{L^2(-1,1)}}{I_j}\left(\frac{2}{2j+1}\right)^{1/2}.$$

Since

$$I_j = \frac{2j(j+1)}{2j+1},$$

one has

$$\frac{1}{I_j}\left(\frac{2}{2j+1}\right)^{1/2} = \frac{\sqrt{2j+1}}{\sqrt{2}\,j(j+1)} \le \frac{\sqrt{3}}{\sqrt{2}}\,j^{-3/2}, \qquad j \ge 1,$$

because $2j+1 \le 3j$ and $j+1 \ge j$. This proves Eq. (351). In particular,

$$\sum_{j=1,3,5,\dots} \big(a_j^{\rm sh}(\eta)\big)^2 < \infty.$$

For each odd j, define

$$\mathbf{B}_{j,\rm E}^{\rm out} = -\nabla\Phi_{j,\rm E}^{\rm out}.$$

The radial component is

$$B_{r,j,\rm E}^{\rm out}(r,\upsilon) = -\partial_r\Phi_{j,\rm E}^{\rm out}(r,\upsilon) = \mu_0 I\,\frac{j+1}{r_*}\,d_j^{\rm E}(\eta)\left(\frac{r_*}{r}\right)^{j+2} P_j(\upsilon).$$

The polar component is

$$B^{\mathrm{out}}_{\vartheta,j,\mathrm{E}}(r,\upsilon) = -\frac{1}{r}\partial_\vartheta \Phi^{\mathrm{out}}_{j,\mathrm{E}}(r,\upsilon).$$

Using $\upsilon = \cos\vartheta$, hence

$$\partial_\vartheta P_j(\upsilon) = -\rho_\perp(\upsilon)\, P_j'(\upsilon),$$

one obtains

$$B^{\mathrm{out}}_{\vartheta,j,\mathrm{E}}(r,\upsilon) = \mu_0 I\, \frac{1}{r_*}\, d^{\mathrm{E}}_j(\eta) \left(\frac{r_*}{r}\right)^{j+2} \rho_\perp(\upsilon)\, P_j'(\upsilon).$$

Therefore

$$\begin{aligned}\int_{\mathbb{S}^2} \left(|B^{\mathrm{out}}_{r,j,\mathrm{E}}|^2 + |B^{\mathrm{out}}_{\vartheta,j,\mathrm{E}}|^2\right) \mathrm{d}\Omega = 2\pi\mu_0^2 I^2\, &\frac{(d^{\mathrm{E}}_j(\eta))^2}{r_*^2} \left(\frac{r_*}{r}\right)^{2j+4} \\ &\times \left[(j+1)^2 \int_{-1}^{1} P_j(\upsilon)^2 \,\mathrm{d}\upsilon + \int_{-1}^{1} (1-\upsilon^2) P_j'(\upsilon)^2 \,\mathrm{d}\upsilon\right].\end{aligned}$$

Using

$$\int_{-1}^{1} P_j(\upsilon)^2 \,\mathrm{d}\upsilon = \frac{2}{2j+1}, \qquad \int_{-1}^{1} (1-\upsilon^2) P_j'(\upsilon)^2 \,\mathrm{d}\upsilon = \frac{2j(j+1)}{2j+1},$$

we obtain

$$\int_{\mathbb{S}^2} \left(|B^{\mathrm{out}}_{r,j,\mathrm{E}}|^2 + |B^{\mathrm{out}}_{\vartheta,j,\mathrm{E}}|^2\right) \mathrm{d}\Omega = 4\pi\mu_0^2 I^2\, (j+1)\, \left(d^{\mathrm{E}}_j(\eta)\right)^2 \frac{r_*^{2j+2}}{r^{2j+4}}.$$

Hence

$$\begin{aligned} U^{\mathrm{out}}_j &= \frac{1}{2\mu_0} \int_{r_*}^{\infty} \int_{\mathbb{S}^2} \left(|B^{\mathrm{out}}_{r,j,\mathrm{E}}|^2 + |B^{\mathrm{out}}_{\vartheta,j,\mathrm{E}}|^2\right) r^2 \,\mathrm{d}\Omega \,\mathrm{d}r \\ &= 2\pi\mu_0 I^2\, (j+1)\, \left(d^{\mathrm{E}}_j(\eta)\right)^2 r_*^{2j+2} \int_{r_*}^{\infty} r^{-2j-2} \,\mathrm{d}r \\ &= 2\pi\mu_0 I^2\, r_*\, \frac{j+1}{2j+1} \left(d^{\mathrm{E}}_j(\eta)\right)^2. \end{aligned}$$

Using Eq. (348), this is exactly Eq. (352).

For $j \neq k$, the angular cross term is

$$\begin{aligned} &\int_{\mathbb{S}^2} \left(B^{\mathrm{out}}_{r,j,\mathrm{E}} B^{\mathrm{out}}_{r,k,\mathrm{E}} + B^{\mathrm{out}}_{\vartheta,j,\mathrm{E}} B^{\mathrm{out}}_{\vartheta,k,\mathrm{E}}\right) \mathrm{d}\Omega \\ &= 2\pi\mu_0^2 I^2\, \frac{d^{\mathrm{E}}_j d^{\mathrm{E}}_k}{r_*^2} \left(\frac{r_*}{r}\right)^{j+k+4} \left[(j+1)(k+1) \int_{-1}^{1} P_j(\upsilon) P_k(\upsilon) \,\mathrm{d}\upsilon \right. \\ &\qquad\qquad \left. + \int_{-1}^{1} (1-\upsilon^2) P_j'(\upsilon) P_k'(\upsilon) \,\mathrm{d}\upsilon\right]. \end{aligned}$$

The first integral vanishes by Legendre orthogonality. For the second integral, integration by parts gives

$$\begin{aligned} \int_{-1}^{1} (1-\upsilon^2) P_j'(\upsilon) P_k'(\upsilon) \,\mathrm{d}\upsilon &= -\int_{-1}^{1} P_k(\upsilon) \frac{d}{d\upsilon}\Big((1-\upsilon^2) P_j'(\upsilon)\Big) \,\mathrm{d}\upsilon \\ &= j(j+1) \int_{-1}^{1} P_j(\upsilon) P_k(\upsilon) \,\mathrm{d}\upsilon = 0, \end{aligned}$$

because $j \neq k$, and because the boundary term vanishes at $\upsilon = \pm 1$. Hence the cross term is zero, and the family $\{\mathbf{B}^{\mathrm{out}}_{j,\mathrm{E}}\}_{j \text{ odd}}$ is orthogonal in the exterior energy inner product.

Since $d_j^{\mathrm{E}}(\eta) = \eta^{-1/2} a_j^{\mathrm{sh}}(\eta)$ and $\frac{j+1}{2j+1} \le 1$, we have

$$\sum_{j=1,3,5,\ldots} U_j^{\mathrm{out}} \le 2\pi\mu_0 I^2\, r_*\, \eta^{-1} \sum_{j=1,3,5,\ldots} \big(a_j^{\mathrm{sh}}(\eta)\big)^2 < \infty.$$

Hence the orthogonal mode family defines a finite exterior energy-dual response norm

$$U^{\mathrm{out}} = \sum_{j=1,3,5,\ldots} U_j^{\mathrm{out}}.$$

Substituting Eq. (352) into Eq. (353) yields Eq. (354). Finally, using

$$\widehat{a}_j(\eta) = 2(j+1)\eta^{-1/2} a_j^{\mathrm{sh}}(\eta),$$

we obtain

$$\Delta\Lambda_{\mathrm{out}}(\eta) = -\pi \sum_{j=1,3,5,\ldots} \frac{\widehat{a}_j(\eta)^2}{(j+1)(2j+1)}.$$

Then

$$J_j^{(\chi)}(\eta) = \sqrt{\frac{2\pi}{(j+1)(2j+1)}}\, \widehat{a}_j(\eta)$$

implies

$$\Delta\Lambda_{\mathrm{out}}(\eta) = -\frac{1}{2} \sum_{j=1,3,5,\ldots} \big(J_j^{(\chi)}(\eta)\big)^2 = -\frac{1}{2}\, \|\mathbf{J}_\chi(\eta)\|_{\ell^2}^2.$$

This proves Eq. (356), and Eq. (355) follows immediately. Since the right-hand side is $-\frac{1}{2}\|\mathbf{J}_\chi(\eta)\|_{\ell^2}^2$, Eq. (357) follows as well. □

Remark. No proxy for $\Delta\Lambda_{\mathrm{out}}$ is used in the exact theorem-level construction of this section. The quantity $\Delta\Lambda_{\mathrm{out}}$ is the shell-normalized energy-dual exterior-response subtraction associated with the exact magnetostatic shell trace. Equivalently, it is the signed quadratic source norm in Eq. (356). The exact tangential shell trace is carried by $\widetilde{b}_\eta(v)$, or equivalently by the flux-compatible datum $\beta_\eta(v) = \rho_\perp(v)\widetilde{b}_\eta(v)$, whereas the coefficients $a_j^{\mathrm{sh}}(\eta)$ are the normalized-shell Riesz-dual source moments seen by the exterior energy.

When numerical tables are written in the physical-shell convention, the displayed amplitude is $a_j^{\mathrm{sh,phys}}(\eta) = \eta^{-(j+1)} a_j^{\mathrm{sh}}(\eta)$. This is only a rescaling convention for the numerical tables and does not alter $\widehat{a}_j(\eta)$, $J_j^{(\chi)}(\eta)$, or $\Delta\Lambda_{\mathrm{out}}(\eta)$. Any lower-dimensional diagnostic formula introduced elsewhere is not part of the exact vector channel constructed here. No measured value of α and no QED benchmark enters the exterior subtraction.

D. Shell-memory operator and exact Galerkin formulation

The local vector load has already been extracted in the previous subsections. What remains is the genuinely nonlocal part of the vector channel. A tangential-transverse (TT) shell field launched by the one-loop branch is extended through the Gaussian near-shell collar, propagated by the renormalized Maxwell kernel, and returned to the matching shell. This renormalized collar-mediated return is the shell-memory effect.

The key point is that the local logarithmic core has already been separated off into Λ_{ind}, and the admitted Gaussian finite part has already been reduced to $\Delta\Lambda_{\mathrm{UV}\to\mathrm{IR}}(\ell_0)$. The operator constructed here therefore does not reinsert the local singular self-coupling. It records only the renormalized nonlocal shell return. No measured value of α, no QED coefficient, and no fitted vector parameter enters this shell-memory construction.

Two logically distinct levels appear below. The finite odd-mode matrix elements R_{jk}^{ren} are defined by absolutely convergent mode-pairing integrals under the endpoint hypotheses stated in proposition 41. The stronger statement that these matrix elements are represented by a compact self-adjoint operator $\mathbb{R}_{\mathrm{sh}}^{\mathrm{ren}}$ on the full Hilbert space $\mathcal{H}_{\mathrm{flux}}^{\mathrm{odd}}$ requires the weighted-kernel hypothesis stated in lemma 25. The exact functional and the exact return factor R_χ are asserted only under that operator hypothesis together with the later contraction hypothesis.

Definition VII.11 (Symmetric shell-normalized azimuthal Maxwell kernel)**.** The azimuthal Maxwell kernel $\mathcal{G}_\varphi$ is the Coulomb-gauge Biot–Savart kernel for the azimuthal component of the vector potential produced by a circular filament. In SI units, $I\,\mathcal{G}_\varphi$ has the units of a vector potential, namely tesla-meter. Hence $\mathcal{G}_\varphi$ has the same dimensions as μ_0, namely tesla-meter per ampere. For $\rho, \rho' > 0$ and $(\rho, z) \neq (\rho', z')$, its shell-normalized dimensionless form is chosen so that the coefficient of the local logarithmic singularity is exactly unity. Explicitly,

$$\widetilde{\mathcal{G}}_\varphi(\rho, z; \rho', z') = \frac{2\pi}{\mu_0}\sqrt{\frac{\rho}{\rho'}}\,\mathcal{G}_\varphi(\rho, z; \rho', z'), \tag{358}$$

where

$$\mathcal{G}_\varphi(\rho, z; \rho', z') = \frac{\mu_0}{\pi k}\sqrt{\frac{\rho'}{\rho}}\left[\left(1 - \frac{k^2}{2}\right)\mathrm{K}_{\mathrm{ell}}(k^2) - \mathrm{E}_{\mathrm{ell}}(k^2)\right], \tag{359}$$

with

$$k^2 = \frac{4\rho\rho'}{(\rho+\rho')^2 + (z-z')^2} \in (0,1).$$

Indeed,

$$1 - k^2 = \frac{(\rho-\rho')^2 + (z-z')^2}{(\rho+\rho')^2 + (z-z')^2} > 0$$

away from the coincidence set $(\rho, z) = (\rho', z')$. Equivalently,

$$\widetilde{\mathcal{G}}_\varphi(\rho, z; \rho', z') = \frac{2}{k}\left[\left(1 - \frac{k^2}{2}\right)\mathrm{K}_{\mathrm{ell}}(k^2) - \mathrm{E}_{\mathrm{ell}}(k^2)\right]. \tag{360}$$

In the normalized form Eq. (360), the kernel depends on the two points only through the symmetric parameter k^2. Hence

$$\widetilde{\mathcal{G}}_\varphi(\rho, z; \rho', z') = \widetilde{\mathcal{G}}_\varphi(\rho', z'; \rho, z)$$

for $\rho, \rho' > 0$ and $(\rho, z) \neq (\rho', z')$.

No value at the cylindrical axis $\rho = 0$ or $\rho' = 0$, and no value on the coincidence set $(\rho, z) = (\rho', z')$, is assigned by Eq. (360). Axis and diagonal values, when needed, are understood only after shell-mode pairing or after the local subtraction of Eq. (361).

Definition VII.12 (Local singular core of the azimuthal kernel)**.** For $\rho, \rho' > 0$ and $(\rho, z) \neq (\rho', z')$, define the dimensionless local singular core by

$$\widetilde{\mathcal{G}}_{\mathrm{loc}}(\rho, z; \rho', z') = \ln\frac{8\sqrt{\rho\rho'}}{\sqrt{(\rho-\rho')^2 + (z-z')^2}} - 2. \tag{361}$$

No value on the cylindrical axis, and no value on the coincidence set $(\rho, z) = (\rho', z')$, is assigned by this expression.

Lemma 21 (Local cancellation of the azimuthal singularity)**.** *Let*

$$d\big((\rho, z), (\rho', z')\big) = \sqrt{(\rho-\rho')^2 + (z-z')^2}.$$

Let

$$K \Subset (0,\infty) \times \mathbb{R}$$

be compact. Then, as $(\rho', z') \to (\rho, z)$ with $(\rho, z), (\rho', z') \in K$ and $(\rho, z) \neq (\rho', z')$, one has

$$\widetilde{\mathcal{G}}_\varphi(\rho, z; \rho', z') = \ln\frac{8\sqrt{\rho\rho'}}{d\big((\rho, z), (\rho', z')\big)} - 2 + O_K\!\left(\frac{d\big((\rho, z), (\rho', z')\big)^2}{\rho\rho'}\,\ln\frac{2\sqrt{\rho\rho'}}{d\big((\rho, z), (\rho', z')\big)}\right). \tag{362}$$

where the remainder is uniform on the chosen compact set K. Consequently,

$$\widetilde{\mathcal{G}}_\varphi - \widetilde{\mathcal{G}}_{\mathrm{loc}}$$

extends continuously across the diagonal on every compact set with $\rho, \rho' > 0$.

Proof. Write $k'^2 := 1 - k^2$. Since

$$(\rho + \rho')^2 + (z - z')^2 = 4\rho\rho' + (\rho - \rho')^2 + (z - z')^2 = 4\rho\rho' + d^2,$$

one has the exact identity

$$k'^2 = \frac{d^2}{4\rho\rho' + d^2}.$$

For $k' \downarrow 0$, the standard elliptic expansions are

$$\mathrm{K}_{\mathrm{ell}}(k^2) = \ln\frac{4}{k'} + O\left(k'^2 \ln\frac{1}{k'}\right),$$

$$\mathrm{E}_{\mathrm{ell}}(k^2) = 1 + O\left(k'^2 \ln\frac{1}{k'}\right), \qquad \frac{1}{k} = 1 + O(k'^2).$$

Substituting these expansions into Eq. (360), and using

$$1 - \frac{k^2}{2} = \frac{1}{2} + \frac{k'^2}{2}, \qquad \frac{1}{k} = 1 + O(k'^2),$$

gives

$$\begin{aligned}\widetilde{\mathcal{G}}_\varphi &= \frac{2}{k}\left[\left(\frac{1}{2} + \frac{k'^2}{2}\right)\mathrm{K}_{\mathrm{ell}}(k^2) - \mathrm{E}_{\mathrm{ell}}(k^2)\right] \\ &= \ln\frac{4}{k'} - 2 + O\left(k'^2 \ln\frac{1}{k'}\right).\end{aligned}$$

Next,

$$k' = \frac{d}{\sqrt{4\rho\rho' + d^2}} = \frac{d}{2\sqrt{\rho\rho'}}\left(1 + \frac{d^2}{4\rho\rho'}\right)^{-1/2},$$

so

$$\ln\frac{4}{k'} = \ln\frac{8\sqrt{\rho\rho'}}{d} + O_K\left(\frac{d^2}{\rho\rho'}\right).$$

Also, using

$$k'^2 = \frac{d^2}{4\rho\rho' + d^2},$$

one obtains, locally uniformly on every compact subset of $\{\rho > 0, \rho' > 0\}$,

$$k'^2 \ln\frac{1}{k'} = O_K\left(\frac{d^2}{\rho\rho'}\ln\frac{2\sqrt{\rho\rho'}}{d}\right).$$

Combining the last two displays yields Eq. (362). Subtracting Eq. (361) removes the logarithmic singularity. The remainder is continuous across the diagonal on every compact set with $\rho, \rho' > 0$. □

Definition VII.13 (Renormalized shell-return kernel)**.** Let

$$X(\upsilon, \xi) = \big(\rho_\perp(\upsilon, \xi), z(\upsilon, \xi)\big) = \big(r_* e^{-\ell_0 \xi}\rho_\perp(\upsilon),\ r_* e^{-\ell_0 \xi}\upsilon\big), \qquad \xi \geq 0. \tag{363}$$

Here ξ is the dimensionless inward collar coordinate, and $e^{-\ell_0 \xi}$ transports the shell point radially inward along the same spherical ray. Although X is written with the physical shell scale r_*, the dimensionless kernels $\widetilde{\mathcal{G}}_\varphi$ and $\widetilde{\mathcal{G}}_{\mathrm{loc}}$ are homogeneous of degree zero under a common scaling of both arguments. Hence the common factor r_* cancels from $K_{\mathrm{sh}}^{\mathrm{ren}}$. Thus $K_{\mathrm{sh}}^{\mathrm{ren}}$ is a renormalized near-shell collar-return kernel. The exterior vacuum energy has already been separated into $\Delta\Lambda_{\mathrm{out}}$, so the present kernel does not reinsert that exterior subtraction. Using the same half-Gaussian collar profile $\varpi_{\mathrm{col}}(\xi)$ already fixed in Eq. (306), define, for $\upsilon, \upsilon' \in (-1,1)$, the renormalized shell-return kernel, whenever the following integral exists as an absolutely convergent improper integral, by

$$K_{\mathrm{sh}}^{\mathrm{ren}}(\upsilon,\upsilon';\eta_0,\ell_0) = \int_0^\infty\int_0^\infty \varpi_{\mathrm{col}}(\xi)\varpi_{\mathrm{col}}(\xi')\Big[\widetilde{\mathcal{G}}_\varphi\big(X(\upsilon,\xi),X(\upsilon',\xi')\big) - \widetilde{\mathcal{G}}_{\mathrm{loc}}\big(X(\upsilon,\xi),X(\upsilon',\xi')\big)\Big]\,\mathrm{d}\xi\,\mathrm{d}\xi'. \tag{364}$$

Whenever the defining integral is absolutely convergent for both ordered pairs (υ,υ') and (υ',υ), the kernel is symmetric:

$$K_{\mathrm{sh}}^{\mathrm{ren}}(\upsilon,\upsilon';\eta_0,\ell_0) = K_{\mathrm{sh}}^{\mathrm{ren}}(\upsilon',\upsilon;\eta_0,\ell_0).$$

This follows by exchanging the collar variables $\xi \leftrightarrow \xi'$ and using the symmetry of both $\widetilde{\mathcal{G}}_\varphi$ and $\widetilde{\mathcal{G}}_{\mathrm{loc}}$.

Endpoint extensions, when needed, are understood through the weighted-kernel hypothesis imposed below.

The exponential radial transport is a positive-radius parametrization of the inward collar. For small $\ell_0\xi$,

$$r_* - r_* e^{-\ell_0\xi} = \sigma_{\mathbb{C}}\xi + O(\ell_0\sigma_{\mathbb{C}}\xi^2),$$

so ξ agrees to leading order with inward depth measured in units of $\sigma_{\mathbb{C}}$.

Remark (Diagonal subtraction versus polar endpoint control). The subtraction $\widetilde{\mathcal{G}}_\varphi - \widetilde{\mathcal{G}}_{\mathrm{loc}}$ is a diagonal finite-part subtraction. Its purpose is to remove the local filamentary logarithm already accounted for by Λ_{ind} and $\Delta\Lambda_{\mathrm{UV}\to\mathrm{IR}}(\ell_0)$. It should not be read as a proof of polar endpoint regularity. Indeed, the local core contains the factor $\ln\sqrt{\rho\rho'}$, so endpoint behavior at $\rho = 0$ or $\rho' = 0$ is a separate question from diagonal cancellation away from the axis. This is why the full Hilbert-space operator statement below is placed under the weighted-kernel hypothesis of lemma 25. The weaker finite-mode matrix elements can remain absolutely convergent even when the unprojected weighted kernel has not yet been certified as Hilbert–Schmidt.

Lemma 22 (Equatorial parity of the renormalized shell-return kernel). *For $\upsilon,\upsilon' \in (-1,1)$, whenever the integral defining $K_{\mathrm{sh}}^{\mathrm{ren}}$ exists, one has*

$$K_{\mathrm{sh}}^{\mathrm{ren}}(-\upsilon,-\upsilon';\eta_0,\ell_0) = K_{\mathrm{sh}}^{\mathrm{ren}}(\upsilon,\upsilon';\eta_0,\ell_0). \tag{365}$$

Consequently, whenever the corresponding flux-return transform with kernel $K_{\mathrm{sh}}^{\mathrm{ren}}$ is well defined on flux-compatible data, it maps even flux-compatible data to even flux-compatible data. Since

$$\mathcal{T}_j(-\upsilon) = (-1)^{j+1}\mathcal{T}_j(\upsilon),$$

the odd-degree modes $j = 1,3,5,\ldots$ are even functions of υ. Therefore, after the odd-degree flux space is introduced below, the resulting operator preserves $\mathcal{H}_{\mathrm{flux}}^{\mathrm{odd}}$.

Proof. First note that

$$\rho_\perp(-\upsilon,\xi) = \rho_\perp(\upsilon,\xi), \qquad z(-\upsilon,\xi) = -z(\upsilon,\xi).$$

Therefore, under the simultaneous equatorial reflection $(\upsilon,\upsilon') \mapsto (-\upsilon,-\upsilon')$, one has

$$\rho_\perp\rho'_\perp \mapsto \rho_\perp\rho'_\perp, \qquad z - z' \mapsto -(z-z'), \qquad (z-z')^2 \mapsto (z-z')^2.$$

Hence the elliptic parameter

$$k^2 = \frac{4\rho_\perp\rho'_\perp}{(\rho_\perp+\rho'_\perp)^2 + (z-z')^2}$$

is unchanged. The normalized Maxwell kernel $\widetilde{\mathcal{G}}_\varphi$ in Eq. (360) and the local core $\widetilde{\mathcal{G}}_{\mathrm{loc}}$ in Eq. (361) are therefore both invariant under this simultaneous reflection. Since the collar weights $\varpi_{\mathrm{col}}(\xi)\varpi_{\mathrm{col}}(\xi')$ are independent of υ and υ', the double integral defining $K_{\mathrm{sh}}^{\mathrm{ren}}$ satisfies

$$K_{\mathrm{sh}}^{\mathrm{ren}}(-\upsilon,-\upsilon';\eta_0,\ell_0) = K_{\mathrm{sh}}^{\mathrm{ren}}(\upsilon,\upsilon';\eta_0,\ell_0).$$

This proves Eq. (365).

Now let f be an even flux-compatible function for which the operator $\mathbb{R}_{\mathrm{sh}}^{\mathrm{ren}} f$ is well defined. Using Eq. (365) and the change of variable $\upsilon'' = -\upsilon'$, one finds

$$\begin{aligned}
(\mathbb{R}_{\mathrm{sh}}^{\mathrm{ren}} f)(-\upsilon) &= \int_{-1}^{1} K_{\mathrm{sh}}^{\mathrm{ren}}(-\upsilon, \upsilon'; \eta_0, \ell_0)\, f(\upsilon')\, \frac{\mathrm{d}\upsilon'}{1-\upsilon'^2} \\
&= \int_{-1}^{1} K_{\mathrm{sh}}^{\mathrm{ren}}(\upsilon, -\upsilon'; \eta_0, \ell_0)\, f(\upsilon')\, \frac{\mathrm{d}\upsilon'}{1-\upsilon'^2} \\
&= \int_{-1}^{1} K_{\mathrm{sh}}^{\mathrm{ren}}(\upsilon, \upsilon''; \eta_0, \ell_0)\, f(-\upsilon'')\, \frac{\mathrm{d}\upsilon''}{1-\upsilon''^2} \\
&= \int_{-1}^{1} K_{\mathrm{sh}}^{\mathrm{ren}}(\upsilon, \upsilon''; \eta_0, \ell_0)\, f(\upsilon'')\, \frac{\mathrm{d}\upsilon''}{1-\upsilon''^2} \\
&= (\mathbb{R}_{\mathrm{sh}}^{\mathrm{ren}} f)(\upsilon).
\end{aligned}$$

Hence $\mathbb{R}_{\mathrm{sh}}^{\mathrm{ren}} f$ is even. Since the odd-degree toroidal modes are even functions of υ, the operator preserves the odd-degree flux sector once that sector is defined below. □

Remark (Branch label and scale invariance of the return kernel). In the displayed definition of $K_{\mathrm{sh}}^{\mathrm{ren}}$, the common scale r_* cancels from the dimensionless Maxwell kernel and from the local core. Thus the return kernel itself depends on the minimal branch through the collar ratio $\ell_0 = \sigma_{\mathbb{C}}/r_*$. The label η_0 is retained only to keep the notation aligned with the branch-fixed source and exterior subtraction, where $\eta_0 = R/r_*$ enters explicitly through $J_\chi(\eta_0)$ and $\Delta\Lambda_{\mathrm{out}}(\eta_0)$.

Definition VII.14 (Normalized odd flux basis and toroidal identification)**.** For odd j, define the normalized flux basis functions

$$e_j(\upsilon) = \frac{\mathcal{T}_j(\upsilon)}{\sqrt{I_j}}, \qquad j = 1, 3, 5, \dots, \tag{366}$$

where $I_j = \frac{2j(j+1)}{2j+1}$. Since

$$\mathcal{T}_j(\upsilon) = (1-\upsilon^2) P_j'(\upsilon), \qquad \mathcal{T}_j(-\upsilon) = (-1)^{j+1} \mathcal{T}_j(\upsilon),$$

each e_j with odd degree j is an even function of υ, vanishes at $\upsilon = \pm 1$, and belongs to the flux-compatible class. Hence $\{e_1, e_3, e_5, \dots\}$ is an orthonormal basis of the closed odd-degree flux subspace

$$\mathcal{H}_{\mathrm{flux}}^{\mathrm{odd}} := \overline{\operatorname{span}}\{e_1, e_3, e_5, \dots\}^{\|\cdot\|_{\mathrm{flux}}}. \tag{367}$$

Here the superscript "odd" refers to the odd harmonic degree, not to odd parity in υ. Under the isometry

$$\mathcal{J} f = \frac{f}{\sqrt{1-\upsilon^2}},$$

the basis vector e_j maps, up to a sign and normalization, to the associated Legendre function P_j^1. By the standard completeness of the fixed-order associated Legendre system, the odd-degree subfamily $j = 1, 3, 5, \dots$ spans the even-parity subspace of $L^2(-1,1)$. Thus, with this standard completeness fact understood, $\mathcal{H}_{\mathrm{flux}}^{\mathrm{odd}}$ may equivalently be identified with the even-parity flux-compatible sector.

Let

$$\mathcal{H}_{\mathrm{tor}}^{\mathrm{ax}}(\Sigma_{r_*}) = \operatorname{Ran} \Pi_{\mathrm{TT}} \subset H_{\tan}^{\mathrm{ax}}(\Sigma_{r_*})$$

be the full axisymmetric tangential divergence-free shell sector, and define the odd toroidal shell sector by

$$\mathcal{H}_{\mathrm{tor}}^{\mathrm{odd}}(\Sigma_{r_*}) := \mathcal{I}_{\mathrm{tor}}(\mathcal{H}_{\mathrm{flux}}^{\mathrm{odd}}) \subset \mathcal{H}_{\mathrm{tor}}^{\mathrm{ax}}(\Sigma_{r_*}). \tag{368}$$

Define

$$(\mathcal{I}_{\mathrm{tor}} f)(\upsilon) = \frac{1}{\sqrt{2\pi}} \frac{f(\upsilon)}{\sqrt{1-\upsilon^2}}\, \hat{\mathbf{e}}_\varphi, \qquad f \in \mathcal{H}_{\mathrm{flux}}^{\mathrm{odd}}. \tag{369}$$

Its inverse on $\mathcal{H}_{\mathrm{tor}}^{\mathrm{odd}}(S_{r_*}^2)$ is

$$\mathcal{I}_{\mathrm{tor}}^{-1}\big(U_\varphi(\upsilon)\hat{\mathbf{e}}_\varphi\big) = \sqrt{2\pi}\, \sqrt{1-\upsilon^2}\, U_\varphi(\upsilon).$$

Definition VII.15 (Renormalized shell-return form and operator)**.** Let

$$\mathcal{D}^{\mathrm{odd}}_{\mathrm{flux}} \coloneqq \operatorname{span}\{e_1, e_3, e_5, \dots\} \subset \mathcal{H}^{\mathrm{odd}}_{\mathrm{flux}}.$$

Assume the parity relation Eq. (365). For $f, g \in \mathcal{D}^{\mathrm{odd}}_{\mathrm{flux}}$, define the renormalized shell-return bilinear form by

$$\mathfrak{r}^{\mathrm{ren}}_{\mathrm{sh}}[f,g] = \int_{-1}^{1}\int_{-1}^{1} \frac{f(\upsilon)\, K^{\mathrm{ren}}_{\mathrm{sh}}(\upsilon,\upsilon';\eta_0,\ell_0)\, g(\upsilon')}{(1-\upsilon^2)(1-\upsilon'^2)}\, \mathrm{d}\upsilon\, \mathrm{d}\upsilon'. \tag{370}$$

For finite odd-mode data the quotients $f(\upsilon)/(1-\upsilon^2)$ and $g(\upsilon)/(1-\upsilon^2)$ are finite linear combinations of Legendre derivatives $P_j'(\upsilon)$. Thus the bilinear form is well defined on $\mathcal{D}^{\mathrm{odd}}_{\mathrm{flux}}$ whenever the endpoint and diagonal hypotheses of proposition 41 hold for each finite mode pair. This finite-mode statement is weaker than the weighted-kernel hypothesis used later to obtain a bounded operator on the full Hilbert space.

Whenever this form is represented by a bounded self-adjoint operator on $\mathcal{H}^{\mathrm{odd}}_{\mathrm{flux}}$, we denote that operator by $\mathbb{R}^{\mathrm{ren}}_{\mathrm{sh}}(\eta_0,\ell_0)$. On finite-mode data for which the pointwise representative belongs to the flux space, its action is

$$(\mathbb{R}^{\mathrm{ren}}_{\mathrm{sh}} f)(\upsilon) = \int_{-1}^{1} K^{\mathrm{ren}}_{\mathrm{sh}}(\upsilon,\upsilon';\eta_0,\ell_0)\, f(\upsilon')\, \frac{\mathrm{d}\upsilon'}{1-\upsilon'^2}. \tag{371}$$

The weighted-kernel hypothesis in lemma 25 is a sufficient condition for this bounded self-adjoint representative to exist.

Lemma 23 (Isometric identification of odd flux space with the odd toroidal shell sector)**.** *The map $\mathcal{I}_{\mathrm{tor}}$ is an isometric isomorphism from $\mathcal{H}^{\mathrm{odd}}_{\mathrm{flux}}$ onto $\mathcal{H}^{\mathrm{odd}}_{\mathrm{tor}}(S^2_{r_*})$. In particular,*

$$\langle \mathcal{I}_{\mathrm{tor}} f, \mathcal{I}_{\mathrm{tor}} g\rangle_{\mathrm{sh}} = \langle f, g\rangle_{\mathrm{flux}}. \tag{372}$$

Proof. For axisymmetric toroidal shell fields

$$U(\vartheta) = U_\varphi(\vartheta)\,\hat{\mathbf{e}}_\varphi, \qquad V(\vartheta) = V_\varphi(\vartheta)\,\hat{\mathbf{e}}_\varphi,$$

the shell pairing Eq. (298), together with Eq. (369), reduces to

$$\langle U, V\rangle_{\mathrm{sh}} = 2\pi \int_0^\pi U_\varphi(\vartheta) V_\varphi(\vartheta) \sin\vartheta\, \mathrm{d}\vartheta.$$

Using $\upsilon = \cos\vartheta$, hence $\mathrm{d}\upsilon = -\sin\vartheta\,\mathrm{d}\vartheta$, we obtain

$$\langle U, V\rangle_{\mathrm{sh}} = 2\pi \int_{-1}^{1} U_\varphi(\upsilon) V_\varphi(\upsilon)\, \mathrm{d}\upsilon.$$

Now set $U = \mathcal{I}_{\mathrm{tor}} f$ and $V = \mathcal{I}_{\mathrm{tor}} g$. Then

$$U_\varphi(\upsilon) = \frac{1}{\sqrt{2\pi}} \frac{f(\upsilon)}{\sqrt{1-\upsilon^2}}, \qquad V_\varphi(\upsilon) = \frac{1}{\sqrt{2\pi}} \frac{g(\upsilon)}{\sqrt{1-\upsilon^2}}.$$

Substituting gives

$$\begin{aligned} \langle \mathcal{I}_{\mathrm{tor}} f, \mathcal{I}_{\mathrm{tor}} g\rangle_{\mathrm{sh}} &= 2\pi \int_{-1}^{1} \left(\frac{1}{\sqrt{2\pi}} \frac{f(\upsilon)}{\sqrt{1-\upsilon^2}}\right)\left(\frac{1}{\sqrt{2\pi}} \frac{g(\upsilon)}{\sqrt{1-\upsilon^2}}\right) \mathrm{d}\upsilon \\ &= \int_{-1}^{1} \frac{f(\upsilon) g(\upsilon)}{1-\upsilon^2}\, \mathrm{d}\upsilon = \langle f, g\rangle_{\mathrm{flux}}. \end{aligned}$$

Hence $\mathcal{I}_{\mathrm{tor}}$ is isometric. The explicit inverse formula shows that its range is exactly $\mathcal{H}^{\mathrm{odd}}_{\mathrm{tor}}(S^2_{r_*})$, so it is an isometric isomorphism. □

Lemma 24 (Odd-degree invariance of the shell-admission operator)**.** *For every $\ell \geq 0$, the shell-admission operator $\mathbb{Q}_\chi(\ell)$ preserves the odd toroidal shell sector $\mathcal{H}^{\mathrm{odd}}_{\mathrm{tor}}(S^2_{r_*})$. Consequently, its flux-space realization preserves the odd-degree flux sector $\mathcal{H}^{\mathrm{odd}}_{\mathrm{flux}}$.*

Proof. On toroidal shell data, Π_{TT} acts as the identity. The operators E_ℓ and E_ℓ^* act only in the collar variable and therefore do not mix angular harmonic degrees. The operator $\mathbb{S}_\ell$ is a bounded Borel function of $-\Delta_{\mathrm{tor}}$, so it preserves each toroidal harmonic sector. Hence

$$\mathbb{Q}_\chi(\ell) = \Pi_{\mathrm{TT}} E_\ell^* \Big(\mathbb{I} - \frac{1}{3}\,\mathbb{S}_\ell\Big) E_\ell \Pi_{\mathrm{TT}}$$

preserves each degree-j toroidal harmonic sector, and therefore preserves the closed direct sum of the odd-degree sectors. This is exactly $\mathcal{H}^{\mathrm{odd}}_{\mathrm{tor}}(S^2_{r_*})$.

Since $\mathcal{I}_{\mathrm{tor}}$ is an isometric isomorphism from $\mathcal{H}^{\mathrm{odd}}_{\mathrm{flux}}$ onto $\mathcal{H}^{\mathrm{odd}}_{\mathrm{tor}}(S^2_{r_*})$, the transported operator $\mathbb{Q}_{\chi,\mathrm{flux}}(\ell) = \mathcal{I}_{\mathrm{tor}}^{-1}\mathbb{Q}_\chi(\ell)\mathcal{I}_{\mathrm{tor}}$ preserves $\mathcal{H}^{\mathrm{odd}}_{\mathrm{flux}}$. □

Definition VII.16 (Flux-space realization of the shell-admission operator)**.** By lemma 24, the shell-space admission operator $\mathbb{Q}_{\chi,\mathrm{sh}}(\ell)$ maps $\mathcal{H}^{\mathrm{odd}}_{\mathrm{tor}}(S^2_{r_*})$ into itself. We may therefore transport it to odd flux space by

$$\mathbb{Q}_{\chi,\mathrm{flux}}(\ell) = \mathcal{I}_{\mathrm{tor}}^{-1}\,\mathbb{Q}_{\chi,\mathrm{sh}}(\ell)\,\mathcal{I}_{\mathrm{tor}}. \tag{373}$$

The normalized shell-space admission operator used in scalar admission quotients is

$$\overline{\mathbb{Q}_{\chi,\mathrm{sh}}}(\ell) \coloneqq N_{\mathrm{col}}^{-1}\mathbb{Q}_{\chi,\mathrm{sh}}(\ell). \tag{374}$$

The normalized flux-space admission operator, when needed, is

$$\overline{\mathbb{Q}_{\chi,\mathrm{flux}}}(\ell) \coloneqq N_{\mathrm{col}}^{-1}\mathbb{Q}_{\chi,\mathrm{flux}}(\ell). \tag{375}$$

Thus $\mathbb{Q}_{\chi,\mathrm{sh}}$, $\mathbb{Q}_{\chi,\mathrm{flux}}$, $\overline{\mathbb{Q}_{\chi,\mathrm{sh}}}$, and $\overline{\mathbb{Q}_{\chi,\mathrm{flux}}}$ are distinct representatives of the same admission construction on different Hilbert spaces or with different normalization.

Remark (Notation for shell, flux, full-load, and TT realizations)*.* The tag sh labels the shell-space realization of an admission operator on $H^{\mathrm{ax}}_{\tan}(S^2_{r_*})$ or on its toroidal shell subspace. The tag flux labels the transported realization on the odd flux space $\mathcal{H}^{\mathrm{odd}}_{\mathrm{flux}}$ under the isometric identification $\mathcal{I}_{\mathrm{tor}}$. Thus

$$\mathbb{Q}_{\chi,\mathrm{flux}}(\ell) = \mathcal{I}_{\mathrm{tor}}^{-1}\,\mathbb{Q}_{\chi,\mathrm{sh}}(\ell)\,\mathcal{I}_{\mathrm{tor}}.$$

The normalized operators $\overline{\mathbb{Q}_{\chi,\mathrm{sh}}}(\ell)$ and $\overline{\mathbb{Q}_{\chi,\mathrm{flux}}}(\ell)$ differ from the corresponding unnormalized operators only by the scalar factor N_{col}^{-1}.

For admitted weights, the tag full denotes normalization by the full shell-load norm of the fixed branch representative, whereas the tag TT denotes normalization by the TT-cleaned norm. In the present minimal-branch numerical realization, the quantity $P^{(\chi)}_{IR}(\ell)$ always means the branch-fixed full-load quotient

$$P^{(\chi)}_{IR}(\ell) \equiv P^{(\chi)}_{IR,\mathrm{full}}(\ell;\mathscr{A}^{\mathrm{coll}}_{\parallel}).$$

Definition VII.17 (Exact shell-memory operator under the return-kernel hypothesis)**.** Assume that the return form of definition VII.15 is represented by a bounded self-adjoint operator $\mathbb{R}^{\mathrm{ren}}_{\mathrm{sh}}(\eta_0,\ell_0)$ on $\mathcal{H}^{\mathrm{odd}}_{\mathrm{flux}}$. This is the return-kernel hypothesis; it is not a numerical fit and not a consequence of the finite mode-pairing formulas alone. By lemma 24 and by the positivity, boundedness, and self-adjointness proved in lemma 14, the flux-space realization $\mathbb{Q}_{\chi,\mathrm{flux}}(\ell_0)$ restricts to a bounded, positive, self-adjoint operator on $\mathcal{H}^{\mathrm{odd}}_{\mathrm{flux}}$. Its unique positive square root on that subspace is therefore well defined. The normalized scalar operator $\overline{\mathbb{Q}_{\chi,\mathrm{sh}}}(\ell_0)$ used in $P^{(\chi)}_{IR,\mathrm{full}}(\ell;\mathscr{A}_{\mathrm{sh}})$ does not enter the present vector-memory definition.

The exact shell-memory operator on $\mathcal{H}^{\mathrm{odd}}_{\mathrm{flux}}$ is

$$\mathbb{G}_{\mathrm{sh}}(\eta_0,\ell_0) \coloneqq \mathbb{Q}_{\chi,\mathrm{flux}}(\ell_0)^{1/2}\,\mathbb{R}^{\mathrm{ren}}_{\mathrm{sh}}(\eta_0,\ell_0)\,\mathbb{Q}_{\chi,\mathrm{flux}}(\ell_0)^{1/2}. \tag{376}$$

In the normalized odd flux basis introduced below, $\mathbb{Q}_{\chi,\mathrm{flux}}(\ell_0)$ acts diagonally with positive eigenvalues $q_j(\ell_0) > 0$, so its positive square root is obtained mode by mode.

Lemma 25 (Basic properties of the shell-memory operator)**.** *Define the weighted kernel*

$$\widehat{K}^{\mathrm{ren}}_{\mathrm{sh}}(\upsilon,\upsilon') = \frac{K^{\mathrm{ren}}_{\mathrm{sh}}(\upsilon,\upsilon';\eta_0,\ell_0)}{\sqrt{1-\upsilon^2}\,\sqrt{1-\upsilon'^2}}. \tag{377}$$

Assume that $\widehat{K}_{\mathrm{sh}}^{\mathrm{ren}}$ is real-valued, symmetric, and belongs to $L^2((-1,1)\times(-1,1))$. Assume moreover that the integral transform with kernel $K_{\mathrm{sh}}^{\mathrm{ren}}$ preserves the even-parity flux-compatible sector; by lemma 22, this follows from the equatorial parity of the kernel. Then the form $\mathfrak{r}_{\mathrm{sh}}^{\mathrm{ren}}$ is represented by a Hilbert–Schmidt, hence compact, self-adjoint operator $\mathbb{R}_{\mathrm{sh}}^{\mathrm{ren}}$ on $\mathcal{H}_{\mathrm{flux}}^{\mathrm{odd}}$. Because $\mathbb{Q}_{\chi,\mathrm{flux}}(\ell_0)$ is bounded, positive, and self-adjoint on the same space, the shell-memory operator

$$\mathbb{G}_{\mathrm{sh}}(\eta_0,\ell_0)=\mathbb{Q}_{\chi,\mathrm{flux}}(\ell_0)^{1/2}\,\mathbb{R}_{\mathrm{sh}}^{\mathrm{ren}}(\eta_0,\ell_0)\,\mathbb{Q}_{\chi,\mathrm{flux}}(\ell_0)^{1/2}$$

is compact and self-adjoint on $\mathcal{H}_{\mathrm{flux}}^{\mathrm{odd}}$.

Proof. Introduce the isometry

$$\mathcal{J}:\mathcal{H}_{\mathrm{flux}}^{\mathrm{odd}}\to L^2(-1,1),\qquad (\mathcal{J}f)(\upsilon)=\frac{f(\upsilon)}{\sqrt{1-\upsilon^2}}.$$

By the completeness statement in definition VII.14, the isometry $\mathcal{J}$ maps $\mathcal{H}_{\mathrm{flux}}^{\mathrm{odd}}$ onto the closed even subspace

$$L^2_{\mathrm{even}}(-1,1)\coloneqq\{g\in L^2(-1,1)\ ;\ g(-\upsilon)=g(\upsilon)\text{ a.e.}\}.$$

Let $T_{\widehat{K}}$ be the integral operator on $L^2(-1,1)$ with kernel $\widehat{K}_{\mathrm{sh}}^{\mathrm{ren}}$,

$$(T_{\widehat{K}}g)(\upsilon)=\int_{-1}^{1}\widehat{K}_{\mathrm{sh}}^{\mathrm{ren}}(\upsilon,\upsilon')\,g(\upsilon')\,\mathrm{d}\upsilon'.$$

Since $\widehat{K}_{\mathrm{sh}}^{\mathrm{ren}}\in L^2((-1,1)^2)$, the operator $T_{\widehat{K}}$ is Hilbert–Schmidt on $L^2(-1,1)$, hence compact. Since $\widehat{K}_{\mathrm{sh}}^{\mathrm{ren}}$ is real-valued and symmetric, $T_{\widehat{K}}$ is self-adjoint.

Let $\mathcal{P}$ be the parity operator on $L^2(-1,1)$,

$$(\mathcal{P}g)(\upsilon)\coloneqq g(-\upsilon).$$

Because the weight $(1-\upsilon^2)^{-1/2}$ is even, the parity relation Eq. (365) implies

$$\widehat{K}_{\mathrm{sh}}^{\mathrm{ren}}(-\upsilon,-\upsilon')=\widehat{K}_{\mathrm{sh}}^{\mathrm{ren}}(\upsilon,\upsilon').$$

Therefore $T_{\widehat{K}}$ commutes with $\mathcal{P}$. Hence $L^2_{\mathrm{even}}(-1,1)$ is a reducing subspace for $T_{\widehat{K}}$, and the restriction

$$T_{\widehat{K}}^{\mathrm{even}}\coloneqq T_{\widehat{K}}\big|_{L^2_{\mathrm{even}}(-1,1)}$$

is again Hilbert–Schmidt, compact, and self-adjoint.

Define

$$\mathbb{R}_{\mathrm{sh}}^{\mathrm{ren}}\coloneqq\mathcal{J}^{-1}T_{\widehat{K}}^{\mathrm{even}}\mathcal{J}\quad\text{on }\mathcal{H}_{\mathrm{flux}}^{\mathrm{odd}}.\tag{378}$$

Then $\mathbb{R}_{\mathrm{sh}}^{\mathrm{ren}}$ is compact and self-adjoint on $\mathcal{H}_{\mathrm{flux}}^{\mathrm{odd}}$.

It remains to verify that $\mathbb{R}_{\mathrm{sh}}^{\mathrm{ren}}$ represents the form $\mathfrak{r}_{\mathrm{sh}}^{\mathrm{ren}}$. Let $f,g\in\mathcal{D}_{\mathrm{flux}}^{\mathrm{odd}}$. Then

$$\begin{aligned}\langle f,\mathbb{R}_{\mathrm{sh}}^{\mathrm{ren}}g\rangle_{\mathrm{flux}}&=\langle\mathcal{J}f,T_{\widehat{K}}^{\mathrm{even}}\mathcal{J}g\rangle_{L^2(-1,1)}\\&=\int_{-1}^{1}\!\!\int_{-1}^{1}\frac{f(\upsilon)\,K_{\mathrm{sh}}^{\mathrm{ren}}(\upsilon,\upsilon';\eta_0,\ell_0)\,g(\upsilon')}{(1-\upsilon^2)(1-\upsilon'^2)}\,\mathrm{d}\upsilon\,\mathrm{d}\upsilon'\\&=\mathfrak{r}_{\mathrm{sh}}^{\mathrm{ren}}[f,g].\end{aligned}$$

Thus $\mathbb{R}_{\mathrm{sh}}^{\mathrm{ren}}$ represents the return form.

The operator $\mathbb{Q}_{\chi,\mathrm{flux}}(\ell_0)^{1/2}$ is bounded and self-adjoint because $\mathbb{Q}_{\chi,\mathrm{flux}}(\ell_0)$ is bounded, positive, and self-adjoint on $\mathcal{H}_{\mathrm{flux}}^{\mathrm{odd}}$. Therefore

$$\mathbb{G}_{\mathrm{sh}}=\mathbb{Q}_{\chi,\mathrm{flux}}(\ell_0)^{1/2}\,\mathbb{R}_{\mathrm{sh}}^{\mathrm{ren}}\,\mathbb{Q}_{\chi,\mathrm{flux}}(\ell_0)^{1/2}$$

is compact as a bounded-compact-bounded product. Its adjoint is

$$\mathbb{G}_{\mathrm{sh}}^{*}=\mathbb{Q}_{\chi,\mathrm{flux}}(\ell_0)^{1/2}\,(\mathbb{R}_{\mathrm{sh}}^{\mathrm{ren}})^{*}\,\mathbb{Q}_{\chi,\mathrm{flux}}(\ell_0)^{1/2}=\mathbb{G}_{\mathrm{sh}},$$

so $\mathbb{G}_{\mathrm{sh}}$ is self-adjoint. □

Definition VII.18 (Flux-space shell source element)**.** By Eq. (355), the normalized shell source coefficients define an element of $\mathcal{H}_{\text{flux}}^{\text{odd}}$. We therefore set

$$J_\chi(\eta) := \sum_{j=1,3,5,\ldots} J_j^{(\chi)}(\eta)\, e_j. \tag{379}$$

Since $\{e_1, e_3, e_5, \ldots\}$ is an orthonormal basis of $\mathcal{H}_{\text{flux}}^{\text{odd}}$, one has

$$\|J_\chi(\eta)\|_{\text{flux}}^2 = \sum_{j=1,3,5,\ldots} \big(J_j^{(\chi)}(\eta)\big)^2 = \|\mathbf{J}_\chi(\eta)\|_{\ell^2}^2.$$

Theorem 13 (Conditional exact vector functional under the contractive shell-memory hypothesis)**.** *Assume the hypotheses under which $\mathbb{G}_{\text{sh}}(\eta_0, \ell_0)$ is a bounded self-adjoint operator on $\mathcal{H}_{\text{flux}}^{\text{odd}}$. In this coordinate display we restrict to the real stationary axisymmetric sector. If the flux space is complexified, the corresponding formulas are understood with the sesquilinear flux pairing and with real variations of the real functional. In the real sector used for the Galerkin matrix realizations, transposes are ordinary matrix transposes.*

$$\mathcal{L}_\Lambda[a] = \Lambda_{\text{ind}} + \Delta\Lambda_{\text{UV}\to\text{IR}}(\ell_0) - \langle J_\chi(\eta_0), a\rangle_{\text{flux}} + \frac{1}{2}\left\langle a,\, \big(\mathbb{I} - \mathbb{G}_{\text{sh}}(\eta_0, \ell_0)\big)a\right\rangle_{\text{flux}}. \tag{380}$$

Assume the contractive shell-memory hypothesis

$$\|\mathbb{G}_{\text{sh}}(\eta_0, \ell_0)\| < 1.$$

This is a sufficient operator-level hypothesis for the exact vector functional. It is not a fitted numerical condition. Then $\mathcal{L}_\Lambda$ is strictly convex on $\mathcal{H}_{\text{flux}}^{\text{odd}}$, it admits the unique stationary point

$$a_* = (\mathbb{I} - \mathbb{G}_{\text{sh}}(\eta_0, \ell_0))^{-1} J_\chi(\eta_0), \tag{381}$$

and the branch geometric constant is

$$\Lambda_{\text{geom}} = \Lambda_{\text{ind}} + \Delta\Lambda_{\text{UV}\to\text{IR}}(\ell_0) - \frac{1}{2}\left\langle J_\chi(\eta_0),\, (\mathbb{I} - \mathbb{G}_{\text{sh}}(\eta_0, \ell_0))^{-1} J_\chi(\eta_0)\right\rangle_{\text{flux}}. \tag{382}$$

If $J_\chi(\eta_0) = 0$, then $a_* = 0$. By Eq. (356), also $\Delta\Lambda_{\text{out}}(\eta_0) = 0$, and

$$\Lambda_{\text{geom}} = \Lambda_{\text{ind}} + \Delta\Lambda_{\text{UV}\to\text{IR}}(\ell_0).$$

If $J_\chi(\eta_0) \neq 0$, define

$$R_\chi := \left\langle \widehat{J}_\chi,\, (\mathbb{I} - \mathbb{G}_{\text{sh}}(\eta_0, \ell_0))^{-1} \widehat{J}_\chi\right\rangle_{\text{flux}}, \qquad \widehat{J}_\chi = \frac{J_\chi(\eta_0)}{\|J_\chi(\eta_0)\|_{\text{flux}}}. \tag{383}$$

Moreover, with

$$\rho_G = \|\mathbb{G}_{\text{sh}}(\eta_0, \ell_0)\| < 1,$$

one has

$$\frac{1}{1+\rho_G} \le R_\chi \le \frac{1}{1-\rho_G}. \tag{384}$$

and then

$$\Lambda_{\text{geom}} = \Lambda_{\text{ind}} + \Delta\Lambda_{\text{UV}\to\text{IR}}(\ell_0) + \Delta\Lambda_{\text{out}}(\eta_0)\, R_\chi. \tag{385}$$

Proof. Let

$$T := \mathbb{I} - \mathbb{G}_{\text{sh}}(\eta_0, \ell_0).$$

By lemma 25, T is self-adjoint. For any $a, h \in \mathcal{H}_{\text{flux}}^{\text{odd}}$ and $\varepsilon \in \mathbb{R}$,

$$\mathcal{L}_\Lambda[a + \varepsilon h] = \Lambda_{\text{ind}} + \Delta\Lambda_{\text{UV}\to\text{IR}}(\ell_0) - \langle J_\chi, a + \varepsilon h\rangle_{\text{flux}} + \frac{1}{2}\langle a + \varepsilon h, T(a + \varepsilon h)\rangle_{\text{flux}}.$$

Expanding the last term and using self-adjointness of T,

$$\langle a+\varepsilon h, T(a+\varepsilon h)\rangle_{\text{flux}} = \langle a, Ta\rangle_{\text{flux}} + 2\varepsilon\langle h, Ta\rangle_{\text{flux}} + \varepsilon^2\langle h, Th\rangle_{\text{flux}}.$$

Hence

$$\mathcal{L}_\Lambda[a+\varepsilon h] = \mathcal{L}_\Lambda[a] + \varepsilon\left\langle h, Ta - J_\chi\right\rangle_{\text{flux}} + \frac{\varepsilon^2}{2}\langle h, Th\rangle_{\text{flux}}.$$

Therefore the first variation vanishes for every h if and only if

$$Ta = J_\chi,$$

namely

$$(\mathbb{I} - \mathbb{G}_{\text{sh}})a = J_\chi.$$

Since $\|\mathbb{G}_{\text{sh}}\| < 1$, one has

$$\langle h, Th\rangle_{\text{flux}} = \langle h, h\rangle_{\text{flux}} - \langle h, \mathbb{G}_{\text{sh}}h\rangle_{\text{flux}} \geq \big(1 - \|\mathbb{G}_{\text{sh}}\|\big)\,\|h\|^2_{\text{flux}}$$

for every $h \in \mathcal{H}^{\text{odd}}_{\text{flux}}$. Hence T is coercive. Moreover, the strict contraction bound gives the convergent Neumann series

$$T^{-1} = (\mathbb{I} - \mathbb{G}_{\text{sh}})^{-1} = \sum_{n=0}^{\infty} \mathbb{G}^n_{\text{sh}} \qquad \text{in operator norm,}$$

and therefore

$$\|T^{-1}\| \leq \frac{1}{1 - \|\mathbb{G}_{\text{sh}}\|}.$$

The quadratic part of $\mathcal{L}_\Lambda$ is thus strictly positive, so $\mathcal{L}_\Lambda$ is strictly convex. The unique stationary point is

$$a_* = T^{-1}J_\chi = (\mathbb{I} - \mathbb{G}_{\text{sh}})^{-1}J_\chi.$$

To evaluate the stationary value, use $Ta_* = J_\chi$ in Eq. (380):

$$\mathcal{L}_\Lambda[a_*] = \Lambda_{\text{ind}} + \Delta\Lambda_{\text{UV}\to\text{IR}}(\ell_0) - \langle J_\chi, a_*\rangle_{\text{flux}} + \frac{1}{2}\langle a_*, Ta_*\rangle_{\text{flux}}.$$

Because $Ta_* = J_\chi$,

$$\langle a_*, Ta_*\rangle_{\text{flux}} = \langle a_*, J_\chi\rangle_{\text{flux}} = \langle J_\chi, a_*\rangle_{\text{flux}}.$$

Hence

$$\mathcal{L}_\Lambda[a_*] = \Lambda_{\text{ind}} + \Delta\Lambda_{\text{UV}\to\text{IR}}(\ell_0) - \frac{1}{2}\langle J_\chi, a_*\rangle_{\text{flux}}.$$

Write, for brevity,

$$J_\chi \coloneqq J_\chi(\eta_0), \qquad \mathbb{G}_{\text{sh}} \coloneqq \mathbb{G}_{\text{sh}}(\eta_0, \ell_0).$$

Substituting

$$a_* = (\mathbb{I} - \mathbb{G}_{\text{sh}})^{-1}J_\chi$$

gives

$$\Lambda_{\text{geom}} = \Lambda_{\text{ind}} + \Delta\Lambda_{\text{UV}\to\text{IR}}(\ell_0) - \frac{1}{2}\big\langle J_\chi,\, (\mathbb{I} - \mathbb{G}_{\text{sh}})^{-1}J_\chi\big\rangle_{\text{flux}}.$$

Now write

$$J_\chi = \|J_\chi\|_{\text{flux}}\,\widehat{J}_\chi.$$

Then

$$\langle J_\chi,\, (\mathbb{I}-\mathbb{G}_{\rm sh})^{-1}J_\chi\rangle_{\rm flux} = \|J_\chi\|^2_{\rm flux}\langle \widehat{J}_\chi,\, (\mathbb{I}-\mathbb{G}_{\rm sh})^{-1}\widehat{J}_\chi\rangle_{\rm flux} = \|J_\chi\|^2_{\rm flux} R_\chi.$$

Because $\{e_1, e_3, e_5, \dots\}$ is an orthonormal basis of $\mathcal{H}^{\rm odd}_{\rm flux}$, one has

$$\|J_\chi(\eta_0)\|^2_{\rm flux} = \sum_{j=1,3,5,\dots} \big(J_j^{(\chi)}(\eta_0)\big)^2 = \|\mathbf{J}_\chi(\eta_0)\|^2_{\ell^2}.$$

Hence, by Eq. (356),

$$\Delta\Lambda_{\rm out}(\eta_0) = -\frac{1}{2}\,\|J_\chi(\eta_0)\|^2_{\rm flux}.$$

Substituting this identity together with

$$\langle J_\chi,\, (\mathbb{I}-\mathbb{G}_{\rm sh})^{-1}J_\chi\rangle_{\rm flux} = \|J_\chi\|^2_{\rm flux}\, R_\chi$$

into Eq. (382) yields Eq. (385).

Since $\mathbb{G}_{\rm sh}$ is self-adjoint and $\|\mathbb{G}_{\rm sh}\| = \rho_G < 1$, the spectrum of $\mathbb{G}_{\rm sh}$ lies in $[-\rho_G, \rho_G]$. Hence the spectrum of $(\mathbb{I}-\mathbb{G}_{\rm sh})^{-1}$ lies in

$$\left[\frac{1}{1+\rho_G}, \frac{1}{1-\rho_G}\right].$$

Applying this spectral bound to the unit vector $\widehat{J}_\chi$ gives Eq. (384). □

Theorem 14 (Exact diagonal action of the shell-admission operator on the odd flux basis)**.** *Here $\mathbb{Q}_{\chi,\rm flux}(\ell)$ denotes the unnormalized flux-space realization of the shell-admission operator introduced in Eq.* (373)*; it is not the normalized scalar-admission operator $\overline{\mathbb{Q}_{\chi,\rm sh}}(\ell) = N_{\rm col}^{-1}\mathbb{Q}_{\chi,\rm sh}(\ell)$ used in Eq.* (313)*. For every odd degree j, the normalized flux basis vector e_j is an eigenvector of $\mathbb{Q}_{\chi,\rm flux}(\ell)$. More precisely,*

$$\mathbb{Q}_{\chi,\rm flux}(\ell)\, e_j = q_j(\ell)\, e_j, \qquad j = 1, 3, 5, \dots. \tag{386}$$

with exact eigenvalue

$$q_j(\ell) = N_{\rm col}\left(1 - \frac{1}{3}\frac{\ell^2 j(j+1)}{1+\ell^2 j(j+1)}\right), \qquad N_{\rm col} = \int_0^\infty \varpi_{\rm col}(\xi)^2\,\mathrm{d}\xi = \sqrt{\frac{2}{\pi}}. \tag{387}$$

In particular, the admission matrix on the odd flux basis is

$$\mathsf{Q}^{(\chi)}_{jk} := \langle e_j, \mathbb{Q}_{\chi,\rm flux}(\ell_0) e_k\rangle_{\rm flux} = q_j(\ell_0)\,\delta_{jk}. \tag{388}$$

Proof. By Eq. (373),

$$\mathbb{Q}_{\chi,\rm flux}(\ell) = \mathcal{I}_{\rm tor}^{-1}\,\mathbb{Q}_{\chi,\rm sh}(\ell)\,\mathcal{I}_{\rm tor}.$$

Here $\mathbb{Q}_{\chi,\rm sh}(\ell)$ is the shell-space operator defined in Eq. (310). For odd j, define the axisymmetric toroidal shell harmonic

$$\mathcal{X}_j(\upsilon) := \sqrt{1-\upsilon^2}\,P_j'(\upsilon)\,\hat{\mathbf{e}}_\varphi.$$

Using $\mathcal{T}_j(\upsilon) = (1-\upsilon^2)P_j'(\upsilon)$ together with Eqs. (366) and (369), one finds

$$\mathcal{I}_{\rm tor} e_j = \frac{1}{\sqrt{2\pi I_j}}\,\mathcal{X}_j.$$

Moreover,

$$\mathcal{X}_j(\vartheta) = \sqrt{1-\upsilon^2}\,P_j'(\upsilon)\,\hat{\mathbf{e}}_\varphi = \sin\vartheta\,P_j'(\cos\vartheta)\,\hat{\mathbf{e}}_\varphi.$$

To compute the toroidal eigenvalue explicitly, let

$$U(\vartheta) = u(\vartheta)\,\hat{\mathbf{e}}_\varphi$$

be a smooth axisymmetric toroidal field on the unit sphere, and identify it with the tangential 1-form

$$\beta_U = u(\vartheta)\sin\vartheta\,\mathrm{d}\varphi.$$

Since β_U is coexact, hence divergence-free, one has

$$\delta\beta_U = 0.$$

Let $\Delta_{\mathrm{H}} = d\delta + \delta d$ denote the nonnegative Hodge Laplacian on one-forms. On this coexact axisymmetric sector,

$$\Delta_{\mathrm{H}}\beta_U = \delta d\beta_U.$$

Our signed toroidal operator is normalized by

$$-\Delta_{\mathrm{tor}} = \Delta_{\mathrm{H}}.$$

A direct calculation gives

$$d\beta_U = \frac{\mathrm{d}}{\mathrm{d}\vartheta}\big(u(\vartheta)\sin\vartheta\big)\,\mathrm{d}\vartheta\wedge\mathrm{d}\varphi,$$

and, with the standard Hodge star on the unit sphere,

$$\star(\mathrm{d}\vartheta\wedge\mathrm{d}\varphi) = \frac{1}{\sin\vartheta}.$$

Hence

$$\star d\beta_U = \frac{1}{\sin\vartheta}\frac{\mathrm{d}}{\mathrm{d}\vartheta}\big(u(\vartheta)\sin\vartheta\big),$$

so

$$\delta d\beta_U = -\star\,\mathrm{d}\bigg(\frac{1}{\sin\vartheta}\frac{\mathrm{d}}{\mathrm{d}\vartheta}\big(u(\vartheta)\sin\vartheta\big)\bigg) = -\frac{\mathrm{d}}{\mathrm{d}\vartheta}\left[\frac{1}{\sin\vartheta}\frac{\mathrm{d}}{\mathrm{d}\vartheta}\big(u(\vartheta)\sin\vartheta\big)\right]\sin\vartheta\,\mathrm{d}\varphi.$$

Therefore the tangential Hodge Laplacian on the axisymmetric toroidal sector is

$$(-\Delta_{\mathrm{tor}}U)(\vartheta) = -\frac{\mathrm{d}}{\mathrm{d}\vartheta}\left[\frac{1}{\sin\vartheta}\frac{\mathrm{d}}{\mathrm{d}\vartheta}\big(u(\vartheta)\sin\vartheta\big)\right]\hat{\mathbf{e}}_\varphi.$$

Apply this to

$$u_j(\vartheta) \coloneqq \sin\vartheta\,P_j'(\cos\vartheta).$$

Writing $x = \cos\vartheta$, one has

$$u_j(\vartheta)\sin\vartheta = (1-x^2)P_j'(x).$$

Therefore

$$\frac{\mathrm{d}}{\mathrm{d}\vartheta}\big(u_j(\vartheta)\sin\vartheta\big) = -\sin\vartheta\,\frac{\mathrm{d}}{\mathrm{d}x}\Big((1-x^2)P_j'(x)\Big).$$

Using the Legendre equation

$$\frac{\mathrm{d}}{\mathrm{d}x}\Big((1-x^2)P_j'(x)\Big) + j(j+1)P_j(x) = 0,$$

we obtain

$$\frac{1}{\sin\vartheta}\frac{\mathrm{d}}{\mathrm{d}\vartheta}\big(u_j(\vartheta)\sin\vartheta\big) = j(j+1)P_j(\cos\vartheta).$$

Differentiating once more yields

$$-\frac{\mathrm{d}}{\mathrm{d}\vartheta}\left[\frac{1}{\sin\vartheta}\frac{\mathrm{d}}{\mathrm{d}\vartheta}\big(u_j(\vartheta)\sin\vartheta\big)\right] = j(j+1)\sin\vartheta\, P_j'(\cos\vartheta) = j(j+1)u_j(\vartheta).$$

Hence

$$-\Delta_{\mathrm{tor}}\mathcal{X}_j = j(j+1)\mathcal{X}_j.$$

Hence

$$\mathbb{S}_\ell\mathcal{X}_j = \frac{\ell^2 j(j+1)}{1+\ell^2 j(j+1)}\,\mathcal{X}_j.$$

Because $\mathcal{X}_j \in \mathcal{H}^{\mathrm{ax}}_{\mathrm{tor}}(S^2_{r_*})$,

$$\Pi_{\mathrm{TT}}\mathcal{X}_j = \mathcal{X}_j.$$

The collar extension acts on shell fields by

$$(E_\ell\mathcal{X}_j)(\xi,\upsilon) = \varpi_{\mathrm{col}}(\xi)\,\mathcal{X}_j(\upsilon),$$

and therefore

$$E_\ell^* E_\ell\mathcal{X}_j = \left(\int_0^\infty \varpi_{\mathrm{col}}(\xi)^2\,\mathrm{d}\xi\right)\mathcal{X}_j = N_{\mathrm{col}}\,\mathcal{X}_j.$$

Combining the previous identities yields

$$\mathbb{Q}_{\chi,\mathrm{sh}}(\ell)\,\mathcal{X}_j = N_{\mathrm{col}}\left(1-\frac{1}{3}\frac{\ell^2 j(j+1)}{1+\ell^2 j(j+1)}\right)\mathcal{X}_j.$$

Applying $\mathcal{I}_{\mathrm{tor}}^{-1}$ gives

$$\mathbb{Q}_{\chi,\mathrm{flux}}(\ell)\,e_j = N_{\mathrm{col}}\left(1-\frac{1}{3}\frac{\ell^2 j(j+1)}{1+\ell^2 j(j+1)}\right)e_j,$$

which is Eq. (386). The matrix identity Eq. (388) then follows from the orthonormality of the basis $\{e_1, e_3, e_5, \dots\}$. ☐

Proposition 41 (Well-defined renormalized shell-return matrix elements)**.** *For odd indices j,k, let*

$$R^{\mathrm{ren}}_{jk} := \frac{1}{\sqrt{I_j I_k}}\int_{-1}^{1}\int_{-1}^{1}\frac{\mathcal{T}_j(\upsilon)\,K^{\mathrm{ren}}_{\mathrm{sh}}(\upsilon,\upsilon';\eta_0,\ell_0)\,\mathcal{T}_k(\upsilon')}{(1-\upsilon^2)(1-\upsilon'^2)}\,\mathrm{d}\upsilon\,\mathrm{d}\upsilon'. \tag{389}$$

Assume that $K^{\mathrm{ren}}_{\mathrm{sh}}$ is symmetric, is continuous across the diagonal away from the shell endpoints, and satisfies the endpoint bound

$$\left|K^{\mathrm{ren}}_{\mathrm{sh}}(\upsilon,\upsilon';\eta_0,\ell_0)\right| \le C_{jk}\left[1+\left|\ln(1-\upsilon^2)\right|+\left|\ln(1-\upsilon'^2)\right|\right] \tag{390}$$

on the endpoint strips relevant to the fixed finite pair (j,k). These are finite-mode hypotheses and do not assert a Hilbert–Schmidt operator on the full flux space. Then the double integral in Eq. (389) *is absolutely convergent. Moreover,*

$$R^{\mathrm{ren}}_{jk} = R^{\mathrm{ren}}_{kj}. \tag{391}$$

If, in addition, the form of Eq. (370) *is represented by a bounded self-adjoint operator $\mathbb{R}^{\mathrm{ren}}_{\mathrm{sh}}(\eta_0,\ell_0)$ on $\mathcal{H}^{\mathrm{odd}}_{\mathrm{flux}}$, then*

$$R^{\mathrm{ren}}_{jk} = \langle e_j, \mathbb{R}^{\mathrm{ren}}_{\mathrm{sh}}(\eta_0,\ell_0)e_k\rangle_{\mathrm{flux}}.$$

Proof. Under the hypotheses of the present proposition, $K^{\mathrm{ren}}_{\mathrm{sh}}(\upsilon,\upsilon';\eta_0,\ell_0)$ is integrable on $[-1,1]^2$. Indeed, on every compact set away from the shell endpoints it is bounded by continuity, while on the endpoint strips its at-most-logarithmic growth is absolutely integrable because

$$\int_0^1 |\ln s|\,\mathrm{d}s < \infty.$$

Using

$$\mathcal{T}_j(\upsilon) = (1-\upsilon^2)P_j'(\upsilon), \qquad \mathcal{T}_k(\upsilon') = (1-\upsilon'^2)P_k'(\upsilon'),$$

the quotient in Eq. (389) satisfies the exact cancellation

$$\frac{\mathcal{T}_j(\upsilon)\mathcal{T}_k(\upsilon')}{(1-\upsilon^2)(1-\upsilon'^2)} = P_j'(\upsilon)P_k'(\upsilon').$$

Hence the integrand is

$$P_j'(\upsilon)\,K^{\mathrm{ren}}_{\mathrm{sh}}(\upsilon,\upsilon';\eta_0,\ell_0)\,P_k'(\upsilon').$$

Since P_j' and P_k' are bounded on $[-1,1]$, the double integral is absolutely convergent.

If $K^{\mathrm{ren}}_{\mathrm{sh}}$ is symmetric, then exchanging $\upsilon \leftrightarrow \upsilon'$ and $j \leftrightarrow k$ gives

$$R^{\mathrm{ren}}_{jk} = R^{\mathrm{ren}}_{kj},$$

which proves Eq. (391).

If the bounded self-adjoint operator $\mathbb{R}^{\mathrm{ren}}_{\mathrm{sh}}(\eta_0,\ell_0)$ representing the form $\mathfrak{r}^{\mathrm{ren}}_{\mathrm{sh}}$ exists, then for the basis vectors $e_j, e_k \in \mathcal{D}^{\mathrm{odd}}_{\mathrm{flux}}$,

$$\langle e_j, \mathbb{R}^{\mathrm{ren}}_{\mathrm{sh}}(\eta_0,\ell_0)e_k\rangle_{\mathrm{flux}} = \mathfrak{r}^{\mathrm{ren}}_{\mathrm{sh}}[e_j,e_k].$$

By the definition of $\mathfrak{r}^{\mathrm{ren}}_{\mathrm{sh}}$ and the explicit form of e_j and e_k, the right-hand side is exactly the integral in Eq. (389). Hence

$$\langle e_j, \mathbb{R}^{\mathrm{ren}}_{\mathrm{sh}}(\eta_0,\ell_0)e_k\rangle_{\mathrm{flux}} = R^{\mathrm{ren}}_{jk}.$$

□

Corollary 6 (Exact Galerkin matrix representation)**.** *Assume the hypotheses of theorem 13 and $J_\chi(\eta_0) \neq 0$. In the normalized odd flux basis Eq.* (366)*, let*

$$\mathcal{H}_N = \mathrm{span}\{e_1, e_3, \ldots, e_{2N-1}\},$$

and let Π_N be the orthogonal projector onto $\mathcal{H}_N$. Then, by theorem 14, the exact Galerkin matrix of the shell-memory operator is

$$(G_N)_{jk} = \langle e_j, \mathbb{G}_{\mathrm{sh}}(\eta_0,\ell_0)e_k\rangle_{\mathrm{flux}} = \sqrt{q_j(\ell_0)}\,R^{\mathrm{ren}}_{jk}\,\sqrt{q_k(\ell_0)}, \qquad R^{\mathrm{ren}}_{jk} := \langle e_j, \mathbb{R}^{\mathrm{ren}}_{\mathrm{sh}}(\eta_0,\ell_0)e_k\rangle_{\mathrm{flux}}, \qquad j,k = 1,3,\ldots,2N-1. \tag{392}$$

The explicit integral formula for R^{ren}_{jk} is given in proposition 41. Let $\widehat{J}_\chi$ be the normalized source from Eq. (383)*, and define its Galerkin coordinates*

$$(J_N)_j = \langle e_j, \widehat{J}_\chi\rangle_{\mathrm{flux}}, \qquad j = 1,3,\ldots,2N-1. \tag{393}$$

Since $\|G_N\| \le \|\mathbb{G}_{\mathrm{sh}}\| < 1$, the matrix $\mathbb{I}_N - G_N$ is invertible, where $\mathbb{I}_N$ denotes the identity matrix in the basis $\{e_1, e_3, \ldots, e_{2N-1}\}$ of $\mathcal{H}_N$. Define

$$R^{(N)}_\chi = J_N^\top(\mathbb{I}_N - G_N)^{-1}J_N. \tag{394}$$

Then the N-mode Galerkin realization of the vector datum is

$$\Lambda^{(N)}_{\mathrm{geom}} = \Lambda_{\mathrm{ind}} + \Delta\Lambda_{\mathrm{UV}\to\mathrm{IR}}(\ell_0) + \Delta\Lambda_{\mathrm{out}}(\eta_0)\,R^{(N)}_\chi. \tag{395}$$

Proof. By theorem 14,

$$\mathbb{Q}_{\chi,\text{flux}}(\ell_0)e_j = q_j(\ell_0)e_j, \qquad \mathbb{Q}_{\chi,\text{flux}}(\ell_0)^{1/2}e_j = \sqrt{q_j(\ell_0)}\, e_j.$$

Therefore

$$\begin{aligned}\langle e_j, \mathbb{G}_{\text{sh}} e_k\rangle_{\text{flux}} &= \left\langle \mathbb{Q}_{\chi,\text{flux}}(\ell_0)^{1/2}e_j,\, \mathbb{R}^{\text{ren}}_{\text{sh}}\, \mathbb{Q}_{\chi,\text{flux}}(\ell_0)^{1/2}e_k\right\rangle_{\text{flux}} \\ &= \sqrt{q_j(\ell_0)}\, \langle e_j, \mathbb{R}^{\text{ren}}_{\text{sh}} e_k\rangle_{\text{flux}}\, \sqrt{q_k(\ell_0)} \\ &= \sqrt{q_j(\ell_0)}\, R^{\text{ren}}_{jk}\, \sqrt{q_k(\ell_0)},\end{aligned}$$

which proves Eq. (392).

Let $a_N \in \mathcal{H}_N$ denote the unique solution of the normalized Galerkin problem

$$\Pi_N(\mathbb{I} - \mathbb{G}_{\text{sh}})\Pi_N a_N = \Pi_N \widehat{J}_\chi.$$

Expanding

$$a_N = \sum_{m=1}^{N} \xi_m^{(N)} e_{2m-1}, \qquad \boldsymbol{\xi}_N = \left(\xi_1^{(N)}, \dots, \xi_N^{(N)}\right)^\top,$$

in the basis $\{e_1, e_3, \dots, e_{2N-1}\}$ gives

$$(\mathbb{I}_N - G_N)\boldsymbol{\xi}_N = J_N,$$

hence

$$\boldsymbol{\xi}_N = (\mathbb{I}_N - G_N)^{-1}J_N, \qquad R_\chi^{(N)} = J_N^\top(\mathbb{I}_N - G_N)^{-1}J_N.$$

Define the truncated stationary geometric value by

$$\Lambda^{(N)}_{\text{geom}} := \Lambda_{\text{ind}} + \Delta\Lambda_{\text{UV}\to\text{IR}}(\ell_0) - \frac{1}{2}\|J_\chi(\eta_0)\|^2_{\text{flux}}\langle \widehat{J}_\chi, a_N\rangle_{\text{flux}}.$$

Because

$$\langle \widehat{J}_\chi, a_N\rangle_{\text{flux}} = J_N^\top(\mathbb{I}_N - G_N)^{-1}J_N = R_\chi^{(N)},$$

one obtains

$$\Lambda^{(N)}_{\text{geom}} = \Lambda_{\text{ind}} + \Delta\Lambda_{\text{UV}\to\text{IR}}(\ell_0) - \frac{1}{2}\|J_\chi(\eta_0)\|^2_{\text{flux}} R_\chi^{(N)}.$$

Finally, using

$$\Delta\Lambda_{\text{out}}(\eta_0) = -\frac{1}{2}\|J_\chi(\eta_0)\|^2_{\text{flux}},$$

we conclude that

$$\Lambda^{(N)}_{\text{geom}} = \Lambda_{\text{ind}} + \Delta\Lambda_{\text{UV}\to\text{IR}}(\ell_0) + \Delta\Lambda_{\text{out}}(\eta_0)\, R_\chi^{(N)},$$

which is Eq. (395). ∎

Theorem 15 (Convergence and explicit error bound for the exact Galerkin truncations)**.** *Assume in addition that* $J_\chi(\eta_0) \neq 0$*, so that*

$$u := \widehat{J}_\chi = \frac{J_\chi(\eta_0)}{\|J_\chi(\eta_0)\|_{\text{flux}}} \tag{396}$$

is well defined. Set

$$G := \mathbb{G}_{\text{sh}}(\eta_0, \ell_0).$$

Assume that G is compact and self-adjoint on $\mathcal{H}^{\mathrm{odd}}_{\mathrm{flux}}$, and that

$$\rho_G := \|G\| < 1.$$

Let Π_N be the orthogonal projector onto

$$\mathcal{H}_N = \operatorname{span}\{e_1, e_3, \ldots, e_{2N-1}\},$$

and define the finite-rank compression on the full flux space by

$$A_N := \Pi_N G \Pi_N.$$

Its matrix in the basis $\{e_1, e_3, \ldots, e_{2N-1}\}$ is exactly the Galerkin matrix G_N of Eq. (392). Then

$$R_\chi^{(N)} \longrightarrow R_\chi, \qquad \Lambda_{\mathrm{geom}}^{(N)} \longrightarrow \Lambda_{\mathrm{geom}}, \qquad N \to \infty. \tag{397}$$

Moreover, with

$$\varepsilon_N := \|(\mathbb{I} - \Pi_N)u\|_{\mathrm{flux}}, \qquad \delta_N := \|G - A_N\|,$$

one has the explicit error bound

$$|R_\chi - R_\chi^{(N)}| \le \frac{2\varepsilon_N + \varepsilon_N^2}{1 - \rho_G} + \frac{\delta_N}{(1 - \rho_G)^2}. \tag{398}$$

Consequently,

$$|\Lambda_{\mathrm{geom}} - \Lambda_{\mathrm{geom}}^{(N)}| \le |\Delta\Lambda_{\mathrm{out}}(\eta_0)| \left[\frac{2\varepsilon_N + \varepsilon_N^2}{1 - \rho_G} + \frac{\delta_N}{(1 - \rho_G)^2} \right]. \tag{399}$$

This estimate becomes fully certified once independent upper bounds for ε_N and δ_N are available.

Proof. Since $\Pi_N \to \mathbb{I}$ strongly and G is compact, the standard compactness lemma for Galerkin compressions gives

$$\delta_N = \|G - \Pi_N G \Pi_N\| \longrightarrow 0.$$

Also,

$$\|A_N\| = \|\Pi_N G \Pi_N\| \le \|G\| = \rho_G < 1.$$

Therefore $\mathbb{I} - A_N$ is invertible for every N, and

$$\|(\mathbb{I} - A_N)^{-1}\| \le \frac{1}{1 - \rho_G}, \qquad \|(\mathbb{I} - G)^{-1}\| \le \frac{1}{1 - \rho_G}.$$

By the resolvent identity,

$$(\mathbb{I} - A_N)^{-1} - (\mathbb{I} - G)^{-1} = (\mathbb{I} - A_N)^{-1}(A_N - G)(\mathbb{I} - G)^{-1}.$$

Hence

$$\|(\mathbb{I} - A_N)^{-1} - (\mathbb{I} - G)^{-1}\| \le \frac{\delta_N}{(1 - \rho_G)^2}. \tag{400}$$

Set

$$T := (\mathbb{I} - G)^{-1}, \qquad T_N := (\mathbb{I} - A_N)^{-1}.$$

Because $A_N = \Pi_N G \Pi_N$ maps $\mathcal{H}_N$ into $\mathcal{H}_N$ and vanishes on $\mathcal{H}_N^\perp$, the operator $T_N = (\mathbb{I} - A_N)^{-1}$ acts as $(\mathbb{I} - G_N)^{-1}$ on $\mathcal{H}_N$ and as the identity on $\mathcal{H}_N^\perp$. Hence

$$R_\chi^{(N)} = \langle \Pi_N u, T_N \Pi_N u \rangle_{\mathrm{flux}}. \tag{401}$$

Now set

$$p_N \coloneqq \Pi_N u, \qquad e_N \coloneqq (\mathbb{I} - \Pi_N)u, \qquad \|e_N\|_{\text{flux}} = \varepsilon_N.$$

Then

$$u = p_N + e_N, \qquad \|p_N\|_{\text{flux}}^2 = 1 - \varepsilon_N^2 \le 1.$$

Using Eq. (401), we write

$$\begin{aligned}
|R_\chi - R_\chi^{(N)}| &= |\langle u, Tu\rangle_{\text{flux}} - \langle p_N, T_N p_N\rangle_{\text{flux}}| \\
&\le |\langle u, Tu\rangle_{\text{flux}} - \langle p_N, T p_N\rangle_{\text{flux}}| + |\langle p_N, (T - T_N) p_N\rangle_{\text{flux}}| \,.
\end{aligned}$$

For the first term,

$$\langle u, Tu\rangle_{\text{flux}} - \langle p_N, Tp_N\rangle_{\text{flux}} = \langle e_N, Tp_N\rangle_{\text{flux}} + \langle p_N, Te_N\rangle_{\text{flux}} + \langle e_N, Te_N\rangle_{\text{flux}}.$$

Therefore

$$\begin{aligned}
|\langle u, Tu\rangle_{\text{flux}} - \langle p_N, Tp_N\rangle_{\text{flux}}| &\le \|T\|\big(2\|p_N\|_{\text{flux}}\|e_N\|_{\text{flux}} + \|e_N\|_{\text{flux}}^2\big) \\
&\le \frac{2\varepsilon_N + \varepsilon_N^2}{1 - \rho_G}.
\end{aligned}$$

For the second term,

$$|\langle p_N, (T - T_N) p_N\rangle_{\text{flux}}| \le \|p_N\|_{\text{flux}}^2 \, \|T - T_N\| \le \frac{\delta_N}{(1 - \rho_G)^2},$$

using Eq. (400). Combining the last two bounds yields Eq. (398). Since $\varepsilon_N \to 0$ and $\delta_N \to 0$, the convergence $R_\chi^{(N)} \to R_\chi$ follows.

Finally, by Eq. (395) and Eq. (385),

$$\Lambda_{\text{geom}}^{(N)} - \Lambda_{\text{geom}} = \Delta\Lambda_{\text{out}}(\eta_0)\big(R_\chi^{(N)} - R_\chi\big).$$

This gives Eq. (399) and proves $\Lambda_{\text{geom}}^{(N)} \to \Lambda_{\text{geom}}$. □

Theorem 16 (Source-cyclic Jacobi representation of the exact return factor)**.** *Assume the hypotheses of theorem 13, and assume in addition that*

$$G \coloneqq \mathbb{G}_{\text{sh}}(\eta_0, \ell_0)$$

is compact on $\mathcal{H}_{\text{flux}}^{\text{odd}}$. Assume also that $J_\chi(\eta_0) \neq 0$, and set

$$u \coloneqq \widehat{J}_\chi = \frac{J_\chi(\eta_0)}{\|J_\chi(\eta_0)\|_{\text{flux}}}.$$

Let

$$\mathcal{K}_J = \overline{\operatorname{span}}\{u, Gu, G^2u, \dots\} \subset \mathcal{H}_{\text{flux}}^{\text{odd}}$$

be the source-cyclic subspace. Then $\mathcal{K}_J$ reduces G, and the restriction $G|_{\mathcal{K}_J}$ is unitarily equivalent to a Jacobi operator

$$J_{\text{cyc}} = \begin{pmatrix} a_0 & b_1 & 0 & \cdots \\ b_1 & a_1 & b_2 & \ddots \\ 0 & b_2 & a_2 & \ddots \\ \vdots & \ddots & \ddots & \ddots \end{pmatrix}.$$

Let $\mathbf{e}_0$ denote the first standard basis vector in the Jacobi representation space; namely $\mathbf{e}_0 = (1, 0, 0, \dots)^\top$ in the nonterminating case and $\mathbf{e}_0 \in \mathbb{R}^d$ in the terminating case. Since

$$\|J_{\text{cyc}}\| = \|G|_{\mathcal{K}_J}\| \le \|G\| < 1,$$

the resolvent $(\mathbb{I}-J_{\mathrm{cyc}})^{-1}$ exists. If the Lanczos process does not terminate, then $b_n>0$ for all $n\geq 1$. If it terminates after d cyclic steps, then J_{cyc} is the finite $d\times d$ Jacobi matrix and the continued fraction below terminates after d levels. In both cases,

$$R_\chi=\langle u,(\mathbb{I}-G)^{-1}u\rangle_{\mathrm{flux}}=\mathbf{e}_0^\top(\mathbb{I}-J_{\mathrm{cyc}})^{-1}\mathbf{e}_0. \tag{402}$$

Equivalently, in the nonterminating case,

$$R_\chi=\cfrac{1}{1-a_0-\cfrac{b_1^2}{1-a_1-\cfrac{b_2^2}{1-a_2-\ddots}}}. \tag{403}$$

The same formula holds in the terminating case with the continued fraction cut off at the last cyclic level. This Jacobi representation is an exact representation of the source-cyclic resolvent element under the stated operator hypotheses; it is not a modal continuation ansatz.

Let

$$m_n=\langle u,G^nu\rangle_{\mathrm{flux}},\qquad n=1,2,3,\ldots.$$

Then

$$a_0=m_1,\qquad b_1^2=m_2-m_1^2. \tag{404}$$

If $b_1>0$, then

$$a_1=\frac{m_3-2m_1m_2+m_1^3}{m_2-m_1^2}. \tag{405}$$

If $b_1=0$, then the cyclic subspace is one-dimensional and

$$R_\chi=\frac{1}{1-a_0}.$$

Proof. First we check that $\mathcal{K}_J$ is a reducing subspace for G. It is invariant by construction, because

$$G(G^nu)=G^{n+1}u.$$

If $h\perp\mathcal{K}_J$, then for every polynomial p,

$$\langle Gh,p(G)u\rangle_{\mathrm{flux}}=\langle h,Gp(G)u\rangle_{\mathrm{flux}}=0,$$

because $Gp(G)u\in\mathcal{K}_J$. Since polynomial vectors $p(G)u$ are dense in $\mathcal{K}_J$ by definition of the cyclic closure, it follows that $Gh\perp\mathcal{K}_J$. Hence $\mathcal{K}_J^\perp$ is invariant. Therefore $\mathcal{K}_J$ reduces G, and $G|_{\mathcal{K}_J}$ is self-adjoint.

We construct the Jacobi basis directly. Set $q_{-1}=0$, $b_0=0$, and $q_0=u$. Once $q_0,\ldots,q_n$ have been constructed, define

$$a_n=\langle q_n,Gq_n\rangle_{\mathrm{flux}},\qquad r_{n+1}=Gq_n-b_nq_{n-1}-a_nq_n.$$

A direct induction gives $r_{n+1}\perp q_m$ for every $0\leq m\leq n$. Indeed, for $m\leq n-2$, self-adjointness gives

$$\langle r_{n+1},q_m\rangle_{\mathrm{flux}}=\langle q_n,Gq_m\rangle_{\mathrm{flux}}=0,$$

because $Gq_m\in\operatorname{span}\{q_{m-1},q_m,q_{m+1}\}$. For $m=n-1$, the term b_nq_{n-1} subtracts $\langle q_n,Gq_{n-1}\rangle_{\mathrm{flux}}=b_n$. For $m=n$, the term a_nq_n subtracts $\langle q_n,Gq_n\rangle_{\mathrm{flux}}=a_n$. If $r_{n+1}=0$, the process terminates. Otherwise set

$$b_{n+1}=\|r_{n+1}\|_{\mathrm{flux}}>0,\qquad q_{n+1}=\frac{r_{n+1}}{b_{n+1}}.$$

Thus, at every nonterminating step,

$$Gq_n=b_nq_{n-1}+a_nq_n+b_{n+1}q_{n+1}.$$

Since $q_0 = u$, the scalar resolvent element is the $(1,1)$-entry of $(\mathbb{I} - J_{\mathrm{cyc}})^{-1}$, namely

$$R_\chi = \langle u, (\mathbb{I} - G)^{-1} u \rangle_{\mathrm{flux}} = \mathbf{e}_0^\top (\mathbb{I} - J_{\mathrm{cyc}})^{-1} \mathbf{e}_0.$$

To derive the continued fraction, write the first Schur split in the nonterminating case as

$$\mathbb{I} - J_{\mathrm{cyc}} = \begin{pmatrix} 1 - a_0 & -b_1 (\mathbf{e}_0^{(1)})^\top \\ -b_1 \mathbf{e}_0^{(1)} & \mathbb{I} - J_{\mathrm{cyc}}^{(1)} \end{pmatrix},$$

where $J_{\mathrm{cyc}}^{(1)}$ is the tail Jacobi operator obtained by deleting the first row and the first column, and $\mathbf{e}_0^{(1)}$ is the first standard vector in the tail space. Since $\|J_{\mathrm{cyc}}^{(1)}\| \le \|J_{\mathrm{cyc}}\| < 1$, the tail resolvent exists. The Schur complement of the lower-right block gives

$$\mathbf{e}_0^\top (\mathbb{I} - J_{\mathrm{cyc}})^{-1} \mathbf{e}_0 = \frac{1}{1 - a_0 - b_1^2 \, (\mathbf{e}_0^{(1)})^\top (\mathbb{I} - J_{\mathrm{cyc}}^{(1)})^{-1} \mathbf{e}_0^{(1)}}.$$

Repeating the same Schur split on each tail gives, for every tail level n,

$$F_n = \frac{1}{1 - a_n - b_{n+1}^2 F_{n+1}}, \qquad F_n \coloneqq (\mathbf{e}_0^{(n)})^\top (\mathbb{I} - J_{\mathrm{cyc}}^{(n)})^{-1} \mathbf{e}_0^{(n)}.$$

In the terminating case of cyclic dimension d, the recursion ends with $F_{d-1} = (1 - a_{d-1})^{-1}$. In the nonterminating case, the continued fraction is obtained as the limit of the finite Schur complements of the principal Jacobi truncations. Let P_n denote the projection onto the first n Jacobi basis vectors. Since $P_n \to \mathbb{I}$ strongly and J_{cyc} is compact,

$$\|J_{\mathrm{cyc}} - P_n J_{\mathrm{cyc}} P_n\| \to 0.$$

Together with $\|J_{\mathrm{cyc}}\| < 1$, the resolvent identity gives

$$\big\|(\mathbb{I} - P_n J_{\mathrm{cyc}} P_n)^{-1} - (\mathbb{I} - J_{\mathrm{cyc}})^{-1}\big\| \le \frac{\|J_{\mathrm{cyc}} - P_n J_{\mathrm{cyc}} P_n\|}{(1 - \|J_{\mathrm{cyc}}\|)^2} \to 0.$$

Hence the finite continued fractions converge to $\mathbf{e}_0^\top (\mathbb{I} - J_{\mathrm{cyc}})^{-1} \mathbf{e}_0$, which proves Eq. (403).

It remains to verify the first moment identities. Since $q_0 = u$,

$$a_0 = \langle q_0, G q_0 \rangle_{\mathrm{flux}} = \langle u, G u \rangle_{\mathrm{flux}} = m_1.$$

The first residual is

$$r_1 \coloneqq G q_0 - a_0 q_0 = G u - m_1 u.$$

Hence

$$b_1^2 = \|r_1\|_{\mathrm{flux}}^2 = \langle G u - m_1 u, G u - m_1 u \rangle_{\mathrm{flux}} = m_2 - m_1^2.$$

If $b_1 = 0$, then $G u = m_1 u$, so $\mathcal{K}_J = \mathrm{span}\{u\}$ and $R_\chi = (1 - a_0)^{-1}$.

If $b_1 > 0$, then

$$q_1 = \frac{G u - m_1 u}{b_1}.$$

Therefore

$$\begin{aligned} a_1 &= \langle q_1, G q_1 \rangle_{\mathrm{flux}} \\ &= \frac{\langle G u - m_1 u, \, G(G u - m_1 u) \rangle_{\mathrm{flux}}}{b_1^2} \\ &= \frac{m_3 - 2 m_1 m_2 + m_1^3}{m_2 - m_1^2}. \end{aligned}$$

This proves Eqs. (404) and (405). $\square$

Corollary 7 (No additional vector-side closure remains after exact Galerkin or Jacobi evaluation)**.** *Assume the hypotheses of theorem 13 and assume $J_\chi(\eta_0) \neq 0$. Once the exact matrix elements R^{ren}_{jk}, the exact admission eigenvalues $q_j(\ell_0)$, and the normalized source coordinates are fixed, the exact return factor R_χ is determined by the Galerkin limit*

$$R_\chi = \lim_{N\to\infty} J_N^\top (\mathbb{I}_N - G_N)^{-1} J_N,$$

where $\mathbb{I}_N$ denotes the identity matrix on $\mathrm{span}\{e_1, e_3, \dots, e_{2N-1}\}$. Equivalently, R_χ is determined by the source-cyclic Jacobi data of $\mathbb{G}_{\mathrm{sh}}(\eta_0, \ell_0)$.

A later reduced spectral measure, modal continuation rule, or low-rank replacement is theorem-level only when its spectral points and weights are derived from this exact Galerkin or Jacobi object, or when its tail error is certified, for example by Eq. (398). Without such a derivation or certification, it is a diagnostic or evaluation proxy and not an independent definition of R_χ. Within the stated vector operator framework, no auxiliary mean geometric constant, modal continuation ansatz, or further vector-side closure is required after the exact Galerkin or source-cyclic evaluation.

Proof. The Galerkin convergence statement is exactly theorem 15, applied to the normalized source $u = \widehat{J}_\chi$. The source-cyclic Jacobi representation is exactly theorem 16. Hence both procedures evaluate the same resolvent matrix element

$$R_\chi = \langle \widehat{J}_\chi, (\mathbb{I} - \mathbb{G}_{\mathrm{sh}})^{-1} \widehat{J}_\chi \rangle_{\mathrm{flux}}.$$

Since Λ_{geom} depends on the vector-memory sector only through this scalar resolvent element, no further vector-side closure remains. Any replacement not derived from these objects, and not supplied with a tail estimate, is a reduced diagnostic rather than an operator-level definition. □

E. Numerical status on the minimal electron branch

This subsection reports the current reduced numerical realization of the vector geometric constant on the minimal electron branch. The theorem-level ingredients fixed earlier are Λ_{ind}, $\Delta\Lambda_{\mathrm{UV}\to\mathrm{IR}}(\ell_0; \mathscr{A}_\parallel^{\mathrm{coll}})$, the infinite-mode exterior subtraction $\Delta\Lambda_{\mathrm{out}}(\eta_0)$, and the exact shell source $J_\chi(\eta_0)$. In the numerical realization reported here, the shell-source norm and $\Delta\Lambda_{\mathrm{out}}$ are evaluated through the stated odd-mode cutoff, whereas the only reduced-model ingredient is the source-weighted return factor $R^{\mathrm{red}}_{\chi,101}$. This factor does not replace the exact operator definition of R_χ in Eq. (383). No scalar-channel target, no measured value of α, no QED coefficient, no electron g-factor benchmark, and no fitted coefficient enters the calculation. The reported reduced realization value is obtained from the factorized theorem-path vector realization

$$\Lambda^{(\mathrm{th})}_{\mathrm{geom}} \equiv \Lambda^{\mathrm{red},[101]}_{\mathrm{geom}} = \Lambda_{\mathrm{ind}} + \Delta\Lambda_{\mathrm{UV}\to\mathrm{IR}}(\ell_0; \mathscr{A}_\parallel^{\mathrm{coll}}) + \Delta\Lambda^{[101]}_{\mathrm{out}}(\eta_0)\, R^{\mathrm{red}}_{\chi,101}. \tag{406}$$

The superscript (th) is a realization label indicating that the local core, the admitted UV load, the Maxwell source formula, and the exterior subtraction formula are inherited from the theorem-level construction above. It does not mean that the shell-return factor has been evaluated as the exact operator resolvent. The displayed value nevertheless remains a reduced cutoff realization. The exterior subtraction is evaluated through the exact partial sum $\Delta\Lambda^{[101]}_{\mathrm{out}}(\eta_0)$, whereas the return factor is the reduced source-weighted realization $R^{\mathrm{red}}_{\chi,101}$. Thus $\Lambda^{(\mathrm{th})}_{\mathrm{geom}}$ is not the exact operator value obtained from Eq. (383), and no convergence claim from theorem 15 is invoked here.

Here $R^{\mathrm{red}}_{\chi,101}$ is the cutoff-101 source-weighted reduced spectral realization defined in definition VII.19. It is distinct from both the exact Galerkin quantity $R^{(N)}_\chi$ of Eq. (394) and the exact operator value R_χ of Eq. (383). All quantities reported below are dimensionless. The exterior subtraction $\Delta\Lambda_{\mathrm{out}}$ and the shell source J_χ are defined from the exact Maxwell shell projection in the energy-dual normalization. The reported numerical values are their stated odd-mode cutoff realizations. When the notation $\Delta\Lambda^{[101]}_{\mathrm{out}}(\eta_0)$ is used below, it denotes the cutoff value obtained from the resolved set $\mathcal{J}_{101}$, not the infinite-mode operator value.

The admitted UV load is evaluated from the exact cyclic admission formula

$$\Delta\Lambda_{\mathrm{UV}\to\mathrm{IR}}(\ell_0; \mathscr{A}_\parallel^{\mathrm{coll}}) = C^{(\mathrm{Gauss})}_{\mathrm{UV}}\, P^{(\chi)}_{IR}(\ell_0), \qquad P^{(\chi)}_{IR}(\ell_0) = \frac{N_{IR}(\ell_0)}{D_{IR}}. \tag{407}$$

Here $y = r/r_*$ is the dimensionless first-node shell coordinate,

$$D_{IR} = \int_0^1 y^2 \sin^2(\pi y)\, \mathrm{d}y,$$

and

$$N_{IR}(\ell_0) = \int_0^1 y^2 \sin^2(\pi y) \left[1 - \frac{1}{3}\,\frac{(1-y)^2}{(1-y)^2 + \ell_0^2}\right] \exp\left[-\left(\frac{1-y}{\ell_0}\right)^2\right] \mathrm{d}y.$$

The reduced source-channel return used in the numerical ledger is introduced once in definition VII.19. It is a source-weighted reduced spectral realization of the exact operator resolvent, not an independent definition of the exact return factor R_χ.

The shell source itself is obtained from the exact Maxwell shell projection in the energy-dual normalization, and the infinite-mode exterior subtraction is defined by the exact quadratic source norm

$$\Delta\Lambda_{\text{out}}(\eta_0) = -\frac{1}{2}\,\|J_\chi(\eta_0)\|^2_{\text{flux}}. \tag{408}$$

For a finite odd-mode ledger cutoff $J_{\max}$, define the cutoff realization by

$$\Delta\Lambda^{[J_{\max}]}_{\text{out}}(\eta_0) := -\frac{1}{2} \sum_{j\in\mathcal{J}_{J_{\max}}} \left(J_j^{(\chi)}(\eta_0)\right)^2. \tag{409}$$

The numerical tables below report the computed value of $\Delta\Lambda^{[101]}_{\text{out}}(\eta_0)$. At the theorem level, this object is the finite partial sum of an absolutely convergent nonnegative series. In the numerical ledger, its displayed value is obtained from the stated quadrature and odd-mode cutoff. Thus the monotonicity statement below applies to the exact partial sums, while the printed decimal remains a quadrature realization of that finite sum. By Eq. (355),

$$0 \le \Delta\Lambda^{[J_{\max}]}_{\text{out}}(\eta_0) - \Delta\Lambda_{\text{out}}(\eta_0) = \frac{1}{2} \sum_{\substack{j \text{ odd} \\ j > J_{\max}}} \left(J_j^{(\chi)}(\eta_0)\right)^2, \qquad \Delta\Lambda^{[J_{\max}]}_{\text{out}}(\eta_0) \downarrow \Delta\Lambda_{\text{out}}(\eta_0) \quad (J_{\max} \to \infty).$$

Thus $\Delta\Lambda^{[101]}_{\text{out}}(\eta_0)$ is the theorem-defined finite partial-sum object at $J_{\max} = 101$, not a new definition of $\Delta\Lambda_{\text{out}}$. Its printed value in the tables is the numerical quadrature realization of that partial sum.

Numerically, the present evaluation uses 100-digit working precision, direct quadrature for the one-dimensional shell-admission integral, Gauss–Legendre quadrature with 512 nodes for the shell-source projections, and odd-mode summation through $j \le 101$ for the shell source and the reduced source-channel return. The resulting $j \le 101$ ledger is reported in Tables X–XVIII.

Closed-form constants listed below are rounded evaluations of exact formulas. Quantities involving the cutoff odd-mode source, the reduced source-channel return, or numerical quadrature are ledger-level numerical realizations of the stated computation. The algebraic residuals printed in the tables certify only internal consistency of the same cutoff realization. They do not provide a rigorous truncation bound for the exact operator-level quantities, and they do not by themselves certify all displayed digits of the cutoff-dependent entries.

Definition VII.19 (Reduced source-weighted vector return used in the numerical ledger)**.** Fix an odd cutoff $J_{\max}$ and set

$$\mathcal{J}_{J_{\max}} = \{1, 3, 5, \ldots, J_{\max}\}.$$

The numerical ledger below uses $J_{\max} = 101$. The theorem-defined Maxwell source coefficients $J_j^{(\chi)}(\eta_0)$ are computed for the modes in this cutoff. Whenever

$$\sum_{k\in\mathcal{J}_{J_{\max}}} \left(J_k^{(\chi)}(\eta_0)\right)^2 > 0,$$

the source weights used in the reduced spectral measure are defined by

$$w_j^{(J_{\max})} = \frac{\left(J_j^{(\chi)}(\eta_0)\right)^2}{\sum_{k\in\mathcal{J}_{J_{\max}}} \left(J_k^{(\chi)}(\eta_0)\right)^2}, \qquad \sum_{j\in\mathcal{J}_{J_{\max}}} w_j^{(J_{\max})} = 1.$$

In the tables, the superscript $(J_{\max})$ is suppressed and w_j denotes $w_j^{(101)}$.

For this ledger-level reduced return model, define the reduced return constants

$$\gamma_{\rm geom} = \frac{1}{2}\,\frac{\sinh\eta_0}{\eta_0}, \qquad A_{\rm ret} \equiv (\ln 2)\eta_0^4, \qquad B_{\rm ret} \equiv \frac{\eta_0^4}{8\pi^2}.$$

These constants belong to the reduced spectral realization used in the numerical ledger; they are not additional operator-level inputs to $\mathbb{G}_{\rm sh}$. Set

$$\beta_\chi = P_{IR}^{(\chi)}(\ell_0)\,\gamma_{\rm geom} + \frac{P_{IR}^{(\chi)}(\ell_0)\,\Delta\Lambda_{\rm UV\to IR}(\ell_0;\mathscr{A}_\parallel^{\rm coll})}{2(1+A_{\rm ret})}. \tag{410}$$

For each odd shell mode define

$$m_j = \frac{j-1}{2}, \qquad \Phi_j = \frac{1+\frac{1}{2}B_{\rm ret}m_j}{1+A_{\rm ret}m_j}, \qquad R_j^{\rm red} = 1+\beta_\chi\Phi_j. \tag{411}$$

Since $A_{\rm ret}>0$, $B_{\rm ret}>0$, and $m_j \geq 0$, one has

$$\Phi_j > 0.$$

In the minimal-branch numerical ledger $\beta_\chi > 0$, and therefore

$$R_j^{\rm red} > 1.$$

Equivalently, introduce the reduced spectral point

$$g_j^{\rm red} = 1 - \frac{1}{R_j^{\rm red}} = \frac{\beta_\chi\Phi_j}{1+\beta_\chi\Phi_j}. \tag{412}$$

Thus

$$0 \leq g_j^{\rm red} < 1, \qquad \frac{1}{1-g_j^{\rm red}} = R_j^{\rm red}. \tag{413}$$

The reduced source-weighted spectral measure and its return factor are

$$\mathrm{d}\mu_{\chi,J_{\max}}^{\rm red}(\lambda) = \sum_{j\in\mathcal{J}_{J_{\max}}} w_j^{(J_{\max})}\,\delta(\lambda - g_j^{\rm red}), \qquad R_{\chi,J_{\max}}^{\rm red} = \int \frac{\mathrm{d}\mu_{\chi,J_{\max}}^{\rm red}(\lambda)}{1-\lambda}. \tag{414}$$

Hence

$$R_{\chi,J_{\max}}^{\rm red} = \sum_{j\in\mathcal{J}_{J_{\max}}} \frac{w_j^{(J_{\max})}}{1-g_j^{\rm red}} = \sum_{j\in\mathcal{J}_{J_{\max}}} w_j^{(J_{\max})}R_j^{\rm red} = 1+\beta_\chi F_{\chi,J_{\max}}, \qquad F_{\chi,J_{\max}} = \sum_{j\in\mathcal{J}_{J_{\max}}} w_j^{(J_{\max})}\Phi_j. \tag{415}$$

In the numerical tables below,

$$R_\chi^{\rm red} \equiv R_{\chi,101}^{\rm red}, \qquad F_\chi \equiv F_{\chi,101}.$$

This construction is a realization-level reduced spectral representation intended to approximate the source-cyclic return factor. It is used only in the numerical tables below and does not redefine the exact operator-level return factor R_χ of Eq. (383). It is not fitted to a measured value of α, to a QED coefficient, or to a scalar-channel target. No convergence statement in $J_{\max}$ is asserted for $R_{\chi,J_{\max}}^{\rm red}$. In particular, $R_{\chi,J_{\max}}^{\rm red}$ is not the exact Galerkin sequence of Eq. (394). A certified replacement of R_χ would require either the exact Galerkin limit or an error bound of the type stated in Eq. (398).

For the numerical ledger, it is convenient to record the physical-shell energy-dual amplitudes rather than the theorem-normalized shell moments. Accordingly, define

$$a_j^{\rm sh,phys}(\eta) \equiv \eta^{-(j+1)}\,a_j^{\rm sh}(\eta), \tag{416}$$

TABLE X. Fixed minimal-branch geometry, theorem-path local constants, and reduced-return ledger constants entering the current vector-channel realization. All quantities are dimensionless and none is an external benchmark.

Item	Symbol / formula	Value
Minimal collar ratio	$\varepsilon_{\mathrm{br},0} = 1/\sqrt{\pi}$	0.564189583547756286948079451561
Minimal branch ratio	$\eta_0 = 1/\pi$	0.318309886183790671537767526745
Minimal shell width	$\ell_0 = \varepsilon_{\mathrm{br},0}\eta_0 = 1/(\pi\sqrt{\pi})$	0.179587122125166561689081983628
Euler–Mascheroni constant	γ_E	0.577215664901532860606512090082
Filamentary reference core	$\Lambda_{\mathrm{ind}} = \ln(8\sqrt{\pi}) - 2$	0.651806484604536015323410040051
Gaussian UV constant	$C_{\mathrm{UV}}^{(\mathrm{Gauss})} = \frac{1}{2}(\ln 2 + \gamma_E)$	0.635181422730739085011872105770
Geometric return prefactor	$\gamma_{\mathrm{geom}} = \frac{1}{2}\sinh(\eta_0)/\eta_0$	0.508486310232226026713244570368
UV return coefficient	$A_{\mathrm{ret}} = (\ln 2)\eta_0^4$	0.007115836655512877336607052631
IR return coefficient	$B_{\mathrm{ret}} = \eta_0^4/(8\pi^2)$	0.000130020184161981537011229704
Collar norm	$N_{\mathrm{col}} = \sqrt{2/\pi}$	0.797884560802865355879892119869

TABLE XI. Closed branch-cyclic normalized χ-admission block on the minimal electron branch. The quotient $P_{IR}^{(\chi)}(\ell_0) = N_{IR}(\ell_0)/D_{IR}$ is evaluated from the one-dimensional branch-cyclic Rayleigh law associated with the normalized shell-space admission operator $\overline{\mathbb{Q}_{\chi,\mathrm{sh}}}(\ell_0)$, and the admitted UV load is $\Delta\Lambda_{\mathrm{UV}\to\mathrm{IR}}(\ell_0;\mathscr{A}_{\parallel}^{\mathrm{coll}}) = C_{\mathrm{UV}}^{(\mathrm{Gauss})}\, P_{IR}^{(\chi)}(\ell_0)$. This table reports an internal vector-admission quantity, not a fitted input.

Item	Symbol / formula	Value
Admission denominator	$D_{IR} = \int_0^1 y^2 \sin^2(\pi y)\,\mathrm{d}y$	0.141336370756082223805696800864
Admission numerator	$N_{IR}(\ell_0)$	0.0121237197662881294096075356310
Shell-admission quotient	$P_{IR}^{(\chi)}(\ell_0) = N_{IR}(\ell_0)/D_{IR}$	0.0857791925845556011097469124949
Admitted UV load	$\Delta\Lambda_{\mathrm{UV}\to\mathrm{IR}}(\ell_0;\mathscr{A}_{\parallel}^{\mathrm{coll}}) = C_{\mathrm{UV}}^{(\mathrm{Gauss})} P_{IR}^{(\chi)}(\ell_0)$	0.0544853495865520906532491466725

where $a_j^{\mathrm{sh}}(\eta)$ is the exact shell-source coefficient from Eq. (342). Equivalently, in SI-normalized physical variables,

$$a_j^{\mathrm{sh,phys}}(\eta) = \frac{r_*}{\mu_0 I\, I_j}\left(\frac{r_*}{R}\right)^{j+1}\int_{-1}^{1} B_\vartheta(r_*, \upsilon; \eta, I)\, \mathcal{T}_j(\upsilon)\,\mathrm{d}\upsilon. \tag{417}$$

The factor $r_*/R = \eta^{-1}$ is geometric and dimensionless. The factor $r_* B_\vartheta/(\mu_0 I)$ is dimensionless in SI units, so Eq. (417) has the same units as Eq. (416), namely none. In terms of these physical-shell amplitudes, the normalized source amplitudes used in the numerical realization are

$$\widehat{a}_j(\eta) = 2(j+1)\,\eta^{j+1/2}\, a_j^{\mathrm{sh,phys}}(\eta), \tag{418}$$

which is equivalent to the theorem normalization Eq. (344). The corresponding exact source coefficients remain

$$J_j^{(\chi)}(\eta) = \sqrt{\frac{2\pi}{(j+1)(2j+1)}}\,\widehat{a}_j(\eta). \tag{419}$$

TABLE XII. High-precision odd-mode cutoff ledger for the Maxwell shell source and exterior subtraction on the minimal electron branch. The exact infinite-mode identity $\Delta\Lambda_{\mathrm{out}}(\eta_0) = -\frac{1}{2}\|J_\chi(\eta_0)\|_{\mathrm{flux}}^2$ is represented at finite cutoff by the theorem-defined partial sum $\Delta\Lambda_{\mathrm{out}}^{[101]}(\eta_0)$ over $j \le 101$. The displayed decimals are quadrature realizations of that cutoff ledger, not certified tail bounds for the exact infinite-mode value.

Item	Symbol / formula	Value
Cutoff source norm	$\|J_\chi^{[101]}(\eta_0)\|_{\mathrm{flux}}^2 = \sum_{j\in\mathcal{J}_{101}} (J_j^{(\chi)})^2$	0.0279343161251718605341693629773
Cutoff exterior subtraction	$\Delta\Lambda_{\mathrm{out}}^{[101]}(\eta_0)$	-0.0139671580625859302670846814886
Cutoff quadratic identity	$-\frac{1}{2}\|J_\chi^{[101]}(\eta_0)\|_{\mathrm{flux}}^2$	-0.0139671580625859302670846814886
Internal check	$\Delta\Lambda_{\mathrm{out}}^{[101]}(\eta_0) + \frac{1}{2}\|J_\chi^{[101]}(\eta_0)\|_{\mathrm{flux}}^2$	1.12×10^{-103}
Source-weight normalization	$\sum_{j\in\mathcal{J}_{101}} w_j$	1

TABLE XIII. Leading odd physical-shell source amplitudes and normalized source coefficients on the minimal electron branch. Here $a_j^{\mathrm{sh,phys}} = \eta_0^{-(j+1)} a_j^{\mathrm{sh}}$ is the physical-shell rescaling of the theorem coefficient Eq. (342). The weights w_j are normalized only on the resolved cutoff set $\mathcal{J}_{101}$; they are therefore ledger weights, not the infinite-mode weights of the exact source.

j	$a_j^{\mathrm{sh,phys}}$	$\widehat{a}_j$	$J_j^{(\chi)}$	w_j
1	0.225035986276	0.161654260600	0.165425122325	0.979636335954
3	−0.345425446938	−0.0502828355856	−0.0238193924124	0.0203106262689
5	0.170500913603	0.00377210398766	0.00116386236000	$4.84914535564 \times 10^{-5}$
7	−0.509958673680	−0.00152416126532	−0.000348762860904	$4.35434082584 \times 10^{-6}$
9	−0.866308418075	−0.000327928180687	−0.0000596337160832	$1.27305070866 \times 10^{-7}$
11	−5.17840859580	−0.000238332912723	−0.0000359599777037	$4.62914499376 \times 10^{-8}$

TABLE XIV. Exact unnormalized admission eigenvalues and reduced low-mode source-channel return data. The numbers $q_j(\ell_0)$ are the exact eigenvalues of the unnormalized flux-space shell-admission operator $\mathbb{Q}_{\chi,\mathrm{flux}}(\ell_0)$ on the odd flux basis. The modal reduced return shape is $\Phi_j = (1 + \frac{1}{2} B_{\mathrm{ret}} m_j)/(1 + A_{\mathrm{ret}} m_j)$, with $m_j = (j-1)/2$.

Mode j	$q_j(\ell_0)$	m_j	Φ_j	$R_j^{\mathrm{red}} = 1 + \beta_\chi \Phi_j$	$w_j R_j^{\mathrm{red}}$
1	0.781768746053826182396	0	1.00000000000000000000	1.04593788859456687671	1.02463876081841962961
3	0.723673573719823330668	1	0.99299891469693625866	1.04561627704465205011	0.0212371214236845937708
5	0.667097270671369973321	2	0.986096220914864547172	1.04529917833991045530	0.0000506880765590558643912
7	0.626703288563007265019	3	0.979289635032263742585	1.04498649815592618788	0.00000455022737137521277154
9	0.600072203619720163839	4	0.972577237345054419302	1.04467814477876873763	$1.32992825253 \times 10^{-7}$
11	0.582512972724815998944	5	0.965957086250438531300	1.04437402901530507301	$4.83455880803 \times 10^{-8}$

TABLE XV. Reduced source-weighted resolvent on the minimal electron branch. The return factor is evaluated as the resolvent of the reduced spectral measure $\mathrm{d}\mu_{\chi,101}^{\mathrm{red}}$. It is a ledger-level reduced realization of the return factor, not the exact operator value R_χ.

Item	Symbol / formula	Value
Source-channel coupling	$\beta_\chi = P_{IR}^{(\chi)}(\ell_0)\gamma_{\mathrm{geom}} + P_{IR}^{(\chi)}(\ell_0)\Delta\Lambda_{\mathrm{UV}\to\mathrm{IR}}(\ell_0; \mathscr{A}_{\parallel}^{\mathrm{coll}})/[2(1 + A_{\mathrm{ret}})]$	0.0459378885945668767059351471824
Weighted return average	$F_\chi = \sum_{j\in\mathcal{J}_{101}} w_j \Phi_j$	0.999857034848837013544434076182
Return factor	$R_\chi^{\mathrm{red}} = 1 + \beta_\chi F_\chi$	1.04593132107737984602098907405
Exterior-memory contribution	$\Delta\Lambda_{\mathrm{out}}^{[101]}(\eta_0) R_\chi^{\mathrm{red}}$	-0.0146086880840970792604994790889

TABLE XVI. Source-cyclic Jacobi audit of the reduced vector-memory factor. Here $g_j^{\mathrm{red}} = 1 - 1/R_j^{\mathrm{red}}$. The rank-two Jacobi continued fraction reproduces R_χ^{red} to the displayed precision for the reduced cutoff spectral measure. This is an audit of that reduced spectral measure, not a proof that the exact operator R_χ has rank two and not a certified truncation estimate for the exact source-cyclic Jacobi tail.

Quantity	Formula	Value
First moment	$m_1 = \sum_{j\in\mathcal{J}_{101}} w_j g_j^{\mathrm{red}}$	0.0439142783548438317181313792328
Second moment	$m_2 = \sum_{j\in\mathcal{J}_{101}} w_j (g_j^{\mathrm{red}})^2$	0.00192846558397150040289752466655
Third moment	$m_3 = \sum_{j\in\mathcal{J}_{101}} w_j (g_j^{\mathrm{red}})^3$	0.0000846873268238501265557698534838
First Jacobi diagonal	$a_0 = m_1$	0.0439142783548438317181313792328
First Jacobi coupling	$b_1^2 = m_2 - m_1^2$	$1.74054479493167290170 \times 10^{-9}$
First Jacobi off-diagonal	$b_1 = \sqrt{b_1^2}$	0.0000417198369475681544363744364556
Second Jacobi diagonal	$a_1 = (m_3 - 2m_1m_2 + m_1^3)/(m_2 - m_1^2)$	0.0436281908997979873706949825675
Rank-two return	$R_\chi^{[2]} = \left(1 - a_0 - b_1^2/(1 - a_1)\right)^{-1}$	1.04593132107737984236690002815
Return residual	$R_\chi^{\mathrm{red}} - R_\chi^{[2]}$	$3.65408904590 \times 10^{-18}$
Geometric impact	$\Delta\Lambda_{\mathrm{out}}^{[101]}(\eta_0)(R_\chi^{\mathrm{red}} - R_\chi^{[2]})$	$-5.10372392788 \times 10^{-20}$

The source-side concentration can be checked internally within the same cutoff ledger, independently of the final

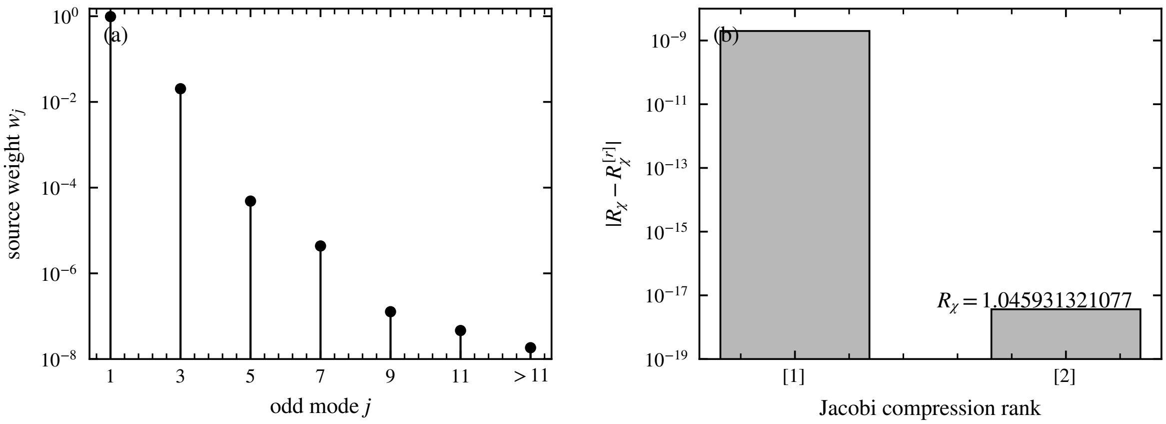

FIG. 9. Diagnostic view of source concentration and source-cyclic Jacobi saturation. Panel (a) shows the normalized resolved odd-sector source weights $w_j = (J_j^{(\chi)})^2 / \sum_{k\in\mathcal{J}_{101}} (J_k^{(\chi)})^2$, with the unresolved tail grouped as $j \geq 13$. The first odd toroidal mode carries nearly all of the resolved source norm. Panel (b) shows the scalar return residual after one and two source-cyclic Jacobi levels for the reduced spectral measure. The two-level continued fraction reproduces $R_\chi^{\rm red}$ at the displayed precision. The figure is diagnostic only; it illustrates the reduced numerical realization and does not replace the exact Galerkin or source-cyclic operator formulation.

scalar–vector lock calculation. On the cutoff $\mathcal{J}_{101}$, the weights

$$w_j = \frac{\left(J_j^{(\chi)}(\eta_0)\right)^2}{\sum_{k\in\mathcal{J}_{101}} \left(J_k^{(\chi)}(\eta_0)\right)^2}, \qquad \sum_{j\in\mathcal{J}_{101}} w_j = 1,$$

show how the theorem-defined Maxwell shell source is distributed over the resolved cutoff odd toroidal sector. The same cutoff-normalized weights define the moments used in the source-cyclic audit of the reduced numerical return law,

$$m_n = \sum_{j\in\mathcal{J}_{101}} w_j \, (g_j^{\rm red})^n, \qquad g_j^{\rm red} = 1 - \frac{1}{R_j^{\rm red}}.$$

Figure 9 displays both diagnostics. The first odd mode carries almost the entire resolved cutoff source norm, and the two-level Jacobi continued fraction reproduces the reported $R_\chi^{\rm red}$ at the displayed precision. This figure is diagnostic only; the exact definition of R_χ remains the operator resolvent in Eq. (383).

TABLE XVII. Top-level contribution breakdown for the current reduced cutoff realization of $\Lambda_{\rm geom}$ on the minimal electron branch. The percentage column reports the signed share of each contribution relative to the final reduced realization value.

Contribution	Formula / factor	Value	Share of $\Lambda_{\rm geom}^{(\rm th)}$
Intrinsic core	$\Lambda_{\rm ind}$	0.651806484604536015323410040051	94.234837%
UV-to-IR shell transfer	$\Delta\Lambda_{\rm UV\to IR}(\ell_0;\mathscr{A}_\parallel^{\rm coll}) = C_{\rm UV}^{(\rm Gauss)} P_{IR}^{(\chi)}(\ell_0)$	0.0544853495865520906532491466725	7.877212%
Exterior-memory contribution	$\Delta\Lambda_{\rm out}^{[101]}(\eta_0) R_\chi^{\rm red}$	-0.01460868880840970792604994790889	-2.112049%
Total reduced geometric constant	$\Lambda_{\rm geom}^{(\rm th)} \equiv \Lambda_{\rm geom}^{\rm red,[101]}$	**0.6916831461069910267161597**	100.000000%

TABLE XVIII. Internal decomposition of the reduced exterior-memory contribution. The cutoff identity used here is $\Delta\Lambda_{\rm out}^{[101]}(\eta_0) R_\chi^{\rm red} = \Delta\Lambda_{\rm out}^{[101]}(\eta_0) + \Delta\Lambda_{\rm out}^{[101]}(\eta_0)(R_\chi^{\rm red} - 1)$.

Contribution inside $\Delta\Lambda_{\rm out}^{[101]}(\eta_0) R_\chi^{\rm red}$	Formula / factor	Value	Share of $\Delta\Lambda_{\rm out}^{[101]}(\eta_0) R_\chi^{\rm red}$
Cutoff bare exterior subtraction	$\Delta\Lambda_{\rm out}^{[101]}(\eta_0)$	-0.0139671580625859302670846814886	95.608572%
Memory correction above cutoff exterior	$\Delta\Lambda_{\rm out}^{[101]}(\eta_0)(R_\chi^{\rm red} - 1)$	-0.000641530021511148993414797600296	4.391428%
Total reduced exterior-memory contribution	$\Delta\Lambda_{\rm out}^{[101]}(\eta_0) R_\chi^{\rm red}$	-0.01460868880840970792604994790889	100.000000%

Remark (Reduced realization and low-mode structure). The reported branch value $\Lambda_{\mathrm{geom}}^{(\mathrm{th})} \equiv \Lambda_{\mathrm{geom}}^{\mathrm{red},[101]}$ is obtained from the reduced vector-channel realization Eq. (406). The admitted weight $P_{IR}^{(\chi)}(\ell_0)$ is evaluated from the exact one-dimensional branch-cyclic Rayleigh law, whereas R_{χ}^{red} is evaluated as the resolvent of the reduced source-weighted spectral measure $\mathrm{d}\mu_{\chi,101}^{\mathrm{red}}$. The low-mode dominance seen in tables XIII and XIV follows from the Maxwell shell projection and the cutoff source normalization on the resolved odd sector. The Jacobi audit in table XVI shows that this reduced spectral measure is reproduced at the displayed precision by its rank-two Jacobi approximant. This statement concerns only the reduced spectral realization, not the exact operator R_{χ}. A full operator-level numerical evaluation would replace R_{χ}^{red} by the Galerkin limit of $\mathbb{G}_{\mathrm{sh}}$ from theorem 15, together with a certified tail bound. No measured value of α, no QED coefficient, and no scalar-channel target is used to tune the displayed vector data.

Part IV

Emergent Alpha

VIII. THE SHELL LOGARITHMIC COEFFICIENT $\mathcal{C}_{\log}$

Within the shell construction, $\mathcal{C}_{\log}$ denotes the coefficient of the canonical single-log response generated by the internal dilatation

$$\rho \mapsto s\rho, \qquad s > 1,$$

on the internal $\mathbb{C}$-plane. The symbol r is reserved for the radial coordinate of the pinned shell in $\mathbb{R}^3$. In Path I this coefficient is read through the infrared reporter

$$a_{\mathrm{rep}} \equiv \frac{g-2}{2},$$

understood only as the dimensionless coefficient of the Pauli slot in the infrared magnetic sector. This reporter is not assigned a measured value, and no perturbative QED coefficient is inserted into it. Its only role is to provide a gauge-invariant scalar readout for the canonical single-log shell response, because it vanishes in the Dirac limit and its leading local magnetic deviation occupies the Pauli slot identified in the infrared theory. After this reporter convention has been fixed, we write a for a_{rep} whenever no confusion can arise.

We use the logarithmic dilatation variable

$$\tau = \ln s.$$

The precise single-log projection used in Path I is stated below in definition VIII.1. Path I uses the retained shell vector polarization and the tangential-transverse shell feed into the scalar block to produce, under the stated Path-I closure assumptions, a remainder-controlled representative for the dependence of the canonical coefficient on the baseline scalar block $\mathcal{D}_{\mathrm{C}}$, the branch-fixed vector input Λ_{geom}, and the geometric shell constants. Thus $\mathcal{C}_{\log}^{(I)}$ is a representative with an explicit remainder, not an independent exact definition of $\mathcal{C}_{\log}$.

Path II computes the same canonical single-log coefficient from shell geometry alone. Within the stated single-polarization shell averaging class it gives

$$\mathcal{C}_{\log}^{(II)} = \frac{1}{3}$$

without using the vector-chain return or the scalar evaluator. The shell lock is the compatibility condition that identifies these two quantities as two readings of the same canonical coefficient. The vector input entering that lock is the already computed operator-level value Λ_{geom}, or a specified reduced realization of it when the numerical lock is evaluated; it is not an averaged or fitted vector input.

The dependency order in this section is as follows. The scalar overlap coefficient $\mathsf{K}_{\mathrm{ALP}}$ is computed from the reduced pinned line. The vector input enters Path I only through the already fixed shell-geometric datum Λ_{geom}, via $\zeta = \mathsf{K}_{\mathrm{ALP}}\Lambda_{\mathrm{geom}}/(2\pi^2)$. The metric toroidal weight C_χ is fixed by the minimal-branch phase-pinning convention. Path I then gives a representative $\mathcal{C}_{\log}^{(I)}(\mathcal{D}_{\mathrm{C}}, \zeta)$ with a controlled remainder. Path II independently gives $\mathcal{C}_{\log}^{(II)} = 1/3$ within the single-polarization shell average. The baseline Alpha Lock Point is obtained only after imposing the zeroth-discrepancy closure, namely after omitting ε_{I} from the primary algebraic lock equation while retaining it as a separate representative-remainder budget.

Remark (Why $a = (g-2)/2$ is a sufficient Path-I reporter). At infrared scales, within the local dimension-five magnetic sector specified in Eq. (138), the leading magnetic deviation from the minimally coupled Dirac branch enters through the Pauli slot. Hence the single dimensionless scalar

$$a \equiv \frac{g-2}{2}$$

records the leading infrared magnetic deviation used in Path I. This use of a is only a reporter convention for extracting the shell logarithm; it is not an external QED input and does not define $\mathcal{C}_{\log}$ independently of the shell response.

A. Path I from shell vector polarization

Path I isolates, within the retained shell-geometric representative, the coefficient of the single logarithm generated when the minimal branch is probed by a slow geometric dilatation on the internal $\mathbb{C}$-plane,

$$\rho \mapsto s\rho.$$

Here ρ denotes the radial coordinate in the internal generator plane, not the cylindrical radius used in the Maxwell shell formulas. The pinned shell in $\mathbb{R}^3$ is not reselected during this probe, and the vector datum Λ_{geom} is not recomputed along the dilatation. The question is how much toroidal tangential-transverse population is admitted by the shell under the internal dilatation and how that admitted population is read by the Coulombic slowdown block $\mathcal{D}_{\mathrm{C}}$. Since the radial half-line is counted with the scale-invariant measure $\mathrm{d}\rho/\rho$, the canonical first-order finite-dilatation count is proportional to $\ln s$. The dimensionless reporter a is used only to read off the corresponding shell logarithm when the canonical single-log projection of definition VIII.1 exists. No measured anomalous moment, QED anomaly coefficient, measured value of α, or fitted benchmark enters this extraction.

Definition VIII.1 (Canonical long piece)**.** Let $s > 1$ denote the geometric stretch $\rho \mapsto s\rho$ on the internal $\mathbb{C}$-plane, and let $a(s)$ denote the value of the dimensionless infrared reporter on the corresponding dilated pinned branch. The reporter is a formal shell-response slot in this subsection; it is not a measured electron anomaly. Let

$$\mathcal{D}_{\mathrm{C}}^{\mathrm{dil}}(s)$$

denote the scalar slowdown response of the already fixed pinned branch under the internal dilatation probe, and let

$$\mathcal{D}_{\mathrm{C}} \equiv \mathcal{D}_{\mathrm{C}}^{\mathrm{dil}}(1) > 0$$

denote the scalar slowdown block of the unscaled pinned branch. This baseline scalar block is held fixed in the normalization of the canonical single-log coefficient.

We say that the reporter admits a canonical single-log expansion if, for s sufficiently close to 1,

$$a(s) - a(1) = \mathcal{D}_{\mathrm{C}}^2\, \mathcal{C}_{\log}\, \ln s + R_{\log}(s), \qquad \lim_{s\to 1^+} \frac{R_{\log}(s)}{\ln s} = 0. \tag{420}$$

The canonical long piece is the term linear in $\ln s$,

$$\Delta a_{\log}(s) \equiv \mathcal{D}_{\mathrm{C}}^2\, \mathcal{C}_{\log}\, \ln s. \tag{421}$$

Equivalently, whenever the limit exists,

$$\mathcal{D}_{\mathrm{C}}^2\, \mathcal{C}_{\log} = \lim_{s\to 1^+} \frac{a(s) - a(1)}{\ln s}. \tag{422}$$

In particular, every contribution proportional to $(\ln s)^q$ with $q \geq 2$ is absorbed into $R_{\log}(s)$, since

$$(\ln s)^q = o(\ln s) \qquad \text{as} \qquad s \to 1^+.$$

Terms proportional to $\ln s$ with higher powers of another small parameter, such as $\zeta^3 \ln s$, are not removed by this projection; they contribute to the exact single-log coefficient unless they are included in a controlled representative remainder. Hence $\Delta a_{\log}(s)$ is the unique first-order logarithmic part of the dilatational response, whenever the limit in Eq. (422) exists.

Remark. The reference value

$$\mathcal{D}_{\mathrm{C}} = \mathcal{D}_{\mathrm{C}}^{\mathrm{dil}}(1)$$

is fixed before the dilatation is applied. This removes any ambiguity between the baseline scalar block and the dilated response $\mathcal{D}_{\mathrm{C}}^{\mathrm{dil}}(s)$ that enters the Path-I scale-flow formulas. The function $\mathcal{D}_{\mathrm{C}}^{\mathrm{dil}}(s)$ is not the scalar coupling branch $\mathcal{D}_{\mathrm{C}}(\alpha)$.

Definition VIII.2 (Reduced pinned line and overlap integrals)**.** On the reduced pinned line, written in the cavity coordinate

$$y = \frac{r}{r_*} \in (0,1), \qquad r \text{ the radial coordinate in } \mathbb{R}^3, \tag{423}$$

let

$$\phi_n(y) = \sqrt{2}\sin(n\pi y), \qquad n \in \mathbb{N}, \tag{424}$$

so that $\{\phi_n\}_{n\geq 1}$ is the Dirichlet eigenbasis of $-\pi^{-2}\partial_y^2$ with eigenvalues n^2. Let ϕ_1 be the minimal pinned mode and define

$$I_n = \int_0^1 y^2 \sin(\pi y)\sin(n\pi y)\,\mathrm{d}y = \frac{1}{2}\,\langle \phi_n, y^2\phi_1\rangle_{L^2(0,1;\mathrm{d}y)}. \tag{425}$$

Remark (Why the internal dilatation is read on the reduced line)*.* The geometric dilatation is imposed on the internal generator sector $\mathbb{C}$, whereas the scalar slowdown block $\mathcal{D}_{\mathrm{C}}$ is defined on the pinned shell in $\mathbb{R}^3$. The reduced line $y = r/r_*$ is the scalar carrier through which that internal shell feed is read on the pinned branch. Path I therefore does not introduce a second scalar problem. It probes how the dilatational shell feed excites the already fixed pinned scalar line above its ground mode.

Proposition 42 (Quadratic reduced-line source in Path I)**.** *In the scalar mother construction associated with the pinned shell in $\mathbb{R}^3$, the reduced bulk load is*

$$V^{\mathrm{red}}_{\mathrm{bulk}}(y) = 3 - y^2. \tag{426}$$

After the uniform part 3 has been separated into the already fixed Coulombic baseline, the first nonuniform shell profile is y^2, and the leading Path-I coupling from the pinned ground line to the excited Dirichlet ladder is

$$\langle \phi_n, y^2\phi_1\rangle_{L^2(0,1;\mathrm{d}y)} = 2I_n, \qquad n \geq 2. \tag{427}$$

If

$$P_\perp u = u - \langle \phi_1, u\rangle_{L^2(0,1;\mathrm{d}y)}\,\phi_1$$

denotes the orthogonal projection onto the excited Dirichlet sector, then the associated second-order admitted susceptibility, normalized by the reduced cavity operator $K_0 = -\pi^{-2}\partial_y^2$, is

$$\begin{aligned} \mathsf{K}_{ALP} &\equiv \frac{2}{\pi^2}\,\big\langle y^2\phi_1,\, P_\perp(K_0 - \mathbb{I}_{\mathrm{cav}})_\perp^{-1} P_\perp y^2\phi_1\big\rangle_{L^2(0,1;\mathrm{d}y)} \\ &= \frac{2}{\pi^2}\sum_{n=2}^{\infty}\frac{(2I_n)^2}{n^2-1}. \end{aligned} \tag{428}$$

Here

$$(K_0 - \mathbb{I}_{\mathrm{cav}})_\perp^{-1}$$

denotes the bounded inverse of $K_0 - \mathbb{I}_{\mathrm{cav}}$ restricted to the excited sector $\mathcal{H}_\perp = \{\phi_1\}^\perp$.

Proof. Equation (426) is the reduced bulk load derived in the scalar mother construction. Splitting

$$V^{\mathrm{red}}_{\mathrm{bulk}}(y) = 3 - y^2$$

into uniform and nonuniform parts, the constant term has no excited-sector matrix element. Indeed, for every $n \geq 2$,

$$\big\langle \phi_n, 3\phi_1\big\rangle_{L^2(0,1)} = 3\int_0^1 \big(\sqrt{2}\sin(n\pi y)\big)\big(\sqrt{2}\sin(\pi y)\big)\,\mathrm{d}y = 3\,\delta_{n1} = 0.$$

Thus the uniform part contributes only to the ground-line Coulombic baseline and does not drive any excited Dirichlet transition. The first nonuniform excited-sector source is therefore

$$P_\perp V^{\mathrm{red}}_{\mathrm{bulk}}\phi_1 = -P_\perp(y^2\phi_1).$$

Since the susceptibility below is quadratic in the transition amplitudes, the sign of this source drops out.

The reduced cavity operator satisfies

$$K_0\phi_n = n^2\phi_n, \qquad n \geq 1.$$

On the excited sector

$$\mathcal{H}_\perp = \{\phi_1\}^\perp \subset L^2(0,1;\mathrm{d}y),$$

the spectral gap is

$$n^2 - 1 \geq 3, \qquad n \geq 2.$$

Hence $K_0 - \mathbb{I}_{\mathrm{cav}}$ is boundedly invertible on $\mathcal{H}_\perp$, with

$$(K_0 - \mathbb{I}_{\mathrm{cav}})_\perp^{-1}\phi_n = \frac{1}{n^2-1}\phi_n, \qquad n \geq 2,$$

and

$$\left\|(K_0 - \mathbb{I}_{\mathrm{cav}})_\perp^{-1}\right\|_{\mathcal{H}_\perp \to \mathcal{H}_\perp} = \sup_{n\geq 2} \frac{1}{n^2-1} = \frac{1}{3}.$$

Since multiplication by y^2 is bounded on $L^2(0,1)$, the source $P_\perp(y^2\phi_1)$ belongs to $\mathcal{H}_\perp$, and its exact Dirichlet expansion is

$$P_\perp(y^2\phi_1) = \sum_{n=2}^{\infty} \langle \phi_n, y^2\phi_1\rangle_{L^2(0,1;\mathrm{d}y)}\, \phi_n$$

with convergence in $L^2(0,1)$. Using the definition of I_n,

$$\langle \phi_n, y^2\phi_1\rangle_{L^2(0,1;\mathrm{d}y)} = 2I_n, \qquad n \geq 2.$$

Therefore

$$\begin{aligned}
&\left\langle y^2\phi_1,\, P_\perp(K_0 - \mathbb{I}_{\mathrm{cav}})^{-1}P_\perp y^2\phi_1\right\rangle_{L^2(0,1;\mathrm{d}y)} \\
&\quad = \sum_{n=2}^{\infty} \frac{\left|\langle \phi_n, y^2\phi_1\rangle_{L^2(0,1;\mathrm{d}y)}\right|^2}{n^2-1} = \sum_{n=2}^{\infty} \frac{(2I_n)^2}{n^2-1}.
\end{aligned}$$

Multiplying by the normalization factor $2/\pi^2$ gives exactly Eq. (428). □

Remark. The role of $\mathsf{K}_{\mathrm{ALP}}$ is precise. It is not borrowed from the later scalar lock and it is not fitted. It is the exact quadratic susceptibility of the minimal pinned ground line under the first nonuniform shell load that remains after the uniform Coulombic part has been separated.

Lemma 26 (Closed form for I_n)**.** *For $n \in \mathbb{N} \setminus \{1\}$,*

$$I_n = -\frac{4(-1)^n n}{\pi^2(n^2-1)^2}. \tag{429}$$

Proof. Using $2\sin A \sin B = \cos(A-B) - \cos(A+B)$, one obtains

$$I_n = \frac{1}{2}\int_0^1 y^2\Big[\cos((n-1)\pi y) - \cos((n+1)\pi y)\Big]\mathrm{d}y.$$

For $m \in \mathbb{N}$, set

$$J_m = \int_0^1 y^2 \cos(m\pi y)\,\mathrm{d}y.$$

Then

$$\begin{aligned}
J_m &= \left[\frac{y^2 \sin(m\pi y)}{m\pi}\right]_0^1 - \frac{2}{m\pi}\int_0^1 y \sin(m\pi y)\,\mathrm{d}y \\
&= -\frac{2}{m\pi}\left\{\left[-\frac{y\cos(m\pi y)}{m\pi}\right]_0^1 + \frac{1}{m\pi}\int_0^1 \cos(m\pi y)\,\mathrm{d}y\right\}.
\end{aligned}$$

The first boundary term in J_m vanishes because $\sin(m\pi) = 0$, and the remaining cosine integral vanishes because

$$\int_0^1 \cos(m\pi y)\,\mathrm{d}y = \left[\frac{\sin(m\pi y)}{m\pi}\right]_0^1 = 0.$$

Therefore

$$J_m = \frac{2\cos(m\pi)}{(m\pi)^2} = \frac{2(-1)^m}{(m\pi)^2}.$$

Substituting $m = n-1$ and $m = n+1$ gives

$$\begin{aligned} I_n &= \frac{1}{2}\big(J_{n-1} - J_{n+1}\big) \\ &= \frac{(-1)^{n-1}}{\pi^2(n-1)^2} - \frac{(-1)^{n+1}}{\pi^2(n+1)^2}. \end{aligned}$$

Since $(-1)^{n-1} = (-1)^{n+1} = -(-1)^n$,

$$\begin{aligned} I_n &= -\frac{(-1)^n}{\pi^2}\left[\frac{1}{(n-1)^2} - \frac{1}{(n+1)^2}\right] \\ &= -\frac{(-1)^n}{\pi^2}\frac{(n+1)^2 - (n-1)^2}{(n^2-1)^2} \\ &= -\frac{4(-1)^n n}{\pi^2(n^2-1)^2}. \end{aligned}$$

This proves Eq. (429). □

Proposition 43 (Closed form and numerical value of K_{ALP})**.** *The series Eq.* (428) *converges absolutely and*

$$\mathsf{K}_{\text{ALP}} = \frac{128}{\pi^6}\sum_{n=2}^{\infty}\frac{n^2}{(n^2-1)^5} = \frac{150\pi^2 - 8\pi^4 - 315}{180\pi^6}. \tag{430}$$

Numerically,

$$\mathsf{K}_{\text{ALP}} = 0.0022315389165319701864087940 52\ldots,$$

where the displayed decimal is the rounded evaluation of the exact closed form Eq. (430)*.*

Proof. From Eq. (429),

$$(2I_n)^2 = \frac{64n^2}{\pi^4(n^2-1)^4}.$$

Thus

$$\mathsf{K}_{\text{ALP}} = \frac{2}{\pi^2}\sum_{n=2}^{\infty}\frac{(2I_n)^2}{n^2-1} = \frac{128}{\pi^6}\sum_{n=2}^{\infty}\frac{n^2}{(n^2-1)^5}.$$

For $n \geq 2$,

$$0 \leq \frac{n^2}{(n^2-1)^5} = \frac{n^2}{(n-1)^5(n+1)^5} \leq \frac{1}{(n-1)^8},$$

so the series converges absolutely by comparison with $\sum_{n\geq 2}(n-1)^{-8}$.

The summand has the partial-fraction decomposition

$$\begin{aligned} \frac{n^2}{(n^2-1)^5} = \frac{5}{256}&\left(\frac{1}{n+1} - \frac{1}{n-1}\right) + \frac{5}{256}\left(\frac{1}{(n+1)^2} + \frac{1}{(n-1)^2}\right) \\ &+ \frac{1}{128}\left(\frac{1}{(n+1)^3} - \frac{1}{(n-1)^3}\right) \\ &- \frac{1}{64}\left(\frac{1}{(n+1)^4} + \frac{1}{(n-1)^4}\right) + \frac{1}{32}\left(\frac{1}{(n-1)^5} - \frac{1}{(n+1)^5}\right). \end{aligned}$$

This identity is verified by multiplying both sides by $(n^2-1)^5$ and comparing the resulting polynomial in n.

Let ζ_{R} denote the Riemann zeta function. The telescoping and zeta sums are

$$\sum_{n=2}^{\infty}\left(\frac{1}{n+1}-\frac{1}{n-1}\right)=-\frac{3}{2},$$

$$\sum_{n=2}^{\infty}\left(\frac{1}{(n+1)^2}+\frac{1}{(n-1)^2}\right)=2\zeta_{\mathrm{R}}(2)-1-\frac{1}{4}=\frac{\pi^2}{3}-\frac{5}{4},$$

$$\sum_{n=2}^{\infty}\left(\frac{1}{(n+1)^3}-\frac{1}{(n-1)^3}\right)=-1-\frac{1}{8}=-\frac{9}{8},$$

$$\sum_{n=2}^{\infty}\left(\frac{1}{(n+1)^4}+\frac{1}{(n-1)^4}\right)=2\zeta_{\mathrm{R}}(4)-1-\frac{1}{16}=\frac{\pi^4}{45}-\frac{17}{16},$$

and

$$\sum_{n=2}^{\infty}\left(\frac{1}{(n-1)^5}-\frac{1}{(n+1)^5}\right)=1+\frac{1}{32}=\frac{33}{32}.$$

Combining these five identities gives

$$\sum_{n=2}^{\infty}\frac{n^2}{(n^2-1)^5}=-\frac{7}{512}+\frac{5\pi^2}{768}-\frac{\pi^4}{2880}.$$

Multiplication by $128/\pi^6$ yields

$$\mathsf{K}_{\text{ALP}}=\frac{150\pi^2-8\pi^4-315}{180\pi^6}.$$

The decimal value follows by direct evaluation. □

Corollary 8 (Exact spectral-overlap coefficient)**.** *Define*

$$\Upsilon_{\mathrm{sp}}=\frac{\mathsf{K}_{ALP}}{2\pi^2}. \tag{431}$$

Then

$$\Upsilon_{\mathrm{sp}}=0.00011305108218347960557155230557406412264 64\ldots,$$

where the displayed decimal is the rounded evaluation of the exact quotient $\Upsilon_{\mathrm{sp}}=\mathsf{K}_{ALP}/(2\pi^2)$.

Proof. This is an immediate consequence of Eq. (430). □

Definition VIII.3 (Vector input and overlap strength)**.** The vector-channel computation supplies the branch-fixed geometric constant Λ_{geom} already determined in the vector section. At the exact operator level this is the vector-side geometric input to the lock. In a finite-rank or theorem-level reduced numerical realization, the same formula is evaluated with the explicitly specified replacement $\Lambda_{\mathrm{geom}}\mapsto\Lambda_{\mathrm{geom}}^{(N)}$ or $\Lambda_{\mathrm{geom}}\mapsto\Lambda_{\mathrm{geom}}^{(\mathrm{th})}$. No averaged Λ, measured α, or QED coefficient enters this input.

With Υ_{sp} fixed by Eq. (431), define the exact overlap strength by

$$\zeta\equiv\zeta_{\mathrm{geom}}=\Upsilon_{\mathrm{sp}}\Lambda_{\mathrm{geom}}=\frac{\mathsf{K}_{\text{ALP}}}{2\pi^2}\Lambda_{\mathrm{geom}}. \tag{432}$$

The scalar ζ is the dimensionless tangential-transverse-to-scalar overlap strength carried by the shell vector channel of the minimal branch in $\mathbb{R}^3$. It is fixed before the Path-I dilatation is applied. Its reduced numerical descendants are obtained only by the explicit replacements of the vector input stated above.

Definition VIII.4 (Minimal toroidal shell weight)**.** Let $\Theta(\phi)$ denote the unwrapped metric phase-length coordinate associated with the one-loop carrier along the pinned shell azimuth ϕ. This coordinate is not the compact generator phase θ_0, and it is not required to close after an integer multiple of 2π when ϕ runs once around the shell. The minimal toroidal shell weight is the metric phase-Jacobian integral

$$C_\chi = \int_0^{2\pi} \frac{\mathrm{d}\Theta}{\mathrm{d}\phi}\,\mathrm{d}\phi. \tag{433}$$

This quantity measures the metric phase weight exported to the toroidal shell channel. It is a geometric weight, not a topological winding number.

Proposition 44 (Pinned value of C_χ)**.** *Adopt the minimal-branch metric phase-pinning convention*

$$R\,\mathrm{d}\Theta = r_*\,\mathrm{d}\phi. \tag{434}$$

This convention identifies the internal phase arc length on the carrier with the corresponding pinned shell azimuthal arc length. Then, since $r_* = \pi R$,

$$\frac{\mathrm{d}\Theta}{\mathrm{d}\phi} = \frac{r_*}{R} = \pi, \qquad C_\chi = 2\pi^2. \tag{435}$$

This is the minimal metric toroidal weight of the baseline branch.

Proof. From Eq. (434),

$$\frac{\mathrm{d}\Theta}{\mathrm{d}\phi} = \frac{r_*}{R}.$$

Using the minimal-branch relation $r_* = \pi R$ from Eq. (139), one obtains

$$\frac{\mathrm{d}\Theta}{\mathrm{d}\phi} = \pi.$$

Inserting this into Eq. (433) gives

$$C_\chi = \int_0^{2\pi} \pi\,\mathrm{d}\phi = 2\pi^2.$$

This proves Eq. (435). □

Remark. The role of C_χ is purely geometric. It supplies the metric toroidal phase weight retained by the minimal shell pinning. Any angular corrugation of the swirl changes this weight only through higher projector contractions and therefore begins beyond the baseline linear TT response.

Definition VIII.5 (Signed admitted toroidal response under dilatation)**.** For a geometric stretch $\rho \mapsto s\rho$ on the internal $\mathbb{C}$-plane, with $s > 1$, the branch-fixed overlap strength ζ is held fixed. Equivalently, the dilatation probe counts the admitted logarithmic population on the already fixed vector-shell datum, rather than recomputing Λ_{geom} along the probe. Here ρ and ρ_0 are internal generator-plane radii. Fix any reference radius $\rho_0 > 0$ and define the signed admitted toroidal response by

$$N_{\mathrm{tor}}(s) = \zeta \int_{\rho_0}^{s\rho_0} \frac{\mathrm{d}\rho}{\rho} \int_0^{2\pi} \frac{\mathrm{d}\Theta}{\mathrm{d}\phi}\,\mathrm{d}\phi. \tag{436}$$

Since the radial measure is scale-invariant,

$$\int_{\rho_0}^{s\rho_0} \frac{\mathrm{d}\rho}{\rho} = \ln s, \tag{437}$$

so $N_{\mathrm{tor}}(s)$ is independent of ρ_0. On the minimal branch, Eq. (435) gives

$$N_{\mathrm{tor}}(s) = C_\chi\,\zeta\,\ln s. \tag{438}$$

Remark. The logarithm is not inserted by hand. It is the unique finite count generated by the scale-invariant radial measure $\mathrm{d}\rho/\rho$ under a finite dilatation on $\mathbb{C}$.

Remark. The use of $\partial_\tau \ln \mathcal{D}_\mathrm{C}$, rather than $\partial_\tau \mathcal{D}_\mathrm{C}$, follows from the role assigned to $\mathcal{D}_\mathrm{C}$ in this retained shell response model. The scalar block is a positive dimensionless slowdown factor, not an extensive energy. Successive dilatations are represented multiplicatively, so the natural first-order scale-flow law is written for $\ln \mathcal{D}_\mathrm{C}$. This is a Path-I closure convention, not a general identity for all scalar-channel realizations.

Definition VIII.6 (Single-log extraction operator)**.** For a function $F(s)$ defined for $s > 1$ sufficiently close to 1, with $F(s) = O(\ln s)$ as $s \to 1^+$, we write

$$\mathsf{L}_1[F](s) = c_1 \ln s$$

whenever the limit

$$c_1 = \lim_{\sigma \to 1^+} \frac{F(\sigma)}{\ln \sigma}$$

exists. Equivalently,

$$F(s) = \mathsf{L}_1[F](s) + o(\ln s) \qquad (s \to 1^+).$$

Thus L_1 keeps only the canonical term linear in $\ln s$ and removes powers $(\ln s)^q$ with $q \geq 2$.

Condition VIII.1 (Retained Path-I multiplicative scale-flow closure)**.** Write

$$\tau = \ln s.$$

Let

$$\mathcal{D}_\mathrm{C}^{\mathrm{dil}}(e^\tau)$$

denote the scalar slowdown response of the already fixed pinned branch under the internal dilatation probe, with baseline value

$$\mathcal{D}_\mathrm{C}^{\mathrm{dil}}(1) = \mathcal{D}_\mathrm{C} > 0.$$

This response variable is distinct from the scalar coupling branch $\mathcal{D}_\mathrm{C}(\alpha)$. In the retained Path-I representative, the signed admitted toroidal response enters the scalar block through the multiplicative shell closure

$$\frac{\mathrm{d}}{\mathrm{d}\tau} \ln\!\big(\mathcal{D}_\mathrm{C}^{\mathrm{dil}}(e^\tau)\big) = \frac{\mathrm{d}}{\mathrm{d}\tau} N_{\mathrm{tor}}(e^\tau) + \mathcal{R}_D(\tau, \zeta), \qquad |\mathcal{R}_D(\tau, \zeta)| \leq C_D |\zeta|^3, \tag{439}$$

uniformly for bounded $|\tau|$. We also assume that the averaged remainder has a right single-log coefficient,

$$r_D^{(1)}(\zeta) := \lim_{\tau \to 0^+} \frac{1}{\tau} \int_0^\tau \mathcal{R}_D(\tau', \zeta)\, \mathrm{d}\tau', \qquad |r_D^{(1)}(\zeta)| \leq C_D |\zeta|^3.$$

The absence of an independent $O(\zeta^2)$ term in this retained scale-flow law is part of the stated Path-I representative closure. It is not imported from QED, not fitted to a measured anomaly, and not used in Path II.

Proposition 45 (Single-log consequence of the retained Path-I scale flow)**.** *Define the finite dilatational scalar-response increment by*

$$\Delta_{\mathrm{dil}} \mathcal{D}_\mathrm{C}(s) := \mathcal{D}_\mathrm{C}^{\mathrm{dil}}(s) - \mathcal{D}_\mathrm{C}.$$

Under Condition VIII.1, and for $s = e^\tau > 1$ with $|\tau|$ in a fixed bounded interval on which Eq. (439) *holds, one has*

$$\frac{\mathrm{d}}{\mathrm{d} \ln s} \ln\!\big(\mathcal{D}_\mathrm{C}^{\mathrm{dil}}(s)\big) = C_\chi\, \zeta + \mathcal{R}_D(\ln s, \zeta), \qquad \big|\mathcal{R}_D(\ln s, \zeta)\big| \leq C_D |\zeta|^3. \tag{440}$$

Moreover, the canonical single-log part of the finite increment is

$$\mathsf{L}_1[\Delta_{\mathrm{dil}} \mathcal{D}_\mathrm{C}](s) = \mathcal{D}_\mathrm{C}\big(C_\chi\, \zeta + r_D^{(1)}(\zeta)\big) \ln s, \qquad \big|r_D^{(1)}(\zeta)\big| \leq C_D |\zeta|^3. \tag{441}$$

Equivalently,

$$|\mathsf{L}_1[\Delta_{\mathrm{dil}} \mathcal{D}_\mathrm{C}](s) - \mathcal{D}_\mathrm{C}\, C_\chi\, \zeta\, \ln s| \leq C_D\, \mathcal{D}_\mathrm{C}\, |\zeta|^3\, |\ln s|.$$

Proof. From Eq. (438),

$$N_{\mathrm{tor}}(e^{\tau}) = C_{\chi}\,\zeta\,\tau.$$

Hence

$$\frac{\mathrm{d}}{\mathrm{d}\tau} N_{\mathrm{tor}}(e^{\tau}) = C_{\chi}\,\zeta.$$

Substituting this into Eq. (439) gives

$$\frac{\mathrm{d}}{\mathrm{d}\tau}\ln\!\big(\mathcal{D}_{\mathrm{C}}^{\mathrm{dil}}(e^{\tau})\big) = C_{\chi}\,\zeta + \mathcal{R}_D(\tau,\zeta), \qquad |\mathcal{R}_D(\tau,\zeta)| \le C_D|\zeta|^3.$$

Integrating from 0 to $\tau = \ln s$ yields

$$\ln\frac{\mathcal{D}_{\mathrm{C}}^{\mathrm{dil}}(s)}{\mathcal{D}_{\mathrm{C}}} = C_{\chi}\,\zeta\,\ln s + \int_0^{\ln s} \mathcal{R}_D(\tau',\zeta)\,\mathrm{d}\tau'.$$

By the definition of $r_D^{(1)}(\zeta)$ in Condition VIII.1,

$$\frac{1}{\ln s}\int_0^{\ln s} \mathcal{R}_D(\tau',\zeta)\,\mathrm{d}\tau' = r_D^{(1)}(\zeta) + o(1) \qquad (s \to 1^+).$$

Therefore

$$\ln\frac{\mathcal{D}_{\mathrm{C}}(s)}{\mathcal{D}_{\mathrm{C}}} = \big(C_{\chi}\,\zeta + r_D^{(1)}(\zeta)\big)\ln s + o(\ln s).$$

Set

$$L(s) \coloneqq \big(C_{\chi}\,\zeta + r_D^{(1)}(\zeta)\big)\ln s + o(\ln s).$$

Then

$$\mathcal{D}_{\mathrm{C}}^{\mathrm{dil}}(s) = \mathcal{D}_{\mathrm{C}}\,e^{L(s)}, \qquad \Delta_{\mathrm{dil}}\mathcal{D}_{\mathrm{C}}(s) = \mathcal{D}_{\mathrm{C}}\big(e^{L(s)} - 1\big).$$

Since $L(s) = O(\ln s)$ as $s \to 1^+$, one has

$$e^{L(s)} - 1 = L(s) + O\big(L(s)^2\big),$$

and therefore

$$\Delta_{\mathrm{dil}}\mathcal{D}_{\mathrm{C}}(s) = \mathcal{D}_{\mathrm{C}}\,L(s) + O\big(\mathcal{D}_{\mathrm{C}}\,L(s)^2\big).$$

Because $L(s)^2 = o(\ln s)$, the quadratic term has zero canonical single-log projection. Hence

$$\mathsf{L}_1[\Delta_{\mathrm{dil}}\mathcal{D}_{\mathrm{C}}](s) = \mathcal{D}_{\mathrm{C}}\big(C_{\chi}\,\zeta + r_D^{(1)}(\zeta)\big)\ln s.$$

The bound

$$\big|r_D^{(1)}(\zeta)\big| \le C_D|\zeta|^3$$

is part of Condition VIII.1, so the displayed estimate for the difference from $\mathcal{D}_{\mathrm{C}}\,C_{\chi}\,\zeta\,\ln s$ follows immediately. □

Remark. Equation (440) is the shell analogue of a leading logarithmic response law. For intuition only, one may compare this with the way single-log terms arise from polarization weights in standard QED. Here the coefficient is not diagrammatic, no QED coefficient is imported, and no measured anomaly is used. It is purely shell-geometric within the retained Path-I representative.

Condition VIII.2 (Retained minimal toroidal synchronization linearization)**.** On the axisymmetric minimal one-loop branch, let H_{tor} denote the leading admitted toroidal TT shell line, equipped with its shell Hilbert inner product $\langle\cdot,\cdot\rangle_{H_{\mathrm{tor}}}$. In the retained Path-I linearization, higher toroidal lines are represented by the explicit controlled remainder below. Let $\psi_{\mathrm{tor}} \in H_{\mathrm{tor}}$ be normalized by

$$\|\psi_{\mathrm{tor}}\|_{H_{\mathrm{tor}}} = 1,$$

and define the rank-one orthogonal projector

$$\Pi_{\mathrm{tor}} u = \langle \psi_{\mathrm{tor}}, u\rangle_{H_{\mathrm{tor}}}\, \psi_{\mathrm{tor}}. \tag{442}$$

The linearized synchronization kernel is

$$\mathsf{K}_{\mathrm{TT}} = \mathbb{I}_{H_{\mathrm{tor}}} + \zeta\,\Pi_{\mathrm{tor}} + \mathcal{E}_{\mathrm{tor}}(\zeta), \qquad \|\mathcal{E}_{\mathrm{tor}}(\zeta)\|_{H_{\mathrm{tor}}\to H_{\mathrm{tor}}} \le C_{\mathrm{tor}}|\zeta|^2. \tag{443}$$

The dressed reporter slope is

$$\left(\frac{\partial a}{\partial \mathcal{D}_{\mathrm{C}}}\right)_{\mathrm{dressed}} = \frac{1}{2}\,\langle \psi_{\mathrm{tor}}, \mathsf{K}_{\mathrm{TT}}\psi_{\mathrm{tor}}\rangle_{H_{\mathrm{tor}}}. \tag{444}$$

Proposition 46 (Dressed slope on the minimal toroidal branch)**.** *Under the retained synchronization model of Eq.* (443)*, one has*

$$\left(\frac{\partial a}{\partial \mathcal{D}_{\mathrm{C}}}\right)_{\mathrm{dressed}} = \frac{1}{2}(1+\zeta) + O(\zeta^2). \tag{445}$$

This is a retained Path-I reporter slope, not a QED anomaly coefficient and not a measured magnetic-moment input.

Proof. Since Π_{tor} is the orthogonal projector onto the one-dimensional span of ψ_{tor},

$$\Pi_{\mathrm{tor}}\psi_{\mathrm{tor}} = \psi_{\mathrm{tor}}.$$

Using $\|\psi_{\mathrm{tor}}\|_{H_{\mathrm{tor}}} = 1$, we obtain

$$\begin{aligned}\langle \psi_{\mathrm{tor}}, \mathsf{K}_{\mathrm{TT}}\psi_{\mathrm{tor}}\rangle_{H_{\mathrm{tor}}} &= \langle \psi_{\mathrm{tor}}, \big(\mathbb{I}_{H_{\mathrm{tor}}} + \zeta\Pi_{\mathrm{tor}} + \mathcal{E}_{\mathrm{tor}}(\zeta)\big)\psi_{\mathrm{tor}}\rangle_{H_{\mathrm{tor}}}\\ &= 1 + \zeta + \langle \psi_{\mathrm{tor}}, \mathcal{E}_{\mathrm{tor}}(\zeta)\psi_{\mathrm{tor}}\rangle_{H_{\mathrm{tor}}}.\end{aligned}$$

The operator bound in Eq. (443) gives

$$|\langle \psi_{\mathrm{tor}}, \mathcal{E}_{\mathrm{tor}}(\zeta)\psi_{\mathrm{tor}}\rangle_{H_{\mathrm{tor}}}| \le \|\mathcal{E}_{\mathrm{tor}}(\zeta)\|_{H_{\mathrm{tor}}\to H_{\mathrm{tor}}}\|\psi_{\mathrm{tor}}\|^2_{H_{\mathrm{tor}}} \le C_{\mathrm{tor}}|\zeta|^2.$$

Hence

$$\langle \psi_{\mathrm{tor}}, \mathsf{K}_{\mathrm{TT}}\psi_{\mathrm{tor}}\rangle_{H_{\mathrm{tor}}} = 1 + \zeta + O(\zeta^2).$$

Inserting this into Eq. (444) gives

$$\left(\frac{\partial a}{\partial \mathcal{D}_{\mathrm{C}}}\right)_{\mathrm{dressed}} = \frac{1}{2}(1+\zeta) + O(\zeta^2).$$

This proves Eq. (445). ☐

Remark. The one-dimensional projector Π_{tor} is not fitted. It selects the leading axisymmetric toroidal TT line of the minimal branch. In the retained Path-I synchronization model, higher toroidal sectors are accounted for by the explicit operator-norm remainder in Eq. (443).

Theorem 17 (Remainder-controlled Path-I formula)**.** *Assume the hypotheses of propositions 45 and 46. Assume moreover that, in the Path-I regime and for* $s > 1$ *sufficiently close to* 1*, the canonical single-log increment of the reporter,* $\Delta a_{\log}(s)$ *from Eq.* (421)*, admits the first-order dressed scalar linearization*

$$\Delta a_{\log}(s) = \left(\frac{\partial a}{\partial \mathcal{D}_{\mathrm{C}}}\right)_{\mathrm{dressed}} \mathsf{L}_1[\Delta_{\mathrm{dil}}\mathcal{D}_{\mathrm{C}}](s) + r_a(s), \qquad |r_a(s)| \le C_a\,\mathcal{D}_{\mathrm{C}}\,|\zeta|^3|\ln s|. \tag{446}$$

If $|\zeta| \le \zeta_0 \le 1$*, then there exists a constant* $C_{\mathrm{I}} > 0$*, depending only on* ζ_0*,* $|C_\chi|$*,* C_a*,* C_{tor}*, and the constants appearing in Condition VIII.1, such that*

$$\left|\Delta a_{\log}(s) - \frac{1}{2}(1+\zeta)\,\mathcal{D}_{\mathrm{C}}\left(C_\chi\,\zeta\,\ln s\right)\right| \le C_{\mathrm{I}}\,\mathcal{D}_{\mathrm{C}}\,|\zeta|^3\,|\ln s| \tag{447}$$

for all $s > 1$ *sufficiently close to* 1 *within that regime.*

Proof. By Eq. (441),

$$\mathsf{L}_1[\Delta\mathcal{D}_{\mathrm{C}}](s) = \mathcal{D}_{\mathrm{C}}\big(C_\chi\,\zeta + r_D^{(1)}(\zeta)\big)\ln s, \qquad |r_D^{(1)}(\zeta)| \le C_D|\zeta|^3.$$

By Eq. (445), there exists r_2 such that

$$\left(\frac{\partial a}{\partial\mathcal{D}_{\mathrm{C}}}\right)_{\text{dressed}} = \frac{1}{2}(1+\zeta) + r_2, \qquad |r_2| \le C_2|\zeta|^2.$$

Using Eq. (446), we obtain

$$\Delta a_{\log}(s) = \left(\frac{1}{2}(1+\zeta) + r_2\right)\mathcal{D}_{\mathrm{C}}\big(C_\chi\,\zeta + r_D^{(1)}(\zeta)\big)\ln s + r_a(s).$$

Subtracting the leading representative term gives

$$\begin{aligned}\Delta a_{\log}(s) - \frac{1}{2}(1+\zeta)\,\mathcal{D}_{\mathrm{C}}\,(C_\chi\,\zeta\,\ln s) = {}& \frac{1}{2}(1+\zeta)\,\mathcal{D}_{\mathrm{C}}\,r_D^{(1)}(\zeta)\,\ln s \\ &+ r_2\,\mathcal{D}_{\mathrm{C}}\,C_\chi\,\zeta\,\ln s + r_2\,\mathcal{D}_{\mathrm{C}}\,r_D^{(1)}(\zeta)\,\ln s + r_a(s).\end{aligned}$$

Since $|\zeta| \le \zeta_0 \le 1$, one has $|1+\zeta| \le 2$. Therefore

$$\left|\frac{1}{2}(1+\zeta)\,\mathcal{D}_{\mathrm{C}}\,r_D^{(1)}(\zeta)\,\ln s\right| \le C_D\,\mathcal{D}_{\mathrm{C}}\,|\zeta|^3|\ln s|,$$

$$|r_2\,\mathcal{D}_{\mathrm{C}}\,C_\chi\,\zeta\,\ln s| \le C_2|C_\chi|\,\mathcal{D}_{\mathrm{C}}\,|\zeta|^3|\ln s|,$$

$$|r_2\,\mathcal{D}_{\mathrm{C}}\,r_D^{(1)}(\zeta)\,\ln s| \le C_2C_D\,\mathcal{D}_{\mathrm{C}}\,|\zeta|^5|\ln s| \le C_2C_D\,\mathcal{D}_{\mathrm{C}}\,|\zeta|^3|\ln s|,$$

and

$$|r_a(s)| \le C_a\,\mathcal{D}_{\mathrm{C}}\,|\zeta|^3|\ln s|.$$

Summing these four bounds yields Eq. (447). □

Corollary 9 (Remainder-controlled Path-I representative)**.** *Assume the hypotheses of theorem 17, with $\mathcal{D}_{\mathrm{C}} > 0$. Define the retained Path-I representative of the canonical logarithmic coefficient by*

$$\mathcal{C}_{\log}^{(I)}(\mathcal{D}_{\mathrm{C}},\zeta) = \frac{C_\chi}{2\mathcal{D}_{\mathrm{C}}}\,\zeta(1+\zeta). \tag{448}$$

Then there exists a constant $C_{\mathrm{I}}' > 0$, depending only on the constants in theorem 17, such that

$$\left|\mathcal{C}_{\log} - \mathcal{C}_{\log}^{(I)}(\mathcal{D}_{\mathrm{C}},\zeta)\right| \le C_{\mathrm{I}}'\,\frac{|\zeta|^3}{\mathcal{D}_{\mathrm{C}}}. \tag{449}$$

In particular, on the minimal pinned-shell baseline where $C_\chi = 2\pi^2$, one obtains

$$\boxed{\mathcal{C}_{\log}^{(I)}(\mathcal{D}_{\mathrm{C}},\zeta) = \frac{\pi^2}{\mathcal{D}_{\mathrm{C}}}\,\zeta(1+\zeta)} \qquad [\ \textbf{Path I}\ ], \qquad \zeta = \frac{\mathsf{K}_{ALP}\Lambda_{\mathrm{geom}}}{2\pi^2}. \tag{450}$$

This is the baseline Path-I representative. In a reduced vector realization, this displayed formula is evaluated only after the explicit replacement

$$\Lambda_{\mathrm{geom}} \longmapsto \Lambda_{\mathrm{geom}}^{(N)} \quad \textit{or} \quad \Lambda_{\mathrm{geom}}^{(\mathrm{th})}$$

has been stated. Such a replacement changes only the vector input used in ζ; it does not redefine the Path-I coefficient formula and it does not introduce a measured value of α.

Proof. By Eq. (421),

$$\Delta a_{\log}(s) = \mathcal{D}_{\mathrm{C}}^2 \mathcal{C}_{\log} \ln s.$$

Combining this exact identity with Eq. (447) gives

$$\left| \mathcal{D}_{\mathrm{C}}^2 \mathcal{C}_{\log} \ln s - \frac{1}{2}(1+\zeta)\, \mathcal{D}_{\mathrm{C}} \left(C_\chi \zeta \ln s \right) \right| \leq C_{\mathrm{I}}\, \mathcal{D}_{\mathrm{C}}\, |\zeta|^3 |\ln s|.$$

For $s > 1$ sufficiently close to 1, one has $\ln s > 0$. Dividing by $\mathcal{D}_{\mathrm{C}}^2 \ln s$, and using $\mathcal{D}_{\mathrm{C}} > 0$, yields

$$\left| \mathcal{C}_{\log} - \frac{C_\chi}{2\mathcal{D}_{\mathrm{C}}}\, \zeta(1+\zeta) \right| \leq C_{\mathrm{I}} \frac{|\zeta|^3}{\mathcal{D}_{\mathrm{C}}}.$$

This proves Eq. (449), with $C'_{\mathrm{I}} = C_{\mathrm{I}}$. Equation (450) follows from Eq. (435). □

Remark. The quantities $\mathsf{K}_{\mathrm{ALP}}$, Υ_{sp}, ζ, and C_χ are geometric inputs of Path I within the stated shell construction. The hypotheses used in Conditions VIII.1 and VIII.2 and theorem 17 are retained Path-I assumptions. Accordingly, $\mathcal{C}_{\log}^{(I)}(\mathcal{D}_{\mathrm{C}}, \zeta)$ is a controlled representative of the canonical logarithmic coefficient, with reporter-level remainder bounded by Eq. (449); it is not an independent exact value of $\mathcal{C}_{\log}$. The vector input remains Λ_{geom} at the exact operator level, with reduced numerical descendants obtained only by explicit replacement of that input. No measured α, QED anomaly coefficient, or fitted reporter datum enters Path I.

B. Path II from shell geometry

Path II is the shell-geometric route that computes the canonical logarithmic coefficient within a specified single-polarization shell averaging class. It does not use Λ_{geom}, $\mathcal{D}_{\mathrm{C}}$, the scalar evaluator, the vector-memory inversion, a measured value of α, or any QED coefficient. Its purpose is to compute the single-log shell average produced by one instantaneous tangential polarization on the matching sphere, integrated against the scale-invariant radial measure $\mathrm{d}\rho/\rho$. Within the stated averaging class, the result is exact and yields the geometric value 1/3. Its later identification with the Path-I representative is a consistency statement, not an input to the present calculation.

Condition VIII.3 (Path-II single-polarization shell averaging class)**.** The Path-II computation uses the following geometric averaging class. The shell normal $\hat{n}$ is averaged uniformly over $\mathbb{S}^2$; the local in-plane polarization phase is averaged uniformly over $[0, 2\pi)$; and the radial dilatation count is taken with the scale-invariant measure $\mathrm{d}\rho/\rho$. Exactly one instantaneous rank-one tangential polarization is counted at each shell point. With the notation defined below in definitions VIII.7 and VIII.8, and with the phase average evaluated in proposition 47, this convention is represented by

$$\left\langle \hat{\tau}(\varphi)\hat{\tau}(\varphi)^\top \right\rangle_\varphi = \frac{1}{2} P_T(\hat{n}), \qquad \langle X \rangle_\varphi \equiv \frac{1}{2\pi} \int_0^{2\pi} X(\varphi)\, \mathrm{d}\varphi.$$

The factor 1/2 is therefore the result of averaging one instantaneous rank-one tangent direction over its in-plane phase, not an externally supplied degeneracy factor. This is the defining Path-II averaging class. It is not imported from QED and it is not a fitted polarization multiplicity.

Definition VIII.7 (Local tangent projector)**.** At a point of the matching shell let $\hat{n} \in \mathbb{S}^2$ be the outward unit normal. The orthogonal projector from $\mathbb{R}^3$ onto the tangent plane $T_{\hat{n}}\mathbb{S}^2$ is

$$P_T(\hat{n}) = \mathbb{I}_3 - \hat{n}\hat{n}^\top. \tag{451}$$

Definition VIII.8 (Instantaneous in-plane polarization direction)**.** Choose any orthonormal basis $\{\hat{\tau}_1, \hat{\tau}_2\}$ of the tangent plane $T_{\hat{n}}\mathbb{S}^2$. For $\varphi \in [0, 2\pi)$, define the unit in-plane polarization direction

$$\hat{\tau}(\varphi) = \cos\varphi\, \hat{\tau}_1 + \sin\varphi\, \hat{\tau}_2. \tag{452}$$

Its associated rank-one projector is

$$\hat{\tau}(\varphi)\hat{\tau}(\varphi)^\top.$$

The angle φ is a local polarization phase. It is distinct from the shell azimuth, from the compact generator phase θ_0, and from any electromagnetic gauge phase used elsewhere in the paper.

Proposition 47 (Uniform in-plane average)**.** *Under the uniform phase average on the tangent plane,*

$$\langle X\rangle_\varphi \equiv \frac{1}{2\pi}\int_0^{2\pi} X(\varphi)\,\mathrm{d}\varphi,$$

one has

$$\left\langle \hat\tau(\varphi)\hat\tau(\varphi)^\top \right\rangle_\varphi = \frac{1}{2}\,P_T(\hat n). \tag{453}$$

In particular, the phase average is intrinsic and does not depend on the chosen orthonormal tangent basis.

Proof. Expanding $\hat\tau(\varphi)\hat\tau(\varphi)^\top$ gives

$$\begin{aligned}\hat\tau(\varphi)\hat\tau(\varphi)^\top =\;& \cos^2\varphi\,\hat\tau_1\hat\tau_1^\top + \sin^2\varphi\,\hat\tau_2\hat\tau_2^\top \\ & + \sin\varphi\cos\varphi\left(\hat\tau_1\hat\tau_2^\top + \hat\tau_2\hat\tau_1^\top\right).\end{aligned}$$

Using

$$\frac{1}{2\pi}\int_0^{2\pi}\cos^2\varphi\,\mathrm{d}\varphi = \frac{1}{2}, \qquad \frac{1}{2\pi}\int_0^{2\pi}\sin^2\varphi\,\mathrm{d}\varphi = \frac{1}{2}, \qquad \frac{1}{2\pi}\int_0^{2\pi}\sin\varphi\cos\varphi\,\mathrm{d}\varphi = 0,$$

one finds

$$\left\langle \hat\tau(\varphi)\hat\tau(\varphi)^\top \right\rangle_\varphi = \frac{1}{2}\left(\hat\tau_1\hat\tau_1^\top + \hat\tau_2\hat\tau_2^\top\right).$$

Since $\{\hat\tau_1, \hat\tau_2\}$ is an orthonormal basis of $T_{\hat n}\mathbb{S}^2$, the sum in parentheses is exactly $P_T(\hat n)$. This proves Eq. (453). $\square$

Definition VIII.9 (Local overlap amplitude and logarithmic density)**.** Fix a unit test vector $\hat u \in \mathbb{R}^3$, independent of the shell normal $\hat n$. The vector $\hat u$ is used only to probe the rotational average. It is not a preferred branch direction and not an empirical polarization axis. For the instantaneous in-plane polarization $\hat\tau(\varphi)$, define the local overlap amplitude

$$A(\hat u, \hat n, \varphi) \equiv \hat u \cdot \hat\tau(\varphi). \tag{454}$$

The local shell overlap density with respect to the logarithmic radial count $\mathrm{d}\rho/\rho$ is the phase-averaged squared overlap

$$W(\hat u, \hat n) \equiv \frac{1}{2\pi}\int_0^{2\pi}\left(A(\hat u, \hat n, \varphi)\right)^2\mathrm{d}\varphi. \tag{455}$$

Proposition 48 (Closed form of the local overlap density)**.** *For every fixed unit vector $\hat u$ and shell normal $\hat n$,*

$$W(\hat u, \hat n) = \hat u^\top\left(\frac{1}{2}P_T(\hat n)\right)\hat u = \frac{1}{2}\Big(1 - (\hat u\cdot\hat n)^2\Big). \tag{456}$$

Proof. Using Eq. (455), one has

$$\begin{aligned}W(\hat u, \hat n) &= \frac{1}{2\pi}\int_0^{2\pi}\left(\hat u\cdot\hat\tau(\varphi)\right)^2\mathrm{d}\varphi \\ &= \frac{1}{2\pi}\int_0^{2\pi}\hat u^\top\hat\tau(\varphi)\hat\tau(\varphi)^\top\hat u\,\mathrm{d}\varphi \\ &= \hat u^\top\left(\frac{1}{2\pi}\int_0^{2\pi}\hat\tau(\varphi)\hat\tau(\varphi)^\top\,\mathrm{d}\varphi\right)\hat u.\end{aligned}$$

By Eq. (453),

$$\frac{1}{2\pi}\int_0^{2\pi}\hat\tau(\varphi)\hat\tau(\varphi)^\top\,\mathrm{d}\varphi = \frac{1}{2}P_T(\hat n).$$

Therefore

$$W(\hat u, \hat n) = \hat u^\top\left(\frac{1}{2}P_T(\hat n)\right)\hat u.$$

Using Eq. (451),

$$\begin{aligned} W(\hat{u},\hat{n}) &= \frac{1}{2}\hat{u}^\top\big(\mathbb{I}_3 - \hat{n}\hat{n}^\top\big)\hat{u} \\ &= \frac{1}{2}\Big(\hat{u}^\top\hat{u} - \hat{u}^\top\hat{n}\hat{n}^\top\hat{u}\Big) \\ &= \frac{1}{2}\Big(1-(\hat{u}\cdot\hat{n})^2\Big), \end{aligned}$$

since $\hat{u}$ is a unit vector. This proves Eq. (456). □

Lemma 27 (Spherical average of the normal dyad and tangent projector)**.** *For any integrable field $F(\hat{n})$ on $\mathbb{S}^2$, define*

$$\langle F\rangle_{\mathbb{S}^2} \equiv \frac{1}{4\pi}\int_{\mathbb{S}^2} F(\hat{n})\,\mathrm{d}\Omega.$$

Then

$$\langle \hat{n}_i\hat{n}_j\rangle_{\mathbb{S}^2} = \frac{1}{3}\delta_{ij}. \tag{457}$$

Consequently,

$$\langle P_T(\hat{n})\rangle_{\mathbb{S}^2} = \mathbb{I}_3 - \big\langle \hat{n}\hat{n}^\top\big\rangle_{\mathbb{S}^2} = \frac{2}{3}\mathbb{I}_3. \tag{458}$$

Proof. Define

$$M_{ij} \coloneqq \frac{1}{4\pi}\int_{\mathbb{S}^2} \hat{n}_i\hat{n}_j\,\mathrm{d}\Omega.$$

For any $R \in SO(3)$, rotational invariance of the normalized spherical measure gives

$$\begin{aligned} M_{ij} &= \frac{1}{4\pi}\int_{\mathbb{S}^2} \hat{n}_i\hat{n}_j\,\mathrm{d}\Omega \\ &= \frac{1}{4\pi}\int_{\mathbb{S}^2} (R\hat{n})_i(R\hat{n})_j\,\mathrm{d}\Omega \\ &= R_{ik}R_{j\ell}\frac{1}{4\pi}\int_{\mathbb{S}^2} \hat{n}_k\hat{n}_\ell\,\mathrm{d}\Omega \\ &= R_{ik}R_{j\ell}M_{k\ell}. \end{aligned}$$

Hence

$$M = RMR^\top \qquad \text{for every } R \in SO(3).$$

Take the three half-turn rotations

$$R_x = \begin{pmatrix} 1 & 0 & 0 \\ 0 & -1 & 0 \\ 0 & 0 & -1 \end{pmatrix}, \qquad R_y = \begin{pmatrix} -1 & 0 & 0 \\ 0 & 1 & 0 \\ 0 & 0 & -1 \end{pmatrix}, \qquad R_z = \begin{pmatrix} -1 & 0 & 0 \\ 0 & -1 & 0 \\ 0 & 0 & 1 \end{pmatrix}.$$

The identities

$$M = R_xMR_x^\top, \qquad M = R_yMR_y^\top, \qquad M = R_zMR_z^\top$$

force every off-diagonal entry of M to vanish. Thus

$$M = \mathrm{diag}(M_{11}, M_{22}, M_{33}).$$

Next take the quarter-turn rotation about the z-axis,

$$R_{z,\pi/2} = \begin{pmatrix} 0 & -1 & 0 \\ 1 & 0 & 0 \\ 0 & 0 & 1 \end{pmatrix}.$$

The identity $M = R_{z,\pi/2} M R_{z,\pi/2}^{\top}$ gives

$$M_{11} = M_{22}.$$

Similarly, the quarter-turn rotation about the x-axis,

$$R_{x,\pi/2} = \begin{pmatrix} 1 & 0 & 0 \\ 0 & 0 & -1 \\ 0 & 1 & 0 \end{pmatrix},$$

gives

$$M_{22} = M_{33}.$$

Hence

$$M = c\,\mathbb{I}_3$$

for some scalar c.

Taking the trace yields

$$3c = \operatorname{tr} M = \frac{1}{4\pi} \int_{\mathbb{S}^2} \hat{n}_i \hat{n}_i \, \mathrm{d}\Omega = \frac{1}{4\pi} \int_{\mathbb{S}^2} |\hat{n}|^2 \, \mathrm{d}\Omega = \frac{1}{4\pi} \int_{\mathbb{S}^2} 1 \, \mathrm{d}\Omega = 1.$$

Therefore $c = 1/3$, which proves Eq. (457). Equation (458) then follows from Eq. (451):

$$\langle P_T(\hat{n}) \rangle_{\mathbb{S}^2} = \langle \mathbb{I}_3 - \hat{n}\hat{n}^{\top} \rangle_{\mathbb{S}^2} = \mathbb{I}_3 - \frac{1}{3}\mathbb{I}_3 = \frac{2}{3}\mathbb{I}_3.$$

□

Theorem 18 (Path II single-polarization shell-geometric value)**.** *Assume the Path-II averaging class of Condition VIII.3, and let $W(\hat{u}, \hat{n})$ be the local overlap density from definition VIII.9, where $\hat{u} \in \mathbb{R}^3$ is any fixed unit test vector. Fix $s > 1$ and a reference scale $\rho_0 > 0$. The variable ρ in this theorem is the positive scale coordinate used in the radial dilatation count. It is not the cylindrical Maxwell radius and it is not the physical shell radius. Define the Path-II geometric annulus response, and hence its single-log coefficient, by*

$$\mathcal{C}_{\log}^{(II)} \ln s \equiv \frac{1}{4\pi} \int_{\mathbb{S}^2} \left(\int_{\rho_0}^{s\rho_0} \frac{\mathrm{d}\rho}{\rho} \right) W(\hat{u}, \hat{n}) \, \mathrm{d}\Omega. \tag{459}$$

Then the result is independent of ρ_0 and of the direction of the fixed unit vector $\hat{u}$. Moreover,

$$\langle W(\hat{u}, \hat{n}) \rangle_{\mathbb{S}^2} = \frac{1}{3}, \tag{460}$$

so that

$$\boxed{\mathcal{C}_{\log}^{(II)} = \frac{1}{3}} \qquad [\ \textbf{Path II}\ ] \tag{461}$$

This is the exact Path-II value within the stated single-polarization averaging class.

Proof. By Eq. (459),

$$\mathcal{C}_{\log}^{(II)} \ln s = \left(\int_{\rho_0}^{s\rho_0} \frac{\mathrm{d}\rho}{\rho} \right) \langle W(\hat{u}, \hat{n}) \rangle_{\mathbb{S}^2}.$$

The radial integral gives the dimensionless scale count

$$\int_{\rho_0}^{s\rho_0} \frac{\mathrm{d}\rho}{\rho} = \int_1^s \frac{\mathrm{d}q}{q} = \ln s, \qquad q := \frac{\rho}{\rho_0}.$$

Hence

$$\mathcal{C}_{\log}^{(II)} = \langle W(\hat{u},\hat{n})\rangle_{\mathbb{S}^2}\,,$$

so the coefficient is independent of ρ_0.

Using Eq. (456),

$$W(\hat{u},\hat{n}) = \frac{1}{2}\Big(1-(\hat{u}\cdot\hat{n})^2\Big).$$

Averaging over the sphere gives

$$\langle W(\hat{u},\hat{n})\rangle_{\mathbb{S}^2} = \frac{1}{2}\left(1-\left\langle(\hat{u}\cdot\hat{n})^2\right\rangle_{\mathbb{S}^2}\right).$$

Now, with repeated Cartesian indices summed,

$$\begin{aligned}\left\langle(\hat{u}\cdot\hat{n})^2\right\rangle_{\mathbb{S}^2} &= \langle(u_i\hat{n}_i)(u_j\hat{n}_j)\rangle_{\mathbb{S}^2}\\ &= u_iu_j\,\langle\hat{n}_i\hat{n}_j\rangle_{\mathbb{S}^2} = u_iu_j\frac{1}{3}\delta_{ij} = \frac{1}{3}\,|\hat{u}|^2 = \frac{1}{3}.\end{aligned}$$

Thus the average depends only on the norm of $\hat{u}$, and since $|\hat{u}|=1$, it is independent of the chosen direction of $\hat{u}$. Therefore

$$\langle W(\hat{u},\hat{n})\rangle_{\mathbb{S}^2} = \frac{1}{2}\left(1-\frac{1}{3}\right) = \frac{1}{3}.$$

This proves Eq. (460), and substituting it back into the definition of $\mathcal{C}_{\log}^{(II)}$ yields Eq. (461). □

Remark. The value 1/3 factorizes as

$$\frac{1}{3} = \frac{1}{2}\cdot\frac{2}{3}.$$

The factor 1/2 comes from the phase average of a single rank-one tangential polarization. The factor 2/3 comes from the spherical average of the tangent projector. Replacing the rank-one phase average by the full tangent projector would give 2/3 instead of 1/3. This would describe two independent tangential polarizations rather than the single instantaneous in-plane polarization tracked in Path II. The distinction belongs to the Path-II averaging class and does not import a QED polarization count.

C. Compatibility of the two paths and the shell lock

We now compare the two routes. Path I gives a remainder-controlled representative of the canonical logarithmic coefficient. Path II gives the exact value of that coefficient within the stated single-polarization shell averaging class. The shell lock is the compatibility statement that both routes refer to the same canonical single-log response, with the only retained discrepancy carried by the explicit Path-I representative remainder.

Condition VIII.4 (Single-log compatibility condition for the two paths)**.** The shell lock compares Path I and Path II only after both have been projected onto the same canonical single-log response under the same internal dilatation variable

$$\tau = \ln s.$$

The comparison uses the same scale-invariant radial count $\mathrm{d}\rho/\rho$ and the same single-polarization convention of Condition VIII.3. Under this compatibility condition, the exact coefficient used in the shell lock is taken from Path II,

$$\mathcal{C}_{\log} = \mathcal{C}_{\log}^{(II)} = \frac{1}{3},$$

whereas Path I supplies the retained representative $\mathcal{C}_{\log}^{(I)}(\mathcal{D}_{\mathrm{C}},\zeta)$ with the explicit bound of Eq. (449). This condition compares the two single-log extractions and is not a numerical fit.

Theorem 19 (Shell lock with controlled representative remainder)**.** *Assume the hypotheses of corollary 9 and theorem 18, with $\mathcal{D}_{\mathrm{C}} > 0$, and impose the single-log equality condition of Condition VIII.4. Define the Path-I representative discrepancy, not as an independent parameter but as the difference between the retained Path-I representative and the Path-II coefficient, by*

$$\varepsilon_{\mathrm{I}} \equiv \mathcal{C}_{\log}^{(I)}(\mathcal{D}_{\mathrm{C}}, \zeta) - \mathcal{C}_{\log}^{(II)}. \tag{462}$$

Then

$$\frac{C_\chi}{2\mathcal{D}_{\mathrm{C}}}\,\zeta(1+\zeta) = \frac{1}{3} + \varepsilon_{\mathrm{I}}, \qquad |\varepsilon_{\mathrm{I}}| \leq C_{\mathrm{I}}' \,\frac{|\zeta|^3}{\mathcal{D}_{\mathrm{C}}}. \tag{463}$$

Proof. By Eq. (449),

$$\left|\mathcal{C}_{\log} - \mathcal{C}_{\log}^{(I)}(\mathcal{D}_{\mathrm{C}}, \zeta)\right| \leq C_{\mathrm{I}}' \,\frac{|\zeta|^3}{\mathcal{D}_{\mathrm{C}}}.$$

By theorem 18,

$$\mathcal{C}_{\log}^{(II)} = \frac{1}{3}.$$

By the same-coefficient identification assumed in the shell lock,

$$\mathcal{C}_{\log} = \mathcal{C}_{\log}^{(II)}.$$

Therefore

$$\left|\mathcal{C}_{\log}^{(I)}(\mathcal{D}_{\mathrm{C}}, \zeta) - \mathcal{C}_{\log}^{(II)}\right| \leq C_{\mathrm{I}}' \,\frac{|\zeta|^3}{\mathcal{D}_{\mathrm{C}}}.$$

Using Eq. (448) and $\mathcal{C}_{\log}^{(II)} = 1/3$, this is precisely

$$\left|\frac{C_\chi}{2\mathcal{D}_{\mathrm{C}}}\,\zeta(1+\zeta) - \frac{1}{3}\right| \leq C_{\mathrm{I}}' \,\frac{|\zeta|^3}{\mathcal{D}_{\mathrm{C}}}.$$

Defining the representative discrepancy ε_{I} by Eq. (462) gives Eq. (463). □

Remark. The shell lock is not an exact equality between the Path-I representative and the Path-II value unless $\varepsilon_{\mathrm{I}} = 0$. It is an equality modulo the explicitly bounded representative remainder ε_{I}. The baseline algebraic lock used below is obtained by omitting this remainder from the primary algebraic equation while retaining it as a separate remainder budget. No parameter is adjusted in this step.

Definition VIII.10 (Baseline shell-lock closure)**.** In the baseline pinned-shell closure used for the primary algebraic extraction, the representative discrepancy ε_{I} in Eq. (463) is omitted from the primary lock equation. Equivalently, the baseline closure retains the zeroth-discrepancy part of the controlled representative expansion. This is a closure convention, not a theorem asserting that ε_{I} vanishes identically, and it does not adjust Λ_{geom}, $\mathcal{D}_{\mathrm{C}}$, $\mathsf{K}_{\mathrm{ALP}}$, C_χ, or any measured benchmark. The baseline lock is the zeroth-discrepancy equation

$$\frac{C_\chi}{2\mathcal{D}_{\mathrm{C}}}\,\zeta(1+\zeta) = \frac{1}{3}. \tag{464}$$

The omitted term ε_{I} is retained only as a separate remainder budget.

Proposition 49 (Remainder-deformed shell lock and relative correction)**.** *Under the hypotheses of theorem 19, the remainder-deformed lock is*

$$\frac{C_\chi}{2\mathcal{D}_{\mathrm{C}}}\,\zeta(1+\zeta) = \frac{1}{3} + \varepsilon_{\mathrm{I}}. \tag{465}$$

If $|3\varepsilon_{\mathrm{I}}| < 1$, then $1 + 3\varepsilon_{\mathrm{I}} > 0$, and define the corresponding positive deformed locked scalar value by

$$\mathcal{D}_{\mathrm{C}}^{\mathrm{lock}}(\varepsilon_{\mathrm{I}}) \equiv \frac{\dfrac{3C_\chi}{2}\,\zeta(1+\zeta)}{1+3\varepsilon_{\mathrm{I}}}. \tag{466}$$

Let

$$\mathcal{D}_{\mathrm{C}}^{\mathrm{base}} \equiv \frac{3C_\chi}{2}\,\zeta(1+\zeta) \tag{467}$$

be the baseline scalar target generated by the zeroth-discrepancy lock. Assume $\mathcal{D}_{\mathrm{C}}^{\mathrm{base}} \neq 0$*, equivalently* $\zeta(1+\zeta) \neq 0$*. Then*

$$\frac{\mathcal{D}_{\mathrm{C}}^{\mathrm{lock}}(\varepsilon_{\mathrm{I}}) - \mathcal{D}_{\mathrm{C}}^{\mathrm{base}}}{\mathcal{D}_{\mathrm{C}}^{\mathrm{base}}} = -\frac{3\varepsilon_{\mathrm{I}}}{1+3\varepsilon_{\mathrm{I}}}, \tag{468}$$

and therefore

$$\left|\frac{\mathcal{D}_{\mathrm{C}}^{\mathrm{lock}}(\varepsilon_{\mathrm{I}}) - \mathcal{D}_{\mathrm{C}}^{\mathrm{base}}}{\mathcal{D}_{\mathrm{C}}^{\mathrm{base}}} + 3\varepsilon_{\mathrm{I}}\right| \leq \frac{9\varepsilon_{\mathrm{I}}^2}{1-3|\varepsilon_{\mathrm{I}}|}. \tag{469}$$

In particular,

$$\frac{\mathcal{D}_{\mathrm{C}}^{\mathrm{lock}}(\varepsilon_{\mathrm{I}}) - \mathcal{D}_{\mathrm{C}}^{\mathrm{base}}}{\mathcal{D}_{\mathrm{C}}^{\mathrm{base}}} = -3\varepsilon_{\mathrm{I}} + O(\varepsilon_{\mathrm{I}}^2) \qquad (\varepsilon_{\mathrm{I}} \to 0).$$

Proof. The identity Eq. (465) is exactly Eq. (463). Rewriting it as

$$\frac{C_\chi}{2\mathcal{D}_{\mathrm{C}}}\,\zeta(1+\zeta) = \frac{1+3\varepsilon_{\mathrm{I}}}{3}$$

and multiplying by $2\mathcal{D}_{\mathrm{C}}$ gives

$$C_\chi\,\zeta(1+\zeta) = \frac{2}{3}\,(1+3\varepsilon_{\mathrm{I}})\,\mathcal{D}_{\mathrm{C}}.$$

Solving for $\mathcal{D}_{\mathrm{C}}$ yields

$$\mathcal{D}_{\mathrm{C}} = \frac{\frac{3C_\chi}{2}\,\zeta(1+\zeta)}{1+3\varepsilon_{\mathrm{I}}}.$$

This is precisely Eq. (466), namely

$$\mathcal{D}_{\mathrm{C}}^{\mathrm{lock}}(\varepsilon_{\mathrm{I}}) = \frac{\mathcal{D}_{\mathrm{C}}^{\mathrm{base}}}{1+3\varepsilon_{\mathrm{I}}}.$$

Hence

$$\frac{\mathcal{D}_{\mathrm{C}}^{\mathrm{lock}}(\varepsilon_{\mathrm{I}}) - \mathcal{D}_{\mathrm{C}}^{\mathrm{base}}}{\mathcal{D}_{\mathrm{C}}^{\mathrm{base}}} = \frac{1}{1+3\varepsilon_{\mathrm{I}}} - 1 = -\frac{3\varepsilon_{\mathrm{I}}}{1+3\varepsilon_{\mathrm{I}}},$$

which proves Eq. (468). Moreover,

$$\begin{aligned}\frac{\mathcal{D}_{\mathrm{C}}^{\mathrm{lock}}(\varepsilon_{\mathrm{I}}) - \mathcal{D}_{\mathrm{C}}^{\mathrm{base}}}{\mathcal{D}_{\mathrm{C}}^{\mathrm{base}}} + 3\varepsilon_{\mathrm{I}} &= -\frac{3\varepsilon_{\mathrm{I}}}{1+3\varepsilon_{\mathrm{I}}} + 3\varepsilon_{\mathrm{I}} \\ &= \frac{9\varepsilon_{\mathrm{I}}^2}{1+3\varepsilon_{\mathrm{I}}}.\end{aligned}$$

If $|3\varepsilon_{\mathrm{I}}| < 1$, then

$$|1+3\varepsilon_{\mathrm{I}}| \geq 1 - 3|\varepsilon_{\mathrm{I}}|,$$

so

$$\left|\frac{\mathcal{D}_{\mathrm{C}}^{\mathrm{lock}}(\varepsilon_{\mathrm{I}}) - \mathcal{D}_{\mathrm{C}}^{\mathrm{base}}}{\mathcal{D}_{\mathrm{C}}^{\mathrm{base}}} + 3\varepsilon_{\mathrm{I}}\right| \leq \frac{9\varepsilon_{\mathrm{I}}^2}{1-3|\varepsilon_{\mathrm{I}}|}.$$

This proves Eq. (469). The final $O(\varepsilon_{\mathrm{I}}^2)$ statement is the Taylor expansion of $(1+3\varepsilon_{\mathrm{I}})^{-1}$ at $\varepsilon_{\mathrm{I}} = 0$. $\square$

Proposition 50 (Asymptotic vanishing of the representative remainder)**.** *Assume the hypotheses of theorem 19, and assume $\zeta > 0$, as in the minimal positive-Λ_{geom} branch realization. For a signed branch with $\zeta < 0$, the corresponding bootstrap statement must be written with the sign of $\zeta(1+\zeta)$ controlled separately. This is an asymptotic statement about the retained Path-I representative remainder. It is not a finite-ζ certification unless the constant C'_{I} has been bounded. Define*

$$\beta(\zeta) \equiv \frac{2C'_{\mathrm{I}}}{3C_\chi}\,\frac{\zeta^2}{1+\zeta}. \tag{470}$$

If $\beta(\zeta) < 1/3$, then

$$|\varepsilon_{\mathrm{I}}| \leq \frac{\beta(\zeta)}{1-3\beta(\zeta)}. \tag{471}$$

In particular,

$$\varepsilon_{\mathrm{I}} = O(\zeta^2) \qquad (\zeta \to 0^+), \tag{472}$$

and therefore

$$\varepsilon_{\mathrm{I}} \to 0 \qquad (\zeta \to 0^+). \tag{473}$$

Proof. From Eq. (463),

$$\frac{C_\chi}{2\mathcal{D}_{\mathrm{C}}}\,\zeta(1+\zeta) = \frac{1}{3} + \varepsilon_{\mathrm{I}} = \frac{1+3\varepsilon_{\mathrm{I}}}{3}.$$

Solving for $\mathcal{D}_{\mathrm{C}}$ gives

$$\mathcal{D}_{\mathrm{C}} = \frac{\dfrac{3C_\chi}{2}\,\zeta(1+\zeta)}{1+3\varepsilon_{\mathrm{I}}}.$$

Since $\mathcal{D}_{\mathrm{C}} > 0$, $\zeta > 0$, and $C_\chi > 0$, this identity implies $1 + 3\varepsilon_{\mathrm{I}} > 0$. Substituting this identity into the remainder bound from Eq. (463) yields

$$|\varepsilon_{\mathrm{I}}| \leq C'_{\mathrm{I}}\,\frac{\zeta^3}{\mathcal{D}_{\mathrm{C}}} = \frac{2C'_{\mathrm{I}}}{3C_\chi}\,\frac{\zeta^2}{1+\zeta}\,|1+3\varepsilon_{\mathrm{I}}|.$$

Using Eq. (470) and the estimate

$$|1+3\varepsilon_{\mathrm{I}}| \leq 1 + 3|\varepsilon_{\mathrm{I}}|,$$

we obtain

$$|\varepsilon_{\mathrm{I}}| \leq \beta(\zeta)\big(1+3|\varepsilon_{\mathrm{I}}|\big).$$

Hence

$$(1-3\beta(\zeta))\,|\varepsilon_{\mathrm{I}}| \leq \beta(\zeta).$$

If $\beta(\zeta) < 1/3$, this gives

$$|\varepsilon_{\mathrm{I}}| \leq \frac{\beta(\zeta)}{1-3\beta(\zeta)},$$

which is Eq. (471).

Since

$$\beta(\zeta) = \frac{2C'_{\mathrm{I}}}{3C_\chi}\,\frac{\zeta^2}{1+\zeta} \to 0 \qquad (\zeta \to 0^+),$$

there exists $\zeta_* > 0$ such that

$$\beta(\zeta) < \frac{1}{3} \qquad \text{for all } 0 < \zeta < \zeta_*.$$

For such ζ, the previous bound applies. Because

$$\frac{x}{1-3x} = O(x) \qquad (x \to 0^+),$$

and because $\beta(\zeta) = O(\zeta^2)$ as $\zeta \to 0^+$, it follows that

$$\varepsilon_{\mathrm{I}} = O(\zeta^2) \qquad (\zeta \to 0^+).$$

Therefore

$$\varepsilon_{\mathrm{I}} \to 0 \qquad (\zeta \to 0^+).$$

□

Theorem 20 (Baseline Alpha Lock Point)**.** *Within the zeroth-discrepancy baseline shell-lock closure Eq.* (464)*, using* $C_\chi = 2\pi^2$ *from Eq.* (435) *and*

$$\zeta = \frac{\mathsf{K}_{ALP}}{2\pi^2}\Lambda_{\mathrm{geom}}$$

from Eq. (432)*, the baseline lock with the exact operator-level vector input fixes the canonical scalar-lock target as*

$$\boxed{\mathfrak{D}_* \equiv \mathfrak{D}_{\mathrm{lock}}(\Lambda_{\mathrm{geom}}) = \frac{3}{2}\,\mathsf{K}_{ALP}\,\Lambda_{\mathrm{geom}}\left(1 + \frac{\mathsf{K}_{ALP}\Lambda_{\mathrm{geom}}}{2\pi^2}\right)} \qquad [\ \textbf{ALP}\text{–}\textit{Alpha Lock Point}\ ] \tag{474}$$

Here $\mathfrak{D}_*$ *is the scalar target obtained from the exact operator-level vector input* Λ_{geom}*, under the baseline zeroth-discrepancy lock. It is not a new scalar branch and not a measured slowdown value; the scalar branch still supplies the function* $\mathcal{D}_{\mathrm{C}}(\alpha)$*, which is then constrained by* $\mathcal{D}_{\mathrm{C}}(\alpha) = \mathfrak{D}_*$*. The scalar slowdown branch supplied by the scalar-sector construction is constrained by the admissible-coupling equation*

$$\mathcal{D}_{\mathrm{C}}(\alpha) = \mathfrak{D}_*. \tag{475}$$

An admissible coupling is a root of this equation in the admissible interval specified later.

In a reduced numerical realization, the same target map is evaluated only after replacing Λ_{geom} *by the specified reduced vector input, for example*

$$\mathfrak{D}_*^{(\mathrm{th})} = \mathfrak{D}_{\mathrm{lock}}\big(\Lambda_{\mathrm{geom}}^{(\mathrm{th})}\big).$$

Proof. Starting from the zeroth-discrepancy baseline lock Eq. (464),

$$\frac{C_\chi}{2\mathcal{D}_{\mathrm{C}}}\,\zeta(1+\zeta) = \frac{1}{3},$$

where the controlled representative discrepancy ε_{I} has been omitted according to definition VIII.10, we multiply both sides by $2\mathcal{D}_{\mathrm{C}}$ and obtain

$$C_\chi\,\zeta(1+\zeta) = \frac{2}{3}\mathcal{D}_{\mathrm{C}}.$$

Hence

$$\mathcal{D}_{\mathrm{C}} = \frac{3C_\chi}{2}\,\zeta(1+\zeta).$$

Using $C_\chi = 2\pi^2$, one obtains

$$\mathcal{D}_{\mathrm{C}} = 3\pi^2\,\zeta(1+\zeta).$$

Now substitute the geometric vector input

$$\zeta = \frac{\mathsf{K}_{\mathrm{ALP}}}{2\pi^2}\Lambda_{\mathrm{geom}}.$$

This yields

$$\begin{aligned}\mathcal{D}_{\mathrm{C}} &= 3\pi^2\left(\frac{\mathsf{K}_{\mathrm{ALP}}\Lambda_{\mathrm{geom}}}{2\pi^2}\right)\left(1+\frac{\mathsf{K}_{\mathrm{ALP}}\Lambda_{\mathrm{geom}}}{2\pi^2}\right)\\ &= \frac{3}{2}\,\mathsf{K}_{\mathrm{ALP}}\,\Lambda_{\mathrm{geom}}\left(1+\frac{\mathsf{K}_{\mathrm{ALP}}\Lambda_{\mathrm{geom}}}{2\pi^2}\right).\end{aligned}$$

By the canonical scalar-lock notation, the right-hand side is

$$\mathfrak{D}_* = \mathfrak{D}_{\mathrm{lock}}(\Lambda_{\mathrm{geom}}) = \frac{3}{2}\,\mathsf{K}_{\mathrm{ALP}}\,\Lambda_{\mathrm{geom}}\left(1+\frac{\mathsf{K}_{\mathrm{ALP}}\Lambda_{\mathrm{geom}}}{2\pi^2}\right).$$

The scalar sector supplies the branch function $\mathcal{D}_{\mathrm{C}}(\alpha)$. Therefore the admissible coupling is selected by the one-variable root equation

$$\mathcal{D}_{\mathrm{C}}(\alpha) = \mathfrak{D}_*,$$

once the admissible interval has been specified. No measured value of α, no QED coefficient, and no benchmark value has entered this derivation. □

Remark. Path II fixes the geometric value 1/3 exactly within the stated single-polarization shell average. Path I converts that benchmark into a relation between the scalar shell block and the independently computed vector input Λ_{geom}, with the controlled representative discrepancy ε_{I} described above. At the baseline closure, this discrepancy is omitted from the primary algebraic equation, so the zeroth-discrepancy Path-I representative is matched to the exact Path-II value,

$$\mathcal{C}_{\log}^{(I)} = \mathcal{C}_{\log}^{(II)} = \frac{1}{3}.$$

This is a baseline closure convention, not a theorem that ε_{I} vanishes identically. Any later comparison with QED is diagnostic only.

IX. GEOMETRIC LOCK AND THE EMERGENT FINE-STRUCTURE ROOT

This section closes the scalar–vector construction at the level of the admissible fine-structure root within the stated shell postulates and baseline lock closure. The scalar sector supplies the shell slowdown branch $\mathcal{D}_{\mathrm{C}}(\alpha)$ through the mother cavity–shell pencil of section VI, where α is the symbolic compact-charge coupling variable and not a measured input. The vector sector supplies an independently computed shell-geometric input. Under the exact operator hypotheses of the vector section this input is Λ_{geom}. At finite Galerkin rank it is represented by $\Lambda_{\mathrm{geom}}^{(N)}$. In the current reduced numerical realization it is represented by $\Lambda_{\mathrm{geom}}^{(\mathrm{th})}$. Once either the exact vector-shell input or a specified reduced representative has been fixed, it enters the scalar lock only as a fixed geometric datum.

Within the baseline shell-lock closure of Eq. (464), once the geometric vector constant has been computed independently, the shell lock is no longer a coupled fixed-point problem. The Alpha Lock Point of Eq. (474) defines the derived baseline scalar target map, written below as $\mathfrak{D}_{\mathrm{lock}}(\Lambda)$ in definition IX.2. Thus any positive vector-shell input or specified representative Λ in the admissible range determines a scalar target $\mathfrak{D}_{\mathrm{lock}}(\Lambda)$, while the scalar mother law converts any admissible α into the corresponding scalar shell slowdown $\mathcal{D}_{\mathrm{C}}(\alpha)$.

When the exact vector input and a chosen exact scalar evaluator are both used, the exact baseline geometric-lock root is obtained, subject to the admissibility conditions below, from the one-variable lock condition

$$\mathcal{D}_{\mathrm{C}}(\alpha) = \mathfrak{D}_{\mathrm{lock}}(\Lambda_{\mathrm{geom}}). \tag{476}$$

The closed inversion formula proved below applies to scalar evaluators whose retained admissible branch has a D-only radicand. If the retained exact scalar law has an explicit x-dependent radicand, the same lock condition remains the defining equation, while the closed algebraic inversion is replaced by the corresponding two-variable scalar equation. In a reduced realization, the same lock equation is evaluated after the explicit replacement

$$\Lambda_{\mathrm{geom}} \mapsto \Lambda_{\mathrm{geom}}^{(N)} \quad \text{or} \quad \Lambda_{\mathrm{geom}} \mapsto \Lambda_{\mathrm{geom}}^{(\mathrm{th})}.$$

Thus the vector geometry fixes the target scalar slowdown, and the scalar mother law supplies the admissible inverse reading of that target.

Throughout this section the minimal electron branch is fixed. Hence

$$\eta = \eta_0 = \frac{1}{\pi}, \qquad \ell = \ell_0 = \frac{1}{\pi\sqrt{\pi}}, \tag{477}$$

and these two geometric ratios are suppressed from the notation whenever no ambiguity can arise.

A. Geometric lock value and scalar inversion

We first collect the scalar and vector objects that enter the baseline lock. The dependency order is fixed as follows. The vector construction supplies either the exact input Λ_{geom} or an explicitly specified reduced representative. The baseline ALP map then produces the scalar target $\mathfrak{D}_{\mathrm{lock}}(\Lambda)$. Only after this target has been fixed is the scalar evaluator inverted through its admissible radicand branch. Thus Λ, $\mathfrak{D}_{\mathrm{lock}}(\Lambda)$, $\mathfrak{D}_*$, and α_* have different logical status. Here Λ is a vector input or representative, $\mathfrak{D}_{\mathrm{lock}}(\Lambda)$ is the derived target map, $\mathfrak{D}_*$ is the fixed target obtained after the exact vector input has been chosen, and α_* is the admissible root of the chosen scalar evaluator at that fixed target.

Definition IX.1 (Vector-shell inputs entering the lock)**.** Throughout this definition,

$$\Delta\Lambda_{\mathrm{UV}\to\mathrm{IR}}(\ell_0) \equiv \Delta\Lambda_{\mathrm{UV}\to\mathrm{IR}}(\ell_0; \mathscr{A}_{\parallel}^{\mathrm{coll}})$$

denotes the admitted Gaussian UV load evaluated on the fixed minimal-branch shell representative. Under the exact vector-operator hypotheses, the geometric vector-shell constant is

$$\Lambda_{\mathrm{geom}} \equiv \Lambda_{\mathrm{ind}} + \Delta\Lambda_{\mathrm{UV}\to\mathrm{IR}}(\ell_0) + \Delta\Lambda_{\mathrm{out}}(\eta_0)\, R_\chi. \tag{478}$$

with finite-rank Galerkin descendants

$$\Lambda_{\mathrm{geom}}^{(N)} = \Lambda_{\mathrm{ind}} + \Delta\Lambda_{\mathrm{UV}\to\mathrm{IR}}(\ell_0) + \Delta\Lambda_{\mathrm{out}}(\eta_0)\, R_\chi^{(N)}. \tag{479}$$

The current reduced vector evaluator used in the numerical ledger is

$$\Lambda_{\mathrm{geom}}^{(\mathrm{th})} \equiv \Lambda_{\mathrm{ind}} + \Delta\Lambda_{\mathrm{UV}\to\mathrm{IR}}(\ell_0) + \Delta\Lambda_{\mathrm{out}}^{[101]}(\eta_0)\, R_\chi^{(\mathrm{th})}. \tag{480}$$

The symbol $R_\chi^{(\mathrm{th})}$ is only an alias for the current reduced ledger value $R_{\chi,101}^{\mathrm{red}}$; it is not an additional theorem-level return factor. Here R_χ is the exact shell-memory resolvent factor, $R_\chi^{(N)}$ is its finite-rank Galerkin descendant, and $R_\chi^{(\mathrm{th})}$ is the current reduced source-weighted resolvent realization used in the numerical ledger. In the notation of the vector ledger,

$$R_\chi^{(\mathrm{th})} \equiv R_\chi^{\mathrm{red}}.$$

The superscript [101] records the odd-mode cutoff used in the present vector ledger for the source norm and exterior subtraction. It is not part of the exact operator-level definition.

Remark (Current reduced vector input and numerical status). The current reduced vector input used in the reported realization is

$$\Lambda_{\mathrm{geom}}^{(\mathrm{th})} = 0.6916831461069910267161597076345744739664. \tag{481}$$

It is not the exact operator-limit value Λ_{geom}. It is the current reduced evaluator based on the theorem-defined shell source, the cutoff exterior subtraction $\Delta\Lambda_{\mathrm{out}}^{[101]}(\eta_0)$, and the current source-weighted vector-memory realization.

The displayed decimal is the working-precision value of the present reduced evaluator. It does not imply that all shown digits are stable digits of the exact operator-limit quantity. Numerical significance beyond the realization-level status stated here requires the separate precision audit. The realization-level uncertainty of this input is controlled by the unresolved vector Galerkin tail, the reduced source-weighted memory replacement, and the finite odd-mode cutoff used in the vector numerics. The number is not tuned to a measured value of α, to a QED coefficient, or to a scalar-channel target.

Definition IX.2 (Baseline scalar target induced by a vector-shell input)**.** Within the baseline shell-lock closure Eq. (464), for any positive vector-shell input or specified representative Λ lying in the range where the scalar evaluator is later admissible, define the derived scalar target map

$$\mathfrak{D}_{\mathrm{lock}}(\Lambda) \equiv \frac{3}{2}\, \mathsf{K}_{\mathrm{ALP}}\, \Lambda \left(1 + \frac{\mathsf{K}_{\mathrm{ALP}}\Lambda}{2\pi^2}\right). \tag{482}$$

When the exact vector input is used, we write

$$\mathfrak{D}_* \equiv \mathfrak{D}_{\mathrm{lock}}(\Lambda_{\mathrm{geom}}). \tag{483}$$

When the current reduced numerical evaluator is used, the corresponding realization-level target value is denoted by

$$\mathfrak{D}_*^{(\mathrm{th})} \equiv \mathfrak{D}_{\mathrm{lock}}(\Lambda_{\mathrm{geom}}^{(\mathrm{th})}). \tag{484}$$

Definition IX.3 (Scalar mother radicand and admissible scalar domain)**.** Let the chosen scalar evaluator, after its stated operator reduction or finite-rank realization has been fixed, be represented on its admissible branch by a D-only radicand of the form

$$D = x\sqrt{\mathfrak{R}_{\mathrm{moth}}(D)}, \qquad x = \frac{\alpha}{\pi}, \tag{485}$$

with

$$\mathfrak{R}_{\mathrm{moth}}(D) \equiv 1 - \Theta_{1,\mathrm{eff}}\, D + D^2\, \Phi_{\mathrm{dyn}}(D). \tag{486}$$

The admissible scalar domain of this evaluator is

$$\mathcal{A}_{\mathrm{scal}} \coloneqq \{D > 0\ ;\ \Phi_{\mathrm{dyn}}(D) \text{ is finite and real}, \quad \mathfrak{R}_{\mathrm{moth}}(D) > 0\}\,. \tag{487}$$

On $\mathcal{A}_{\mathrm{scal}}$, the square root in Eq. (485) is the principal positive square root. Here

$$\Theta_{1,\mathrm{eff}} \equiv \Theta_{1,\mathrm{core}} + B_{11}^{(\mathrm{eval})}, \tag{488}$$

and $\Phi_{\mathrm{dyn}}(D)$ denotes the dynamic response retained by the chosen scalar evaluator. In the current article realization this is the visible dynamic block; in a refined scalar realization it is the corresponding realization-level dynamic block.

This definition covers the scalar evaluators used in the present lock calculation, including the current visible dynamic realization and the refined realization-level dynamic block, whenever their retained branch has been reduced to the displayed D-only radicand. A scalar Schur law whose radicand retains an explicit x-dependence must instead be written as $\mathfrak{R}_{\mathrm{moth}}(D, x)$. In that case the closed algebraic inversion in proposition 51 is replaced by the corresponding two-variable scalar equation.

Remark. The symbol $B_{11}^{(\mathrm{eval})}$ denotes the effective static shell load of the chosen scalar evaluator. In the current article scalar realization one uses $B_{11}^{(\mathrm{eval})} = B_{11}^{\mathrm{glue}}$. In the refined no-free-parameter scalar realization one instead uses $B_{11}^{(\mathrm{eval})} = B_{11}^{(3,\rho)}$.

Remark. Equation (485) is the scalar mother law rewritten as an inverse reading of the scalar slowdown target on the chosen admissible branch. The scalar sector enters through the gauge-invariant shell slowdown D, while the vector sector enters through the fixed scalar target $\mathfrak{D}_{\mathrm{lock}}(\Lambda)$. This separation is the reason why the baseline root extraction reduces to a one-variable admissible-root problem once the vector input or specified reduced representative has been fixed.

Proposition 51 (Algebraic inversion of the scalar mother law)**.** *Assume that $D > 0$ and $\mathfrak{R}_{\mathrm{moth}}(D) > 0$. Then the scalar mother law Eq.* (485) *implies*

$$\alpha^2 = \pi^2\, \frac{D^2}{\mathfrak{R}_{\mathrm{moth}}(D)}. \tag{489}$$

The associated squared equation has the two algebraic branches

$$\alpha_\pm(D) = \pm\, \pi\, \frac{D}{\sqrt{\mathfrak{R}_{\mathrm{moth}}(D)}}. \tag{490}$$

Since the mother law Eq. (485) *uses the principal positive square root, and since $D > 0$, the branch compatible with the original scalar mother law and with positive coupling is*

$$\alpha_{\mathrm{phys}}(D) = \pi\, \frac{D}{\sqrt{\mathfrak{R}_{\mathrm{moth}}(D)}}. \tag{491}$$

Proof. Squaring Eq. (485) gives

$$D^2 = x^2\,\mathfrak{R}_{\mathrm{moth}}(D) \qquad \Longleftrightarrow \qquad \left(\frac{\alpha}{\pi}\right)^2 = \frac{D^2}{\mathfrak{R}_{\mathrm{moth}}(D)},$$

which is Eq. (489). The corresponding squared equation has the two algebraic branches Eq. (490). Since $\sqrt{\mathfrak{R}_{\mathrm{moth}}(D)} > 0$ and $D > 0$, the right-hand side of Eq. (485) has the same sign as $x = \alpha/\pi$. Hence the original mother law admits only the positive branch $\alpha_{\mathrm{phys}}(D)$, which is Eq. (491). □

Theorem 21 (Existence and uniqueness of the admissible baseline lock root)**.** *Let a positive vector-shell input or specified representative $\Lambda > 0$ be fixed, and let*

$$\mathfrak{D}_{\mathrm{lock}}(\Lambda)$$

be given by Eq. (482). The exact vector-input case is obtained by taking $\Lambda = \Lambda_{\mathrm{geom}}$, whereas a reduced numerical realization is obtained by taking the corresponding reduced representative. Assume that

$$\mathfrak{D}_{\mathrm{lock}}(\Lambda) \in \mathcal{A}_{\mathrm{scal}}, \qquad 0 < \pi\,\frac{\mathfrak{D}_{\mathrm{lock}}(\Lambda)}{\sqrt{\mathfrak{R}_{\mathrm{moth}}(\mathfrak{D}_{\mathrm{lock}}(\Lambda))}} < 1. \tag{492}$$

Then, for the chosen scalar evaluator on the admissible D-only radicand branch of definition IX.3, the one-variable lock equation

$$\mathcal{D}_{\mathrm{C}}(\alpha) = \mathfrak{D}_{\mathrm{lock}}(\Lambda)$$

has exactly one admissible root in the interval $0 < \alpha < 1$, namely

$$\alpha_*(\Lambda) = \pi\,\frac{\mathfrak{D}_{\mathrm{lock}}(\Lambda)}{\sqrt{\mathfrak{R}_{\mathrm{moth}}(\mathfrak{D}_{\mathrm{lock}}(\Lambda))}}. \tag{493}$$

In particular,

$$\alpha_* \equiv \alpha_*(\Lambda_{\mathrm{geom}})$$

in the exact vector-input case, and

$$\mathcal{D}_{\mathrm{C}}(\alpha_*) = \mathfrak{D}_*$$

when the exact target notation $\mathfrak{D}_* \equiv \mathfrak{D}_{\mathrm{lock}}(\Lambda_{\mathrm{geom}})$ is used.

Proof. Since $\mathfrak{D}_{\mathrm{lock}}(\Lambda) \in \mathcal{A}_{\mathrm{scal}}$, the quantity

$$\sqrt{\mathfrak{R}_{\mathrm{moth}}(\mathfrak{D}_{\mathrm{lock}}(\Lambda))}$$

is finite, real, and strictly positive. At the fixed target value $D = \mathfrak{D}_{\mathrm{lock}}(\Lambda)$, the original scalar mother law on the chosen admissible branch is

$$\mathfrak{D}_{\mathrm{lock}}(\Lambda) = \left(\frac{\alpha}{\pi}\right)\sqrt{\mathfrak{R}_{\mathrm{moth}}(\mathfrak{D}_{\mathrm{lock}}(\Lambda))}.$$

Since the factor multiplying α/π is strictly positive, this is a linear equation in α with exactly one real solution, namely

$$\alpha = \pi\,\frac{\mathfrak{D}_{\mathrm{lock}}(\Lambda)}{\sqrt{\mathfrak{R}_{\mathrm{moth}}(\mathfrak{D}_{\mathrm{lock}}(\Lambda))}}.$$

The squared equation has the two formal branches

$$\alpha_{\pm} = \pm\,\pi\,\frac{\mathfrak{D}_{\mathrm{lock}}(\Lambda)}{\sqrt{\mathfrak{R}_{\mathrm{moth}}(\mathfrak{D}_{\mathrm{lock}}(\Lambda))}},$$

while only the positive branch solves the original principal-root equation, because $\mathfrak{D}_{\mathrm{lock}}(\Lambda) > 0$. The admissibility condition Eq. (492) places this positive branch inside the admissible interval $0 < \alpha < 1$.

Conversely, substituting

$$\alpha_*(\Lambda) = \pi \frac{\mathfrak{D}_{\rm lock}(\Lambda)}{\sqrt{\mathfrak{R}_{\rm moth}(\mathfrak{D}_{\rm lock}(\Lambda))}}$$

into the mother law Eq. (485) at $D = \mathfrak{D}_{\rm lock}(\Lambda)$ gives

$$\mathfrak{D}_{\rm lock}(\Lambda) = \left(\frac{\alpha_*(\Lambda)}{\pi}\right)\sqrt{\mathfrak{R}_{\rm moth}(\mathfrak{D}_{\rm lock}(\Lambda))} = \left(\frac{\mathfrak{D}_{\rm lock}(\Lambda)}{\sqrt{\mathfrak{R}_{\rm moth}(\mathfrak{D}_{\rm lock}(\Lambda))}}\right)\sqrt{\mathfrak{R}_{\rm moth}(\mathfrak{D}_{\rm lock}(\Lambda))} = \mathfrak{D}_{\rm lock}(\Lambda).$$

Hence the displayed branch is indeed a solution of the one-variable lock equation. Uniqueness within the retained D-only branch has already been proved from the fixed-target linear equation above. Therefore the admissible baseline lock root is exactly Eq. (493). □

Proposition 52 (Sensitivity of the geometric-lock root)**.** *Let* $\Lambda_{\rm in} > 0$ *and set*

$$D_{\rm in} := \mathfrak{D}_{\rm lock}(\Lambda_{\rm in}).$$

Assume that $D_{\rm in} \in \mathcal{A}_{\rm scal}$*, that* $\Phi_{\rm dyn}$ *is differentiable on an open neighborhood of* $D_{\rm in}$*, and that* $\mathfrak{R}_{\rm moth}(D) > 0$ *on that neighborhood. Then*

$$\mathfrak{R}'_{\rm moth}(D) = -\Theta_{1,\rm eff} + 2D\,\Phi_{\rm dyn}(D) + D^2\,\Phi'_{\rm dyn}(D). \tag{494}$$

Let

$$\alpha(D) = \pi D\,\mathfrak{R}_{\rm moth}(D)^{-1/2}. \tag{495}$$

Then

$$\frac{{\rm d}\alpha}{{\rm d}D} = \pi\,\frac{1 - \dfrac{D}{2}\dfrac{\mathfrak{R}'_{\rm moth}(D)}{\mathfrak{R}_{\rm moth}(D)}}{\sqrt{\mathfrak{R}_{\rm moth}(D)}}. \tag{496}$$

Moreover, along the scalar target curve $D = \mathfrak{D}_{\rm lock}(\Lambda)$*,*

$$\frac{\rm d}{{\rm d}\Lambda}\mathfrak{D}_{\rm lock}(\Lambda) = \frac{3}{2}\,\mathsf{K}_{ALP}\left(1 + \frac{\mathsf{K}_{ALP}\Lambda}{\pi^2}\right), \tag{497}$$

and, wherever the admissible root function

$$\alpha_*(\Lambda) := \alpha(\mathfrak{D}_{\rm lock}(\Lambda))$$

is defined on a neighborhood of $\Lambda_{\rm in}$*, one has*

$$\left.\frac{{\rm d}\alpha_*}{{\rm d}\Lambda}\right|_{\Lambda=\Lambda_{\rm in}} = \left.\frac{{\rm d}\alpha}{{\rm d}D}\right|_{D=\mathfrak{D}_{\rm lock}(\Lambda_{\rm in})}\left.\frac{\rm d}{{\rm d}\Lambda}\mathfrak{D}_{\rm lock}(\Lambda)\right|_{\Lambda=\Lambda_{\rm in}}. \tag{498}$$

The exact vector input corresponds to $\Lambda_{\rm in} = \Lambda_{\rm geom}$*, whereas the current reduced numerical realization corresponds to* $\Lambda_{\rm in} = \Lambda^{\rm (th)}_{\rm geom}$*.*

Proof. Differentiating Eq. (486) gives

$$\frac{\rm d}{{\rm d}D}\left(1 - \Theta_{1,\rm eff}D + D^2\Phi_{\rm dyn}(D)\right) = -\Theta_{1,\rm eff} + 2D\Phi_{\rm dyn}(D) + D^2\Phi'_{\rm dyn}(D),$$

which proves Eq. (494). Next, differentiating Eq. (495) directly yields

$$\frac{{\rm d}\alpha}{{\rm d}D} = \pi\,\mathfrak{R}_{\rm moth}(D)^{-1/2} - \frac{\pi D}{2}\,\mathfrak{R}_{\rm moth}(D)^{-3/2}\,\mathfrak{R}'_{\rm moth}(D).$$

Factoring out $\pi\mathfrak{R}_{\mathrm{moth}}(D)^{-1/2}$ gives

$$\frac{\mathrm{d}\alpha}{\mathrm{d}D}=\pi\,\frac{1-\dfrac{D}{2}\dfrac{\mathfrak{R}'_{\mathrm{moth}}(D)}{\mathfrak{R}_{\mathrm{moth}}(D)}}{\sqrt{\mathfrak{R}_{\mathrm{moth}}(D)}},$$

which is Eq. (496). Differentiating Eq. (482) gives

$$\frac{\mathrm{d}}{\mathrm{d}\Lambda}\mathfrak{D}_{\mathrm{lock}}(\Lambda)=\frac{3}{2}\mathsf{K}_{\mathrm{ALP}}+\frac{3}{2}\mathsf{K}_{\mathrm{ALP}}\,\frac{\mathsf{K}_{\mathrm{ALP}}\Lambda}{\pi^2}=\frac{3}{2}\mathsf{K}_{\mathrm{ALP}}\left(1+\frac{\mathsf{K}_{\mathrm{ALP}}\Lambda}{\pi^2}\right),$$

which is Eq. (497).

By the admissibility assumption at Λ_{in}, together with the local differentiability of Φ_{dyn} and the local positivity of $\mathfrak{R}_{\mathrm{moth}}$, the composed root function

$$\alpha_*(\Lambda)=\alpha(\mathfrak{D}_{\mathrm{lock}}(\Lambda))$$

is well defined and differentiable on a neighborhood of Λ_{in}. Applying the ordinary chain rule at $\Lambda=\Lambda_{\mathrm{in}}$ gives Eq. (498). □

B. Operational meaning of the geometric lock

The baseline geometric lock has the following operational reading. For every positive vector-shell input or specified representative Λ, the baseline shell closure defines the scalar target map

$$\mathfrak{D}_{\mathrm{lock}}(\Lambda)=\frac{3}{2}\,\mathsf{K}_{\mathrm{ALP}}\,\Lambda\left(1+\frac{\mathsf{K}_{\mathrm{ALP}}\Lambda}{2\pi^2}\right).$$

This algebraic target is defined for every $\Lambda>0$. The scalar admissibility requirement enters only when one asks whether this target is attained on the retained scalar branch. For scalar evaluators covered by definition IX.3, theorem 21 applies whenever

$$\mathfrak{D}_{\mathrm{lock}}(\Lambda)\in\mathcal{A}_{\mathrm{scal}},\qquad 0<\pi\,\frac{\mathfrak{D}_{\mathrm{lock}}(\Lambda)}{\sqrt{\mathfrak{R}_{\mathrm{moth}}(\mathfrak{D}_{\mathrm{lock}}(\Lambda))}}<1.$$

Under these conditions the admissible lock root is unique and is given by

$$\alpha_*(\Lambda)=\pi\,\frac{\mathfrak{D}_{\mathrm{lock}}(\Lambda)}{\sqrt{\mathfrak{R}_{\mathrm{moth}}(\mathfrak{D}_{\mathrm{lock}}(\Lambda))}}.$$

In particular, in the exact vector-input case one may write

$$\mathfrak{D}_*\equiv\mathfrak{D}_{\mathrm{lock}}(\Lambda_{\mathrm{geom}}),\qquad \alpha_*\equiv\alpha_*(\Lambda_{\mathrm{geom}}).$$

If the same admissibility conditions hold at $\Lambda=\Lambda^{(\mathrm{th})}_{\mathrm{geom}}$, then the corresponding reduced numerical realization is

$$\mathfrak{D}^{(\mathrm{th})}_*\equiv\mathfrak{D}_{\mathrm{lock}}(\Lambda^{(\mathrm{th})}_{\mathrm{geom}}),\qquad \alpha^{(\mathrm{th})}_*\equiv\alpha_*(\Lambda^{(\mathrm{th})}_{\mathrm{geom}}).$$

Remark. For scalar evaluators covered by definition IX.3, the baseline lock is the one-variable equation

$$\mathcal{D}_{\mathrm{C}}(\alpha)=\mathfrak{D}_{\mathrm{lock}}(\Lambda),$$

supplemented by the admissibility conditions

$$\mathfrak{D}_{\mathrm{lock}}(\Lambda)\in\mathcal{A}_{\mathrm{scal}},\qquad 0<\pi\,\frac{\mathfrak{D}_{\mathrm{lock}}(\Lambda)}{\sqrt{\mathfrak{R}_{\mathrm{moth}}(\mathfrak{D}_{\mathrm{lock}}(\Lambda))}}<1.$$

The exact vector-input case is obtained by setting $\Lambda=\Lambda_{\mathrm{geom}}$, equivalently

$$\mathcal{D}_{\mathrm{C}}(\alpha)=\mathfrak{D}_*,\qquad \mathfrak{D}_*\equiv\mathfrak{D}_{\mathrm{lock}}(\Lambda_{\mathrm{geom}}).$$

The current reduced numerical realization is obtained by setting $\Lambda=\Lambda^{(\mathrm{th})}_{\mathrm{geom}}$, equivalently

$$\mathcal{D}_{\mathrm{C}}(\alpha)=\mathfrak{D}^{(\mathrm{th})}_*,\qquad \mathfrak{D}^{(\mathrm{th})}_*\equiv\mathfrak{D}_{\mathrm{lock}}(\Lambda^{(\mathrm{th})}_{\mathrm{geom}}).$$

The distinction is essential. The first equation uses the exact vector input, whereas the second uses the current reduced numerical representative. Neither equation uses a measured value of α, a QED coefficient, or a fitted benchmark target.

X. NUMERICAL REALIZATION AND EXTERNAL DIAGNOSTIC COMPARISONS

This section records the numerical output of the baseline geometric lock in the current article realization and compares it with external benchmark values only after the internal computation has been completed. The numerical flow is split into the reduced geometric vector input, the derived scalar target, intermediate shell quantities, the resulting lock root, and reference-only diagnostics. Throughout this section, the word "current" refers to the specified reduced vector ledger and the rank-5 scalar evaluator used in this realization; it does not refer to an exact operator-limit value.

The quantity reported here is not presented as the final exact value of the physical fine-structure constant. It is the baseline-lock output obtained by combining the reduced vector representative $\Lambda^{(\mathrm{th})}_{\mathrm{geom}}$ with the current rank-5 scalar evaluator for $\mathcal{D}_{\mathrm{C}}(\alpha)$. Benchmark values of α, QED coefficients, and measured magnetic-moment data enter only after the internal lock has been computed, as external diagnostics. Future operator-level refinements of the vector or scalar shell sectors may shift the realized number. The purpose of the present section is numerical accounting of this specified realization and of the internal shell quantities that control it.

The dependency order in this section is fixed. First, the reduced vector input $\Lambda^{(\mathrm{th})}_{\mathrm{geom}}$ is taken from the vector numerical ledger. Second, the baseline ALP map produces the reduced scalar target

$$\mathfrak{D}^{(\mathrm{th})}_{*} \equiv \mathfrak{D}_{\mathrm{lock}}\big(\Lambda^{(\mathrm{th})}_{\mathrm{geom}}\big).$$

Third, the rank-5 scalar evaluator is inverted on its admissible branch at the target $\mathfrak{D}^{(\mathrm{th})}_{*}$ to obtain $\alpha^{(\mathrm{th})}_{*}$. External benchmark values are introduced only after these three internal steps have been completed and are used only in the diagnostic comparison table.

Remark (Numerical protocol and displayed precision)*.* The numerical values in this section are central values of the current reduced realization. The audit computation uses high-precision arithmetic, the odd vector-source cutoff $j \le 101$, Gauss–Legendre shell quadrature, and a scalar-root tolerance far below the displayed digits. In the reproducibility ledger used for the present tables, the working precision is 100 decimal digits, the shell-source quadrature uses 512 nodes, and the scalar root tolerance is 10^{-95}. The displayed residuals therefore certify the arithmetic solution of the stated reduced equations. They do not certify the unresolved operator-level tail of the exact scalar or vector problem. Derived table rows, such as inverse values, differences, relative deviations, and sigma counts, are evaluated from the full-precision internal ledger before rounding. Consequently, exact cross-row reconstruction from the truncated printed entries is not guaranteed at the last displayed digits.

Remark (External benchmark used only for the diagnostic comparison)*.* For the diagnostic comparison table only, we use the CODATA 2022 inverse-form benchmark

$$\alpha^{-1}_{\mathrm{ref}} = 137.035999177, \qquad u\big(\alpha^{-1}\big) = 2.1 \times 10^{-8}. \tag{499}$$

This is an external benchmark value. It is not used in $\Lambda^{(\mathrm{th})}_{\mathrm{geom}}$, $\mathfrak{D}^{(\mathrm{th})}_{*}$, the scalar inversion, or the selection of α_*. The corresponding direct-alpha value and propagated one-sigma uncertainty are

$$\alpha_{\mathrm{ref}} = \frac{1}{\alpha^{-1}_{\mathrm{ref}}}, \qquad u(\alpha) = \left|\frac{\mathrm{d}}{\mathrm{d}x}\, x^{-1}\right|_{x=\alpha^{-1}_{\mathrm{ref}}} u\big(\alpha^{-1}\big) = \frac{u(\alpha^{-1})}{(\alpha^{-1}_{\mathrm{ref}})^2}. \tag{500}$$

This benchmark is an external diagnostic datum and is not used in the lock computation, in the construction of $\mathfrak{D}^{(\mathrm{th})}_{*}$, or in the evaluation of $\Lambda^{(\mathrm{th})}_{\mathrm{geom}}$. The uncertainty $u(\alpha)$ propagated in Eq. (500) is only the quoted external benchmark uncertainty; it does not include any realization-level uncertainty of the present shell computation.

A. Inputs, intermediate quantities, and current article lock output

Proposition 53 (Lock output in the current reduced realization)**.** *Using the current reduced vector representative* $\Lambda^{(\mathrm{th})}_{\mathrm{geom}}$ *together with the current rank-*5 *glued-shell scalar evaluator for* $\mathcal{D}_{\mathrm{C}}(\alpha)$*, define*

$$\mathfrak{D}^{(\mathrm{th})}_{*} \equiv \mathfrak{D}_{\mathrm{lock}}\big(\Lambda^{(\mathrm{th})}_{\mathrm{geom}}\big) = \frac{3}{2}\,\mathsf{K}_{ALP}\,\Lambda^{(\mathrm{th})}_{\mathrm{geom}}\left(1 + \frac{\mathsf{K}_{ALP}\Lambda^{(\mathrm{th})}_{\mathrm{geom}}}{2\pi^2}\right). \tag{501}$$

The current numerical lock equation is

$$\mathcal{D}_{\mathrm{C}}(\alpha) = \mathfrak{D}^{(\mathrm{th})}_{*}. \tag{502}$$

This equation is imposed on the chosen rank-5 scalar evaluator on its retained admissible branch. For this numerical input, the admissibility conditions of Eq. (492) *are satisfied, and the audit bracket*

$$10^{-3} \le \alpha \le 2 \times 10^{-2}$$

contains the unique admissible reduced root $\alpha_*^{(\mathrm{th})}$*. The current reduced root value and its inverse are reported in table XIX. The external diagnostic comparison is reported separately in table XX.*

Proof. Substituting the current reduced vector input Eq. (481) into Eq. (501) gives

$$\begin{aligned}\mathfrak{D}_*^{(\mathrm{th})} &= \frac{3}{2}\,\mathsf{K}_{\mathrm{ALP}}\,\Lambda_{\mathrm{geom}}^{(\mathrm{th})}\left(1 + \frac{\mathsf{K}_{\mathrm{ALP}}\Lambda_{\mathrm{geom}}^{(\mathrm{th})}}{2\pi^2}\right)\\ &= 0.00231545783196185938805\ldots > 0.\end{aligned}$$

For the chosen rank-5 scalar evaluator, the retained dynamic term $\Phi_{\mathrm{dyn}}(\mathfrak{D}_*^{(\mathrm{th})})$ is finite and real at this point. Direct evaluation of the retained mother radicand gives

$$\begin{aligned}\mathfrak{R}_{\mathrm{moth}}(\mathfrak{D}_*^{(\mathrm{th})}) &= 1 - \Theta_{1,\mathrm{eff}}\mathfrak{D}_*^{(\mathrm{th})} + \big(\mathfrak{D}_*^{(\mathrm{th})}\big)^2\Phi_{\mathrm{dyn}}(\mathfrak{D}_*^{(\mathrm{th})})\\ &= 0.99367151249618252037\ldots > 0.\end{aligned}$$

Hence

$$\mathfrak{D}_*^{(\mathrm{th})} \in \mathcal{A}_{\mathrm{scal}}.$$

On this D-only admissible branch, the scalar mother equation at the fixed target $D = \mathfrak{D}_*^{(\mathrm{th})}$ is

$$\mathfrak{D}_*^{(\mathrm{th})} = \left(\frac{\alpha}{\pi}\right)\sqrt{\mathfrak{R}_{\mathrm{moth}}(\mathfrak{D}_*^{(\mathrm{th})})}.$$

Since $\mathfrak{D}_*^{(\mathrm{th})} > 0$ and $\sqrt{\mathfrak{R}_{\mathrm{moth}}(\mathfrak{D}_*^{(\mathrm{th})})} > 0$, the original principal-root equation has exactly one positive solution,

$$\alpha_*^{(\mathrm{th})} = \pi\,\frac{\mathfrak{D}_*^{(\mathrm{th})}}{\sqrt{\mathfrak{R}_{\mathrm{moth}}(\mathfrak{D}_*^{(\mathrm{th})})}}.$$

Substitution of the current numerical values gives

$$\alpha_*^{(\mathrm{th})} = 0.0072973525650506003338\ldots.$$

Therefore

$$10^{-3} < \alpha_*^{(\mathrm{th})} < 2 \times 10^{-2} < 1,$$

so the stated audit bracket contains the admissible positive-branch root. The inverse value

$$\big(\alpha_*^{(\mathrm{th})}\big)^{-1} = 137.035999163494704022\ldots$$

is the direct reciprocal of the same reduced root. No external benchmark enters any step of this computation. □

Definition X.1 (Diagnostic operational bridge used in the numerical audit)**.** For audit purposes only, after the current reduced target

$$\mathfrak{D}_*^{(\mathrm{th})} \equiv \mathfrak{D}_{\mathrm{lock}}\big(\Lambda_{\mathrm{geom}}^{(\mathrm{th})}\big)$$

and the associated overlap strength

$$\zeta_* \equiv \frac{\mathsf{K}_{\mathrm{ALP}}}{2\pi^2}\,\Lambda_{\mathrm{geom}}^{(\mathrm{th})}$$

Item	Symbol	Value
Current reduced lock output	$\alpha_*^{(\mathrm{th})}$	**0.0072973525650506003338**
Inverse reduced lock output	$\left(\alpha_*^{(\mathrm{th})}\right)^{-1}$	**137.035999163494704022**
Current reduced vector representative	$\Lambda_{\mathrm{geom}}^{(\mathrm{th})}$	0.6916831461069910267161597076345744739664
Vector overlap strength	ζ_*	$7.8195528195469174163 \times 10^{-5}$
Current reduced scalar target	$\mathfrak{D}_*^{(\mathrm{th})}$	0.00231545783196185938806
Current scalar radicand	$\mathfrak{R}_{\mathrm{moth}}(\mathfrak{D}_*^{(\mathrm{th})})$	0.993671512496182520379
Scalar block at the reduced lock output	$\mathcal{D}_{\mathrm{C}}\left(\alpha_*^{(\mathrm{th})}\right)$	0.00231545783196185938806
Baseline ALP check	$\pi^2\zeta_*(1+\zeta_*)/\mathfrak{D}_*^{(\mathrm{th})}$	0.333333333333333333333
Diagnostic bridge value	$\mathcal{D}_{\mathrm{total}}^{\mathrm{audit}}\left(\alpha_*^{(\mathrm{th})}\right)$	0.00231527620142896854289
Numerical scalar lock residual	$\mathcal{D}_{\mathrm{C}}\left(\alpha_*^{(\mathrm{th})}\right) - \mathfrak{D}_*^{(\mathrm{th})}$	$-2.3887201124972 \times 10^{-96}$

TABLE XIX. Internal values for the current reduced baseline-lock realization. These values are outputs of the present rank-5 scalar evaluator with the reduced vector representative $\Lambda_{\mathrm{geom}}^{(\mathrm{th})}$. They are not fitted inputs, and no external benchmark is used in producing them.

have been fixed, define

$$\mathcal{D}_{\mathrm{total}}^{\mathrm{audit}}(\alpha) \equiv \mathfrak{D}_*^{(\mathrm{th})} - x(\alpha)\,\zeta_* + \frac{x(\alpha)^2\zeta_*^2}{4\mathfrak{D}_*^{(\mathrm{th})}}, \qquad x(\alpha) = \frac{\alpha}{\pi}. \tag{503}$$

This bridge value is not used to select α_*. The root is selected solely by

$$\mathcal{D}_{\mathrm{C}}(\alpha) = \mathfrak{D}_*^{(\mathrm{th})}.$$

The quantity $\mathcal{D}_{\mathrm{total}}^{\mathrm{audit}}(\alpha_*)$ is reported only to audit the operational slowdown map used later in reference-only comparisons.

Proposition 54 (Associated shell quantities at the current reduced lock output)**.** *At the current reduced lock output $\alpha_*^{(\mathrm{th})}$, let*

$$\mathfrak{D}_*^{(\mathrm{th})} \equiv \mathfrak{D}_{\mathrm{lock}}\big(\Lambda_{\mathrm{geom}}^{(\mathrm{th})}\big).$$

Then the associated shell quantities are

$$\zeta_* = \frac{\mathsf{K}_{ALP}}{2\pi^2}\,\Lambda_{\mathrm{geom}}^{(\mathrm{th})}, \tag{504}$$

$$\mathcal{D}_{\mathrm{C}}\left(\alpha_*^{(\mathrm{th})}\right) = \mathfrak{D}_*^{(\mathrm{th})}, \tag{505}$$

and

$$\mathcal{D}_{\mathrm{total}}^{\mathrm{audit}}\left(\alpha_*^{(\mathrm{th})}\right) = \mathfrak{D}_*^{(\mathrm{th})} - x_*\zeta_* + \frac{x_*^2\zeta_*^2}{4\mathfrak{D}_*^{(\mathrm{th})}}, \qquad x_* = \frac{\alpha_*^{(\mathrm{th})}}{\pi}. \tag{506}$$

Their current numerical values are reported in table XIX.

Proof. Equation (504) is Eq. (432) evaluated at the current reduced vector input $\Lambda_{\mathrm{geom}}^{(\mathrm{th})}$, with the central ALP coefficient written as $\mathsf{K}_{\mathrm{ALP}}$. Equation (505) is the lock identity Eq. (502). Equation (506) is the diagnostic bridge Eq. (503) evaluated at $\alpha = \alpha_*^{(\mathrm{th})}$. □

Remark (Current numerical status). The present numerical output is determined by two ingredients; the reduced vector representative $\Lambda_{\mathrm{geom}}^{(\mathrm{th})}$ and the current rank-5 scalar evaluator for $\mathcal{D}_{\mathrm{C}}(\alpha)$. It should therefore be read as the reduced lock output of this article realization, namely $\alpha_*^{(\mathrm{th})}$. Reference-only QED-induced scalar branches and external benchmark values are useful diagnostics, yet they do not enter the primary lock. Future operator-level refinements of the vector input or of the scalar evaluator may shift the realized number. The main point of the present section is to make the internal lock accounting explicit, including the distinction between arithmetic residuals and unresolved realization-level uncertainty.

Item	Symbol	Value
Adopted benchmark in inverse form	$\alpha_{\mathrm{ref}}^{-1}$	137.035999177
Quoted one-sigma uncertainty	$u(\alpha^{-1})$	2.1×10^{-8}
Derived benchmark in direct form	α_{ref}	0.00729735256433142503025
Propagated one-sigma uncertainty	$u(\alpha)$	$1.11827844341124 \times 10^{-12}$
Difference in inverse form	$\Delta(\alpha^{-1}) = \left(\alpha_*^{(\mathrm{th})}\right)^{-1} - \alpha_{\mathrm{ref}}^{-1}$	$-1.3505295978180 \times 10^{-8}$
Difference in direct form	$\Delta\alpha = \alpha_*^{(\mathrm{th})} - \alpha_{\mathrm{ref}}$	$7.1917530313216 \times 10^{-13}$
Relative difference in parts per trillion	$10^{12}\Delta\alpha/\alpha_{\mathrm{ref}}$	98.55290625
Deviation in sigma units	$z_\sigma(\alpha) = \Delta\alpha/u(\alpha)$	**0.6431093324**

TABLE XX. Diagnostic external comparison of the current reduced baseline-lock realization against the adopted benchmark. This table is included for orientation only. It does not promote $\alpha_*^{(\mathrm{th})}$ to a final physical value, and it does not feed back into the lock computation. The digits shown beyond the benchmark uncertainty are arithmetic guard digits used to make the comparison reproducible. The displayed sigma count uses only the quoted external benchmark uncertainty and does not include a realization-level uncertainty of the shell computation.

B. Local sensitivities

The differential dependence of the baseline lock root on the vector-shell input variable has already been derived in proposition 52. Here we record only its local evaluation at the reduced vector input used in the current realization. This is a realization-level sensitivity. It is not an operator-level uncertainty certificate and not an external benchmark comparison.

Proposition 55 (Local sensitivity at the current reduced vector input)**.** *Assume the hypotheses of proposition 52 at* $\Lambda_{\mathrm{in}} = \Lambda_{\mathrm{geom}}^{(\mathrm{th})}$. *Assume moreover that there exists an open interval* $I_\Lambda \subset (0,\infty)$ *containing* $\Lambda_{\mathrm{geom}}^{(\mathrm{th})}$ *such that*

$$\mathfrak{D}_{\mathrm{lock}}(\Lambda) \in \mathcal{A}_{\mathrm{scal}}, \qquad 0 < \pi\,\frac{\mathfrak{D}_{\mathrm{lock}}(\Lambda)}{\sqrt{\mathfrak{R}_{\mathrm{moth}}(\mathfrak{D}_{\mathrm{lock}}(\Lambda))}} < 1 \qquad \textit{for all } \Lambda \in I_\Lambda.$$

Define

$$\mathfrak{D}_*^{(\mathrm{th})} \equiv \mathfrak{D}_{\mathrm{lock}}(\Lambda_{\mathrm{geom}}^{(\mathrm{th})}), \qquad \alpha_*^{(\mathrm{th})} \equiv \alpha_*(\Lambda_{\mathrm{geom}}^{(\mathrm{th})}) = \pi\,\frac{\mathfrak{D}_*^{(\mathrm{th})}}{\sqrt{\mathfrak{R}_{\mathrm{moth}}(\mathfrak{D}_*^{(\mathrm{th})})}}.$$

Then the admissible positive branch

$$\alpha_*(\Lambda) = \pi\,\frac{\mathfrak{D}_{\mathrm{lock}}(\Lambda)}{\sqrt{\mathfrak{R}_{\mathrm{moth}}(\mathfrak{D}_{\mathrm{lock}}(\Lambda))}}$$

is differentiable at $\Lambda = \Lambda_{\mathrm{geom}}^{(\mathrm{th})}$. *Evaluating Eq.* (498) *at the current reduced vector input* $\Lambda_{\mathrm{geom}}^{(\mathrm{th})}$*, one obtains*

$$\left.\frac{\mathrm{d}\alpha_*(\Lambda)}{\mathrm{d}\Lambda}\right|_{\Lambda=\Lambda_{\mathrm{geom}}^{(\mathrm{th})}} = 0.0105843988474707163121, \tag{507}$$

and the corresponding logarithmic sensitivity

$$\left.\frac{\mathrm{d}\ln\alpha_*}{\mathrm{d}\ln\Lambda}\right|_{\Lambda=\Lambda_{\mathrm{geom}}^{(\mathrm{th})}} = \frac{\Lambda_{\mathrm{geom}}^{(\mathrm{th})}}{\alpha_*^{(\mathrm{th})}}\left.\frac{\mathrm{d}\alpha_*}{\mathrm{d}\Lambda}\right|_{\Lambda=\Lambda_{\mathrm{geom}}^{(\mathrm{th})}} = 1.00324744202885998923. \tag{508}$$

Proof. Let

$$\mathfrak{D}_*^{(\mathrm{th})} \equiv \mathfrak{D}_{\mathrm{lock}}(\Lambda_{\mathrm{geom}}^{(\mathrm{th})}).$$

By Eq. (494), the radicand derivative at this point is

$$\mathfrak{R}'_{\mathrm{moth}}\big(\mathfrak{D}_*^{(\mathrm{th})}\big) = -\Theta_{1,\mathrm{eff}} + 2\mathfrak{D}_*^{(\mathrm{th})}\,\Phi_{\mathrm{dyn}}\big(\mathfrak{D}_*^{(\mathrm{th})}\big) + \big(\mathfrak{D}_*^{(\mathrm{th})}\big)^2\Phi'_{\mathrm{dyn}}\big(\mathfrak{D}_*^{(\mathrm{th})}\big).$$

Therefore, by Eq. (496),

$$\left.\frac{\mathrm{d}\alpha}{\mathrm{d}D}\right|_{D=\mathfrak{D}_*^{(\mathrm{th})}} = \pi\,\frac{1-\dfrac{\mathfrak{D}_*^{(\mathrm{th})}}{2}\dfrac{\mathfrak{R}'_{\mathrm{moth}}(\mathfrak{D}_*^{(\mathrm{th})})}{\mathfrak{R}_{\mathrm{moth}}(\mathfrak{D}_*^{(\mathrm{th})})}}{\sqrt{\mathfrak{R}_{\mathrm{moth}}(\mathfrak{D}_*^{(\mathrm{th})})}}.$$

Also, by Eq. (497),

$$\left.\frac{\mathrm{d}}{\mathrm{d}\Lambda}\mathfrak{D}_{\mathrm{lock}}(\Lambda)\right|_{\Lambda=\Lambda_{\mathrm{geom}}^{(\mathrm{th})}} = \frac{3}{2}\,\mathsf{K}_{\mathrm{ALP}}\left(1+\frac{\mathsf{K}_{\mathrm{ALP}}\Lambda_{\mathrm{geom}}^{(\mathrm{th})}}{\pi^2}\right).$$

Hence the chain rule gives

$$\left.\frac{\mathrm{d}\alpha_*}{\mathrm{d}\Lambda}\right|_{\Lambda=\Lambda_{\mathrm{geom}}^{(\mathrm{th})}} = \left.\frac{\mathrm{d}\alpha}{\mathrm{d}D}\right|_{D=\mathfrak{D}_*^{(\mathrm{th})}}\left.\frac{\mathrm{d}}{\mathrm{d}\Lambda}\mathfrak{D}_{\mathrm{lock}}(\Lambda)\right|_{\Lambda=\Lambda_{\mathrm{geom}}^{(\mathrm{th})}}.$$

Substituting the current reduced numerical data for $\Lambda_{\mathrm{geom}}^{(\mathrm{th})}$, $\mathfrak{D}_*^{(\mathrm{th})}$, $\mathfrak{R}_{\mathrm{moth}}(\mathfrak{D}_*^{(\mathrm{th})})$, and $\mathfrak{R}'_{\mathrm{moth}}(\mathfrak{D}_*^{(\mathrm{th})})$ gives

$$\left.\frac{\mathrm{d}}{\mathrm{d}\Lambda}\mathfrak{D}_{\mathrm{lock}}(\Lambda)\right|_{\Lambda=\Lambda_{\mathrm{geom}}^{(\mathrm{th})}} = 0.0033478318638907561668\ldots,$$

and

$$\left.\frac{\mathrm{d}\alpha}{\mathrm{d}D}\right|_{D=\mathfrak{D}_*^{(\mathrm{th})}} = 3.1615682261802195882\ldots.$$

Therefore

$$\begin{aligned}\left.\frac{\mathrm{d}\alpha_*}{\mathrm{d}\Lambda}\right|_{\Lambda=\Lambda_{\mathrm{geom}}^{(\mathrm{th})}} &= \left.\frac{\mathrm{d}\alpha}{\mathrm{d}D}\right|_{D=\mathfrak{D}_*^{(\mathrm{th})}}\left.\frac{\mathrm{d}}{\mathrm{d}\Lambda}\mathfrak{D}_{\mathrm{lock}}(\Lambda)\right|_{\Lambda=\Lambda_{\mathrm{geom}}^{(\mathrm{th})}}\\ &= 0.010584398847470716312\mathrm{1}.\end{aligned}$$

The logarithmic sensitivity is then

$$\left.\frac{\mathrm{d}\ln\alpha_*}{\mathrm{d}\ln\Lambda}\right|_{\Lambda=\Lambda_{\mathrm{geom}}^{(\mathrm{th})}} = \frac{\Lambda_{\mathrm{geom}}^{(\mathrm{th})}}{\alpha_*^{(\mathrm{th})}}\left.\frac{\mathrm{d}\alpha_*}{\mathrm{d}\Lambda}\right|_{\Lambda=\Lambda_{\mathrm{geom}}^{(\mathrm{th})}},$$

and direct evaluation gives

$$\left.\frac{\mathrm{d}\ln\alpha_*}{\mathrm{d}\ln\Lambda}\right|_{\Lambda=\Lambda_{\mathrm{geom}}^{(\mathrm{th})}} = 1.0032474420288599892\mathrm{3}.$$

No external benchmark value is used in this evaluation. □

Remark. The logarithmic sensitivity is close to unity. For perturbations $\delta\Lambda$ such that $\Lambda_{\mathrm{geom}}^{(\mathrm{th})}+\delta\Lambda$ remains in the same admissible local branch interval, one has

$$\frac{\alpha_*(\Lambda_{\mathrm{geom}}^{(\mathrm{th})}+\delta\Lambda)-\alpha_*^{(\mathrm{th})}}{\alpha_*^{(\mathrm{th})}} = 1.00324744202885998923\,\frac{\delta\Lambda}{\Lambda_{\mathrm{geom}}^{(\mathrm{th})}} + O\left(\left|\frac{\delta\Lambda}{\Lambda_{\mathrm{geom}}^{(\mathrm{th})}}\right|^2\right)\qquad\left(\frac{\delta\Lambda}{\Lambda_{\mathrm{geom}}^{(\mathrm{th})}}\to 0\right). \tag{509}$$

Thus any future certified small error bound on the reduced vector input transfers to the reported reduced root through this local factor. Scalar-evaluator uncertainties and nonlocal operator-tail uncertainties must still be accounted for separately. In this one-parameter vector-input direction, the realized root is locally close to proportional to the input.

Year	External diagnostic method	Ref.	$\alpha_{\rm ref}$	$u_{\rm ref}$	$\Delta\alpha$	z_σ
2006	Rb recoil (Bloch)	[21]	0.007297352585472213	4.84587×10^{-11}	-2.04216×10^{-11}	-0.42
2008	Rb recoil + Ramsey–Bordé	[22]	0.007297352549793805	3.30158×10^{-11}	$+1.52568 \times 10^{-11}$	$+0.46$
2011	Rb recoil	[4]	0.007297352571786615	4.84587×10^{-12}	-6.73601×10^{-12}	-1.39
2018	Cs recoil	[5]	0.007297352571307352	1.43779×10^{-12}	-6.25675×10^{-12}	-4.35
2020	Rb recoil	[6]	0.007297352562787136	5.85765×10^{-13}	$+2.26346 \times 10^{-12}$	$+3.86$
2022	CODATA 2022 adjustment	[8]	0.007297352564331425	1.11828×10^{-12}	$+7.19175 \times 10^{-13}$	$+0.64$
2023	e^- moment with QED-derived α	[7]	0.007297352564917190	7.98770×10^{-13}	$+1.33410 \times 10^{-13}$	$+0.17$

TABLE XXI. External benchmark values of α compared with the current reduced lock output $\alpha_*^{(\rm th)}$. The rows mix recoil determinations, the CODATA adjustment, and a QED-mediated electron-moment benchmark; they are shown together only for external orientation. For each row, the central direct-form value $\alpha_{\rm ref}$ is obtained exactly from the quoted inverse-form datum, whereas the listed direct-form uncertainty $u_{\rm ref} \equiv u(\alpha_{\rm ref})$ is the corresponding first-order propagated one-standard-deviation uncertainty. Here $\Delta\alpha \equiv \alpha_*^{(\rm th)} - \alpha_{\rm ref}$ and $z_\sigma \equiv \Delta\alpha/u_{\rm ref}$. The table is purely diagnostic. The displayed digits in $\alpha_{\rm ref}$, $u_{\rm ref}$, and $\Delta\alpha$ include arithmetic guard digits for reproducible comparison. They do not imply benchmark precision beyond the quoted external uncertainty. The value z_σ uses only the quoted external uncertainty; no realization-level shell uncertainty is included, and no external reference value enters the primary geometric lock.

C. Reference-only comparison with external benchmarks

This subsection records post hoc external diagnostics of the current reduced lock output. These comparisons do not enter the internal geometric lock or its numerical realization.

Remark (Conventions for the comparison table). For the reference-only diagnostic rows based on atomic recoil, electron-moment determinations, and CODATA adjustments, the source data are treated in inverse form as α^{-1}. For each row, the direct benchmark value is obtained exactly by inversion,

$$\alpha_{\rm ref} = \frac{1}{\alpha_{\rm ref}^{-1}},$$

whereas the quoted direct-form one-standard-deviation uncertainty is propagated at first order as

$$u_{\rm ref} \equiv u(\alpha_{\rm ref}) = \frac{u(\alpha^{-1})}{(\alpha_{\rm ref}^{-1})^2},$$

in accordance with Eq. (500). The comparison quantities are

$$\Delta\alpha \equiv \alpha_*^{(\rm th)} - \alpha_{\rm ref}, \qquad z_\sigma \equiv \frac{\Delta\alpha}{u_{\rm ref}}.$$

This convention keeps the direct-form benchmark values, the propagated uncertainties, and the reported z_σ entries numerically self-consistent.

The displayed z_σ values use only the quoted external uncertainty. They do not include a realization-level uncertainty for the present shell computation, so they should not be read as a statistical global-fit or tension claim. The rows are external diagnostics introduced only after the internal lock output has been obtained. They do not enter $\Lambda_{\rm geom}^{(\rm th)}$, $\mathfrak{D}_*^{(\rm th)}$, the scalar inversion, or the selection of $\alpha_*^{(\rm th)}$.

D. Graphical diagnostics of the geometric lock

To complement the numerical tables, we display graphical diagnostics of the baseline geometric lock for the reduced realization used in this article. The figures in this subsection are diagnostic only. They introduce no new lock equation, scalar evaluator, or vector input. They visualize the same one-variable baseline lock already defined in the preceding sections.

Recall the baseline target map

$$\mathfrak{D}_{\rm lock}(\Lambda) \equiv \frac{3}{2}\,\mathsf{K}_{\rm ALP}\,\Lambda\left(1 + \frac{\mathsf{K}_{\rm ALP}\Lambda}{2\pi^2}\right), \tag{510}$$

which is the same algebraic map as in Eq. (482), now viewed as a function of a scanned positive geometric input Λ. The scan is diagnostic only and is not a refit of Λ. In the current reduced realization, the plotted vector input is

$$\Lambda_{\rm geom}^{(\rm th)},$$

and the corresponding fixed scalar target is

$$\mathfrak{D}_*^{(\mathrm{th})} \equiv \mathfrak{D}_{\mathrm{lock}}\big(\Lambda_{\mathrm{geom}}^{(\mathrm{th})}\big).$$

For diagnostic purposes, and using the same scalar evaluator as in the current numerical lock, define the scalar residual on the admissible real branch by

$$\Delta_*(\alpha;\Lambda) \equiv \mathcal{D}_{\mathrm{C}}(\alpha) - \mathfrak{D}_{\mathrm{lock}}(\Lambda). \tag{511}$$

Fix $\Lambda > 0$. If

$$\mathfrak{D}_{\mathrm{lock}}(\Lambda) \in \mathcal{A}_{\mathrm{scal}}, \qquad 0 < \pi\,\frac{\mathfrak{D}_{\mathrm{lock}}(\Lambda)}{\sqrt{\mathfrak{R}_{\mathrm{moth}}(\mathfrak{D}_{\mathrm{lock}}(\Lambda))}} < 1, \tag{512}$$

then theorem 21 gives exactly one admissible zero of $\Delta_*(\alpha;\Lambda)$ in the interval $0 < \alpha < 1$. On this admissible scan set, the induced lock map is therefore defined by

$$\mathcal{D}_{\mathrm{C}}\big(\alpha_*(\Lambda)\big) = \mathfrak{D}_{\mathrm{lock}}(\Lambda), \qquad 0 < \alpha_*(\Lambda) < 1, \tag{513}$$

with $\alpha_*(\Lambda)$ the unique admissible solution.

The cumulative geometric stages marked in the current reduced plot are

$$\Lambda_1 \equiv \Lambda_{\mathrm{ind}}, \qquad \Lambda_2 \equiv \Lambda_{\mathrm{ind}} + \Delta\Lambda_{\mathrm{UV}\to\mathrm{IR}}(\ell_0), \tag{514}$$

$$\begin{aligned} \Lambda_3 &\equiv \Lambda_{\mathrm{ind}} + \Delta\Lambda_{\mathrm{UV}\to\mathrm{IR}}(\ell_0) + \Delta\Lambda_{\mathrm{out}}^{[101]}(\eta_0), \\ \Lambda_4 &\equiv \Lambda_{\mathrm{geom}}^{(\mathrm{th})} = \Lambda_{\mathrm{ind}} + \Delta\Lambda_{\mathrm{UV}\to\mathrm{IR}}(\ell_0) + \Delta\Lambda_{\mathrm{out}}^{[101]}(\eta_0)\, R_\chi^{(\mathrm{th})}, \\ R_\chi^{(\mathrm{th})} &\equiv R_\chi^{\mathrm{red}}. \end{aligned} \tag{515}$$

Thus Λ_3 shows the local vector load together with the cutoff bare exterior subtraction before the current source-weighted memory factor is applied, whereas Λ_4 is the current reduced geometric vector representative used in the numerical lock.

Figures 10 and 11 summarize these diagnostics. Figure 10a shows $\mathfrak{D}_{\mathrm{lock}}(\Lambda)$ over the scanned geometric interval and marks the current reduced input $\Lambda_{\mathrm{geom}}^{(\mathrm{th})}$. Figure 10b shows the corresponding residual $\Delta_*(\alpha;\Lambda_{\mathrm{geom}}^{(\mathrm{th})})$ on the admissible real branch. Its unique admissible zero in the displayed scan interval gives the current reduced lock output $\alpha_*^{(\mathrm{th})}$, in accordance with theorem 21.

XI. REFERENCE-ONLY QED-INDUCED SCALAR BRANCH AND INVERSE-α DIAGNOSTIC

This section performs a one-way external diagnostic based only on a retained universal pure-photonic benchmark series. QED does not define the primary scalar branch, the geometric vector input, or the Alpha Lock Point. Leptonic mass-ratio, hadronic, and electroweak contributions are excluded from the present diagnostic. The retained coefficients are treated only as external dimensionless coefficients of a reference pure-photonic series.

We consider only the inverse diagnostic problem. A reference scalar branch is reconstructed from the retained pure-photonic benchmark series and then evaluated against the same current reduced scalar target used in section X. This determines the fine-structure coupling associated with that reference branch. No coefficient reconstructed in this section is fed back into the primary geometric-lock output.

The dependency order is one-way. First, the current reduced scalar target $\mathfrak{D}_*^{(\mathrm{th})}$ has already been fixed by the no-QED geometric lock. Second, the retained external QED benchmark coefficients are mapped through the operational bridge to a formal reference scalar branch $D_{\mathrm{QED}}(x)$. Third, the truncated reference branch is inverted against the already fixed target $\mathfrak{D}_*^{(\mathrm{th})}$. None of these reference coefficients modifies the primary scalar evaluator $\mathcal{D}_{\mathrm{C}}(\alpha)$, the vector representative $\Lambda_{\mathrm{geom}}^{(\mathrm{th})}$, the target $\mathfrak{D}_*^{(\mathrm{th})}$, or the reported reduced lock output $\alpha_*^{(\mathrm{th})}$.

A. Recovering a reference scalar series from a retained QED benchmark

Let

$$g_{e,2}^{\mathrm{QED}}(x) \equiv \frac{g_e^{\mathrm{QED}}(x)}{2} = 1 + a_e^{\mathrm{QED}}(x), \qquad a_e^{\mathrm{QED}}(x) = \sum_{n\geq 1} a_n^{\mathrm{QED}} x^n, \qquad x = \frac{\alpha}{\pi}. \tag{516}$$

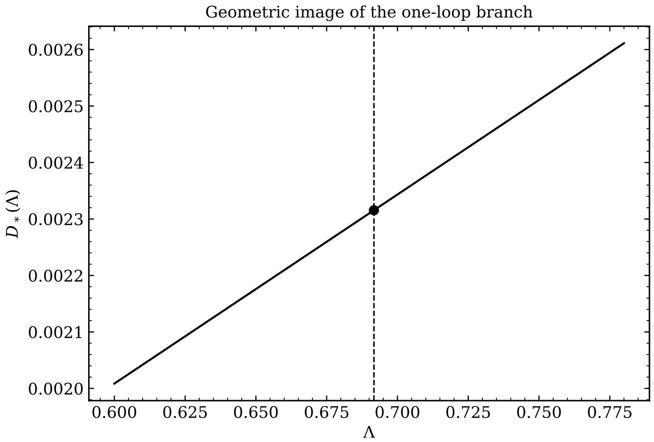

(a) Baseline target map $\mathfrak{D}_{\mathrm{lock}}(\Lambda)$ over the scanned geometric interval. The dashed vertical line marks the current reduced vector input $\Lambda_{\mathrm{geom}}^{(\mathrm{th})}$, and the filled point marks the corresponding fixed scalar target $\mathfrak{D}_*^{(\mathrm{th})}$.

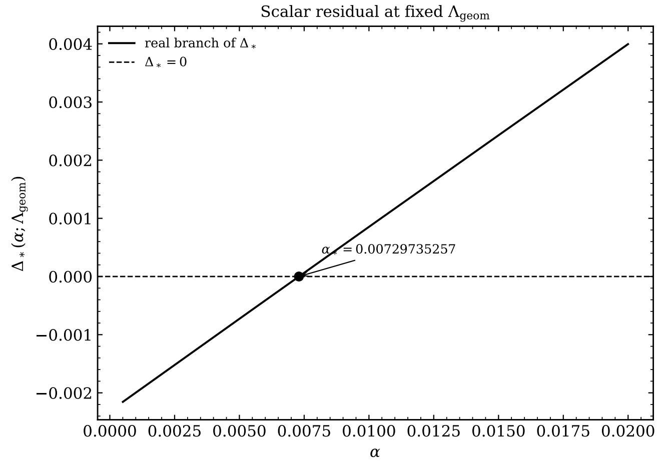

(b) Scalar residual at the current reduced vector input. The solid curve is the admissible real branch of $\Delta_*(\alpha; \Lambda_{\mathrm{geom}}^{(\mathrm{th})})$. Its unique admissible zero, under the admissibility conditions stated in theorem 21, gives the current reduced lock output $\alpha_*^{(\mathrm{th})}$. If an off-branch continuation is shown, it is plotted as the modulus of an analytic continuation and is used only for visual continuity.

FIG. 10. Two complementary graphical diagnostics of the geometric lock. Panel (a) shows the target map $\mathfrak{D}_{\mathrm{lock}}(\Lambda)$ and identifies the fixed scalar target associated with the current reduced vector input. Panel (b) shows the corresponding residual $\Delta_*(\alpha; \Lambda_{\mathrm{geom}}^{(\mathrm{th})})$, whose zero on the admissible real branch yields the current reduced lock output $\alpha_*^{(\mathrm{th})}$ in the displayed scan range. Neither panel introduces a new equation or an external calibration.

In this section $g_{e,2}^{\mathrm{QED}}$ denotes the retained external universal pure-photonic benchmark series used only for reference, and $g_{e,2}$ denotes $g_e/2$, so that $a_e = g_{e,2} - 1$. The coefficients a_n^{QED} are dimensionless retained benchmark coefficients. They are not the full measured electron anomaly and are not used to define the primary scalar evaluator. The operational Relator bridge used in the numerical audit is

$$g_{e,2}(x) = \frac{1}{\sqrt{1 - \mathcal{D}_{\mathrm{total}}(x)}}. \tag{517}$$

Hence the retained-QED-induced total slowdown series is

$$\mathcal{D}_{\mathrm{total}}^{\mathrm{QED}}(x) = 1 - \left(g_{e,2}^{\mathrm{QED}}(x)\right)^{-2}. \tag{518}$$

On the Relator side, the diagnostic inversion uses the same operational bridge map as in the numerical audit,

$$D_{\mathrm{bridge}}(x, D) \equiv D - x\,\zeta(D) + \frac{x^2 \zeta(D)^2}{4D}, \tag{519}$$

where $\zeta(D)$ is the branch analytic at $D = 0$ of the algebraic relation

$$D = 3\pi^2 \zeta(1 + \zeta),$$

and is characterized by

$$\zeta(0) = 0, \qquad \zeta'(0) = \frac{1}{3\pi^2}.$$

For real $D \geq 0$, this is the nonnegative real branch. Explicitly,

$$\zeta(D) = \frac{1}{2}\left(\sqrt{1 + \frac{4D}{3\pi^2}} - 1\right). \tag{520}$$

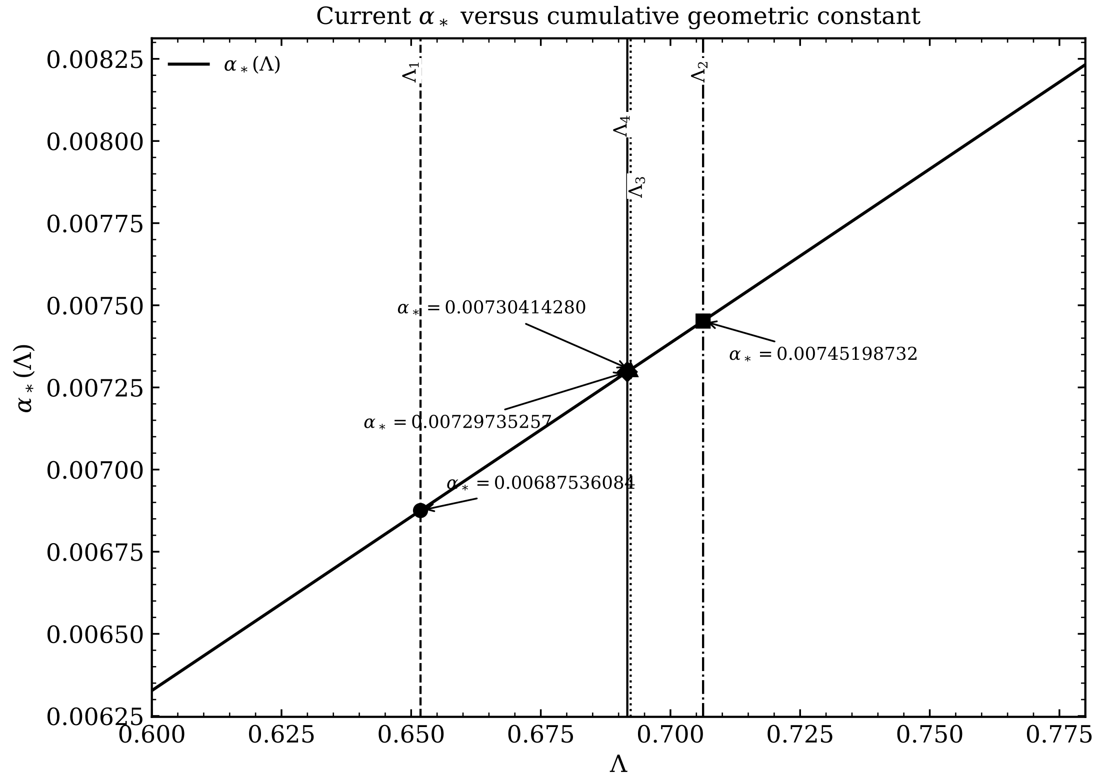

FIG. 11. Induced admissible-root map as a function of the cumulative geometric input, using the same scalar evaluator throughout the scan. The solid curve is the admissible-branch map $\alpha_*(\Lambda)$ on the scanned subset for which the admissibility conditions of theorem 21 hold. The vertical markers identify the cumulative geometric stages Λ_1, Λ_2, Λ_3, and $\Lambda_4 = \Lambda_{\rm geom}^{(\rm th)}$, as defined in Eqs. (514) and (515). The marked point at Λ_4 corresponds to the current reduced output $\alpha_*^{(\rm th)}$. The dotted horizontal line marks the external benchmark $\alpha_{\rm ref}$ for orientation only and is not used in constructing the curve.

The apparent singularity of $D_{\rm bridge}(x, D)$ at $D = 0$ is understood by formal power-series continuation, since $\zeta(D) = D\,h(D)$ with h analytic at the origin. We define the reference QED-induced scalar branch $D_{\rm QED}(x)$, used only in this external diagnostic, as the formal solution of

$$\mathcal{D}_{\rm total}^{\rm QED}(x) = D_{\rm bridge}\big(x, D_{\rm QED}(x)\big). \tag{521}$$

This branch is not the primary scalar shell branch $\mathcal{D}_{\rm C}(\alpha)$, and it is not used in the construction of $\mathfrak{D}_*^{(\rm th)}$. Write

$$D_{\rm QED}(x) = \sum_{n\geq 1} c_n^{\rm QED} x^n, \qquad \mathcal{D}_{\rm total}^{\rm QED}(x) = \sum_{n\geq 1} d_n^{\rm QED} x^n. \tag{522}$$

Lemma 28 (Formal solvability of the reference QED-induced scalar branch)**.** *Let the retained benchmark series satisfy*

$$a_e^{\rm QED}(x) \in x\,\mathbb{R}[[x]].$$

Then there exists a unique formal power series

$$D_{\rm QED}(x) = \sum_{n\geq 1} c_n^{\rm QED} x^n$$

satisfying Eq. (521) *in the ring* $\mathbb{R}[[x]]$*. This is a reference branch determined by the retained benchmark series and the bridge map, not a defining scalar-shell evaluator. If, in addition,*

$$a_1^{\rm QED} = \frac{1}{2},$$

then

$$c_1^{\rm QED} = 1. \tag{523}$$

Proof. Since $a_e^{\mathrm{QED}}(x) = O(x)$, the formal inverse $\left(1 + a_e^{\mathrm{QED}}(x)\right)^{-2}$ exists in $\mathbb{R}[[x]]$, and

$$\mathcal{D}_{\mathrm{total}}^{\mathrm{QED}}(x) = 1 - \left(1 + a_e^{\mathrm{QED}}(x)\right)^{-2} = 2a_e^{\mathrm{QED}} - 3(a_e^{\mathrm{QED}})^2 + 4(a_e^{\mathrm{QED}})^3 - 5(a_e^{\mathrm{QED}})^4 + \cdots . \tag{524}$$

Therefore

$$\mathcal{D}_{\mathrm{total}}^{\mathrm{QED}}(x) = \sum_{n \geq 1} d_n^{\mathrm{QED}} x^n \in x\,\mathbb{R}[[x]].$$

Because $a_1^{\mathrm{QED}} = 1/2$, its linear coefficient is

$$d_1^{\mathrm{QED}} = 2a_1^{\mathrm{QED}} = 1.$$

The function $\zeta(D)$ is analytic at $D = 0$. Its Taylor expansion is

$$\zeta(D) = \frac{D}{3\pi^2} - \frac{D^2}{9\pi^4} + \frac{2D^3}{27\pi^6} - \frac{5D^4}{81\pi^8} + \frac{14D^5}{243\pi^{10}} + O(D^6). \tag{525}$$

Hence

$$\zeta(D) = \sum_{m \geq 1} z_m D^m \in D\,\mathbb{R}[[D]], \qquad z_1 = \frac{1}{3\pi^2}.$$

Since $\zeta(D) \in D\,\mathbb{R}[[D]]$, there is a unique $h(D) \in \mathbb{R}[[D]]$ such that

$$\zeta(D) = D\,h(D), \qquad h(0) = \frac{1}{3\pi^2}.$$

Hence

$$\frac{\zeta(D)^2}{D} = D\,h(D)^2 \in D\,\mathbb{R}[[D]].$$

Define the formal bridge by its removable continuation

$$D_{\mathrm{bridge}}(x, D) \equiv D - x\,\zeta(D) + \frac{x^2}{4}\,D\,h(D)^2. \tag{526}$$

This element belongs to $\mathbb{R}[[x, D]]$, has zero constant term, and agrees with

$$D - x\,\zeta(D) + \frac{x^2 \zeta(D)^2}{4D}$$

whenever $D \neq 0$.

Now seek a formal solution in the form

$$D_{\mathrm{QED}}(x) = \sum_{n \geq 1} c_n^{\mathrm{QED}} x^n.$$

Substitute this series into $D_{\mathrm{bridge}}(x, D)$. For each $n \geq 1$, the coefficient of x^n in $D_{\mathrm{bridge}}(x, D_{\mathrm{QED}}(x))$ has the form

$$c_n^{\mathrm{QED}} + F_n\big(c_1^{\mathrm{QED}}, \ldots, c_{n-1}^{\mathrm{QED}}\big),$$

where F_n is a polynomial expression determined by the already known coefficients z_m. Indeed, $D_{\mathrm{QED}}(x)$ contributes c_n^{QED} directly; the term $x\,\zeta(D_{\mathrm{QED}}(x))$ contributes the coefficient of x^{n-1} in $\zeta(D_{\mathrm{QED}}(x))$, which depends only on $c_1^{\mathrm{QED}}, \ldots, c_{n-1}^{\mathrm{QED}}$ because $\zeta(D)$ has no constant term; and the term

$$x^2 \frac{\zeta(D_{\mathrm{QED}}(x))^2}{4D_{\mathrm{QED}}(x)}$$

contributes the coefficient of x^{n-2} in $\zeta(D_{\mathrm{QED}}(x))^2/D_{\mathrm{QED}}(x)$, which depends only on $c_1^{\mathrm{QED}}, \ldots, c_{n-2}^{\mathrm{QED}}$ because $\zeta(D)^2/D \in D\,\mathbb{R}[[D]]$.

Equating coefficients in

$$\mathcal{D}_{\text{total}}^{\text{QED}}(x) = D_{\text{bridge}}\big(x, D_{\text{QED}}(x)\big)$$

therefore gives the recursion

$$c_n^{\text{QED}} = d_n^{\text{QED}} - F_n\big(c_1^{\text{QED}}, \ldots, c_{n-1}^{\text{QED}}\big), \qquad n \geq 1.$$

Thus the coefficients c_n^{QED} are determined successively and uniquely. This proves existence and uniqueness of the formal series $D_{\text{QED}}(x)$.

At order x, the terms $x\,\zeta(D_{\text{QED}}(x))$ and $x^2 D_{\text{QED}}(x) h(D_{\text{QED}}(x))^2/4$ start at orders x^2 and x^3, respectively. Therefore the coefficient of x in the bridge is only c_1^{QED}. Hence

$$c_1^{\text{QED}} = d_1^{\text{QED}} = 2a_1^{\text{QED}}.$$

Under the retained benchmark normalization $a_1^{\text{QED}} = 1/2$, this gives

$$c_1^{\text{QED}} = 1.$$

This proves Eq. (523). □

Proposition 56 (First reference scalar coefficients induced by the retained QED set)**.** *Using the retained external pure-photonic benchmark central coefficient set*

$$a_1^{\text{QED}} = \frac{1}{2}, \qquad a_2^{\text{QED}} = -0.328478965579193, \qquad a_3^{\text{QED}} = 1.181241456587, \tag{527}$$

and

$$a_4^{\text{QED}} = -1.9122457649264455741526471531265, \qquad a_5^{\text{QED}} = 5.891. \tag{528}$$

The fifth retained coefficient is the central value of the selected tenth-order pure-photonic benchmark set used in this diagnostic. It is not used as a fitted scalar-shell input, and choosing a different published tenth-order benchmark set would define a different external reference diagnostic branch. the corresponding reference scalar coefficients, evaluated from the retained decimal input set Eqs. (527) *and* (528)*, are*

$$c_1^{\text{QED}} = 1, \qquad c_2^{\text{QED}} = -1.3731842032776067428520401789\,3, \tag{529}$$

$$c_3^{\text{QED}} = 3.8001164294311902844982323641\,0, \qquad c_4^{\text{QED}} = -8.8578834082191700324558812351\,9, \tag{530}$$

and

$$c_5^{\text{QED}} = 24.735181450506472598325174337\,7. \tag{531}$$

These displayed decimals are deterministic algebraic outputs of the retained input set. Their benchmark-precision status is discussed in the remark immediately following the proof.

Proof. First expand

$$\mathcal{D}_{\text{total}}^{\text{QED}}(x) = 1 - \big(1 + a_e^{\text{QED}}(x)\big)^{-2} = \sum_{n \geq 1} d_n^{\text{QED}} x^n.$$

Since

$$1 - (1 + a)^{-2} = 2a - 3a^2 + 4a^3 - 5a^4 + 6a^5 + O(a^6),$$

the first five coefficients are

$$d_1^{\text{QED}} = 2a_1^{\text{QED}}, \qquad d_2^{\text{QED}} = 2a_2^{\text{QED}} - 3(a_1^{\text{QED}})^2, \tag{532}$$

$$d_3^{\text{QED}} = 2a_3^{\text{QED}} - 6a_1^{\text{QED}} a_2^{\text{QED}} + 4(a_1^{\text{QED}})^3, \tag{533}$$

$$d_4^{\mathrm{QED}} = 2a_4^{\mathrm{QED}} - 6a_1^{\mathrm{QED}}a_3^{\mathrm{QED}} - 3(a_2^{\mathrm{QED}})^2 + 12(a_1^{\mathrm{QED}})^2 a_2^{\mathrm{QED}} - 5(a_1^{\mathrm{QED}})^4, \tag{534}$$

and

$$\begin{aligned} d_5^{\mathrm{QED}} &= 2a_5^{\mathrm{QED}} - 6a_1^{\mathrm{QED}}a_4^{\mathrm{QED}} - 6a_2^{\mathrm{QED}}a_3^{\mathrm{QED}} + 12(a_1^{\mathrm{QED}})^2 a_3^{\mathrm{QED}} \\ &\quad + 12a_1^{\mathrm{QED}}(a_2^{\mathrm{QED}})^2 - 20(a_1^{\mathrm{QED}})^3 a_2^{\mathrm{QED}} + 6(a_1^{\mathrm{QED}})^5. \end{aligned} \tag{535}$$

Next set

$$D_{\mathrm{QED}}(x) = x + c_2^{\mathrm{QED}}x^2 + c_3^{\mathrm{QED}}x^3 + c_4^{\mathrm{QED}}x^4 + c_5^{\mathrm{QED}}x^5 + O(x^6).$$

Using the Taylor expansion of $\zeta(D)$ from Eq. (525), direct composition gives

$$\begin{aligned} D_{\mathrm{bridge}}\big(x, D_{\mathrm{QED}}(x)\big) = x &+ \left(c_2^{\mathrm{QED}} - \frac{1}{3\pi^2}\right)x^2 \\ &+ \left(c_3^{\mathrm{QED}} - \frac{c_2^{\mathrm{QED}}}{3\pi^2} + \frac{5}{36\pi^4}\right)x^3 \\ &+ \left(c_4^{\mathrm{QED}} - \frac{c_3^{\mathrm{QED}}}{3\pi^2} + \frac{c_2^{\mathrm{QED}}}{4\pi^4} - \frac{5}{54\pi^6}\right)x^4 \\ &+ \left(c_5^{\mathrm{QED}} - \frac{c_4^{\mathrm{QED}}}{3\pi^2} + \frac{c_3^{\mathrm{QED}}}{4\pi^4} + \frac{(c_2^{\mathrm{QED}})^2}{9\pi^4} - \frac{7c_2^{\mathrm{QED}}}{27\pi^6} + \frac{25}{324\pi^8}\right)x^5 \\ &+ O(x^6). \end{aligned}$$

Equating this series with

$$\mathcal{D}_{\mathrm{total}}^{\mathrm{QED}}(x) = d_1^{\mathrm{QED}}x + d_2^{\mathrm{QED}}x^2 + d_3^{\mathrm{QED}}x^3 + d_4^{\mathrm{QED}}x^4 + d_5^{\mathrm{QED}}x^5 + O(x^6)$$

yields

$$c_1^{\mathrm{QED}} = d_1^{\mathrm{QED}} = 1, \qquad c_2^{\mathrm{QED}} = d_2^{\mathrm{QED}} + \frac{1}{3\pi^2}, \tag{536}$$

$$c_3^{\mathrm{QED}} = d_3^{\mathrm{QED}} + \frac{c_2^{\mathrm{QED}}}{3\pi^2} - \frac{5}{36\pi^4} = d_3^{\mathrm{QED}} + \frac{d_2^{\mathrm{QED}}}{3\pi^2} - \frac{1}{36\pi^4}, \tag{537}$$

$$c_4^{\mathrm{QED}} = d_4^{\mathrm{QED}} + \frac{c_3^{\mathrm{QED}}}{3\pi^2} - \frac{c_2^{\mathrm{QED}}}{4\pi^4} + \frac{5}{54\pi^6} = d_4^{\mathrm{QED}} + \frac{d_3^{\mathrm{QED}}}{3\pi^2} - \frac{5d_2^{\mathrm{QED}}}{36\pi^4}, \tag{538}$$

and

$$\begin{aligned} c_5^{\mathrm{QED}} &= d_5^{\mathrm{QED}} + \frac{c_4^{\mathrm{QED}}}{3\pi^2} - \frac{c_3^{\mathrm{QED}}}{4\pi^4} - \frac{(c_2^{\mathrm{QED}})^2}{9\pi^4} + \frac{7c_2^{\mathrm{QED}}}{27\pi^6} - \frac{25}{324\pi^8} \\ &= d_5^{\mathrm{QED}} + \frac{d_4^{\mathrm{QED}}}{3\pi^2} - \frac{5d_3^{\mathrm{QED}}}{36\pi^4} - \frac{(d_2^{\mathrm{QED}})^2}{9\pi^4} + \frac{d_2^{\mathrm{QED}}}{18\pi^6} + \frac{5}{1296\pi^8}. \end{aligned} \tag{539}$$

Substituting Eqs. (527) and (528) into Eqs. (532) to (535), and then substituting the resulting values of d_n^{QED} into Eqs. (536) to (539), gives the coefficients in Eqs. (529) to (531). The calculation is purely algebraic in the retained decimal input set; no value of α_{ref}, $\alpha_*^{(\mathrm{th})}$, or $\mathfrak{D}_*^{(\mathrm{th})}$ enters these coefficients. □

Remark (Precision status of the retained-QED-induced coefficients). The coefficients $\{c_n^{\mathrm{QED}}\}$ above are exact algebraic outputs of the retained benchmark coefficient set written in Eqs. (527) and (528). In particular, the displayed digits of c_5^{QED} inherit the retained central value and retained precision of a_5^{QED}. They should therefore be read as the numerical output of the rounded retained input, not as an independent uncertainty statement for the full pure-photonic benchmark coefficient. The same caution applies to any quantity propagated algebraically from this retained set, including the later diagnostic value $\alpha_{\mathrm{QED}\to\mathrm{D}}^{[5]}$. None of these propagated reference quantities is fed back into the primary scalar branch or the geometric lock.

B. Inverse-α diagnostic at fixed reduced scalar target

Definition XI.1 (Truncated reference QED-induced diagnostic branch)**.** For any truncation order $M \geq 1$ for which the retained reference coefficients $c_1^{\mathrm{QED}}, \ldots, c_M^{\mathrm{QED}}$ have been specified, define

$$D_{\mathrm{QED}}^{[M]}(x) \equiv \sum_{n=1}^{M} c_n^{\mathrm{QED}} x^n. \tag{540}$$

This truncated series is a reference diagnostic branch. It is not the primary scalar evaluator $\mathcal{D}_{\mathrm{C}}(\alpha)$.

Proposition 57 (Retained-QED inverse-α diagnostic at fixed reduced scalar target)**.** *Let*

$$\mathfrak{D}_*^{(\mathrm{th})} \equiv \mathfrak{D}_{\mathrm{lock}}\big(\Lambda_{\mathrm{geom}}^{(\mathrm{th})}\big)$$

denote the same current reduced scalar target used in section X. This is the value defined in Eq. (501) *from the fixed reduced geometric input $\Lambda_{\mathrm{geom}}^{(\mathrm{th})}$. The retained-QED inverse-α diagnostic is defined by the reference root condition*

$$D_{\mathrm{QED}}^{[M]}\Big(\frac{\alpha}{\pi}\Big) = \mathfrak{D}_*^{(\mathrm{th})}. \tag{541}$$

This equation is not the primary lock equation. It is a one-way diagnostic obtained by replacing the article scalar evaluator with the retained QED-induced reference branch after the target has already been fixed. Using the retained central coefficients Eqs. (529) *to* (531) *through $M = 5$, the resulting quintic polynomial*

$$F_5(x) \equiv D_{\mathrm{QED}}^{[5]}(x) - \mathfrak{D}_*^{(\mathrm{th})}$$

has exactly one diagnostic root in the audit bracket

$$I_x = [0.00232281,\, 0.00232282].$$

This is a local uniqueness statement for the retained quintic on I_x only. No global root count outside I_x is claimed, and no statement is made about the untruncated reference series without a separate truncation audit. Denote the unique root of the retained $M = 5$ polynomial on this bracket by $x_{\mathrm{QED}\to D}^{[5]}$, and set

$$\alpha_{\mathrm{QED}\to D}^{[5]} = \pi x_{\mathrm{QED}\to D}^{[5]}.$$

Its numerical value is reported in table XXII.

Proof. Define

$$F_5(x) \equiv D_{\mathrm{QED}}^{[5]}(x) - \mathfrak{D}_*^{(\mathrm{th})}, \qquad x = \frac{\alpha}{\pi}.$$

Using Eqs. (540) and (541), this is a quintic polynomial in x. On the audit bracket

$$I_x = [0.00232281,\, 0.00232282],$$

direct high-precision evaluation of the retained quintic gives

$$F_5(0.00232281) = -9.40444687761024564638 \times 10^{-9} < 0,$$

and

$$F_5(0.00232282) = 5.32370762942082549273 \times 10^{-10} > 0.$$

Thus at least one retained-QED diagnostic zero lies in I_x.

Moreover,

$$F_5'(x) = \frac{\mathrm{d}}{\mathrm{d}x} D_{\mathrm{QED}}^{[5]}(x) = \sum_{n=1}^{5} n\, c_n^{\mathrm{QED}} x^{n-1}.$$

Diagnostic row	$\alpha_{\rm row}$	$\Delta_{\rm ref}\alpha$	z_σ
Current reduced article lock output	**0.0072973525650506003338**	$7.1917530313 \times 10^{-13}$	0.643109
Retained-QED diagnostic	**0.00729735256448495394237**	$1.5352891212 \times 10^{-13}$	0.137290

TABLE XXII. Comparison of the current article baseline lock output and the retained-QED inverse-α diagnostic against the same adopted external benchmark $\alpha_{\rm ref}$ from Eqs. (499) and (500). For each row, $\Delta_{\rm ref}\alpha \equiv \alpha_{\rm row} - \alpha_{\rm ref}$, where $\alpha_{\rm row}$ denotes the value listed in that row, and $z_\sigma \equiv \Delta_{\rm ref}\alpha/u_{\rm ref}$, with $u_{\rm ref} \equiv u(\alpha_{\rm ref})$ the propagated benchmark uncertainty. The displayed z_σ values use only the external benchmark uncertainty and do not include a realization-level uncertainty for either row. The retained-QED row is a central-value diagnostic built from the retained central benchmark coefficients; its last digits should be read with the retained uncertainty of $a_5^{\rm QED}$ and the truncation order $M = 5$ in mind. The retained-QED row is not used as an input to the primary lock, and the current article row is shown here only as the already-computed primary output being compared.

Let

$$a = 0.00232281, \qquad b = 0.00232282.$$

On $I_x = [a, b]$, the retained coefficients have signs

$$c_1^{\rm QED} > 0, \qquad c_2^{\rm QED} < 0, \qquad c_3^{\rm QED} > 0, \qquad c_4^{\rm QED} < 0, \qquad c_5^{\rm QED} > 0.$$

Since $x \mapsto x^m$ is increasing on $[a, b]$ for every integer $m \geq 1$, these sign facts imply, for every $x \in I_x$,

$$2c_2^{\rm QED}x \geq 2c_2^{\rm QED}b, \qquad 3c_3^{\rm QED}x^2 \geq 3c_3^{\rm QED}a^2,$$

$$4c_4^{\rm QED}x^3 \geq 4c_4^{\rm QED}b^3, \qquad 5c_5^{\rm QED}x^4 \geq 5c_5^{\rm QED}a^4.$$

Therefore, for every $x \in I_x$,

$$F_5'(x) \geq 1 + 2c_2^{\rm QED}b + 3c_3^{\rm QED}a^2 + 4c_4^{\rm QED}b^3 + 5c_5^{\rm QED}a^4.$$

Evaluating the right-hand side gives

$$1 + 2c_2^{\rm QED}b + 3c_3^{\rm QED}a^2 + 4c_4^{\rm QED}b^3 + 5c_5^{\rm QED}a^4 = 0.99368175005568340322\ldots > 0.$$

Hence $F_5'(x) > 0$ on I_x, so F_5 is strictly increasing there. Together with the endpoint sign change, the intermediate value theorem yields exactly one zero in I_x. Denote this zero by $x^{[5]}_{\rm QED\to D}$. The corresponding retained-QED diagnostic coupling is

$$\alpha^{[5]}_{\rm QED\to D} = \pi x^{[5]}_{\rm QED\to D}.$$

The numerical root reported in table XXII is obtained by interval bisection on the bracket I_x, with the residual checked against the same fixed target $\mathfrak{D}_*^{(\rm th)}$. This proves existence and uniqueness of the retained diagnostic root on the stated audit bracket. No uniqueness statement outside I_x, no claim about the untruncated reference series, and no uncertainty statement beyond the retained benchmark-coefficient precision and the truncation order $M = 5$, is made here. □

Remark. The retained-QED branch is diagnostic only. It is reconstructed from the retained benchmark coefficients and then inverted against the already fixed reduced target $\mathfrak{D}_*^{(\rm th)}$. It does not replace the primary scalar evaluator $\mathcal{D}_{\rm C}(\alpha)$, and it does not modify the current reduced primary lock output $\alpha_*^{(\rm th)}$.

The difference between the two central values in table XXII is

$$\alpha_*^{(\rm th)} - \alpha^{[5]}_{{\rm QED}\to D} = 5.6564639101 \times 10^{-13}. \tag{542}$$

Correspondingly,

$$10^{12}\,\frac{\alpha_*^{(\rm th)} - \alpha^{[5]}_{{\rm QED}\to D}}{\alpha_*^{(\rm th)}} = 77.51391837. \tag{543}$$

Both numbers are computed from the same central row values shown in table XXII. If a higher-precision internal ledger is used, the subtraction and the relative spread must be recomputed from that ledger before additional digits are displayed. These quantities measure the current central diagnostic spread between the article scalar evaluator and the retained-QED reference branch at the same fixed reduced target. They are not uncertainty estimates and they are not used to adjust either branch.

Part V
Running Alpha

XII. HEAVY-SHELL DECOUPLING ON THE ELECTRON BRANCH AT FIXED GEOMETRIC DATUM

Throughout this part the vector-shell input entering the lock is held fixed before any family deformation is applied. At the exact operator level this input is Λ_{geom}; in a finite Galerkin realization it may be replaced by $\Lambda_{\mathrm{geom}}^{(N)}$; and in the current numerical realization it may be replaced by $\Lambda_{\mathrm{geom}}^{(\mathrm{th})}$. When no distinction is needed, we write Λ_{fix} for the chosen fixed input. No equation in this part recomputes, renormalizes, or benchmark-calibrates that quantity.

In this part, the phrase "running of α" is used only in a fixed-geometry internal sense. It does not denote an independent renormalization-group flow, a QED vacuum-polarization running law, or an experimentally fitted running coupling. It denotes the re-extracted solution of the same fixed geometric lock after the universal scalar branch has been replaced, for the electron diagnostic, by a retained family-resolved effective branch.

We write the scalar branch as a function of

$$x = \frac{\alpha}{\pi}$$

by the convention

$$\mathcal{D}_{\mathrm{C}}(x) \equiv \mathcal{D}_{\mathrm{C}}(\alpha)\big|_{\alpha=\pi x}.$$

All derivatives of $\mathcal{D}_{\mathrm{C}}(x)$ appearing in the fixed-geometry running discussion are derivatives with respect to x, not with respect to α.

The status of the results in this part is the following. The heavy-shell correction on the electron branch is theorem-level only within the retained single-excursion inter-shell channel and under the hypotheses stated below and in the inter-shell appendix. The fixed-geometry shift of the electron root is a local perturbative consequence of that retained channel. Muon and tau running branches are not asserted here. Contributions from lighter-shell resonance on the muon and tau branches would require a closed family-level scalar–vector mother operator, which is not constructed in the present paper.

The dependency order in this section is therefore

$$\Lambda_{\mathrm{fix}} \longrightarrow \mathfrak{D}_{\mathrm{lock,fix}} \equiv \mathfrak{D}_{\mathrm{lock}}(\Lambda_{\mathrm{fix}}) \longrightarrow x_* \longrightarrow \Delta D_e^{\mathrm{H}}(x) \longrightarrow x_e^{\mathrm{run}},\ \alpha_e^{\mathrm{run}}.$$

Here x_* denotes the baseline root associated with the same fixed vector input,

$$\mathcal{D}_{\mathrm{C}}(x_*) = \mathfrak{D}_{\mathrm{lock,fix}}, \qquad \alpha_* = \pi x_*.$$

If the current reduced realization is used, this means $\Lambda_{\mathrm{fix}} = \Lambda_{\mathrm{geom}}^{(\mathrm{th})}$ and $x_* = x_*^{(\mathrm{th})}$. The baseline extraction $\mathfrak{D}_{\mathrm{lock,fix}} \mapsto x_*$ uses the universal scalar branch $\mathcal{D}_{\mathrm{C}}(x)$, whereas the family-resolved extraction to x_e^{run} uses the effective branch $D_e^{\mathrm{eff}}(x)$. In both cases the vector input remains fixed at Λ_{fix}.

Proposition 58 (Compton-baseline rest scale and heavy-shell ratio)**.** *For a charged-lepton branch i labelled by a rest-mass parameter m_i, in the Compton-baseline free rest normalization, the rest scale is*

$$R_i = \frac{\hbar}{m_i c}, \qquad r_*^{(i)} = \pi R_i. \tag{544}$$

The mass parameters m_i are branch labels in this theorem. Their numerical values, if inserted later, are external family data and are not derived by the present shell-lock construction. The family labels are ordered by increasing rest mass; thus $j > i$ means $m_j > m_i$, equivalently $R_j < R_i$ in the Compton-baseline normalization.

For a heavier virtual shell $j > i$, define the dimensionless Compton-baseline rest-scale ratio and the retained heavy-shell decoupling factor by

$$\varrho_{ij}^{\mathrm{H}} := \frac{R_j}{R_i} = \frac{m_i}{m_j}, \qquad \mathfrak{h}_{ij}^{\mathrm{H}} := \left(\varrho_{ij}^{\mathrm{H}}\right)^2 = \left(\frac{m_i}{m_j}\right)^2. \tag{545}$$

Hence, for a genuinely heavier shell,

$$0 < \varrho_{ij}^{\mathrm{H}} < 1, \qquad 0 < \mathfrak{h}_{ij}^{\mathrm{H}} < 1. \tag{546}$$

The symbol $\mathfrak{h}_{ij}^{\mathrm{H}}$ is a geometric decoupling factor. It is not a frequency, not a running coupling, and not an independently fitted strength.

Proof. This is the species-resolved Compton-baseline form of the rest-branch argument used in proposition 28. Replacing the inertial parameter m in that baseline normalization by the lepton branch label m_i gives

$$R_i = \frac{\hbar}{m_i c}.$$

The first-node pinning relation on the same branch then yields

$$r_*^{(i)} = \pi R_i.$$

Therefore, for a heavier shell $j > i$,

$$\varrho_{ij}^{\mathrm{H}} = \frac{R_j}{R_i} = \frac{\hbar/(m_j c)}{\hbar/(m_i c)} = \frac{m_i}{m_j}.$$

Since $m_j > m_i > 0$, one has

$$0 < \frac{m_i}{m_j} < 1,$$

and therefore

$$0 < \varrho_{ij}^{\mathrm{H}} < 1.$$

Squaring the ratio gives

$$\mathfrak{h}_{ij}^{\mathrm{H}} = \left(\varrho_{ij}^{\mathrm{H}}\right)^2 = \left(\frac{m_i}{m_j}\right)^2,$$

and hence

$$0 < \mathfrak{h}_{ij}^{\mathrm{H}} < 1.$$

This proves Eqs. (545) and (546). □

Theorem 22 (Conditional exact reduced law for the retained heavy-shell channel)**.** *Let i be an external shell and let $j > i$, meaning $m_j > m_i$, be a heavier virtual shell. Assume the retained single-excursion inter-shell variational channel of appendix D, including the Hilbert-space, domain, positivity, bounded-gluing, and source-injection hypotheses stated there. Let $x > 0$ lie in the domain of the fixed reference scalar branch, and write*

$$D_i^0(x) = x\,\kappa_i^0(x), \qquad \kappa_i^0(x) > 0.$$

The branch D_i^0 is an input to this conditional family extension. It is not determined by the inter-shell variational elimination.

Within the retained single-excursion channel $i \to j \to i$, the heavy-shell correction to the reference scalar branch $D_i^0(x)$ has the exact reduced form

$$\Delta D^{(i\leftarrow j)}(x) = \frac{x^2}{\kappa_i^0(x)}\,\mathcal{K}_{ij}^{\mathrm{H}}\big(D_i^0(x)\big), \tag{547}$$

where the physical heavy-shell kernel in shell-i units satisfies

$$\mathcal{K}_{ij}^{\mathrm{H}}(D) = \mathfrak{h}_{ij}^{\mathrm{H}}\,\mathcal{M}_{ij}^{\mathrm{H}}(D), \qquad D \geq 0. \tag{548}$$

The normalized memory function $\mathcal{M}_{ij}^{\mathrm{H}}$ is non-negative and completely monotone on $[0, \infty)$. It is strictly positive whenever the injected inter-shell ground-line datum is nonzero, namely whenever

$$\tau_{ij}\phi_i \neq 0.$$

The leading numerical value of its zeroth moment is not fixed by this theorem; it is supplied only after the retained quadrupolar normalization is imposed.

Proof. The retained inter-shell variational channel is constructed in appendix D. In that appendix, the virtual inter-shell field is eliminated exactly in lemma 30. After this elimination, the reduced single-excursion law on the pinned ground line is theorem 25. Applying that theorem to the fixed reference branch

$$D_i^0(x) = x\,\kappa_i^0(x), \qquad \kappa_i^0(x) > 0,$$

gives

$$\Delta D^{(i\leftarrow j)}(x) = \frac{x^2}{\kappa_i^0(x)}\,\mathcal{K}_{ij}^{\mathrm{H}}\big(D_i^0(x)\big),$$

which is exactly Eq. (547).

The kernel factorization in shell-i units is the one obtained from the exact shell-rescaling of the inter-shell resolvent in proposition 75 and from the definition of the normalized heavy-shell memory in definition D.5. Namely, for every $D \geq 0$,

$$\mathcal{K}_{ij}^{\mathrm{H}}(D) = \mathfrak{h}_{ij}^{\mathrm{H}}\,\mathcal{M}_{ij}^{\mathrm{H}}(D).$$

This proves Eq. (548).

Finally, the Stieltjes representation and complete monotonicity of $\mathcal{M}_{ij}^{\mathrm{H}}$ are proved in proposition 76 and corollary 12. In particular, there exists a positive finite Borel measure ν_{ij}^{H} such that

$$\mathcal{M}_{ij}^{\mathrm{H}}(D) = \int_0^\infty \frac{\mathrm{d}\nu_{ij}^{\mathrm{H}}(s)}{1+sD}, \qquad D \geq 0.$$

Under the bounded inter-shell operator hypotheses of the appendix, there exists $S_{ij} < \infty$ such that

$$\operatorname{supp}\nu_{ij}^{\mathrm{H}} \subset [0, S_{ij}].$$

Since $(1+sD)^{-1} \geq 0$ for $D \geq 0$ and $s \geq 0$, this gives

$$\mathcal{M}_{ij}^{\mathrm{H}}(D) \geq 0, \qquad D \geq 0.$$

Moreover, for each $n \geq 1$ and each fixed $D \geq 0$,

$$0 \leq \frac{s^n}{(1+sD)^{n+1}} \leq S_{ij}^n \qquad \text{for } s \in \operatorname{supp}\nu_{ij}^{\mathrm{H}},$$

and the right-hand side is ν_{ij}^{H}-integrable. Dominated convergence therefore justifies differentiation under the integral sign and yields

$$(-1)^n \frac{\mathrm{d}^n}{\mathrm{d}D^n}\mathcal{M}_{ij}^{\mathrm{H}}(D) = n!\int_0^\infty \frac{s^n\,\mathrm{d}\nu_{ij}^{\mathrm{H}}(s)}{(1+sD)^{n+1}} \geq 0, \qquad D \geq 0.$$

Together with the case $n = 0$, this gives complete monotonicity. If $\tau_{ij}\phi_i \neq 0$, then

$$\widehat{\psi}_{ij}^{\mathrm{H}} = (\widehat{\mathbb{L}}_{ij}^{\mathrm{int}})^{-1/2}\tau_{ij}\phi_i \neq 0,$$

because $\widehat{\mathbb{L}}_{ij}^{\mathrm{int}}$ is strictly positive and hence its inverse square root is injective. Therefore

$$\mathcal{M}_{ij}^{\mathrm{H}}(D) = \left\|\big(\mathbb{I} + \mathfrak{h}_{ij}^{\mathrm{H}} D\,\mathbf{S}_{ij}^{\mathrm{H}}\big)^{-1/2}\widehat{\psi}_{ij}^{\mathrm{H}}\right\|^2 > 0, \qquad D \geq 0.$$

This proves the stated positivity, strict positivity, and complete monotonicity. □

Corollary 10 (Conditional leading heavy-shell kernel)**.** *Assume the hypotheses of theorem 22 and, in addition, the retained leading quadrupolar normalization condition of Condition E.1. Then, for each fixed ordered pair (i,j) with $m_j > m_i$, there exist pair-dependent constants $D_{ij}^{\mathrm{loc}} > 0$ and $C_{ij} < \infty$ such that, for $0 \leq D \leq D_{ij}^{\mathrm{loc}}$,*

$$\mathcal{K}_{ij}^{\mathrm{H}}(D) = \mathfrak{h}_{ij}^{\mathrm{H}}\left(\frac{2}{45} + \mathcal{E}_{ij}^{\mathrm{H}}(D)\right), \qquad |\mathcal{E}_{ij}^{\mathrm{H}}(D)| \leq C_{ij} D. \tag{549}$$

This is a retained shell-kernel expansion and is not imported from a QED vacuum-polarization coefficient.

Proof. By theorem 22, the physical heavy-shell kernel factorizes as

$$\mathcal{K}^{\mathrm{H}}_{ij}(D) = \mathfrak{h}^{\mathrm{H}}_{ij}\,\mathcal{M}^{\mathrm{H}}_{ij}(D), \qquad D \ge 0.$$

Under the retained leading quadrupolar normalization, corollary 14 gives constants $D^{\mathrm{loc}}_{ij} > 0$, $C_{ij} < \infty$, and a remainder $\mathcal{E}^{\mathrm{H}}_{ij}$ such that

$$\mathcal{M}^{\mathrm{H}}_{ij}(D) = \frac{2}{45} + \mathcal{E}^{\mathrm{H}}_{ij}(D), \qquad |\mathcal{E}^{\mathrm{H}}_{ij}(D)| \le C_{ij} D, \qquad 0 \le D \le D^{\mathrm{loc}}_{ij}.$$

Multiplying this identity by $\mathfrak{h}^{\mathrm{H}}_{ij}$ yields Eq. (549). □

Theorem 23 (Heavy-shell decoupling on the electron branch)**.** *Assume positive ordered family mass labels*

$$0 < m_e < m_\mu < m_\tau.$$

Let

$$\mathfrak{h}^{\max}_e := \left(\frac{m_e}{m_\mu}\right)^2 = \max\left\{\left(\frac{m_e}{m_\mu}\right)^2, \left(\frac{m_e}{m_\tau}\right)^2\right\}. \tag{550}$$

This symbol is a bookkeeping scale for the retained heavy-shell expansion on the electron branch; it is not a new coupling, not a frequency, and not a running parameter. Let $x = \alpha/\pi$, and let $\mathcal{D}_{\mathrm{C}}(x)$ denote the universal electron scalar branch expressed as a function of x under the convention stated at the beginning of this section. Assume that this reference branch satisfies

$$\mathcal{D}_{\mathrm{C}}(x) = x + O(x^2) \qquad (x \downarrow 0). \tag{551}$$

Assume, in addition, the hypotheses of theorem 22 for the two ordered pairs $(i,j) = (e,\mu)$ and $(i,j) = (e,\tau)$, and assume the retained leading quadrupolar normalization of Condition E.1. Within the retained single-excursion heavy-shell channel, set

$$\Delta D^{\mathrm{H}}_e(x) \equiv \sum_{j=\mu,\tau} \Delta D^{(e\leftarrow j)}(x).$$

Define the family-resolved effective electron branch by

$$D^{\mathrm{eff}}_e(x) := \mathcal{D}_{\mathrm{C}}(x) + \Delta D^{\mathrm{H}}_e(x). \tag{552}$$

Then, as $x \downarrow 0$ with m_e, m_μ, m_τ fixed,

$$\boxed{D^{\mathrm{eff}}_e(x) = \mathcal{D}_{\mathrm{C}}(x) + \frac{2}{45}\left[\left(\frac{m_e}{m_\mu}\right)^2 + \left(\frac{m_e}{m_\tau}\right)^2\right] x^2 + O\big(\mathfrak{h}^{\max}_e x^3\big)}. \tag{553}$$

The $O\big(\mathfrak{h}^{\max}_e x^3\big)$ remainder is taken in the limit $x \downarrow 0$, with m_e, m_μ, m_τ fixed. Its implicit constant is independent of x and depends only on the fixed mass labels, on the pair-dependent local kernel constants from corollary 10 for the pairs (e,μ) and (e,τ), and on a local small-x bound for the reference branch $\mathcal{D}_{\mathrm{C}}(x)$. This remainder is local to the retained single-excursion heavy-shell channel. It does not include repeated inter-shell excursions, lighter-shell resonances, or a complete family-level scalar–vector closure.

Proof. For each $j \in \{\mu,\tau\}$, apply Eq. (547) to the electron reference branch $D^0_e(x) = \mathcal{D}_{\mathrm{C}}(x)$. Then

$$\Delta D^{(e\leftarrow j)}(x) = \frac{x^2}{\kappa^0_e(x)}\,\mathcal{K}^{\mathrm{H}}_{ej}\big(\mathcal{D}_{\mathrm{C}}(x)\big), \qquad \kappa^0_e(x) = \frac{\mathcal{D}_{\mathrm{C}}(x)}{x}. \tag{554}$$

Since $\mathcal{D}_{\mathrm{C}}(x) = x + O(x^2)$ as $x \downarrow 0$, there exist $x_1 > 0$ and $C_{\mathrm{ref}} < \infty$ such that

$$|\mathcal{D}_{\mathrm{C}}(x) - x| \le C_{\mathrm{ref}}\, x^2 \qquad \text{for } 0 < x \le x_1.$$

Therefore, for $0 < x \le x_1$,

$$\kappa_e^0(x) = \frac{\mathcal{D}_{\mathrm{C}}(x)}{x} = 1 + r(x), \qquad |r(x)| \le C_{\mathrm{ref}}\, x.$$

Choose $x_2 \in (0, x_1]$ such that $C_{\mathrm{ref}} x_2 \le \frac{1}{2}$. Then, for $0 < x \le x_2$,

$$\kappa_e^0(x) \ge \frac{1}{2}, \qquad \left| \frac{1}{\kappa_e^0(x)} - 1 \right| = \frac{|r(x)|}{|1 + r(x)|} \le 2C_{\mathrm{ref}}\, x.$$

Hence

$$\big(\kappa_e^0(x)\big)^{-1} = 1 + O(x) \qquad (x \downarrow 0). \tag{555}$$

For each $j \in \{\mu, \tau\}$, corollary 10 gives constants $D_{ej}^{\mathrm{loc}} > 0$, $C_{ej} < \infty$, and a remainder $\mathcal{E}_{ej}^{\mathrm{H}}$ such that

$$\mathcal{K}_{ej}^{\mathrm{H}}(D) = \mathfrak{h}_{ej}^{\mathrm{H}} \left(\frac{2}{45} + \mathcal{E}_{ej}^{\mathrm{H}}(D) \right), \qquad |\mathcal{E}_{ej}^{\mathrm{H}}(D)| \le C_{ej} D, \qquad 0 \le D \le D_{ej}^{\mathrm{loc}}.$$

Since $\mathcal{D}_{\mathrm{C}}(x) \to 0$ as $x \downarrow 0$, and since the previous bound gives $\kappa_e^0(x) \ge 1/2$ for $0 < x \le x_2$, choose $x_3 \in (0, x_2]$ so small that

$$\mathcal{D}_{\mathrm{C}}(x) \le \min\{D_{e\mu}^{\mathrm{loc}}, D_{e\tau}^{\mathrm{loc}}\} \qquad \text{for } 0 < x \le x_3.$$

Then, for the same range of x,

$$\mathcal{D}_{\mathrm{C}}(x) = x\, \kappa_e^0(x) \ge \frac{x}{2} > 0,$$

and hence

$$0 < \mathcal{D}_{\mathrm{C}}(x) \le \min\{D_{e\mu}^{\mathrm{loc}}, D_{e\tau}^{\mathrm{loc}}\} \qquad \text{for } 0 < x \le x_3.$$

Therefore, for $0 < x \le x_3$,

$$\mathcal{K}_{ej}^{\mathrm{H}}\big(\mathcal{D}_{\mathrm{C}}(x)\big) = \mathfrak{h}_{ej}^{\mathrm{H}} \left(\frac{2}{45} + \mathcal{E}_{ej}^{\mathrm{H}}\big(\mathcal{D}_{\mathrm{C}}(x)\big) \right),$$

with

$$\big|\mathcal{E}_{ej}^{\mathrm{H}}\big(\mathcal{D}_{\mathrm{C}}(x)\big)\big| \le C_{ej}\, \mathcal{D}_{\mathrm{C}}(x) = O(x) \qquad (x \downarrow 0).$$

Combining this with Eq. (554) and Eq. (555), we obtain, for $0 < x \le x_0 := \min\{x_2, x_3\}$,

$$\begin{aligned} \Delta D^{(e \leftarrow j)}(x) &= x^2 \big(\kappa_e^0(x)\big)^{-1} \mathfrak{h}_{ej}^{\mathrm{H}} \left(\frac{2}{45} + \mathcal{E}_{ej}^{\mathrm{H}}\big(\mathcal{D}_{\mathrm{C}}(x)\big) \right) \\ &= \frac{2}{45}\, \mathfrak{h}_{ej}^{\mathrm{H}} x^2 + x^2 \mathfrak{h}_{ej}^{\mathrm{H}} \left[\frac{2}{45} \left(\big(\kappa_e^0(x)\big)^{-1} - 1 \right) + \big(\kappa_e^0(x)\big)^{-1} \mathcal{E}_{ej}^{\mathrm{H}}\big(\mathcal{D}_{\mathrm{C}}(x)\big) \right]. \end{aligned}$$

For $0 < x \le x_0$, the bounds above give

$$\left| \big(\kappa_e^0(x)\big)^{-1} - 1 \right| \le 2C_{\mathrm{ref}} x, \qquad \big(\kappa_e^0(x)\big)^{-1} \le 2,$$

and, for a constant $C'_{ej} < \infty$,

$$\big|\mathcal{E}_{ej}^{\mathrm{H}}\big(\mathcal{D}_{\mathrm{C}}(x)\big)\big| \le C'_{ej} x.$$

Therefore the bracket satisfies

$$\left| \frac{2}{45} \left(\big(\kappa_e^0(x)\big)^{-1} - 1 \right) + \big(\kappa_e^0(x)\big)^{-1} \mathcal{E}_{ej}^{\mathrm{H}}\big(\mathcal{D}_{\mathrm{C}}(x)\big) \right| \le \left(\frac{4C_{\mathrm{ref}}}{45} + 2C'_{ej} \right) x.$$

Hence

$$\Delta D^{(e\leftarrow j)}(x) = \frac{2}{45}\,\mathfrak{h}^{\mathrm{H}}_{ej}x^2 + O\big(\mathfrak{h}^{\mathrm{H}}_{ej}x^3\big) \qquad (x\downarrow 0).$$

Summing over the two retained heavier charged leptons $j=\mu,\tau$ gives

$$\Delta D^{\mathrm{H}}_e(x) = \frac{2}{45}\left[\left(\frac{m_e}{m_\mu}\right)^2 + \left(\frac{m_e}{m_\tau}\right)^2\right]x^2 + \sum_{j=\mu,\tau} O\big(\mathfrak{h}^{\mathrm{H}}_{ej}x^3\big)\,.$$

Since there are only two fixed heavy species and $\mathfrak{h}^{\mathrm{H}}_{ej} \le \mathfrak{h}^{\max}_e$ for $j=\mu,\tau$, the sum of the two remainder terms is $O(\mathfrak{h}^{\max}_e x^3)$. Therefore

$$\Delta D^{\mathrm{H}}_e(x) = \frac{2}{45}\left[\left(\frac{m_e}{m_\mu}\right)^2 + \left(\frac{m_e}{m_\tau}\right)^2\right]x^2 + O\big(\mathfrak{h}^{\max}_e x^3\big) \qquad (x\downarrow 0).$$

Using

$$D^{\mathrm{eff}}_e(x) = \mathcal{D}_{\mathrm{C}}(x) + \Delta D^{\mathrm{H}}_e(x),$$

this is exactly Eq. (553). □

Remark (Scope of the retained family channel). The theorem above concerns only the retained heavy-shell single-excursion channel. Repeated heavy excursions and higher inter-shell contractions are not used in the present paper. In the bookkeeping adopted here, such terms are assigned beyond the retained leading electron deformation. They are therefore not part of the load-bearing universal electron-α extraction, and no complete estimate of the full family correction is claimed here. The correction ΔD^{H}_e is used only for the fixed-geometry family diagnostic developed in the following section.

Remark (Why only the electron branch is theorem-level here). The electron branch is the only one for which the retained family channel contains exclusively heavier virtual shells. No lower-shell resonance exists below the electron. A muon- or tau-branch extension would require a common family-level scalar–vector mother operator, a rule for lighter-shell resonance admission, and control of repeated inter-shell excursions. Without those ingredients, inserting $i=\mu$ or $i=\tau$ into the present heavy-shell formulas yields only partial diagnostics rather than complete running branches or predicted muon/tau fine-structure roots.

XIII. FIXED-GEOMETRY ELECTRON α SHIFT

The meaning of the fixed-geometry electron α-shift used in this section is as follows. The vector-shell input entering the geometric target is held fixed before any family deformation is applied. At the exact operator level this input is Λ_{geom}; in a finite Galerkin realization it may be replaced by $\Lambda^{(N)}_{\mathrm{geom}}$; and in the current reduced numerical realization it may be replaced by $\Lambda^{(\mathrm{th})}_{\mathrm{geom}}$. We write Λ_{fix} for whichever one of these fixed vector-shell inputs has been chosen. No equation in this section recomputes, renormalizes, or benchmark-calibrates Λ_{fix}.

For the electron family diagnostic, the universal scalar branch is compared with the retained family-resolved effective branch, and the same fixed geometric target is solved again using that effective branch. The resulting local root displacement is the fixed-geometry electron α-shift studied here. It is not an independent renormalization-group flow law and it does not replace the primary baseline root.

In this section we write

$$\mathcal{D}_{\mathrm{C}}(x) \equiv \mathcal{D}_{\mathrm{C}}(\alpha)\big|_{\alpha=\pi x}, \qquad x = \frac{\alpha}{\pi},$$

and all derivatives such as $\mathcal{D}'_{\mathrm{C}}(x_*)$ are derivatives with respect to the variable x, not with respect to α.

Definition XIII.1 (Baseline and re-extracted roots at fixed geometric datum)**.** Let

$$\mathfrak{D}_{\mathrm{lock,fix}} \equiv \mathfrak{D}_{\mathrm{lock}}(\Lambda_{\mathrm{fix}})$$

denote the fixed scalar target determined by the baseline geometric lock. Let x_* be the baseline electron root defined by

$$\mathcal{D}_{\mathrm{C}}(x_*) = \mathfrak{D}_{\mathrm{lock,fix}}, \qquad \alpha_* = \pi x_*. \tag{556}$$

With the retained effective electron branch $D_e^{\mathrm{eff}}(x)$ defined in Eq. (552), the fixed-geometry re-extracted root x_e^{run} is defined by

$$D_e^{\mathrm{eff}}\big(x_e^{\mathrm{run}}\big) = \mathfrak{D}_{\mathrm{lock,fix}}. \tag{557}$$

The corresponding fixed-geometry re-extracted coupling is

$$\alpha_e^{\mathrm{run}} \coloneqq \pi x_e^{\mathrm{run}}. \tag{558}$$

Theorem 24 (Linearized electron shift at fixed geometric datum)**.** *Assume that $\mathcal{D}_{\mathrm{C}} \in C^2(I_*)$ on an open interval $I_* \ni x_*$, with*

$$\mathcal{D}_{\mathrm{C}}(x_*) = \mathfrak{D}_{\mathrm{lock,fix}}, \qquad \mathcal{D}_{\mathrm{C}}'(x_*) \neq 0.$$

Assume also that $\Delta D_e^{\mathrm{H}} \in C^1(I_*)$, and that there is a small bookkeeping parameter $\delta_{\mathrm{H}} > 0$ such that

$$\sup_{x\in I_*} \big(|\Delta D_e^{\mathrm{H}}(x)| + |(\Delta D_e^{\mathrm{H}})'(x)|\big) \leq C_{\mathrm{H}}\delta_{\mathrm{H}}, \tag{559}$$

with C_{H} independent of δ_{H}. Then there exists a closed interval $J_* \subset I_*$, centered at x_*, such that for sufficiently small δ_{H} the Eq. (557) has a unique root $x_e^{\mathrm{run}} \in J_*$. Writing

$$\delta x_e = x_e^{\mathrm{run}} - x_*, \qquad \delta\alpha_e = \alpha_e^{\mathrm{run}} - \alpha_*,$$

one has, as $\delta_{\mathrm{H}} \downarrow 0$ with J_*, x_*, and the reference branch $\mathcal{D}_{\mathrm{C}}$ fixed,

$$\boxed{\delta x_e = -\frac{\Delta D_e^{\mathrm{H}}(x_*)}{\mathcal{D}_{\mathrm{C}}'(x_*)} + O_{\mathrm{loc}}(\delta_{\mathrm{H}}^2), \qquad \delta\alpha_e = -\pi\,\frac{\Delta D_e^{\mathrm{H}}(x_*)}{\mathcal{D}_{\mathrm{C}}'(x_*)} + O_{\mathrm{loc}}(\delta_{\mathrm{H}}^2)}. \tag{560}$$

Proof. Define

$$F_0(x) \equiv \mathcal{D}_{\mathrm{C}}(x) - \mathfrak{D}_{\mathrm{lock,fix}}, \qquad \Phi_e(x) \equiv F_0(x) + \Delta D_e^{\mathrm{H}}(x).$$

Since

$$F_0(x_*) = 0, \qquad F_0'(x_*) = \mathcal{D}_{\mathrm{C}}'(x_*) \neq 0,$$

continuity of $\mathcal{D}_{\mathrm{C}}'$ yields $r > 0$ and $c_0 > 0$ such that

$$J_* = [x_* - r, x_* + r] \subset I_*, \qquad |\mathcal{D}_{\mathrm{C}}'(x)| \geq 2c_0 \quad \text{for every } x \in J_*.$$

Since $\mathcal{D}_{\mathrm{C}}'$ is continuous and does not vanish on J_*, its sign is constant on J_*. Hence $F_0' = \mathcal{D}_{\mathrm{C}}'$ has a fixed sign on J_*, and F_0 is strictly monotone there. Moreover,

$$F_0(x_* - r) = -\int_{x_*-r}^{x_*} \mathcal{D}_{\mathrm{C}}'(u)\,\mathrm{d}u, \qquad F_0(x_* + r) = \int_{x_*}^{x_*+r} \mathcal{D}_{\mathrm{C}}'(u)\,\mathrm{d}u.$$

Since $\mathcal{D}_{\mathrm{C}}'$ has a fixed nonzero sign on J_*, these two endpoint values have opposite signs. Therefore

$$F_0(x_* - r)\,F_0(x_* + r) < 0.$$

Set

$$m_0 \coloneqq \min\big\{|F_0(x_* - r)|,\ |F_0(x_* + r)|\big\} > 0.$$

If δ_{H} is so small that

$$C_{\mathrm{H}}\delta_{\mathrm{H}} < m_0, \qquad C_{\mathrm{H}}\delta_{\mathrm{H}} \leq c_0,$$

then

$$|\Delta D_e^{\mathrm{H}}(x)| \leq \|\Delta D_e^{\mathrm{H}}\|_{C^0(I_*)} \leq C_{\mathrm{H}}\delta_{\mathrm{H}} < |F_0(x)|$$

at the two endpoints $x = x_* - r$ and $x = x_* + r$. Therefore $\Phi_e(x_* - r)$ and $\Phi_e(x_* + r)$ have the same signs as $F_0(x_* - r)$ and $F_0(x_* + r)$, respectively. In particular,

$$\Phi_e(x_* - r)\,\Phi_e(x_* + r) < 0.$$

By the intermediate value theorem, Φ_e has at least one zero in J_*.

Next, for every $x \in J_*$,

$$|\Phi_e'(x)| = |\mathcal{D}_{\mathrm{C}}'(x) + (\Delta D_e^{\mathrm{H}})'(x)| \geq |\mathcal{D}_{\mathrm{C}}'(x)| - |(\Delta D_e^{\mathrm{H}})'(x)| \geq 2c_0 - C_{\mathrm{H}}\delta_{\mathrm{H}} \geq c_0.$$

Hence Φ_e' never vanishes on J_*. Since Φ_e' is continuous, its sign is constant on J_*. Therefore Φ_e is strictly monotone on J_*, and the zero obtained by the intermediate value theorem is unique. Denote it by x_e^{run}.

Since $\Phi_e(x_e^{\mathrm{run}}) = 0$, the mean-value theorem applied to Φ_e on the interval with endpoints x_* and x_e^{run} gives a point ξ_e between them such that

$$-\Phi_e(x_*) = \Phi_e'(\xi_e)\,(x_e^{\mathrm{run}} - x_*).$$

Since $F_0(x_*) = 0$, one has

$$\Phi_e(x_*) = \Delta D_e^{\mathrm{H}}(x_*).$$

Therefore

$$|\delta x_e| = \frac{|\Phi_e(x_*)|}{|\Phi_e'(\xi_e)|} \leq \frac{|\Delta D_e^{\mathrm{H}}(x_*)|}{c_0} \leq \frac{C_{\mathrm{H}}}{c_0}\,\delta_{\mathrm{H}},$$

so

$$\delta x_e = O_{\mathrm{loc}}(\delta_{\mathrm{H}}).$$

Now write

$$x_e^{\mathrm{run}} = x_* + \delta x_e.$$

Since x_e^{run} is a root of Φ_e,

$$0 = \Phi_e(x_* + \delta x_e) = \mathcal{D}_{\mathrm{C}}(x_* + \delta x_e) - \mathcal{D}_{\mathrm{C}}(x_*) + \Delta D_e^{\mathrm{H}}(x_* + \delta x_e) - \Delta D_e^{\mathrm{H}}(x_*) + \Delta D_e^{\mathrm{H}}(x_*).$$

Taylor's theorem with remainder for $\mathcal{D}_{\mathrm{C}} \in C^2(I_*)$ gives, for some $\xi_{\mathcal{D}_{\mathrm{C}}}$ between x_* and $x_* + \delta x_e$,

$$\mathcal{D}_{\mathrm{C}}(x_* + \delta x_e) - \mathcal{D}_{\mathrm{C}}(x_*) = \mathcal{D}_{\mathrm{C}}'(x_*)\,\delta x_e + \frac{1}{2}\,\mathcal{D}_{\mathrm{C}}''(\xi_{\mathcal{D}_{\mathrm{C}}})\,\delta x_e^2.$$

The mean-value theorem for $\Delta D_e^{\mathrm{H}} \in C^1(I_*)$ gives, for some ξ_{H} between x_* and $x_* + \delta x_e$,

$$\Delta D_e^{\mathrm{H}}(x_* + \delta x_e) - \Delta D_e^{\mathrm{H}}(x_*) = (\Delta D_e^{\mathrm{H}})'(\xi_{\mathrm{H}})\,\delta x_e.$$

Substituting these two identities into the previous equation yields

$$0 = \Delta D_e^{\mathrm{H}}(x_*) + \mathcal{D}_{\mathrm{C}}'(x_*)\,\delta x_e + \frac{1}{2}\,\mathcal{D}_{\mathrm{C}}''(\xi_{\mathcal{D}_{\mathrm{C}}})\,\delta x_e^2 + (\Delta D_e^{\mathrm{H}})'(\xi_{\mathrm{H}})\,\delta x_e.$$

Because J_* is compact and $\mathcal{D}_{\mathrm{C}}''$ is continuous, $\mathcal{D}_{\mathrm{C}}''$ is bounded on J_*. Because

$$\|\Delta D_e^{\mathrm{H}}\|_{C^1(I_*)} \leq C_{\mathrm{H}}\delta_{\mathrm{H}},$$

one has

$$|(\Delta D_e^{\mathrm{H}})'(\xi_{\mathrm{H}})| \leq C_{\mathrm{H}}\delta_{\mathrm{H}}.$$

Together with $\delta x_e = O_{\mathrm{loc}}(\delta_{\mathrm{H}})$, this gives

$$\frac{1}{2}\,\mathcal{D}_{\mathrm{C}}''(\xi_{\mathcal{D}_{\mathrm{C}}})\,\delta x_e^2 = O_{\mathrm{loc}}(\delta_{\mathrm{H}}^2), \qquad (\Delta D_e^{\mathrm{H}})'(\xi_{\mathrm{H}})\,\delta x_e = O_{\mathrm{loc}}(\delta_{\mathrm{H}}^2).$$

Therefore

$$0 = \Delta D_e^{\mathrm{H}}(x_*) + \mathcal{D}'_{\mathrm{C}}(x_*)\,\delta x_e + O_{\mathrm{loc}}(\delta_{\mathrm{H}}^2),$$

and hence

$$\delta x_e = -\frac{\Delta D_e^{\mathrm{H}}(x_*)}{\mathcal{D}'_{\mathrm{C}}(x_*)} + O_{\mathrm{loc}}(\delta_{\mathrm{H}}^2).$$

Multiplying by π and using $\delta\alpha_e = \pi\delta x_e$ gives

$$\delta\alpha_e = -\pi\,\frac{\Delta D_e^{\mathrm{H}}(x_*)}{\mathcal{D}'_{\mathrm{C}}(x_*)} + O_{\mathrm{loc}}(\delta_{\mathrm{H}}^2).$$

This proves Eq. (560). □

Corollary 11 (Leading fixed-geometry electron shift from heavy shells)**.** *Under the hypotheses of theorems 23 and 24, and assuming that the expansion of $\Delta D_e^{\mathrm{H}}(x)$ and the corresponding first-derivative expansion are both valid uniformly on the local interval J_* of theorem 24, define*

$$S_e \equiv \left(\frac{m_e}{m_\mu}\right)^2 + \left(\frac{m_e}{m_\tau}\right)^2.$$

Then one has

$$\delta\alpha_e = -\frac{2\pi}{45}\,\frac{S_e x_*^2}{\mathcal{D}'_{\mathrm{C}}(x_*)} + O_{\mathrm{loc}}\big(\mathfrak{h}_e^{\max} x_*^3\big) + O_{\mathrm{loc}}\big((\mathfrak{h}_e^{\max})^2 x_*^2\big)\,. \tag{561}$$

If, in addition, the bookkeeping regime is such that

$$(\mathfrak{h}_e^{\max})^2 x_*^2 \le C_{\mathrm{bk}}\,\mathfrak{h}_e^{\max} x_*^3, \qquad \textit{equivalently} \qquad \mathfrak{h}_e^{\max} \le C_{\mathrm{bk}}\,x_*,$$

for some fixed constant $C_{\mathrm{bk}} > 0$, then the previous estimate reduces to the optional simplified form

$$\delta\alpha_e = -\frac{2\pi}{45}\,\frac{\left[\left(\frac{m_e}{m_\mu}\right)^2 + \left(\frac{m_e}{m_\tau}\right)^2\right] x_*^2}{\mathcal{D}'_{\mathrm{C}}(x_*)} + O_{\mathrm{loc}}\big(\mathfrak{h}_e^{\max} x_*^3\big)\,. \tag{562}$$

This last display is a conditional bookkeeping simplification and is not used unless the domination condition is verified for the chosen numerical regime.

Remark. The sign of the fixed-geometry shift is determined by the sign of $\mathcal{D}'_{\mathrm{C}}(x_*)$ together with the sign of $\Delta D_e^{\mathrm{H}}(x_*)$. Under the retained heavy-shell hypotheses of theorem 23, $\Delta D_e^{\mathrm{H}}(x_*) \ge 0$. Therefore, if the chosen scalar evaluator is locally increasing at x_*, namely if $\mathcal{D}'_{\mathrm{C}}(x_*) > 0$, the leading fixed-geometry electron shift is negative. No sign statement is made without this local monotonicity condition.

Proof. Since $x_* > 0$ and J_* is a closed interval centered at x_*, after possibly shrinking J_* one may assume

$$0 < \frac{x_*}{2} \le x \le \frac{3x_*}{2} \qquad \text{for every } x \in J_*.$$

Define

$$S_e := \left(\frac{m_e}{m_\mu}\right)^2 + \left(\frac{m_e}{m_\tau}\right)^2.$$

By theorem 23, and by the assumed uniform validity of the small-x expansion on J_*, one has

$$\Delta D_e^{\mathrm{H}}(x) = \frac{2}{45}\,S_e\,x^2 + O_{\mathrm{loc}}\big(\mathfrak{h}_e^{\max} x^3\big) \qquad \text{uniformly for } x \in J_*.$$

Evaluating at $x = x_*$ gives

$$\Delta D_e^{\mathrm{H}}(x_*) = \frac{2}{45}\,S_e\,x_*^2 + O_{\mathrm{loc}}\big(\mathfrak{h}_e^{\max} x_*^3\big)\,.$$

By the assumed uniform validity of the differentiated expansion,

$$(\Delta D_e^{\mathrm{H}})'(x) = \frac{4}{45}\, S_e\, x + O_{\mathrm{loc}}\big(\mathfrak{h}_e^{\max} x^2\big) \qquad \text{uniformly for } x \in J_*.$$

Since $S_e \le 2\mathfrak{h}_e^{\max}$ and $x \asymp x_*$ on J_*, this implies

$$\sup_{x\in J_*} |(\Delta D_e^{\mathrm{H}})'(x)| = O_{\mathrm{loc}}(\mathfrak{h}_e^{\max} x_*)\,,$$

and likewise

$$\sup_{x\in J_*} |\Delta D_e^{\mathrm{H}}(x)| = O_{\mathrm{loc}}\big(\mathfrak{h}_e^{\max} x_*^2\big)\,.$$

After shrinking J_* if necessary so that $x \le 1$ on J_*, the bound for the C^0 part is dominated by the bound for the derivative part. Therefore there exists a local constant $C_* < \infty$, independent of x on J_*, such that

$$\sup_{x\in J_*} \big(|\Delta D_e^{\mathrm{H}}(x)| + |(\Delta D_e^{\mathrm{H}})'(x)|\big) \le C_*\, \mathfrak{h}_e^{\max} x_*.$$

Thus the hypothesis of theorem 24 applies on J_* with the local bookkeeping scale

$$\delta_{\mathrm{H}}^{\mathrm{loc}} = \mathfrak{h}_e^{\max} x_*.$$

Applying Eq. (560) with this local scale yields

$$\delta\alpha_e = -\pi\, \frac{\Delta D_e^{\mathrm{H}}(x_*)}{\mathcal{D}_{\mathrm{C}}'(x_*)} + O_{\mathrm{loc}}\Big(\big(\mathfrak{h}_e^{\max} x_*\big)^2\Big)\,.$$

Equivalently,

$$O_{\mathrm{loc}}\Big(\big(\mathfrak{h}_e^{\max} x_*\big)^2\Big) = O_{\mathrm{loc}}\big((\mathfrak{h}_e^{\max})^2 x_*^2\big)\,.$$

Using the explicit value of $\Delta D_e^{\mathrm{H}}(x_*)$ computed above, one obtains

$$\delta\alpha_e = -\frac{2\pi}{45}\, \frac{S_e x_*^2}{\mathcal{D}_{\mathrm{C}}'(x_*)} + O_{\mathrm{loc}}\big(\mathfrak{h}_e^{\max} x_*^3\big) + O_{\mathrm{loc}}\big((\mathfrak{h}_e^{\max})^2 x_*^2\big)\,.$$

Replacing S_e by its definition gives Eq. (561).

If, in addition,

$$(\mathfrak{h}_e^{\max})^2 x_*^2 = O_{\mathrm{loc}}\big(\mathfrak{h}_e^{\max} x_*^3\big)\,,$$

then the quadratic-root remainder is absorbed into the $O_{\mathrm{loc}}(\mathfrak{h}_e^{\max} x_*^3)$ term, and Eq. (562) follows. □

Remark (What is and is not claimed here). The fixed-geometry shift $\delta\alpha_e$ is the precise mathematical content of the fixed-geometry electron α-shift considered here. It is a family-resolved re-extraction of the same fixed ALP target after the scalar branch is deformed by the retained heavy-shell channel. It is not a new renormalization-group law, not a scale-dependent flow of Λ_{geom}, and not a replacement for the primary universal extraction of α_* quoted earlier in the paper. The primary lock output remains the baseline universal value; the present shift is a fixed-geometry family diagnostic.

Remark (Optional fixed-α reading). The same scalar correction can also be read at fixed x as a reflected shift of the auxiliary ALP image Λ_{ALP}. That algebraic reflection, together with the downstream lift to $\mathcal{D}_{\mathrm{total}}$ and to the g_2-proxy, is recorded in appendix F. Those formulas are optional diagnostics only. They are not load-bearing for the extraction of α_*, they do not define a running law, and Λ_{ALP} is only the inverse image of a scalar value under the diagnostic ALP map. It should not be identified with the fixed vector-shell datum Λ_{geom}.

Part VI
Validation and physical consequences

XIV. SCOPE, INFRARED COMPATIBILITY, AND FALSIFIABLE CONSEQUENCES

This section records the scope of the result as explicitly as possible. Its purpose is twofold; first, to separate the assumptions of the construction from the statements derived within those assumptions, and second, to identify the sharpest conditional falsifiability tests of the present shell realization. The emphasis remains on the conditional geometric selection of the admissible coupling α_*. Nothing in this section changes the derivation; it clarifies the logical status of the result and its testable content. Detailed audits of sensitivity, truncation, and numerical robustness are deferred to appendix C.

A. What is derived and what remains postulated

The logical value of the construction depends as much on what it does *not* claim as on what it does claim. We therefore separate the standing inputs from the outputs derived from them.

Proposition 59 (Logical layers of the construction)**.** *The present paper contains three logically distinct layers.*

1. *Standing postulates*
   - *(a) the split arena* $\mathbb{C} \oplus \mathbb{R}^3$*;*
   - *(b) the* Relator *lock* $R\omega = c$*;*
   - *(c) the shell admissibility, analyticity, exterior-regularity, and gauge-regularity assumptions stated in the opening postulate and notation sections.*
2. *Branch selections and shell constructions below the lock*
   - *(a) the maximum-entropy Gaussian generator sheet at fixed second moment, together with the branch width fixed after the minimal one-loop calibration,*
   $$\sigma_{\mathbb{C}} = \frac{R}{\sqrt{\pi}};$$
   - *(b) the minimal branch geometry and matching shell obtained after the minimal winding choice and the first-node shell selection,*
   $$r_* = \pi R, \qquad \eta = \frac{1}{\pi}, \qquad \ell = \frac{1}{\pi\sqrt{\pi}};$$
   - *(c) the quantized charge slot after canonical quantization of the compact phase sector, the infrared Dirac limit under the minimal spinorial completion, and the tree-level value* $g = 2$ *under the calibrated effective spin normalization;*
   - *(d) the scalar shell block* $\mathcal{D}_{\mathrm{C}}(\alpha)$*, defined by the cavity–shell mother pencil, together with finite-rank or reduced scalar evaluators stated separately when numerical values are quoted;*
   - *(e) the vector shell-memory return factor* R_χ*, defined under the shell-memory hypotheses stated in section VII, and the associated geometric vector constant* Λ_{geom}*, with finite-rank and reduced numerical representatives stated separately;*
   - *(f) the shell-geometric logarithmic coefficient in the single-polarization Path-II shell average,*
   $$\mathcal{C}_{\log}^{(II)} = \frac{1}{3},$$
   together with the Path-I/Path-II same-coefficient compatibility statement and the explicit Path-I representative remainder budget.
3. *Baseline lock relation, realized roots, and downstream secondary outputs*

(a) the geometric target map

$$\mathfrak{D}_{\rm lock}(\Lambda) = \frac{3}{2}\,\mathsf{K}_{ALP}\,\Lambda\left(1 + \frac{\mathsf{K}_{ALP}\Lambda}{2\pi^2}\right);$$

(b) the admissible lock equation, after a vector-shell input or specified representative has been fixed,

$$\mathcal{D}_{\rm C}(\alpha) = \mathfrak{D}_{\rm lock}(\Lambda);$$

(c) for a specified scalar evaluator and a fixed vector-shell input, the realized admissible root α_*, with exact, finite-rank, or reduced status inherited from those inputs;

(d) in a later construction, provided the stated analytic hypotheses of the downstream coefficient map hold, the scalar branch can be lifted through the diagnostic ALP image map and the operational orbital slowdown map to produce a secondary realization-level mass-independent electron–photon coefficient sequence $\widehat{A}_1^{(2n)}$. This sequence is conditional on that evaluator and is not used to define or select the primary lock root.

Proof. Item 1 is exactly the standing postulate set assumptions 1 to 4.

In item 2, the Gaussian generator sheet and the width relation $\sigma_{\mathbb{C}} = R/\sqrt{\pi}$ are established in theorem 3 and proposition 12; the minimal branch geometry (r_*, η, ℓ) is fixed in proposition 17 and corollary 2; the quantized charge slot, the infrared Dirac limit, and the tree-level value $g = 2$ are established in theorems 4 to 6 and corollary 3; the scalar shell block is fixed by the mother-pencil construction in definition VI.13 and theorem 7; the exact vector return factor and geometric constant are fixed, under the stated shell-memory hypotheses, by Eqs. (383) and (385); and the shell-geometric logarithmic coefficient together with the baseline shell lock are fixed in theorems 18 and 20.

In item 3, the baseline shell lock is fixed in theorem 20, the target map is definition IX.2, the admissible lock root is given by theorem 21, and the current realization-level root is reported in proposition 53. The last item is a forward summary of the later construction in section XV; it is not used elsewhere in the present section. □

Remark. The most important point in proposition 59 is that the reported value α_* is *not* postulated. The symbol α appears earlier as the symbolic coupling variable of the scalar branch, while the selected value appears only after the shell geometry, the scalar block, the vector geometry, and the logarithmic lock have all been fixed. In a numerical realization, the status of the reported digits is inherited from the chosen scalar evaluator and vector-shell representative.

The paper also does not claim more than it proves. It does not derive the full Standard Model. It does not reproduce the full perturbative apparatus of QED. It does not claim a complete family-level or scale-complete running law. The claim is narrower. Within the stated shell postulates, the baseline lock closure, and a specified scalar–vector realization, the admissible coupling is selected — whenever the admissibility and uniqueness hypotheses of the chosen scalar evaluator hold — as the shell equilibrium of the fixed geometric closure on the minimal electron branch. If the same scalar evaluator also satisfies the analytic hypotheses of the downstream diagnostic lift, it then yields a definite mass-independent electron–photon coefficient sequence as a secondary realization-level consequence.

Remark (Dependency order). The dependency order is

$$\text{standing postulates} \longrightarrow \text{branch selection} \longrightarrow \mathcal{D}_{\rm C},\ \Lambda_{\rm geom},\ \mathcal{C}_{\rm log}^{(II)} \longrightarrow \text{shell lock} \longrightarrow \mathfrak{D}_{*,\rm in} = \mathfrak{D}_{\rm lock}(\Lambda_{\rm in}) \longrightarrow \alpha_*.$$

Reduced numerical representatives, external benchmark values, retained QED coefficient data, and reference-only QED-induced branches enter only after this chain has been fixed. They do not define the postulates, the primary scalar branch, the vector input, the scalar target map, or the Alpha Lock Point.

B. Relation to standard infrared physics

The present construction is not presented as a replacement for standard infrared physics. Rather, within the stated shell postulates and branch selections, it supplies an upstream shell-geometric account of the infrared charged-particle structures recovered in the paper and used, where needed, in the lock construction.

Proposition 60 (Infrared compatibility)**.** *On the minimal charged branch, and within the gauge, sign, compact-phase, spinorial-completion, and retained infrared operator conventions fixed in the paper, the shell construction is compatible with the following standard low-energy charged-particle structures, together with the restricted Pauli-slot statement used in the reporter sector.*

1. the worldline gauge coupling

$$S_{\rm int} = -Q \int A_\mu \, \mathrm{d}x^\mu ;$$

2. the quantized charge slot obtained after canonical quantization of the compact phase sector,

$$Q = kq_0, \qquad k \in \mathbb{Z};$$

3. the minimally coupled Dirac infrared equation obtained under the minimal spinorial infrared completion,

$$(\gamma^\mu \Pi_\mu - mc)\Psi = 0;$$

4. the tree-level magnetic normalization with

$$g = 2,$$

under the calibrated effective spin normalization and, independently, by the Pauli reduction of the minimally coupled Dirac equation, with the two derivations agreeing at the coefficient level;

5. in the retained parity-even magnetic sector classified as mass dimension five in the natural-unit counting convention of definition V.9, and under the restriction that no derivatives act on Ψ or on $F_{\mu\nu}$, the Pauli bilinear

$$\bar{\Psi}\, \sigma^{\mu\nu} F_{\mu\nu} \Psi$$

is the unique retained local Lorentz- and gauge-invariant slot through which a leading magnetic deviation may enter.

Proof. Item 1 is the worldline interaction derived in proposition 20. Item 2 is the compact-phase charge spectrum of theorem 4. Item 3 is the infrared Dirac limit of theorem 5. Item 4 is the coefficient-level agreement between the geometric normalization of corollary 3 and the Pauli reduction of theorem 6. Item 5 is the restricted parity-even no-derivative Pauli-slot uniqueness statement of proposition 27. These references establish the listed infrared structures, and the stated restricted operator classification, under the hypotheses fixed earlier in the paper. □

Remark. The relation to accepted infrared physics is straightforward. Standard local relativistic gauge theory appears here as the infrared description of the shell branch. The present construction adds an upstream geometric statement that perturbative QED does not by itself supply, namely a conditional shell closure that selects an admissible value of a dimensionless coupling variable within the specified shell realization. QED remains the accepted perturbative framework for high-accuracy infrared radiative calculations. The present construction does not replace that framework. Within the specified shell realization, it supplies a shell invariant that selects an admissible value of the dimensionless coupling variable used by the infrared theory and, secondarily, generates a definite pure-photonic coefficient sequence through the specified scalar evaluator.

Remark (Why $g-2$ is only a reporter). The use of

$$a = \frac{g-2}{2}$$

as an infrared reporter does not make the construction $g-2$-centric. It is legitimate because, within the local infrared operator class singled out in definition V.9, namely the retained parity-even mass-dimension-five magnetic sector with no derivatives acting on Ψ or $F_{\mu\nu}$, the leading magnetic deviation from the Dirac value enters through the Pauli term and is therefore encoded by a single gauge-invariant dimensionless scalar. The shell coefficient $\mathcal{C}_{\log}$ is primary; a is only one convenient infrared reporter of it. No measured value of a, no QED anomaly coefficient, and no benchmark $g-2$ datum is used in the primary shell lock.

C. Primary lock output and falsifiable consequences

The present paper separates the internal lock output from the sharpest realization-level falsifiability tests. The currently reported value of α_* in the article realization is a no-QED output of the specified scalar–vector realization of the geometric lock. It is not presented here as an operator-complete final numerical prediction of the physical fine-structure constant. At the present stage, the sharpest conditional falsifiability tests lie in the higher pure-photonic coefficients, in the electron-anomaly normalization, generated from the same specified scalar-shell evaluator by the later lift described below.

Proposition 61 (Internal lock output and realization-level pure-photonic continuation)**.** *Assume that the admissibility hypotheses of theorem 21 hold for the chosen scalar evaluator and the fixed vector-shell input described below. For a specified scalar evaluator and a fixed geometric vector-shell input, computed independently of QED benchmarks, the primary internal output of that realization is the admissible lock root α_*. Let $\Lambda_{\rm in}$ denote that fixed vector-shell input. At exact vector-operator level,*

$$\Lambda_{\rm in} = \Lambda_{\rm geom}.$$

In a finite-rank or reduced realization, $\Lambda_{\rm in}$ is the specified fixed representative used in that realization. For this fixed input define

$$\mathfrak{D}_{*,\rm in} \equiv \mathfrak{D}_{\rm lock}(\Lambda_{\rm in}).$$

Then the lock root is determined by

$$\mathcal{D}_{\rm C}(\alpha_*) = \mathfrak{D}_{*,\rm in}. \tag{563}$$

Equivalently, for the same fixed vector-shell input $\Lambda_{\rm in}$, define

$$\zeta_* = \frac{\mathsf{K}_{ALP}\Lambda_{\rm in}}{2\pi^2}.$$

Then the same baseline target obeys the algebraic identity

$$\frac{\pi^2}{\mathfrak{D}_{*,\rm in}}\,\zeta_*(1+\zeta_*) = \frac{1}{3}. \tag{564}$$

For the current article realization, the corresponding reduced numerical value is $\alpha_*^{(\rm th)}$, as reported in proposition 53.

At the present stage, the sharpest realization-level falsifiability test lies in the mass-independent electron–photon A_1 sector. If the same specified scalar evaluator satisfies the analytic hypotheses of the later coefficient map, then its diagnostic lift through the ALP image map and the operational orbital slowdown map gives the secondary realization-level coefficient sequence

$$g_{e,2}^{\rm Rel}(x) = 1 + \sum_{n\geq 1} \widehat{A}_1^{(2n)} x^n, \qquad x = \frac{\alpha}{\pi}. \tag{565}$$

The higher entries of this sequence, from $\widehat{A}_1^{(12)}$ onward, are conditional forward outputs of the specified no-free-parameter scalar-shell realization; see section XV. The intended falsifiable comparison, once independent benchmark calculations are available in the same A_1 normalization, is with the corresponding mass-independent pure-photonic QED coefficients. Agreement or disagreement must be assessed against the stated realization, truncation, and independent-calculation error budgets.

Proof. By theorem 21, once the chosen scalar evaluator and the fixed vector-shell input $\Lambda_{\rm in}$ satisfy the admissibility hypotheses, there exists exactly one admissible lock root α_*, and it satisfies Eq. (563).

Next, by Eq. (482),

$$\mathfrak{D}_{*,\rm in} = \frac{3}{2}\,\mathsf{K}_{\rm ALP}\,\Lambda_{\rm in}\left(1 + \frac{\mathsf{K}_{\rm ALP}\Lambda_{\rm in}}{2\pi^2}\right).$$

With

$$\zeta_* = \frac{\mathsf{K}_{\rm ALP}\Lambda_{\rm in}}{2\pi^2},$$

this becomes

$$\mathfrak{D}_{*,\rm in} = 3\pi^2\,\zeta_*(1+\zeta_*).$$

Dividing both sides by $3\mathfrak{D}_{*,\rm in}$ gives

$$\frac{\pi^2}{\mathfrak{D}_{*,\rm in}}\,\zeta_*(1+\zeta_*) = \frac{1}{3},$$

which is Eq. (564).

The current numerical realization is the one reported in proposition 53, together with the associated shell data of proposition 54. The final paragraph is a conditional forward summary of the later construction in section XV; it is not used in the derivation of α_* in the present section. □

Remark (Error budget and present status of the α value). The currently reported value $\alpha_*^{(\mathrm{th})}$ is a primary no-QED output of the current scalar–vector realization of the geometric lock. It is not an operator-complete exact value of the physical fine-structure constant. Its remaining realization-level uncertainty enters at least through two channels. The first is the vector-geometric input used in the realization: Λ_{geom} at exact operator level, or the specified fixed representative Λ_{in} in a finite-rank or reduced realization. Future independent evaluations of the shell-matrix resolvent, higher-mode tail, and exterior-memory functional can sharpen that input. The second is the scalar evaluator $\mathcal{D}_{\mathrm{C}}(\alpha)$; its operator-level completion can be tested by rank stability, by independent scalar-shell calculations, and by reference-only comparison with the universal pure-photonic $g-2$ coefficients.

If universal QED coefficients are used to tune or replace the scalar evaluator, the resulting number should be reported as a reference-assisted realization, not as the primary no-QED extraction. In the present paper, the quoted α_* remains independent of QED benchmarks. For this reason it is best read as the current internal lock output rather than as the final operator-complete prediction of the physical fine-structure constant. A future operator-complete scalar and vector realization, with certified scalar and vector error budgets, would be the appropriate setting in which to report the same mechanism as a direct numerical prediction of α.

Remark (Falsifiable content at the present stage). The cleanest present falsifiability test is not the last printed digit of $\alpha_*^{(\mathrm{th})}$. It is the higher mass-independent electron–photon A_1 coefficient sequence generated by the specified no-free-parameter scalar-shell realization. The coefficients $\widehat{A}_1^{(2n)}$ with $n \geq 6$, corresponding to $A_1^{(12)}$ and higher in standard QED notation, are not used as inputs and are not obtained from perturbative QED. Agreement of future independent high-order pure-photonic QED calculations with these values within the combined realization, truncation, and independent-calculation error budgets would provide nontrivial support for this specified realization. Disagreement beyond those combined budgets would falsify the specified realization, not every possible operator completion of the broader framework.

The computational scale of this test is substantial. The independent evaluation of the five-loop universal coefficient $A_1^{(10)}$ already required large-scale multi-loop numerical work [23]. The next coefficients, beginning with $A_1^{(12)}$, therefore constitute demanding future comparisons rather than routine checks.

Scale-dependent shells, non-electronic lepton branches, and precision atomic windows are natural next extensions of the framework, yet they are not needed for the present claim. At the current stage, the article is most sharply falsifiable through the higher mass-independent A_1 universal coefficients, while the no-QED value $\alpha_*^{(\mathrm{th})}$ records the internal numerical state of the present geometric-lock realization together with its unresolved scalar–vector realization-level error budget.

Part VII
Cross-checks and higher-order universal predictions

XV. MASS-INDEPENDENT A_1 ELECTRON ANOMALY; DIAGNOSTIC COMPARISON AND CONDITIONAL HIGHER-ORDER OUTPUTS

Throughout this section we restrict attention to the mass-independent universal electron coefficient sequence, customarily denoted by $A_1^{(2n)}$ in QED. This is the one-lepton universal sector used as an external benchmark. It excludes mass-dependent insertions carrying the scales m_μ and m_τ, as well as hadronic and electroweak contributions. Closed electron subgraphs that belong to the universal one-lepton coefficient are therefore part of the benchmark convention used here.

To avoid terminology ambiguity, the shorthand "pure-photonic" in this section means the mass-independent one-lepton electron–photon benchmark sector just described, in the A_1 convention. It does not mean the narrower no-closed-lepton-loop subset unless that restriction is stated explicitly.

The primary aim of the present paper is the construction of the scalar slowdown block $\mathcal{D}_{\rm C}(\alpha)$ and its lock to the matching-shell geometry within the stated shell postulates. The electron anomalous magnetic moment is therefore not the primary target of the paper. Once a scalar evaluator has been fixed, however, the Relator framework yields a secondary consequence; it produces an α-dependent operational slowdown and hence a realization-level coefficient sequence for the mass-independent electron quantity

$$g_{e,2}(x) \equiv \frac{g_e(x)}{2} = 1 + a_e(x), \qquad a_e(x) \equiv \frac{g_e(x)-2}{2}, \qquad x \equiv \frac{\alpha}{\pi}. \tag{566}$$

Here g_e denotes the positive gyromagnetic-ratio magnitude used in the anomaly expansion. The sign of the electron charge has already been fixed in the branch current convention and is not reintroduced in this diagnostic ratio. This section records that consequence as a numerical diagnostic comparison for the scalar-shell construction and as a source of conditional higher-order outputs for the universal A_1 coefficients.

This restriction is conceptual, not merely numerical. The scalar-shell realization used in this section contains only electron-branch geometric and dynamical data. The additional mass scales associated with μ and τ are therefore not absorbed into the present scalar-shell analysis. They belong to a separate family extension. Accordingly, the external benchmark used below is the mass-independent QED sequence customarily denoted by $A_1^{(2n)}$ in the standard electron-anomaly literature [23, 24].

In standard notation the mass-independent QED expansion of the electron anomaly is

$$a_e^{(A_1)}(x) = \sum_{n\geq 1} A_1^{(2n)} x^n, \qquad g_{e,2}^{(A_1)}(x) = 1 + \sum_{n\geq 1} A_1^{(2n)} x^n. \tag{567}$$

The Relator coefficient extraction below is independent of perturbative QED. QED enters only at the comparison stage. Operationally, the specified scalar evaluator together with the diagnostic ALP image map and the orbital slowdown map acts as a low-dimensional nonlinear generator for a coefficient sequence that can be compared with the retained mass-independent A_1 benchmark sequence.

Throughout this section we write

$$\mathcal{D}_{\rm C}(x) \equiv \mathcal{D}_{\rm C}(\alpha)\big|_{\alpha=\pi x}.$$

The scalar channel determines this function. In order to obtain the operational anomaly map used in the comparison, one must also reconstruct an auxiliary α-dependent overlap image. For this purpose we use only the diagnostic algebraic ALP image associated with Eq. (474), not the fixed-geometric lock equation itself. The diagnostic image relation is

$$\mathcal{D}_{\rm C} = 3\pi^2\zeta(1+\zeta). \tag{568}$$

On the nonnegative branch, this yields

$$\zeta(\mathcal{D}_{\rm C}) = \frac{\sqrt{1+\dfrac{4\mathcal{D}_{\rm C}}{3\pi^2}}-1}{2}. \tag{569}$$

The corresponding auxiliary ALP image is then reconstructed by

$$\Lambda_{\mathrm{ALP}}(x) = \frac{2\pi^2}{\mathsf{K}_{\mathrm{ALP}}}\,\zeta\big(\mathcal{D}_{\mathrm{C}}(x)\big). \tag{570}$$

This auxiliary image is recorded only as a downstream diagnostic of the scalar branch. It does not enter $\mathcal{D}_{\mathrm{total}}(x)$ as an independent input. The operational map $\mathcal{D}_{\mathrm{total}}(x)$ depends directly on $\mathcal{D}_{\mathrm{C}}(x)$ and on the same algebraic overlap image $\zeta(\mathcal{D}_{\mathrm{C}}(x))$, not on a separately supplied vector-shell datum. The label "ALP" refers only to the algebraic Alpha-Lock-Point inversion used in this diagnostic map. The quantity $\Lambda_{\mathrm{ALP}}(x)$ is not a vector-shell datum, not a new geometric input, and not a pion or hadronic quantity.

Remark (Diagnostic status of $\Lambda_{\mathrm{ALP}}(x)$). The auxiliary image $\Lambda_{\mathrm{ALP}}(x)$ of Eq. (570) is not the fixed vector-shell datum Λ_{geom} used in the primary extraction of α. The primary lock uses

$$\Lambda_{\mathrm{geom}} \longmapsto \mathfrak{D}_{\mathrm{lock}}(\Lambda_{\mathrm{geom}}) \longmapsto \alpha_*,$$

with Λ_{geom} fixed before the scalar inversion. By contrast, the diagnostic map in this section first takes the already chosen scalar evaluator, computes $\mathcal{D}_{\mathrm{C}}(x)$, and then reconstructs $\Lambda_{\mathrm{ALP}}(x)$ from the algebraic ALP image. Thus $\Lambda_{\mathrm{ALP}}(x)$ is downstream of $\mathcal{D}_{\mathrm{C}}(x)$, whereas Λ_{geom} is upstream of the primary lock. No value of $\Lambda_{\mathrm{ALP}}(x)$, no QED coefficient, and no electron anomaly datum is fed back into the primary Alpha Lock Point.

For the present realization-level comparison we use the operational orbital slowdown map

$$\mathcal{D}_{\mathrm{total}}(x) = \mathcal{D}_{\mathrm{C}}(x) - x\,\zeta\big(\mathcal{D}_{\mathrm{C}}(x)\big) + \frac{x^2\zeta\big(\mathcal{D}_{\mathrm{C}}(x)\big)^2}{4\mathcal{D}_{\mathrm{C}}(x)} \quad \text{for } \mathcal{D}_{\mathrm{C}}(x) > 0. \tag{571}$$

At $x = 0$, and more generally at any point where the displayed quotient is written with $\mathcal{D}_{\mathrm{C}}(x) = 0$, the last term is defined by analytic continuation. Indeed,

$$\zeta(D) = D\,h(D), \qquad h(D) = \frac{1}{3\pi^2} - \frac{D}{9\pi^4} + \frac{2D^2}{27\pi^6} - \frac{5D^3}{81\pi^8} + O(D^4), \tag{572}$$

so that

$$\frac{x^2\zeta(\mathcal{D}_{\mathrm{C}}(x))^2}{4\mathcal{D}_{\mathrm{C}}(x)} = \frac{x^2\mathcal{D}_{\mathrm{C}}(x)\,h(\mathcal{D}_{\mathrm{C}}(x))^2}{4}, \tag{573}$$

which is analytic wherever $\mathcal{D}_{\mathrm{C}}(x)$ is analytic. The corresponding realization-level Relator map for the electron ratio $g_e/2$ is

$$g_{e,2}^{\mathrm{Rel}}(x) = \frac{1}{\sqrt{1-\mathcal{D}_{\mathrm{total}}(x)}}, \qquad a_e^{\mathrm{Rel}}(x) = g_{e,2}^{\mathrm{Rel}}(x) - 1 \tag{574}$$

The square root is the principal positive branch. As a formal coefficient map, this equation is read on the analytic branch near $x = 0$, where $\mathcal{D}_{\mathrm{total}}(0) = 0$. For numerical evaluation at a physical point, it is used only where $1 - \mathcal{D}_{\mathrm{total}}(x) > 0$. Thus the diagnostic cross-check relations are

$$\mathcal{D}_{\mathrm{C}}(x) \longrightarrow \zeta\big(\mathcal{D}_{\mathrm{C}}(x)\big), \qquad \zeta\big(\mathcal{D}_{\mathrm{C}}(x)\big) \longrightarrow \Lambda_{\mathrm{ALP}}(x), \qquad \big(\mathcal{D}_{\mathrm{C}}(x), \zeta\big(\mathcal{D}_{\mathrm{C}}(x)\big)\big) \longrightarrow \mathcal{D}_{\mathrm{total}}(x) \longrightarrow g_{e,2}^{\mathrm{Rel}}(x),\ a_e^{\mathrm{Rel}}(x).$$

At the external reference point, used only for physical-point comparison and not for constructing the scalar evaluator or selecting a rank,

$$\alpha_{\mathrm{ref}}^{-1} = 137.035999177, \qquad \alpha_{\mathrm{ref}} \equiv \big(\alpha_{\mathrm{ref}}^{-1}\big)^{-1}, \qquad x_{\mathrm{ref}} \equiv \frac{\alpha_{\mathrm{ref}}}{\pi}. \tag{575}$$

For a retained benchmark truncation order M, write

$$g_{e,2}^{(A_1,[M])}(x) = 1 + \sum_{n=1}^{M} A_1^{(2n)} x^n.$$

In the numerical tables below $M = 5$. We define the retained physical-point discrepancy by

$$\Delta g_{e,2}^{[5]}(x_{\mathrm{ref}}) \equiv g_{e,2}^{\mathrm{Rel}}(x_{\mathrm{ref}}) - g_{e,2}^{(A_1,[5])}(x_{\mathrm{ref}}). \tag{576}$$

TABLE XXIII. Mass-independent A_1 rank summary for the current article evaluator and the refined no-free-parameter mother truncation, evaluated at the external reference point $x_{\rm ref}$. The refined rows use the diagnostic $g-2$ dynamic-kernel convention of Eq. (578). The quantity $\Delta g^{[5]}_{e,2}(x_{\rm ref})$ is defined relative to the retained five-term mass-independent A_1 benchmark truncation $g^{(A_1,[5])}_{e,2}(x_{\rm ref})$, not to an all-orders QED value. The coefficient max norm is formed from the retained central coefficient discrepancies through $n=5$, whenever those benchmark coefficients are specified. Both diagnostics are post-computation comparisons and are not fitting criteria.

Model	$\mathcal{D}_{\rm C}(x_{\rm ref})$	$g^{\rm Rel}_{e,2}(x_{\rm ref})$	$\Delta g^{[5]}_{e,2}(x_{\rm ref})$	$\max_{1\le n\le 5}\lvert\Delta A_1^{(2n)}\rvert$
Current rank-1	$2.3154578363279683401\times10^{-3}$	1.0011596521781891656	$2.21797065495\times10^{-12}$	$2.31712269445\times10^{-3}$
Refined rank-1	$2.3154578364863156687\times10^{-3}$	1.0011596521782686088	$2.29741384877\times10^{-12}$	$2.31715274729\times10^{-3}$
Current rank-3	$2.3154578318351729839\times10^{-3}$	1.0011596521759351206	$-3.60743961731\times10^{-14}$	$4.21146202143\times10^{-4}$
Refined rank-3	$2.3154578320016569938\times10^{-3}$	1.0011596521760186460	$4.74509881361\times10^{-14}$	$4.18472779052\times10^{-4}$
Current rank-5	$2.3154578317343851564\times10^{-3}$	1.0011596521758845551	$-8.66398650485\times10^{-14}$	$4.73632414272\times10^{-5}$
Refined rank-5	$2.3154578319065179530\times10^{-3}$	1.0011596521759709145	$-2.80472391650\times10^{-16}$	$5.19137462830\times10^{-5}$
Current rank-100	$2.3154578317316878604\times10^{-3}$	1.0011596521758832019	$-8.79931042139\times10^{-14}$	$7.47379106462\times10^{-5}$
Refined rank-100	$2.3154578319042056856\times10^{-3}$	1.0011596521759697544	$-1.44054186275\times10^{-15}$	$7.94163636274\times10^{-5}$

Whenever an external benchmark coefficient $A_1^{(2n)}$ has been specified, define the coefficient discrepancy by

$$\Delta A_1^{(2n)} \equiv \widehat{A}_1^{(2n)} - A_1^{(2n)}. \tag{577}$$

The rank parameter entering the glued-shell scalar evaluator is a truncation index of the excited shell tower, not a loop order. Two no-free-parameter diagnostic families are relevant below.

First, the current article-consistent evaluator is retained as a baseline. Within that family, rank $N=5$ is the scalar evaluator fixed by the article construction before the $g-2$ comparison is made. Its coefficient-space discrepancies relative to the first five retained benchmark orders are reported only after this evaluator has been fixed. They are not used to select $N=5$ and are not a fitting criterion.

Second, the refined no-free-parameter mother truncation supplements the same scalar branch by the three-channel static completion and the no-free-parameter visible dynamic renormalization. For the $g-2$ diagnostic tables only, we use the explicitly stated realized diagnostic convention

$$\Phi^{(\text{refined},g2)}_{\rm dyn}(D) = \big(\lambda_u^{(N)}\big)^2\Phi^{(\text{visible},N)}_{\rm dyn}(D). \tag{578}$$

This convention is not used in the primary extraction of α_*. It is also distinct from the scalar-reporting convention in which one power of $\lambda_u^{(N)}$ is used. Therefore every numerical value in the refined $g-2$ tables is conditional on the diagnostic convention Eq. (578). This convention is specified before the comparison with the A_1 benchmark table and is not a fit to the retained coefficients. Within the realized $g-2$ convention, the central physical-point discrepancy and the first two nontrivial universal coefficient discrepancies are reduced relative to the current rank-5 baseline. Rank $N=100$ is used as the highest-rank finite-rank representative reported in the current numerical ledger.

For that reason table XXIII reports both families explicitly. In the detailed benchmark table below, the current rank-5 branch is kept as the article baseline already fixed in table XXIII, while the refined rank-100 branch is used for the quoted higher-order conditional outputs.

The quantity $\max_{1\le n\le 5}\lvert\Delta A_1^{(2n)}\rvert$ is reported only as an external diagnostic; it is not used as a fitting criterion. In particular, the refined rank-100 branch is not selected by minimizing this five-order central max norm, and the displayed central values show that it is not the minimizer of that diagnostic. This is not a defect of the refined branch as a diagnostic representative, because the fifth mass-independent benchmark is much less sharply known than the first four. The refined branch nevertheless reduces the central physical-point discrepancy and the first two nontrivial universal coefficient discrepancies relative to the current rank-5 baseline.

At this same reference point, the refined rank-100 branch, used here as the highest-rank finite-rank no-free-parameter representative reported in the current numerical ledger, gives the values listed in table XXIV. These numbers are obtained directly from the specified scalar shell evaluator and the algebraic diagnostic maps Eqs. (568) to (571) and (574).

The numerical ledger was evaluated with high-precision arithmetic. The displayed digits are central arithmetic digits of the specified finite-rank evaluator. They certify only the numerical solution of the stated finite-rank algebraic realization at the reported working precision. They do not constitute a certified operator-level tail bound, a realized uncertainty interval, or a rank-to-infinity error estimate for the refined rank-100 realization. Accordingly, digits beyond the cross-rank agreement visible in table XXIII should be read as finite-rank ledger digits rather than as certified

TABLE XXIV. Physical-point values entering the pure-photonic Relator diagnostic for the electron anomalous magnetic moment, evaluated on the refined rank-100 branch.

Quantity	Value
$\mathcal{D}_{\mathrm{C}}(x_{\mathrm{ref}})$	$2.3154578319042056856 \times 10^{-3}$
$\zeta(\mathcal{D}_{\mathrm{C}}(x_{\mathrm{ref}}))$	$7.8195528193522298180 \times 10^{-5}$
$\Lambda_{\mathrm{ALP}}(x_{\mathrm{ref}})$	0.69168314608976982065
$\mathcal{D}_{\mathrm{total}}(x_{\mathrm{ref}})$	$2.3152762013713372625 \times 10^{-3}$
$g_{e,2}^{\mathrm{Rel}}(x_{\mathrm{ref}})$	1.0011596521759697544
$a_e^{\mathrm{Rel}}(x_{\mathrm{ref}})$	$1.1596521759697544408 \times 10^{-3}$

operator-level digits. Benchmark uncertainties, when present, are external and are not included in the displayed Relator-side digits.

Remark. The numerical proximity between $\Lambda_{\mathrm{ALP}}(x_{\mathrm{ref}})$ and $\Lambda_{\mathrm{geom}}^{(\mathrm{th})}$ in table XXIV is a downstream consequence of evaluating the diagnostic ALP image near the already locked physical point. It is not an identity, it is not imposed as a constraint, and it is not used in the construction of $\mathcal{D}_{\mathrm{total}}(x)$ or $g_{e,2}^{\mathrm{Rel}}(x)$.

Proposition 62 (Coefficient map from the scalar branch to the anomaly sequence)**.** *Assume that the chosen scalar evaluator is analytic in a neighborhood of $x = 0$, with*

$$\mathcal{D}_{\mathrm{C}}(x) = \sum_{n\geq 1} c_n x^n, \qquad c_1 = 1. \tag{579}$$

Define

$$Z(x) \equiv \zeta(\mathcal{D}_{\mathrm{C}}(x)) = \sum_{n\geq 1} z_n x^n, \qquad \bar{D}(x) \equiv \frac{\mathcal{D}_{\mathrm{C}}(x)}{x} = \sum_{n\geq 0} c_{n+1} x^n, \tag{580}$$

and define the analytically continued quotient

$$U(x) \equiv \frac{Z(x)^2}{\bar{D}(x)} = \sum_{n\geq 0} u_n x^n. \tag{581}$$

Since $\bar{D}(0) = c_1 = 1$, the quotient defining $U(x)$ is analytic near $x = 0$. Then the coefficients d_n of

$$\mathcal{D}_{\mathrm{total}}(x) = \sum_{n\geq 1} d_n x^n$$

are

$$d_n = c_n - z_{n-1} + \frac{1}{4} u_{n-1}, \qquad n \geq 1, \tag{582}$$

where $z_0 = 0$. The Relator anomaly coefficients are then obtained from

$$g_{e,2}^{\mathrm{Rel}}(x) = \big(1 - \mathcal{D}_{\mathrm{total}}(x)\big)^{-1/2} = 1 + \sum_{n\geq 1} \widehat{A}_1^{(2n)} x^n. \tag{583}$$

Equivalently,

$$\widehat{A}_1^{(2n)} = \sum_{k=1}^{n} \frac{\binom{2k}{k}}{4^k} \sum_{\substack{m_1+\cdots+m_k=n \\ m_a\geq 1}} d_{m_1} \cdots d_{m_k}. \tag{584}$$

In particular,

$$\widehat{A}_1^{(2)} = \frac{1}{2}d_1, \tag{585}$$
$$\widehat{A}_1^{(4)} = \frac{1}{2}d_2 + \frac{3}{8}d_1^2, \tag{586}$$
$$\widehat{A}_1^{(6)} = \frac{1}{2}d_3 + \frac{3}{4}d_1 d_2 + \frac{5}{16}d_1^3, \tag{587}$$
$$\widehat{A}_1^{(8)} = \frac{1}{2}d_4 + \frac{3}{4}d_1 d_3 + \frac{3}{8}d_2^2 + \frac{15}{16}d_1^2 d_2 + \frac{35}{128}d_1^4, \tag{588}$$
$$\widehat{A}_1^{(10)} = \frac{1}{2}d_5 + \frac{3}{4}d_1 d_4 + \frac{3}{4}d_2 d_3 + \frac{15}{16}d_1^2 d_3 + \frac{15}{16}d_1 d_2^2 + \frac{35}{32}d_1^3 d_2 + \frac{63}{256}d_1^5. \tag{589}$$

Proof. Since $c_1 = 1$, the scalar branch satisfies

$$\mathcal{D}_{\mathrm{C}}(x) = x + O(x^2) \qquad (x \to 0),$$

and therefore

$$\bar{D}(x) = \frac{\mathcal{D}_{\mathrm{C}}(x)}{x} = 1 + O(x), \qquad \bar{D}(0) = 1.$$

By Eq. (569), the nonnegative ALP image

$$\zeta(D) = \frac{\sqrt{1 + \dfrac{4D}{3\pi^2}} - 1}{2}$$

is analytic at $D = 0$, with

$$\zeta(0) = 0, \qquad \zeta'(0) = \frac{1}{3\pi^2}.$$

Hence

$$Z(x) = \zeta(\mathcal{D}_{\mathrm{C}}(x)) = O(x) \qquad (x \to 0).$$

Since $\bar{D}(0) = 1 \neq 0$, the reciprocal $\bar{D}(x)^{-1}$ is analytic in a neighborhood of $x = 0$. Therefore

$$U(x) = \frac{Z(x)^2}{\bar{D}(x)}$$

is analytic near $x = 0$. Because $Z(x) = O(x)$, one also has

$$U(x) = O(x^2), \qquad u_0 = u_1 = 0.$$

Using

$$\mathcal{D}_{\mathrm{C}}(x) = x\bar{D}(x),$$

the quotient term in the orbital slowdown map has the analytic form

$$\frac{x^2 Z(x)^2}{4\mathcal{D}_{\mathrm{C}}(x)} = \frac{x^2 Z(x)^2}{4x\bar{D}(x)} = \frac{x}{4}\,\frac{Z(x)^2}{\bar{D}(x)} = \frac{x}{4}\,U(x).$$

Hence the analytically continued orbital slowdown map is

$$\mathcal{D}_{\mathrm{total}}(x) = \mathcal{D}_{\mathrm{C}}(x) - xZ(x) + \frac{x}{4}U(x).$$

Hence $\mathcal{D}_{\mathrm{total}}(x)$ is analytic near $x = 0$, and

$$\mathcal{D}_{\mathrm{total}}(0) = 0.$$

TABLE XXV. Comparison of the first five nontrivial coefficients of the pure-photonic electron anomaly. The current rank-5 branch is retained as the article baseline reported in table XXIII, while the refined rank-100 branch is the highest-rank finite-rank no-free-parameter representative reported in the current numerical ledger. For $n = 5$, the displayed $\Delta A_1^{(10)}$ values subtract the central benchmark value 5.891; the comparison should be read at the uncertainty scale stated in Eq. (590).

n	$A_1^{(2n)}$ (pure QED)	$\widehat{A}_1^{(2n)}$ (current rank-5)	$\widehat{A}_1^{(2n)}$ (refined rank-100)	$\Delta A_1^{(2n)}$ (current rank-5)	$\Delta A_1^{(2n)}$ (refined rank-100)
1	0.5	0.5	0.5	0	0
2	-0.328478965579193	-0.3284789802289695381	-0.3284789655084229695	$-1.46497765381 \times 10^{-8}$	$7.07700304874 \times 10^{-11}$
3	1.181241456587	1.1812409955772212510	1.1812414773240741611	$-4.61009778749 \times 10^{-7}$	$2.07370741611 \times 10^{-8}$
4	-1.9122457649264456	-1.9122320381250895959	-1.9122411411271610819	$1.37268013560 \times 10^{-5}$	$4.62379928449 \times 10^{-6}$
5	5.891(61)	5.8910473632414271894	5.8910794163636274299	$4.73632414272 \times 10^{-5}$	$7.94163636274 \times 10^{-5}$

Expanding

$$\mathcal{D}_{\mathrm{C}}(x) = \sum_{n\geq 1} c_n x^n, \qquad Z(x) = \sum_{n\geq 1} z_n x^n, \qquad U(x) = \sum_{n\geq 0} u_n x^n,$$

and comparing the coefficient of x^n gives

$$d_n = c_n - z_{n-1} + \frac{1}{4} u_{n-1}, \qquad n \geq 1,$$

with $z_0 = 0$. This proves Eq. (582).

Because $\mathcal{D}_{\mathrm{total}}(0) = 0$, the principal branch

$$(1-y)^{-1/2} = 1 + \sum_{k\geq 1} \frac{\binom{2k}{k}}{4^k} y^k$$

is analytic at $y = 0$, and substitution $y = \mathcal{D}_{\mathrm{total}}(x)$ is valid in a neighborhood of $x = 0$. Thus

$$g_{e,2}^{\mathrm{Rel}}(x) = (1 - \mathcal{D}_{\mathrm{total}}(x))^{-1/2} = 1 + \sum_{k\geq 1} \frac{\binom{2k}{k}}{4^k} \left(\sum_{m\geq 1} d_m x^m \right)^k .$$

Extracting the coefficient of x^n yields Eq. (584). The displayed formulas Eqs. (585) to (589) are the cases $n = 1, \ldots, 5$. $\square$

The following benchmark coefficients are external retained comparison data. They are not used in constructing $\mathcal{D}_{\mathrm{C}}(x)$, Λ_{geom}, $\mathfrak{D}_*$, α_*, the rank choice, or the diagnostic kernel convention. For $n = 1, \ldots, 4$ we use the standard mass-independent A_1 values summarized in the electron anomaly review of Aoyama, Kinoshita, and Nio [24]. For $n = 5$, corresponding to the tenth-order coefficient $A_1^{(10)}$, we use the retained central benchmark

$$A_1^{(10)} = 5.891(61), \tag{590}$$

from Volkov [23]. In the coefficient tables below, the central value 5.891 is used only for displaying central discrepancies. The $n = 5$ comparison, corresponding to the tenth-order benchmark $A_1^{(10)}$, must therefore be read at the quoted 6.1×10^{-2} coefficient uncertainty scale. It should not be used as a sharp discriminator between nearby finite-rank Relator realizations.

In the notation of this table, the row $n = 6$ corresponds to the twelfth-order mass-independent coefficient $A_1^{(12)}$, not to the standard sixth-order coefficient $A_1^{(6)}$, which is the $n = 3$ row. No independent benchmark for $A_1^{(12)}$ or for the higher A_1 coefficients listed below is used in this article. This is a substantial computational gap rather than a matter of notation; even the five-loop coefficient $A_1^{(10)}$ required large-scale numerical work and has served as a high-precision benchmark problem. Consequently, the entries with $n \geq 6$ in table XXVI are conditional forward outputs of the specified Relator realization. Agreement of future independent high-order calculations of the universal A_1 sequence with these values within the combined realization, truncation, and independent-calculation error budgets would provide nontrivial support for this specified realization. Disagreement outside those combined budgets would falsify the specified realization, not every possible operator completion of the broader shell framework.

TABLE XXVI. First ten nontrivial coefficients of the refined rank-100 Relator output for the mass-independent electron–photon series. The first five entries are compared with the retained universal benchmark coefficients $A_1^{(2n)}$, with the fifth entry read at the uncertainty stated in Eq. (590). The last five entries are conditional outputs of the present no-free-parameter scalar-shell realization under the diagnostic $g-2$ convention of Eq. (578). The printed digits are central finite-rank ledger digits of the specified rank-100 realization. No operator-level tail bound is claimed for the rows $n \geq 6$.

n	$\widehat{A}_1^{(2n)}$ (Relator)	$A_1^{(2n)}$ (pure QED)	Status
1	0.5	0.5	benchmarked
2	−0.3284789655084229695	−0.328478965579193	benchmarked
3	1.1812414773240741611	1.181241456587	benchmarked
4	−1.9122411411271610819	−1.9122457649264456	benchmarked
5	5.8910794163636274299	5.891(61)	benchmarked
6	−14.2482848504641364623	—	conditional prediction
7	43.3967102259713990944	—	conditional prediction
8	−126.0356609136404213802	—	conditional prediction
9	396.2530199554764995308	—	conditional prediction
10	−1248.0206243076369262343	—	conditional prediction

In particular, the refined rank-100 realization changes $\Delta A_1^{(4)}$ from $-1.46497765381\times10^{-8}$ to $7.07700304874\times10^{-11}$, and $\Delta A_1^{(6)}$ from $-4.61009778749\times10^{-7}$ to $2.07370741611\times10^{-8}$. The first two nontrivial universal coefficient discrepancies are therefore reduced by roughly two orders of magnitude and one order of magnitude, respectively, relative to the current rank-5 baseline.

At the same physical point, the central retained benchmark value used here, obtained from the pure-photonic QED coefficients through $n=5$, is

$$g_{e,2}^{(A_1,[5])}(x_{\rm ref}) = 1.00115965217597119498265100941, \qquad a_e^{(A_1,[5])}(x_{\rm ref}) = 1.15965217597119498265100940 63\times10^{-3}. \tag{591}$$

The corresponding central retained physical-point discrepancy of the refined rank-100 realization, relative to the five-term benchmark truncation and not to an all-orders QED value, is

$$\Delta g_{e,2}^{[5]}(x_{\rm ref}) = g_{e,2}^{\rm Rel}(x_{\rm ref}) - g_{e,2}^{(A_1,[5])}(x_{\rm ref}) = -1.44054186275\times10^{-15}. \tag{592}$$

The retained uncertainty in the fifth benchmark coefficient alone gives

$$u_{A_1^{(10)}}\left(g_{e,2}^{(A_1,[5])}\right) = 0.061\,x_{\rm ref}^5 = 4.12484010134\times10^{-15}. \tag{593}$$

Thus the central discrepancy in Eq. (592) should be read at least on the uncertainty scale of Eq. (593), before any realization-level uncertainty of the Relator scalar evaluator is considered. This comparison is a diagnostic cross-check only. It is not an input to the primary Alpha Lock Point.

The refined rank-100 branch, taken here as the highest-rank finite-rank no-free-parameter representative reported in the current numerical ledger, yields a definite realization-level continuation of the pure-photonic coefficient sequence beyond the benchmarked orders used in this article. We therefore write the Taylor expansion of the specified realization through tenth order as

$$g_{e,2}^{\rm Rel}(x) = 1 + \sum_{n=1}^{10} \widehat{A}_1^{(2n)} x^n + O(x^{11}), \tag{594}$$

and list the first ten coefficients in table XXVI. The first five rows are comparisons with the retained pure-photonic QED benchmarks. The last five rows are conditional Relator outputs in the mass-independent electron–photon A_1 sector.

Proposition 63 (Higher-order universal coefficients as conditional falsifiable outputs)**.** *Assume that the specified refined rank-*100 *diagnostic realization, together with the $g-2$ dynamic-kernel convention of Eq.* (578)*, satisfies the analyticity hypotheses of proposition 62. Equivalently, assume that its scalar branch $\mathcal{D}_{\rm C}(x)$ is analytic near $x=0$ with $\mathcal{D}_{\rm C}(x) = x + O(x^2)$, and that the diagnostic maps Eqs.* (569)*,* (571) *and* (574) *are read on their analytic branches near $x=0$. Then the coefficients $\widehat{A}_1^{(2n)}$ with $n \geq 6$ are uniquely determined algebraic outputs of that finite-rank realization in the mass-independent A_1 sector. Since no benchmark values for these coefficients are used in this article, the values listed in table XXVI for $n = 6,\ldots,10$ are not benchmarked inputs.*

These entries are conditional falsifiable outputs of the specified finite-rank realization, not theorem-level values of an operator-complete shell theory. A future operator-level scalar completion or a different stated diagnostic kernel convention may shift them. A certified finite-rank tail estimate would not by itself redefine the displayed finite-rank central values; it would instead quantify the gap between those values and the corresponding operator-level values of the same stated convention.

Proof. Under the stated analyticity hypotheses, proposition 62 applies to the refined rank-100 realization. Hence the Taylor series

$$g_{e,2}^{\mathrm{Rel}}(x) = 1 + \sum_{n\geq 1} \widehat{A}_1^{(2n)} x^n$$

exists and its coefficients are uniquely determined by the Taylor coefficients of the specified finite-rank scalar branch $\mathcal{D}_{\mathrm{C}}(x)$ through the algebraic maps

$$\mathcal{D}_{\mathrm{C}}(x) \longmapsto \zeta(\mathcal{D}_{\mathrm{C}}(x)) \longmapsto \mathcal{D}_{\mathrm{total}}(x) \longmapsto g_{e,2}^{\mathrm{Rel}}(x).$$

The first five coefficients are compared with retained external benchmarks only after the sequence has been generated. The coefficients with $n \geq 6$ are not benchmark inputs in this article and therefore provide conditional falsifiable outputs of the specified finite-rank realization. □

Remark (Firewall between the primary lock and the $g-2$ diagnostic)*.* The interpretation of this section is intentionally narrow. The primary extraction of α_* is completed before any benchmark value of $A_1^{(2n)}$, any measured electron anomaly, or any QED perturbative coefficient is introduced. The QED coefficient tables enter only after the scalar evaluator has been fixed and only as external comparison data.

Thus this section does not tune the scalar evaluator, does not redefine Λ_{geom}, does not modify the fixed scalar target $\mathfrak{D}_*$, and does not feed back into the Alpha Lock Point. It records a secondary realization-level consequence; after $\mathcal{D}_{\mathrm{C}}(x)$ has been fixed, the algebraic ALP image and the orbital slowdown map generate a coefficient sequence $\widehat{A}_1^{(2n)}$. The agreement or disagreement of this sequence with external A_1 benchmarks tests the specified scalar-shell realization and the stated diagnostic map used in this section. It is not an input to the primary geometric derivation.

XVI. CONCLUSION

Within the stated Relator shell postulates, we have constructed a shell-geometric closure in which the fine-structure coupling is not inserted as a primitive numerical input. The construction begins from the split arena $\mathbb{C} \oplus \mathbb{R}^3$ and the Relator lock $R\omega = c$, fixes the minimal pinned electron branch, derives the matching-shell geometry, builds the scalar cavity–shell slowdown block $\mathcal{D}_{\mathrm{C}}(\alpha)$, constructs the vector shell datum Λ_{geom}, and computes, within the Path-II single-polarization shell averaging class, the logarithmic coefficient

$$\mathcal{C}_{\log}^{(II)} = \frac{1}{3}.$$

The same-coefficient compatibility condition is imposed only afterward, when this Path-II value is compared with the Path-I representative in the baseline shell lock. The baseline shell closure is the Alpha Lock Point. Under this baseline closure convention, the theorem path defines the target map

$$\mathfrak{D}_{\mathrm{lock}}(\Lambda) = \frac{3}{2}\,\mathsf{K}_{\mathrm{ALP}}\,\Lambda\left(1 + \frac{\mathsf{K}_{\mathrm{ALP}}\Lambda}{2\pi^2}\right),$$

while the vector construction supplies the branch-fixed input Λ. When the admissibility hypotheses of theorem 21 hold for the exact vector input Λ_{geom} and for the chosen scalar evaluator, the admissible coupling is then selected by the one-variable lock equation

$$\mathcal{D}_{\mathrm{C}}(\alpha_*) = \mathfrak{D}_{\mathrm{lock}}(\Lambda_{\mathrm{geom}}).$$

In a finite-rank or reduced realization, the same lock equation is read only after the explicit replacement

$$\Lambda_{\mathrm{geom}} \mapsto \Lambda_{\mathrm{geom}}^{(N)} \quad \text{or} \quad \Lambda_{\mathrm{geom}} \mapsto \Lambda_{\mathrm{geom}}^{(\mathrm{th})}.$$

Thus, within the stated shell postulates, a specified scalar evaluator, and an independently computed vector-shell input, the coupling appears as the compatibility value at which the scalar slowdown law and the shell geometry close on the same minimal branch. It is not borrowed from experiment and it is not inferred from QED coefficients.

The logical status of the construction is intentionally narrow and explicit. The paper does not claim to derive the full Standard Model, the full perturbative machinery of QED, or a complete renormalization-group flow across all scales. It also does not claim that the current finite-rank realization is already the last possible operator completion of the scalar or vector shell sectors. What has been established is more specific and more structural. Once the standing shell assumptions, the minimal branch, the matching-shell geometry, the scalar evaluator, the fixed vector-shell input, and the baseline logarithmic lock are fixed, the closure contains an internal scalar target and hence an internally selected dimensionless coupling. In this sense, within the present shell construction, the fine-structure constant is no longer a bare insertion. It is the value at which the scalar and vector shell sectors close on the same pinned branch.

The current numerical realization illustrates the construction without defining it. The primary computation of $\Lambda_{\mathrm{geom}}^{(\mathrm{th})}$, $\mathfrak{D}_*^{(\mathrm{th})}$, and $\alpha_*^{(\mathrm{th})}$ is separated from all reference data; no measured value of α, no QED anomaly coefficient, and no fitted coefficient enters the primary lock. External values enter only afterward, as diagnostic comparisons. With the current rank-5 scalar evaluator and the current reduced vector representative, the lock output gives the reduced central value reported in the numerical section. Its displayed digits are realization-level ledger digits of that finite-rank computation and do not, by themselves, constitute a certified operator-level uncertainty interval. Independently, the refined no-free-parameter scalar realization, read under the stated diagnostic $g-2$ kernel convention, provides a secondary mass-independent A_1 electron-anomaly diagnostic whose first retained benchmark rows are compared with the universal QED sequence in the coefficient tables, with the displayed central discrepancies read at their stated benchmark- and realization-level status. These two facts should be kept distinct. The first concerns the primary lock output of the current realization. The second concerns the quality of a stronger realization-level continuation of the same shell framework.

The sharpest present conditional falsifiability test lies in the mass-independent one-lepton A_1 sector. Once a scalar evaluator is fixed, the ALP map and the operational slowdown map generate a definite series

$$g_{e,2}^{\mathrm{Rel}}(x) = 1 + \sum_{n\geq 1} \widehat{A}_1^{(2n)} x^n, \qquad x = \frac{\alpha}{\pi}.$$

For the refined no-free-parameter rank-100 realization, read with the diagnostic $g-2$ kernel convention fixed earlier, the first retained benchmark coefficients agree with the universal pure-photonic QED values at the levels displayed in table XXV, and the higher coefficients beginning with $A_1^{(12)}$ become conditional forward outputs of that specified realization; see table XXVI. In particular, under the stated refined rank-100 diagnostic convention, the finite-rank realization yields a definite higher-order continuation of the universal mass-independent A_1 sequence, beginning with the ledger value

$$\widehat{A}_1^{(12)} = -14.2482848504641364623,$$

and continuing through the higher coefficients listed in table XXVI. These numbers are not QED inputs and are not benchmark-fitted outputs. They are realization-level Taylor coefficients of the specified Relator map once the scalar evaluator, the diagnostic kernel convention, and the operational lift have been fixed.

This yields a demanding falsifiability test. The independent pure-photonic five-loop coefficient $A_1^{(10)}$ already required large-scale multi-loop numerical work and remains a precision benchmark problem [23, 24]. The next coefficients, beginning with $A_1^{(12)}$, are therefore substantial future targets. Agreement of independent high-order calculations of the same mass-independent A_1 QED sequence with the Relator values, within the combined realization-level, truncation, and independent-calculation error budgets, would provide nontrivial support for the specified scalar-shell realization. Disagreement outside those combined budgets would falsify that specified realization. The framework therefore exposes the present finite-rank evaluator to a concrete computational test.

The mass-dependent discussion has the same restricted meaning. The primary result of the paper is the universal electron lock on the minimal one-loop branch at a fixed vector-shell datum; namely Λ_{geom} at exact operator level, or the explicitly specified reduced representative in a realization. Heavy-shell effects from μ and τ enter only through the retained single-excursion heavy-shell channel as a family-resolved deformation of the electron scalar branch. Their role here is diagnostic; they are not load-bearing for the quoted one-loop extraction of α_*. The analysis shows, within that retained channel, how such corrections decouple through squared mass ratios and how, at fixed geometric datum, they would shift a re-extracted coupling. It does not replace the full scale-dependent running structure of QED.

The conceptual outcome is direct. Within the present framework, the origin problem for α is reformulated as a shell-consistency problem rather than a numerical insertion. Within the stated shell postulates, the baseline shell-lock closure, the chosen scalar evaluator, and the chosen vector-shell input, and whenever the admissibility conditions of the selected scalar branch hold, the coupling is selected by the compatibility of a scalar slowdown law, a vector shell geometry, and the Path-II logarithmic coefficient used in the same-coefficient lock. The empirical future of the construction is also clear; improved operator realizations can sharpen the lock, and independent high-order pure-photonic calculations can test the predicted continuation. Either outcome is informative. Agreement within the combined realization, truncation, and independent-calculation budgets would provide nontrivial support for the specified realization. Disagreement outside those budgets would identify where that realization fails. In both cases, within this construction the fine-structure constant is no longer treated as an unexplained numerical input. It becomes a shell-matching and branch-compatibility problem governed by geometry, scalar slowdown, and infrared consistency.

Appendices

Appendix A: Decoupled two-pole approximation of the scalar mother law

This appendix records a deliberately simplified approximation of the scalar mother law. It is not an additional scalar evaluator and it is not used in the primary geometric lock. Its only purpose is to show how the familiar two-pole formula is obtained from the same mother-law structure after explicit simplifying assumptions are imposed.

The active scalar mother branch has the form

$$D = x\sqrt{1-\Theta_{1,\mathrm{eff}}D + D^2\Phi_{\mathrm{dyn}}(D)}, \qquad x = \frac{\alpha}{\pi}, \tag{A1}$$

with the principal positive square root on the admissible branch. In the current finite-rank realization, the dynamic block is the visible glued two-mode block

$$\Phi^{(N)}_{\mathrm{dyn}}(D) = u_N^\top\big(\mathbb{I}_2 + DS_N\big)^{-1}u_N, \qquad u_N = \begin{pmatrix}\sqrt{A^{(N)}_{\mathrm{uv}}}\\ \sqrt{A^{(N)}_{\mathrm{ir}}}\end{pmatrix}, \qquad S_N = \begin{pmatrix} s_{\mathrm{uv}} & \chi_N\\ \chi_N & s_{\mathrm{ir}}\end{pmatrix}. \tag{A2}$$

Here $A^{(N)}_{\mathrm{uv}} \geq 0$ and $A^{(N)}_{\mathrm{ir}} \geq 0$, and the displayed expression is read on the domain where $\mathbb{I}_2 + DS_N$ is invertible. Equivalently, whenever

$$\Delta_N(D) \equiv (1+s_{\mathrm{uv}}D)(1+s_{\mathrm{ir}}D) - \chi_N^2D^2 \neq 0,$$

one has

$$\Phi^{(N)}_{\mathrm{dyn}}(D) = \frac{A^{(N)}_{\mathrm{uv}}(1+s_{\mathrm{ir}}D) + A^{(N)}_{\mathrm{ir}}(1+s_{\mathrm{uv}}D) - 2\chi_N D\sqrt{A^{(N)}_{\mathrm{uv}}A^{(N)}_{\mathrm{ir}}}}{(1+s_{\mathrm{uv}}D)(1+s_{\mathrm{ir}}D) - \chi_N^2D^2}. \tag{A3}$$

The decoupled two-pole approximation is obtained by imposing the following explicit simplifications on the active mother-law data:

$$B^{(\mathrm{eval})}_{11} = B^{\mathrm{glue}}_{11} \longmapsto \Theta^{(\mathrm{coll})}_1 + \Theta^{(\mathrm{log})}_1, \qquad \Theta_{1,\mathrm{eff}} \longmapsto \Theta^{\mathrm{dec}}_1, \tag{A4}$$

with

$$A^{(N)}_{\mathrm{uv}} \longmapsto A_{\mathrm{vis},0}, \qquad A^{(N)}_{\mathrm{ir}} \longmapsto A_{\mathrm{vis},0}, \qquad \chi_N \longmapsto 0. \tag{A5}$$

Thus the static collar–log Schur contraction is replaced by the uncoupled collar-plus-log first-moment sum, the UV and IR visible amplitudes are replaced by a common baseline amplitude, and the dynamic cross-correlation between the two visible poles is neglected. The common visible baseline is

$$A_{\mathrm{vis},0} \equiv \pi^2C_{11}(\ell_0) + \frac{\gamma_{\mathrm{E}}}{4}. \tag{A6}$$

The two pole scales are

$$s_{\mathrm{uv}} \equiv \ln 2, \qquad s_{\mathrm{ir}} \equiv \frac{1}{8\pi^2}. \tag{A7}$$

The corresponding approximate effective first-moment coefficient is

$$\Theta^{\mathrm{dec}}_1 \equiv \Theta_{1,\mathrm{core}} + \Theta^{(\mathrm{coll})}_1 + \Theta^{(\mathrm{log})}_1. \tag{A8}$$

Definition A.1 (Decoupled two-pole scalar approximation)**.** The decoupled two-pole dynamic approximation is

$$\Phi^{(2\mathrm{p})}_{\mathrm{dec}}(D) \equiv A_{\mathrm{vis},0}\left(\frac{1}{1+s_{\mathrm{uv}}D} + \frac{1}{1+s_{\mathrm{ir}}D}\right). \tag{A9}$$

The associated approximate scalar branch is the analytic branch near $x=0$ with $D^{(2\mathrm{p})}_{\mathrm{dec}}(0) = 0$, defined by

$$D^{(2\mathrm{p})}_{\mathrm{dec}}(x) = x\sqrt{1-\Theta^{\mathrm{dec}}_1D^{(2\mathrm{p})}_{\mathrm{dec}}(x) + \big(D^{(2\mathrm{p})}_{\mathrm{dec}}(x)\big)^2\Phi^{(2\mathrm{p})}_{\mathrm{dec}}\big(D^{(2\mathrm{p})}_{\mathrm{dec}}(x)\big)}. \tag{A10}$$

As a formal series, this equation is read on the branch determined in proposition 64. For real numerical evaluation, it is used only where the displayed radicand is positive and the principal positive square root is real. It is an approximation obtained from Eq. (A1); it is not the active scalar evaluator used for the article lock.

Proposition 64 (Local analytic branch of the decoupled approximation)**.** *The decoupled two-pole scalar law Eq.* (A10) *has a unique analytic solution near $x = 0$ satisfying*

$$D^{(2p)}_{\mathrm{dec}}(0) = 0, \qquad \frac{\mathrm{d}}{\mathrm{d}x} D^{(2p)}_{\mathrm{dec}}(0) = 1.$$

In particular,

$$D^{(2p)}_{\mathrm{dec}}(x) = x + O(x^2) \qquad (x \to 0).$$

Proof. Define the decoupled radicand

$$\mathcal{R}_{\mathrm{dec}}(D) = 1 - \Theta_1^{\mathrm{dec}} D + D^2 \Phi^{(2p)}_{\mathrm{dec}}(D).$$

Since

$$\Phi^{(2p)}_{\mathrm{dec}}(D) = A_{\mathrm{vis},0} \left(\frac{1}{1 + s_{\mathrm{uv}} D} + \frac{1}{1 + s_{\mathrm{ir}} D} \right),$$

and since both denominators equal 1 at $D = 0$, $\Phi^{(2p)}_{\mathrm{dec}}$ is analytic in a neighborhood of $D = 0$. Hence $\mathcal{R}_{\mathrm{dec}}$ is analytic near $D = 0$, with

$$\mathcal{R}_{\mathrm{dec}}(0) = 1.$$

The principal square root is therefore analytic near $D = 0$, and

$$\sqrt{\mathcal{R}_{\mathrm{dec}}(0)} = 1.$$

Set

$$F(D, x) = D - x\sqrt{\mathcal{R}_{\mathrm{dec}}(D)}.$$

Then

$$F(0,0) = 0, \qquad \frac{\partial F}{\partial D}(0,0) = 1 - x \left. \frac{\mathcal{R}'_{\mathrm{dec}}(D)}{2\sqrt{\mathcal{R}_{\mathrm{dec}}(D)}} \right|_{(D,x)=(0,0)} = 1.$$

The analytic implicit-function theorem gives a unique analytic function $D^{(2p)}_{\mathrm{dec}}(x)$ near $x = 0$ such that $F(D^{(2p)}_{\mathrm{dec}}(x), x) = 0$ and $D^{(2p)}_{\mathrm{dec}}(0) = 0$. Differentiating

$$D^{(2p)}_{\mathrm{dec}}(x) = x\sqrt{\mathcal{R}_{\mathrm{dec}}\big(D^{(2p)}_{\mathrm{dec}}(x)\big)}$$

and setting $x = 0$ gives

$$\frac{\mathrm{d}}{\mathrm{d}x} D^{(2p)}_{\mathrm{dec}}(0) = \sqrt{\mathcal{R}_{\mathrm{dec}}(0)} = 1.$$

Therefore

$$D^{(2p)}_{\mathrm{dec}}(x) = x + O(x^2),$$

which proves the claim. □

Proposition 65 (Reduction of the active visible block to the two-pole form)**.** *Under the approximation map Eqs.* (A4) *and* (A5)*, the active visible dynamic quotient Eq.* (A3) *reduces exactly to Eq.* (A9)*. Consequently, the mother law Eq.* (A1) *reduces to the approximate scalar law Eq.* (A10)*.*

Proof. Under the approximation map,

$$u_N \longmapsto \sqrt{A_{\mathrm{vis},0}} \begin{pmatrix} 1 \\ 1 \end{pmatrix}, \qquad S_N \longmapsto \begin{pmatrix} s_{\mathrm{uv}} & 0 \\ 0 & s_{\mathrm{ir}} \end{pmatrix}.$$

Hence

$$\mathbb{I}_2 + DS_N \longmapsto \begin{pmatrix} 1+s_{\rm uv}D & 0 \\ 0 & 1+s_{\rm ir}D \end{pmatrix},$$

and therefore

$$\big(\mathbb{I}_2 + DS_N\big)^{-1} \longmapsto \begin{pmatrix} (1+s_{\rm uv}D)^{-1} & 0 \\ 0 & (1+s_{\rm ir}D)^{-1} \end{pmatrix},$$

on the domain where the two displayed denominators are nonzero. Substitution into the matrix form of the active block gives the full chain

$$\begin{aligned}\Phi^{(N)}_{\rm dyn}(D) &\longmapsto A_{\rm vis,0}\begin{pmatrix}1 & 1\end{pmatrix}\begin{pmatrix} (1+s_{\rm uv}D)^{-1} & 0 \\ 0 & (1+s_{\rm ir}D)^{-1} \end{pmatrix}\begin{pmatrix}1\\1\end{pmatrix}\\ &= A_{\rm vis,0}\left(\frac{1}{1+s_{\rm uv}D}+\frac{1}{1+s_{\rm ir}D}\right).\end{aligned}$$

This is Eq. (A9).

The same conclusion follows from the quotient form. Indeed, after inserting

$$A^{(N)}_{\rm uv} = A^{(N)}_{\rm ir} = A_{\rm vis,0}, \qquad \chi_N = 0,$$

the numerator of Eq. (A3) becomes

$$A_{\rm vis,0}(1+s_{\rm ir}D) + A_{\rm vis,0}(1+s_{\rm uv}D),$$

while the denominator becomes

$$(1+s_{\rm uv}D)(1+s_{\rm ir}D).$$

Thus

$$\begin{aligned}\Phi^{(N)}_{\rm dyn}(D) &\longmapsto A_{\rm vis,0}\left[\frac{1+s_{\rm ir}D}{(1+s_{\rm uv}D)(1+s_{\rm ir}D)}+\frac{1+s_{\rm uv}D}{(1+s_{\rm uv}D)(1+s_{\rm ir}D)}\right]\\ &= A_{\rm vis,0}\left(\frac{1}{1+s_{\rm uv}D}+\frac{1}{1+s_{\rm ir}D}\right).\end{aligned}$$

Finally, the static replacement

$$\Theta_{1,\rm eff} \longmapsto \Theta_1^{\rm dec}$$

changes the active radicand

$$1-\Theta_{1,\rm eff}D + D^2\Phi^{(N)}_{\rm dyn}(D)$$

into

$$1-\Theta_1^{\rm dec}D + D^2\Phi^{(2\rm p)}_{\rm dec}(D).$$

Substituting $D = D^{(2\rm p)}_{\rm dec}(x)$ in the mother law gives exactly Eq. (A10). □

Remark (Status of the approximation)*.* The approximation in this appendix does not remove the static first-moment sector. It replaces the glued static Schur load $B^{\rm glue}_{11}$ by the uncoupled collar-plus-log sum

$$\Theta_1^{(\rm coll)} + \Theta_1^{(\rm log)}.$$

It also suppresses the finite-rank hidden-mode corrections entering $A^{(N)}_{\rm uv}$ and $A^{(N)}_{\rm ir}$, sets the dynamic cross-correlation χ_N to zero, and omits any operator-level tail of the full scalar bath. The current numerical lock reported in the paper is not computed from $D^{(2\rm p)}_{\rm dec}$. It uses the current rank-5 scalar evaluator with $B^{\rm glue}_{11}$, $A^{(5)}_{\rm uv}$, $A^{(5)}_{\rm ir}$, and χ_5, together with the fixed reduced vector input $\Lambda^{(\rm th)}_{\rm geom}$. The two-pole formula above is therefore only a compact analytic limiting case of the same mother-law architecture.

Appendix B: Explicit glued-shell overlap formulas and finite-rank Schur evaluation

This appendix records the implementation-level formulas used in the finite-rank evaluation of the glued-shell scalar block of section VI. It introduces no new physical input and no independent scalar law. Its role is to make explicit the retained rank-one overlap, trace matrices, and Schur-complement formulas that underlie the glued-shell dynamic evaluation used in the scalar sector.

In logical-status terms, the overlap data $\psi_{\mathrm{coll},\ell}$, $\psi_{\log,D}$, $g_{c\ell}(D)$, and $\mathsf{G}_{c\ell}(D)$ are evaluation-level definitions. The closed form of $g_{c\ell}(D)$, the block-resolvent identities, and the finite Schur formulas are derived implementation statements. The finite correction $\delta\mathcal{G}^{\mathrm{gl},N}_{e\gamma}$ is a diagnostic Schur term. It is not a postulate, it does not introduce an external benchmark, and it does not define a second scalar evaluator.

1. Rank-one gluing of the collar and the logarithmic line

Definition B.1 (Retained rank-one gluing data)**.** Fix $\ell > 0$ and $D \geq 0$. In this appendix, D denotes the scalar evaluation parameter. To avoid a notation clash, we write $H^{\mathrm{Dir}}_{\mathrm{coll},\ell}$ for the Dirichlet collar operator denoted elsewhere by $H^{\mathrm{D}}_{\mathrm{coll}}$. The superscript Dir records the boundary condition and is unrelated to the scalar parameter D. The half-line coordinate ξ used here is a dummy collar variable and is unrelated to the generator radius ρ on $\mathbb{C}$.

The underlying half-line Hilbert spaces are

$$\mathcal{H}_{\mathrm{coll}} = L^2(\mathbb{R}_+, \mathrm{d}\xi), \qquad \mathcal{H}_{\log} = L^2(\mathbb{R}_+, \mathrm{d}t).$$

The two diagonal bath operators are

$$H^{\mathrm{Dir}}_{\mathrm{coll},\ell} = \ell^{-2}\big(-\partial_\xi^2 + \xi^2\big),$$

with

$$\mathrm{Dom}\big(H^{\mathrm{Dir}}_{\mathrm{coll},\ell}\big) = \Big\{u \in H^1_0(\mathbb{R}_+)\ ;\ -u'' + \xi^2 u \in L^2(\mathbb{R}_+)\Big\}.$$

Equivalently,

$$\mathrm{Dom}\big(H^{\mathrm{Dir}}_{\mathrm{coll},\ell}\big) = \Big\{u \in H^2(\mathbb{R}_+) \cap H^1_0(\mathbb{R}_+)\ ;\ \xi^2 u \in L^2(\mathbb{R}_+)\Big\}.$$

The logarithmic half-line operator is

$$L_{\log} = -\partial_t^2 + \frac{1}{4}, \qquad \mathrm{Dom}(L_{\log}) = H^2(\mathbb{R}_+) \cap H^1_0(\mathbb{R}_+).$$

In the minimal electron-branch evaluation one sets $\ell = \ell_0$, although the overlap formula is written for general $\ell > 0$. Define

$$\kappa(D) \equiv \sqrt{D + \frac{1}{4}}. \tag{B1}$$

The retained normalized collar and logarithmic directions are

$$\psi_{\mathrm{coll},\ell}(\xi) = \left(\frac{2}{\sqrt{\pi}\,\ell}\right)^{1/2} \exp\!\left(-\frac{\xi^2}{2\ell^2}\right), \qquad \xi \in \mathbb{R}_+,$$

and

$$\psi_{\log,D}(t) = \sqrt{2\kappa(D)}\, e^{-\kappa(D)t}, \qquad t \in \mathbb{R}_+.$$

These satisfy

$$\|\psi_{\mathrm{coll},\ell}\|_{L^2(\mathbb{R}_+,\mathrm{d}\xi)} = 1, \qquad \|\psi_{\log,D}\|_{L^2(\mathbb{R}_+,\mathrm{d}t)} = 1.$$

The retained scalar gluing amplitude is

$$g_{c\ell}(D) \equiv \int_0^\infty \exp\!\left[-\left(\frac{s}{\ell}\right)^2\right] e^{-\kappa(D)s}\,\mathrm{d}s. \tag{B2}$$

The scalar coefficient $g_{c\ell}(D)$ is built from the unnormalized raw collar and logarithmic profiles. The normalized channel vectors enter separately through the rank-one operator

$$\mathsf{G}_{c\ell}(D) \equiv g_{c\ell}(D)\,|\psi_{\mathrm{coll},\ell}\rangle\langle\psi_{\log,D}|. \tag{B3}$$

Thus $\mathsf{G}_{c\ell}(D)$ maps $\mathcal{H}_{\log}$ to $\mathcal{H}_{\mathrm{coll}}$, and its adjoint maps $\mathcal{H}_{\mathrm{coll}}$ to $\mathcal{H}_{\log}$. This is a D-parametrized retained gluing operator used in the finite-rank evaluation. It is not the D-independent abstract glued-bath operator of the mother scalar law.

The same evaluation parameter D enters both the retained gluing operator $\mathsf{G}_{c\ell}(D)$ and the shifted resolvent

$$\big(\mathbb{L}^{\mathrm{gl}}_{\mathrm{sh},\ell}(D) + D\mathbb{I}\big)^{-1}.$$

Remark. The vectors $\psi_{\mathrm{coll},\ell}$ and $\psi_{\log,D}$ are retained channel directions rather than exact eigenfunctions of the full glued bath. The scalar amplitude $g_{c\ell}(D)$ is built from the raw Gaussian collar profile and the raw decaying logarithmic profile. It is not a Hilbert inner product of the two unit vectors, since those vectors live on different half-lines. Accordingly, $\mathsf{G}_{c\ell}(D)$ is an evaluation-level rank-one gluing model and not a new microscopic shell postulate.

Lemma 29 (Closed form of the gluing amplitude)**.** *For every $\ell > 0$ and $D \geq 0$,*

$$g_{c\ell}(D) = \frac{\sqrt{\pi}\,\ell}{2}\exp\left[\frac{\ell^2}{4}\left(D + \frac{1}{4}\right)\right]\operatorname{erfc}\left(\frac{\ell}{2}\sqrt{D + \frac{1}{4}}\right). \tag{B4}$$

Proof. Set

$$\kappa \equiv \kappa(D) = \sqrt{D + \frac{1}{4}}.$$

Then

$$g_{c\ell}(D) = \int_0^\infty \exp\left[-\frac{s^2}{\ell^2} - \kappa s\right] \mathrm{d}s.$$

Complete the square in the exponent:

$$-\frac{s^2}{\ell^2} - \kappa s = -\frac{1}{\ell^2}\left(s + \frac{\kappa\ell^2}{2}\right)^2 + \frac{\kappa^2\ell^2}{4}.$$

Hence

$$g_{c\ell}(D) = \exp\left(\frac{\kappa^2\ell^2}{4}\right)\int_0^\infty \exp\left[-\frac{1}{\ell^2}\left(s + \frac{\kappa\ell^2}{2}\right)^2\right] \mathrm{d}s.$$

Introduce

$$u = \frac{1}{\ell}\left(s + \frac{\kappa\ell^2}{2}\right), \qquad \mathrm{d}s = \ell\,\mathrm{d}u.$$

When $s = 0$, one has $u = \kappa\ell/2$, and when $s \to \infty$, one has $u \to \infty$. Therefore

$$g_{c\ell}(D) = \ell\exp\left(\frac{\kappa^2\ell^2}{4}\right)\int_{\kappa\ell/2}^\infty e^{-u^2}\,\mathrm{d}u.$$

Using

$$\operatorname{erfc}(z) = \frac{2}{\sqrt{\pi}}\int_z^\infty e^{-u^2}\,\mathrm{d}u,$$

we obtain

$$g_{c\ell}(D) = \frac{\sqrt{\pi}\,\ell}{2}\exp\left(\frac{\kappa^2\ell^2}{4}\right)\operatorname{erfc}\left(\frac{\kappa\ell}{2}\right).$$

Since $\kappa^2 = D + \frac{1}{4}$, this is exactly Eq. (B4). □

Definition B.2 (Retained rank-one glued shell bath)**.** For a fixed bandwidth ratio $\ell > 0$ and fixed evaluation parameter $D \geq 0$, the retained rank-one implementation-level glued shell operator is

$$\mathbb{L}^{\mathrm{gl}}_{\mathrm{sh},\ell}(D) \equiv \begin{pmatrix} H^{\mathrm{Dir}}_{\mathrm{coll},\ell} & \mathsf{G}_{c\ell}(D) \\ \mathsf{G}_{c\ell}(D)^* & L_{\log} \end{pmatrix}, \tag{B5}$$

with domain

$$\mathrm{Dom}\big(\mathbb{L}^{\mathrm{gl}}_{\mathrm{sh},\ell}(D)\big) = \mathrm{Dom}\big(H^{\mathrm{Dir}}_{\mathrm{coll},\ell}\big) \oplus \mathrm{Dom}(L_{\log}). \tag{B6}$$

On the minimal branch, the shorthand

$$\mathbb{L}^{\mathrm{gl}}_{\mathrm{sh}}(D) \equiv \mathbb{L}^{\mathrm{gl}}_{\mathrm{sh},\ell_0}(D)$$

is used. This shorthand is local to this implementation appendix and denotes the retained D-parametrized evaluation operator, not the abstract glued bath of the main scalar mother law.

Proposition 66 (Basic operator properties of the retained glued bath)**.** *For each fixed $D \geq 0$, the operator $\mathsf{G}_{c\ell}(D)$ is bounded and rank one. Consequently, $\mathbb{L}^{\mathrm{gl}}_{\mathrm{sh},\ell}(D)$ is self-adjoint on*

$$\mathrm{Dom}\big(\mathbb{L}^{\mathrm{gl}}_{\mathrm{sh},\ell}(D)\big).$$

No positivity or invertibility of $\mathbb{L}^{\mathrm{gl}}_{\mathrm{sh},\ell}(D)$ is asserted by this statement alone.

Proof. Let

$$\mathbb{L}_{\mathrm{diag},\ell} = \begin{pmatrix} H^{\mathrm{Dir}}_{\mathrm{coll},\ell} & 0 \\ 0 & L_{\log} \end{pmatrix}.$$

By the self-adjointness of the two diagonal summands on their stated domains, $\mathbb{L}_{\mathrm{diag},\ell}$ is self-adjoint on

$$\mathrm{Dom}\big(H^{\mathrm{Dir}}_{\mathrm{coll},\ell}\big) \oplus \mathrm{Dom}(L_{\log}).$$

Since $\psi_{\mathrm{coll},\ell}$ and $\psi_{\log,D}$ are unit vectors,

$$\|\mathsf{G}_{c\ell}(D)\| = |g_{c\ell}(D)|.$$

By Eq. (B4), one has

$$|g_{c\ell}(D)| < \infty \qquad \text{for every } \ell > 0,\ D \geq 0.$$

Hence $\mathsf{G}_{c\ell}(D)$ is bounded and rank one, with

$$\|\mathsf{G}_{c\ell}(D)\| = |g_{c\ell}(D)|.$$

The off-diagonal perturbation

$$\mathbb{B}(D) = \begin{pmatrix} 0 & \mathsf{G}_{c\ell}(D) \\ \mathsf{G}_{c\ell}(D)^* & 0 \end{pmatrix}$$

is therefore bounded and symmetric. Since

$$\mathbb{L}^{\mathrm{gl}}_{\mathrm{sh},\ell}(D) = \mathbb{L}_{\mathrm{diag},\ell} + \mathbb{B}(D),$$

the bounded-perturbation theorem yields self-adjointness of $\mathbb{L}^{\mathrm{gl}}_{\mathrm{sh},\ell}(D)$ on the stated domain. This argument uses only boundedness and symmetry of the rank-one off-diagonal perturbation. It does not by itself give a coercive lower bound for the glued operator. □

Proposition 67 (Block-resolvent formulas)**.** *Assume $D \geq 0$ and assume that*

$$\mathbb{L}^{\mathrm{gl}}_{\mathrm{sh},\ell}(D) + D\mathbb{I}$$

is boundedly invertible on $\mathcal{H}_{\mathrm{coll}} \oplus \mathcal{H}_{\mathrm{log}}$. Set

$$A = H^{\mathrm{Dir}}_{\mathrm{coll},\ell} + D\mathbb{I}_{\mathrm{coll}}, \qquad B = \mathsf{G}_{c\ell}(D), \qquad E = L_{\mathrm{log}} + D\mathbb{I}_{\mathrm{log}}.$$

Then

$$A \geq (\ell^{-2} + D)\mathbb{I}_{\mathrm{coll}}, \qquad E \geq \left(D + \frac{1}{4}\right)\mathbb{I}_{\mathrm{log}},$$

so A and E are boundedly invertible. The Schur complements

$$S_c(D) = A - BE^{-1}B^*, \qquad \mathrm{Dom}(S_c(D)) = \mathrm{Dom}(A),$$

and

$$S_\ell(D) = E - B^*A^{-1}B, \qquad \mathrm{Dom}(S_\ell(D)) = \mathrm{Dom}(E),$$

are boundedly invertible as closed operators from their domains onto the corresponding Hilbert spaces. Moreover,

$$\mathbb{R}^{\mathrm{gl}}_\ell(D) \equiv \left(\mathbb{L}^{\mathrm{gl}}_{\mathrm{sh},\ell}(D) + D\mathbb{I}\right)^{-1} = \begin{pmatrix} R^{\mathrm{gl}}_{cc}(D) & R^{\mathrm{gl}}_{c\ell}(D) \\ R^{\mathrm{gl}}_{\ell c}(D) & R^{\mathrm{gl}}_{\ell\ell}(D) \end{pmatrix} \tag{B7}$$

satisfies

$$R^{\mathrm{gl}}_{cc}(D) = S_c(D)^{-1}, \tag{B8}$$

$$R^{\mathrm{gl}}_{\ell\ell}(D) = S_\ell(D)^{-1}, \tag{B9}$$

and

$$\begin{aligned} R^{\mathrm{gl}}_{c\ell}(D) &= -S_c(D)^{-1}BE^{-1} = -A^{-1}B\,S_\ell(D)^{-1}, \\ R^{\mathrm{gl}}_{\ell c}(D) &= -E^{-1}B^*S_c(D)^{-1} = -S_\ell(D)^{-1}B^*A^{-1}. \end{aligned} \tag{B10}$$

Proof. The lower bounds for the two diagonal half-line operators follow directly from their Dirichlet quadratic forms. For $v \in \mathrm{Dom}(L_{\mathrm{log}})$, integration by parts gives

$$\langle v, L_{\mathrm{log}}v\rangle = \int_0^\infty \left(|v'(t)|^2 + \frac{1}{4}|v(t)|^2\right)\mathrm{d}t \geq \frac{1}{4}\|v\|^2_{L^2(\mathbb{R}_+)}.$$

Hence

$$L_{\mathrm{log}} \geq \frac{1}{4}\mathbb{I}_{\mathrm{log}}.$$

For the collar operator, first take $u \in C^\infty_c(0,\infty)$. Then

$$\begin{aligned} \int_0^\infty |u'(\xi) + \xi u(\xi)|^2\,\mathrm{d}\xi &= \int_0^\infty \left(|u'(\xi)|^2 + \xi^2|u(\xi)|^2\right)\mathrm{d}\xi + \int_0^\infty \xi\,\partial_\xi|u(\xi)|^2\,\mathrm{d}\xi \\ &= \int_0^\infty \left(|u'(\xi)|^2 + \xi^2|u(\xi)|^2\right)\mathrm{d}\xi - \int_0^\infty |u(\xi)|^2\,\mathrm{d}\xi. \end{aligned}$$

The boundary term vanishes because u is compactly supported in $(0,\infty)$. Therefore

$$\int_0^\infty \left(|u'(\xi)|^2 + \xi^2|u(\xi)|^2\right)\mathrm{d}\xi = \int_0^\infty |u'(\xi) + \xi u(\xi)|^2\,\mathrm{d}\xi + \int_0^\infty |u(\xi)|^2\,\mathrm{d}\xi \geq \|u\|^2_{L^2(\mathbb{R}_+)}.$$

By closure of the Dirichlet oscillator form, the same bound holds on the form domain of $H^{\mathrm{Dir}}_{\mathrm{coll},\ell}$. Hence

$$H^{\mathrm{Dir}}_{\mathrm{coll},\ell} \geq \ell^{-2}\mathbb{I}_{\mathrm{coll}}.$$

Consequently,

$$A \geq (\ell^{-2} + D)\mathbb{I}_{\mathrm{coll}}, \qquad E \geq \left(D + \frac{1}{4}\right)\mathbb{I}_{\log},$$

and both A and E are boundedly invertible.

Let $f \in \mathcal{H}_{\mathrm{coll}}$ and $g \in \mathcal{H}_{\log}$. Write

$$\begin{pmatrix} u \\ v \end{pmatrix} = \mathbb{R}_{\ell}^{\mathrm{gl}}(D)\begin{pmatrix} f \\ g \end{pmatrix}.$$

Then $(u, v) \in \mathrm{Dom}(A) \oplus \mathrm{Dom}(E)$ solves

$$Au + Bv = f, \qquad B^*u + Ev = g. \tag{B11}$$

Since E is invertible, the second equation gives

$$v = E^{-1}(g - B^*u).$$

Substituting into the first equation yields

$$\big(A - BE^{-1}B^*\big)u = f - BE^{-1}g,$$

namely

$$S_c(D)u = f - BE^{-1}g.$$

We now prove that $S_c(D)$ is boundedly invertible. If $S_c(D)u = 0$, set

$$v = -E^{-1}B^*u.$$

Then (u, v) solves Eq. (B11) with $f = g = 0$. Since $\mathbb{L}_{\mathrm{sh},\ell}^{\mathrm{gl}}(D) + D\mathbb{I}$ is invertible, one gets $u = 0$ and $v = 0$. Thus $S_c(D)$ is injective. For surjectivity, let $h \in \mathcal{H}_{\mathrm{coll}}$. Solve

$$\big(\mathbb{L}_{\mathrm{sh},\ell}^{\mathrm{gl}}(D) + D\mathbb{I}\big)\begin{pmatrix} u \\ v \end{pmatrix} = \begin{pmatrix} h \\ 0 \end{pmatrix}.$$

Eliminating v as above gives $S_c(D)u = h$. Hence $S_c(D)$ is surjective. Since $S_c(D)$ is closed and bijective, its inverse is bounded by the closed graph theorem. Therefore

$$u = S_c(D)^{-1}(f - BE^{-1}g) = S_c(D)^{-1}f - S_c(D)^{-1}BE^{-1}g.$$

This proves

$$R_{cc}^{\mathrm{gl}}(D) = S_c(D)^{-1}, \qquad R_{c\ell}^{\mathrm{gl}}(D) = -S_c(D)^{-1}BE^{-1}.$$

Next eliminate u. Since A is invertible, the first equation in Eq. (B11) gives

$$u = A^{-1}(f - Bv).$$

Substituting into the second equation yields

$$\big(E - B^*A^{-1}B\big)v = g - B^*A^{-1}f,$$

namely

$$S_\ell(D)v = g - B^*A^{-1}f.$$

The same injectivity, surjectivity, and closed-graph argument shows that $S_\ell(D)$ is boundedly invertible. Hence

$$v = S_\ell(D)^{-1}(g - B^*A^{-1}f) = -S_\ell(D)^{-1}B^*A^{-1}f + S_\ell(D)^{-1}g.$$

Therefore

$$R^{\mathrm{gl}}_{\ell\ell}(D) = S_\ell(D)^{-1}, \qquad R^{\mathrm{gl}}_{\ell c}(D) = -S_\ell(D)^{-1} B^* A^{-1}.$$

Finally, substituting the formula for u into $v = E^{-1}(g - B^* u)$ gives

$$v = -E^{-1} B^* S_c(D)^{-1} f + \big(E^{-1} + E^{-1} B^* S_c(D)^{-1} B E^{-1}\big) g.$$

Comparing the coefficient of f gives

$$R^{\mathrm{gl}}_{\ell c}(D) = -E^{-1} B^* S_c(D)^{-1}.$$

Likewise, substituting the formula for v into $u = A^{-1}(f - Bv)$ gives

$$R^{\mathrm{gl}}_{c\ell}(D) = -A^{-1} B\, S_\ell(D)^{-1}.$$

This proves Eqs. (B8) to (B10). $\square$

2. Glued trace matrix and finite-rank Schur data

Definition B.3 (Collar and logarithmic derivative traces)**.** For the reduced Dirichlet basis

$$\phi_n(y) = \sqrt{2}\sin(n\pi y),$$

define the boundary derivative

$$T_\partial \phi_n \equiv \phi_n'(1^-) = \sqrt{2}\, n\pi(-1)^n. \tag{B12}$$

On the minimal branch we now set $\ell = \ell_0$. From this point on, unless a general ℓ is displayed explicitly, we use the local shorthand

$$\mathbb{L}^{\mathrm{gl}}_{\mathrm{sh}}(D) \equiv \mathbb{L}^{\mathrm{gl}}_{\mathrm{sh},\ell_0}(D), \qquad \mathbb{R}^{\mathrm{gl}}(D) \equiv \mathbb{R}^{\mathrm{gl}}_{\ell_0}(D).$$

This shorthand is confined to the present appendix. It denotes the D-parametrized finite-rank evaluation operator and its resolvent, whereas the main text uses $\mathbb{L}^{\mathrm{gl}}_{\mathrm{sh}}$ for the abstract D-independent mother bath.

The collar and logarithmic trace sources are the shell-bath functions

$$\tau_n^{\mathrm{coll}}(\xi) \equiv \frac{1}{\pi}\exp\!\left[-\frac{\xi^2}{2\ell_0^2}\right] T_\partial\phi_n, \qquad \xi \in \mathbb{R}_+, \tag{B13}$$

and

$$\tau_n^{\log}(t; D) \equiv \eta_0\, T_\partial\phi_n\, e^{-\sqrt{D+1/4}\,t}, \qquad t \in \mathbb{R}_+, \qquad \eta_0 = \frac{1}{\pi}. \tag{B14}$$

The D-dependence of $\tau_n^{\log}$ is part of the finite-rank dynamic evaluation. It is unrelated to the Dirichlet label Dir in $H^{\mathrm{Dir}}_{\mathrm{coll},\ell}$.

Remark. The source enters only through the boundary derivative $T_\partial\phi_n$. The value trace vanishes on the pinned Dirichlet basis, since

$$\phi_n(1) = \sqrt{2}\sin(n\pi) = 0.$$

The glued shell therefore couples to the cavity line through a derivative trace rather than through a value trace.

Definition B.4 (Glued trace matrix)**.** For all $m, n \geq 1$ and for every evaluation parameter $D \geq 0$ for which $\mathbb{R}^{\mathrm{gl}}(D)$ exists, define

$$\widetilde{C}^{\mathrm{gl}}_{mn}(D) \equiv \left\langle \begin{bmatrix} \tau_m^{\mathrm{coll}} \\ \tau_m^{\log}(\cdot; D) \end{bmatrix}, \mathbb{R}^{\mathrm{gl}}(D) \begin{bmatrix} \tau_n^{\mathrm{coll}} \\ \tau_n^{\log}(\cdot; D) \end{bmatrix} \right\rangle_{\mathcal{H}_{\mathrm{coll}} \oplus \mathcal{H}_{\log}}. \tag{B15}$$

Equivalently,

$$\begin{aligned} \widetilde{C}^{\mathrm{gl}}_{mn}(D) = {} & \big\langle \tau_m^{\mathrm{coll}}, R^{\mathrm{gl}}_{cc}(D)\tau_n^{\mathrm{coll}} \big\rangle_{L^2(\mathbb{R}_+, \mathrm{d}\xi)} + \left\langle \tau_m^{\mathrm{coll}}, R^{\mathrm{gl}}_{c\ell}(D)\tau_n^{\log}(\cdot; D) \right\rangle_{L^2(\mathbb{R}_+, \mathrm{d}\xi)} \\ & + \left\langle \tau_m^{\log}(\cdot; D), R^{\mathrm{gl}}_{\ell c}(D)\tau_n^{\mathrm{coll}} \right\rangle_{L^2(\mathbb{R}_+, \mathrm{d}t)} + \left\langle \tau_m^{\log}(\cdot; D), R^{\mathrm{gl}}_{\ell\ell}(D)\tau_n^{\log}(\cdot; D) \right\rangle_{L^2(\mathbb{R}_+, \mathrm{d}t)}. \end{aligned} \tag{B16}$$

Proposition 68 (Well-definedness and symmetry of the glued trace matrix)**.** *Assume $D \geq 0$ and that*

$$\mathbb{L}^{\mathrm{gl}}_{\mathrm{sh}}(D) + D\mathbb{I}$$

is boundedly invertible. Then, for all $m, n \geq 1$, the quantity $\widetilde{C}^{\mathrm{gl}}_{mn}(D)$ is finite. Moreover,

$$\widetilde{C}^{\mathrm{gl}}_{mn}(D) = \overline{\widetilde{C}^{\mathrm{gl}}_{nm}(D)}. \tag{B17}$$

If the retained directions and the trace sources are real-valued, then $\widetilde{C}^{\mathrm{gl}}_{mn}(D) \in \mathbb{R}$ and the matrix is symmetric.

Proof. By Eq. (B13),

$$\begin{aligned}\|\tau^{\mathrm{coll}}_n\|^2_{L^2(\mathbb{R}_+,\mathrm{d}\xi)} &= \frac{|T\partial\phi_n|^2}{\pi^2}\int_0^\infty e^{-\xi^2/\ell_0^2}\,\mathrm{d}\xi \\ &= \frac{|T\partial\phi_n|^2}{\pi^2}\frac{\sqrt{\pi}\,\ell_0}{2} < \infty.\end{aligned}$$

By Eq. (B14),

$$\begin{aligned}\|\tau^{\log}_n(\cdot;D)\|^2_{L^2(\mathbb{R}_+,\mathrm{d}t)} &= \eta_0^2|T\partial\phi_n|^2\int_0^\infty e^{-2\sqrt{D+1/4}\,t}\,\mathrm{d}t \\ &= \frac{\eta_0^2|T\partial\phi_n|^2}{2\sqrt{D+1/4}} < \infty.\end{aligned}$$

Hence

$$\begin{bmatrix}\tau^{\mathrm{coll}}_m \\ \tau^{\log}_m(\cdot;D)\end{bmatrix} \in L^2(\mathbb{R}_+,\mathrm{d}\xi) \oplus L^2(\mathbb{R}_+,\mathrm{d}t)$$

for every $m \geq 1$. Since $\mathbb{R}^{\mathrm{gl}}(D)$ is bounded, the pairing in Eq. (B15) is finite for every $m, n \geq 1$.

Because $\mathbb{L}^{\mathrm{gl}}_{\mathrm{sh}}(D)$ is self-adjoint and the shifted operator $\mathbb{L}^{\mathrm{gl}}_{\mathrm{sh}}(D) + D\mathbb{I}$ is assumed boundedly invertible, the shifted inverse $\mathbb{R}^{\mathrm{gl}}(D)$ is self-adjoint. Therefore

$$\begin{aligned}\widetilde{C}^{\mathrm{gl}}_{mn}(D) &= \left\langle \begin{bmatrix}\tau^{\mathrm{coll}}_m \\ \tau^{\log}_m(\cdot;D)\end{bmatrix}, \mathbb{R}^{\mathrm{gl}}(D)\begin{bmatrix}\tau^{\mathrm{coll}}_n \\ \tau^{\log}_n(\cdot;D)\end{bmatrix}\right\rangle \\ &= \overline{\left\langle \begin{bmatrix}\tau^{\mathrm{coll}}_n \\ \tau^{\log}_n(\cdot;D)\end{bmatrix}, \mathbb{R}^{\mathrm{gl}}(D)\begin{bmatrix}\tau^{\mathrm{coll}}_m \\ \tau^{\log}_m(\cdot;D)\end{bmatrix}\right\rangle} \\ &= \overline{\widetilde{C}^{\mathrm{gl}}_{nm}(D)}.\end{aligned}$$

This proves Eq. (B17). If the retained directions and the trace sources are real-valued, complex conjugation drops out and the matrix is real symmetric. □

Definition B.5 (Finite-rank Schur data)**.** Fix an integer $N \geq 2$. Let

$$\Delta_n \equiv n^2 - 1, \qquad n \geq 2.$$

Define

$$v^{\mathrm{gl}}_n(D) \equiv \frac{\widetilde{C}^{\mathrm{gl}}_{1n}(D)}{\sqrt{\Delta_n}}, \qquad \mathbf{v}^{\mathrm{gl}}_E(D) \equiv \big(v^{\mathrm{gl}}_2(D), \ldots, v^{\mathrm{gl}}_N(D)\big)^\top, \tag{B18}$$

and

$$\big[\mathbb{M}^{\mathrm{gl}}_{EE}(D)\big]_{mn} \equiv \frac{\widetilde{C}^{\mathrm{gl}}_{mn}(D)}{\Delta_m\Delta_n}, \qquad m, n = 2, \ldots, N. \tag{B19}$$

Proposition 69 (Finite-rank glued Schur correction)**.** *Assume that $\mathbb{I}+\mathbb{M}^{\rm gl}_{EE}(D)$ is invertible on $\mathbb{C}^{N-1}$. Define the finite-dimensional block matrix*

$$\mathbb{K}^{\rm gl}_N(D) \equiv \begin{pmatrix} 0 & \big(\mathbf{v}^{\rm gl}_E(D)\big)^* \\ \mathbf{v}^{\rm gl}_E(D) & \mathbb{I}+\mathbb{M}^{\rm gl}_{EE}(D) \end{pmatrix} \tag{B20}$$

on $\mathbb{C}\oplus\mathbb{C}^{N-1}$. Then the Schur complement of the excited block is

$$\mathrm{Schur}_E\big(\mathbb{K}^{\rm gl}_N(D)\big) = -\big(\mathbf{v}^{\rm gl}_E(D)\big)^*\big(\mathbb{I}+\mathbb{M}^{\rm gl}_{EE}(D)\big)^{-1}\mathbf{v}^{\rm gl}_E(D). \tag{B21}$$

With the fixed implementation normalization $\gamma_{\rm E}/\pi^2$, define the finite-rank glued-shell dynamic Schur correction as the negative normalized Schur complement:

$$\delta\mathcal{G}^{{\rm gl},N}_{e\gamma}(D) = -\frac{\gamma_{\rm E}}{\pi^2}\,\mathrm{Schur}_E\big(\mathbb{K}^{\rm gl}_N(D)\big) = \frac{\gamma_{\rm E}}{\pi^2}\,\big(\mathbf{v}^{\rm gl}_E(D)\big)^*\big(\mathbb{I}+\mathbb{M}^{\rm gl}_{EE}(D)\big)^{-1}\mathbf{v}^{\rm gl}_E(D). \tag{B22}$$

If, in addition, $\mathbb{I}+\mathbb{M}^{\rm gl}_{EE}(D)$ is Hermitian positive definite, then

$$\delta\mathcal{G}^{{\rm gl},N}_{e\gamma}(D) \geq 0. \tag{B23}$$

This quantity is the excited-sector dynamic correction extracted from the finite-rank glued higher-mode block with the stated normalization. It is an implementation-level diagnostic Schur term. It should be kept distinct from the reduced visible two-mode evaluator $\mathcal{G}^{{\rm gl},N}_{e\gamma}(D)$ of Eqs. (233) and (235), which is the scalar evaluator used in the main text.

Proof. Let $a,b\in\mathbb{C}$ and $\xi,\eta\in\mathbb{C}^{N-1}$. Consider the block system

$$\mathbb{K}^{\rm gl}_N(D)\begin{pmatrix} a \\ \xi \end{pmatrix} = \begin{pmatrix} b \\ \eta \end{pmatrix}. \tag{B24}$$

This is

$$\big(\mathbf{v}^{\rm gl}_E(D)\big)^*\xi = b, \qquad \mathbf{v}^{\rm gl}_E(D)a + \big(\mathbb{I}+\mathbb{M}^{\rm gl}_{EE}(D)\big)\xi = \eta.$$

Since $\mathbb{I}+\mathbb{M}^{\rm gl}_{EE}(D)$ is invertible, the second equation gives

$$\xi = \big(\mathbb{I}+\mathbb{M}^{\rm gl}_{EE}(D)\big)^{-1}\big(\eta - \mathbf{v}^{\rm gl}_E(D)a\big).$$

Substituting this into the first equation yields

$$b = \big(\mathbf{v}^{\rm gl}_E(D)\big)^*\big(\mathbb{I}+\mathbb{M}^{\rm gl}_{EE}(D)\big)^{-1}\eta - \big(\mathbf{v}^{\rm gl}_E(D)\big)^*\big(\mathbb{I}+\mathbb{M}^{\rm gl}_{EE}(D)\big)^{-1}\mathbf{v}^{\rm gl}_E(D)\,a.$$

Therefore the scalar Schur complement of the excited block is exactly

$$-\big(\mathbf{v}^{\rm gl}_E(D)\big)^*\big(\mathbb{I}+\mathbb{M}^{\rm gl}_{EE}(D)\big)^{-1}\mathbf{v}^{\rm gl}_E(D),$$

which proves Eq. (B21). Multiplying by the fixed positive normalization $\gamma_{\rm E}/\pi^2$ gives Eq. (B22).

If $\mathbb{I}+\mathbb{M}^{\rm gl}_{EE}(D)$ is Hermitian positive definite, then its inverse is Hermitian positive definite. Hence

$$\big(\mathbf{v}^{\rm gl}_E(D)\big)^*\big(\mathbb{I}+\mathbb{M}^{\rm gl}_{EE}(D)\big)^{-1}\mathbf{v}^{\rm gl}_E(D) \geq 0.$$

Since $\gamma_{\rm E}/\pi^2 > 0$, this yields

$$\delta\mathcal{G}^{{\rm gl},N}_{e\gamma}(D) \geq 0,$$

which proves Eq. (B23). No further identification is made here. In particular, the present Schur correction is not a second definition of the main-text quantity $\mathcal{G}^{{\rm gl},N}_{e\gamma}(D)$. □

Remark (Derived diagnostics). Quantities such as $\Delta A^{(N)}_{\rm mix}$, $\delta A^{(N)}_0$, χ_N, $\Delta A^{(N)}_{\rm diag}$, and $\delta A^{(N)}_{\rm off}$ should be regarded as diagnostics extracted from the exact finite inverse

$$\big(\mathbb{I}+\mathbb{M}^{\rm gl}_{EE}(D)\big)^{-1},$$

not as primitive defining inputs. If, for a given D,

$$\|\mathbb{M}^{\rm gl}_{EE}(D)\| < 1, \tag{B25}$$

then the inverse also admits the convergent Neumann expansion

$$\big(\mathbb{I} + \mathbb{M}^{\rm gl}_{EE}(D)\big)^{-1} = \sum_{k=0}^{\infty}\big(-\mathbb{M}^{\rm gl}_{EE}(D)\big)^{k} \tag{B26}$$

in operator norm on the finite excited block. The diagonal and off-diagonal excited-line corrections therefore arise from the single inverse in Eq. (B22). Any Neumann-series interpretation is valid only under the convergence condition Eq. (B25).

3. Numerical orientation and link to the main scalar ledger

Remark. The numerical values of ℓ_0, η_0, $g_{c\ell}(0)$, and $B^{\rm glue}_{11}$ are already recorded in the main scalar numerical ledger; see in particular table IV. This appendix adds no independent numerical datum. Its role is purely implementation-level. It makes explicit the retained overlap, trace-matrix, and Schur-complement formulas that underlie the glued-shell evaluation.

Appendix C: Sensitivity and numerical precision of the geometric lock

This appendix audits the realized geometric-lock evaluation at the levels of local sensitivity, truncation status, and arithmetic precision. The main text shows that, for the frozen D-only scalar-radicand realization used in the present audit, once a vector-shell representative and a scalar evaluator have been fixed, the realized lock output is obtained by algebraic inversion of the scalar shell law. No coupled fixed-point solve remains in this frozen D-only realization. The audit therefore separates exact closed-form ingredients from finite-rank or representative inputs and then quantifies the local response of α_* to each class of data.

The realized error budget has two sources. The first is the vector-shell representative used for $\Lambda_{\rm geom}$; it can be sharpened by improved evaluations of the shell-matrix resolvent, the large-mode tail, and the exterior-memory functional. The second is the scalar evaluator $\mathcal{D}_{\rm C}(\alpha)$; its realization accuracy can be improved by operator-level completion of the scalar branch and can be assessed externally, without entering the primary lock, by comparison with the universal pure-photonic $g-2$ coefficients. The value of α_* audited here is computed without QED coefficients and without the measured fine-structure constant.

1. Closed-form ingredients and truncation map

Throughout this appendix, let $\Lambda_{\rm in}$ denote the vector-shell input actually used in the audit. In the current article realization,

$$\Lambda_{\rm in} = \Lambda^{\rm (th)}_{\rm geom},$$

while at the exact operator level one would set $\Lambda_{\rm in} = \Lambda_{\rm geom}$. This local notation prevents the exact vector-shell object $\Lambda_{\rm geom}$ from being conflated with the reduced representative used in the numerical lock. All formulas in this appendix use $\Lambda_{\rm in}$ unless the exact operator-limit object is named explicitly. The first point that must be kept explicit is the distinction between quantities evaluated by closed formulas and quantities entering through finite-rank representatives or external truncations.

Proposition 70 (Closed-form and representative quantities in the realized lock audit)**.** *In the realized geometric-lock evaluation, the following quantities are exact closed-form ingredients and require no numerical root search.*

$$\eta_0 = \frac{1}{\pi}, \qquad \ell_0 = \frac{1}{\pi\sqrt{\pi}}, \qquad \mathsf{K}_{ALP} = \frac{150\pi^2 - 8\pi^4 - 315}{180\pi^6}, \tag{C1}$$

On the minimal branch, where $\ell = \ell_0$, the collar–log overlap is

$$g_{c\ell}(D) = \frac{\sqrt{\pi}\,\ell_0}{2}\exp\Big[\frac{\ell_0^2}{4}\Big(D + \frac{1}{4}\Big)\Big]\,\mathrm{erfc}\Big(\frac{\ell_0}{2}\sqrt{D + \frac{1}{4}}\Big), \tag{C2}$$

$$\mathfrak{D}_{\text{lock}}(\Lambda) = \frac{3}{2}\,\mathsf{K}_{ALP}\,\Lambda\left(1 + \frac{\mathsf{K}_{ALP}\Lambda}{2\pi^2}\right), \tag{C3}$$

$$\zeta(D) = \frac{1}{2}\left(\sqrt{1 + \frac{4D}{3\pi^2}} - 1\right). \tag{C4}$$

Within a chosen static completion, the coefficients B_{11}^{glue} and $B_{11}^{(3,\rho)}$ are closed realization-level quantities once the raw static traces and the corresponding finite static block have been fixed. More precisely, they are obtained from explicit special-function expressions and finite-dimensional matrix algebra inside the chosen static completion. This does not make either coefficient an operator-exact invariant of the full scalar shell theory.

After the realized scalar evaluator has been frozen, the following are closed algebraic evaluation maps within that fixed evaluator on every interval $I \subset (0,\infty)$ where $\mathfrak{R}_{\text{moth}}(D) > 0$.

$$\alpha(D) = \pi\,\frac{D}{\sqrt{\mathfrak{R}_{\text{moth}}(D)}}, \qquad x(D) = \frac{\alpha(D)}{\pi} = \frac{D}{\sqrt{\mathfrak{R}_{\text{moth}}(D)}}, \tag{C5}$$

$$\mathcal{D}_{\text{total}}(D) = D - x(D)\zeta(D) + \frac{x(D)^2\zeta(D)^2}{4D}, \qquad D > 0. \tag{C6}$$

If one wishes to include $D = 0$, the last term is understood by removable singularity. Indeed, in the realized scalar evaluator $\mathfrak{R}_{\text{moth}}(0) = 1$, so $x(D) = D/\sqrt{\mathfrak{R}_{\text{moth}}(D)}$ extends smoothly to $D = 0$ on any neighborhood where the radicand remains positive. Since $\zeta(D) = D\,h(D)$ with h analytic at $D = 0$, one has

$$\frac{x(D)^2\zeta(D)^2}{4D} = \frac{x(D)^2\,D\,h(D)^2}{4}, \tag{C7}$$

which has a smooth extension to $D = 0$. By contrast, the following quantities are representative, finite-rank, or reference-only quantities rather than operator-exact closed forms of the full shell theory:

$$\Lambda_{\text{in}}, \qquad A_{\text{uv}}^{(N)},\ A_{\text{ir}}^{(N)},\ \chi_N, \qquad D_{\text{QED}}^{[5]}(x),\ \alpha_{\text{QED}\to\text{D}}^{[5]}. \tag{C8}$$

Here Λ_{in} is the vector-shell input used in the audit. In the current numerical realization it is the reduced geometry-only representative $\Lambda_{\text{geom}}^{(\text{th})}$, not the exact operator-limit vector constant. The triple $(A_{\text{uv}}^{(N)}, A_{\text{ir}}^{(N)}, \chi_N)$ belongs to the current finite-rank scalar evaluator. The quantities $D_{\text{QED}}^{[5]}$ and $\alpha_{\text{QED}\to\text{D}}^{[5]}$ belong to the reference-only layer and contain an explicit external QED truncation at order $M = 5$.

Proof. The identities in Eq. (C1) are direct consequences of the pinned minimal-shell geometry and of the closed expression for K_{ALP}. The overlap formula Eq. (C2) is exactly the closed complementary-error-function form of the retained collar–log overlap evaluated on the minimal branch. Its value at $D = 0$ gives the static overlap used in the static ledger. Equation (C3) is the Alpha Lock Point written as a function of the vector-shell constant. Equation (C5) is the algebraic inversion of the scalar mother law.

On every interval $I \subset (0,\infty)$ where $\mathfrak{R}_{\text{moth}}(D) > 0$, the functions $\alpha(D)$ and $x(D)$ are real-valued algebraic evaluation maps. The bridge quantity $\zeta(D)$ is also algebraic, and the last term in Eq. (C6) has only a removable singularity at $D = 0$. Indeed, since

$$\zeta(D) = D\,h(D),$$

with $h(D)$ analytic at $D = 0$, one has

$$\frac{x(D)^2\zeta(D)^2}{4D} = \frac{x(D)^2\,D\,h(D)^2}{4},$$

which extends continuously to $D = 0$. Hence $\zeta(D)$ and $\mathcal{D}_{\text{total}}(D)$ are explicit closed evaluations within the fixed realized scalar evaluator. Therefore no numerical root-finding enters this algebraic evaluation stage.

The quantities B_{11}^{glue} and $B_{11}^{(3,\rho)}$ are closed special-function or finite-dimensional matrix expressions in the chosen static shell data, so they are closed within that chosen static completion. The objects listed in Eq. (C8) are of a different nature. In the current audit, Λ_{in} is the reduced geometry-only numerical representative $\Lambda_{\text{geom}}^{(\text{th})}$, rather than a full operator-level closed form. The visible dynamic block $(A_{\text{uv}}^{(N)}, A_{\text{ir}}^{(N)}, \chi_N)$ is explicitly finite-rank. The QED-induced quantities are not part of the primary lock at all; they are explicitly truncated at order $M = 5$ and belong to the reference-only diagnostic layer. This proves the claimed distinction. □

Ingredient	Status	Comment
$\eta_0, \ell_0, \mathsf{K}_{\text{ALP}}$	exact closed	no truncation
$g_{c\ell}(D)$ with $\ell = \ell_0$	exact closed	complementary-error-function formula
B_{11}^{glue}	closed in visible static block	visible 2-channel realization
$B_{11}^{(3,\rho)}$	closed in chosen completion	canonical 3-channel static lift
$\mathfrak{D}_{\text{lock}}(\Lambda)$	closed target map	realization status inherited from Λ; no root search
$\alpha(D)$	closed within fixed evaluator	once $\mathfrak{R}_{\text{moth}}$ is fixed
$\zeta(D), \mathcal{D}_{\text{total}}(D)$	closed within fixed evaluator	algebraic Relator bridge
Λ_{in}	current representative	$\Lambda_{\text{geom}}^{(\text{th})}$ in the present audit
$(A_{\text{uv}}^{(N)}, A_{\text{ir}}^{(N)}, \chi_N)$	finite-rank	visible dynamic block
$D_{\text{QED}}^{[5]}, \alpha_{\text{QED}\to\text{D}}^{[5]}$	external truncated	reference-only QED cross-check

TABLE XXVII. Status of the quantities used in the realized geometric-lock audit. Only the shell quantities enter the primary lock; the QED-induced quantities are reference-only diagnostics.

2. Closed sensitivity identities within the frozen lock realization

Let

$$\mathfrak{D}_{*,\text{in}} = \mathfrak{D}_{\text{lock}}(\Lambda_{\text{in}}), \qquad \mathfrak{R}_* = \mathfrak{R}_{\text{moth}}(\mathfrak{D}_{*,\text{in}}), \qquad \alpha_* = \pi\,\frac{\mathfrak{D}_{*,\text{in}}}{\sqrt{\mathfrak{R}_*}}. \tag{C9}$$

Here Λ_{in} is the vector-shell input used in the audit. In the current realization $\Lambda_{\text{in}} = \Lambda_{\text{geom}}^{(\text{th})}$; at exact operator level one would instead set $\Lambda_{\text{in}} = \Lambda_{\text{geom}}$, provided the exact vector hypotheses are satisfied. For the fixed scalar evaluator used in this audit, the realized scalar radicand is

$$\mathfrak{R}_{\text{moth}}(D) = 1 - \Theta_{1,\text{eff}} D + D^2 \Phi_{\text{dyn}}(D), \tag{C10}$$

with

$$\Phi_{\text{dyn}}(D) = \kappa_{\text{dyn}}\,\frac{N(D)}{Q(D)}. \tag{C11}$$

For the current article scalar evaluator, $\kappa_{\text{dyn}} = 1$. In a different fixed scalar realization, κ_{dyn} is the kernel scale specified by that realization. It is not varied as an additional fit parameter in the present audit. The numerator and denominator are

$$N(D) = A_{\text{uv}}^{(N)}(1 + s_{\text{ir}} D) + A_{\text{ir}}^{(N)}(1 + s_{\text{uv}} D) - 2\chi_N D\sqrt{A_{\text{uv}}^{(N)} A_{\text{ir}}^{(N)}}, \tag{C12}$$

$$Q(D) = (1 + s_{\text{uv}} D)(1 + s_{\text{ir}} D) - \chi_N^2 D^2. \tag{C13}$$

It is useful to define

$$\rho_{\text{dyn}} = \frac{\chi_N}{\sqrt{s_{\text{uv}} s_{\text{ir}}}}. \tag{C14}$$

Proposition 71 (Regularity of the realized dynamic denominator). *Assume*

$$\chi_N \in \mathbb{R}, \qquad |\rho_{\text{dyn}}| < 1, \qquad s_{\text{uv}} > 0, \qquad s_{\text{ir}} > 0. \tag{C15}$$

Then, for every $D \geq 0$,

$$Q(D) > 0. \tag{C16}$$

If, in addition,

$$A_{\text{uv}}^{(N)} > 0, \qquad A_{\text{ir}}^{(N)} > 0, \qquad \kappa_{\text{dyn}} \in \mathbb{R}, \qquad \Theta_{1,\text{eff}} \in \mathbb{R},$$

then $N(D)$, $\Phi_{\text{dyn}}(D)$, and $\mathfrak{R}_{\text{moth}}(D)$ are real-valued wherever the quotient is defined. Consequently,

$$\Phi_{\text{dyn}} \in C^\infty([0,\infty);\mathbb{R}). \tag{C17}$$

Hence the realized radicand

$$\mathfrak{R}_{\text{moth}}(D) = 1 - \Theta_{1,\text{eff}} D + D^2 \Phi_{\text{dyn}}(D) \tag{C18}$$

is a real-valued C^∞ function on $[0,\infty)$.

Proof. Expanding Eq. (C13) gives

$$Q(D) = 1 + (s_{\rm uv} + s_{\rm ir})D + \bigl(s_{\rm uv}s_{\rm ir} - \chi_N^2\bigr)D^2.$$

From Eq. (C14), and using $\chi_N \in \mathbb{R}$, one has

$$s_{\rm uv}s_{\rm ir} - \chi_N^2 = s_{\rm uv}s_{\rm ir}\bigl(1 - \rho_{\rm dyn}^2\bigr).$$

Under Eq. (C15), this coefficient is strictly positive. Since $s_{\rm uv} > 0$, $s_{\rm ir} > 0$, and $D \geq 0$, the linear and quadratic coefficients of $Q(D)$ are nonnegative and the constant term is 1. Therefore

$$Q(D) \geq 1 > 0, \qquad D \geq 0.$$

This proves Eq. (C16).

Since $N(D)$ and $Q(D)$ are real polynomials in D, and $Q(D) > 0$ on $[0,\infty)$, the quotient

$$\Phi_{\rm dyn}(D) = \kappa_{\rm dyn}\frac{N(D)}{Q(D)}$$

is real-valued and C^∞ on $[0,\infty)$. Therefore

$$\mathfrak{R}_{\rm moth}(D) = 1 - \Theta_{1,\rm eff}D + D^2\Phi_{\rm dyn}(D)$$

is also real-valued and C^∞ on $[0,\infty)$. This proves the final claim. □

Proposition 72 (Closed differential identities at the lock point)**.** *Assume that the scalar evaluator is fixed. Let* $\Lambda_{\rm in} > 0$*, set*

$$\mathfrak{D}_{*,\rm in} := \mathfrak{D}_{\rm lock}(\Lambda_{\rm in}),$$

and assume that

$$\mathfrak{D}_{*,\rm in} \in I \subset (0,\infty),$$

where I *is an interval on which*

$$Q(D) > 0, \qquad \mathfrak{R}_{\rm moth}(D) > 0, \qquad \kappa_{\rm dyn} \in \mathbb{R}. \tag{C19}$$

For the target map $\mathfrak{D}_{\rm lock}(\Lambda)$*, with* K_{ALP} *and* Λ *treated as independent variables for differentiation, one has*

$$\frac{\mathrm{d}\mathfrak{D}_{\rm lock}}{\mathrm{d}\Lambda} = \frac{3}{2}\,\mathsf{K}_{ALP}\left(1 + \frac{\mathsf{K}_{ALP}\Lambda}{\pi^2}\right), \tag{C20}$$

$$\frac{\mathrm{d}\mathfrak{D}_{\rm lock}}{\mathrm{d}\mathsf{K}_{ALP}} = \frac{3}{2}\,\Lambda\left(1 + \frac{\mathsf{K}_{ALP}\Lambda}{\pi^2}\right), \tag{C21}$$

and the scalar inversion satisfies

$$\frac{\mathrm{d}\alpha}{\mathrm{d}D} = \pi\,\frac{1 - \dfrac{D}{2}\dfrac{\mathfrak{R}'_{\rm moth}(D)}{\mathfrak{R}_{\rm moth}(D)}}{\sqrt{\mathfrak{R}_{\rm moth}(D)}}, \tag{C22}$$

where

$$\mathfrak{R}'_{\rm moth}(D) = -\Theta_{1,\rm eff} + 2D\Phi_{\rm dyn}(D) + D^2\Phi'_{\rm dyn}(D), \tag{C23}$$

with

$$\Phi'_{\rm dyn}(D) = \kappa_{\rm dyn}\,\frac{N'(D)Q(D) - N(D)Q'(D)}{Q(D)^2}, \tag{C24}$$

$$N'(D) = A_{\rm uv}^{(N)} s_{\rm ir} + A_{\rm ir}^{(N)} s_{\rm uv} - 2\chi_N \sqrt{A_{\rm uv}^{(N)} A_{\rm ir}^{(N)}}, \tag{C25}$$

$$Q'(D) = s_{\rm uv} + s_{\rm ir} + 2D(s_{\rm uv}s_{\rm ir} - \chi_N^2), \tag{C26}$$

Consequently, holding the scalar evaluator and K_{ALP} fixed,

$$\frac{\mathrm{d}\alpha_*}{\mathrm{d}\Lambda_{\rm in}} = \left.\frac{\mathrm{d}\alpha}{\mathrm{d}D}\right|_{D=\mathfrak{D}_{*,\rm in}} \left.\frac{\mathrm{d}\mathfrak{D}_{\rm lock}}{\mathrm{d}\Lambda}\right|_{\Lambda=\Lambda_{\rm in}}, \tag{C27}$$

and, holding the scalar evaluator and $\Lambda_{\rm in}$ fixed,

$$\frac{\mathrm{d}\alpha_*}{\mathrm{d}\mathsf{K}_{ALP}} = \left.\frac{\mathrm{d}\alpha}{\mathrm{d}D}\right|_{D=\mathfrak{D}_{*,\rm in}} \left.\frac{\mathrm{d}\mathfrak{D}_{\rm lock}}{\mathrm{d}\mathsf{K}_{ALP}}\right|_{\Lambda=\Lambda_{\rm in}}. \tag{C28}$$

Proof. All differentiations below are taken on the interval I, where $Q(D) > 0$ and $\mathfrak{R}_{\rm moth}(D) > 0$, so every displayed quotient and square root is well defined.

Differentiating

$$\mathfrak{D}_{\rm lock}(\Lambda) = \frac{3}{2}\,\mathsf{K}_{\rm ALP}\,\Lambda\left(1 + \frac{\mathsf{K}_{\rm ALP}\Lambda}{2\pi^2}\right)$$

with respect to Λ gives Eq. (C20). Differentiating the same expression with respect to $\mathsf{K}_{\rm ALP}$, while holding Λ fixed, gives Eq. (C21).

For the scalar inversion, write

$$\alpha(D) = \pi D\,\mathfrak{R}_{\rm moth}(D)^{-1/2}.$$

Then

$$\frac{\mathrm{d}\alpha}{\mathrm{d}D} = \pi\,\mathfrak{R}_{\rm moth}(D)^{-1/2} - \frac{\pi D}{2}\,\mathfrak{R}_{\rm moth}(D)^{-3/2}\,\mathfrak{R}'_{\rm moth}(D),$$

which is exactly Eq. (C22).

Equation (C23) follows by differentiating Eq. (C10). Since

$$\Phi_{\rm dyn}(D) = \kappa_{\rm dyn}\frac{N(D)}{Q(D)},$$

with $\kappa_{\rm dyn}$ independent of D, the quotient rule yields Eq. (C24). The derivatives Eqs. (C25) and (C26) follow by direct differentiation of Eqs. (C12) and (C13).

Finally, Eqs. (C27) and (C28) are immediate chain-rule evaluations at the lock point

$$(D,\Lambda) = (\mathfrak{D}_{*,\rm in}, \Lambda_{\rm in}).$$

$\square$

Proposition 73 (Fixed-lock scalar-parameter response)**.** *Assume*

$$\mathfrak{R}_* = \mathfrak{R}_{\rm moth}(\mathfrak{D}_{*,\rm in}) > 0. \tag{C29}$$

Let q be any differentiable scalar-evaluator parameter that enters only through $\mathfrak{R}_{\rm moth}(D)$ and not through $\mathfrak{D}_{*,\rm in}$. Then, at fixed target value $\mathfrak{D}_{*,\rm in}$, one has

$$\frac{\partial\alpha_*}{\partial q} = -\frac{\alpha_*}{2\mathfrak{R}_*}\left.\frac{\partial\mathfrak{R}_{\rm moth}(D)}{\partial q}\right|_{D=\mathfrak{D}_{*,\rm in}}. \tag{C30}$$

In particular, if $\Theta_{1,\rm eff} > 0$, then

$$\frac{\partial\alpha_*}{\partial\Theta_{1,\rm eff}} = \frac{\alpha_*\mathfrak{D}_{*,\rm in}}{2\mathfrak{R}_*}, \qquad \frac{\partial\ln\alpha_*}{\partial\ln\Theta_{1,\rm eff}} = \Theta_{1,\rm eff}\,\frac{\mathfrak{D}_{*,\rm in}}{2\mathfrak{R}_*}. \tag{C31}$$

If

$$\Theta_{1,\mathrm{eff}} = \Theta_{1,\mathrm{core}} + B_{11}^{(\mathrm{eval})}, \tag{C32}$$

and $B_{11}^{(\mathrm{eval})}$ *does not enter* $\Phi_{\mathrm{dyn}}(D)$*, and if*

$$B_{11}^{(\mathrm{eval})} > 0, \tag{C33}$$

then

$$\frac{\partial \ln \alpha_*}{\partial \ln B_{11}^{(\mathrm{eval})}} = B_{11}^{(\mathrm{eval})} \frac{\mathfrak{D}_{*,\mathrm{in}}}{2\mathfrak{R}_*}. \tag{C34}$$

Proof. At fixed $\mathfrak{D}_{*,\mathrm{in}}$, the only dependence of α_* on q comes through the radicand,

$$\alpha_* = \pi \mathfrak{D}_{*,\mathrm{in}}\, \mathfrak{R}_{\mathrm{moth}}(\mathfrak{D}_{*,\mathrm{in}})^{-1/2}.$$

Differentiating with respect to q gives

$$\frac{\partial \alpha_*}{\partial q} = -\frac{\pi \mathfrak{D}_{*,\mathrm{in}}}{2}\, \mathfrak{R}_{\mathrm{moth}}(\mathfrak{D}_{*,\mathrm{in}})^{-3/2}\, \frac{\partial \mathfrak{R}_{\mathrm{moth}}(D)}{\partial q}\bigg|_{D=\mathfrak{D}_{*,\mathrm{in}}}.$$

Using

$$\alpha_* = \frac{\pi \mathfrak{D}_{*,\mathrm{in}}}{\sqrt{\mathfrak{R}_*}}, \qquad \mathfrak{R}_* = \mathfrak{R}_{\mathrm{moth}}(\mathfrak{D}_{*,\mathrm{in}}),$$

this becomes Eq. (C30).

For $q = \Theta_{1,\mathrm{eff}}$, one has

$$\partial_{\Theta_{1,\mathrm{eff}}} \mathfrak{R}_{\mathrm{moth}}(D) = -D,$$

which yields Eq. (C31).

Under Eq. (C32), the derivative with respect to $B_{11}^{(\mathrm{eval})}$ is the same as the derivative with respect to $\Theta_{1,\mathrm{eff}}$, provided $B_{11}^{(\mathrm{eval})}$ enters the radicand only through $\Theta_{1,\mathrm{eff}}$. If moreover $B_{11}^{(\mathrm{eval})} > 0$, multiplying by $B_{11}^{(\mathrm{eval})}/\alpha_*$ gives Eq. (C34). □

Quantity	Value
$\mathfrak{D}_{*,\mathrm{in}} = \mathfrak{D}_{\mathrm{lock}}(\Lambda_{\mathrm{in}})$	0.002315457831961859388055180838225655037164
$\mathfrak{R}_* = \mathfrak{R}_{\mathrm{moth}}(\mathfrak{D}_{*,\mathrm{in}})$	0.9936715124961825203792602609712460860095
$\mathrm{d}\mathfrak{D}_{\mathrm{lock}}/\mathrm{d}\Lambda$	0.003347831863890756166833390212679253971757
$\mathrm{d}\mathfrak{D}_{\mathrm{lock}}/\mathrm{d}\mathsf{K}_{\mathrm{ALP}}$	1.037686978747347760197771044955982368875
$\mathrm{d}\alpha/\mathrm{d}D$ at $\mathfrak{D}_{*,\mathrm{in}}$	3.161568226180219588210396780642174986292
$\mathrm{d}\alpha_*/\mathrm{d}\Lambda_{\mathrm{in}}$	0.01058439884747071631208203873195519178583
$\mathrm{d}\alpha_*/\mathrm{d}\mathsf{K}_{\mathrm{ALP}}$	3.280718180728563480414678180833963545929
$\partial \ln \alpha_*/\partial \ln \Lambda_{\mathrm{in}}$	1.003247442028859989232465858598685031103
$\partial \ln \alpha_*/\partial \ln \mathsf{K}_{\mathrm{ALP}}$	1.003247442028859989232465858598685031103
$\partial \alpha_*/\partial \Theta_{1,\mathrm{eff}}$	$8.502161900006311283571535347498921474059 \times 10^{-6}$
$\partial \ln \alpha_*/\partial \ln \Theta_{1,\mathrm{eff}}$	0.003199800080873844445610073237844962628056
$\partial \ln \alpha_*/\partial \ln B_{11}^{(\mathrm{eval})}$	$3.383597525937520272758965249350957221989 \times 10^{-5}$

TABLE XXVIII. Closed sensitivities at the geometric lock within the frozen realization. These values are obtained directly from Eqs. (C20) to (C22), (C27), (C28), (C31) and (C34) and contain no numerical root search. For the current article scalar evaluator, $B_{11}^{(\mathrm{eval})} = B_{11}^{\mathrm{glue}}$. The rows involving $\mathsf{K}_{\mathrm{ALP}}$ are diagnostic sensitivities of the algebraic target map. They are not additional realization-level uncertainties in the closed coefficient $\mathsf{K}_{\mathrm{ALP}}$.

3. Numerical sensitivities of the realized scalar evaluator

For the finite-rank quantities that belong to the current article scalar evaluator, it is convenient to evaluate logarithmic sensitivities directly at the lock point by a symmetric multiplicative perturbation.

Definition C.1 (Symmetric logarithmic sensitivity estimator)**.** Let $q > 0$ be a parameter of the realized scalar evaluator. Let $\alpha(q)$ denote the lock output obtained after varying only this parameter, while holding the target $\mathfrak{D}_{*,\mathrm{in}}$ and all other scalar-evaluator parameters fixed. Assume that $\alpha(\cdot)$ is defined and positive on an open interval $I_q \subset (0,\infty)$ containing q. For $\varepsilon \in (0,1)$ such that

$$q(1-\varepsilon) \in I_q, \qquad q(1+\varepsilon) \in I_q,$$

define

$$S_q^{(\varepsilon)} \equiv \frac{\ln \alpha(q(1+\varepsilon)) - \ln \alpha(q(1-\varepsilon))}{\ln(1+\varepsilon) - \ln(1-\varepsilon)}. \tag{C35}$$

Proposition 74 (Limit and local error of the symmetric logarithmic estimator)**.** *Assume that $\alpha(\cdot)$ is positive on an open interval $I_q \subset (0,\infty)$ containing q, and that $\alpha \in C^3(I_q)$. Then*

$$S_q^{(\varepsilon)} = \frac{q}{\alpha(q)} \frac{\partial \alpha}{\partial q}(q) + O_q(\varepsilon^2) \qquad (\varepsilon \to 0), \tag{C36}$$

where the implied constant depends on q and on a local C^3-bound for α. In particular,

$$\lim_{\varepsilon \to 0} S_q^{(\varepsilon)} = \frac{q}{\alpha(q)} \frac{\partial \alpha}{\partial q}(q).$$

Proof. Set

$$g(u) := \ln \alpha(u).$$

Since $\alpha > 0$ and $\alpha \in C^3(I_q)$, one has $g \in C^3(I_q)$. Define

$$f(t) := g(qe^t)$$

for t in a neighborhood of 0. Then $f \in C^3$ near 0, and

$$f'(0) = q\, g'(q) = \frac{q}{\alpha(q)} \frac{\partial \alpha}{\partial q}(q).$$

Next set

$$a_\varepsilon := \ln(1-\varepsilon), \qquad b_\varepsilon := \ln(1+\varepsilon),$$

so that

$$S_q^{(\varepsilon)} = \frac{f(b_\varepsilon) - f(a_\varepsilon)}{b_\varepsilon - a_\varepsilon}.$$

Write

$$m_\varepsilon := \frac{a_\varepsilon + b_\varepsilon}{2} = \frac{1}{2}\ln(1-\varepsilon^2), \qquad h_\varepsilon := \frac{b_\varepsilon - a_\varepsilon}{2} = \frac{1}{2}\big(\ln(1+\varepsilon) - \ln(1-\varepsilon)\big).$$

Then

$$a_\varepsilon = m_\varepsilon - h_\varepsilon, \qquad b_\varepsilon = m_\varepsilon + h_\varepsilon.$$

Since

$$m_\varepsilon = O(\varepsilon^2), \qquad h_\varepsilon = \varepsilon + O(\varepsilon^3),$$

it remains to expand the symmetric difference quotient of f about m_ε.

Parameter	$S_q^{(10^{-8})}$
$\Theta_{1,\mathrm{eff}}$	0.00319980008087384433895444
$A_{\mathrm{uv}}^{(5)}$	$-7.71320934913998665044942 \times 10^{-6}$
$A_{\mathrm{ir}}^{(5)}$	$-7.69070828972777109005450 \times 10^{-6}$
χ_5	$1.47021060626261554821047 \times 10^{-12}$
s_{uv}	$1.23595014089731614720138 \times 10^{-8}$
s_{ir}	$2.25528122964264145769737 \times 10^{-10}$

TABLE XXIX. Numerical logarithmic sensitivities of the current article scalar evaluator, evaluated by the symmetric estimator Eq. (C35) at the current geometric lock with the scalar target $\mathfrak{D}_{*,\mathrm{in}}$ held fixed.

By Taylor's theorem with remainder, there exist $\xi_{\varepsilon,+}$ and $\xi_{\varepsilon,-}$ between m_ε and $m_\varepsilon \pm h_\varepsilon$ such that

$$f(m_\varepsilon + h_\varepsilon) = f(m_\varepsilon) + h_\varepsilon f'(m_\varepsilon) + \frac{h_\varepsilon^2}{2} f''(m_\varepsilon) + \frac{h_\varepsilon^3}{6} f'''(\xi_{\varepsilon,+}),$$

$$f(m_\varepsilon - h_\varepsilon) = f(m_\varepsilon) - h_\varepsilon f'(m_\varepsilon) + \frac{h_\varepsilon^2}{2} f''(m_\varepsilon) - \frac{h_\varepsilon^3}{6} f'''(\xi_{\varepsilon,-}).$$

Subtracting and dividing by $2h_\varepsilon$ gives

$$S_q^{(\varepsilon)} = f'(m_\varepsilon) + \frac{h_\varepsilon^2}{12}\big(f'''(\xi_{\varepsilon,+}) + f'''(\xi_{\varepsilon,-})\big).$$

Since f''' is locally bounded near 0, the second term is $O(h_\varepsilon^2) = O(\varepsilon^2)$. Also, because $f' \in C^1$ near 0 and $m_\varepsilon = O(\varepsilon^2)$,

$$f'(m_\varepsilon) = f'(0) + O(m_\varepsilon) = f'(0) + O(\varepsilon^2).$$

Therefore

$$S_q^{(\varepsilon)} = f'(0) + O(\varepsilon^2) = \frac{q}{\alpha(q)} \frac{\partial \alpha}{\partial q}(q) + O_q(\varepsilon^2),$$

which proves Eq. (C36). □

In the numerical audit we use $\varepsilon = 10^{-8}$, working precision 120 decimal digits, and evaluate all local scalar-parameter sensitivities at the current article lock point determined by the realized vector input $\Lambda_{\mathrm{in}} = \Lambda_{\mathrm{geom}}^{(\mathrm{th})}$ and the rank-5 article scalar evaluator. The perturbations are chosen small enough to preserve the positivity and admissibility conditions of the evaluator.

Remark. The hierarchy in table XXIX is diagnostically informative. The realized lock output is much more sensitive to the geometric target itself than to the detailed finite-rank parameters of the visible dynamic scalar block. In particular, the response to χ_5 is numerically negligible at the displayed precision, and the responses to s_{uv} and s_{ir} are tiny. This is one of the numerical reasons why the current article lock is stable under the visible dynamic scalar completion.

The row for $\Theta_{1,\mathrm{eff}}$ provides an internal consistency check. Its numerical value agrees with the corresponding closed logarithmic sensitivity reported in table XXVIII up to the $O(\varepsilon^2)$ truncation error of the symmetric estimator Eq. (C35), with $\varepsilon = 10^{-8}$, together with the arithmetic rounding error of the finite-difference evaluation.

4. Precision and rank-stability audit

Once the realized vector input Λ_{in} and the chosen scalar evaluator have been fixed, the lock output is obtained algebraically from

$$\mathfrak{D}_{*,\mathrm{in}} = \mathfrak{D}_{\mathrm{lock}}(\Lambda_{\mathrm{in}}), \qquad \alpha_* = \pi \frac{\mathfrak{D}_{*,\mathrm{in}}}{\sqrt{\mathfrak{R}_*}}, \qquad \mathfrak{R}_* = \mathfrak{R}_{\mathrm{moth}}(\mathfrak{D}_{*,\mathrm{in}}).$$

Accordingly, the present subsection does not audit an iterative solve. It separates two different numerical issues; realization resolution, coming from the finite-rank and representative character of the current scalar and vector inputs, and arithmetic resolution, coming from finite working precision.

Remark. The two stability tables show that the dominant uncertainty in the current realization does not come from arithmetic precision. The current lock output α_* is stable at the displayed prefix once the working precision is moderate. The visible source of approximation is instead the finite-rank and representative nature of the current scalar and vector inputs, which is why those ingredients were isolated in table XXVII.

Rank N	$\alpha_*^{(N)}$	$\alpha_*^{(N)} - \alpha_*^{(100)}$
1	0.007297352550527673778111395432000269	$-1.4531454240513 \times 10^{-11}$
3	0.007297352564731952740369293989053486	$-3.2717527825504 \times 10^{-13}$
5	0.007297352565050600333377958762732712	$-8.5276852463781 \times 10^{-15}$
100	0.007297352565059128018624336814032979	0

TABLE XXX. Rank-stability of the geometric-lock output within the current article scalar family, with the realized vector input $\Lambda_{\rm in} = \Lambda_{\rm geom}^{(\rm th)}$ held fixed. The primary article value quoted in the main text is the rank-5 output. The rank-100 row is included only as a high-rank finite representative for stability diagnostics within the same current scalar family. It is not used as an operator-limit value.

Working precision	stable displayed prefix of α_*	absolute drift from 300 dps
50 dps	0.007297352565050600333377958762732711688845043386975	$-1.4583663120557 \times 10^{-53}$
80 dps	0.007297352565050600333377958762732711688845043386975	$3.6058576503830 \times 10^{-83}$
120 dps	0.007297352565050600333377958762732711688845043386975	$-2.1241709388290 \times 10^{-123}$
200 dps	0.007297352565050600333377958762732711688845043386975	$1.0788773409699 \times 10^{-203}$
300 dps	0.007297352565050600333377958762732711688845043386975	0

TABLE XXXI. Arithmetic-precision audit of the current article geometric-lock output. The middle column reports a stable displayed prefix shared by all runs listed in the table. It is not a certification that every displayed digit is individually justified at the smaller working precisions. The shared prefix shown here contains 49 significant digits. The final column reports the absolute difference between the value returned at the stated working precision and the 300-dps reference run. This table is therefore an arithmetic-stability diagnostic, not an operator-level error bar.

5. Reproducibility protocol and optional diagnostic plots

The numerical checks reported in tables XXVIII to XXXI were generated by the companion Python audit script used for this appendix. The same script can also generate two diagnostic plots; the curve $\alpha_*(\Lambda)$ in a small neighborhood of the realized geometric input $\Lambda_{\rm in}$, and, separately, the reference-only quintic residual

$$F_5(x) = D_{\rm QED}^{[5]}(x) - \mathfrak{D}_{*,\rm in}$$

near the QED-induced cross-check root. These plots are not needed for the derivation. The first audits local monotonicity and conditioning of the primary algebraic lock, whereas the second belongs only to the external QED-induced diagnostic layer.

Remark. In the frozen D-only scalar-radicand realization audited here, the primary geometric-lock evaluation requires no iterative solve after the scalar evaluator and the vector input have been fixed. The only root-finding step in the audit script belongs to the external QED-induced cross-check, where the retained quintic equation is solved on a validated physical bracket by monotone bisection. This separation keeps the audited primary output algebraic and confines numerical root-finding to the external consistency test.

Appendix D: Inter-shell variational channel and heavy-shell resolvent

This appendix gives the operator-theoretic variational reduction behind the heavy-shell correction law used in the main text. Under the inter-shell hypotheses stated below, it derives the retained single-excursion channel $i \to j \to i$ before any low-energy expansion is taken. The inter-shell operator, the derivative-trace injection, and the single-excursion reduction are not additional standing postulates of the primary one-loop construction. They are retained hypotheses used only for the conditional heavy-shell extension.

Definition D.1 (Inter-shell Hilbert space). For a pair of branch labels $i < j$, ordered by increasing rest mass and hence by decreasing Compton-baseline radius, let $\mathcal{H}_{ij}^{\rm coll}$ and $\mathcal{H}_{ij}^{\rm log}$ be complex Hilbert spaces with inner products conjugate-linear in the first entry. Define the inter-shell Hilbert space by

$$\mathcal{H}_{ij}^{\rm int} = \mathcal{H}_{ij}^{\rm coll} \oplus \mathcal{H}_{ij}^{\rm log}, \tag{D1}$$

with inner product

$$\langle (\xi_c, \xi_\ell), (\zeta_c, \zeta_\ell) \rangle_{\mathcal{H}_{ij}^{\rm int}} = \langle \xi_c, \zeta_c \rangle_{\mathcal{H}_{ij}^{\rm coll}} + \langle \xi_\ell, \zeta_\ell \rangle_{\mathcal{H}_{ij}^{\rm log}}. \tag{D2}$$

Definition D.2 (Shell-j-normalized inter-shell operator hypothesis)**.** On $\mathcal{H}_{ij}^{\mathrm{int}}$, let

$$\widehat{G}_{c\ell,ij} := \widehat{\mathsf{G}}_{c\ell,ij}.$$

The shell-j-normalized inter-shell operator is

$$\widehat{\mathbb{L}}_{ij}^{\mathrm{int}} = \begin{pmatrix} \widehat{H}_{ij}^{\mathrm{coll}} & \widehat{G}_{c\ell,ij} \\ \widehat{G}_{c\ell,ij}^{*} & \widehat{L}_{ij}^{\log} \end{pmatrix}, \qquad \mathrm{Dom}(\widehat{\mathbb{L}}_{ij}^{\mathrm{int}}) = \mathrm{Dom}(\widehat{H}_{ij}^{\mathrm{coll}}) \oplus \mathrm{Dom}(\widehat{L}_{ij}^{\log}). \tag{D3}$$

where $\widehat{H}_{ij}^{\mathrm{coll}}$ and $\widehat{L}_{ij}^{\log}$ are non-negative self-adjoint operators on their respective Hilbert spaces, and

$$\widehat{G}_{c\ell,ij} : \mathcal{H}_{ij}^{\log} \to \mathcal{H}_{ij}^{\mathrm{coll}}$$

is bounded. The off-diagonal block operator

$$\widehat{G}_{c\ell,ij}^{\mathrm{off}} := \begin{pmatrix} 0 & \widehat{G}_{c\ell,ij} \\ \widehat{G}_{c\ell,ij}^{*} & 0 \end{pmatrix}$$

is bounded and self-adjoint on $\mathcal{H}_{ij}^{\mathrm{int}}$. Hence $\widehat{\mathbb{L}}_{ij}^{\mathrm{int}}$ is self-adjoint on the stated domain by the bounded self-adjoint perturbation theorem. In addition, assume strict positivity; namely, there exists $c_{ij} > 0$ such that

$$\langle \xi, \widehat{\mathbb{L}}_{ij}^{\mathrm{int}} \xi \rangle \geq c_{ij} \|\xi\|^2 \qquad \text{for all } \xi \in \mathrm{Dom}(\widehat{\mathbb{L}}_{ij}^{\mathrm{int}}). \tag{D4}$$

Remark. The reduction in this appendix uses only positivity, self-adjointness, and bounded gluing. A more microscopic model for $\widehat{H}_{ij}^{\mathrm{coll}}$, $\widehat{L}_{ij}^{\log}$, and $\widehat{\mathsf{G}_{c\ell,ij}}$ may later specialize these objects, provided the stated operator hypotheses remain valid.

Definition D.3 (Derivative trace injection)**.** Let ϕ_i denote the normalized reduced pinned cavity ground line of the external shell i. After reduction to the universal cavity coordinate $y = r/r_*^{(i)}$, this line is the Dirichlet ground mode

$$\phi_i(y) = \phi_1(y) = \sqrt{2}\sin(\pi y), \qquad \|\phi_i\|_{L^2(0,1)} = 1.$$

On the reduced Dirichlet cavity line,

$$K_0 = -\pi^{-2}\partial_y^2, \qquad \mathrm{Dom}(K_0) = H^2(0,1) \cap H_0^1(0,1),$$

define the graph-norm continuous derivative trace

$$T_\partial u = u'(1^-), \qquad u \in \mathrm{Dom}(K_0). \tag{D5}$$

Let $J_{ij} : \mathbb{C} \to \mathcal{H}_{ij}^{\mathrm{int}}$ be a bounded injection, fixed as part of the retained inter-shell channel rather than derived from the self-shell scalar bath. Since the domain is one-dimensional, any bounded linear map is determined by the source vector $j_{ij} = J_{ij}(1) \in \mathcal{H}_{ij}^{\mathrm{int}}$, and the injection condition is equivalent to

$$j_{ij} \neq 0.$$

The inter-shell derivative-trace map is

$$\tau_{ij} = J_{ij} T_\partial : \mathrm{Dom}(K_0) \to \mathcal{H}_{ij}^{\mathrm{int}}. \tag{D6}$$

Equip $\mathrm{Dom}(K_0)$ with the graph norm

$$\|u\|_{\mathrm{gr}(K_0)} := \|u\|_{L^2(0,1)} + \|K_0 u\|_{L^2(0,1)}.$$

To see the continuity directly, write

$$u = \sum_{n=1}^{\infty} u_n \phi_n, \qquad K_0 u = \sum_{n=1}^{\infty} n^2 u_n \phi_n, \qquad \sum_{n=1}^{\infty} n^4 |u_n|^2 < \infty.$$

Since

$$T_\partial \phi_n = \sqrt{2}\, n\pi(-1)^n,$$

the Cauchy–Schwarz inequality gives

$$\begin{aligned}|T_\partial u| &= \left|\sqrt{2}\,\pi \sum_{n=1}^{\infty}(-1)^n n u_n\right| \\ &= \sqrt{2}\,\pi \left|\sum_{n=1}^{\infty}(n^2 u_n)\,\frac{(-1)^n}{n}\right| \\ &\le \sqrt{2}\,\pi \left(\sum_{n=1}^{\infty} n^4 |u_n|^2\right)^{1/2} \left(\sum_{n=1}^{\infty}\frac{1}{n^2}\right)^{1/2} = \frac{\pi^2}{\sqrt{3}}\,\|K_0 u\|_{L^2(0,1)}.\end{aligned}$$

Therefore, for every $u \in \mathrm{Dom}(K_0)$,

$$\|\tau_{ij}u\|_{\mathcal{H}_{ij}^{\mathrm{int}}} \le \|J_{ij}\|\,|T_\partial u| \le \|J_{ij}\|\,\frac{\pi^2}{\sqrt{3}}\,\|u\|_{\mathrm{gr}(K_0)}.$$

Since

$$T_\partial \phi_i = \phi_1'(1^-) = -\sqrt{2}\,\pi,$$

the injected ground-line datum is

$$\tau_{ij}\phi_i = -\sqrt{2}\,\pi\, j_{ij} \in \mathcal{H}_{ij}^{\mathrm{int}}. \tag{D7}$$

In particular, under the injection condition $j_{ij} \neq 0$, one has

$$\tau_{ij}\phi_i \neq 0.$$

Remark. The coupling enters through the derivative trace rather than through a value trace because the pinned cavity line vanishes at the matching shell. This is the same mechanism that generates the self-shell memory in the universal scalar law.

Definition D.4 (Physical inter-shell operator in shell-i units)**.** Let $\mathbb{L}_{ij}^{\dim}$ denote a dimensional representative of the retained inter-shell operator of the channel $i \to j \to i$, with physical dimension L^{-2}, acting on the same inter-shell Hilbert space. This is a unit convention for comparing shell-j and shell-i normalizations; it is not a second dynamical input beyond the retained operator $\widehat{\mathbb{L}}_{ij}^{\mathrm{int}}$. The shell-$j$-normalized operator and the shell-i-normalized operator are defined by

$$\widehat{\mathbb{L}}_{ij}^{\mathrm{int}} \equiv R_j^2\,\mathbb{L}_{ij}^{\dim}, \qquad \mathbb{L}_{ij}^{\mathrm{phys}} \equiv R_i^2\,\mathbb{L}_{ij}^{\dim}. \tag{D8}$$

These two dimensionless realizations have the same operator domain,

$$\mathrm{Dom}(\mathbb{L}_{ij}^{\mathrm{phys}}) = \mathrm{Dom}(\widehat{\mathbb{L}}_{ij}^{\mathrm{int}}). \tag{D9}$$

Proposition 75 (Exact shell-rescaling of the inter-shell operator)**.** *Let $i < j$ be ordered by increasing rest mass, so that $m_j > m_i$ and therefore $R_j < R_i$. Set*

$$\varrho_{ij}^{\mathrm{H}} = \frac{R_j}{R_i}, \qquad 0 < \varrho_{ij}^{\mathrm{H}} < 1. \tag{D10}$$

Then, as self-adjoint operators on the common domain $\mathrm{Dom}(\widehat{\mathbb{L}}_{ij}^{\mathrm{int}})$*,*

$$\mathbb{L}_{ij}^{\mathrm{phys}} = \left(\varrho_{ij}^{\mathrm{H}}\right)^{-2}\widehat{\mathbb{L}}_{ij}^{\mathrm{int}}. \tag{D11}$$

In particular,

$$\mathbb{L}_{ij}^{\mathrm{phys}} \ge \left(\varrho_{ij}^{\mathrm{H}}\right)^{-2} c_{ij}\mathbf{1}. \tag{D12}$$

Consequently, for every dimensionless shell-i spectral parameter $D \ge 0$,

$$(\mathbb{L}_{ij}^{\mathrm{phys}} + D\mathbf{1})^{-1} = \left(\varrho_{ij}^{\mathrm{H}}\right)^{2}\left(\widehat{\mathbb{L}}_{ij}^{\mathrm{int}} + \left(\varrho_{ij}^{\mathrm{H}}\right)^{2} D\mathbf{1}\right)^{-1}. \tag{D13}$$

Proof. By Eq. (D8),

$$\widehat{\mathbb{L}}_{ij}^{\mathrm{int}} = R_j^2\,\mathbb{L}_{ij}^{\mathrm{dim}}, \qquad \mathbb{L}_{ij}^{\mathrm{phys}} = R_i^2\,\mathbb{L}_{ij}^{\mathrm{dim}}.$$

Eliminating $\mathbb{L}_{ij}^{\mathrm{dim}}$ on the common operator domain gives

$$\mathbb{L}_{ij}^{\mathrm{phys}}\xi = \frac{R_i^2}{R_j^2}\,\widehat{\mathbb{L}}_{ij}^{\mathrm{int}}\xi = \big(\varrho_{ij}^{\mathrm{H}}\big)^{-2}\,\widehat{\mathbb{L}}_{ij}^{\mathrm{int}}\xi, \qquad \xi \in \mathrm{Dom}(\widehat{\mathbb{L}}_{ij}^{\mathrm{int}}).$$

This proves Eq. (D11). Since $\widehat{\mathbb{L}}_{ij}^{\mathrm{int}} \geq c_{ij}\mathbf{1}$, one also has

$$\mathbb{L}_{ij}^{\mathrm{phys}} \geq \big(\varrho_{ij}^{\mathrm{H}}\big)^{-2}\,c_{ij}\mathbf{1},$$

which proves Eq. (D12).

Next,

$$\mathbb{L}_{ij}^{\mathrm{phys}} + D\mathbf{1} = \big(\varrho_{ij}^{\mathrm{H}}\big)^{-2}\big(\widehat{\mathbb{L}}_{ij}^{\mathrm{int}} + \big(\varrho_{ij}^{\mathrm{H}}\big)^{2}\,D\mathbf{1}\big).$$

The shifted operator in parentheses is boundedly invertible for every $D \geq 0$, because it is bounded below by $c_{ij}\mathbf{1}$. Inverting the previous identity yields Eq. (D13). □

Definition D.5 (Normalized heavy-shell memory and physical kernel)**.** Let

$$\mathfrak{h}_{ij}^{\mathrm{H}} = \big(\varrho_{ij}^{\mathrm{H}}\big)^{2}, \qquad \mathbf{S}_{ij}^{\mathrm{H}} = (\widehat{\mathbb{L}}_{ij}^{\mathrm{int}})^{-1}, \qquad \widehat{\psi}_{ij}^{\mathrm{H}} = (\widehat{\mathbb{L}}_{ij}^{\mathrm{int}})^{-1/2}\tau_{ij}\phi_i. \tag{D14}$$

The factor $\mathfrak{h}_{ij}^{\mathrm{H}}$ is therefore the dimensionless heavy-shell decoupling factor forced by shell rescaling. It is not a frequency, not a running parameter, and not an independently fitted kernel strength.

The inverse square root is bounded because $\widehat{\mathbb{L}}_{ij}^{\mathrm{int}} \geq c_{ij}\mathbf{1}$ with $c_{ij} > 0$. In particular, $(\widehat{\mathbb{L}}_{ij}^{\mathrm{int}})^{-1/2}$ is bounded and injective. For $D \geq 0$, define the normalized heavy-shell memory by

$$\mathcal{M}_{ij}^{\mathrm{H}}(D) = \Big\langle \widehat{\psi}_{ij}^{\mathrm{H}},\, \big(\mathbf{1} + \mathfrak{h}_{ij}^{\mathrm{H}} D\,\mathbf{S}_{ij}^{\mathrm{H}}\big)^{-1}\widehat{\psi}_{ij}^{\mathrm{H}} \Big\rangle_{\mathcal{H}_{ij}^{\mathrm{int}}}. \tag{D15}$$

The corresponding physical heavy-shell kernel in shell-i units is

$$\mathcal{K}_{ij}^{\mathrm{H}}(D) = \mathfrak{h}_{ij}^{\mathrm{H}}\,\mathcal{M}_{ij}^{\mathrm{H}}(D). \tag{D16}$$

Definition D.6 (Inter-shell action)**.** For $x > 0$, $\kappa > 0$, $u_i \in \mathrm{Dom}(K_0)$, and $\xi_{ij} \in \mathrm{Dom}(\mathbb{L}_{ij}^{\mathrm{phys}})$, define the real quadratic functional, viewed on the complex Hilbert space by real variations. The source term is well defined because $\tau_{ij}u_i \in \mathcal{H}_{ij}^{\mathrm{int}}$ and $\xi_{ij} \in \mathcal{H}_{ij}^{\mathrm{int}}$:

$$\mathcal{L}_{ij}^{\mathrm{int}}[u_i, \xi_{ij}; \kappa, x] \equiv \frac{x^2}{\kappa}\left(\Big\langle \xi_{ij}, (\mathbb{L}_{ij}^{\mathrm{phys}} + x\kappa\mathbf{1})\xi_{ij} \Big\rangle_{\mathcal{H}_{ij}^{\mathrm{int}}} + 2\,\Re\,\langle \tau_{ij}u_i, \xi_{ij}\rangle_{\mathcal{H}_{ij}^{\mathrm{int}}}\right). \tag{D17}$$

Remark. The prefactor x^2 is the lowest order retained for a single virtual excursion $i \to j \to i$. The heavy-shell suppression $\mathfrak{h}_{ij}^{\mathrm{H}}$ is not inserted here by hand; it emerges from the operator rescaling in Eq. (D13). This keeps the retained single-excursion order counting unambiguous.

Lemma 30 (Exact elimination of the virtual inter-shell field)**.** *For fixed $u_i \in \mathrm{Dom}(K_0)$, $x > 0$, and $\kappa > 0$, the map $\xi_{ij} \mapsto \mathcal{L}_{ij}^{\mathrm{int}}[u_i, \xi_{ij}; \kappa, x]$ is strictly convex on $\mathrm{Dom}(\mathbb{L}_{ij}^{\mathrm{phys}})$, viewed as a real affine space with its graph topology, and is uniquely minimized at*

$$\xi_{ij}^{\mathrm{crit}} = -(\mathbb{L}_{ij}^{\mathrm{phys}} + x\kappa\mathbf{1})^{-1}\tau_{ij}u_i. \tag{D18}$$

At this critical point,

$$\mathcal{L}_{ij}^{\mathrm{int}}[u_i, \xi_{ij}^{\mathrm{crit}}; \kappa, x] = -\frac{x^2}{\kappa}\,\langle \tau_{ij}u_i, (\mathbb{L}_{ij}^{\mathrm{phys}} + x\kappa\mathbf{1})^{-1}\tau_{ij}u_i\rangle_{\mathcal{H}_{ij}^{\mathrm{int}}}. \tag{D19}$$

Proof. Set

$$\mathbb{A}_{ij}(x,\kappa) = \mathbb{L}_{ij}^{\text{phys}} + x\kappa\mathbf{1}.$$

By Eqs. (D4) and (D11), $\mathbb{L}_{ij}^{\text{phys}}$ is strictly positive and self-adjoint. Since $x > 0$ and $\kappa > 0$, the shifted operator $\mathbb{A}_{ij}(x,\kappa)$ is strictly positive and self-adjoint. Hence $\mathbb{A}_{ij}(x,\kappa)^{-1}$ is a bounded operator on $\mathcal{H}_{ij}^{\text{int}}$, with range contained in $\mathrm{Dom}(\mathbb{A}_{ij}(x,\kappa))$. Writing

$$b_{ij} = \tau_{ij}u_i,$$

the action becomes

$$\mathcal{L}_{ij}^{\text{int}}[u_i,\xi_{ij};\kappa,x] = \frac{x^2}{\kappa}\left(\langle\xi_{ij},\mathbb{A}_{ij}\xi_{ij}\rangle_{\mathcal{H}_{ij}^{\text{int}}} + 2\,\Re\langle b_{ij},\xi_{ij}\rangle_{\mathcal{H}_{ij}^{\text{int}}}\right).$$

Complete the square. Since the inner product is conjugate-linear in the first entry and $\mathbb{A}_{ij}$ is self-adjoint,

$$\begin{aligned}&\Big\langle \xi_{ij} + \mathbb{A}_{ij}^{-1}b_{ij}, \mathbb{A}_{ij}\big(\xi_{ij} + \mathbb{A}_{ij}^{-1}b_{ij}\big)\Big\rangle_{\mathcal{H}_{ij}^{\text{int}}}\\ &\qquad = \langle\xi_{ij},\mathbb{A}_{ij}\xi_{ij}\rangle + \langle\xi_{ij},b_{ij}\rangle + \langle b_{ij},\xi_{ij}\rangle + \langle b_{ij},\mathbb{A}_{ij}^{-1}b_{ij}\rangle.\end{aligned}$$

Hence

$$\begin{aligned}\langle\xi_{ij},\mathbb{A}_{ij}\xi_{ij}\rangle + 2\,\Re\langle b_{ij},\xi_{ij}\rangle &= \Big\langle \xi_{ij} + \mathbb{A}_{ij}^{-1}b_{ij}, \mathbb{A}_{ij}\big(\xi_{ij} + \mathbb{A}_{ij}^{-1}b_{ij}\big)\Big\rangle_{\mathcal{H}_{ij}^{\text{int}}}\\ &\quad - \langle b_{ij},\mathbb{A}_{ij}^{-1}b_{ij}\rangle_{\mathcal{H}_{ij}^{\text{int}}}.\end{aligned}$$

Moreover, by Eq. (D12),

$$\langle\zeta,\mathbb{A}_{ij}\zeta\rangle \geq \left[\left(\varrho_{ij}^{\mathrm{H}}\right)^{-2}c_{ij} + x\kappa\right]\|\zeta\|^2, \qquad \zeta\in\mathrm{Dom}(\mathbb{A}_{ij}).$$

Hence the quadratic part is strictly convex. The first term in the completed square is nonnegative and vanishes if and only if

$$\xi_{ij} = -\mathbb{A}_{ij}^{-1}b_{ij},$$

which is exactly Eq. (D18). Because $\mathbb{A}_{ij}^{-1}$ is bounded and maps $\mathcal{H}_{ij}^{\text{int}}$ into $\mathrm{Dom}(\mathbb{A}_{ij})$, this critical point belongs to the variational domain. Evaluating the action at this unique minimizer gives Eq. (D19). ☐

Corollary 12 (Unscaled spectral form, positivity, and complete monotonicity)**.** *For every $D \geq 0$, the normalized heavy-shell memory function $\mathcal{M}_{ij}^{\mathrm{H}}(D)$ is non-negative. It is strictly positive whenever $\tau_{ij}\phi_i \neq 0$. Under the injection convention of definition D.3, this nonzero condition is automatic, because*

$$\tau_{ij}\phi_i = -\sqrt{2}\,\pi\,j_{ij}, \qquad j_{ij}\neq 0.$$

More precisely, the spectral measure of $\mathbf{S}_{ij}^{\mathrm{H}}$ associated with $\widehat{\psi}_{ij}^{\mathrm{H}}$ defines a canonical positive finite Borel measure μ_{ij}^{H} on $[0,\|\mathbf{S}_{ij}^{\mathrm{H}}\|]$ such that

$$\mathcal{M}_{ij}^{\mathrm{H}}(D) = \int_{[0,\|\mathbf{S}_{ij}^{\mathrm{H}}\|]} \frac{\mathrm{d}\mu_{ij}^{\mathrm{H}}(\sigma)}{1+\mathfrak{h}_{ij}^{\mathrm{H}}D\sigma}. \tag{D20}$$

This is the unscaled spectral representation. The standard Stieltjes representation with denominator $1+sD$ is obtained in proposition 76 by the push-forward $s = \mathfrak{h}_{ij}^{\mathrm{H}}\sigma$, and that pushed-forward normalization is the one used for the moments and for the retained quadrupolar normalization in Condition E.1.

Consequently,

$$(-1)^n\frac{\mathrm{d}^n}{\mathrm{d}D^n}\mathcal{M}_{ij}^{\mathrm{H}}(D) \geq 0, \qquad D\geq 0, \quad n = 0,1,2,\ldots, \tag{D21}$$

with derivatives at $D=0$ understood by the compactly supported spectral integral. Thus $\mathcal{M}_{ij}^{\mathrm{H}}$ is completely monotone on $[0,\infty)$.

Proof. By Eq. (D14),

$$\mathbf{S}^{\mathrm{H}}_{ij} = (\widehat{\mathbb{L}}^{\mathrm{int}}_{ij})^{-1}.$$

Since $\widehat{\mathbb{L}}^{\mathrm{int}}_{ij}$ is strictly positive and self-adjoint, $\mathbf{S}^{\mathrm{H}}_{ij}$ is bounded, positive, injective, and self-adjoint on $\mathcal{H}^{\mathrm{int}}_{ij}$. By the spectral theorem there exists a projection-valued measure E_{ij} on $[0, \|\mathbf{S}^{\mathrm{H}}_{ij}\|]$ such that

$$\mathbf{S}^{\mathrm{H}}_{ij} = \int_{[0,\|\mathbf{S}^{\mathrm{H}}_{ij}\|]} \sigma \, \mathrm{d}E_{ij}(\sigma).$$

Define the positive finite Borel measure

$$\mu^{\mathrm{H}}_{ij}(B) \equiv \langle \widehat{\psi}^{\mathrm{H}}_{ij}, E_{ij}(B)\widehat{\psi}^{\mathrm{H}}_{ij} \rangle, \qquad B \subset [0, \|\mathbf{S}^{\mathrm{H}}_{ij}\|] \text{ Borel}.$$

Then

$$\big(\mathbf{1} + \mathfrak{h}^{\mathrm{H}}_{ij} D\, \mathbf{S}^{\mathrm{H}}_{ij}\big)^{-1} = \int_{[0,\|\mathbf{S}^{\mathrm{H}}_{ij}\|]} \frac{1}{1 + \mathfrak{h}^{\mathrm{H}}_{ij} D s} \, \mathrm{d}E_{ij}(s),$$

and therefore

$$\mathcal{M}^{\mathrm{H}}_{ij}(D) = \int_{[0,\|\mathbf{S}^{\mathrm{H}}_{ij}\|]} \frac{\mathrm{d}\mu^{\mathrm{H}}_{ij}(s)}{1 + \mathfrak{h}^{\mathrm{H}}_{ij} D s},$$

which proves Eq. (D20). Non-negativity follows from the positivity of the measure. Moreover,

$$\mathcal{M}^{\mathrm{H}}_{ij}(D) = \Big\| \big(\mathbf{1} + \mathfrak{h}^{\mathrm{H}}_{ij} D\, \mathbf{S}^{\mathrm{H}}_{ij}\big)^{-1/2} \widehat{\psi}^{\mathrm{H}}_{ij} \Big\|^2_{\mathcal{H}^{\mathrm{int}}_{ij}}.$$

Thus $\mathcal{M}^{\mathrm{H}}_{ij}(D) > 0$ for every $D \geq 0$ whenever $\widehat{\psi}^{\mathrm{H}}_{ij} \neq 0$. Since $(\widehat{\mathbb{L}}^{\mathrm{int}}_{ij})^{-1/2}$ is bounded and injective by strict positivity, this holds whenever $\tau_{ij}\phi_i \neq 0$.

For every integer $n \geq 0$, compact support gives the uniform bound

$$0 \leq \frac{\sigma^n}{(1 + \mathfrak{h}^{\mathrm{H}}_{ij} D\sigma)^{n+1}} \leq \|\mathbf{S}^{\mathrm{H}}_{ij}\|^n, \qquad D \geq 0,$$

which is integrable with respect to the finite measure μ^{H}_{ij}. Hence dominated convergence justifies differentiation under the integral sign, including right derivatives at $D = 0$, and gives

$$\frac{\mathrm{d}^n}{\mathrm{d}D^n} \mathcal{M}^{\mathrm{H}}_{ij}(D) = (-1)^n n! \, (\mathfrak{h}^{\mathrm{H}}_{ij})^n \int_{[0,\|\mathbf{S}^{\mathrm{H}}_{ij}\|]} \frac{\sigma^n \, \mathrm{d}\mu^{\mathrm{H}}_{ij}(\sigma)}{(1 + \mathfrak{h}^{\mathrm{H}}_{ij} D\sigma)^{n+1}}.$$

The integrand is nonnegative for $D \geq 0$. Hence

$$(-1)^n \frac{\mathrm{d}^n}{\mathrm{d}D^n} \mathcal{M}^{\mathrm{H}}_{ij}(D) \geq 0,$$

which proves Eq. (D21). ☐

Theorem 25 (Conditional exact reduced law for the retained heavy-shell channel)**.** *Fix $i < j$, ordered by increasing rest mass. Assume the inter-shell Hilbert space, operator, strict-positivity, shell-rescaling, derivative-trace injection, normalized-memory, and single-excursion action structure specified in definitions D.1 to D.6. Let $x > 0$ belong to the domain of a fixed reference scalar branch and write*

$$D^0_i(x) = x\kappa^0_i(x), \qquad \kappa^0_i(x) > 0.$$

The branch $D^0_i(x)$ is an input to this conditional inter-shell extension. It is not determined by the variational elimination below and is not recomputed by the virtual shell j. Let ϕ_i be the normalized external pinned cavity ground line from definition D.3. Then the eliminated virtual field contributes a non-positive Schur term to the inter-shell action. The retained single-excursion slowdown convention defines the positive slowdown increment by

$$\Delta D^{(i\leftarrow j)}(x) := -\mathcal{L}^{\mathrm{int}}_{ij}[\phi_i, \xi^{\mathrm{crit}}_{ij}; \kappa^0_i(x), x]. \tag{D22}$$

Under this convention, the induced correction is

$$\Delta D^{(i\leftarrow j)}(x) = \frac{x^2}{\kappa^0_i(x)} \, \mathcal{K}^{\mathrm{H}}_{ij}\big(D^0_i(x)\big). \tag{D23}$$

Proof. Set

$$u_i = \phi_i, \qquad \kappa = \kappa_i^0(x), \qquad D_i^0(x) = x\kappa_i^0(x) = x\kappa.$$

Since $\phi_i = \phi_1 \in \mathrm{Dom}(K_0)$, $x > 0$, and $\kappa_i^0(x) > 0$, one has $D_i^0(x) > 0$. Applying lemma 30 with these values gives

$$\mathcal{L}_{ij}^{\mathrm{int}}[\phi_i, \xi_{ij}^{\mathrm{crit}}; \kappa_i^0(x), x] = -\frac{x^2}{\kappa_i^0(x)} \big\langle \tau_{ij}\phi_i,\, (\mathbb{L}_{ij}^{\mathrm{phys}} + D_i^0(x)\mathbf{1})^{-1}\tau_{ij}\phi_i \big\rangle_{\mathcal{H}_{ij}^{\mathrm{int}}}. \tag{D24}$$

For

$$A_{ij}^0(x) = \mathbb{L}_{ij}^{\mathrm{phys}} + D_i^0(x)\mathbf{1},$$

strict positivity gives

$$\big\langle f, (A_{ij}^0(x))^{-1} f \big\rangle_{\mathcal{H}_{ij}^{\mathrm{int}}} = \big\| (A_{ij}^0(x))^{-1/2} f \big\|_{\mathcal{H}_{ij}^{\mathrm{int}}}^2 \geq 0, \qquad f = \tau_{ij}\phi_i.$$

Thus the Schur-complement term in Eq. (D24) is non-positive. By the retained single-excursion slowdown convention Eq. (D22),

$$\Delta D^{(i\leftarrow j)}(x) = -\mathcal{L}_{ij}^{\mathrm{int}}[\phi_i, \xi_{ij}^{\mathrm{crit}}; \kappa_i^0(x), x] \geq 0.$$

Therefore

$$\Delta D^{(i\leftarrow j)}(x) = \frac{x^2}{\kappa_i^0(x)} \big\langle \tau_{ij}\phi_i,\, (\mathbb{L}_{ij}^{\mathrm{phys}} + D_i^0(x)\mathbf{1})^{-1}\tau_{ij}\phi_i \big\rangle_{\mathcal{H}_{ij}^{\mathrm{int}}}. \tag{D25}$$

It remains to identify the quadratic form in Eq. (D25) with the physical heavy-shell kernel. By Eq. (D13), for every $D \geq 0$,

$$(\mathbb{L}_{ij}^{\mathrm{phys}} + D\mathbf{1})^{-1} = \mathfrak{h}_{ij}^{\mathrm{H}} \big(\widehat{\mathbb{L}}_{ij}^{\mathrm{int}} + \mathfrak{h}_{ij}^{\mathrm{H}} D\mathbf{1}\big)^{-1}. \tag{D26}$$

Since $\widehat{\mathbb{L}}_{ij}^{\mathrm{int}} \geq c_{ij}\mathbf{1}$ with $c_{ij} > 0$, the operators $(\widehat{\mathbb{L}}_{ij}^{\mathrm{int}})^{-1}$ and $(\widehat{\mathbb{L}}_{ij}^{\mathrm{int}})^{-1/2}$ are bounded. Also

$$\mathbf{1} + \mathfrak{h}_{ij}^{\mathrm{H}} D\, \mathbf{S}_{ij}^{\mathrm{H}} \geq \mathbf{1},$$

so its inverse is bounded. By the spectral theorem, the scalar identity

$$(\lambda + \mathfrak{h}_{ij}^{\mathrm{H}} D)^{-1} = \lambda^{-1/2} \big(1 + \mathfrak{h}_{ij}^{\mathrm{H}} D\, \lambda^{-1}\big)^{-1} \lambda^{-1/2}, \qquad \lambda \in [c_{ij}, \infty),$$

lifts to the operator identity

$$\big(\widehat{\mathbb{L}}_{ij}^{\mathrm{int}} + \mathfrak{h}_{ij}^{\mathrm{H}} D\mathbf{1}\big)^{-1} = (\widehat{\mathbb{L}}_{ij}^{\mathrm{int}})^{-1/2} \big(\mathbf{1} + \mathfrak{h}_{ij}^{\mathrm{H}} D\, \mathbf{S}_{ij}^{\mathrm{H}}\big)^{-1} (\widehat{\mathbb{L}}_{ij}^{\mathrm{int}})^{-1/2}. \tag{D27}$$

Using

$$\widehat{\psi}_{ij}^{\mathrm{H}} = (\widehat{\mathbb{L}}_{ij}^{\mathrm{int}})^{-1/2} \tau_{ij}\phi_i,$$

we obtain the chain

$$\begin{aligned}
&\big\langle \tau_{ij}\phi_i,\, (\mathbb{L}_{ij}^{\mathrm{phys}} + D\mathbf{1})^{-1}\tau_{ij}\phi_i \big\rangle_{\mathcal{H}_{ij}^{\mathrm{int}}} \\
&\quad = \mathfrak{h}_{ij}^{\mathrm{H}} \big\langle \tau_{ij}\phi_i,\, \big(\widehat{\mathbb{L}}_{ij}^{\mathrm{int}} + \mathfrak{h}_{ij}^{\mathrm{H}} D\mathbf{1}\big)^{-1} \tau_{ij}\phi_i \big\rangle_{\mathcal{H}_{ij}^{\mathrm{int}}} \\
&\quad = \mathfrak{h}_{ij}^{\mathrm{H}} \Big\langle \widehat{\psi}_{ij}^{\mathrm{H}},\, \big(\mathbf{1} + \mathfrak{h}_{ij}^{\mathrm{H}} D\, \mathbf{S}_{ij}^{\mathrm{H}}\big)^{-1} \widehat{\psi}_{ij}^{\mathrm{H}} \Big\rangle_{\mathcal{H}_{ij}^{\mathrm{int}}} \\
&\quad = \mathfrak{h}_{ij}^{\mathrm{H}}\, \mathcal{M}_{ij}^{\mathrm{H}}(D) = \mathcal{K}_{ij}^{\mathrm{H}}(D),
\end{aligned}$$

where the last two equalities use Eqs. (D15) and (D16). This identifies the quadratic form generated by the eliminated inter-shell field with the physical heavy-shell kernel in shell-i units. Substituting this identity into Eq. (D25) with $D = D_i^0(x)$ gives

$$\Delta D^{(i\leftarrow j)}(x) = \frac{x^2}{\kappa_i^0(x)}\, \mathcal{K}_{ij}^{\mathrm{H}}\big(D_i^0(x)\big),$$

which is Eq. (D23). □

Remark (Status of the retained inter-shell channel). The theorem derives the exact reduced law for the retained single-excursion channel under the operator hypotheses of this appendix. It does not construct a complete family-level scalar–vector mother operator, does not include repeated inter-shell excursions, and does not fix the leading quadrupolar normalization of the heavy-shell measure. That normalization is a separate retained input recorded in Condition E.1. The heavy-shell correction used in the main text is therefore theorem-level only within this retained channel. It should not be read as a complete running-coupling theory, and it does not feed back into the fixed vector-shell datum or the primary baseline value of α_*.

Appendix E: Stieltjes memory and quadrupolar normalization

This appendix records the positivity structure of the normalized heavy-shell memory and states the leading isotropic quadrupolar normalization retained in the main text as an explicit input. The Stieltjes representation and moment expansion are derived consequences of the retained inter-shell operator hypotheses. By contrast, the leading quadrupolar value of the zeroth memory moment is a normalization condition on the retained channel, not a consequence of the spectral theorem alone.

The logical roles in this appendix are separated as follows. The measure ν_{ij}^{H} is the pushed-forward spectral measure of $\mathbf{S}_{ij}^{\mathrm{H}}$ associated with the injected vector $\widehat{\psi}_{ij}^{\mathrm{H}}$. The moments $h_{ij,m}$, complete monotonicity, and the moment expansion are derived from the retained inter-shell operator and injection of appendix D. The value $h_{ij,0} = 2/45$ is not supplied by those spectral arguments; it is a retained leading quadrupolar normalization condition that fixes the zeroth moment, equivalently the norm of the injected heavy-shell datum. The higher moments and the detailed spectral distribution remain unspecified in the present paper.

Proposition 76 (Stieltjes representation of the normalized heavy-shell memory)**.** *Let $i < j$ be a retained heavier-shell pair in the Compton-baseline ordering, so that $m_j > m_i$ and*

$$\mathfrak{h}_{ij}^{\mathrm{H}} = \left(\frac{R_j}{R_i}\right)^2 = \left(\frac{m_i}{m_j}\right)^2 \in (0,1).$$

Assume the retained inter-shell operator, injection, and normalized-memory hypotheses of definitions D.2, D.3 and D.5. Then there exists a unique positive finite Borel measure ν_{ij}^{H} on $[0,\infty)$ such that the normalized memory has the Stieltjes form

$$\mathcal{M}_{ij}^{\mathrm{H}}(D) = \int_0^\infty \frac{\mathrm{d}\nu_{ij}^{\mathrm{H}}(s)}{1+sD}, \qquad D \geq 0. \tag{E1}$$

This measure is the push-forward, under

$$s = \mathfrak{h}_{ij}^{\mathrm{H}}\sigma,$$

of the scalar spectral measure of $\mathbf{S}_{ij}^{\mathrm{H}}$ associated with $\widehat{\psi}_{ij}^{\mathrm{H}}$. Its support is contained in the compact interval

$$\operatorname{supp}\nu_{ij}^{\mathrm{H}} \subset \big[0, \mathfrak{h}_{ij}^{\mathrm{H}}\|\mathbf{S}_{ij}^{\mathrm{H}}\|\big]. \tag{E2}$$

Proof. Because $\widehat{\mathbb{L}}_{ij}^{\mathrm{int}}$ is strictly positive and self-adjoint, the operator

$$\mathbf{S}_{ij}^{\mathrm{H}} = (\widehat{\mathbb{L}}_{ij}^{\mathrm{int}})^{-1}$$

is bounded, positive, injective, and self-adjoint. By the heavier-shell ordering assumed in the statement,

$$\mathfrak{h}_{ij}^{\mathrm{H}} \in (0,1).$$

Let E_{ij} be the projection-valued spectral measure of $\mathbf{S}_{ij}^{\mathrm{H}}$. Since $\mathbf{S}_{ij}^{\mathrm{H}}$ is bounded and positive, the spectral theorem gives

$$\mathbf{S}_{ij}^{\mathrm{H}} = \int_{[0,\|\mathbf{S}_{ij}^{\mathrm{H}}\|]} \sigma\,\mathrm{d}E_{ij}(\sigma).$$

Define the positive finite Borel measure

$$\mu_{ij}^{\mathrm{H}}(B) \equiv \langle \widehat{\psi}_{ij}^{\mathrm{H}}, E_{ij}(B)\widehat{\psi}_{ij}^{\mathrm{H}} \rangle_{\mathcal{H}_{ij}^{\mathrm{int}}}, \qquad B \subset [0, \|\mathbf{S}_{ij}^{\mathrm{H}}\|] \text{ Borel.}$$

By functional calculus,

$$\left(\mathbf{1} + \mathfrak{h}_{ij}^{\mathrm{H}} D\, \mathbf{S}_{ij}^{\mathrm{H}}\right)^{-1} = \int_{[0,\|\mathbf{S}_{ij}^{\mathrm{H}}\|]} \frac{1}{1 + \mathfrak{h}_{ij}^{\mathrm{H}} D\, \sigma}\, \mathrm{d}E_{ij}(\sigma).$$

Hence the normalized memory defined by Eq. (D15) satisfies

$$\mathcal{M}_{ij}^{\mathrm{H}}(D) = \int_{[0,\|\mathbf{S}_{ij}^{\mathrm{H}}\|]} \frac{\mathrm{d}\mu_{ij}(\sigma)}{1 + \mathfrak{h}_{ij}^{\mathrm{H}} D\, \sigma}.$$

Push μ_{ij} forward under the map

$$\sigma \longmapsto s = \mathfrak{h}_{ij}^{\mathrm{H}} \sigma.$$

Define ν_{ij}^{H} by

$$\nu_{ij}^{\mathrm{H}}(B) = \mu_{ij}^{\mathrm{H}}\left(\{\sigma \in [0, \|\mathbf{S}_{ij}^{\mathrm{H}}\|]\ ;\ \mathfrak{h}_{ij}^{\mathrm{H}}\sigma \in B\}\right), \qquad B \subset [0,\infty) \text{ Borel.}$$

Then ν_{ij}^{H} is positive and finite, with

$$\nu_{ij}^{\mathrm{H}}([0,\infty)) = \mu_{ij}\left([0, \|\mathbf{S}_{ij}^{\mathrm{H}}\|]\right) = \|\widehat{\psi}_{ij}^{\mathrm{H}}\|_{\mathcal{H}_{ij}^{\mathrm{int}}}^2 < \infty.$$

Its support obeys

$$\operatorname{supp} \nu_{ij}^{\mathrm{H}} \subset \left[0, \mathfrak{h}_{ij}^{\mathrm{H}} \|\mathbf{S}_{ij}^{\mathrm{H}}\|\right],$$

which is Eq. (E2). The change of variables gives

$$\mathcal{M}_{ij}^{\mathrm{H}}(D) = \int_0^\infty \frac{\mathrm{d}\nu_{ij}^{\mathrm{H}}(s)}{1 + sD}, \qquad D \geq 0,$$

which proves existence.

It remains to prove uniqueness. Suppose that another positive finite Borel measure $\widetilde{\nu}$ on $[0,\infty)$ satisfies

$$\int_0^\infty \frac{\mathrm{d}\widetilde{\nu}(s)}{1 + sD} = \int_0^\infty \frac{\mathrm{d}\nu_{ij}^{\mathrm{H}}(s)}{1 + sD} \qquad \text{for all } D > 0.$$

Let

$$\lambda = \widetilde{\nu} - \nu_{ij}^{\mathrm{H}}.$$

Then λ is a finite signed Borel measure on $[0,\infty)$. Its Stieltjes transform

$$F(D) := \int_0^\infty \frac{\mathrm{d}\lambda(s)}{1 + sD}$$

vanishes for every $D > 0$. Since λ is finite and $(1 + sD)^{-1} \to 1$ pointwise as $D \downarrow 0$, dominated convergence gives

$$\lambda([0,\infty)) = \int_0^\infty \mathrm{d}\lambda(s) = \lim_{D \downarrow 0} F(D) = 0.$$

For each integer $n \geq 0$, differentiation under the integral sign is justified at $D = 1$. Indeed, on every compact interval $D \in [1/2, 3/2]$,

$$\left| \frac{\partial^n}{\partial D^n} \frac{1}{1 + sD} \right| = n!\, \frac{s^n}{(1 + sD)^{n+1}} \leq n!\, \frac{s^n}{(1 + s/2)^{n+1}}.$$

With $u = s/2$, the last factor satisfies

$$\frac{s^n}{(1+s/2)^{n+1}} = 2^n \frac{u^n}{(1+u)^{n+1}} \le 2^n, \qquad s \ge 0.$$

Since $|\lambda|$ is finite, the constant $n!2^n$ is $|\lambda|$-integrable. Hence

$$0 = F^{(n)}(1) = (-1)^n n! \int_0^\infty \frac{s^n}{(1+s)^{n+1}} \,\mathrm{d}\lambda(s), \qquad n = 0, 1, 2, \ldots.$$

Push λ forward under the continuous map

$$u = \frac{s}{1+s} \in [0, 1).$$

We regard the resulting finite signed Borel measure $\widetilde{\lambda}$ as a measure on $[0, 1]$, with no mass at $u = 1$. Then

$$\int_{[0,1]} u^n (1-u) \,\mathrm{d}\widetilde{\lambda}(u) = 0, \qquad n = 0, 1, 2, \ldots,$$

and

$$\widetilde{\lambda}([0, 1]) = \lambda([0, \infty)) = 0.$$

We now prove by induction that

$$\int_{[0,1]} u^n \,\mathrm{d}\widetilde{\lambda}(u) = 0 \qquad \text{for all } n \ge 0.$$

The case $n = 0$ is the total-mass identity above. If it holds for some $n \ge 0$, then

$$0 = \int_{[0,1]} u^n (1-u) \,\mathrm{d}\widetilde{\lambda}(u) = \int_{[0,1]} u^n \,\mathrm{d}\widetilde{\lambda}(u) - \int_{[0,1]} u^{n+1} \,\mathrm{d}\widetilde{\lambda}(u) = -\int_{[0,1]} u^{n+1} \,\mathrm{d}\widetilde{\lambda}(u),$$

so the claim follows for $n + 1$. Therefore $\widetilde{\lambda}$ annihilates every polynomial on $[0, 1]$. By the Weierstrass approximation theorem, polynomials are uniformly dense in $C([0, 1])$. Since $\widetilde{\lambda}$ is finite, it annihilates every continuous function on $[0, 1]$. By the Riesz representation theorem for finite signed regular Borel measures on the compact interval $[0, 1]$, this implies

$$\widetilde{\lambda} = 0.$$

Since $s \mapsto s/(1 + s)$ is injective on $[0, \infty)$, the vanishing of the push-forward implies $\lambda = 0$. Thus $\widetilde{\nu} = \nu^{\mathrm{H}}_{ij}$, and the representing measure is unique. □

Corollary 13 (Positivity and complete monotonicity)**.** *For every retained inter-shell channel satisfying the hypotheses above,*

$$\mathcal{M}^{\mathrm{H}}_{ij}(D) \ge 0 \qquad (D \ge 0). \tag{E3}$$

If $\tau_{ij}\phi_i \ne 0$, then this inequality is strict. Under the retained injection convention of definition D.3, this nonzero condition is automatic whenever $j_{ij} = J_{ij}(1) \ne 0$, because

$$\tau_{ij}\phi_i = T_\partial \phi_i \, j_{ij} = -\sqrt{2}\,\pi \, j_{ij}.$$

In that case,

$$\mathcal{M}^{\mathrm{H}}_{ij}(D) > 0 \qquad (D \ge 0). \tag{E4}$$

Moreover, for every integer $m \ge 0$,

$$(-1)^m \frac{\mathrm{d}^m}{\mathrm{d}D^m} \mathcal{M}^{\mathrm{H}}_{ij}(D) \ge 0, \qquad D > 0, \tag{E5}$$

where the case $m=0$ is the non-negativity statement above. The one-sided derivatives at $D=0$ exist and satisfy

$$(-1)^m \, \frac{\mathrm{d}^m}{\mathrm{d}D^m}\mathcal{M}^{\mathrm{H}}_{ij}(D)\bigg|_{D=0^+} = m! \int_0^\infty s^m \, \mathrm{d}\nu^{\mathrm{H}}_{ij}(s) \geq 0.$$

In the notation introduced later in definition E.1, this is

$$(-1)^m \, \frac{\mathrm{d}^m}{\mathrm{d}D^m}\mathcal{M}^{\mathrm{H}}_{ij}(D)\bigg|_{D=0^+} = m! \, h_{ij,m}.$$

Thus $\mathcal{M}^{\mathrm{H}}_{ij}$ is completely monotone on $[0,\infty)$, with complete monotonicity at the endpoint understood in this one-sided sense.

Proof. From Eq. (E1),

$$\mathcal{M}^{\mathrm{H}}_{ij}(D) = \int_0^\infty \frac{\mathrm{d}\nu^{\mathrm{H}}_{ij}(s)}{1+sD}, \qquad D \geq 0.$$

Since ν^{H}_{ij} is a positive measure, one has

$$\mathcal{M}^{\mathrm{H}}_{ij}(D) \geq 0.$$

Because $\widehat{\mathbb{L}}^{\mathrm{int}}_{ij}$ is strictly positive, the operator $(\widehat{\mathbb{L}}^{\mathrm{int}}_{ij})^{-1/2}$ is bounded and injective. Hence

$$\tau_{ij}\phi_i \neq 0 \qquad \Longrightarrow \qquad \widehat{\psi}^{\mathrm{H}}_{ij} = (\widehat{\mathbb{L}}^{\mathrm{int}}_{ij})^{-1/2}\tau_{ij}\phi_i \neq 0.$$

Therefore

$$\nu^{\mathrm{H}}_{ij}([0,\infty)) = \|\widehat{\psi}^{\mathrm{H}}_{ij}\|^2 > 0,$$

so ν^{H}_{ij} is not the zero measure. Since the integrand $(1+sD)^{-1}$ is strictly positive for $D \geq 0$, this implies

$$\mathcal{M}^{\mathrm{H}}_{ij}(D) > 0.$$

The case $m=0$ in Eq. (E5) is exactly $\mathcal{M}^{\mathrm{H}}_{ij}(D) \geq 0$. Now fix $m \geq 1$. By Eq. (E2), the measure ν^{H}_{ij} has compact support, say in $[0, s^{\max}_{ij}]$. For $D \geq 0$, and for right derivatives when $D=0$,

$$\left| \frac{\mathrm{d}^m}{\mathrm{d}D^m}\frac{1}{1+sD} \right| = m! \, \frac{s^m}{(1+sD)^{m+1}} \leq m! \, (s^{\max}_{ij})^m.$$

The right-hand side is ν^{H}_{ij}-integrable because ν^{H}_{ij} is finite. Therefore differentiation under the integral sign is justified by dominated convergence, and

$$\frac{\mathrm{d}^m}{\mathrm{d}D^m}\mathcal{M}^{\mathrm{H}}_{ij}(D) = \int_0^\infty \frac{\mathrm{d}^m}{\mathrm{d}D^m}\left(\frac{1}{1+sD}\right) \mathrm{d}\nu^{\mathrm{H}}_{ij}(s).$$

Using

$$\frac{\mathrm{d}^m}{\mathrm{d}D^m}\frac{1}{1+sD} = (-1)^m m! \, \frac{s^m}{(1+sD)^{m+1}},$$

we obtain

$$(-1)^m \frac{\mathrm{d}^m}{\mathrm{d}D^m}\mathcal{M}^{\mathrm{H}}_{ij}(D) = m! \int_0^\infty \frac{s^m \, \mathrm{d}\nu^{\mathrm{H}}_{ij}(s)}{(1+sD)^{m+1}} \geq 0, \qquad D > 0.$$

Taking the right limit $D \downarrow 0$ inside the integral, again by dominated convergence and compact support of ν^{H}_{ij}, gives

$$(-1)^m \, \frac{\mathrm{d}^m}{\mathrm{d}D^m}\mathcal{M}^{\mathrm{H}}_{ij}(D)\bigg|_{D=0^+} = m! \int_0^\infty s^m \, \mathrm{d}\nu^{\mathrm{H}}_{ij}(s),$$

which is nonnegative. This proves Eq. (E5). □

Definition E.1 (Heavy-shell moments)**.** Define the heavy-shell moments by

$$h_{ij,m} \equiv \int_0^\infty s^m \,\mathrm{d}\nu_{ij}^{\mathrm{H}}(s), \qquad m = 0, 1, 2, \ldots. \tag{E6}$$

In particular,

$$h_{ij,0} = \nu_{ij}^{\mathrm{H}}([0,\infty)) = \|\widehat{\psi}_{ij}^{\mathrm{H}}\|^2. \tag{E7}$$

Proposition 77 (Moment expansion of the normalized heavy-shell memory)**.** *Because $\mathbf{S}_{ij}^{\mathrm{H}}$ is bounded, the measure ν_{ij}^{H} has compact support. Hence all moments $\{h_{ij,m}\}_{m\geq 0}$ are finite. Let*

$$s_{ij}^{\max} \equiv \sup \operatorname{supp} \nu_{ij}^{\mathrm{H}} < \infty, \tag{E8}$$

with the convention $s_{ij}^{\max} = 0$ if ν_{ij}^{H} is the zero measure. If $s_{ij}^{\max} > 0$, then for real or complex D satisfying

$$|D| < \frac{1}{s_{ij}^{\max}}, \tag{E9}$$

the normalized memory admits the absolutely convergent power series

$$\mathcal{M}_{ij}^{\mathrm{H}}(D) = h_{ij,0} - h_{ij,1}D + h_{ij,2}D^2 - h_{ij,3}D^3 + \cdots. \tag{E10}$$

If $s_{ij}^{\max} = 0$, then ν_{ij}^{H} is supported at $s = 0$, possibly as the zero measure, and

$$\mathcal{M}_{ij}^{\mathrm{H}}(D) \equiv h_{ij,0}. \tag{E11}$$

In the strictly injected case $\tau_{ij}\phi_i \neq 0$, the measure is nonzero. Since $\mathbf{S}_{ij}^{\mathrm{H}}$ is injective, this degenerate zero-support case cannot occur for a nonzero injected datum.

Proof. By Eq. (E2), the measure ν_{ij}^{H} has compact support, hence every polynomial is ν_{ij}^{H}-integrable. This proves finiteness of the moments Eq. (E6).

If $s_{ij}^{\max} = 0$, then ν_{ij}^{H} is supported on $\{0\}$, with the zero-measure case included, so

$$\mathcal{M}_{ij}^{\mathrm{H}}(D) = \int_0^\infty \frac{\mathrm{d}\nu_{ij}^{\mathrm{H}}(s)}{1+sD} = \int_0^\infty \mathrm{d}\nu_{ij}^{\mathrm{H}}(s) = h_{ij,0}.$$

If, in addition, $\tau_{ij}\phi_i \neq 0$, then $\widehat{\psi}_{ij}^{\mathrm{H}} \neq 0$. Let μ_{ij} denote the scalar spectral measure of $\mathbf{S}_{ij}^{\mathrm{H}}$ associated with $\widehat{\psi}_{ij}^{\mathrm{H}}$, so that ν_{ij}^{H} is the push-forward of μ_{ij} under

$$s = \mathfrak{h}_{ij}^{\mathrm{H}}\sigma.$$

Since $\mathfrak{h}_{ij}^{\mathrm{H}} > 0$, support on $s = 0$ implies that μ_{ij}^{H} is supported on $\sigma = 0$. Hence

$$\widehat{\psi}_{ij}^{\mathrm{H}} = E_{ij}(\{0\})\widehat{\psi}_{ij}^{\mathrm{H}}.$$

By the spectral theorem,

$$\mathbf{S}_{ij}^{\mathrm{H}}\widehat{\psi}_{ij}^{\mathrm{H}} = \int \sigma \,\mathrm{d}E_{ij}(\sigma)\widehat{\psi}_{ij}^{\mathrm{H}} = 0.$$

Since $\mathbf{S}_{ij}^{\mathrm{H}}$ is injective, this implies $\widehat{\psi}_{ij}^{\mathrm{H}} = 0$, a contradiction. Therefore the degenerate zero-support case cannot occur for a nonzero injected datum. There is nothing further to prove in the zero-support case.

Assume now that $s_{ij}^{\max} > 0$. If $|D| < 1/s_{ij}^{\max}$, choose $q \in (0,1)$ such that

$$|D|\, s_{ij}^{\max} \leq q.$$

Then, for every $s \in \operatorname{supp} \nu_{ij}^{\mathrm{H}}$,

$$|sD| \leq q < 1.$$

Hence the geometric series

$$\frac{1}{1+sD}=\sum_{m=0}^{\infty}(-1)^m s^m D^m$$

converges absolutely and uniformly on $\operatorname{supp}\nu_{ij}^{\mathrm{H}}$. Moreover,

$$\sum_{m=0}^{\infty}|sD|^m \le \sum_{m=0}^{\infty} q^m = \frac{1}{1-q}.$$

Since ν_{ij}^{H} is finite, dominated convergence justifies termwise integration, and

$$\begin{aligned}\mathcal{M}_{ij}^{\mathrm{H}}(D) &= \int_0^\infty \frac{\mathrm{d}\nu_{ij}^{\mathrm{H}}(s)}{1+sD} \\ &= \int_0^\infty \left(\sum_{m=0}^{\infty}(-1)^m s^m D^m\right)\mathrm{d}\nu_{ij}^{\mathrm{H}}(s) \\ &= \sum_{m=0}^{\infty}(-1)^m D^m \int_0^\infty s^m\,\mathrm{d}\nu_{ij}^{\mathrm{H}}(s) \\ &= \sum_{m=0}^{\infty}(-1)^m h_{ij,m} D^m,\end{aligned}$$

which is exactly Eq. (E10). □

Lemma 31 (Isotropic fourth moment)**.** *Let $\langle\cdot\rangle$ denote the normalized rotationally invariant average on the unit sphere $\mathbb{S}^2$, so that $\langle 1\rangle = 1$. Then*

$$\langle \hat{n}_a\hat{n}_b\hat{n}_c\hat{n}_d\rangle = \frac{1}{15}\left(\delta_{ab}\delta_{cd}+\delta_{ac}\delta_{bd}+\delta_{ad}\delta_{bc}\right). \tag{E12}$$

Proof. Set

$$T_{abcd} \equiv \langle \hat{n}_a\hat{n}_b\hat{n}_c\hat{n}_d\rangle .$$

Rotational invariance implies that T_{abcd} is an isotropic rank-four tensor. Since no Levi–Civita tensor can occur in a fully symmetric parity-even fourth moment, the most general form is

$$T_{abcd} = A\,\delta_{ab}\delta_{cd} + B\,\delta_{ac}\delta_{bd} + C\,\delta_{ad}\delta_{bc}$$

for some scalars A, B, C. Because the product $\hat{n}_a\hat{n}_b\hat{n}_c\hat{n}_d$ is symmetric under every permutation of the indices, the coefficients of the three invariant tensors must agree:

$$A = B = C.$$

Therefore

$$T_{abcd} = A\left(\delta_{ab}\delta_{cd}+\delta_{ac}\delta_{bd}+\delta_{ad}\delta_{bc}\right).$$

Contracting with $\delta_{ab}\delta_{cd}$ gives

$$\begin{aligned}1 = \left\langle(\hat{n}\cdot\hat{n})^2\right\rangle &= T_{abcd}\delta_{ab}\delta_{cd} \\ &= A\left(\delta_{ab}\delta_{ab}\,\delta_{cd}\delta_{cd} + \delta_{ac}\delta_{bd}\delta_{ab}\delta_{cd} + \delta_{ad}\delta_{bc}\delta_{ab}\delta_{cd}\right) \\ &= A(9+3+3) = 15A.\end{aligned}$$

Hence $A = 1/15$, which proves Eq. (E12). □

Lemma 32 (Isotropic quadrupolar eigenvalue)**.** *Let $S_{cd} = S_{dc}$ and $S_{cc} = 0$. Then*

$$\langle \hat{n}_a\hat{n}_b\hat{n}_c\hat{n}_d\rangle\, S_{cd} = \frac{2}{15}\, S_{ab}. \tag{E13}$$

Proof. Using Eq. (E12),

$$\langle \hat{n}_a \hat{n}_b \hat{n}_c \hat{n}_d \rangle \, S_{cd} = \frac{1}{15} \left(\delta_{ab} S_{cc} + S_{ab} + S_{ab} \right) \\ = \frac{2}{15} \, S_{ab},$$

since $S_{cc} = 0$. This proves Eq. (E13). □

Condition E.1 (Retained leading quadrupolar normalization)**.** For any specified inter-shell operator and injection, the measure ν^{H}_{ij} and its zeroth moment $h_{ij,0}$ are fixed by the spectral construction above. The condition below is therefore an explicit normalization of the retained channel, equivalently of the norm of the injected heavy-shell datum. It is not implied by the spectral theorem alone. The present paper does not construct a closed family-level mother operator that would fix this normalization from first principles.

In the bookkeeping used here, the monopole sector is already absorbed into the universal scalar law, while the centered rest branch excludes the dipole sector by parity. The first retained inter-shell channel is retained in the symmetric traceless $l = 2$ sector. Its zeroth memory moment is fixed by

$$h_{ij,0} = \frac{2}{15} \, \mathcal{C}^{(II)}_{\log} = \frac{2}{45}, \tag{E14}$$

using the Path-II single-polarization shell-geometric value

$$\mathcal{C}^{(II)}_{\log} = \frac{1}{3}.$$

Equivalently, after the retained inter-shell source direction has been fixed, this condition fixes its normalization by requiring

$$\| \widehat{\psi}^{\mathrm{H}}_{ij} \|^2 = \frac{2}{45}$$

in the leading isotropic quadrupolar channel. Thus the spectral construction determines the measure from the chosen normalized source, while this condition chooses the retained source normalization used in the heavy-shell channel.

Remark. The factor $2/15$ is the isotropic quadrupolar projector eigenvalue from Eq. (E13). The factor $1/3$ is the Path-II single-polarization shell-geometric logarithmic weight derived earlier. Their product fixes only the retained leading isotropic quadrupolar zeroth moment. It does not specify the spectral distribution of ν^{H}_{ij}, the higher moments $h_{ij,m}$ for $m \geq 1$, or any full microscopic family-level heavy-shell operator.

Corollary 14 (Leading heavy-shell kernel expansion)**.** *Under the retained quadrupolar normalization Eq.* (E14)*, define*

$$\mathcal{E}^{\mathrm{H}}_{ij}(D) \coloneqq \mathcal{M}^{\mathrm{H}}_{ij}(D) - h_{ij,0}.$$

Then, for each fixed retained pair (i, j)*,*

$$\mathcal{K}^{\mathrm{H}}_{ij}(D) = \mathfrak{h}^{\mathrm{H}}_{ij} \left(\frac{2}{45} + \mathcal{E}^{\mathrm{H}}_{ij}(D) \right), \qquad |\mathcal{E}^{\mathrm{H}}_{ij}(D)| \leq h_{ij,1} D, \qquad D \geq 0. \tag{E15}$$

The leading coefficient $2/45$ *is fixed by the retained quadrupolar normalization. The correction is controlled by the first heavy-shell moment* $h_{ij,1}$*. The estimate is pairwise in* (i, j)*; no pair-uniform bound over all heavy shells is asserted unless additional uniform moment bounds are supplied. Equivalently, for the same fixed pair,*

$$\mathcal{K}^{\mathrm{H}}_{ij}(D) = \frac{2}{45} \, \mathfrak{h}^{\mathrm{H}}_{ij} + \mathcal{R}^{\mathrm{H}}_{ij}(D), \qquad |\mathcal{R}^{\mathrm{H}}_{ij}(D)| \leq \mathfrak{h}^{\mathrm{H}}_{ij} h_{ij,1} D, \qquad D \geq 0. \tag{E16}$$

This equivalent form makes the remainder explicit in shell-i units.

Proof. From the Stieltjes representation,

$$\mathcal{M}^{\mathrm{H}}_{ij}(D) - h_{ij,0} = \int_0^\infty \left(\frac{1}{1 + sD} - 1 \right) \mathrm{d}\nu^{\mathrm{H}}_{ij}(s) = -D \int_0^\infty \frac{s}{1 + sD} \, \mathrm{d}\nu^{\mathrm{H}}_{ij}(s).$$

Therefore, for $D \geq 0$,

$$\left|\mathcal{M}^{\mathrm{H}}_{ij}(D) - h_{ij,0}\right| \leq D \int_0^\infty s \, \mathrm{d}\nu^{\mathrm{H}}_{ij}(s) = h_{ij,1} D.$$

The retained quadrupolar normalization Eq. (E14) gives

$$h_{ij,0} = \frac{2}{45}.$$

Since

$$\mathcal{E}^{\mathrm{H}}_{ij}(D) = \mathcal{M}^{\mathrm{H}}_{ij}(D) - h_{ij,0},$$

the estimate above gives

$$|\mathcal{E}^{\mathrm{H}}_{ij}(D)| \leq h_{ij,1} D, \qquad D \geq 0.$$

Using the physical kernel definition Eq. (D16),

$$\mathcal{K}^{\mathrm{H}}_{ij}(D) = \mathfrak{h}^{\mathrm{H}}_{ij} \, \mathcal{M}^{\mathrm{H}}_{ij}(D),$$

one obtains

$$\mathcal{K}^{\mathrm{H}}_{ij}(D) = \mathfrak{h}^{\mathrm{H}}_{ij} \left(\frac{2}{45} + \mathcal{E}^{\mathrm{H}}_{ij}(D) \right), \qquad |\mathcal{E}^{\mathrm{H}}_{ij}(D)| \leq h_{ij,1} D.$$

This proves Eq. (E15).

Equivalently, set

$$\mathcal{R}^{\mathrm{H}}_{ij}(D) \coloneqq \mathfrak{h}^{\mathrm{H}}_{ij} \, \mathcal{E}^{\mathrm{H}}_{ij}(D).$$

Then

$$\mathcal{K}^{\mathrm{H}}_{ij}(D) = \frac{2}{45} \, \mathfrak{h}^{\mathrm{H}}_{ij} + \mathcal{R}^{\mathrm{H}}_{ij}(D),$$

and

$$|\mathcal{R}^{\mathrm{H}}_{ij}(D)| \leq \mathfrak{h}^{\mathrm{H}}_{ij} h_{ij,1} D, \qquad D \geq 0.$$

This is Eq. (E16). □

Appendix F: Downstream diagnostic maps and a conditional family extension

The formulas in this appendix are not used in the derivation of the primary one-loop electron value α_*. They record diagnostic algebraic maps that become available once a family-dependent scalar deformation $\Delta\mathcal{D}^{(i)}_{\mathrm{C}}(x)$ has been specified. These maps leave the fixed geometric lock unchanged, do not redefine Λ_{geom}, and do not provide an independent running law. Every map below is therefore downstream of a chosen scalar deformation rather than a new postulate of the primary shell closure.

The index i is only a family label in this appendix. To avoid a double-subscript clash with the primary scalar-block symbol $\mathcal{D}_{\mathrm{C}}$, the family-resolved scalar branches are written in this appendix with superscript family labels as

$$\mathcal{D}^{(i),0}_{\mathrm{C}}(x), \qquad \mathcal{D}^{(i),\mathrm{eff}}_{\mathrm{C}}(x), \qquad \Delta\mathcal{D}^{(i)}_{\mathrm{C}}(x),$$

with

$$\mathcal{D}^{(i),\mathrm{eff}}_{\mathrm{C}}(x) = \mathcal{D}^{(i),0}_{\mathrm{C}}(x) + \Delta\mathcal{D}^{(i)}_{\mathrm{C}}(x).$$

These are downstream family-level inputs. They are not new definitions of the primary electron scalar block $\mathcal{D}_{\mathrm{C}}(x)$, except in the special case where the family label is explicitly specialized to the electron branch.

Definition F.1 (ALP image map)**.** Recall the downstream ALP target map

$$\mathfrak{D}_{\text{lock}}(\Lambda) \equiv \frac{3}{2}\,\mathsf{K}_{\text{ALP}}\,\Lambda\left(1+\frac{\mathsf{K}_{\text{ALP}}\Lambda}{2\pi^2}\right), \qquad \Lambda \geq 0, \tag{F1}$$

together with its inverse-branch parametrization

$$\zeta(D) \equiv \frac{1}{2}\left(\sqrt{1+\frac{4D}{3\pi^2}}-1\right), \qquad \Lambda_{\text{ALP}}(D) \equiv \frac{2\pi^2}{\mathsf{K}_{\text{ALP}}}\,\zeta(D), \qquad D \geq 0. \tag{F2}$$

In this appendix, $\mathfrak{D}_{\text{lock}}$ and Λ_{ALP} are used as diagnostic coordinate maps. The value $\Lambda_{\text{ALP}}(\mathcal{D}_{\text{C}})$ reconstructed from a scalar branch is not, by definition, the fixed vector datum Λ_{geom}. The label "ALP" in Λ_{ALP} is only a mnemonic for the algebraic Alpha-Lock-Point image used in this inverse map. It has no relation to pion or hadronic physics.

Proposition 78 (Inverse-map identities for the ALP image)**.** *Since $\mathsf{K}_{ALP} > 0$ by proposition 43, the map $\mathfrak{D}_{\text{lock}}$: $[0,\infty) \to [0,\infty)$ is a smooth strictly increasing bijection. Its inverse on $[0,\infty)$ is Λ_{ALP}. Thus, for all $D \geq 0$ and $\Lambda \geq 0$,*

$$\mathfrak{D}_{\text{lock}}\big(\Lambda_{\text{ALP}}(D)\big) = D, \qquad \Lambda_{\text{ALP}}\big(\mathfrak{D}_{\text{lock}}(\Lambda)\big) = \Lambda. \tag{F3}$$

Moreover,

$$\mathfrak{D}'_{\text{lock}}(\Lambda) = \frac{3}{2}\,\mathsf{K}_{ALP}\left(1+\frac{\mathsf{K}_{ALP}\Lambda}{\pi^2}\right) > 0, \tag{F4}$$

and

$$\Lambda'_{\text{ALP}}(D) = \frac{2}{3\mathsf{K}_{ALP}}\,\frac{1}{\sqrt{1+\dfrac{4D}{3\pi^2}}} = \frac{1}{\mathfrak{D}'_{\text{lock}}\big(\Lambda_{\text{ALP}}(D)\big)}. \tag{F5}$$

Proof. First,

$$\frac{\mathsf{K}_{\text{ALP}}\Lambda_{\text{ALP}}(D)}{2\pi^2} = \zeta(D).$$

Hence

$$\begin{aligned}\mathfrak{D}_{\text{lock}}\big(\Lambda_{\text{ALP}}(D)\big) &= \frac{3}{2}\,\mathsf{K}_{\text{ALP}}\,\frac{2\pi^2}{\mathsf{K}_{\text{ALP}}}\,\zeta(D)\,(1+\zeta(D)) \\ &= 3\pi^2\,\zeta(D)\big(1+\zeta(D)\big).\end{aligned}$$

Using

$$\zeta(\mathcal{D}_{\text{C}}) = \frac{1}{2}\left(\sqrt{1+\frac{4\mathcal{D}_{\text{C}}}{3\pi^2}}-1\right), \qquad 1+\zeta(\mathcal{D}_{\text{C}}) = \frac{1}{2}\left(\sqrt{1+\frac{4\mathcal{D}_{\text{C}}}{3\pi^2}}+1\right),$$

one obtains the first-principles chain

$$\begin{aligned}3\pi^2\,\zeta(\mathcal{D}_{\text{C}})\big(1+\zeta(\mathcal{D}_{\text{C}})\big) &= 3\pi^2\,\frac{\left(\sqrt{1+\frac{4\mathcal{D}_{\text{C}}}{3\pi^2}}-1\right)\left(\sqrt{1+\frac{4\mathcal{D}_{\text{C}}}{3\pi^2}}+1\right)}{4} \\ &= \frac{3\pi^2}{4}\left[\left(1+\frac{4\mathcal{D}_{\text{C}}}{3\pi^2}\right)-1\right] \\ &= \mathcal{D}_{\text{C}}.\end{aligned}$$

This proves the first identity in Eq. (F3).

For the second identity, set

$$\mathcal{D}_{\text{C}} = \mathfrak{D}_{\text{lock}}(\Lambda) = \frac{3}{2}\,\mathsf{K}_{\text{ALP}}\,\Lambda\left(1+\frac{\mathsf{K}_{\text{ALP}}\Lambda}{2\pi^2}\right).$$

Then

$$1+\frac{4\mathcal{D}_{\rm C}}{3\pi^2}=1+\frac{4}{3\pi^2}\left[\frac{3}{2}\,\mathsf{K}_{\rm ALP}\,\Lambda\left(1+\frac{\mathsf{K}_{\rm ALP}\Lambda}{2\pi^2}\right)\right]$$
$$=1+\frac{2\mathsf{K}_{\rm ALP}\Lambda}{\pi^2}+\frac{\mathsf{K}_{\rm ALP}^2\Lambda^2}{\pi^4}$$
$$=\left(1+\frac{\mathsf{K}_{\rm ALP}\Lambda}{\pi^2}\right)^2.$$

Since $\Lambda \geq 0$ and $\mathsf{K}_{\rm ALP} > 0$, the positive square root gives

$$\sqrt{1+\frac{4\mathcal{D}_{\rm C}}{3\pi^2}}=1+\frac{\mathsf{K}_{\rm ALP}\Lambda}{\pi^2}.$$

Therefore

$$\zeta(\mathcal{D}_{\rm C})=\frac{1}{2}\left(1+\frac{\mathsf{K}_{\rm ALP}\Lambda}{\pi^2}-1\right)=\frac{\mathsf{K}_{\rm ALP}\Lambda}{2\pi^2}.$$

Hence

$$\Lambda_{\rm ALP}(\mathcal{D}_{\rm C})=\frac{2\pi^2}{\mathsf{K}_{\rm ALP}}\,\zeta(\mathcal{D}_{\rm C})=\Lambda.$$

Differentiating Eq. (F1) gives

$$\mathfrak{D}'_{\rm lock}(\Lambda)=\frac{3}{2}\,\mathsf{K}_{\rm ALP}\left(1+\frac{\mathsf{K}_{\rm ALP}\Lambda}{\pi^2}\right),$$

which is strictly positive for $\Lambda \geq 0$. Therefore $\mathfrak{D}_{\rm lock}$ is strictly increasing on $[0,\infty)$. Also,

$$\mathfrak{D}_{\rm lock}(0)=0,\qquad \lim_{\Lambda\to\infty}\mathfrak{D}_{\rm lock}(\Lambda)=\infty,$$

so $\mathfrak{D}_{\rm lock}$ maps $[0,\infty)$ onto $[0,\infty)$. Smoothness is immediate from its polynomial form. Thus it is a smooth strictly increasing bijection.

Differentiating Eq. (F2) gives

$$\Lambda'_{\rm ALP}(\mathcal{D}_{\rm C})=\frac{2}{3\mathsf{K}_{\rm ALP}}\frac{1}{\sqrt{1+\frac{4\mathcal{D}_{\rm C}}{3\pi^2}}}.$$

Using

$$1+\frac{\mathsf{K}_{\rm ALP}\Lambda_{\rm ALP}(\mathcal{D}_{\rm C})}{\pi^2}=1+2\zeta(\mathcal{D}_{\rm C})=\sqrt{1+\frac{4\mathcal{D}_{\rm C}}{3\pi^2}},$$

one obtains

$$\Lambda'_{\rm ALP}(\mathcal{D}_{\rm C})=\frac{1}{\mathfrak{D}'_{\rm lock}\big(\Lambda_{\rm ALP}(\mathcal{D}_{\rm C})\big)}.$$

This proves Eqs. (F4) and (F5). □

Proposition 79 (Fixed-x reflection on the ALP image)**.** *Fix x. Assume that*

$$\mathcal{D}_{\rm C}^{(i),0}(x)\geq 0,\qquad \mathcal{D}_{\rm C}^{(i),\rm eff}(x)=\mathcal{D}_{\rm C}^{(i),0}(x)+\Delta\mathcal{D}_{\rm C}^{(i)}(x)\geq 0, \tag{F6}$$

and let $K_x \subset [0,\infty)$ be a compact interval containing the segment joining $\mathcal{D}_{\rm C}^{(i),0}(x)$ and $\mathcal{D}_{\rm C}^{(i),\rm eff}(x)$. The constants in the remainder estimates below are allowed to depend on K_x, but not on $\Delta\mathcal{D}_{\rm C}^{(i)}(x)$ once K_x has been fixed. Define

$$\delta\Lambda_{\rm ALP}^{(i)}(x)=\Lambda_{\rm ALP}\big(\mathcal{D}_{\rm C}^{(i),\rm eff}(x)\big)-\Lambda_{\rm ALP}\big(\mathcal{D}_{\rm C}^{(i),0}(x)\big).$$

Then, with x fixed and with the implicit constants depending only on a compact $\mathcal{D}_{\mathrm{C}}$-interval containing the segment between $\mathcal{D}_{\mathrm{C}}^{(i),0}(x)$ and $\mathcal{D}_{\mathrm{C}}^{(i),\mathrm{eff}}(x)$,

$$\delta\Lambda_{\mathrm{ALP}}^{(i)}(x) = \Lambda'_{\mathrm{ALP}}\big(\mathcal{D}_{\mathrm{C}}^{(i),0}(x)\big)\,\Delta\mathcal{D}_{\mathrm{C}}^{(i)}(x) + O\big(|\Delta\mathcal{D}_{\mathrm{C}}^{(i)}(x)|^2\big), \tag{F7}$$

and equivalently

$$\delta\Lambda_{\mathrm{ALP}}^{(i)}(x) = \frac{\Delta\mathcal{D}_{\mathrm{C}}^{(i)}(x)}{\mathfrak{D}'_{\mathrm{lock}}\big(\Lambda_{\mathrm{ALP}}(\mathcal{D}_{\mathrm{C}}^{(i),0}(x))\big)} + O\big(|\Delta\mathcal{D}_{\mathrm{C}}^{(i)}(x)|^2\big). \tag{F8}$$

This is a fixed-x coordinate reflection of the scalar deformation. It is not the fixed-Λ_{geom} root re-extraction used for the load-bearing electron shift.

Proof. The function $\Lambda_{\mathrm{ALP}}(\mathcal{D}_{\mathrm{C}})$ is the restriction to $[0,\infty)$ of a C^∞ function on the open interval $(-3\pi^2/4,\infty)$. Therefore Taylor's theorem at the point $\mathcal{D}_{\mathrm{C}}^{(i),0}(x)$ gives

$$\begin{aligned}\Lambda_{\mathrm{ALP}}\big(\mathcal{D}_{\mathrm{C}}^{(i),0}(x)+\Delta\mathcal{D}_{\mathrm{C}}^{(i)}(x)\big) &= \Lambda_{\mathrm{ALP}}\big(\mathcal{D}_{\mathrm{C}}^{(i),0}(x)\big) + \Lambda'_{\mathrm{ALP}}\big(\mathcal{D}_{\mathrm{C}}^{(i),0}(x)\big)\,\Delta\mathcal{D}_{\mathrm{C}}^{(i)}(x)\\ &\quad+\frac{1}{2}\Lambda''_{\mathrm{ALP}}\big(\mathcal{D}_{\mathrm{C}}^{(i),0}(x)+\theta_x\Delta\mathcal{D}_{\mathrm{C}}^{(i)}(x)\big)\,\big(\Delta\mathcal{D}_{\mathrm{C}}^{(i)}(x)\big)^2,\end{aligned}$$

for some $\theta_x\in[0,1]$. Subtracting $\Lambda_{\mathrm{ALP}}(\mathcal{D}_{\mathrm{C}}^{(i),0}(x))$ from both sides gives Eq. (F7), provided Λ''_{ALP} stays bounded on the segment joining $\mathcal{D}_{\mathrm{C}}^{(i),0}(x)$ and $\mathcal{D}_{\mathrm{C}}^{(i),\mathrm{eff}}(x)$.

Now

$$\Lambda_{\mathrm{ALP}}(\mathcal{D}_{\mathrm{C}}) = \frac{\pi^2}{\mathsf{K}_{\mathrm{ALP}}}\left(\sqrt{1+\frac{4\mathcal{D}_{\mathrm{C}}}{3\pi^2}}-1\right),$$

so

$$\Lambda'_{\mathrm{ALP}}(\mathcal{D}_{\mathrm{C}}) = \frac{2}{3\mathsf{K}_{\mathrm{ALP}}}\frac{1}{\sqrt{1+\dfrac{4\mathcal{D}_{\mathrm{C}}}{3\pi^2}}},$$

and

$$\Lambda''_{\mathrm{ALP}}(\mathcal{D}_{\mathrm{C}}) = -\frac{4}{9\mathsf{K}_{\mathrm{ALP}}\pi^2}\left(1+\frac{4\mathcal{D}_{\mathrm{C}}}{3\pi^2}\right)^{-3/2}.$$

Hence Λ''_{ALP} is continuous on $[0,\infty)$, so it is bounded on every compact interval. This yields the stated $O\big(|\Delta\mathcal{D}_{\mathrm{C}}^{(i)}(x)|^2\big)$ remainder.

Finally, by Eq. (F5),

$$\Lambda'_{\mathrm{ALP}}\big(\mathcal{D}_{\mathrm{C}}^{(i),0}(x)\big) = \frac{1}{\mathfrak{D}'_{\mathrm{lock}}\big(\Lambda_{\mathrm{ALP}}(\mathcal{D}_{\mathrm{C}}^{(i),0}(x))\big)},$$

which converts Eq. (F7) into Eq. (F8). ☐

Definition F.2 (Operational total slowdown and anomaly proxy)**.** Given a scalar branch $\mathcal{D}_{\mathrm{C}}^{(i)}(x)$, define the operational total slowdown wherever $\mathcal{D}_{\mathrm{C}}^{(i)}(x)>0$ by

$$\mathcal{D}_{\mathrm{total}}^{(i)}(x) \equiv \mathcal{D}_{\mathrm{C}}^{(i)}(x) - x\,\zeta\big(\mathcal{D}_{\mathrm{C}}^{(i)}(x)\big) + \frac{x^2\zeta\big(\mathcal{D}_{\mathrm{C}}^{(i)}(x)\big)^2}{4\mathcal{D}_{\mathrm{C}}^{(i)}(x)}. \tag{F9}$$

At points where $\mathcal{D}_{\mathrm{C}}^{(i)}(x)=0$, this expression is defined by the removable extension. Indeed, writing the scalar argument as D,

$$\zeta(D) = D\,h(D), \qquad h(D) = \frac{1}{3\pi^2}+O(D), \qquad D\to 0,$$

gives

$$\frac{x^2\zeta(D)^2}{4D} = \frac{x^2 D\, h(D)^2}{4} \longrightarrow 0 \qquad (D \to 0). \tag{F10}$$

Whenever formal expansions around $x = 0$ are used below, the last term is understood through this extension.

When $\mathcal{D}^{(i)}_{\text{total}}(x) < 1$, define the corresponding real anomaly-like proxy by

$$g^{\text{Rel}}_{i,2}(x) \equiv \frac{1}{\sqrt{1 - \mathcal{D}^{(i)}_{\text{total}}(x)}}. \tag{F11}$$

The superscript Rel marks the downstream RELATOR diagnostic map. It does not insert QED data into the primary shell lock, and the proxy is not a new definition of the physical anomaly outside the stated downstream map.

Proposition 80 (First-order propagation through the operational lift)**.** *Fix x. Assume*

$$\mathcal{D}^{(i),0}_{\text{C}}(x) > 0, \qquad \mathcal{D}^{(i),\text{eff}}_{\text{C}}(x) = \mathcal{D}^{(i),0}_{\text{C}}(x) + \Delta\mathcal{D}^{(i)}_{\text{C}}(x) > 0, \tag{F12}$$

and assume that $|\Delta\mathcal{D}^{(i)}_{\text{C}}(x)|$ is sufficiently small. Set

$$F_x(\mathcal{D}_{\text{C}}) = \mathcal{D}_{\text{C}} - x\zeta(\mathcal{D}_{\text{C}}) + \frac{x^2\zeta(\mathcal{D}_{\text{C}})^2}{4\mathcal{D}_{\text{C}}}, \qquad \mathcal{D}_{\text{C}} > 0.$$

Define

$$\mathcal{D}^{(i),0}_{\text{total}}(x) = F_x\big(\mathcal{D}^{(i),0}_{\text{C}}(x)\big), \qquad \mathcal{D}^{(i),\text{eff}}_{\text{total}}(x) = F_x\big(\mathcal{D}^{(i),\text{eff}}_{\text{C}}(x)\big).$$

Then

$$\mathcal{D}^{(i),\text{eff}}_{\text{total}}(x) - \mathcal{D}^{(i),0}_{\text{total}}(x) = J_{\text{total}}\big(x, \mathcal{D}^{(i),0}_{\text{C}}(x)\big)\,\Delta\mathcal{D}^{(i)}_{\text{C}}(x) + O\big(|\Delta\mathcal{D}^{(i)}_{\text{C}}(x)|^2\big), \tag{F13}$$

where, for $D > 0$,

$$J_{\text{total}}(x, D) = 1 - x\,\zeta'(D) + \frac{x^2}{2D}\,\zeta(D)\zeta'(D) - \frac{x^2}{4D^2}\,\zeta(D)^2. \tag{F14}$$

The same formula has a removable extension to $D = 0$, namely

$$J_{\text{total}}(x, 0) = 1 - \frac{x}{3\pi^2} + \frac{x^2}{36\pi^4}.$$

If $1 - \mathcal{D}^{(i),0}_{\text{total}}(x) > 0$, then, after possibly decreasing the smallness threshold on $|\Delta\mathcal{D}^{(i)}_{\text{C}}(x)|$, both proxy values are real. Define

$$g^{\text{Rel},0}_{i,2}(x) = \big(1 - \mathcal{D}^{(i),0}_{\text{total}}(x)\big)^{-1/2}, \qquad g^{\text{Rel,eff}}_{i,2}(x) = \big(1 - \mathcal{D}^{(i),\text{eff}}_{\text{total}}(x)\big)^{-1/2}.$$

Then

$$\begin{aligned} &g^{\text{Rel,eff}}_{i,2}(x) - g^{\text{Rel},0}_{i,2}(x) \\ &\quad = \frac{1}{2}\big(1 - \mathcal{D}^{(i),0}_{\text{total}}(x)\big)^{-3/2}\Big[\mathcal{D}^{(i),\text{eff}}_{\text{total}}(x) - \mathcal{D}^{(i),0}_{\text{total}}(x)\Big] + O\big(|\Delta\mathcal{D}^{(i)}_{\text{C}}(x)|^2\big). \end{aligned} \tag{F15}$$

Proof. Set

$$D_0 = \mathcal{D}^{(i),0}_{\text{C}}(x), \qquad \delta D = \Delta\mathcal{D}^{(i)}_{\text{C}}(x), \qquad D_{\text{eff}} = D_0 + \delta D.$$

By Eq. (F12), both D_0 and D_{eff} are strictly positive. Hence F_x is C^∞ on a neighborhood of D_0. Taylor's theorem gives

$$F_x(D_0 + \delta D) - F_x(D_0) = F'_x(D_0)\,\delta D + O\big(|\delta D|^2\big).$$

By definition,

$$\mathcal{D}^{(i),\mathrm{eff}}_{\mathrm{total}}(x) = F_x(D_{\mathrm{eff}}), \qquad \mathcal{D}^{(i),0}_{\mathrm{total}}(x) = F_x(D_0),$$

so this is exactly Eq. (F13) once $F'_x(\mathcal{D}_{\mathrm{C}})$ is computed.

Direct differentiation gives, for $D > 0$,

$$\begin{aligned} F'_x(D) &= 1 - x\,\zeta'(D) + \frac{x^2}{4}\,\frac{\mathrm{d}}{\mathrm{d}D}\left(\frac{\zeta(D)^2}{D}\right) \\ &= 1 - x\,\zeta'(D) + \frac{x^2}{4}\left(\frac{2\zeta(D)\zeta'(D)}{D} - \frac{\zeta(D)^2}{D^2}\right) \\ &= 1 - x\,\zeta'(\mathcal{D}_{\mathrm{C}}) + \frac{x^2}{2\mathcal{D}_{\mathrm{C}}}\,\zeta(\mathcal{D}_{\mathrm{C}})\zeta'(\mathcal{D}_{\mathrm{C}}) - \frac{x^2}{4\mathcal{D}_{\mathrm{C}}^2}\,\zeta(\mathcal{D}_{\mathrm{C}})^2, \end{aligned}$$

which proves Eq. (F14).

Now define

$$h(u) = (1-u)^{-1/2}.$$

If $1 - \mathcal{D}^{(i),0}_{\mathrm{total}}(x) > 0$, then h is C^∞ at $u = \mathcal{D}^{(i),0}_{\mathrm{total}}(x)$. Therefore

$$h(u+\delta u) - h(u) = h'(u)\,\delta u + O(|\delta u|^2), \qquad h'(u) = \frac{1}{2}(1-u)^{-3/2}.$$

Apply this with

$$u = \mathcal{D}^{(i),0}_{\mathrm{total}}(x), \qquad \delta u = \mathcal{D}^{(i),\mathrm{eff}}_{\mathrm{total}}(x) - \mathcal{D}^{(i),0}_{\mathrm{total}}(x).$$

Since F_x is C^1 on a compact neighborhood of D_0, the first part of the proof gives

$$\delta u = O(\delta D).$$

Because $1 - \mathcal{D}^{(i),0}_{\mathrm{total}}(x) > 0$, there exists $\varepsilon_x > 0$ such that

$$|\delta u| < \frac{1}{2}\big(1 - \mathcal{D}^{(i),0}_{\mathrm{total}}(x)\big) \qquad \text{whenever } |\delta D| < \varepsilon_x.$$

For such δD,

$$1 - \mathcal{D}^{(i),\mathrm{eff}}_{\mathrm{total}}(x) = 1 - \mathcal{D}^{(i),0}_{\mathrm{total}}(x) - \delta u > \frac{1}{2}\big(1 - \mathcal{D}^{(i),0}_{\mathrm{total}}(x)\big) > 0,$$

so both proxy values are real. Hence the remainder $O(|\delta u|^2)$ is also $O(|\delta D|^2)$. This yields Eq. (F15). □

Figure 12 summarizes two coordinate readings of the same family-dependent scalar deformation. At fixed x, the deformation is reflected through the inverse ALP image Λ_{ALP}, as in Eq. (F8). At a fixed geometric datum Λ_{fix}, which may be the exact vector input or a specified reduced representative, the same deformation is re-read as a shifted root of

$$\mathcal{D}^{(i),\mathrm{eff}}_{\mathrm{C}}(x) = D^{\mathrm{fix}}_{\mathrm{lock}}, \qquad D^{\mathrm{fix}}_{\mathrm{lock}} \equiv \mathfrak{D}_{\mathrm{lock}}(\Lambda_{\mathrm{fix}}).$$

Whenever the undeformed family branch is used in this reading, we denote its corresponding baseline root by x^0_i. Thus

$$\mathcal{D}^{(i),0}_{\mathrm{C}}(x^0_i) = D^{\mathrm{fix}}_{\mathrm{lock}},$$

whenever such a root exists. For the electron branch this is precisely the fixed-geometry running shift discussed in Eq. (560). The lower box records the optional downstream lift to $\mathcal{D}^{(i)}_{\mathrm{total}}$ and to the proxy $g^{\mathrm{Rel}}_{i,2}$. In the present paper, only the electron fixed-Λ_{geom} re-extraction is used in the main argument. The generic family label i is included only as diagnostic notation, and the downstream proxy does not enter the primary extraction of α_*.

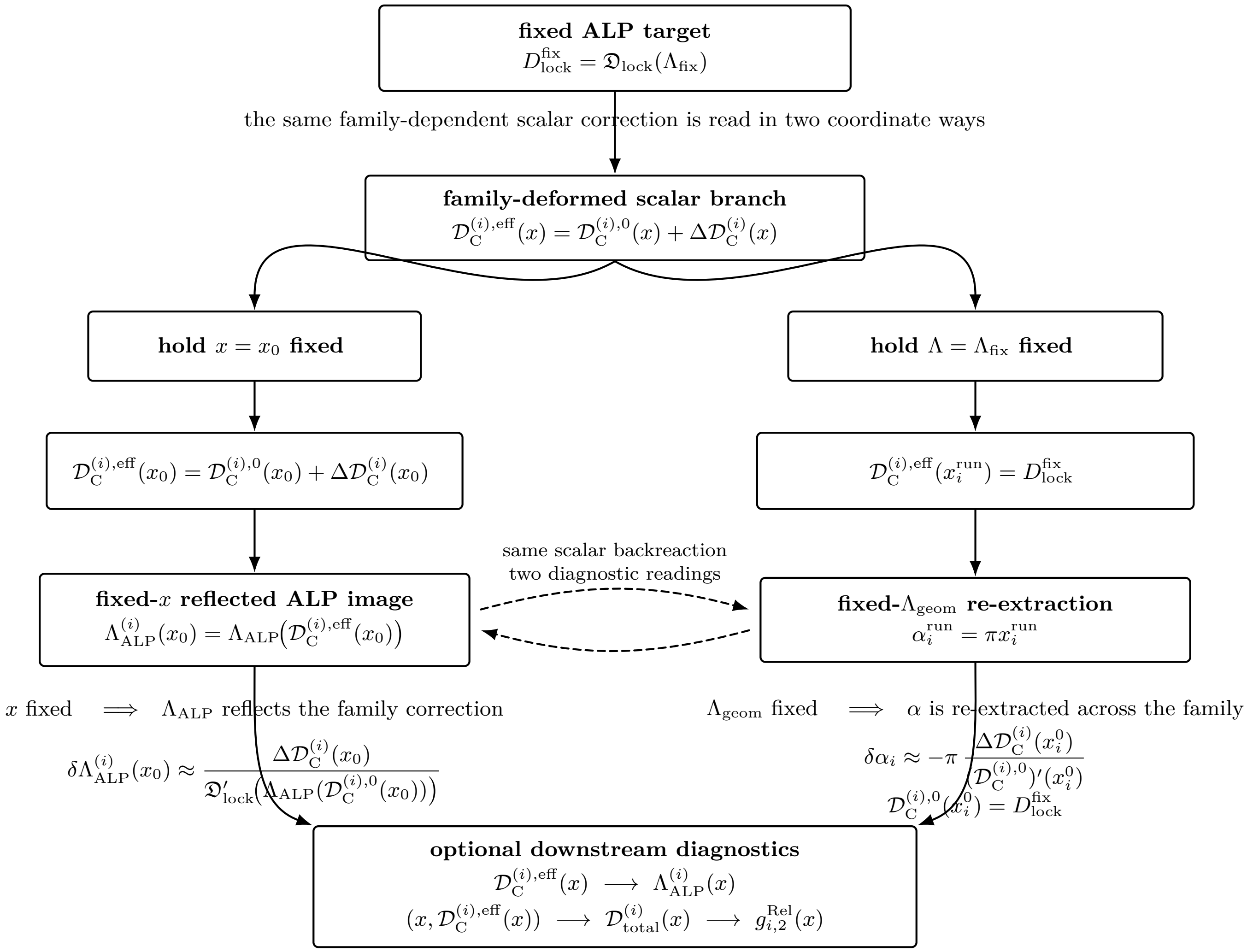

FIG. 12. Two coordinate diagnostic readings of the same family-dependent scalar deformation. The top box shows the fixed ALP target $D_{\rm lock}^{\rm fix} = \mathfrak{D}_{\rm lock}(\Lambda_{\rm fix})$. The center box shows the deformed scalar branch $\mathcal{D}_{\rm C}^{(i),\rm eff}(x) = \mathcal{D}_{\rm C}^{(i),0}(x) + \Delta\mathcal{D}_{\rm C}^{(i)}(x)$. The left column shows the fixed-x reflection on the ALP image $\Lambda_{\rm ALP}$. The right column shows the fixed-$\Lambda_{\rm geom}$ re-extraction of $x_i^{\rm run}$ and $\alpha_i^{\rm run}$. The lower box records the optional downstream lift to $\mathcal{D}_{\rm total}^{(i)}$ and to the proxy $g_{i,2}^{\rm Rel}$. The figure is diagnostic only. In the present paper, only the electron fixed-$\Lambda_{\rm geom}$ re-extraction is used in the main argument, while the generic family label i is retained only as diagnostic notation.

Definition F.3 (Optional coefficient map)**.** Near $x = 0$, and as formal power series unless convergence is stated separately, write the baseline operational total slowdown in the form

$$\mathcal{D}_{\rm total}^{(i),0}(x) = d_{i,1}x + d_{i,2}x^2 + d_{i,3}x^3 + O(x^4), \tag{F16}$$

The induced operational contribution is

$$\Delta\mathcal{D}_{\rm total}^{(i)}(x) \equiv \mathcal{D}_{\rm total}^{(i),\rm eff}(x) - \mathcal{D}_{\rm total}^{(i),0}(x).$$

The displayed form assumes that the retained deformation begins at order x^2, as in the heavy-shell channel used in the electron diagnostic. Accordingly, we write

$$\Delta\mathcal{D}_{\rm total}^{(i)}(x) = m_{i,2}x^2 + m_{i,3}x^3 + m_{i,4}x^4 + O(x^5). \tag{F17}$$

Define the baseline anomaly-like proxy by

$$a_i^{\rm Rel,0}(x) \equiv \frac{1}{\sqrt{1 - \mathcal{D}_{\rm total}^{(i),0}(x)}} - 1 = \sum_{n\geq 1} A_i^{(2n)} x^n, \tag{F18}$$

and define the deformed anomaly-like proxy by

$$a_i^{\mathrm{Rel,eff}}(x) \equiv \frac{1}{\sqrt{1-\mathcal{D}_{\mathrm{total}}^{(i),0}(x)-\Delta\mathcal{D}_{\mathrm{total}}^{(i)}(x)}}-1=\sum_{n\geq 1}\big(A_i^{(2n)}+\Delta C_i^{(2n)}\big)x^n. \tag{F19}$$

The coefficients $A_i^{(2n)}$ and $\Delta C_i^{(2n)}$ in this optional map are internal proxy coefficients. The family index i is not the QED universal subscript in $A_1^{(2n)}$. These coefficients are not external QED benchmark coefficients unless a separate comparison layer explicitly identifies them with such a benchmark.

Proposition 81 (First optional deformation-dependent coefficient shifts)**.** *As formal coefficient identities for the optional proxy Eq.* (F19)*, the deformation does not shift the leading coefficient,*

$$\Delta C_i^{(2)} = 0. \tag{F20}$$

The first nonzero deformation-dependent shifts are

$$\Delta C_i^{(4)} = \frac{m_{i,2}}{2}, \tag{F21}$$

$$\Delta C_i^{(6)} = \frac{3}{4}d_{i,1}m_{i,2}+\frac{1}{2}m_{i,3}, \tag{F22}$$

and

$$\Delta C_i^{(8)} = \frac{3}{8}m_{i,2}^2+\left(\frac{3}{4}d_{i,2}+\frac{15}{16}d_{i,1}^2\right)m_{i,2}+\frac{3}{4}d_{i,1}m_{i,3}+\frac{1}{2}m_{i,4}. \tag{F23}$$

Proof. Set

$$U(x)=\mathcal{D}_{\mathrm{total}}^{(i),0}(x), \qquad M(x)=\Delta\mathcal{D}_{\mathrm{total}}^{(i)}(x).$$

Then

$$\sum_{n\geq 1}\Delta C_i^{(2n)}x^n=(1-U-M)^{-1/2}-(1-U)^{-1/2}.$$

Since $U(x)=O(x)$ and $M(x)=O(x^2)$, the binomial expansion gives

$$(1-U-M)^{-1/2}=1+\frac{1}{2}(U+M)+\frac{3}{8}(U+M)^2+\frac{5}{16}(U+M)^3+\frac{35}{128}(U+M)^4+O(x^5),$$

and

$$(1-U)^{-1/2}=1+\frac{1}{2}U+\frac{3}{8}U^2+\frac{5}{16}U^3+\frac{35}{128}U^4+O(x^5).$$

Hence

$$\begin{aligned}(1-U-M)^{-1/2}-(1-U)^{-1/2}&=\frac{1}{2}M+\frac{3}{8}\left[(U+M)^2-U^2\right]\\&\quad+\frac{5}{16}\left[(U+M)^3-U^3\right]\\&\quad+\frac{35}{128}\left[(U+M)^4-U^4\right]+O(x^5).\end{aligned}$$

Since $U=O(x)$ and $M=O(x^2)$,

$$(U+M)^2-U^2=2UM+M^2,$$

$$(U+M)^3-U^3=3U^2M+3UM^2+M^3=3U^2M+O(x^5),$$

and

$$(U+M)^4 - U^4 = 4U^3M + 6U^2M^2 + 4UM^3 + M^4 = O(x^5).$$

Therefore

$$(1-U-M)^{-1/2} - (1-U)^{-1/2} = \frac{1}{2}M + \frac{3}{8}\big(2UM + M^2\big) + \frac{5}{16}\big(3U^2M\big) + O(x^5).$$

Now insert

$$U(x) = d_{i,1}x + d_{i,2}x^2 + d_{i,3}x^3 + O(x^4), \qquad M(x) = m_{i,2}x^2 + m_{i,3}x^3 + m_{i,4}x^4 + O(x^5).$$

Then

$$\frac{1}{2}M = \frac{1}{2}m_{i,2}x^2 + \frac{1}{2}m_{i,3}x^3 + \frac{1}{2}m_{i,4}x^4 + O(x^5),$$

$$\frac{3}{8}(2UM) = \frac{3}{4}d_{i,1}m_{i,2}x^3 + \frac{3}{4}\big(d_{i,1}m_{i,3} + d_{i,2}m_{i,2}\big)x^4 + O(x^5),$$

$$\frac{3}{8}M^2 = \frac{3}{8}m_{i,2}^2x^4 + O(x^5),$$

and

$$\frac{5}{16}(3U^2M) = \frac{15}{16}d_{i,1}^2m_{i,2}x^4 + O(x^5).$$

There is no term of order x, because $M(x) = O(x^2)$. Hence

$$\Delta C_i^{(2)} = 0.$$

Collecting the coefficients of x^2, x^3, and x^4 gives

$$\Delta C_i^{(4)} = \frac{m_{i,2}}{2},$$

$$\Delta C_i^{(6)} = \frac{3}{4}d_{i,1}m_{i,2} + \frac{1}{2}m_{i,3},$$

and

$$\Delta C_i^{(8)} = \frac{3}{8}m_{i,2}^2 + \left(\frac{3}{4}d_{i,2} + \frac{15}{16}d_{i,1}^2\right)m_{i,2} + \frac{3}{4}d_{i,1}m_{i,3} + \frac{1}{2}m_{i,4}.$$

This proves Eqs. (F21) to (F23). □

Remark (Conditional extension to the muon and tau). The present paper does not derive theorem-level reference branches for the muon or tau. If such branches are constructed later from a closed family-level scalar–vector system, then, for heavier virtual shells $j > i$, the retained heavy-shell kernel $\mathcal{K}_{ij}^{\mathrm{H}}$ and the same fixed-geometry re-extraction map apply in the single-excursion channel already derived for heavy shells. What changes is the reference scalar branch $\mathcal{D}_{\mathrm{C}}^{(i),0}(x)$, not the algebraic form of the downstream map. This statement is conditional on the later construction of those reference branches and on the absence, or separate treatment, of lighter-shell resonance channels. Such resonance channels require a separate family-level construction and are not supplied by the heavy-shell kernel alone.

Remark (Two coordinate diagnostic readings). Given a scalar deformation $\Delta\mathcal{D}_{\mathrm{C}}^{(i)}(x)$, one may either keep x fixed and read the effect as a reflected shift of the ALP image Λ_{ALP}, or keep Λ_{geom} fixed and read the effect as a re-extracted shift of the coupling root. These are two coordinate readings of the same scalar backreaction rather than two independent dynamical effects. In the present paper, only the fixed-Λ_{geom} electron re-extraction is used in the main argument. The fixed-x ALP reflection and the downstream $g_{i,2}^{\mathrm{Rel}}$ proxy remain diagnostic.

Appendix G: Diagnostic visualizations of the theorem-level shell source

This appendix gives a compact visual audit of the theorem-level odd shell source used in the vector-shell ledger. The figures are diagnostic. They do not introduce a new vector datum, do not modify $\Lambda_{\rm geom}$, and do not enter the scalar lock or the extraction of α_*. Their purpose is to show how the exact Maxwell shell trace, its odd source coefficients, and the resulting toroidal source field appear on the matching sphere.

Throughout this appendix the minimal electron-branch ratios are fixed,

$$\eta_0 = \frac{1}{\pi}, \qquad \ell_0 = \frac{1}{\pi\sqrt{\pi}},$$

and the plotted finite source cutoff is

$$J_{\max} = 101.$$

The shell variable is

$$\upsilon = \cos\vartheta, \qquad \rho_\perp(\upsilon) = \sqrt{1-\upsilon^2}.$$

The symbol $\rho_\perp(\upsilon)$ is the normalized cylindrical radius on the shell. It is used here to avoid overloading the generator-space radial coordinate ρ.

The exact tangential Maxwell shell trace plotted in fig. 13 is

$$\widetilde{b}_{\eta_0}(\upsilon) = \upsilon\,\mathcal{B}_\rho(\eta_0;\upsilon) - \rho_\perp(\upsilon)\,\mathcal{B}_z(\eta_0;\upsilon), \tag{G1}$$

where $\mathcal{B}_\rho$ and $\mathcal{B}_z$ are the dimensionless cylindrical and axial Biot–Savart shell components of the circular carrier at $R/r_* = \eta_0$, as defined in Eqs. (334) and (335). The common SI factor $\mu_0 I/r_*$ has already been removed in these dimensionless shell profiles. The odd source coefficients are then computed from

$$a_j^{\rm sh} = \frac{1}{I_j}\int_{-1}^{1} \widetilde{b}_{\eta_0}(\upsilon)(1-\upsilon^2)P_j'(\upsilon)\,\mathrm{d}\upsilon, \qquad I_j = \frac{2j(j+1)}{2j+1}, \tag{G2}$$

for odd j, followed by

$$\widehat{a}_j = 2(j+1)\eta_0^{-1/2}a_j^{\rm sh}, \qquad J_j^{(\chi)} = \left[\frac{2\pi}{(j+1)(2j+1)}\right]^{1/2}\widehat{a}_j. \tag{G3}$$

The finite odd toroidal source field displayed on the matching sphere Σ_{r_*} is

$$\mathbf{U}_\chi^{[J_{\max}]}(\vartheta,\varphi) = U_\varphi^{[J_{\max}]}(\vartheta)\,\hat{\mathbf{e}}_\varphi, \tag{G4}$$

with

$$U_\varphi^{[J_{\max}]}(\vartheta) = \frac{1}{\sqrt{2\pi}} \sum_{\substack{1\le j\le J_{\max}\\ j\ \text{odd}}} J_j^{(\chi)}\,\frac{\sin\vartheta\,P_j'(\cos\vartheta)}{\sqrt{I_j}}. \tag{G5}$$

The plotted figures use the normalized shell $r_* = 1$, while the identities below keep the explicit r_*-factor.

Proposition 82 (Divergence and scalar curl of the finite odd source)**.** *The field $\mathbf{U}_\chi^{[J_{\max}]}$ is tangential, axisymmetric, and divergence-free on Σ_{r_*}. More precisely,*

$$\operatorname{div}_{\Sigma_{r_*}}\mathbf{U}_\chi^{[J_{\max}]} = \frac{1}{r_*\sin\vartheta}\,\frac{\partial U_\varphi^{[J_{\max}]}}{\partial\varphi} = 0. \tag{G6}$$

Its scalar surface curl is

$$\operatorname{curl}_{\Sigma_{r_*}}\mathbf{U}_\chi^{[J_{\max}]} = \frac{1}{r_*\sin\vartheta}\frac{\partial}{\partial\vartheta}\left(\sin\vartheta\,U_\varphi^{[J_{\max}]}(\vartheta)\right), \tag{G7}$$

and equivalently

$$\operatorname{curl}_{\Sigma_{r_*}}\mathbf{U}_\chi^{[J_{\max}]} = \frac{1}{r_*\sqrt{2\pi}} \sum_{\substack{1\le j\le J_{\max}\\ j\ \text{odd}}} J_j^{(\chi)}\,\frac{j(j+1)P_j(\cos\vartheta)}{\sqrt{I_j}}. \tag{G8}$$

Proof. On a sphere of radius r_*, the surface divergence of a tangential field $A_\vartheta \hat{\mathbf{e}}_\vartheta + A_\varphi \hat{\mathbf{e}}_\varphi$ is

$$\operatorname{div}_{\Sigma_{r_*}} \mathbf{A} = \frac{1}{r_* \sin\vartheta} \frac{\partial}{\partial\vartheta}\big(\sin\vartheta\, A_\vartheta\big) + \frac{1}{r_* \sin\vartheta} \frac{\partial A_\varphi}{\partial\varphi}.$$

For $\mathbf{U}_\chi^{[J_{\max}]}$, one has

$$A_\vartheta = 0, \qquad A_\varphi = U_\varphi^{[J_{\max}]}(\vartheta),$$

so

$$\operatorname{div}_{\Sigma_{r_*}} \mathbf{U}_\chi^{[J_{\max}]} = \frac{1}{r_* \sin\vartheta} \frac{\partial U_\varphi^{[J_{\max}]}}{\partial\varphi} = 0,$$

because $U_\varphi^{[J_{\max}]}$ is independent of φ.

The scalar surface curl is the radial component of the three-dimensional curl restricted to the sphere. For a tangential field it is

$$\operatorname{curl}_{\Sigma_{r_*}} \mathbf{A} = \frac{1}{r_* \sin\vartheta} \frac{\partial}{\partial\vartheta}\big(\sin\vartheta\, A_\varphi\big) - \frac{1}{r_* \sin\vartheta} \frac{\partial A_\vartheta}{\partial\varphi}.$$

With $A_\vartheta = 0$ and $A_\varphi = U_\varphi^{[J_{\max}]}(\vartheta)$, this gives Eq. (G7).

It remains to evaluate the derivative. Set

$$u = \cos\vartheta.$$

For one mode,

$$\sin\vartheta \, \frac{\sin\vartheta\, P_j'(\cos\vartheta)}{\sqrt{I_j}} = \frac{(1-u^2)P_j'(u)}{\sqrt{I_j}}.$$

Since

$$\frac{\mathrm{d}}{\mathrm{d}\vartheta} = -\sin\vartheta \, \frac{\mathrm{d}}{\mathrm{d}u},$$

and the Legendre equation gives

$$\frac{\mathrm{d}}{\mathrm{d}u}\left[(1-u^2)P_j'(u)\right] = -j(j+1)P_j(u),$$

we obtain the chain

$$\frac{1}{\sin\vartheta}\frac{\mathrm{d}}{\mathrm{d}\vartheta}\left[(1-u^2)P_j'(u)\right] = -\frac{\mathrm{d}}{\mathrm{d}u}\left[(1-u^2)P_j'(u)\right] = j(j+1)P_j(u).$$

Substituting this identity term by term into Eq. (G7) gives Eq. (G8). □

The intensity shown in the figures is the pointwise squared shell amplitude

$$I_\chi(\vartheta) = \left| U_\varphi^{[J_{\max}]}(\vartheta) \right|^2. \tag{G9}$$

It is dimensionless in the normalization of Eqs. (G1) and (G3).

Remark. The figures in this appendix are intended to make the source geometry transparent. They are not used to define the source, to choose the cutoff, or to fit the vector input. The source sequence and its finite toroidal reconstruction are defined by Eqs. (G1) to (G3) and (G5), while the figures only display that reconstruction. Increasing $J_{\max}$ changes the finite diagnostic reconstruction and the finite-cutoff ledger quantities. Replacing the reduced vector ledger by an operator-limit computation would change the images only through the corresponding change in the underlying source data.

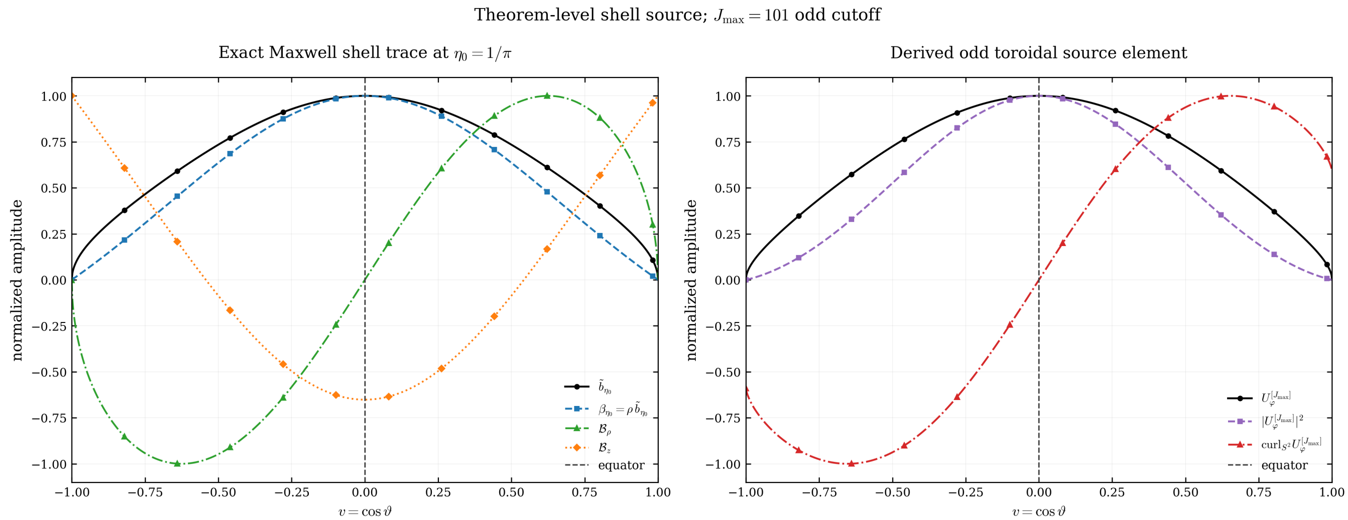

FIG. 13. Exact shell trace and derived odd toroidal source. The left panel shows the normalized Maxwell shell trace $\widetilde{b}_{\eta_0}$, the weighted trace $\beta_{\eta_0} = \rho_\perp(\upsilon)\widetilde{b}_{\eta_0}$, and the two field components $\mathcal{B}_\rho$ and $\mathcal{B}_z$, all as functions of the plotted variable $v = \upsilon = \cos\vartheta$. The right panel shows the finite odd-source reconstruction $U_\varphi^{[J_{\max}]}$, its intensity, and its scalar surface curl.

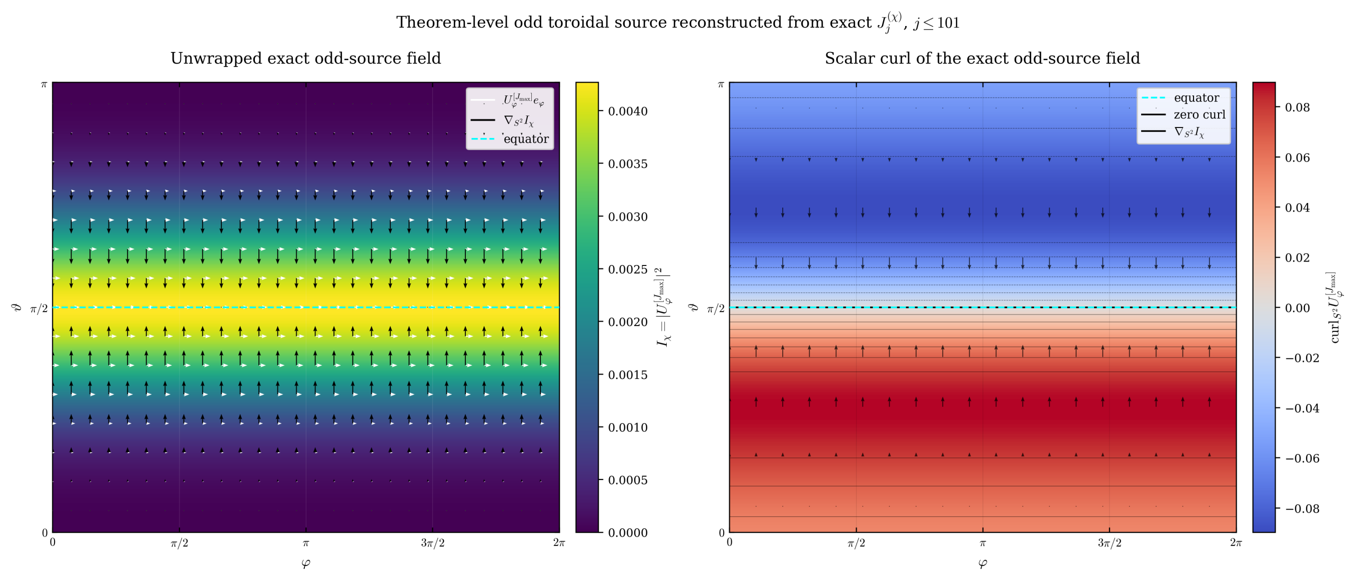

FIG. 14. Unwrapped view of the theorem-level odd toroidal source on the shell. The horizontal coordinate is φ, and the vertical coordinate is ϑ. The left panel shows the source intensity $I_\chi = |U_\varphi^{[J_{\max}]}|^2$. White arrows show the toroidal direction $U_\varphi^{[J_{\max}]}\hat{\mathbf{e}}_\varphi$, while black arrows show the angular gradient $\nabla_{\mathbb{S}^2} I_\chi$ on the normalized shell. The right panel shows the scalar curl field, with the zero-curl contour and the same equator marker. The plot makes the two separate roles visible; the toroidal source is divergence-free, while the scalar curl changes sign across the equatorial symmetry line.

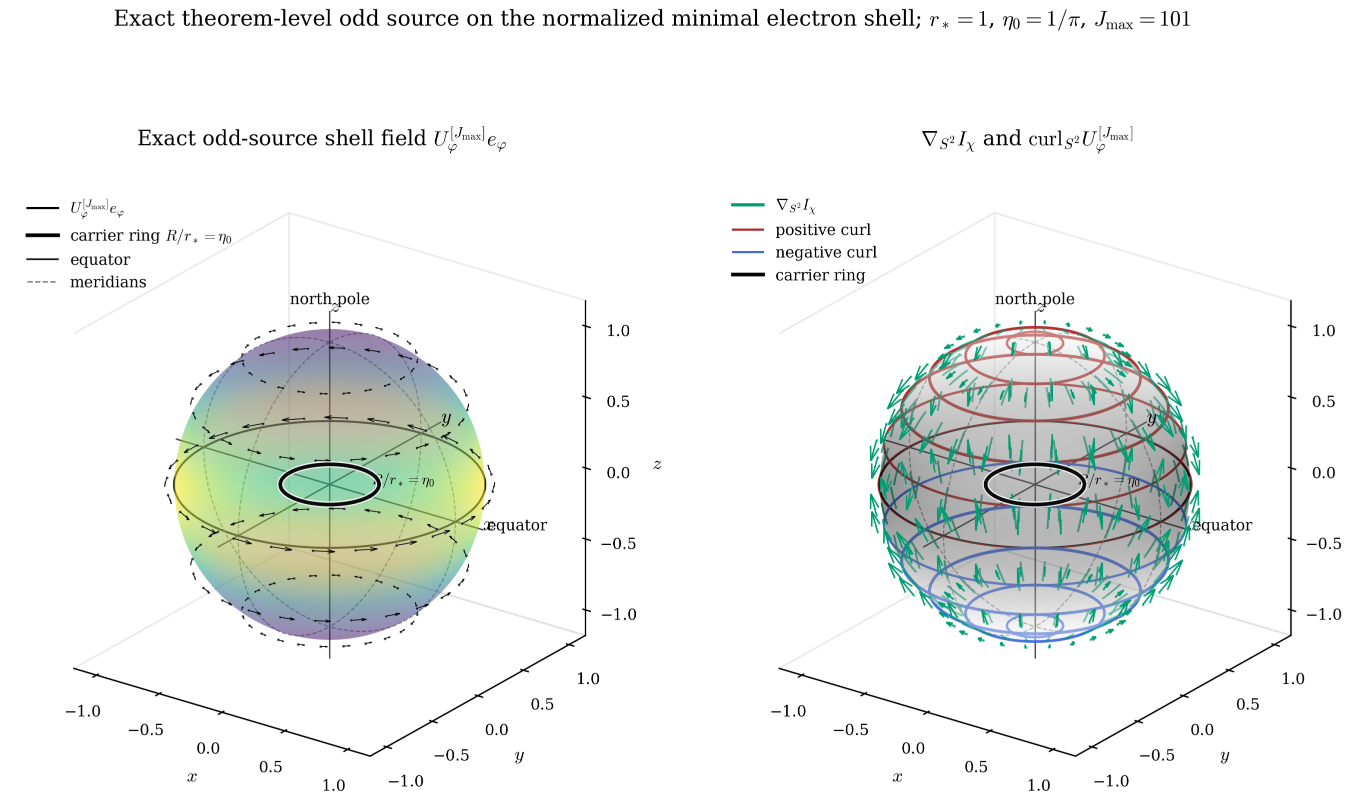

FIG. 15. Three-dimensional shell visualization of the same finite odd-source field. The left panel shows the toroidal field $U_\varphi^{[J_{\max}]}\hat{\mathbf{e}}_\varphi$ on the normalized matching sphere $r_* = 1$, with the carrier ring $R/r_* = \eta_0$ shown in black. The right panel shows the surface-gradient direction $\nabla_{\mathbb{S}^2} I_\chi$ together with latitude rings colored by the sign of the scalar curl of $\mathbf{U}_\chi^{[J_{\max}]}$. Red rings denote positive scalar curl and blue rings denote negative scalar curl. The figure is a geometric visualization of the finite odd-mode source and is not a replacement for the numerical vector ledger.

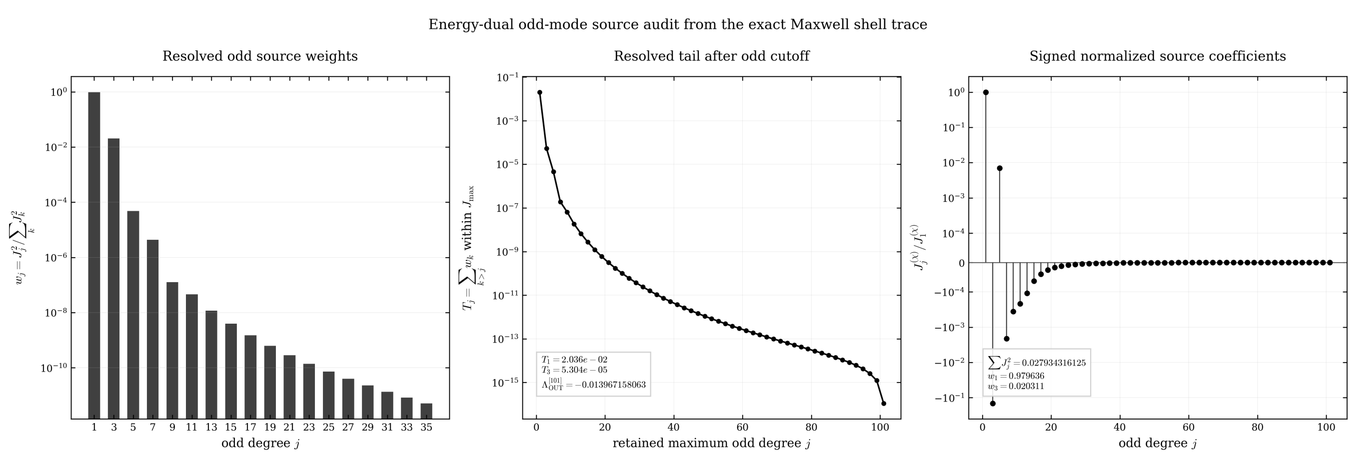

FIG. 16. Odd-mode source audit for the finite cutoff $J_{\max} = 101$. The left panel shows the resolved weights $w_j = J_j^2/\sum_k J_k^2$. The middle panel shows the remaining resolved tail $T_j = \sum_{k>j} w_k$ inside the same finite cutoff. The right panel shows the signed normalized coefficients $J_j^{(\chi)}/J_1^{(\chi)}$ on a symmetric logarithmic scale. These diagnostics indicate that the finite source is dominated by the lowest odd modes and that the high-mode tail is numerically small within the displayed cutoff. The number displayed for $\Delta\Lambda_{\mathrm{out}}^{[101]}(\eta_0)$ is the finite-cutoff ledger value entering the reduced vector realization.

[1] A. Sommerfeld, Zur quantentheorie der spektrallinien, Annalen der Physik **356**, 1 (1916).

[2] P. A. M. Dirac, The quantum theory of the electron, Proceedings of the Royal Society A **117**, 610 (1928).

[3] R. P. Feynman, R. B. Leighton, and M. Sands, *The Feynman Lectures on Physics, Vol. I*, Vol. 17 (Addison–Wesley, Reading, MA, 1964) pp. 45–46, see Ch. 2 for the 1/137 coupling remark.

[4] R. Bouchendira, P. Cladé, S. Guellati-Khélifa, F. Nez, and F. Biraben, New determination of the fine structure constant and test of the quantum electrodynamics, Physical Review Letters **106**, 080801 (2011).

[5] R. H. Parker, C. Yu, W. Zhong, B. Estey, and H. Müller, Measurement of the fine-structure constant as a test of the standard model, Science **360**, 191 (2018).

[6] L. Morel, Z. Yao, P. Cladé, and S. Guellati-Khélifa, Determination of the fine-structure constant with an accuracy of 81 parts per trillion, Nature **588**, 61 (2020).

[7] X. Fan, T. G. Myers, B. A. D. Sukra, and G. Gabrielse, Measurement of the electron magnetic moment, Physical Review Letters **130**, 071801 (2023), arXiv:2209.13084 [physics.atom-ph].

[8] E. Tiesinga, J. W. Pratt, P. J. Mohr, and D. B. Newell, Codata recommended values of the fundamental physical constants: 2022, Reviews of Modern Physics **97**, 025002 (2025).

[9] E. Schrödinger, An undulatory theory of the mechanics of atoms and molecules, Physical Review **28**, 1049 (1926).

[10] C. E. Shannon, A mathematical theory of communication, Bell System Technical Journal **27**, 379 (1948).

[11] E. T. Jaynes, Information theory and statistical mechanics, Physical Review **106**, 620 (1957).

[12] W. V. D. Hodge, *The Theory and Applications of Harmonic Integrals* (Cambridge University Press, Cambridge, 1941).

[13] R. G. Barrera, G. A. Estévez, and J. Giraldo, Vector spherical harmonics and their application to magnetostatics, European Journal of Physics **6**, 287 (1985).

[14] J. D. Jackson, *Classical Electrodynamics*, 3rd ed. (Wiley, New York, 1998).

[15] T. Kaluza, Zum unitätsproblem der physik, Sitzungsberichte der Königlich Preussischen Akademie der Wissenschaften **122**, 966 (1921), english transl. available; see arXiv:1803.08616.

[16] O. Klein, Quantum theory and five-dimensional relativity, Zeitschrift für Physik **37**, 895 (1926), eng. transl. in: *The Oskar Klein Memorial Lectures*, World Scientific (2014).

[17] J. D. Bjorken and S. D. Drell, *Relativistic Quantum Mechanics* (McGraw-Hill, New York, 1964).

[18] H. B. Lawson and M.-L. Michelsohn, *Spin Geometry* (Princeton University Press, Princeton, 1989).

[19] W. Pauli, Zur quantenmechanik des magnetischen elektrons, Zeitschrift für Physik **43**, 601 (1927).

[20] L. L. Foldy and S. A. Wouthuysen, On the dirac theory of spin 1/2 particles and its non-relativistic limit, Physical Review **78**, 29 (1950).

[21] P. Cladé, E. de Mirandes, M. Cadoret, S. Guellati-Khélifa, C. Schwob, F. Nez, L. Julien, and F. Biraben, Determination of the fine structure constant based on bloch oscillations of ultracold atoms, Physical Review Letters **96**, 033001 (2006).

[22] M. Cadoret, E. de Mirandes, P. Cladé, S. Guellati-Khélifa, C. Schwob, F. Nez, L. Julien, and F. Biraben, Combination of bloch oscillations with a ramsey–bordé interferometer: New determination of the fine structure constant, Physical Review Letters **101**, 230801 (2008).

[23] S. Volkov, Calculation of the total 10th order qed contribution to the electron anomalous magnetic moment, Phys. Rev. D **110**, 036001 (2024), arXiv:2404.00649 [hep-ph].

[24] T. Aoyama, T. Kinoshita, and M. Nio, Theory of the anomalous magnetic moment of the electron, Atoms **7**, 28 (2019).

Author's note. The manuscript focuses on the emergent-α mechanism and on the universal pure-photonic electron $g-2$ coefficients that follow from the specified scalar-shell realization. Possible extensions to charged-particle mass hierarchies and family spectra are left to separate work.